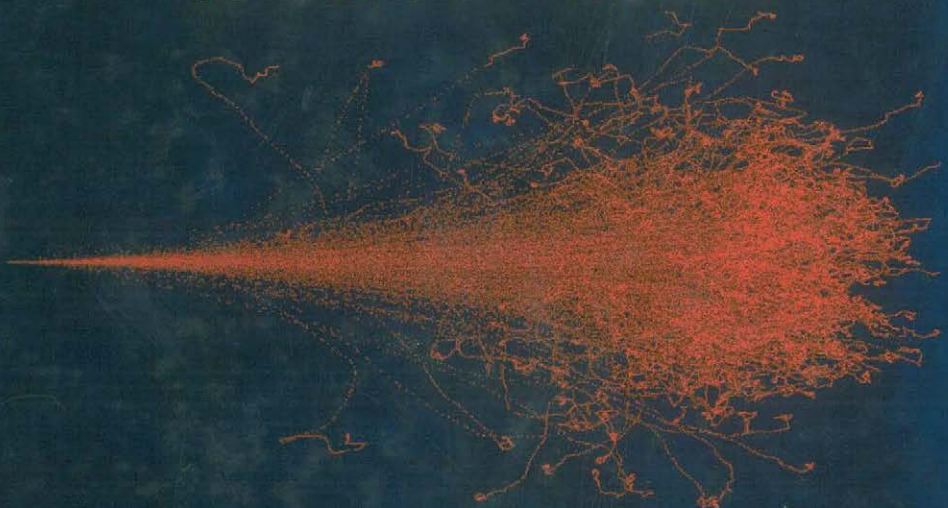


SRIM

The Stopping and Range of Ions in Matter



J. F. Ziegler
J. P. Biersack
M. D. Ziegler

S

R

I

M

7

Dedicated to my sons,
Samuel and Matthias,
and to the
Love of My Life
Ann Ziegler

SRIM

The Stopping and Range of Ions in Matter

James F. Ziegler

United States Naval Academy

Annapolis, MD, 21402, USA

Ziegler@SRIM.org

Jochen P. Biersack

Hahn-Meitner Institute

I Berlin 39, Germany

Matthias D. Ziegler

University of California at Los Angeles

Los Angeles, CA, 90066, USA

MZiegler@SRIM.org

*The version number of this book is shown on the book's spine
Full details of changes are listed in this book's last pages*

(www.SRIM.org)

SRIM Co.
2835 Cox Neck Rd.
Chester, Maryland, 21619
U.S.A.
www.SRIM.org

Library of Congress Cataloging-in-Publication Data

SRIM - THE STOPPING AND RANGE OF IONS IN MATTER

J. F. Ziegler, J. P. Biersack and M. D. Ziegler

398p. 21.6 x 27.9 cm.

Includes Index.

ISBN -13: 978-0-9654207-1-6

1. SRIM, 2 Ziegler, J. F. (James F.)

QC702.7.I55H38 2008

530.4'16 -- dc20

ISBN-13: 978-0-9654207-1-6

ISBN: 0-9654207-1-X

EAN: 9780965420716

© 2008, SRIM Co., All rights reserved.

Version Number – See Version Comments on last page of this book. The version number of this book is shown as a number on its spine.

No part of this publication may be reproduced, stored in a retrieval system or transmitted in any form or by any means, electronic, mechanical, photocopying, scanned, recording or otherwise, without the prior written permission of the publisher, SRIM Co., Copyright & Permissions Department, 2835 Cox Neck Rd., Chester, MD, 21619, U.S.A.

Special regulations for readers in the U.S.A.: This publication is being registered with the Copyright Clearance Center Inc. (CCC), Salem, MA. Information can be obtained from the CCC about conditions under which photocopies of parts of the publication may be made in the U.S.A. All other copyright questions, including photocopying outside of the U.S. A., should be referred to the copyright owner, SRIM Co., unless otherwise specified.

No responsibility is assumed by the Publisher for any injury and/or damage to persons or property as a matter of products liability, negligence or otherwise, or from any use or operation of any methods, products, instruction or ideas contained in the material herein.

Other Books by J. F. Ziegler

- "*Inelastic Electron Scattering by Nuclei*" (1967)
- "*Ion Beam Surface Layer Analysis*" (1973)
- "*New Uses of Ion Accelerators*" (1975)
- "*Hydrogen Stopping Powers and Ranges in all Elements*" (1977)
- "*Bibliography of Experimental Range / Stopping Power Data*" (1977)
- "*Helium Stopping and Ranges in all Elements*" (1978)
- "*Handbook of Heavy Ion Stopping in all Elements*" (1980)
- "*Handbook of the Range Distributions of Energetic Ions*" (1980)
- "*Ion Implantation - Science and Technology*" (1984)
- "*Ion Implantation Equipment and Techniques*" (1985)
- "*The Stopping and Range of Ions in Solids*" (1985)
- "*Ion Implantation - Science and Technology, 2nd Edition*" (1988)
- "*Ion Beam Analysis*" (1990)
- "*Handbook of Ion Implantation Technology*" (1994)
- "*Ion Implantation - Science and Technology, 6th Edition*" (1998)
- "*Ion Implantation - Science and Technology, 2000 Edition*" (2000)
- "*Ion Implantation - Science and Technology, 2002 Edition*" (2002)
- "*The Stopping and Range of Ions in Solids*" (2002)
- "*Soft Fails – History, Trends and Challenges*" (2004)
- "*Ion Implantation - Science and Technology, 2004 Edition*" (2004)
- "*Ion Implantation - Science and Technology, 2006 Edition*" (2006)

SRIM

The Stopping and Range of Ions in Matter

Ch 1 - Historical Review

Ch 2 - Nuclear Stopping of Ions

Ch 3 - Electronic Stopping of Ions

Ch 4 - Stopping of Energetic Light Ions

Ch 5 - Stopping of Ions in Compounds

Ch 6 - Ion Straggling

Ch 7 - TRIM : Scientific Background

Ch 8 - TRIM : Setup and Input

Ch 9 - TRIM : Output Files

Ch 10 - Stopping and Range Tables

Ch 11 - SRIM Tutorials

Ch 12 - References and Index



The Stopping and Range of Ions in Matter

Preface

This book covers the physical phenomena associated with the penetration of energetic ions into matter. It is primarily concerned with the quantitative evaluation of how ions lose energy into matter and the final distribution of these ions after they stop within the target. Also considered are the first order effects of the atoms on solids, particularly the electronic excitation of the atoms, the displacement of lattice atoms by energetic collisions (lattice damage) and the production of plasmons and phonons within the solid by the passing ions. No evaluation is made of thermal effects in the solid, especially redistribution of lattice atoms or implanted ions by thermal or vacancy induced diffusions.

The scientific literature contains a large amount of experimentally determined stopping powers and ion range distributions. These are not, however, so accurate or dense that direct interpolation to other systems is usually possible. The main goal of this work is to establish methods for determining the stopping and range of ions based on accurate experimental data and extending these values using unified theoretical concepts.

The theoretical chapters of this book are Chapters 2 (Nuclear Stopping in Matter) and 3 (Electronic Stopping in Matter) and they are presented in an elementary tutorial style which needs little background. Chapters 3 and 4 presents the traditional stopping of point charges in matter which can be quite accurate for energetic H or He ions (>2 MeV/u) in targets.

Chapter 5 discusses the important matter of variations in stopping in targets in various phases (solid, liquid and gas) and the effects of chemical binding on stopping in compounds.

Chapter 6 is a chapter on the most challenging subject of this book – straggling. It considers the variations of stopping and ranges of ions about their mean values. It is recommended for those who like deep mathematical challenges.

Chapters 7-9 discuss the TRIM software code. Chapter 7 gives the scientific and mathematical background. Chapter 8 discusses how to set TRIM up for a wide range of problems. And Chapter 9 evaluates the various types of output files, and what they mean.

Chapter 10 is a discussion of PRAL, and transport calculation for quick tables of the range of ions in targets.

Chapter 11 is a set of Tutorials to help students and new users to be come used to SRIM.

Each chapter has its own list of citations, and these are all brought together at the end of this book. Finally, an Index is included of the most important subjects in the book.

Nomenclature:

For about a century, the energy loss of ions in matter has been called the ion's Stopping Power. In the 1990's, Peter Sigmund, one of the most distinguished theorists in this field, suggested that the term be changed to ***Stopping Force***, since this is consistent with the units of stopping, which normally are the energy loss per unit path length. This suggestion was both logical and reasonable, but changing such a phrase after a century of use was possibly more difficult than one suggestion, no matter how reasonable, could achieve. Sigmund has recently suggested that such a change would probably be glacially slow (2006a). This book is a textbook, and we need to help students learn from classical papers which almost always use the traditional phrase. Hence, we shall use ***Stopping Power***, but in various places have explained that this is an historical phrase, and ***Stopping Force*** would be more accurate.

A second suggestion by Sigmund concerned the ***Barkas Effect***. This name came from an early paper by Barkas (1963) that showed that the pions appeared to have two different ranges in photographic emulsion, and it was postulated that one range was related to π^+ particles and one to π^- particles. Since the π^- particles would be attracted towards the nucleus of atoms, and π^+ particles repelled, the π^- particles would transit a more dense cloud of electrons and have greater stopping powers, and hence lower ranges. A later paper by Andersen et al. (1969) evaluated the stopping of protons, deuterons and alpha particles in metals. They showed that there was a distinct difference in stopping for high velocity particles that couldn't be accounted for by traditional Bethe-Bloch formalism (see Chapter 4), and that it was necessary to include a Z_i^3 term. This is the same conclusion that would be reached by analysis of the earlier Barkas effect experiments. Sigmund suggested that the traditional name for the "***Barkas Effect***", be called the "***Barkas-Andersen Effect***" since Andersen's work was much clearer in suggesting the cause of the variations observed. We agree with this, and have used the "***Barkas-Andersen Effect***" for the Z_i^3 term in the Bethe-Bloch formalism for high velocity stopping.

1 - Introduction and Historical Review

Chapter Contents

1 - INTRODUCTION AND HISTORICAL REVIEW	1-1
Historical Summary.....	1-1
Quantum Mechanics and Stopping Theory (1930 - 1935).....	1-8
Analysis of Fission Fragments (1938 - 1941)	1-8
Particle Stopping in a Free Electron Gas (1947 - 1960)	1-12
Theories for Stopping & Ranges of Heavy Ions (1963 - 1985).....	1-16
“Stopping Power” vs. “Stopping Force”	1-18
Citations for Chapter 1.....	1-19

Historical Summary

The history of the penetration of a particle into matter might begin 400 years ago with the study of projectile ballistics, since the understanding of cannonballs in a viscous medium might be considered similar to the penetration of particles in matter.¹ However, in this chapter, we shall review only the last century, from the discovery of radioactive particles (1895). Certain terminology is traditional, and we shall use it from the beginning:

Ion	The moving atom, whether it is charged or neutral. Its atomic number is Z_1 , its mass is M_1 , its energy is E , and its velocity is E/M_1 . This velocity is only used to compare relative velocities, so the fact that it is squared is usually ignored
Atom	Any target atom, with atomic number, Z_2 , and mass, M_2
Stopping Power	The rate of energy loss by the ion in the target, defined as dE/dx , the energy loss per unit distance, x . Some authors use <i>stopping cross-sections</i> , <i>stopping force</i> , or <i>inelastic losses</i> or similar descriptions for the same concept. See discussion at end of this chapter.

The development of the theory of an ion slowing in a solid has been difficult because the problem of describing both the ion and the target is complex. Once the ion penetrates a solid, it is quickly stripped of some of its electrons, and its charge state becomes a function of the target. The target

¹A study was done by Leonardo DaVinci on catapults and how to increase the range of the projectiles (~1580). Unfortunately, his knowledge of dynamics was not as good as his analysis of static structures (levers, etc.) and he began with the unfortunate premise that the velocity of a projectile was proportional to the maximum force exerted on it, and hence what he actually derived was an early version of GIGO (Garbage In → Garbage Out). Other studies were published by Galileo and Newton. But of special note was the analysis by a British vicar, Benjamin Robins, who attempted to help his Navy design better cannons during the Napoleonic Wars. His treatise, published in 1804, was called “New Principles of Gunnery” and reached the important conclusion that the energy loss of a projectile in a viscous medium was proportional to its velocity (see ref. 1804). This result was widely discussed and criticized, until Robins invented a ballistic pendulum apparatus to measure the effect. Since his result is similar to the quantum mechanical solution for the energy loss of charged particles in an electron gas, developed 130 years later, it is worth noting Robins’s major scientific contribution. Similar studies were published by Euler, Laplace and Lavoisier, all of whom reached the same conclusion as Robins for low speed projectiles.

feels the ion coming, and its electrons polarize around the moving ion. The charge state of the ion is modified by the polarized target, which then further affects the target. The merging of the incident ion's electrons with the electrons of target atoms causes quantum exclusions of some available states – a complicated matter which is very important in evaluating energy transfer from the ion to the target.. Finally, all of these effects depend on the constantly changing ion velocity.

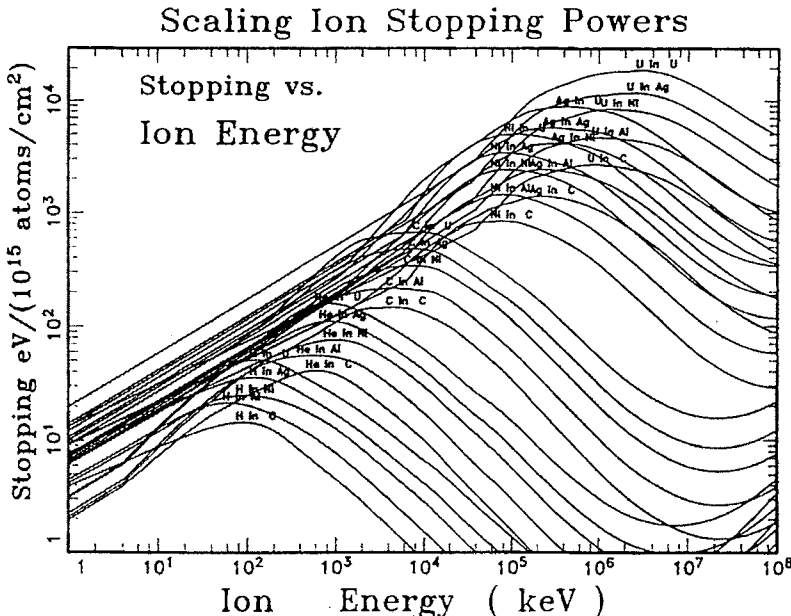


Figure 1-1 The Stopping of Ions in Various Solids

This figure shows the stopping power of ions from H to U in various elemental targets from C to U. The stopping is in units of $eV/(10^{15} \text{ atoms}/\text{cm}^2)$, which is approximately the energy loss per monolayer of a solid. The ion energies extend over eight orders of magnitude, which covers most scientific applications. The data in this figure will be used later in this chapter to illustrate advances in stopping theory.

In order to understand historical conceptual advances, it is illustrative to show how new ideas affect the scaling of stopping powers, i.e. the relative change of stopping between ions or targets or as a function of ion energy. Shown in Figure 1-1. are the stopping powers of various ions (H, He, C, Ni, Ag and U) in various solids (C, Al, Ni, Ag, U) over 8 decades of energy. The stopping powers range over a factor of 10,000. We shall use this figure to show how new ideas affect the scaling of these curves, and with simple rules the total variation reduces to less than a factor of 2.

Early Studies with Radioactive Particles (1899 - 1920)

Soon after the discovery of energetic particle emission from radioactive materials, there was interest in how these corpuscles were slowed down in traversing matter. From her work in 1898-1899, Marie Curie stated the hypothesis that "les rayons alpha sont des projectiles materiels susceptibles de perdre de leur vitesse en traversant la matiere." (00a). Figure 1-2 shows her apparatus, in which particles emitted from radium (source A) went through thin metallic films (at T) and were counted by using an electrometer (P).

By varying the thickness of the metallic film, she was able to find the energy loss of the particles as a function of the density of the metal. Many scientists immediately realized that since these particles could penetrate thin films, such experiments might finally unravel the secrets of the atom. Early attempts to create a particle energy loss theory were inconclusive for there was not yet an accurate proposed model of the atom.

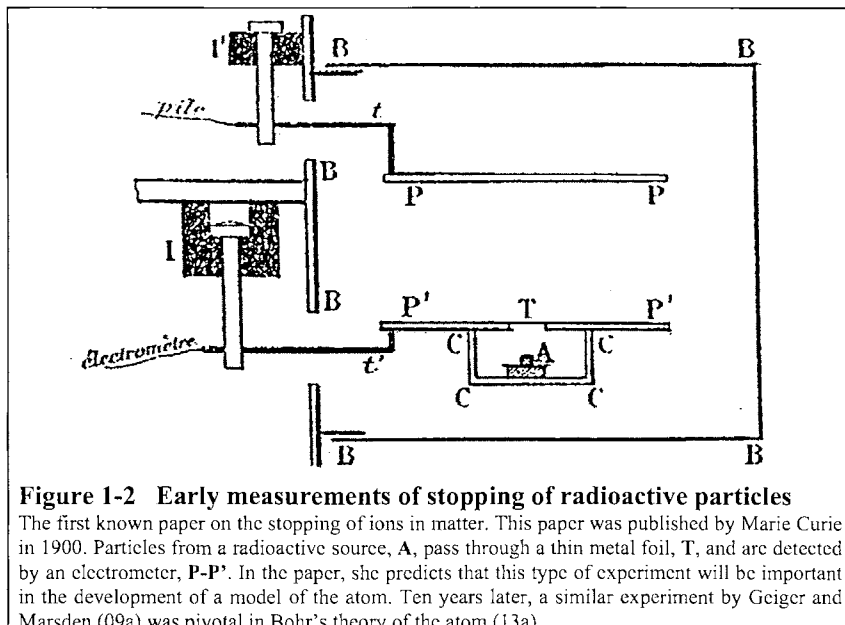


Figure 1-2 Early measurements of stopping of radioactive particles

The first known paper on the stopping of ions in matter. This paper was published by Marie Curie in 1900. Particles from a radioactive source, A, pass through a thin metal foil, T, and are detected by an electrometer, P-P'. In the paper, she predicts that this type of experiment will be important in the development of a model of the atom. Ten years later, a similar experiment by Geiger and Marsden (09a) was pivotal in Bohr's theory of the atom (13a).

The theoretical treatment for the scattering of two point charges was derived by J. J. Thomson in his classic book on electricity (03a), see Figure 1-3. Much of the traditional particle energy-loss symbolism can be traced to this book which introduced a comprehensive treatment for classical Coulombic scattering between energetic charged particles. This work, however, did not attempt to calculate actual stopping powers.

THE
LONDON, EDINBURGH, AND DUBLIN
PHILOSOPHICAL MAGAZINE
AND
JOURNAL OF SCIENCE.

[SIXTH SERIES.]

APRIL 1912.

XLII. *Ionization by Moving Electrified Particles.*
By Sir J. J. THOMSON.*

THE theory developed in this paper is based on the following assumptions:—

1. Cathode or positive rays when they pass through an atom repel or attract the corpuscles in it and thereby give to them kinetic energy.
2. When the energy imparted to a corpuscle is greater than a certain definite value—the value required to ionize the atom—a corpuscle escapes from the atom, and a free corpuscle and positively charged atom are produced.

We must first find under what circumstances a cathode ray moving with a given velocity will lose when it passes by a corpuscle a quantity of energy greater than the amount required to ionize an atom.

In my ‘Conduction of Electricity through Gases’ it is shown that when a body with a charge E_1 in electrostatic units and mass M_1 is projected with a velocity V towards a body with a charge E_2 and mass M_2 at rest, the energy Q transferred to the latter is given by the equation

$$Q = \frac{4M_1 M_2}{(M_1 + M_2)^2} T \sin^2 \theta,$$

* Communicated by the Author.

Phil. Mag. S. 6. Vol. 23. No. 136. April 1912. 2 H

Figure 1-3 J. J. Thomson's first paper on stopping theory

A reproduction of the first extended theoretical paper on the energy loss of charge particles in matter. Many of the symbol conventions used in stopping theory originate from this paper.

Enough experimental evidence of radioactive particle interactions with matter was collected in the next decade to make stopping power theory one of the central concerns of those attempting to develop an atomic model. In 1909 Geiger and Marsden were studying the penetration of alpha-particles through thin foils, and the spread of the trajectories after emerging from the back side. They hoped to determine the distribution of charges within the foil by the angular spread of the transmitted beam. There are conflicting histories as to who made the suggestion that they look for backscattered particles - but the subsequent startling data reversed the current thought on atomic structure. They reported that about .01% of the heavy alpha-particles were scattered back from the target, and from an analysis of the data statistics such backscattered events had to be from isolated single collisions. Two years later, Rutherford was able to demonstrate theoretically (11a) that the backscattering was indeed due to a single event, and by analyzing this and electron scattering data he was able to first calculate that the *nucleus* of Al atoms must have a charge of about 22 and platinum would have a charge of 138 !

J. J. Thomson, director of the prestigious Cavendish Laboratory, and Niels Bohr, a fresh post-doctoral scientist who had left the Cavendish lab for Rutherford's Manchester Laboratory, published almost simultaneously (12a,13a) an analysis of the stopping of charged particles by matter, see Figure 1-4 . These papers illustrate much of their divergent ideas on the model of an atom. Thomson incredibly ignored in his paper the alpha-particle backscattering measurements of Geiger (09a) and the Rutherford heavy-particle scattering theory (11a) which emphasized the atomic positive charge must be concentrated within the atom. But the nuclear atom with a heavy positively-charged core was the basis of Bohr's ideas. (13a,15a).

Bohr's early work is instructive because for the first time a unified theory of stopping was attempted, and we can see in this and in similar works the essential problems of stopping theory:

- How does an energetic charged particle (a point charge) lose energy to the quantized electron plasma of a solid (inelastic energy loss)?
- How do you incorporate into this interaction simultaneous distortion of the electron plasma caused by the particle (target polarization)?
- How can you extend the point charge-plasma interaction to that for a finite moving atom in a plasma?
- How do you estimate the degree of ionization of the moving atom and describe its electrons when it is both ionized and within an electron plasma?
- How do you calculate the screened Coulomb scattering of the moving atom with each heavy target nucleus it passes?
- How do you include relativistic corrections to all of the above?

This is a brief list of the major problems encountered, and scientific interest shifts back and forth between them over the decades because of external scientific tidal forces. Examples might be (a) the development of quantal scattering in the 1920's, (b) the study of nuclear fission in the 1930's and 1940's, (c) the study of nuclear physics in the 1950's, (d) the technological applications of ion implantation for material modification in the 1960's, (e) the use of ion beams in material analysis in the 1970's, and (f) the use of ion beams in radiation oncology in the 1980's and 1990's. This ebb and flow of interest continues because of the recurrent importance of the problem, and the difficulty of calculating the penetration of energetic atoms in solids from first principles. We briefly review some of the historical milestones in this field below.

THE
LONDON, EDINBURGH, AND DUBLIN
PHILOSOPHICAL MAGAZINE
AND
JOURNAL OF SCIENCE.

[SIXTH SERIES.]

JANUARY 1913.

II. On the Theory of the Decrease of Velocity of Moving Electrified Particles in passing through Matter. By N. BOHR, Dr. phil. Copenhagen*.

WHEN cathode-rays or α - and β -rays penetrate through matter their velocity decreases. A theory of this phenomena was first given by Sir J. J. Thomson†. In the calculation of this author the cathode- and β -rays are assumed to lose their velocity by collisions with the electrons contained in the atoms of the matter. The form of the law, found by this calculation, connecting the velocity of the particles and the thickness of matter traversed, has been recently shown by Whiddington‡ to be in good agreement with experiments. Somewhat different conceptions are used in the calculation of Sir J. J. Thomson on the absorption of α -rays, as the latter, on account of their supposed greater dimensions, are assumed to lose their velocity by collisions, not with the single electrons but with the atoms of the matter considered as entities.

According to the theory given by Professor Rutherford § of the scattering of α -rays by matter, the atoms of the matter are supposed to consist of a cluster of electrons kept together by attractive forces from a nucleus. This nucleus, which possesses a positive charge equal to the sum of the negative charges on the electrons, is further supposed to be the seat of the essential part of the mass of the atom, and to have dimensions which are exceedingly small compared with the dimensions of the atom. According to this theory an α -particle consists simply of the nucleus of a helium atom. We see that after such a conception there is no reason to discriminate materially between the collisions of an atom with an α - or β -particle—apart of course from the differences due to the difference in their charge and mass.

An elaborate theory of the absorption and scattering of α -rays, based on Professor Rutherford's conception of the constitution of atoms, was recently published by C. G. Darwin||. In the theory of this author the α -particles simply penetrate the atoms and act upon the single electrons contained in them, by forces varying inversely as the square

* Communicated by Prof. E. Rutherford, F.R.S.
† J. J. Thomson, "Conduction of Electricity through Gases," pp. 570-82.

‡ H. Whiddington, Proc. Roy. Soc. A, xxvii, p. 360 (1912).

§ E. Rutherford, Phil. Mag. xli, p. 693 (1911).

|| C. G. Darwin, Phil. Mag. xxiii, p. 907 (1912).

THE
LONDON, EDINBURGH, AND DUBLIN
PHILOSOPHICAL MAGAZINE
AND
JOURNAL OF SCIENCE.

[SIXTH SERIES.]

OCTOBER 1915.

LX. On the Decrease of Velocity of Swiftly Moving Electrified Particles in passing through Matter. By N. BOHR, Dr. Phil. Copenhagen; p. l. Reader in Mathematical Physics, University of Manchester*.

THE object of the present paper is to continue some calculations on the decrease of velocity of α and β rays, published by the writer in a previous paper in this magazine†. This paper was concerned only with the mean value of the ratio of decrease of velocity of the swiftly moving particles, but from a closer comparison with the measurements it appears necessary, especially for β rays, to consider the probability distribution of the loss of velocity suffered by the single particles. This problem has been discussed briefly by K. Hersfeld‡, but on assumptions as to the mechanism of decrease of velocity essentially different from those used in the following*. Another question which will be considered more fully in the present paper is the effect of the velocity of β rays being comparable with the velocity of light. These calculations are contained in the first three sections. In the two next sections the theory is compared with the measurements. It will be shown that the approximate agreement obtained in the former paper is improved by the closer theoretical discussion, as well as by using the recent more accurate measurements. Section 6 contains some considerations on the ionization produced by α and β rays. A theory for this phenomenon has been given by Sir J. J. Thomson†.

§ 1. The average value of the rate of decrease of velocity.

For the sake of clearness it is desirable to give a brief summary of the calculations in the former paper. References to the previous literature on the subject will be found in that paper.

Following Sir Ernest Rutherford, we shall assume that the atom consists of a central nucleus carrying a positive charge and surrounded by a cluster of electrons kept together by the attractive forces from the nucleus. The nucleus is the seat of practically the entire mass of the atom, and has dimensions exceedingly small compared with the dimensions of the surrounding cluster of electrons. If an α - or β particle passes through a sheet of matter it will penetrate

Figure 1-4 The two most important papers in early ion stopping theory

Shown are reproductions of the first two papers by Niels Bohr on the stopping of charged particles in matter. Bohr had finished his Ph.D. in 1911. After an unsympathetic visit with J. J. Thomson, Bohr went to work with Rutherford at the Manchester Laboratory and produced these papers. Between these papers he also developed and published his theory of the atom which suggested the quantization of angular momentum.

Both Thomson and Bohr concluded that the particle's velocity was more important than its energy, see Figure 1-5.

One of Bohr's original conclusions was that the energy loss of ions passing through matter could be divided into two components: nuclear stopping (energy loss to the medium's atomic positive cores) and electronic stopping (energy loss to the medium's light electrons). Bohr, in his first papers, correctly deduced that the electronic stopping would be far greater than the nuclear stopping for energetic light ions such as are emitted by radioactive sources. This conclusion was based on recoil kinematics considering only the relative masses and abundance of the target electrons and nuclei.

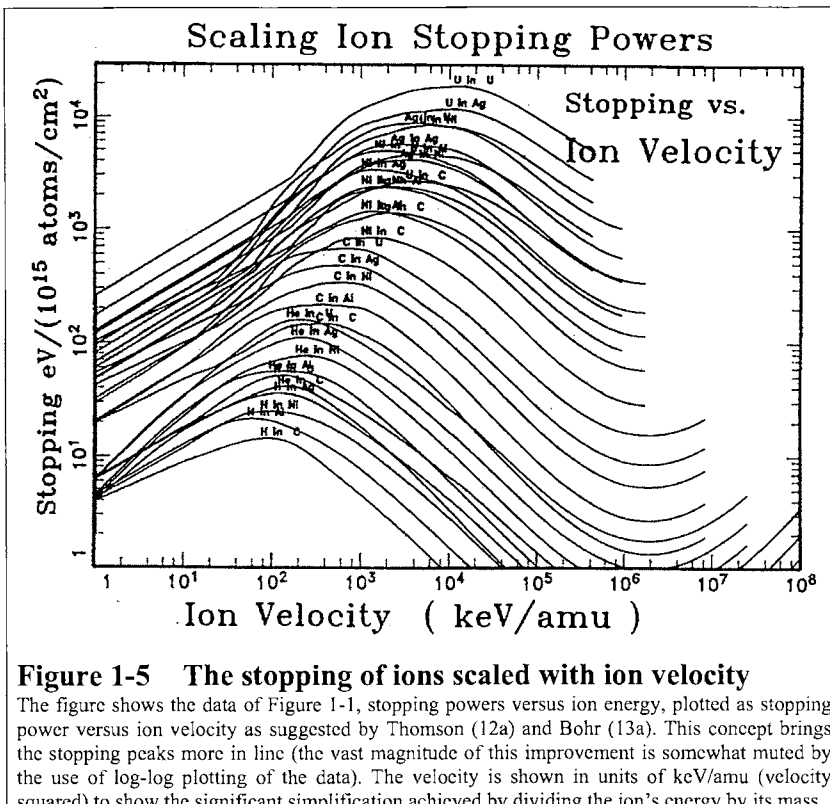


Figure 1-5 The stopping of ions scaled with ion velocity

The figure shows the data of Figure 1-1, stopping powers versus ion energy, plotted as stopping power versus ion velocity as suggested by Thomson (12a) and Bohr (13a). This concept brings the stopping peaks more in line (the vast magnitude of this improvement is somewhat muted by the use of log-log plotting of the data). The velocity is shown in units of keV/amu (velocity squared) to show the significant simplification achieved by dividing the ion's energy by its mass.

Bohr further introduced atomic structure into stopping theory by giving target electrons the orbit frequencies obtained from optical spectra and calculating the energy transferred to such harmonic oscillators. He noted that the experimentally reported stopping powers for heavy atom targets indicated that many electrons in these targets must be more tightly bound than the optical data suggested. He also realized that his accounting of the energy loss process was seriously limited

by a lack of knowledge of the charge state of the ion inside the matter, i.e., its effective charge in its interaction with the target medium.

Quantum Mechanics and Stopping Theory (1930 - 1935)

A major advance in understanding stopping powers came 20 years later when Bethe (30a,32a,34a) and Bloch (33a,33b) restated the problems from the perspective of quantum mechanics, and derived in the Born approximation the fundamental equations for the stopping of very fast particles in a quantized medium, see Figure 1-6. This theoretical approach remains the basic method for evaluating the energy loss of light particles with velocities of 10 MeV/amu - 2 GeV/amu. This restriction in velocity is because below these velocities the ion projectile may not be fully stripped of its electrons (which is assumed by the theory), and above this velocity there are additional relativistic corrections.

Analysis of Fission Fragments (1938 - 1941)

In the late 1930's a renewed interest was taken in energy loss with the discovery of nuclear fission and the energetic heavy particles which resulted from nuclear disintegration, see Hahn and Strassmann paper which led to their Nobel Prize (39b). Various theoretical studies were published by Bohr (40d), Lamb (40b), Knipp (41b), Teller and Fermi (40c), see Figure 1-7 and Figure 1-8.

The problem presented by the fission fragment data was how to treat the interaction of a *partially stripped* heavy ion. This is called the 'effective-charge' problem, for it was hoped that if a degree of ionization for the projectile could be estimated, then the traditional stopping power theories could be used. Bohr suggested (40d,41a) that the ion be considered to be stripped of all electrons with velocities lower than the ion velocity, and using the Thomas Fermi atom he could show that

$$\text{Eq. 1-1:} \quad Z_1^* = Z_1^{1/3} V / V_0$$

where Z_1 is the atomic number of the ion, and Z_1^* is its effective charge in energy loss to the target electrons, V is the ion velocity and V_0 is the Bohr velocity ($\approx 2 \times 10^8$ cm/sec). Lamb (40b) considered the same problem as Bohr, and suggested a similar effective charge approximation, but based on the energy rather than the velocity of the ion's electrons. Lamb also got a similar, but less detailed, expression for stopping power assuming Thomas-Fermi atoms. He suggested that the target electron velocity distribution would significantly alter the stopping of the fission fragments, see Figure 1-8.

Fermi (40c) considered the same points as Lamb and Bohr, but concentrated upon evaluating the interaction of a charged particle with the dielectric plasma of a solid, and the electric polarization of the medium by the particle. This polarization of the target medium had been suggested first by Swann (38a), and Fermi was able to reduce this difficult problem to a form which could be calculated. He showed that stopping powers were universally proportional to target density, on an equal - mass - traversed basis.

A detailed suggestion for scaling stopping powers was shown by Knipp and Teller (41b), who successfully used the effective charge concept of Bohr and Lamb to scale H stopping values to equivalent He ion stopping powers. These theoretical studies had only limited success with the fission fragment problem, and the primary practical result was to provide scaling relationships for the heavy ion stopping and ranges. That is, it allowed for interpolation and modest extrapolation from existing data into systems with different ions/targets/energies. Basically, the dominant effects were the target material and the ion's velocity. If you knew the stopping of one ion, say a proton, at two velocities in a material, and you knew the stopping of a heavy ion in that material

at one of these velocities, then its stopping at the second velocity would be a direct proportionality. This law was applicable over a wide variety of velocities and ions. In fact it became so widely used that it stimulated several papers of objections to its theoretical shortcomings (63b,72b).

ZEITSCHRIFT FÜR PHYSIK

HERAUSGEGEBEN UNTER MITWIRKUNG
DER
DEUTSCHEN PHYSIKALISCHEN GESELLSCHAFT

Bremsformel für Elektronen
relativistischer Geschwindigkeit.

Von H. Bethe, zurück in Rom.

(Eingegangen am 4. Mai 1932.)

Aus der Theorie von Möller^[1]) wird der Energieverlust von Elektronen relativistischer Geschwindigkeit beim Durchgang durch Materie abgeleitet. Der Energieverlust pro Zentimeter Weg erreicht bei etwa 96% der Lichtgeschwindigkeit ein Minimum und steigt bei höheren Geschwindigkeiten wieder an; für Elektronen verschiedener Massen und Werte bedingt die Abhängigkeit pro Zentimeter Wasser. Eine Tabelle des theoretischen Energieverlustes von Elektronen und Protonen der theoretischen Geschwindigkeit wird gegeben.

1. Bis vor kurzem war es nicht möglich, die Streuung von Elektronen sehr hoher Geschwindigkeit quantenmechanisch zu behandeln, weil die bekannten Ansätze für die Wechselwirkungsenergie zweier Elektronen^[2]) nur bis zur Größenordnung α^4/c^4 exakt waren ($\alpha = \text{Elektronen-}e = \text{Lichtgeschwindigkeit}$). Inzwischen hat Möller^[1]) in einer wichtigen Arbeit die Frage der Wechselwirkungsenergie sehr einfach und befriedigend geklärt, und es ist nunmehr möglich, die Bremsformel für beliebig rasche Elektronen anzugeben, was für die Deutung der Experimente über die körnige Hohenstrahlung von Wichtigkeit ist.

Ein Teilchen der Ladung e möge sich mit der Geschwindigkeit v durch eine Substanz hindurchbewegen, welche in der Volumeneinheit N Atome der Ordnungszahl Z enthält. Dann verliert das Teilchen pro Zentimeter Weg die Energie

$$-\frac{dT}{dx} = \frac{2\pi e^4 N Z v^2}{mc^2} \left(\ln \frac{2mv^2 W}{E^4 (1 - \frac{v^2}{c^2})} - \frac{v^2}{c^2} \right). \quad (1)$$

Bremsvermögen von Atomen mit mehreren Elektronen.

Von F. Bloch in Leipzig.

Mit 3 Abbildungen. (Eingegangen am 22. Dezember 1932.)

Das Bremsvermögen komplizierterer Atome wird nach der Methode von Thomas-Fermi berechnet. Es ergibt sich ein einfacher Gang mit der Ordnungszahl, der im guten Einklang mit der Erfahrung steht.

f 1. Erläuterung. Das Problem, die Bremsung rasch bewegter elektrischer Teilchen bei ihrem Durchgang durch Materie zu berechnen, kann im Prinzip als gelöst bezeichnet werden^[4]). Man erhält für die pro Zentimeter Wegstrecke an die Atome übertragene Energie (l. e.)

$$\frac{dT}{dx} = N \cdot \frac{4\pi e^4 E^4}{mc^2} \sum_n f_n \left\{ \ln \frac{(2)^{n_e} v^2}{h\omega_n} - \frac{1}{2} \ln \left(1 - \frac{v^2}{c^2} \right) \right\}$$

Figure 1-6 Applying quantum mechanics to ion stopping theory

This reproduction of two articles from *Zeitschrift für Physik* illustrate the intense interest in Germany in the 1930s to apply quantum mechanics and relativistic theory to the stopping of particles in matter. These and several similar papers established the quantum mechanical aspects of the stopping of high velocity particles.

THE PHYSICAL REVIEW

A Journal of Experimental and Theoretical Physics Established by E. L. Nichols in 1893

MARCH 18, 1940

PHYSICAL REVIEW

VOLUME 57

The Ionization Loss of Energy in Gases and in Condensed Materials*

ENRICO FERMI

Pupin Physics Laboratories, Columbia University, New York, New York

(Received January 22, 1940)

It is shown that the loss of energy of a fast charged particle due to the ionization of the material through which it is passing is considerably affected by the density of the material. The effect is due to the alteration of the electric field of the passing particle by the electric polarization of the medium. A theory based on classical electrodynamics shows that by equal mass of material traversed, the loss is

larger in a rarefied substance than in a condensed one. The application of these results to cosmic radiation problems is discussed especially in view of the possible explanation on this basis of part of the difference in the absorption of mesotrons in air and in condensed materials that is usually interpreted as evidence for a spontaneous decay of the mesotron.

THE determination of the energy lost by a fast charged particle by ionization and

* Publication assisted by the Ernest Kempton Adams Fund for Physical Research of Columbia University.

excitation of the atoms through or near which it is passing has been the object of several theoretical investigations. The essential features of the phenomenon are explained as well known

OCTOBER 1, 1940

PHYSICAL REVIEW

VOLUME 58

Scattering and Stopping of Fission Fragments

N. BOHR

Institute of Theoretical Physics, University of Copenhagen, Copenhagen, Denmark

(Received July 9, 1940)

THE cloud-chamber pictures of tracks of uranium fission fragments in gases obtained by Broström, Bøggild and Lauritsen¹ have revealed a number of interesting differences between such tracks and those of protons and alpha-particles. These differences may be simply shown to be caused by the comparatively high charge and mass of the fission fragments, which imply that nuclear collisions play a much greater part in the phenomenon than is the case for the ordinary light particles.

will have orbital velocities greater than or equal to V .

In an encounter between the fragment and a heavy atom possessing electrons lightly bound and also electrons with velocities greater than V , we may, moreover, assume that only the former electrons, in approximate number V/V_s , will be effective in the stopping. This is true since the faster electrons, just as the electrons carried with the fragment, will be merely adiabatically influenced during the encounter and will therefore

Figure 1-7 Stopping of fission fragments in matter

Reproductions of typical articles from The Physical Review in 1940-1941 which shows that interest had now shifted to the stopping of heavy fission fragments and the development of heavy ion stopping-power scaling theory.

Passage of Uranium Fission Fragments Through Matter*

WILLIS E. LAMB, JR.
Columbia University, New York, New York
 (Received July 19, 1940)

The ranges and rates of energy loss of the fission fragments of uranium are calculated on the basis of a model in which the charge of the fragment is obtained from its energy and its successive ionization potentials. The energy loss cross section for protons of the same velocity is then used to calculate the ranges of the two groups of fragments. For ($Z_1=42, A_1=100$) and ($Z_2=50, A_2=136$) these are found to be 2.42 cm and 2.08 cm, respectively, for a total assumed kinetic energy of 188 Mev and a final kinetic energy of the lighter fragment of 5 Mev (corresponding to ionization-chamber background). These are in fair agreement with the observed ranges of 2.2 cm and 1.5 cm. The experimental and theoretical range-energy relations are also in fair agreement. The validity of the model is discussed in detail, and it appears that it should be fairly good for fragments above 5 Mev. The initial charges of the fission fragments are found to be 17 and 13, respectively, and these are given as a function of the fragment energy in Table I. The density of ionization is found to decrease along the track, in marked contrast to the behavior for protons and alpha-particles.

Velocity-Range Relation for Fission Fragments

N. BOHR
Institute of Theoretical Physics, University of Copenhagen, Copenhagen, Denmark
 (Received November 28, 1940)

Considerations indicated in an earlier note as regards the rate of velocity loss of fission fragments along the range are developed in greater detail and a comparison is given between the calculations and more recent experiments. Especially is a more precise estimate given for the charge effective in electronic encounters which are determining for the stopping effect over the first part of range, and for the screening distance in nuclear collisions which are responsible for the ultimate stopping. In the estimate of the effect of electronic interactions, use is made of a comparison with the stopping of α -particles of the same velocities. In this connection, however, a certain correction is necessary due to an intrinsic difference in the stopping formulae to be applied in the two cases. Moreover, fission fragment tracks show, in contrast to α -rays, a considerable range straggling originating in the end part of the range. It is shown that in this respect also the calculation agrees closely with the experimental data.

On the Energy Loss of Heavy Ions

JULIAN KNAPP, *Purdue University, Lafayette, Indiana*

AND

EDWARD TELLER, *George Washington University, Washington, D. C.*
 (Received February 28, 1941)

The energy loss of heavy ions is due to collisions with electrons and with nuclei. The first process is essentially determined by the ionic charge, which in turn depends on the ratio of the velocities of the most loosely bound electron within the ion, and of the ion. The former velocity is calculated from the Thomas-Fermi model while the ratio of the two velocities is adjusted to empirical data. The nuclear contribution to the stopping cross section is calculated by the known classical method. Though approximations could not be avoided, the procedure lends itself to the systematization of experimental data on intermediate and heavy ions.

Figure 1-8 Stopping of fission-fragments in matter

Further reproductions of typical articles from The Physical Review in 1940-1941 which shows that interest had now shifted to the stopping of heavy fission fragments and the development of heavy ion stopping-power scaling theory.

Scaling Ion Stopping Powers

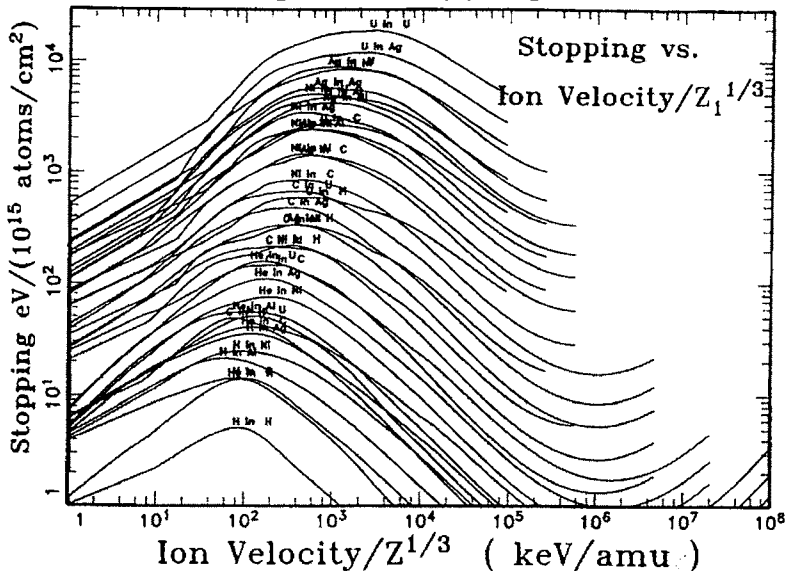


Figure 1-9 Scaling of ion stopping with reduced ion velocity ($V_1/Z_1^{1/3}$)
 The analysis of the energy-loss of fission fragments showed that it increased only slowly with the fragment's mass. Several authors in the papers of Figure 1-7 and Figure 1-8 indicated that reasonable scaling could be obtained by scaling with the cube root of the fragment's atomic number, $Z_1^{1/3}$. The arguments were varied, but this scaling of fission fragments, typically with masses of 50-80 amu, and with very high velocities, seemed to work. See improvement compared that of Figure 1-1

Particle Stopping in a Free Electron Gas (1947 - 1960)

During the 1950's there were fundamental papers on evaluating both the energy transfer from slow particles to quantized electron plasmas, and in the energy loss to target nuclei. The study of particle stopping in a free electron gas is the first step in calculating the energy loss of an ion to a target's electrons. This problem was evaluated in Bohr's earliest papers (13a,15a) where he considered the electrons to be charged harmonic oscillators, with orbit frequencies established by the analysis of optical data. This interaction of a particle with an electron plasma was extended to quantized plasmas and then to Thomas-Fermi atoms by Bethe (30a,32a) and Bloch (33a,33b). An excellent review of relativistic particle (>10 MeV/amu) stopping powers was made by Ahlen (80c) and this chapter will not cover in detail this subject. For energies above 10 MeV/amu one should consult ref. (80a).

Fermi then considered how the fast charged particle would polarize a classical electron medium of the target and hence modify the particle/plasma interaction (40c). This work was extended by Fermi and Teller (47b) to a degenerate free electron gas and they found that for slow particles the

energy loss would be directly proportional to the particle's velocity. Bohr pointed out (48a) that behind the particle there would be an oscillating wake of charge, and this was evaluated more rigorously by Bohr (48b), and by Neufeld and Ritchie (55a). A full treatment of a charged particle penetrating a quantized electron plasma was presented at about the same time by Lindhard (54a), Neufeld and Ritchie (55a) and Fano (56c). The Lindhard approach concentrates on non-relativistic particle interactions with a free-electron gas and provides a full general treatment with the following assumptions:

- The free electron gas consists of electrons at zero temperature (single electrons are described by plane waves) on a fixed uniform positive background with overall charge neutrality.
- The initial electron gas is of constant density, which is considered to be a close approximation to the conduction electrons in metals.
- The interaction of the charged particle on the homogenous electron gas is a small perturbation.
- All particles are non-relativistic.

The Lindhard approach is widely cited in the literature as it formed part of the first unified theory of ion penetration of solids (63a), and it has been widely used as the basis for calculating the electronic stopping of ions in matter (see, for example, 67a, 70b, 72f, 74a, 75k, 77h, 78a, 79d), see Figure 1-10.

Before the widespread use of computers in physics, the energy loss to target nuclei was basically the study of screened Coulomb collisions between two colliding atoms. In the 1950's, major advances were made in the elastic energy loss of the ion to target nuclei. Bohr summarized much of the earlier work in 1948 (48a) which used the Thomas Fermi model to estimate the screened Coulomb potential, $V(r)$ between atoms:

$$\text{Eq. 1-2:} \quad V(r) = (Z_1 Z_2 e^2 / r) \exp(-r/a)$$

where Z_1 and Z_2 are the atomic numbers, r is their separation, and a is a "screening parameter". This screening parameter is an important concept in much of the theory which follows. It essentially increases the size of an atom by moderating the effect of the nuclear positive charge on the outer electrons because the inner electrons shield some of the nuclear charge. This screening parameter then leads to a "screening function" which is the reduction of potential at a point due to the inner electron screening. Once the screening parameter is specified, then the classical scattering and energy transfer can be calculated. Bohr argued that a reasonable approximation might be (48a):

$$\text{Eq. 1-3:} \quad a = a_0 / (Z_1^{2/3} + Z_2^{2/3})^{1/2}$$

but this approximation was not derived. (Note: a_0 is the "Bohr radius", $a_0 = \hbar^2/mc^2 = 0.529 \times 10^{-10} \text{ m} = 0.529 \text{ \AA}$).

Firsov took a more practical approach and used numerical techniques to derive the interatomic potentials of two colliding Thomas-Fermi atoms (58a,b). After finding the numeric values of the potentials as a function of the atomic separation he then fitted these potentials using the Thomas-Fermi screening length and found that the best fit was obtained with:

$$\text{Eq. 1-4:} \quad a = a_0 / (Z_1^{1/3} + Z_2^{1/3})^{2/3}$$

MATHEMATISK-FYSISKE
MEDDELELSE

DET KOL. DANSKE VIDENSKABERNES SELSKAB

THE PENETRATION OF ATOMIC
PARTICLES THROUGH MATTER

BY

NIELS BOHR

Matematisk-fysiske Meddelelser **XVIII**, 8.

ON THE
PROPERTIES OF A GAS OF
CHARGED PARTICLES

BY

J. LINDHARD

Dan. Mat. Fys. Medd. **25**, no. 8 (1954)

RANGE CONCEPTS
AND HEAVY ION RANGES
(NOTES ON ATOMIC COLLISIONS, II)

BY

J. LINDHARD, M. SCHARFF(†) AND H. E. SCHIÖTT

Mat. Fys. Medd. Dan. Vid. Selsk. **25**, no. 14 (1955)

Figure 1-10 Title pages from major papers by Bohr and Lindhard

Reproductions of the articles in the Danish journal of mathematical physics. After World War II, Niels Bohr settled in Copenhagen and created a broad interest in the theory of stopping and range of ions in matter; of special note are the many papers by his student, Jens Lindhard, and his collaborators.

Another problem which received wide attention in the 1950's was the degree of ionization of the ion as it goes through materials. As we noted before, Bohr and others suggested that one simple criterion would be to assume that ions lose electrons with orbital velocities less than the ion velocity. He suggested that the ion charge fraction, Z_1^* / Z_1 , would be :

$$\text{Eq. 1-5: } Z_1^* / Z_1 = V / (V_e Z_1^{2/3})$$

This relation comes from the Thomas-Fermi atom which assumes the electronic charge densities of atoms are similar with a common unit of length being proportional to $Z^{-1/3}$. The charge density is proportional to Z^2 , and the total binding energy scales as $Z^{7/3}$. Therefore the binding per electron scales as $Z^{4/3}$ and the electron velocities are proportional to $Z^{2/3}$. This concept is illustrated in Figure 1-11. Lamb had proposed (40b) the electron binding energy was the important stripping criterion, while Bohr suggested it was the electron velocity. A definitive clarification was made by Northcliffe (60c) who scaled a wide variety of experimental data by dividing each ion/target/energy experimental stopping power by the stopping power of protons in the same target and at the same velocity. In perturbation theory this ratio should scale as $(Z_1^*)^2$ where Z^* is the number of electrons left on the ion. He found a large amount of data could be accurately described using the relation:

$$\text{Eq. 1-6: } (Z^* / Z) = 1 - a \exp\left[\frac{b}{Z^{2/3}} \cdot \frac{v}{v_o}\right]$$

where a and b are fitting constants. The expression expands to be the Bohr relationship (assuming $a = 1$). By the end of the 1950's the status may be summarized as:

Scaling Ion Stopping Powers

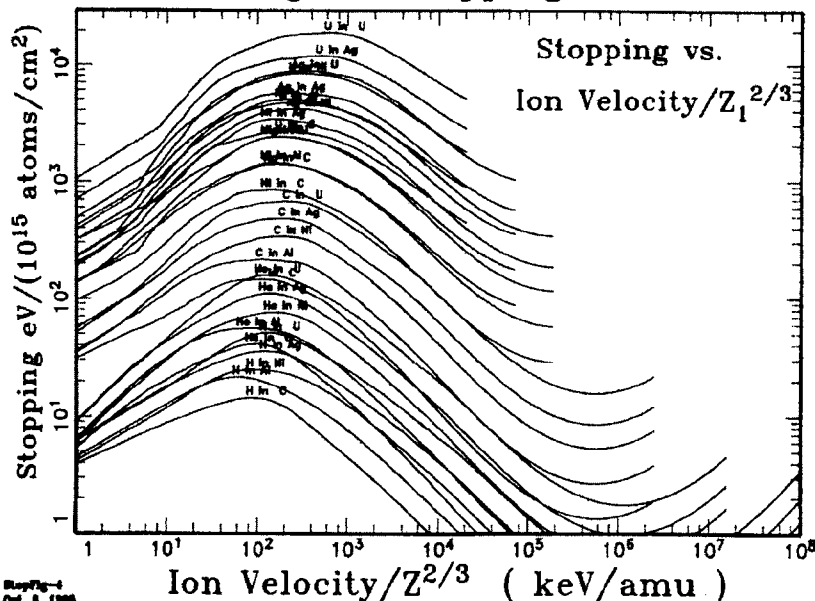


Figure 1-11 Scaling of ion stopping with reduced ion velocity ($V_1/Z_1^{2/3}$)

Bohr (and others) suggested that the charge-state of an ion could be estimated by assuming that it would lose all of its electrons with orbital velocity less than the ion velocity (40d, 41a). The orbital velocity of electrons was considered to be proportional to $Z_1^{2/3}$, so this concept can be illustrated by plotting stopping versus an ion velocity reduced by this electron velocity factor.

- A good treatment of the energy loss of a charged particle to a quantized electron plasma. The theory includes both polarization of the medium about the charge, and discussions of extensions of particle interactions with electron plasmas to electrons in atomic matter.
- A good calculation of interatomic potentials and the energy transferred during a scattering collision between two atoms.
- A good evaluation of the effective charge of heavy ions in solids for the intermediate velocity range ($3 v_0 < v_1 < 30 v_0$), where v_1 is the ion velocity, and v_0 is the Bohr velocity.

Problems left to be solved included:

- How to extend the electron plasma point-charge interaction theory to the interaction with a finite sized ion?
- How to derive fundamentally the effective charge of a moving ion (where effective charge is defined as a combination of ion charge state plus target polarization)?
- And finally, how to modify all of the above to use more realistic Hartree-Fock atoms rather than statistical atoms?

Theories for Stopping & Ranges of Heavy Ions (1963 - 1985)

In 1963 the first unified approach to stopping and range theory was made by Lindhard, Scharff and Schiott (63a) and their approach is commonly called the LSS-theory. This work brought together all the pieces, and bridging approximations were made so that calculations of stopping and range distributions could, for the first time, be made within a single model. This remarkable achievement was the result of over a decade of study by Lindhard and collaborators (53b, 54a, 63a, 64a, 68a, 68b), with the later publications deriving in detail some of the major equations of LSS theory. LSS theory was the peak of stopping and range theory based on statistical atoms. With this theory it was possible to predict the range of ions in solids within a factor of two - a remarkable achievement considering it was applicable over the entire range of atomic species and energies up to the stopping power maximum (70a, 70f, 75c, 75f, 75g, 77a). Since it was based on Thomas-Fermi atoms it was most accurate for atoms with many electrons in the intermediate range where they are neither fully stripped nor almost neutral. The theory naturally shows no shell effects.

During the 1960's and 70's the primary advances came by applying numerical methods to traditional theoretical approaches. The use of computers permitted the incorporation of more realistic Hartree-Fock atoms into the theory and gave significant improvements. These important steps were initiated by Rousseau, Chu and Powers (70b) in electronic stopping, and Wilson, Haggmark and Biersack (77c) in nuclear stopping.

One way to evaluate these theoretical steps is to estimate the accuracy with which one can calculate stopping powers. After the work by Bethe-Bloch in the 1930's, the stopping of high velocity protons could be calculated to about 20%. By the late 1950's, the excellent review article by Whaling (58c) pointed out that little could be calculated for anything heavier than a proton. This changed abruptly with the LSS theory in 1963 (63a), which created a unified approach to the stopping of low energy heavy ions. With this approach, most stopping powers could be estimated within a factor of two or three, and the ranges of these ions in single-element targets could be calculated within a factor of two.

The LSS theory was the last of the comprehensive theories based on statistical models of atom-atom collisions. Improvements in calculating stopping and ranges over the next twenty years were made by using numerical techniques and removing some of the approximations used by Bohr, Firsov and Lindhard. One new theoretical insight which has had profound implications was made by Brandt and Kitagawa (82a) where they revised the Bohr suggestion of the degree of ionization of ions traveling within solids. Bohr had suggested that the ion's electrons which had orbital velocities less than the instantaneous velocity of the ion would be stripped off, leaving the ion only with its inner high-velocity electrons. Brandt and Kitagawa suggested that this stripping criteria should be modified to consider the ion's electron velocity only relative to the Fermi velocity of the solid. They then proceeded to develop the formalism to allow the full evaluation of this new concept which has proved to be quite accurate. This concept is illustrated in Figure 1-12.

Current stopping powers can now be calculated with an average accuracy of better than 10% for low energy heavy ions, and to better than 2% for high velocity light ions. Range distributions for amorphous elemental targets have about the same accuracy.

Scaling Ion Stopping Powers

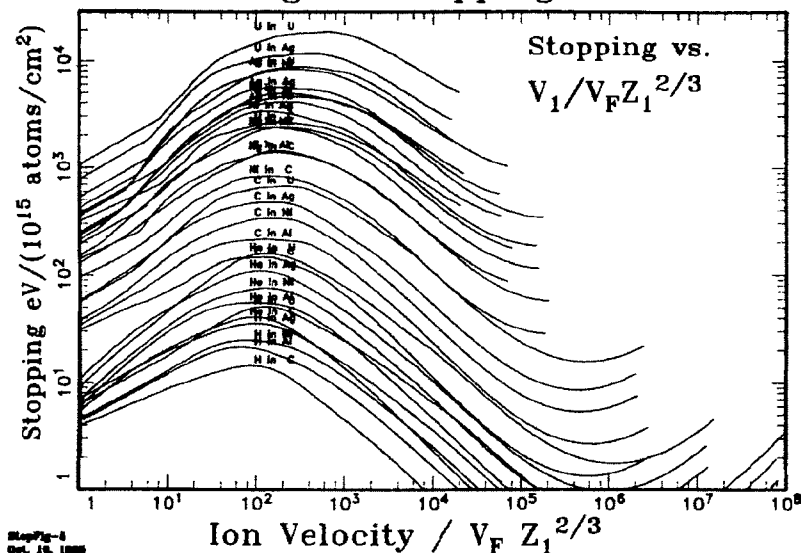


Figure 1-12 Scaling of ion stopping to reduced ion velocity ($V_1/V_F Z_1^{2/3}$)
 Bohr estimated the charge state of an ion by assuming it was stripped of any of its electrons whose orbital velocity was less than its velocity, see Figure 1-11. This concept lasted for thirty years because of its elegant simplicity. Brandt extended this idea to relate the ion velocity (and its electrons) to the electron velocity of the medium in which it was passing (75c, 81c, 82a). Ziegler took this concept and made an explicit formulation that the reduced ion velocity would take the form of $V_1/V_F Z_1^{2/3}$ (85a).

For extended reading in the field of the stopping and range of ions in matter, the following scientific papers are recommended. The classic review by Bohr (48a) encompasses almost everything learned in the first 50 years of study, and it is relatively easy to understand. Other reviews have been made by Whaling (58c), Fano (63b), Jackson (62a, 75a), Bichsel (70e), Sigmund (75b), Ahlen (80e), Ziegler, et al. (78a, 80a, 80b, 82b, 84a), and the International Commission on Radiation Units and Measurements (84d, 93d). For original sources, the theoretical treatment of the stopping of ions in matter is due greatly to the work of Bohr (13a, 15a, 48a), Bethe (30a, 32a, 34a), Bloch (33a, 33b), Firsov (57a, 57b, 58a, 58b) and Lindhard (53b, 54a, 63a, 64a, 68a, 68b).

For more recent works, see the Citation List of this chapter for important papers and books published since 1985.

Scaling Ion Stopping Powers

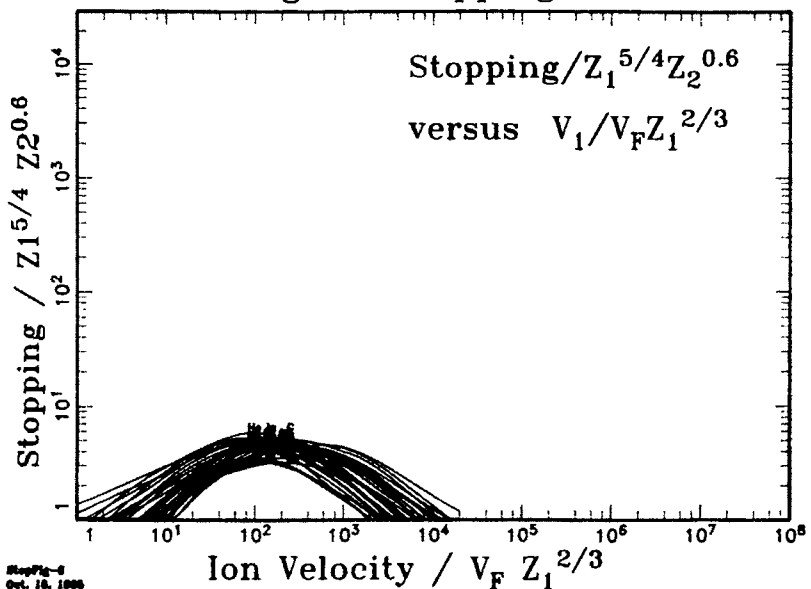


Figure 1-13 Scaling of ion stopping to reduced ion velocity

The previous simplifications of scaling stopping powers were concerned with functions of the ion atomic number, Z_1 . A final simplification can be made by reducing the stopping by applying a function based on the relative magnitudes of Z_1 and Z_2 . The ordinate in the above plot shows the same stopping powers as before, but reduces them by dividing the stopping by $Z_1^{5/4} Z_2^{0.6}$. There is no physics in this approximation; it just collapses all the curves to a shallow grouping. So with minor insights into physics one can predict stopping powers of any ion and target combination, over many orders of ion velocity, with modest accuracy.

"Stopping Power" vs. "Stopping Force"

For about a century, the energy loss of ions in matter has been called the ion's **Stopping Power**. In the 1990's, Peter Sigmund, one of the most distinguished theorists in this field, suggested that the term be changed to **Stopping Force**, since this is consistent with the units of stopping, which normally are the energy loss per unit path length. This suggestion was both logical and reasonable, but changing such a phrase after a hundred years of use was possibly more difficult than one suggestion, no matter how reasonable, could achieve. Sigmund has recently suggested that such a change would probably be glacially slow (2006a). This book is a textbook, and we need to help students learn from classical papers which almost always use the traditional phrase. Hence, we shall use **Stopping Power**, but in various places have explained that this is an historical phrase, and **Stopping Force** would be more accurate.

Citations for Chapter 1

Although this brief Historical Review ends about 1985, there have been many papers since then which have made major contributions to understanding the stopping and range of ions in matter. The authors include fifty-five additional citations which they have found particularly helpful.

- 1804 Benjamin Robins, "New Principles in Gunnery", London (1807). The only copy available in the United States is the 2nd Edition (1842) at the United States Military Academy, West Point, NY.
- 00a Mme. Pierre Curie, Comptes Rendus, 130, 76 (1900).
- 03a J. J. Thomson, "Conduction of Electricity Through Gases," Cambridge University Press, (1903).
- 05a W. H. Bragg and R. Kleeman, Phil. Mag., 10, 318 (1905).
- 09a H. Geiger and E. Marsden, Proc. Roy. Soc., 82, 495 (1909).
- 11a E. Rutherford, Phil. Mag., 21, 212 (1911); *ibid*, 21, 699 (1911).
- 12a J. J. Thomson, Phil. Mag., 6-23, 449 (1912).
- 12b J. Stark, Z. f. Physik, 13, 973 (1912).
- 12c C. G. Darwin, Phil. Mag., 23, 901 (1912).
- 13a N. Bohr, Phil. Mag., 25, 10 (1913).
- 14a L. Flamm, Sitzungsber. d. K. Akad. d. Wiss. Wien, Mat.-nat. Kl., 123, 1393 (1914).
- 15a N. Bohr, Phil. Mag., 30, 581 (1915).
- 27a E. Fermi, Z. f. Physik, 29, 315 (1927).
- 30a H. A. Bethe, Ann. Physik, 5, 325 (1930).
- 31a N. F. Mott, Proc. Camb. Phil. Soc., 27, 553 (1931).
- 32a H. A. Bethe, Z. f. Physik, 26, 293 (1932).
- 32b A. Sommerfeld, Z. f. Physik, 78, 283 (1932).
- 32c W. Lenz, Z. f. Physik, 77, 713 (1932); H. Jensen, Z. f. Physik, 77, 722 (1932).
- 32d C. Moller, Ann. Physik, 14, 531 (1932).
- 32e A. Sommerfeld, Z. f. Physik, 78, 283 (1932).
- 32f W. Lenz, Z. f. Physik, 77, 722 (1932).
- 32g H. Jensen, Z. f. Physik, 77, 722 (1932).
- 33a F. Bloch, Ann. Physik, 16, 287 (1933).
- 33b F. Bloch, Z. f. Physik, 81, 363 (1933).
- 34a H. A. Bethe and W. Heitler, Proc. Roy. Soc., A146, 83 (1934).
- 38a W. F. G. Swann, J. Frank. Inst., 226, 598 (1938).
- 39a E. J. Williams, Proc. Roy. Soc., 169 (1939).
- 39b O. Hahn and F. Strassmann, Naturwiss., 27, 11 (1939).
- 40a L. A. Turner, Rev. Mod. Phys., 12, 1 (1940).
- 40b W. E. Lamb, Phys. Rev., 58, 696 (1940).
- 40c E. Fermi, Phys. Rev., 57, 485 (1940).
- 40d N. Bohr, Phys. Rev., 58, 654 (1940).
- 40e E. J. Williams, Phys. Rev., 58, 292 (1940).
- 41a N. Bohr, Phys. Rev., 59, 270 (1941).
- 41b J. Knipp and E. Teller, Phys. Rev., 59, 659 (1941).

- 41c J. H. M. Brunnings, J. Knipp and E. Teller, Phys. Rev. 60, 657 (1941).
- 47a G. Moliere, Z. f. Naturforschung, A2, 133 (1947).
- 47b E. Fermi and E. Teller, Phys. Rev., 72, 399 (1947).
- 48a N. Bohr, Mat. Fys. Medd. Dan. Vid. Selsk., 18, No. 8 (1948).
- 48b A. Bohr, Mat. Fys. Medd. Dan. Vid. Selsk., 24, No. 19 (1948).
- 49a P. Gombas, "Dic Statistische Theorie des Atoms und hire Anwendungen," Springer-Verlag, Austria (1949).
- 50a T. Hall, Phys. Rev. 79, 504 (1950).
- 50b N. H. Marich, Proc. Cambridge Phil. Soc., 46, 356 (1950).
- 52a M. C. Walske, Phys. Rev. 88, 1283 (1952).
- 53a H. A. Bethe, Phys. Rev. 89, 1256 (1953).
- 53b J. Lindhard and M. Scharff, Mat. Fys. Medd. Kgl. Dan. Vid. Selsk., 27, No 15 (1953).
- 54a J. Lindhard, Mat. Fys. Medd. Dan. Vid. Selsk., 28, No. 8 (1954).
- 54b N. Bohr and J. Lindhard, Mat. Fys. Medd. Dan. Vid. Selsk., 28, No. 7 (1954).
- 54 c A. Erdelyi, "Table of Integral Transforms", McGraw-Hill, London (1954).
- 55 a J. Neufeld and R. H. Ritchie, Phys. Rev., 98, 1632 (1955); ibid. 99, 1125 (1955).
- 55 b J. A. Philips, Phys. Rev., 97, 404 (1955).
- 55 c Kinchin and R. S. Pease, Rep. Prog. Phys., 18, 1 (1955).
- 56 a W. Brandt, Phys. Rev. 104, 691 (1956).
- 56 b M. C. Walske, Phys. Rev. 101, 940 (1956).
- 56 c U. Fano, Phys. Rev., 103, 1202 (1956).
- 56 d W. Barkas, W. Birnbaum and F. M. Smith, Phys. Rev., 101, 778 (1956).
- 56 e P. Gambas, "Statistische Behandlung des Atoms", in *Encyclopedia of Physics*, 36, (1956).
- 57 a O. B. Firsov, Zh. Eksp. Teor. Fiz., 32, 1464 (1957).
- 57 b O. B. Firsov, Zh. Eksp. Teor. Fiz., 33, 696 (1957).
- 57 c H. Bichsel, R. F. Mozley and W. A. Aron, Phys. Rev., 105, 1788 (1957).
- 58 a O. B. Firsov, Zh. Eksp. Teor. Fiz., 34, 447 (1958).
- 58 b O. B. Firsov, JETP., 7, 308 (1958).
- 58 c W. Whaling, "Handbuch der Physik, Bd. XXXIV, 13, Springer-Verlag, Berlin
- 58 d S. K. Allison, Rev. Mod. Phys., 30, 1137 (1958).
- 59 a O. B. Firsov, Zh. Eksp. Teor. Fiz., (Transl.: Sov. Phys. JETP, 9, 1076 (1959)).
- 59 b R. H. Ritchie, Phys. Rev., 114, 644 (1959).
- 59 c O. B. Firsov, Zh. Eksp. Teor. Fiz., 36, 1517 (1959).
- 60 a H. Bichsel and E. A. Uehling, Phys. Rev., 119, 1670 (1960).
- 60 b R. M. Sternheimer, Phys. Rev., 117, 485 (1960).
- 60 c L. C. Northcliffe, Phys. Rev., 120, 1744 (1960).
- 60 d J. A. Davies, J. Friesen and J. D. McIntyre, Can. J. of Chem., 38, 1526 (1960).
- 61 a H. Bichsel, Tech. Report #3, Dept. of Physics, Univ. of So. Calif. (1961).
- 61 b J. Lindhard and M. Scharff, Phys. Rev., 124, 128 (1961).
- 62 a F. W. Martin and L. C. Northcliffe, Phys. Rev., 128, 1166 (1962).
- 62 b J. D. Jackson, "Classical Electrodynamics," Chapt. 13, Wiley, New York (1962, 1975).
- 63 a J. Lindhard, M. Scharff and H. E. Schiott, Mat. Fys. Medd. Dan. Vid. Selsk., 33, No. 14 (1963).
- 63 b U. Fano, Ann. Rev. Nucl. Sci., 13, 1 (1963).
- 63 c L. C. Northcliffe, Ann. Rev. Nucl. Sci., 13, 67 (1963).
- 63 d F. Herman and S. Skillmann, "Atomic Structure Calculations," Prentice-Hall (1963).
- 63 e M. T. Robinson and O. S. Oen, Appl. Phys. Lett., 2, 30 (1963).

- 63 f** W. Mechback and S. K. Allison, Phys. Rev., 132, 294 (1963).
- 63g** J. Lindhard, V. Nielsen, M. Scharff and P. V. Thomsen, Dansk Videnskab. Mat.-Fys. Medd., 33, no. 10 (1963).
- 64a** J. Lindhard and A. Winther, Mat. Fys. Medd. Dan. Vid. Selsk., 34, No. 4 (1964).
- 68a** J. Lindhard, V. Nielsen and M. Scharff, Mat. Fys. Medd. Dan. Vid. Selsk., 36, No. 10 (1968).
- 68a** J. Lindhard, V. Nielsen and M. Scharff, Mat. Fys. Medd. Dan. Vid. Selsk., 36, No. 10 (1968).
- 68b** J. Lindhard, V. Nielsen, M. Scharff and P. V. Thomsen, Mat. Fys. Medd. Dan. Vid. Selsk., 33, No. 10 (1968).
- 68b** J. Lindhard, V. Nielsen, M. Scharff and P. V. Thomsen, Mat. Fys. Medd. Dan. Vid. Selsk., 33, No. 10 (1968).
- 70a** L. C. Northcliffe and R. F. Schilling, Nucl. Data Tables, 7, 233 (1970).
- 70b** C. C. Rousseau, W. K. Chu and D. Powers, Phys. Rev., A4, 1066 (1970).
- 70e** H. Bichsel, Amer. Inst. of Phys. Handbook, 3rd. Ed. (1970).
- 70f** W. S. Johnson and J. F. Gibbons, "Projected Range Statistics in Semiconductors," Stanford University Bookstore, Stanford, CA, 1970 (out of print).
- 75a** J. D. Jackson, "Classical Electrodynamics," Chapt. 13, Wiley, New York (1962, 1975).
- 75b** P. Sigmund, Chapt. 1, "Radiation Damage Processes in Materials," ed. by C. H. S. Du Puy, Noordhoff, Leyden (1975).
- 75e** D. K. Brice, "Ion Implantation Range and Energy Deposition Distributions, vol. 1, High Energies," Plenum Press, New York (1975).
- 75f** K. B. Winterbon, "Ion Implantation Range and Energy Deposition Distributions, vol. 2, Low Energies," Plenum Press, New York (1975).
- 75g** J. F. Gibbons, W. S. Johnson and S. W. Mylroie, "Projected Range Statistics: Semiconductors and Related Materials," 2nd Edition, Halsted Press, Stroudsbury, PA, USA (1975).
- 77a** H. H. Andersen and J. F. Ziegler, "Hydrogen Stopping Powers and Ranges in All Elements," vol. 3 of series "Stopping and Ranges of Ions in Matter," Pergamon Press, New York (1977).
- 77c** W. D. Wilson, L. G. Hagmark and J. P. Biersack, Phys. Rev., 15B, 2458 (1977).
- 78a** J. F. Ziegler, "Helium Stopping Powers and Ranges in All Elements," vol. 4 of series "Stopping and Ranges of Ions in Matter," Pergamon Press, New York (1978).
- 80a** J. F. Ziegler, "Handbook of Stopping Cross Sections for Energetic Ions in All Elements," vol. 5 of series "Stopping and Ranges of Ions in Matter," Pergamon Press, New York (1980).
- 80b** U. Littmark and J. F. Ziegler, "Handbook of Range Distributions for Energetic Ions in All Elements," vol. 6 of series "Stopping and Ranges of Ions in Matter," Pergamon Press, New York (1980).
- 80e** S. P. Ahlen, Rev. Mod. Phys., 52, 121 (1980).
- 82b** J. P. Biersack and J. F. Ziegler, "Ion Implantation Techniques," Springer-Verlag, p. 122 (1982).
- 84a** J. F. Ziegler, J. P. Biersack, U. Littmark, "The Stopping and Range of Ions in Solids," vol. 1 of series "Stopping and Ranges of Ions in Matter," Pergamon Press, New York (1984).
- 84d** M. J. Berger et al., "Stopping Powers and Electrons and Positrons", ICRU-37.

The following citations are valuable additions to the understanding of the stopping of ions in matter. Many of these will be discussed in later chapters in this book.

- 90a A. Narman, R. Monreal, P. M. Echenique, F. Flores, W. Heiland and S. Schubert, Phys. Rev. Lett., 64, 1601 (1990).
90b A. Arnau, M. Penalba, P. M. Echenique, F. Flores and R. H. Ritchie, Phys. Rev. Lett., 65, 1024 (1990).
90c P. M. Echenique, F. Flores and R. H. Ritchie, Sol. State Phys., 43, 229 (1990).
90d M. Hasagawa, T. Uchida, K. Kimura and M. Mannami, Phys. Lett., A-145, 182 (1990).
90f T. Iiaka, Y. H. Ohtsuki, A. Koyama and H. Ishikawa, Phys. Rev. Lett., 65, 3160 (1990).
90g A. Koyama, Y. Sasa, H. Ishikawa, A. Misu, K. Ishii, T. Iitaka, Y. H. Ohtsuki and M. Uda, Phys. Rev. Lett., 65, 3156 (1990).
90h Y. Susuki, H. Mukai, K. Kimura and M. Mannami, Nucl. Inst. and Meth., B48, 347 (1990).
90i H. Esbensen and P. Sigmund, Ann. Phys., 201, 152 (1990).
90j A. H. Sorensen, Nucl. Inst. and Meth., B48, 10 (1990).
90k H. Bichsel, Phys. Rev., A41, 3642 (1990).
91a A. Narmann, W. Heiland, R. Monreal, F. Flores, P. M. Echenique, Phys. Rev., 44B, 2003 (1991).
91b A. Narmann, Mod. Phys. Lett., B5, 561 (1991).
91c R. Medenwalt, S. P. Moller, E. Uggerhoj, T. Worm, P. Hvelplund, H. Knudsen, K. Elsener and E. Morenzoni, Nucl. Inst. and Meth., B58, 1 (1991).
91d K. Shima, N. Kuno, M. Yamanouchi and H. Tawara, Natl. Inst. for Fusion Sci., #NJFS-DATA-10, (1991).
91f S. A. Cruz and J. Souillard, Nucl. Inst. and Meth., B61, 433 (1991).
91g W. Eckstein, "Computer Simulation of Ion-Solid Interactions", Springer-Verlag, Berlin (1991).
91h H. Paul, D. Semrad and A. Swilinger, Nucl. Inst. and Meth., B61, 261 (1991).
92a M. Penalba, A. Arnau and P. M. Echenique, Nucl. Inst. and Meth., B67, 66 (1992).
92b M. Penalba, A. Arnau, P. M. Echenique, F. Flores and R. H. Ritchie, Europhysics Lett., 19, 45 (1992).
92c F. J. Garcia de Abajo and P. M. Echenique, Phys. Rev., 46, 2663 (1992).
92d A. Narmann, H. Franke, K. Schmidt, A. Arnau and W. Heiland, Nucl. Inst. and Meth., B69, 158 (1992).
92f A. Arnau, M. Penalba, P. M. Echenique and F. Flores, Nucl. Inst. and Meth., B69, 102 (1992).
92g S. A. Cruz and J. Souillard, Nucl. Inst. and Meth., B71, 387 (1992).
92h H. Bichsel, Phys. Rev., 46A, 5761 (1992).
92i H. Bichsel and T. Hiroka, Nucl. Inst. and Meth., B66, 345 (1992).
92j P. Bauer, W. Rossler and P. Mertins, Nucl. Inst. and Meth., B69, 46 (1992).
93a J. M. Pitärke, R. H. Ritchie, P. M. Echenique and E. Zaremba, Europhysics Lett., 24, 7 (1993).
93b J. M. Pitärke, R. H. Ritchie and P. M. Echenique, Nucl. Inst. and Meth., B79, 209 (1993).
93c P. M. Echenique and A. Arnau, Phys. Scripta, T49, 677 (1993).
93d M. J. Berger et al., "Stopping Powers and Ranges for Protons and Alpha Particles",

ICRU-49, International Commission on Radiation Units, Bethesda, MD, USA (1993).
See pages 82-105 for a length discussion of experimental methods and their limitations.

- 94a P. Sigmund, Phys. Rev. A, **50**, 3197-3201 (1994).
94b A. N. Narmann and P. Sigmund, Phys. Rev. A, **49**, 4709-4715 (1994).
95a P. Sigmund and A. N. Narmann, Laser and Part. Beams, **13**, 281-292 (1995).
95b Turner, J. E., "Atoms, Radiation and Radiation Protection", Wiley, New York, 2nd Ed.
97a L. Glazov and P. Sigmund, Nucl. Inst. Methods, B125, 110-115 (1997).
98a P. Sigmund, Nucl. Inst. Methods, **135B**, 1-15 (1998).
98b P. Sigmund and L. Glazov, Nucl. Inst. Methods, B136-138 (1998)
2000a Bransden B. H. and Joachain C. J., "Quantum Mechanics", Prentice Hall, Harlow, 2nd Ed. (2000).
2000b Sigmund P. and Schinner A., "Binary Stopping Theory for Swift Heavy Ions", Europ. Phys. J. D12, 425-434, (2000)
2000c Sigmund P., "Shell Correction in Bohr Stopping Theory", Europ. Phys., D12, 111-116 (2000)
2000d Schinner A. and Sigmund P., "Polarization Effect in Stopping of Swift Partially Screened Heavy Ions: Perturbative Theory", Nucl. Inst. Meth., B164-165, 220-229 (2000)
2000e Pitarke J. M. and Campillo I., "Band Structure Effects on the Interaction of Charged Particles with Solids", Nucl. Inst. Meth., B164, 147-160 (2000)
2001a Wieszczycka W. and Scharf W. H., "Proton Radiotherapy Accelerators", World Scientific, New Jersey, USA (2001).
2002a Sigmund, P. and Schinner A., "Binary Theory of Electronic Stopping", Nucl. Inst. Meth.m, B195, 64-90 (2002).
2002b Bichsel H., "Shell Corrections in Stopping Powers", Phys. Rev. A-65, 1-11 (2002).
2002c Arista N. R., "Energy Loss of Heavy Ions in Solids: Non-Linear Calculations for Slow and Swift Ions", Nucl. Inst. Meth., B195, 91-105 (2002).
2002d Grande P. L. and Schiwietz G., "The Unitary Convolution Approximation for Heavy Ions", Nucl. Inst. Meth., B195, 55-63 (2002).
2003a Cohen S. M., "Bethe Stopping Power Theory for Heavy Element Targets and Relativistic Projectiles", Phys. Rev., A 68, 12720 (2003).
2004a Cabrera-Trujillo R. and Sabin, J. R., Ed. "Theory of the Interaction of Swift Ions with Matter", Part 1, vo. 45, , Adv. Quantum Chem., Elsevier, Amsterdam (2004).
2004b Cabrera-Trujillo R. and Sabin, J. R., Ed. "Theory of the Interaction of Swift Ions with Matter", Part 2 vo. 46 , Adv. Quantum Chem., Elsevier, Amsterdam (2004).
2004c Sigmund, P., "Stopping of Heavy Ions", vol. 204 of Springer Tracts of Modern Physics, Springer Co., Berlin.
2004d Cohen S. M., "Aspects of Relativistic Sum Rules", Adv. Quantum Chem., 46, 241-265
2005a ICRU, Vol. 73 of ICRU Reports, "Stopping of Ions Heavier than Helium", Oxford Univ. Press, Oxford, UK (2005).
2005b Basko M. M., "On the Low-Velocity Limit of the Bohr Stopping Formula", Europ. Phys. J. D 32, 9-17 (2005).
2005c Sigmund P., Sharma A., Schinner A. and Fettouhi A., "Valence Structure Effects in the Stopping of Swift Ions", Nucl. Inst. Meth., B230, 1-6 (2005).
2005d Cohen S. M., "Simple and Accurate Sum Rules for Highly Relativistic Systems", J. Chem. Phys., 122, 104-105 (2005).
2006a Sigmund, P., "Particle Penetration and Radiation Effects", vol. 151 of Springer Tracts of Solid State Sciences, Springer Co., Berlin (2006).
2006b Sigmund P. and Schinner A., "Sheil Correction in Stopping Theory", Nucl. Inst.

Collections of Experimental Data

There are two large and comprehensive databases for publications about the experimental studies of the stopping of ions in matter. There is no similar database for ranges.

On the SRIM website, www.SRIM.org, there are plots of the experimental data for most ions in elemental targets, and also in simple compounds. Shown on these are SRIM calculations so its accuracy can be evaluated. There are also tabulations of the citations of the original papers for these data..

Professor Helmut Paul (Univ. Linz) has digitized and plotted most existing experimental data of the stopping powers of ions in matter. His work has made accessible a century of experimental results, and this is a major contribution to the understanding of the stopping of ions in matter. See his website :

www.exphys.uni-linz.ac.at/Stopping/

2. NUCLEAR STOPPING OF IONS

Chapter Abstract

As Bohr suggested in 1913, it is convenient to divide the energy loss of an ion in matter into the losses to the heavy target nuclei, and to the target electrons. This is possible because the nuclei can be assumed to be slowly recoiling for most of the collision, while the electrons will move quickly and often collectively, in response to the charges on the incoming ion. This chapter will cover energy loss by the ion to the target nuclei, and the next chapter will discuss target electrons.

In this section we shall review the mathematics of the collision of two charged point-particles and then the collisional scattering of two atoms, with electrons screening the central nucleus, with emphasis on the elastic energy transferred to the stationary atom. The collision kinematics are calculated from what are called *atom-atom interatomic potentials*. We discuss various models of atoms and show their potentials and their interatomic potentials. Finally, a detailed calculation is reviewed for hundreds of interatomic potentials using modern solid-state atomic models. These are reduced to a single analytic function which is called a universal interatomic potential. This function is applied to generate new universal nuclear stopping cross-sections and scattering functions which can be used to calculate the physics of ion penetration of solids.

Chapter Contents

2. Nuclear Stopping of Ions	2-1
INTRODUCTION TO TWO ATOM SCATTERING.....	2-1
Defining Center-of-Mass Coordinate System.....	2-2
TWO-BODY CENTRAL FORCE SCATTERING.....	2-8
INTERATOMIC POTENTIALS.....	2-10
Model for Calculating Interatomic Potentials.....	2-12
The Charge Distribution of Solid-State Targets	2-16
Single Atom Potentials	2-17
Interatomic Potentials	2-21
Accuracy of Interatomic Potential Calculation.....	2-26
Universal Interatomic Potential	2-28
Energy Transfer from Projectile Atom to Target Atom.....	2-33
Universal Nuclear Stopping Powers	2-34
Nuclear Straggling	2-37
Universal Scattering Formula	2-38
APPENDIX TO CHAPTER	2-44
Accuracy of Universal Interatomic Potentials	2-44
CITATIONS TO CHAPTER 2.....	2-48

INTRODUCTION TO TWO ATOM SCATTERING

The classical transfer of energy between a moving and a stationary charged particle depends only on the mass and charge of the two particles, and the moving particle's initial speed and direction. While the moving charge passes through the material, the stationary particle recoils and absorbs

energy and the moving particle is deflected. The final velocities and trajectories can be simply found from the conservation of momentum and energy of the system. Mathematically this problem is called the asymptotic orbit problem, and it has analytical solutions for simple screened potentials between the particles. Numerical techniques have been developed to evaluate the more complex collision of quantal atoms with shell effects, and the absorption of energy into the Pauli promotion of the electrons as will be discussed later.

Defining Center-of-Mass Coordinate System

The Center-of-Mass coordinate system (CM) is the traditional way to derive two-body scattering. This transformation is used because no matter how complex the force is between the two particles, so long as it acts only along the line joining them (no transverse forces), ***the relative motion of the two particles can be reduced to that of a single particle moving in a central potential (called the interatomic potential)*** centered at the origin of the center-of-mass coordinates. This simplification is essential to the rest of this chapter.

We will first summarize the equations relating the initial and final states of the elastic scattering of two particles. For convenience we shall call the incident particle an '**ion**' and the stationary particle an '**atom**'. This will allow a smooth transition from this section to the later physics of full ion/target atom collisions. In classical non-relativistic elastic collisions, the following relations hold for laboratory coordinates, see Figure 2-1

Conservation of Energy :

$$\text{Eq. 2-1:} \quad E_0 = \frac{1}{2} M_1 V_0^2 = \frac{1}{2} M_1 V_1^2 + \frac{1}{2} M_2 V_2^2$$

where E_0 is the initial ion kinetic energy, V_0 is the incident velocity of the ion with mass M_1 , and V_1 is the ion's final velocity after striking the target atom of mass M_2 , which recoils with velocity V_2 .

Conservation of Momentum :

$$\text{Eq. 2-2:} \quad \text{Longitudinal:} \quad M_1 V_0 = M_1 V_1 \cos \theta + M_2 V_2 \cos \phi$$

$$\text{Eq. 2-3:} \quad \text{Lateral :} \quad 0 = M_1 V_1 \sin \theta + M_2 V_2 \sin \phi$$

where θ is the final angle of deflection of the ion and ϕ is the final recoil angle of the target ion.

The solution of these equations can be made in various forms depending on which variables are canceled by substitution. For example, eliminating the target recoil angle, ϕ , we have:

$$\text{Eq. 2-4:} \quad \left(\frac{V_1}{V_2} \right)^2 - 2 \left(\frac{V_1}{V_0} \right) \frac{M_1}{M_1 + M_2} \cos \theta - \frac{M_2 - M_1}{M_2 + M_1} = 0$$

which is independent of the way the forces between the particles vary with separation.

We will now restate the above in center-of-mass (CM) coordinates. The main advantage of introducing the CM-system arises in cases where the mutual interaction of the two colliding

particles can be described by a force-field, $V(r)$, which only depends on the absolute value of the interatomic separations, r . The motion of both particles can be reduced to a single equation of motion. This equation has r as the independent variable and describes a particle moving in the central force field, $V(r)$. This central force field is a combined field from the two particles, and is called the Interatomic Potential. The derivation of this new field is discussed in detail later.

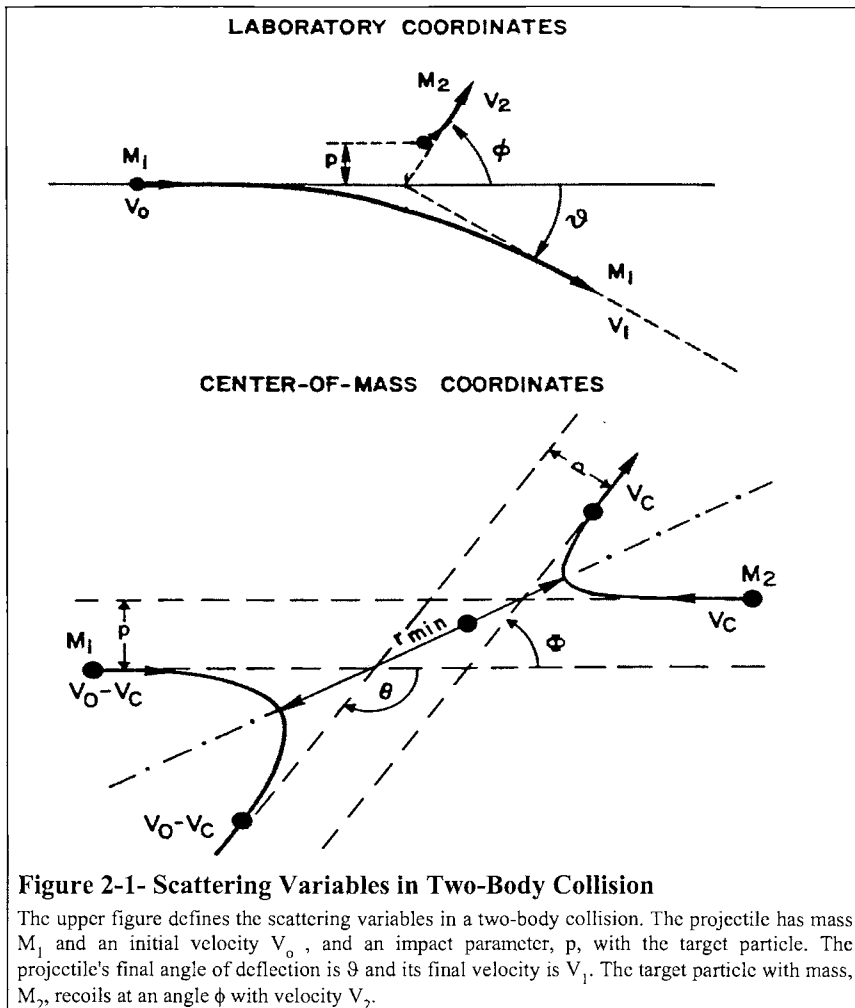


Figure 2-1- Scattering Variables in Two-Body Collision

The upper figure defines the scattering variables in a two-body collision. The projectile has mass M_1 and an initial velocity V_0 , and an impact parameter, p , with the target particle. The projectile's final angle of deflection is θ and its final velocity is V_1 . The target particle with mass, M_2 , recoils at an angle ϕ with velocity V_2 .

The lower figure is the same scattering in center-of-mass (CM) coordinates in which the *total momentum of the system is zero*. The coordinate system moves with velocity V_C relative to the laboratory coordinates, and the new angles of scatter and recoil are Θ and Φ .

For center-of-mass (CM) coordinates we define the system velocity, V_C , such that in this coordinate system there is *zero net momentum*, see Figure 2-1:

$$\text{Eq. 2-5:} \quad M_1 V_0 = (M_1 + M_2) V_C$$

$$\text{Eq. 2-6:} \quad \text{or we define: } V_C \equiv \frac{M_1 V_0}{M_1 + M_2}$$

We shall now derive several variations of the relation of CM coordinates to laboratory coordinates which will be used later. For convenience, we also define in CM coordinates a reduced mass, M_C , by the relation:

$$\text{Eq. 2-7:} \quad (1/M_C) = (1/M_1) + (1/M_2)$$

or we define M_C as:

$$\text{Eq. 2-8:} \quad M_C \equiv M_1 M_2 / (M_1 + M_2)$$

We can now solve for the CM velocity as

$$\text{Eq. 2-9:} \quad V_C = V_0 M_C / M_2$$

The ion and atom velocities can now be restated in CM coordinates:

$$\text{Eq. 2-10:} \quad V_{\text{ion}} = V_0 - V_C = V_0 M_C / M_1$$

$$\text{Eq. 2-11:} \quad V_{\text{atom}} = V_C = V_0 M_C / M_2$$

This relation shows an advantage of using CM coordinates - the system velocity remains constant and is independent of the final angle of scatter between the two particles. Hence, the total linear momentum of the system is always zero, and the particle velocities are inversely proportional to their masses, see Figure 2-1:

$$\text{Eq. 2-12} \quad \frac{V_0 - V_c}{V_c} = \frac{M_2}{M_1}$$

and the CM total kinetic energy, E_C , is equal to the CM initial kinetic energy:

$$\text{Eq. 2-13:} \quad E_C \equiv \frac{1}{2} M_C V_0^2$$

Further, the angular momentum, J_C , is identical in both systems and is simply related to the impact parameter, p , see Figure 2-1:

$$\text{Eq. 2-14:} \quad J_C \equiv M_C V_0 p$$

Using these equations, we can find many relations between the initial parameters and the final scattering angles.

The conversion of scattering angles from the CM system to the laboratory system is shown in Figure 2-2 and Figure 2-3. In Figure 2-2 the conversion for the target-particle recoil is shown to

be very simple because its initial laboratory velocity is zero. Hence its laboratory final velocity vector, v_2 , is related to its CM velocity vector, v_c , by the translation vector between the two systems, v_c . This translation vector, v_c , was defined in Eq. 2-5 to make the total momentum of the system to be zero. As shown in the figure, the vector triangle is isosceles with two sides equal to v_c , so we relate the two recoil angles as

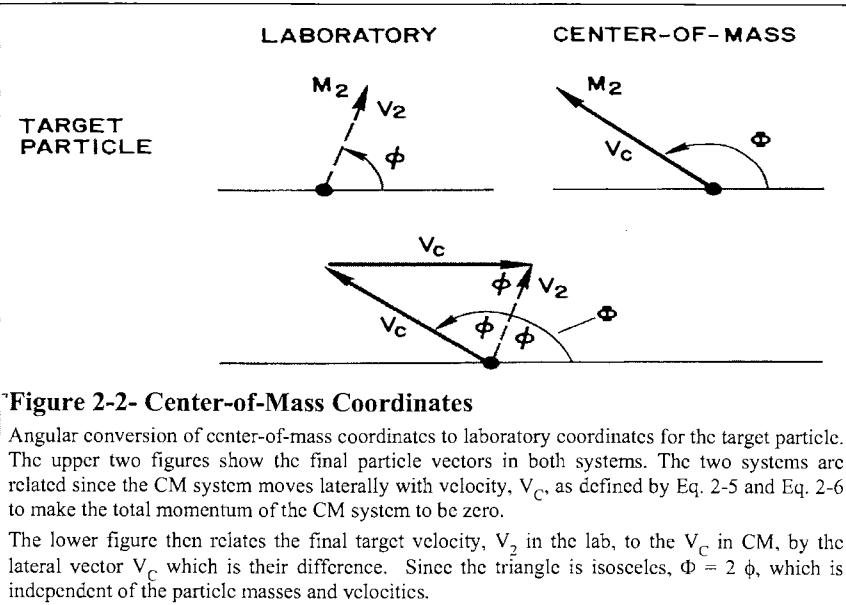


Figure 2-2- Center-of-Mass Coordinates

Angular conversion of center-of-mass coordinates to laboratory coordinates for the target particle. The upper two figures show the final particle vectors in both systems. The two systems are related since the CM system moves laterally with velocity, v_c , as defined by Eq. 2-5 and Eq. 2-6 to make the total momentum of the CM system to be zero.

The lower figure then relates the final target velocity, v_2 in the lab, to the v_c in CM, by the lateral vector v_c which is their difference. Since the triangle is isosceles, $\Phi = 2\phi$, which is independent of the particle masses and velocities.

$$\text{Eq. 2-15:} \quad \Phi = 2\phi$$

where Φ is the CM recoil angle, and ϕ is the laboratory recoil angle. This can be related to the projectile CM angle using Figure 2-1 and we find:

$$\text{Eq. 2-16:} \quad \Phi = \pi - \Theta = 2\phi$$

Another useful relation can be derived from Figure 2-2 by applying the law of cosines:

$$\text{Eq. 2-17:} \quad v_2^2 = v_c^2 + v_c^2 - 2v_c^2 \cos(\pi - \Phi) = 2v_c^2(1 - \cos \Theta)$$

This final recoil velocity can be simplified using Eq. 2-8: $M_C \equiv M_1 M_2 / (M_1 + M_2)$, and Eq. 2-16 : $\Phi = \pi - \Theta = 2\phi$ to obtain:

$$\text{Eq. 2-18:} \quad v_2 = 2 V_0 \frac{M_C}{M_2} \cos \phi$$

which relates the final recoil velocity to the laboratory angle of recoil.

Using this relation, the energy transferred, T, in the collision from the incident projectile to the target particle can be evaluated:

$$\text{Eq. 2-19: } T = \frac{1}{2} M_2 V_2^2$$

$$\text{Eq. 2-20: } T = \frac{M_2}{2} \left(\frac{2 V_0 M_c \cos \phi}{M_2} \right)^2$$

$$\text{Eq. 2-21: } T = \frac{2}{M_2} (V_0 M_c \cos \phi)^2$$

This can be related to the angle of scatter of the projectile : $2\phi = (\pi - \Theta)$, giving the relations :

$$\text{Eq. 2-22: } T = \frac{2}{M_2} \left(V_0 M_c \sin \frac{\Theta}{2} \right)^2$$

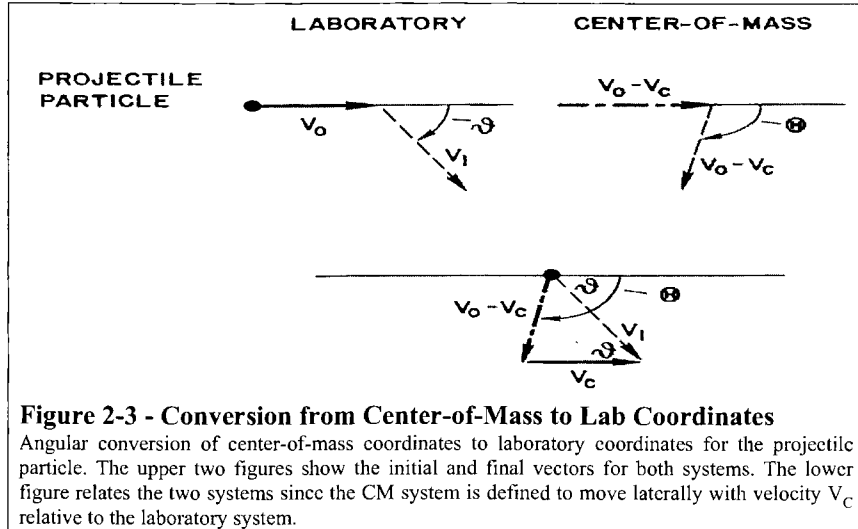


Figure 2-3 - Conversion from Center-of-Mass to Lab Coordinates

Angular conversion of center-of-mass coordinates to laboratory coordinates for the projectile particle. The upper two figures show the initial and final vectors for both systems. The lower figure relates the two systems since the CM system is defined to move laterally with velocity V_c relative to the laboratory system.

$$\text{Eq. 2-23: } T = \frac{4 E_c M_c \sin^2 \frac{\Theta}{2}}{M_2}$$

$$\text{Eq. 2-24: } T = \frac{4 E_0 M_1 M_2 \sin^2 \frac{\Theta}{2}}{(M_1 + M_2)^2}$$

These relations contain the energy lost by the projectile and hence will lead to the stopping power of the projectile when we evaluate the energy loss cross-section.

Similarly, the projectile parameter conversion is shown in Figure 2-3, but it is more complicated because of the initial velocity, V_0 , of the projectile. The relation of the scattering angles can be derived from Figure 2-3 to be :

$$\text{Eq. 2-25:} \quad \tan \theta = \frac{(V_0 - V_c) \sin \Theta}{V_c + (V_0 - V_c) \cos \Theta}$$

but we may use Eq. 2-12 which relates $(V_0 - V_c) / V_c = M_2 / M_1$, which simplifies the angular relationship to :

$$\text{Eq. 2-26:} \quad \tan \theta = \frac{(M_2 / M_1) \sin \Theta}{1 + (M_2 / M_1) \cos \Theta}$$

$$\text{Eq. 2-27:} \quad \text{or : } \tan \theta = \frac{M_2 \sin \Theta}{M_1 + M_2 \cos \Theta}$$

Another way to analyze this relationship is to evaluate Figure 2-3 using the law of sines, and we can obtain the equivalent relation :

$$\text{Eq. 2-28:} \quad \frac{\sin(\Theta - \vartheta)}{\sin \vartheta} = \frac{V_c}{V_0 - V_c}$$

which can be rearranged using Eq. 2-12 to be

$$\text{Eq. 2-29:} \quad \sin(\Theta - \vartheta) = \frac{M_1}{M_2} \sin \vartheta$$

Thus the CM to laboratory angular conversion is shown by Eq. 2-15 for the target particle, and by Eq. 2-28 or Eq. 2-29 for the projectile. The relation between each of these scattering angle pairs can be made with equation $\Phi = (\pi - \Theta)$.

The discussion above concerns asymptotic values, and is valid for all symmetric elastic forces between particles. If the force is electrostatic, falling off as $1/r^2$, then the total path of the two particles can be determined to be hyperbolas. The only part of the path which will interest us later is the closest point of approach between of the two particles.

Defining this minimum radius of separation, r_{\min} , we can show for repulsive inverse square fields that this point is where the potential energy between the two particles exactly equals the initial CM kinetic energy (not the total kinetic energy, but the CM initial energy):

$$\text{Eq. 2-30:} \quad \frac{1}{2} M_c V_0^2 = \frac{2 Z_1 Z_2 e^2}{d}$$

where d is called the *collision diameter* and relates the Coulomb energy to the kinetic energy of the system as shown above and where Z_1 and Z_2 are the number of charges on the two particles. The collision diameter, d , can be considered to be defined by Eq. 2-30:

$$\text{Eq. 2-31:} \quad \text{Collision Diameter} \equiv d = \frac{4 Z_1 Z_2 e^2}{M_c V_0^2}$$

For the minimum separation during the scattering, r_{\min} , we can similarly find from just the collision diameter, d , and the final angle of scatter :

$$\text{Eq. 2-32:} \quad \text{Minimum Separation} \equiv r_{\min} = \frac{d}{2} \left(\csc \frac{\Theta}{2} \pm 1 \right)$$

where the \pm sign is for repulsive (+) or attractive (-) potential.

For a head-on repulsive collision we have the condition for closest approach, r_{\min} , for which the kinetic energy has all been converted to Coulomb energy and $r_{\min} = d$.

TWO-BODY CENTRAL FORCE SCATTERING

The above discussion reviewed the elastic scattering of two particles and the final-state formulae are valid for all such collisions which have conservation of energy and momentum. The equations above that are most applicable to stopping powers are Eq. 2-22 and Eq. 2-24 which show the energy loss from the projectile particle to the target particle during a scattering event. But to get the *cross-section* for the energy transferred we need to know the probability for each final scattering angle, and this is obtained only by evaluating the details of the scattering trajectory and hence the probability of scatter into each scattering angle.

The most important simplification of this problem is to assume that the force between the two particles acts only along the line joining them, and there are no transverse forces. Then, as discussed above, the use of center-of-mass (CM) coordinates reduces any two-body problem to a one-body problem, namely the interaction of a particle with mass, M_c , and velocity, V_c , with a static potential field centered at the origin of the CM coordinates. This is because in the CM system *the total linear momentum of the particles is always zero*, the paths of the two particles are symmetric as shown in Figure 2-1, and the evaluation of one particle's path directly gives the path of the other particle. The conversion from CM scattering angles to laboratory angles is then done with relations such as Eq. 2-16 and Eq. 2-27.

The derivation of the complete particle scattering path is usually done using Lagrangian mechanics in polar coordinates. Since we are dealing with only two particles and no transverse forces, the problem is two-dimensional with the plane defined by the projectile's initial velocity vector and the initial target particle position. We call the azimuthal polar coordinate, Θ , and the radial coordinate, r , in the following discussion.

Only two new equations are needed to determine the trajectory of the particle in the CM coordinate system. We use the notation of $\dot{r} = dr/dt$ and $\dot{\Theta} = d\Theta/dt$ for the time differentials of motion in polar coordinates. From conservation of energy we have for the system

$$\text{Eq. 2-33: } E_C = \frac{1}{2} M_C (\dot{r}^2 + r^2 \dot{\Theta}^2) + V(r)$$

where E_C is the CM energy, defined by Eq. 2-13 to be $E_C = 1/2 M_C V_0^2$, and this is merely restated in Eq. 2-33 with CM polar coordinates.

The second equation states the conservation of angular momentum for the system, and in CM coordinates this is :

$$\text{Eq. 2-34: } J_C = M_C r^2 \dot{\Theta}$$

where J_C is the constant of angular momentum. This is the polar coordinate relation which found previously, in Eq. 2-14, to be a constant of motion with the value :

$$\text{Eq. 2-35: } J_C = M_C V_0 p$$

where p is the impact parameter defined in Figure 2-1.

With these three equations we can solve, for example, for $d\Theta$ as a function of dr . This relation is most important for it will then allow us to calculate directly the energy transferred in any collision for any central force potential, $V(r)$.

We substitute Eq. 2-35 into Eq. 2-34 to remove the variable J_C , then we insert this into Eq. 2-33 and solve for \dot{r} . The result is the radial equation of motion and it can take the form :

$$\text{Eq. 2-36: } \dot{r} = \frac{dr}{dt} = V_0 \left[1 - \frac{V(r)}{E_c} - \left(\frac{p}{r} \right)^2 \right]^{1/2}$$

From the equations above the angular coordinate will be determined by .

$$\text{Eq. 2-37: } \dot{\Theta} = \frac{d\Theta}{dt} = \frac{V_0 p}{r^2}$$

Combining Eq. 2-36 and Eq. 2-37 we have the result :

$$\text{Eq. 2-38: } \frac{d\Theta}{dr} = \frac{d\Theta}{dt} \frac{dt}{dr} = \frac{\dot{\Theta}}{\dot{r}} = \frac{p}{r^2 \left[1 - \frac{V(r)}{E_c} - \frac{p^2}{r^2} \right]^{1/2}}$$

Integrating this over the entire collision path, and taking into account the initial value of $\Theta = \pi$, we have the final relations:

$$\text{Eq. 2-39: } \Theta = \pi - \int_{-\infty}^{\infty} \frac{p dr}{r^2 \left[1 - \frac{V(r)}{E_c} - \frac{p^2}{r^2} \right]^{1/2}}$$

$$\text{Eq. 2-40: } \Theta = \pi - 2 \int_{r_{\min}}^{\infty} \frac{p dr}{r^2 \left[1 - \frac{V(r)}{E_c} - \frac{p^2}{r^2} \right]^{1/2}}$$

This equation allows us to evaluate the final angle of scatter, Θ , in terms of the initial CM energy, E_c , the potential, $V(r)$, and the impact parameter, p .

Later, we will use this equation to calculate the energy transferred to the target atom using Eq. 2-24, and then evaluate the cross-section for such scattering by integrating over all impact parameters using Eq. 2-40. Eq. 2-40 is called the general orbit equation for two-body central force scattering. The only conditions on its applicability are, essentially, that the central force potentials of each particle must not vary with time, nor depend on the particle's motion. The potentials must be spherically symmetric. Finally, the laws of conservation of energy and momentum must hold for the system as a whole.

INTERATOMIC POTENTIALS

As discussed in the preceding section, the scattering of two particles can be reduced to a single equation by transforming the particles motion to a Center-of-Mass coordinate system. The potentials of the two particles are also reduced to a single potential field called the *Interatomic Potential*. After solving the scattering of the two particles using CM coordinates, the final asymptotic solutions (energy transferred and final trajectory angles) are found by converting back from CM coordinates to laboratory coordinates.

In this section we shall consider the case of a moving atom (which we will call the *ion* henceforth) passing a stationary target *atom*. The transfer of energy from the ion to the atom is complicated by the complex electronic screening of the two nuclei, and we must consider the physics of quantized screened Coulomb collisions. We shall first describe in detail our method for calculation of screened collisions between atoms. We shall then calculate the nuclear stopping as the average energy loss of all possible types of these collisions, weighted by their relative probability. We then demonstrate that the screened scattering of two atoms at the limit of very high velocities is the same as the Rutherford scattering of two point charges. Most of the prior published theoretical work has been done using classical universal atomic screening, such as the Thomas-Fermi atom, since these atomic models scale simply from one atomic number to another. Since 1978, Hartree-Fock charge distributions have been used in stopping and collision theory (78a). In this book we present the results of the first potentials derived from solid-state charge distributions. We shall show examples of how these solid-state results compare to those obtained using traditional universal-atom screening. Finally, in order to use Monte-Carlo programs to follow ion trajectories in solids, it is necessary to simplify the

calculation of the ion's deflection as it passes an atom. This is done using a Magic Formula (a phrase used by several authors) where the ion's angle of scatter is calculated analytically by a simple algorithm dependent on the ion's initial velocity and impact parameter.

Because of their universal applicability, statistical models of interatomic interaction have been widely used in calculating nuclear stopping. The most widely used is the Sommerfeld approximation to the Thomas-Fermi potential (32b), the Molicre approximation (47a), the Lenz-Jensen (32c), and the Bohr potential (48a). Each of these potentials may be considered as a Coulombic term ($1/r$) multiplied by a "screening" function. The Coulombic term arises from the positive point nucleus, and the electronic screening reduces its value for all radii. The screening function may be defined as the ratio of the actual atomic potential at some radius to the potential caused by an unscreened nucleus:

$$\text{Eq. 2-41: } \Phi = \frac{V(r)}{(Ze/r)}$$

where Φ is the screening function, $V(r)$ is the potential at radius r , Z is the atomic number and e is the electronic charge. The implications of the spherical symmetry of this definition are discussed in the section on Solid State Charged Distributions.

There are three general approaches which have been used to calculate screening functions (and hence interatomic potentials). One way is to use experimental data and to try to work back to the potential. A second is to incorporate full quantal treatments for all collisional interactions. A third way is to isolate the few interactions of importance to energetic collisions and to estimate the potential from limited calculations. These techniques are described below.

First, the interatomic potential can be derived from crystal data such as phonon dispersion curves, elastic constants, compressibility and the x-ray lattice constants. Although one can obtain excellent potentials for atoms at normal solid-state separations, this method can not be used in obtaining potentials for the small nuclear separations which one finds in atomic collisions. Further, the only potentials which can be obtained are those for atoms of materials which can be fabricated in crystalline form, i.e. for like-atom collisions, e.g. Si-Si, and for the few binary crystals such as GaAs. Finally, the technique can only be applied to stable crystal elements, and has not been used for H or He atoms. The various methods which have been developed to obtain potentials from crystal data has been reviewed by Johnson (73c).

The second technique is at the opposite extreme of computational difficulty. One begins with two Hartree-Fock atoms and as they merge one recalculates the electronic orbits based, for example, on multi-configurational self-consistent-field methods. This type of calculation is the most accurate known and can treat all atomic combinations. It further allows for the treatment of excited and ionized states in either of the atoms. This approach is overly-sophisticated for collisional studies, but it can be used to obtain bench-marks to establish the accuracy of simpler approaches. That is, the complete calculation can be made for a few systems, and we can require that any simpler approach should produce potentials which agree closely to the best calculation which can be done.

A third technique is to use the simplified quantum-mechanical approach which was suggested by Gombas (49a). One of the earliest calculations using this approach was by Wedepohl (67c), and a wide study was made by Wilson, Haggmark and Biersack (77c). This method begins with two

atomic charge distributions, and for the calculation of the interatomic potential the local electron distribution is assumed to remain fixed without any reconfiguration of the atomic structures as a whole. For any volume element of either atom, the number of its electrons in that volume does not change as the two atoms merge. The actual number of electrons in a specific volume element may change if it is part of the overlap volume of the two atoms. For this overlap volume there will be electrons from both atoms, and these are treated as a free electron gas within the volume element. All overlap volumes absorb energy (decrease the attractive potential) because the Pauli principle demands that for an increased electron density there must be promotion of electrons into higher energy levels (i.e. into higher velocities).

This approximate interatomic potential calculation therefore has two parts: one is the Coulombic interaction between all the electrons and the two nuclei, and the second is the increased quantal energy which goes into excitation and exchange effects for the electrons in the volume of atomic overlap. And because the exchange energy is treated in the Slater approximation, a form of correlation is also taken into account.

Model for Calculating Interatomic Potentials

Each atom is assumed to be a spherically symmetric charge distribution, $\rho(r)$, with a central point charge of Z_c , and with the volume normalization $Z = \int 4\pi r^2 \rho(r) dr$. We assume the atom is in a solid and its electrons are confined to a spatially limited cell. When the ion and the atom begin to merge, we assume there is no spatial distortion of the electron clouds, and that each nucleus stays at the center of its electron sphere. The total interaction potential energy is:

$$\text{Eq. 2-42:} \quad V = V_{nn} + V_{en} + V_{ee} + V_k + V_a$$

where V_{nn} is the electrostatic potential energy between the nuclei, V_{ee} is the pure electrostatic interaction energy between the two electron distributions, V_{en} is the interaction energy between each nucleus and the other electron distribution, V_k is the increase in kinetic energy of the electrons in the overlap region due to Pauli excitation and V_a is the increase in exchange energy of these electrons.

The first component of the interatomic potential, V_{nn} , can be described as:

$$\text{Eq. 2-43:} \quad V_{nn} = Z_1 Z_2 e^2 / r_{12}$$

where Z_1 and Z_2 are the atomic numbers of the ion and target atom, e is the electronic charge, and r_{12} is the distance between the two nuclei.

For the term V_{en} , consider the general case where the ion's nucleus, Z_1 , has partially penetrated the electron cloud of the target atom 2, see Figure 2-4. The potential energy gained by this nucleus can be simply divided into two parts:

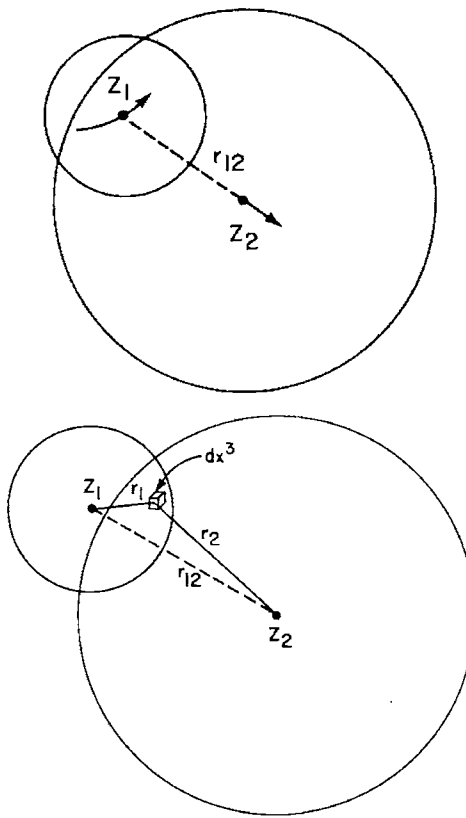


Figure 2-4 - The Calculation of Interatomic Potentials

Figure 2-4a, above, the atom with atomic number, Z_1 , is separated by a distance, r_{12} , from the atom of atomic number, Z_2 . In the simplified calculation of the interatomic potential, no distortion is allowed for the spherically symmetric electron distributions, however the electrons in the volume of overlap of the two atoms absorb energy by Pauli promotion.

Figure 2-4b, below, shows the geometric variables for the calculation of interatomic potentials. The atoms, Z_1 and Z_2 , are separated by a distance r_{12} between their centers. In their region of electronic overlap, the volume element, dx^3 , is a radial distance, r_1 , from atom Z_1 and a radial distance, r_2 , from atom Z_2 . The electrons in volume dx^3 absorb energy by Pauli promotion if this volume is part of the electronic overlap volume of the two atoms.

$$\text{Eq. 2-44: } V_{\text{en}} = -Z_1 e^2 \left[\int_{r_{12}}^{\infty} \frac{(4\pi r^2 \rho_2) dr}{r} + \frac{1}{r_{12}} \int_0^{r_{12}} (4\pi r^2 \rho_2) dr \right]$$

where the first term in the brackets is a potential term at point r_{12} from the electron shell of atom 2 *outside* radius r_{12} ; the second term in the brackets is the potential term for the electrons of atom 2 *within* the sphere of radius r_{12} . We define for later use:

$$\text{Eq. 2-45: } Q_2(r_0) = \int_0^{r_0} 4\pi r^2 \rho_2 dr$$

$$\text{Eq. 2-46: } \Psi_2(r_0) = \int_{r_0}^{\infty} \frac{4\pi r^2 \rho_2 dr}{r}$$

Therefore we have:

$$\text{Eq. 2-47: } V_{\text{en}} = -Z_1 e^2 [\Psi_2(r_{12}) + Q_2(r_{12}) / r_{12}]$$

For the interaction energy, V_{ee} , we use the same approach as for V_{en} , but now we must integrate over the electron distributions of both the target and the ion. We must define new distances in order to express the interaction concisely, see Figure 2-4. For a volume element of the ion, dx^3 , we define r_1 as its distance from nucleus Z_1 , r_2 as its distance from Z_2 , and r is the perpendicular distance from the line joining Z_1 and Z_2 . The energy of the volume element is:

$$\text{Eq. 2-48: } dV_{\text{ee}} = e^2 \left[\psi_2(r_2) + \frac{Q_2(r_2)}{r_2} \right] \rho_1 dx^3$$

and the total energy is the integration over the ion's charge distribution:

$$\text{Eq. 2-49: } V_{\text{ee}} = e^2 \int \left[\psi_2(r_2) + \frac{Q_2(r_2)}{r_2} \right] \rho_1 dx^3$$

The expansion of this equation to more formal spherical coordinates is straightforward, but lengthy. See Ref. 67c for complete expansions.

For potentials V_k and V_a , we consider that, in the region of the electronic overlap, the electronic energy must change because of the Pauli principle. If we treat this volume as a totally degenerate free electron gas, the kinetic energy is given by:

$$\text{Eq. 2-50: } V_k(\text{total}) = \left[\frac{3}{5} \frac{\hbar^2 \pi^2}{2m} \left(\frac{3}{\pi} \right)^{2/3} \right] \int \rho^{5/3} dx^3$$

where m is the electron mass, and $\rho = \rho_1 + \rho_2$, the combined electron density at volume element dx^3 . The factors preceding the integral are usually noted as κ_k and has the numeric value of 21.88

eV-Å². Since we allow no distortion of either charge distribution, the excess kinetic energy is the new energy minus the two original electron energies

$$\text{Eq. 2-51: } V_k = \kappa_k \int \left[(\rho_1 + \rho_2)^{5/3} - (\rho_1^{5/3} + \rho_2^{5/3}) \right] dx^3$$

where the integral is over the overlap volume.

The exchange energy, E_a, can be understood by noting that in the vicinity of each electron the density of electrons with the same spin direction is substantially less than in the case of a uniform distribution. A partial electron depletion thus arises in the vicinity of each electron, caused by the "repulsion" of other electrons with like spin. This leads to a "local" decrease in electronic density which lowers the energy of the system when compared to that of a continuous electronic density. This decrease is identical to what is usually called *the exchange energy*. The total exchange energy of the overlap of atomic electronic densities is, approximately:

$$\text{Eq. 2-52: } V_a(\text{total}) = - \left[\frac{3e^2}{4} \left(\frac{3}{\pi} \right)^{1/3} \right] \int \rho^{4/3} dx^3$$

where the term of constants is usually designated as κ_a and has the value of 10.635 eV-Å. The net increase of energy for the overlap region is

$$\text{Eq. 2-53: } V_a = - \kappa_a \int \left[(\rho_1 + \rho_2)^{4/3} - (\rho_1^{4/3} + \rho_2^{4/3}) \right] dx^3$$

The interatomic potential for two atoms is now completely described, with the basic contributions being classified as Coulombic, kinetic and exchange energies:

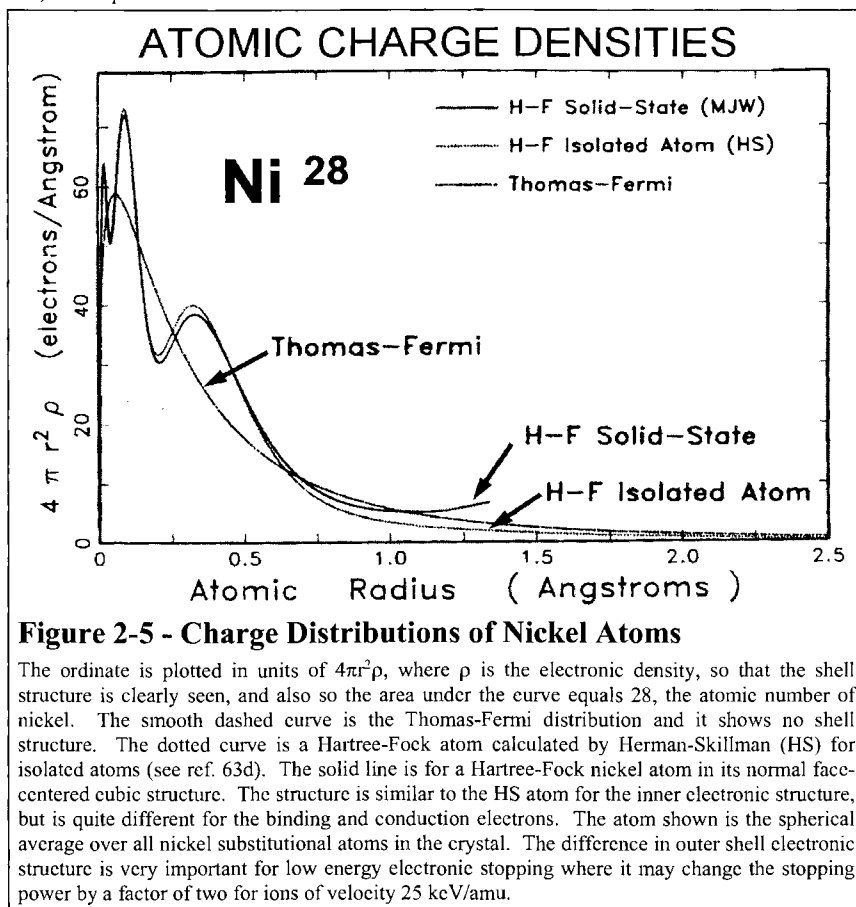
$$\text{Eq. 2-54: } V = V_c + V_k + V_a$$

where V_c is defined as the sum of Eq. 2-43, Eq. 2-47 and Eq. 2-49. V_k is defined by Eq. 2-51. V_a is defined by Eq. 2-53.

One should note that this approach might be considered rather primitive in light of the possible quantum-mechanical effects and polarization which have been omitted in our two atom potential. The main attraction of this procedure is that it can be applied to any two atoms with the only input being the two charge distributions. Further, since we are going to use these interatomic potentials in calculating the stopping and range of ions in matter, we will be averaging over many collisions and small details will blur out. We shall further show that when these results are compared to those of detailed and much more complex calculations, the error is acceptable for interatomic potentials above a few eV. This corresponds to the general experience in quantum mechanics that accurate values for the change in energy can be obtained without changing the electronic distribution in the sense of first order perturbations theory.

The Charge Distribution of Solid-State Targets

The electronic charge distribution of the target is the fundamental input to the calculation of interatomic potentials. The target charge distributions for most solid state targets are distributions which we have constructed using Hartree-Fock-Slater atomic distributions (63d) to make first-order solids by the techniques outlined in reference 67d. More accurate solid-state charge distributions were used for targets with atomic numbers 2-5, 11-13, 19-31 and 27-29. These were constructed using the local density approximation for exchange and correlation effects (78d), and we call these MJW distributions after the authors Moruzzi, Janak and Williams. In all cases the crystalline structures used for the elements corresponded to those tabulated in reference 78d and 76j. In the cases where two crystalline structures are possible at room temperature, such as Sn and Pb, the simpler structure was used.



An example of the various charge-distributions is shown in Figure 2-5, where the classical Thomas-Fermi distribution for nickel is shown by a dotted curve, the Hartree-Fock isolated-atom charge distribution is shown by a dashed line, and the solid-state distribution by a solid line.

One problem in constructing solid-state charge distributions is how to evaluate the interstitial charge region. Once the basic solid is constructed using spherically symmetric atoms in the proper crystalline structure, there is usually about one electron which remains to be distributed in the non-spherically symmetric region between the lattice atoms (which we call the interstitial region). The extra charge is often called a conduction electron. We have tried three standard techniques for distributing this interstitial charge: (a) assuming uniform charge density in each of the interstitial regions of the solid, (b) assuming the charge density *gradient* remains constant from the edge of the muffin-tin atom into the interstitial region until the necessary interstitial electron charge is accounted for, and (c) assuming that the charge density remains constant from the edge of the muffin-tin atom into the interstitial region. (A muffin-tin potential uses individual-atom potentials distributed using specific crystalline atom locations.) The interstitial charge distribution of type (a) is the one we prefer, and it is derived by determining the number of electrons per atom not accounted for within the muffin-tin radius and dividing this charge by the unit crystal volume not filled by the muffin tin solid. This interstitial charge density is usually discontinuous from the muffin-tin distribution.

Each atom of the solid is then made into a spherical distribution (which is required by the mathematics of our interatomic potential scattering) by taking the distributions for atoms in each possible lattice site, averaging their distributions over all spatial orientations, and then finding a mean atom by averaging over the various lattice types weighted by their relative abundance in the solid.

Single Atom Potentials

In order to calculate interatomic potentials, the only physical quantities required are the charge distributions of the colliding atoms. A large body of work has evaluated potentials using classical charge distributions such as those of Bohr (48a), Thomas-Fermi (32b), Lenz-Jensen (32c) and Moliere (47a). For convenience, we shall call these *classical* atomic models henceforth to differentiate them from recent Hartree-Fock or solid-state atomic models. These classical distributions scale simply with atomic number and do not include any explicit shell structure. Although these distributions can be used to provide most of the basic insight into interatomic potentials, the use of Hartree-Fock charge distributions create significant changes in the details of the interaction potentials.

For illustration, we shall use both types of screening to calculate typical interatomic potentials. When we use the classical atom descriptions, we shall be calculating the scattering of two isolated atoms. For the Hartree-Fock distributions, we use the charge distribution of solid matter with normal crystal structure for each element (78d).

For the charge distribution of the ion a problem arises. If we use the Hartree-Fock charge distribution for an isolated atom, then electrons extend out to 5 or 6 Å. However, this is much greater than the mean distance between atoms in a solid, and so these outer electrons would not orbit the ion while it penetrates the solid. Further, there will be some coalescence of the solid's electron sea about the ion, which is called *polarization*, increasing the target's local charge distribution. Analogous to this is a hydrogen atom at rest in a metal where the normal orbit of its electron is beyond the nearest metal atoms. The conduction electrons will compress about the H

nucleus, screening it without necessarily being in a closed orbit. In the spirit of these arguments, we have used solid-state charge distributions for the ion as well as the target atom in order to remove the distant electrons and approximate the polarization of the solid's electrons about the ion.

Shown in Figure 2-5 are various types of charge distributions for atoms. The ordinate is $4\pi r^2 \rho(r)$ in terms of $\text{electrons}/\text{\AA}^3$. The area under the curve equals 28, the atomic number of nickel. The dashed curve is the classical charge distribution of a Thomas-Fermi atom (32b) which has no shell structure. The dotted curve was an early Hartree-Fock-Slater atomic calculation by Hermann and Skillman (63d). This calculation was for isolated atoms and like the Thomas-Fermi atom, the electron distributions extend far out from the nucleus. An example of a modern solid-state charge distribution is shown in Figure 2-6 as a solid line, and it was constructed by Moruzzi, Janak and Williams (78d) using a local density approximation for exchange and correlation effects. This model shows shell structure, and also a sharply truncated charge distribution at 1.3 Å.

Next we consider the calculations of atomic potentials. Normally we might show such a potential in energy units such as eV vs. atomic radius. Instead of potential, there is a long tradition to use a *screening function*, Φ , defined as the ratio of the atomic potential, V , to the potential of an unscreened nucleus:

$$\text{Eq. 2-55:} \quad \Phi = \frac{V(r)}{(Ze/r)} \quad (\text{Definition of Screening Function})$$

here Z is the atom's atomic number, e is the electronic charge and r is the radial coordinate. Traditionally, the radial abscissa is restated using a *reduced radius*, x , which is the atomic radius divided by a quantity called the screening length, which describes the radial gradient of the potential. It will become clear that this reduced radius allows simple comparison of interatomic potentials from various models of the atom. The simplest example is the classic potential for a Bohr atom, which is a simple exponential:

$$\text{Eq. 2-56:} \quad \Phi(\text{Bohr}) = \exp(-r/a_0) = \exp(-x)$$

where the Bohr radius, $a_0 = \hbar^2/me^2 = 0.529 \times 10^{-10} \text{ m} = 0.529 \text{ pm} = 0.529 \text{ \AA}$

For other classical atom models, a similar analytic expression can usually be derived (although it may be an approximation). The Thomas-Fermi atom has been studied by many authors (see reference 49a for a thorough review), and it is traditionally described by defining the reduced radius, x , and a different screening length, a_{TF} , using the expression:

$$\text{Eq. 2-57:} \quad x \equiv \frac{r}{a_{TF}}$$

where a_{TF} , the *Thomas-Fermi screening length*, has been defined as:

$$\text{Eq. 2-58:} \quad a_{TF} \equiv \frac{1}{4} \left(\frac{9\pi^2}{2} \right)^{1/3} \left(\frac{\hbar^2}{m_e^2} \right) \frac{1}{Z^{1/3}}$$

$$\text{Eq. 2-59: } = \frac{.8853 a_0}{Z^{1/3}}$$

The concept of *screening length* is sometimes difficult to grasp, but it is simply a parameter which defines the radial spread of the electronic charge about the nucleus. The constants in Eq. 2-58 are derived from the basic concepts of the Thomas-Fermi atom and are derived in detail in Ref. 49a.

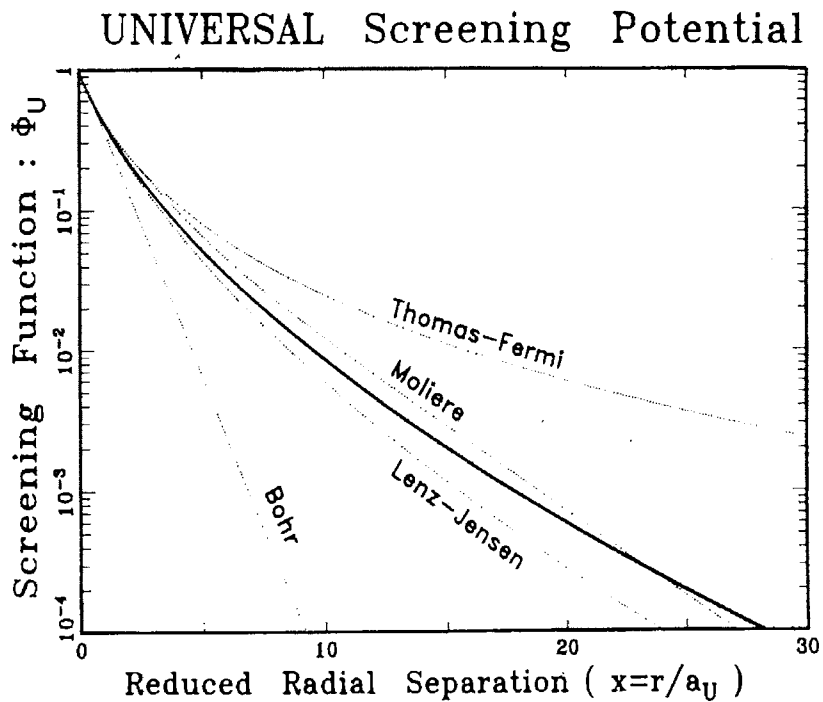


Figure 2-6 Classic Atomic Potentials

Potentials of four models of a statistical atom are shown with the ordinate being the screening function, defined as the ratio of the atomic potential divided by the potential of a bare unscreened nucleus, Eq. 2-55. The abscissa is a reduced radial coordinate defined as the radius divided by the Thomas-Fermi screening length, Eq. 2-58. In these coordinates the atomic potential for each atom is a single line, independent of the atomic number. The Thomas-Fermi atom has the greatest electronic contributions far from the nucleus, so its nucleus is less shielded and has greater scattering potential than the others. The equations for the four classical screening functions can be found in equations Eq. 2-56, and Eq. 2-60 to Eq. 2-63. Also shown as a solid line is the new "Universal" potential described in this chapter (see Figure 2-17).

When we use these reduced coordinates, the Thomas-Fermi potential distribution becomes independent of the atom's atomic number, i.e. all atoms are represented by the same screen function. And, to a reasonable approximation, the other classical potentials are also universal in these coordinates, and a single plot can show their potential distributions for all atoms, see Figure 2-6. Using the notation $x = r / a_{TF}$, the screening function for a Thomas-Fermi atom can not be solved analytically, but various authors have created close approximations:

$$\text{Eq. 2-60: } \Phi(\text{Thomas-Fermi}) = \left[1 + \left(\frac{x}{\alpha} \right)^\lambda \right]^{-\frac{3}{\lambda}} = \left[1 + \left(\frac{x^3}{144} \right)^{\frac{\lambda}{3}} \right]^{-\frac{3}{\lambda}}$$

where the first expression is by Sommerfeld (37c) and the latter is an evaluation by March (50b) using the parameters:

$$\text{Eq. 2-61: } \lambda = 0.8034 \quad \text{and} \quad \alpha = 12^{2/3}$$

These two expressions are almost identical.

Moliere also evaluated the Thomas Fermi atom, and found that this function, for large values of x , deviated from the asymptotical behavior of quantum mechanical wave functions. These functions decay exponentially. Moliere derived an expansion to include this exponential decay, and it was different enough for it to be traditionally called the Moliere Potential, although it also was derived from the Thomas-Fermi atom (47c):

$$\text{Eq. 2-62: } \Phi(\text{Moliere}) = [0.35 \exp(-0.3x)] + [5.5 \exp(-1.2x)] + [0.1 \exp(-6.0x)]$$

Another classical atom often used is the Lenz-Jensen atom (described in 32f and 32g) and we have evaluated its potential to obtain a version in the same functional form as those above:

$$\text{Eq. 2-63: } \Phi(\text{Lenz-Jensen}) = [.7466 \exp(-1.038x)] + [.2433 \exp(-.3876x)] + [.01018 \exp(-.206x)]$$

For the case of the Thomas-Fermi atom, the charge distribution shown in Figure 2-5 can be simply calculated using the Thomas-Fermi differential equation to obtain:

$$\text{Eq. 2-64: } 4\pi r^2 \rho_{TF} = (Z/r) (x \Phi_{TF})^{3/2}$$

where Z is the atomic number of the atom. In general, we have by virtue of the Poisson equation, the relation:

$$\text{Eq. 2-65: } 4\pi\rho = (Z/r) d\Phi^2 / dr^2$$

The screening functions of Eq. 2-56 to Eq. 2-63 are plotted in Figure 2-7 as dotted lines, which shows the effect of the various electron distributions on the atomic potential.

Plotted in Figure 2-7 are representative potentials of the solid-state atoms which we will use in this book. Shown in solid lines are the screening functions of atoms in solid forms of boron, nickel and gold. These screening functions can not be represented well by the classical models

except for the innermost electron shells, i.e. closer than $x = 3$ (which is 0.8, 0.5 and 0.3 Angstroms for B, Ni and Au respectively).

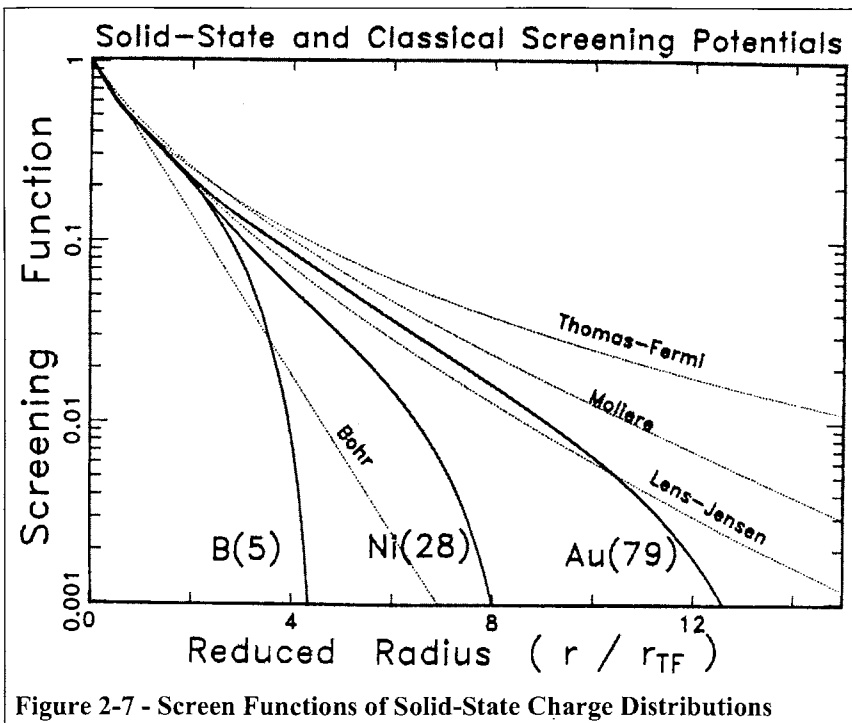


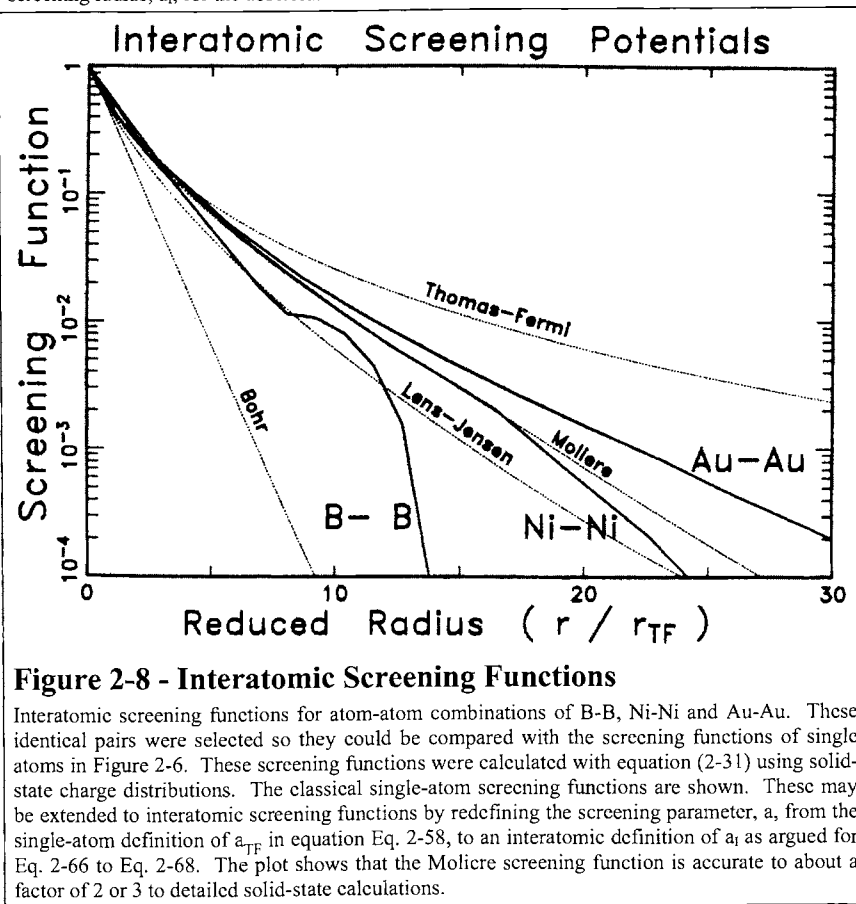
Figure 2-7 - Screen Functions of Solid-State Charge Distributions

Shown are the screening functions of three solid-state atomic charge distributions and four classical screening functions. The nickel and gold atoms are from f.c.c. structures, while the gold is from a hexagonal structure. The screening functions are calculated using equation (2-44). For the inner shells, these atoms are well described by the Moliere and Lenz-Jensen atoms. Beyond the L-shell, none of the classical screening functions adequately describe the solid-state screening.

Interatomic Potentials

We have previously discussed the definition of interatomic potentials and how they may be calculated. The broad spectrum of the possible interatomic potentials of two colliding atoms is more complicated to illustrate than the potentials of single atoms as above, because the interatomic potential depends on the potentials of each of the colliding particles, and the number of possible pairs of atoms approaches 10^4 . We will show how to calculate these potentials (or their equivalent screening functions) for both classical atoms and HFS solid-state charge distributions. We show in Figure 2-8 results from using classical atoms and also using Eq. 2-42 for the solid-state collisions of B-B, Ni-Ni and Au-Au.

The historical approach to creating *interatomic* screening functions for classical atoms is to use the simple *atomic* potentials, and to adjust the definition of the screening length to approximate for the two-atom potential. So the classical curves in Figure 2-8 are identical to those of Figure 2-6 but the conversion from these reduced units to physical units requires a redefined interatomic screening radius, a_i , for the abscissa.



The creation of a universal reduced coordinate for interatomic potential has been more argued than derived. Bohr suggested (40d, 41a) a form:

$$\text{Eq. 2-66: } a_i(\text{Bohr}) = \frac{a_0}{\left(Z_1^{2/3} + Z_2^{2/3}\right)^{1/2}}$$

where a_0 is the Bohr radius, and Z_1 and Z_2 are the atomic numbers of the two atoms. Firsov made extensive computer calculations (57a, 58b) based upon merging two Thomas-Fermi atoms and suggested that the interatomic potential would be best described by the neutral atomic Thomas-Fermi screening functions, 58, but with the reduced radius being defined as

$$\text{Eq. 2-67: } a_{\text{I}}(\text{Firsov}) = \frac{0.8853 a_0}{(Z_1^{1/2} + Z_2^{1/2})^{2/3}}$$

where the constant, 0.8853, is derived from the Thomas-Fermi atom, see Eq. 2-58 and Eq. 2-59.

Lindhard suggested also using the atomic Thomas-Fermi screening function for the interatomic screening function, but with a slightly different variation:

$$\text{Eq. 2-68: } a_{\text{I}}(\text{Lindhard}) = \frac{0.8853 a_0}{(Z_1^{2/3} + Z_2^{2/3})^{1/2}}$$

which numerically does not differ significantly from the other suggestions. These proposals clearly scale the screening length approximately with $Z^{1/3}$ of the colliding atoms. For the purposes of calculating stopping powers and ranges, we shall end up with summing many collisions, and any of the above approximations might be adequate. In Figure 2-8 the light atom scattering, B-B, is closest to Lens-Jensen screening estimates, while the heavy atom screening, Au-Au, lies between Moliere and Thomas-Fermi screening. Although there are large deviations from any of the universal curves and some of the solid-state calculated curves, it will not be clear until later how significantly these errors will affect stopping powers and ranges. In converting Figure 2-8 from reduced to real units, we must use the *interatomic* screening function definition

$$\text{Eq. 2-69: } \Phi_1 = \frac{V(r)}{Z_1 Z_2 (e^2 / r)}$$

which relates the interatomic screening function, Φ_1 , with the potential, $V(r)$. Also we would have to use some conversion from the reduced radius, a_{I} , to physical interatomic separation, r , using some variation as shown in Eq. 2-66 to Eq. 2-68.

The numeric calculation of an interatomic potential using solid-state charge distributions is shown in detail in Figure 2-9 for two boron atoms. In the upper left part of the plot are listed the potentials as a function of the nuclear separation, r_{12} , tabulated in Angstroms. Column 2 shows the Coulomb potential between all the charges and it is equal to the sum of Eq. 2-43, Eq. 2-44 and Eq. 2-49. This potential is zero at maximum separation, starts negative (attractive) and then turns positive for small separations. This potential is plotted in the lower left plot as the dotted line labeled V_c . The next column is V_k , Eq. 2-51, the energy absorbed in Pauli promotion of the electrons in the volume of overlap of the two atoms. This energy is always positive and increases as the distance between the atoms decreases. Finally the exchange energy, V_a , Eq. 2-53, is tabulated and this energy is always negative.

When the potentials are summed the total interatomic potential, V , is obtained in column four. This total potential is plotted in the upper-right figure.

In column six is tabulated the screening function defined in Eq. 2-69, Φ , and in column seven is the reduced radial coordinate defined using Eq. 2-57, $x = r/a_{\text{TF}}$. The screening function is plotted versus reduced radial separation in the lower right plot. As indicated in Eq. 2-60 through Eq. 2-63, the classical atom interatomic screening functions are single curves in the coordinate system

Atoms = B⁵ and B⁵	r₁₂	V_c	V_k	V_a	V	Phi	r₁₂/a_{TF}
.05	4901.84	688.15	-47.65	5342.34	7696	.2098	
.10	1892.51	542.23	-41.40	2193.34	6093	.5795	
.15	828.12	392.51	-34.56	1184.27	4934	.8693	
.20	459.71	273.77	-28.14	734.34	4091	1.1591	
.40	115.56	87.87	-15.64	187.79	.2067	2.3161	
.60	23.42	59.92	-12.05	71.29	.1188	3.4772	
.80	-7.68	46.04	-9.57	28.79	.0640	4.6363	
1.00	-14.86	34.46	-7.30	12.30	.0342	5.7954	
1.20	-11.69	22.20	-5.00	5.52	.0184	6.9544	
1.40	-4.75	10.85	-2.98	2.92	.0114	8.1135	
1.60	-1.12	5.90	-1.76	2.37	.0105	9.2726	
1.80	- .54	3.06	- .95	1.59	.0080	10.4317	
2.00	- .11	1.34	- .42	.80	.0044	11.5907	
2.20	- .01	.39	- .12	.25	.0015	12.7496	
2.40	.00	.02	- .01	.01	.0001	13.9089	

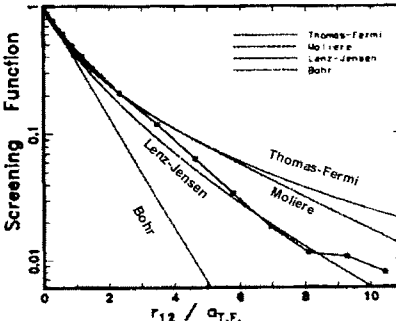
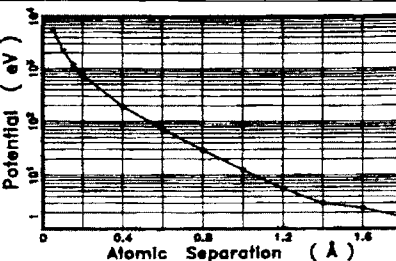
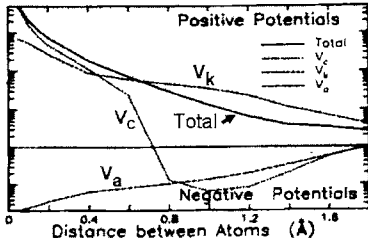


Figure 2-9 - Calculation of Solid-State Interatomic Potentials: B⁵ - B⁵

In the upper left are shown the values of the various potentials for increasing nuclear separation distances, r_{12} , in units of Angstroms. The various potentials are described in the text and are known as V_C , the Coulomb interaction; V_K , the electron excitation energy (kinetic energy of electrons); V_a , the exchange energy between electrons; and V , the total interaction, $V_C + V_K + V_a$, in units of eV (see Eq. 2-42 and following). The next column labeled "Phi" is called the screening function, Φ , and is the summed potential V divided by the potential of the two bare nuclei at the same separation without any electron screening, Eq. 2-55. This screening function goes from unity (at zero separation) to zero at the point where both atoms are totally separate and completely screened from each other. The final column of tabulated numbers is labeled r_{12}/a_{TF} , which is the atom separation, r_{12} , reduced after the manner of Firsov by the Thomas-Fermi screening distance of the two atoms, Eq. 2-57 and Eq. 2-67. This final unit is useful in comparing these results with traditional potentials based upon statistical models of the atoms such as the Thomas-Fermi atom.

The lower left plot shows the four individual contributions to the potential tabulated above. Of particular interest is how the Coulomb energy goes from repulsive to attractive as a function of interatomic separation. Note further that the total potential, V , shown as a solid curve, is greater than any of its components for small separations, but once the Coulomb potential goes negative it becomes less than V_K . The upper right figure shows the final interatomic potential in the physical units of eV versus Angstroms. The lower right figure compares this calculation with those using traditional models such as the Thomas-Fermi, the Moliere, the Lenz-Jensen and the Bohr. The radial separation units are the reduced units based on Firsov theory as described above, and it can be seen that the B-B atom potential lies between the Lenz-Jensen and the Moliere potentials.

Atoms = Au ⁷⁹ and Au ⁷⁹						
r ₁₂	V _a	V _K	V _a	V	Phi	r ₁₂ /a _{TF}
.05	794324.45	222335.36	-5299.29	291013580.51	5839.7271	
.10	206787.30	121722.94	-2385.03	326125.25	3629.14542	
.15	75607.03	74524.96	-1800.39	148332.48	2478.21813	
.20	27971.41	52204.85	-1424.27	78752.29	1753.29085	
.40	449.89	12330.80	-340.57	12420.32	0553.5.8186	
.80	-732.95	2012.20	-154.04	1125.21	0100.11.8339	
1.00	-406.53	941.29	-89.03	443.73	0049.14.5223	
1.20	-236.76	485.16	-53.41	165.01	0026.17.4508	
1.40	-147.33	272.64	-32.63	92.68	0014.20.3593	
1.60	-67.44	132.24	-19.01	45.80	0006.23.2677	
1.80	-21.99	54.18	-10.45	21.74	0000.26.1762	
2.00	-7.51	24.75	-5.64	11.10	0002.29.0846	
2.20	-2.47	10.67	-2.90	5.30	0001.31.9931	
2.40	-1.74	4.55	-1.40	2.40	0001.34.9016	
2.60	-1.18	1.83	-0.61	1.04	0000.37.8100	
2.80	-0.93	0.62	-0.22	0.58	0000.40.7185	
3.00	-0.00	0.10	-0.03	0.06	0000.43.6270	

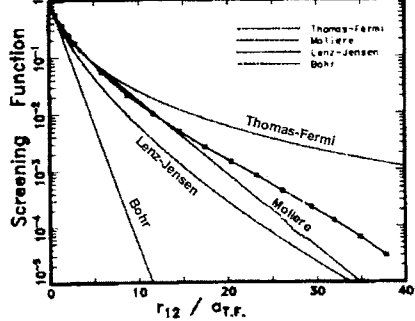
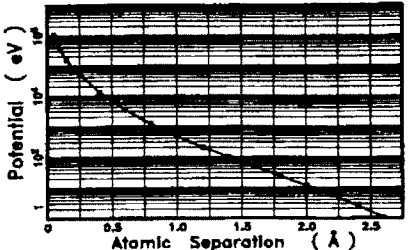
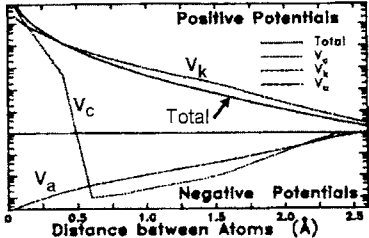


Figure 2-10 - Calculation of Solid-State Interatomic Potentials: Au⁷⁹ - Au⁷⁹

In the upper left arc shown the values of the various potentials for increasing nuclear separation distances, r_{12} , in units of Angstroms. The various potentials are described in the text and are known as V_C , the Coulomb interaction; V_K , the electron excitation energy (kinetic energy of electrons); V_a , the exchange energy between electrons; and V , the total interaction, $V_C + V_K + V_a$, in units of eV (see Eq. 2-42 and following). The next column labeled "Phi" is called the screening function, Φ , and is the summed potential divided by the potential of the two bare nuclei at the same separation without any electron screening, Eq. 2-55. This screening function goes from unity (at zero separation) to zero at the point where both atoms are totally separate and completely screened from each other. The final column of tabulated numbers is labeled r_{12}/a_{TF} , which is the atom separation, r_{12} , reduced after the manner of Firsov by the Thomas-Fermi screening distance of the two atoms, Eq. 2-57 and Eq. 2-67. This final unit is useful in comparing these results with traditional potentials based upon statistical models of the atoms such as the Thomas-Fermi atom.

The lower left plot shows the four individual contributions to the potential tabulated above. Of particular interest is how the Coulomb energy goes from repulsive to attractive as a function of interatomic separation. Note further that the total potential, V , shown as a solid curve, is greater than any of its components for small separations, but once the Coulomb potential goes negative it becomes less than V_K . The upper right figure shows the final interatomic potential in the physical units of eV versus Angstroms. The lower right figure compares this calculation with those using traditional models such as the Thomas-Fermi, the Moliere, the Lenz-Jensen and the Bohr. The radial separation units are the reduced units based on Firsov theory as described above, and it can be seen that the Au-Au atom potential lies between the Thomas-Fermi and the Moliere potentials.

shown (they are independent of Z_1 and Z_2 in these coordinates). The calculated points are shown and connected by a solid line. It can be seen that each of the classical potentials are accurate for only a small span of atomic separation, and differences as large as a factor of two exists between the calculated values and the Moliere and Thomas-Fermi lines, but reasonable agreement is made with the Lenz-Jensen line.

As another example we can take the heavy atom case of Au on Au shown in Figure 2-10. The separate potentials tabulated show marked changes from the B-B pair in Figure 2-9. The maximum radial separation between the atoms extends twice as far before atom overlap ceases. More important, the shapes of V_k and V_a are quite different for separations below 1 Å. Finally, looking at the lower right screening function you can see that for small separations the calculation for Au-Au is reasonably in agreement with the Moliere curve, but for large reduced radial separations, $r_{12} / a_{TF} > 12$, there is a wide divergence of the calculated curve from any of the statistical model interatomic screening functions. For the Au-Au case this region covers all collisions with potentials below 500 eV, which constitutes most collisions for a Au ion penetrating a solid of gold.

Accuracy of Interatomic Potential Calculation

The type of interatomic potential calculation discussed here has been extensively reviewed by many authors, e.g. 49a, 67c, 70i, 71a, 71b, 72h, 74d, 78e, 79f, 79g, 81h, 82f. The early papers compare various types of calculations using statistical models such as the Thomas Fermi atom. The papers published in the 1970's used isolated atom Hartree-Fock orbitals and found significant differences from the previous potentials calculated with statistical atoms. The papers ranged from broad surveys such as 77f which considered a score of atom/atom combinations, to calculations which included very complex accounting for the modified electron orbitals during a collision and devoted their entire effort to a single element, e.g. Al in Ref. 79f. We show in Figure 2-11 the results of the Sabelli et al. calculation (79f) for the interatomic calculation for Al - Al atoms and the results of our calculation. There is good agreement between the two calculations. The Sabelli et al. work shows that polarization effects and correlation of the combined molecular orbitals can be large effects, but when everything is averaged out there is not a significant difference in screening functions for hard collisions (i.e. for interatomic potentials above a few eV).

It is difficult to compare interatomic potentials directly to experimental data. In papers such as Loftager et al. (79g) the data is the angular distribution of an ion scattered by a single collision with a gaseous atom. They find good agreement between their scattering data and calculations similar to ours, but the data oscillates about the mean values of the calculation. The authors suggest that in these hard collisions there may be coupled a significant inelastic energy loss to the atomic electrons which would modify the classical elastic-scattering trajectories. Thus to directly compare single scattering events to calculations it would be necessary to unfold the correlated inelastic contributions which, unfortunately, would introduce a new modeling effect. This subject of coupled large elastic and inelastic energy losses during a single collision has been discussed in length by Mcyer et al. (77), Biersack and Mertens (83a), Lennard et al. (83b), Ishiwari et al. (82i) and Jakas et al. (83c).

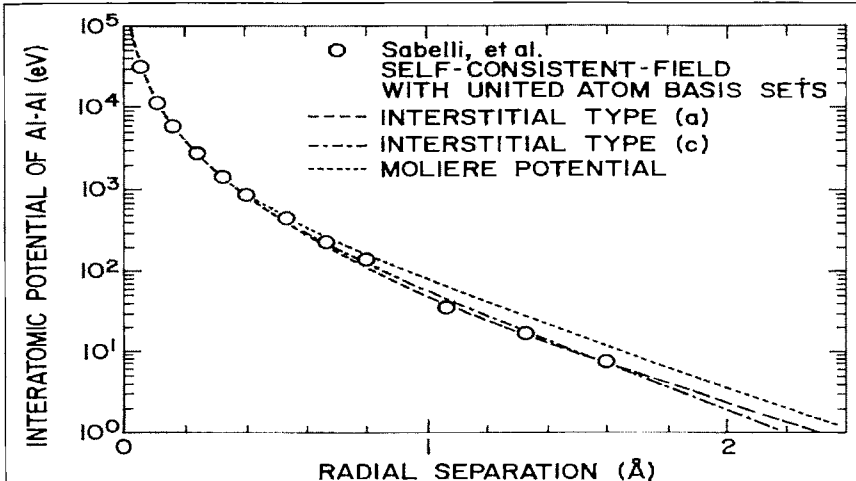


Figure 2-11 - Comparison with Self-Consistent Field Interatomic Potentials

Comparison of intratomic potential calculation between Sabelli et al. and this work using three types of charge distributions. The Sabelli calculation was a self-consistent-field calculation with basis sets consisting of scaled even-tempered Slater orbitals, augmented by diffuse equations, with the addition of united atom basis sets. This detailed calculation is compared with this work, Eq. 2-41 and Eq. 2-42, using solid state charge distributions with interstitial electrons of type (a) and (c) as discussed in the text. The Sabelli calculations shows a 20% undulation about the curves of this work, which accurately depicts a mean value. The differences between the potentials of the two interstitial types is not significant.

Also shown for comparison is the Moliere potential, extended to units of Angstroms with the Firsov relation, Eq. 2-62.

Extensive comparisons of experimental data to our type of calculation has been made by Gordon and Kim (72h, 74d). They studied rare gas molecules and alkali halide molecules and found that the calculation predicted accurately the molecular bond energies, bond lengths and vibrational frequencies. They pointed out that the molecules selected were special in that they were not covalently bonded nor was any atomic polarization expected to be important.

Comparisons to data evaluating the more gentle collisions between atoms can also be found in these papers (72h, 74d) and they indicate that collisions with interatomic potentials below a few eV can not be accurately described without including precise orbital calculations. In our work on solid targets such low potentials would only exist in the lowest density compounds, thus this restriction is generally inapplicable to the ion/target combinations of this book.

In summary, many papers have evaluated the accuracy of the interatomic potentials calculated in first order perturbation theory by considering unpolarized atoms merging without distortion. They find good agreement with both experimental data and with more extensive and sophisticated theoretical treatments of the problem. However, several limitations exist: (a) Our study includes only neutral atoms with the assumption that the degree of ionization of the ion is partially

compensated by polarization of the target; (b) Polarization effects between the two atoms are assumed to be negligible (both atoms remain spherically symmetric during the collision); (c) There are no correlated inelastic processes during the collision; and (d) The energy in elastic electron promotion is assumed to be accurately described by the local density approximation (free electron-gas model) applied to the volume of overlap of the two atoms.

Universal Interatomic Potential

Within the framework of our model, we have attempted to find an analytic function which accurately predicts the interatomic potential between atoms. If a single analytic function could be found, then we could derive a single formula for nuclear stopping and for atom-atom collisional scattering. Without such a formula we would have to store the interatomic potential coefficients for all 8×10^3 atom-atom combinations - a procedure which is possible but cumbersome.

First we needed a representative group of interatomic potentials. The atom pairs chosen are shown in Figure 2-12 where we *randomly* selected 261 pairs from all stable atomic numbers. Since all collisions are symmetrical (ion and target are interchangeable) this gives 522 pairs of atoms (6% of the total possible). This final number was chosen warily as each calculation takes about an hour. (Authors note: the number of H atoms, atomic number = 1, appears over-represented in our random sample).

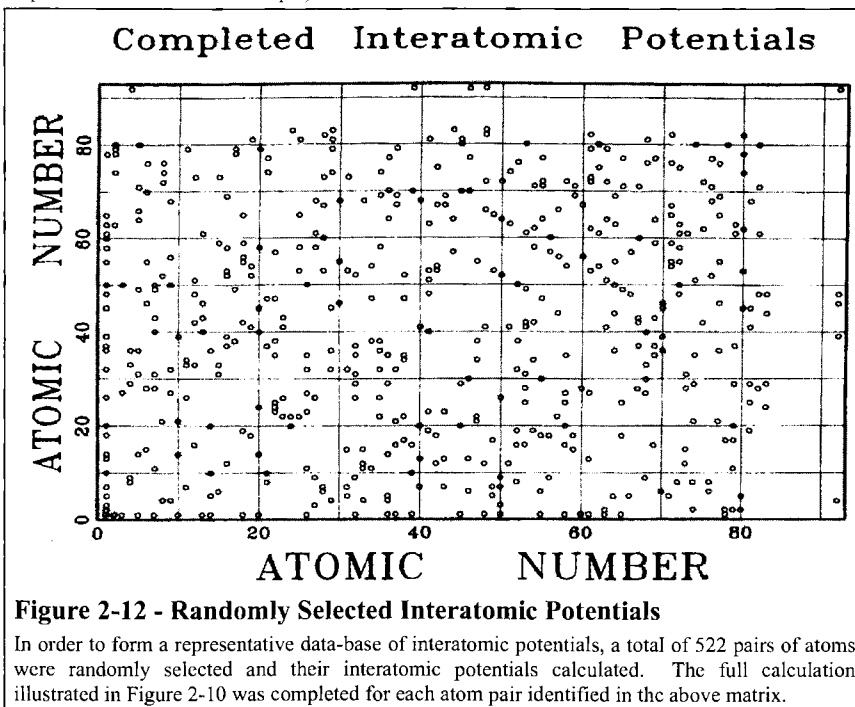


Figure 2-12 - Randomly Selected Interatomic Potentials

In order to form a representative data-base of interatomic potentials, a total of 522 pairs of atoms were randomly selected and their interatomic potentials calculated. The full calculation illustrated in Figure 2-10 was completed for each atom pair identified in the above matrix.

Each interatomic screening function was then fit with a series of three exponentials:

$$\text{Eq. 2-70: } \Phi(x) = \sum_{i=1}^3 a_i \exp(-b_i x)$$

where $x = r_{12}/a_1$, Eq. 2-57, a_i and b_i are fitting coefficients, and the “ a_i ” coefficients are normalized so that:

$$\sum_{i=1}^3 a_i = 1$$

and for the limit of $x=0$, the screening function is unity, $\Phi(x)=1$. Examples of this procedure are shown in Figure 2-13 for B + B and Au + Au atomic pairs. The circles are calculated points, and the line is the fitted curve. The coefficients are shown just above the curve. All fits averaged better than 10% to the calculated points.

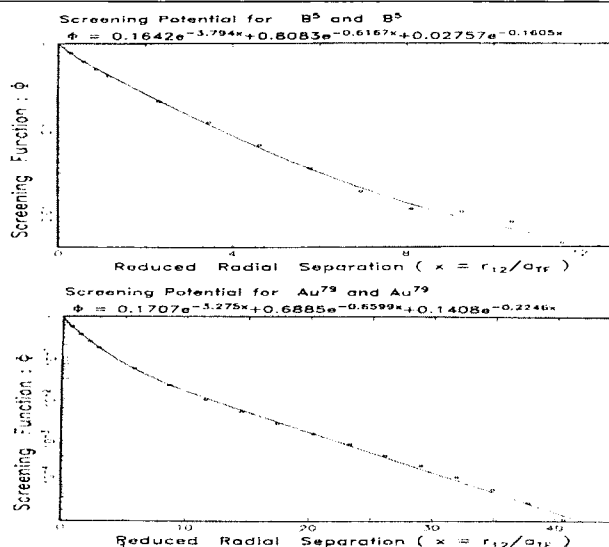


Figure 2-13 - Screening Function for Interatomic Potentials

The screening function for each atomic pair identified in Figure 2-12 was fitted with a series of exponential terms. Typical accuracy of the fits are shown in the above plots for B-B and Au-Au atomic pairs. The final analytic equation for each pair is shown above the plot. The six coefficients for all calculations are tabulated in the Appendix of [84a].

The result of the calculations is shown in Figure 2-14 where the 261 screening functions are plotted versus the separation between the atoms. These screening functions are plotted in Figure 2-15 with the Firsov reduced radial coordinate obtained by dividing the interatomic distance by the screening length:

$$\text{Eq. 2-71: } a_1(\text{Firsov}) = 0.8853 a_0 / (Z_1^{1/2} + Z_2^{1/2})^{2/3}$$

and the lower figure shows these screening functions versus the Lindhard et al. screening length

Interatomic Screening Potentials

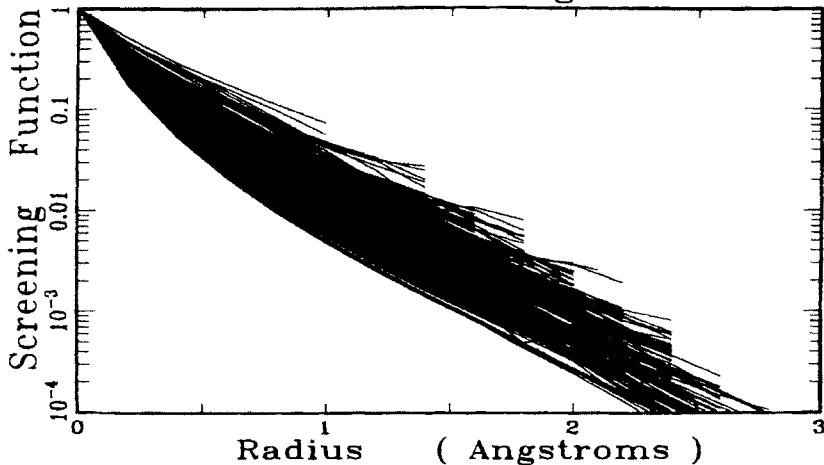


Figure 2-14 - Interatomic Screening Functions for 522 Pairs of Atoms

The calculated screening functions of all atomic pairs identified in Figure 2-12. The problem is to find a coordinate system in which all these lines will collapse into a single tight grouping so that a single analytic expression can be found to calculate them. We show in Figure 2-15 the two most important past attempts to do this.

$$\text{Eq. 2-72:} \quad a_1(\text{Lindhard}) = 0.8853 a_0 / (Z_1^{2/3} + Z_2^{2/3})^{1/2}$$

Both results considerably compress the screening functions to a scatter of about a factor of ($\sigma \approx 44\%$). Both figures have one feature in common, i.e. the light ion-target combinations are systematically lower than the heavy ones just opposite to Figure 2-14. This suggests that the overall Z dependence (hidden in $a_i \sim Z^{1/3}$) was too strong and a smaller exponential factor would be more accurate. We have tried many ways to improve upon these earlier suggestions, and finally found a type of reduced radial coordinate which created a much tighter grouping:

$$\text{Eq. 2-73:} \quad a_U = 0.8853 a_0 / (Z_1^{23} + Z_2^{23})$$

The screening functions are shown plotted with this screening length in Figure 2-16. We call this a universal screening length for it will be the basis of our later universal nuclear stopping function. The scatter of screening lengths in this coordinate system has a standard deviation of $\sigma \approx 18\%$ for interatomic potentials above 2 eV. For potentials below 2 eV there is virtually no convergence in any reduced coordinate system.

The new reduced screening functions were then fit similarly to the individual ones with a series of exponentials to obtain a universal screening potential:

Interatomic Screening Potentials

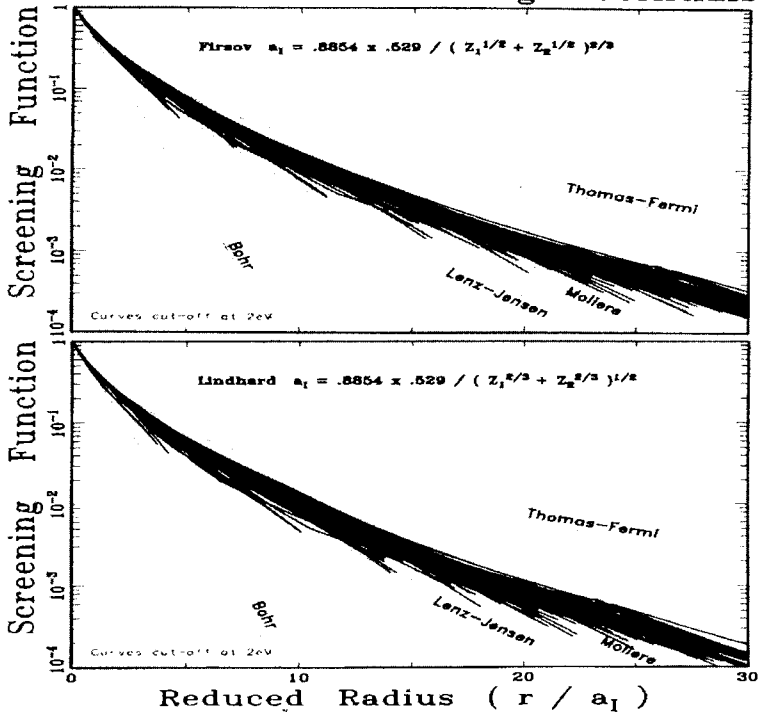


Figure 2-15 - Analytic Approximations to Screening Functions by Firsov and Lindhard

The screening functions of Figure 2-14 are compacted by introducing a reduced radius, r/a_1 , where a_1 is specified by Firsov by Eq. 2-67 and is shown in the upper plot. Lindhard et al. suggested a modified Bohr reduction, Eq. 2-68, and the results are shown in the lower plot. Here, the screening length is calculated using atomic numbers, Z_1 , and Z_2 , raised to the power of $1/3$. This correction is too great since the light atom screening functions are consistently lower than those for heavy atom pairs. The compressed screening functions have a scatter of about $2\sigma \approx 44\%$.

$$\text{Eq. 2-74: } \Phi_U = .1818 \exp(-3.2x) + .5099 \exp(-.9423x) + .2802 \exp(-.4028x) + .2817 \exp(-.2016x)$$

This curve is shown in Figure 2-17 with the statistical atom screening functions. This universal screening function is an improvement to one found by Wilson et al. (77f) which they identify as a C-Kr potential. This universal screening function has been further reviewed (85a) by comparing 106 experimentally determined potentials with theoretical ones. Their results are shown in the following table:

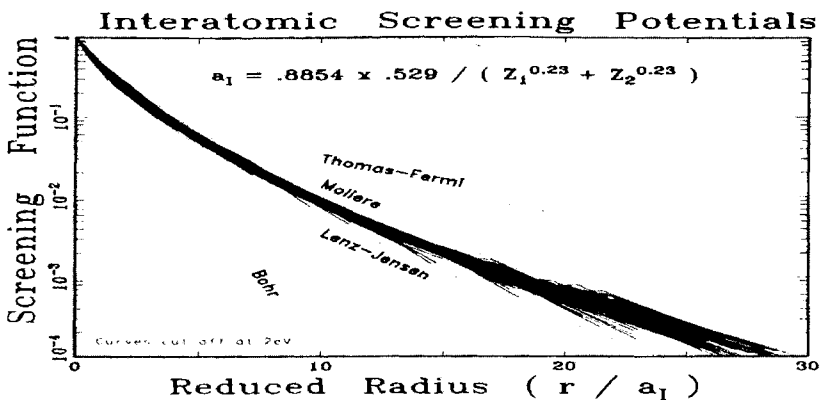


Figure 2-16 - ZBL Universal Interatomic Screening Function

The screening functions of Figure 2-14 are compacted further by introducing the new screening factor shown above, which calculates the screening length by using a factor of 0.23 for Z_1 and Z_2 . The grouping is quite tight, with a standard deviation, $\sigma \approx 18\%$. With this new screening distance, a_1 , all the interatomic potentials can be calculated with reasonable accuracy. Further, this screening length can now be used to generate universal nuclear stopping powers with a simple analytic expression.

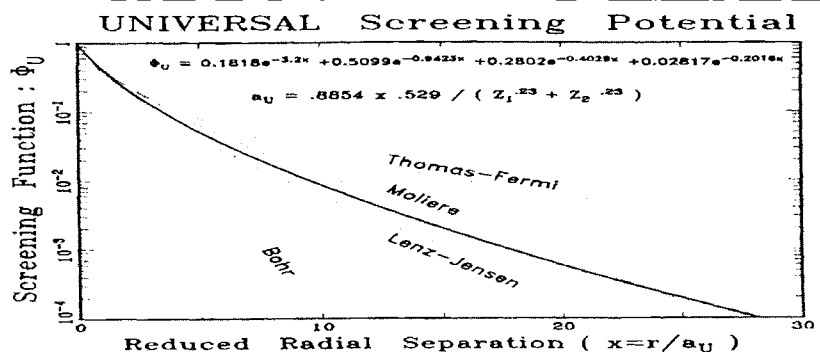


Figure 2-17 - ZBL Universal Screening vs. Classical Screening Models

The reduced screening function have been fitted to the analytic expression shown above with four exponential terms. This screening function is identified as Φ_U , a universal screening function with its argument, x , being defined as $x \equiv r / a_U$, where a_U is the universal screening length shown above. This screening length is important in converting the screening function, Φ , back to the real potential, V , using Eq. 2-69.

Potential Type	Screening Length	Theory / Experiment Standard Deviation
Moliere	a _I	237%
Lenz-Jensen	a _I	142%
C-Kr	a _U	7%
Universal	a _U	5%

Energy Transfer from Projectile Atom to Target Atom

We shall first briefly review the formulae we will need which were derived at the beginning of this chapter. The energy transferred during the screened Coulomb collision of two atoms will be described as a function of two variables, the projectile atom's initial energy, E, and its impact parameter, p. These are identified in Figure 2-1, with p being defined as the projected offset of the original path of Z₁ from Z₂. If these two variables are known, then the scattering angle in the CM system, Θ, can be determined using Eq. 2-40. From this the energy transfer, T, to the target atom can be determined simply from conservation of energy and momentum, as was shown in the derivation of the general orbit equation, Eq. 2-24:

$$\text{Eq. 2-75: } T = \frac{2}{M_2} \left(V_0 M_c \sin \frac{\Theta}{2} \right)^2 = \frac{4E_c M_c}{M_2} \sin^2 \frac{\Theta}{2} = \frac{4E_0 M_1 M_2}{(M_1 + M_2)^2} \sin^2 \frac{\Theta}{2}$$

where M₁ and M₂ are the masses of atoms, Z₁ and Z₂, and where Θ is the projectile's scattering angle in center-of-mass coordinates, which is related to the lab frame by:

$$\text{Eq. 2-76: } \theta = \tan^{-1} [\sin \Theta / (\cos \Theta + M_1/M_2)]$$

where θ is the laboratory final deflection angle of the projectile, see Eq. 2-27.

As discussed at the beginning of this chapter, the problem of a two body collision may be reduced to that of a particle in a single central-force field if the following conditions are met: (a) The potentials are spherically symmetric and do not vary with time or with either particle's velocity, and (b) The laws of the conservation of energy and momentum are conserved for the system as a whole. With these conditions, the scattering angle of deflection, Θ, was derived in Eq. 2-40 to be:

$$\text{Eq. 2-77: } \Theta = \pi - 2 \int_{r_{\min}}^{\infty} \frac{p dr}{r^2 \left[1 - \frac{V(r)}{E_c} - \frac{p^2}{r^2} \right]^{1/2}}$$

where V(r) is the interatomic potential of the two atoms and E_C is the center-of-mass energy defined

$$\text{Eq. 2-78: } E_C \equiv E_0 M_2 / (M_1 + M_2)$$

and r_{\min} is the distance of closest approach during the collision, see Eq. 2-32. Eq. 2-77 is the general solution for a particle in a spherically symmetric central force field and the difficult problem of two atom scattering has been reduced to this simple form. The energy transferred to the target atom is now a function p and E , and is found by inserting the solution of Eq. 2-77 into Eq. 2-75.

In order to solve Eq. 2-77 in an universal way, especially in a way independent of the ion-target combination, we use the substitutions: $x = r/a$, $b = p/a$, and $\epsilon = E_c / (Z_1 Z_2 c^2 / a)$ and obtain:

$$\text{Eq. 2-79: } \Theta = \pi - 2 \int_{x_0}^{\infty} \frac{b dx}{x^2 \left[1 - \frac{\Phi(x)}{x\epsilon} - \frac{b^2}{x^2} \right]^{1/2}}$$

where we have also replaced the interatomic potential with the previously discussed screening function $V = (Z_1 Z_2 e^2 / r) \Phi(r/a)$, see Eq. 2-69. Now Eq. 2-79 allows the calculation of the final scattering angle with the new parameters ϵ and b , and the individual atomic variables, Z_1 , Z_2 , M_1 and M_2 have been eliminated (see further comments on this derivation in references (57a,b, 63a, and 64c)).

A brief survey of the accuracy of the universal interatomic potential is included as an Appendix to this Chapter.

Universal Nuclear Stopping Powers

The energy lost by the ion per unit path length is defined as dE/dR . This is related to the nuclear stopping cross-section, $S_n(E)$, by the relation $dE/dR = N S_n(E)$, where N = the atomic density of the target. The nuclear stopping power, $S_n(E)$, is the average energy transferred when summed over all impact parameters, so using Eq. 2-75 we have :

$$\text{Eq. 2-80: } S_n(E) = \int_0^{\infty} T d\sigma = \int_0^{\infty} T(E, p) 2\pi p dp = 2\pi \gamma E \int_0^{p_{\max}} \sin^2 \frac{\Theta}{2} p dp$$

with the integration's upper limit being the sum of the two atomic radii, p_{\max} , beyond which the interatomic potential, and T , is zero. We now define a CM to lab transformation unit, γ , which will be used below :

$$\text{Eq. 2-81: } \gamma \equiv 4 M_1 M_2 / (M_1 + M_2)^2$$

In order to show clearly the results of using classical charge distributions and also those using solid state distributions, it is easiest to again plot the nuclear stopping in reduced units in which a single curve describes all combinations of classical atom-atom collision. Lindhard et al. have discussed at length the calculation of nuclear stopping using Thomas-Fermi atoms (63a, 68a). They suggested a reduced coordinate system for nuclear stopping which we will extend to our new calculations. Using the formalism of Lindhard we define :

$$\text{Eq. 2-82: } S_n(\varepsilon) = \frac{\varepsilon}{\pi a_U^2 \gamma E_0} S_n(E)$$

where ε is a *reduced energy* introduced by Lindhard et al. (63a, 68a) defined as

$$\text{Eq. 2-83: } \varepsilon \equiv a_U M_2 E_0 / Z_1 Z_2 e^2 (M_1 + M_2)$$

and a_U is the universal screening length of Eq. 2-73.

Eq. 2-80 defines nuclear stopping in physical units, and Eq. 2-82 - Eq. 2-83 converts it to LSS reduced units.

We show in Figure 2-18 the reduced nuclear stopping based on the four classical atom screening functions and for the universal screening function. The universal nuclear stopping is calculated by restating Eq. 2-80 in reduced units using the reduced impact parameter

$$b = p/a_U$$

$$\text{Eq. 2-84: } S_n(\varepsilon) = \varepsilon \int_0^\infty \sin^2 \frac{\Theta}{2} d(b^2)$$

which is now independent of the chosen screening length, since Θ is a function of ε and b only because of Eq. 2-79 (see, for example, ref. 68a or 77f for expansions of this equation).

The dotted lines in Figure 2-18 reproduce within a few percent the similar calculations of ref. 77f for the classical interatomic potentials and confirm the accuracy of our computer program. The small circles on the plot are solutions of Eq. 2-84 using the universal screening function, Eq. 2-74. The solid line is an analytic expression fitted to the points with the form :

$$\text{Eq. 2-85: } S_n(\varepsilon) = \frac{\ln(1+a\varepsilon)}{2(\varepsilon+b\varepsilon^c+d\varepsilon^{1/2})}$$

where a , b , c and d are fitting coefficients as shown on the Figure 2-18. This equation does not have accurate high energy properties where nuclear stopping must become like Rutherford scattering. So for reduced energies, ε , above 30, it may be simplified to the unscreened form of nuclear stopping :

$$\text{Eq. 2-86: } S_n(\varepsilon) = (\ln \varepsilon) / 2\varepsilon$$

Figure 2-18 shows for all potentials the nuclear stopping is identical for $\varepsilon > 10$. For lower values of epsilon the universal stopping curve falls between the Moliere and Lenz-Jensen curves.

For practical calculations, the universal nuclear stopping is

$$\text{Eq. 2-87: } S_n(E_0) = \frac{8.462 \times 10^{-15} Z_1 Z_2 M_1 S_n(\varepsilon)}{(M_1 + M_2)(Z_1^{23} + Z_2^{23})} \text{ eV / (atom / cm}^2\text{)}$$

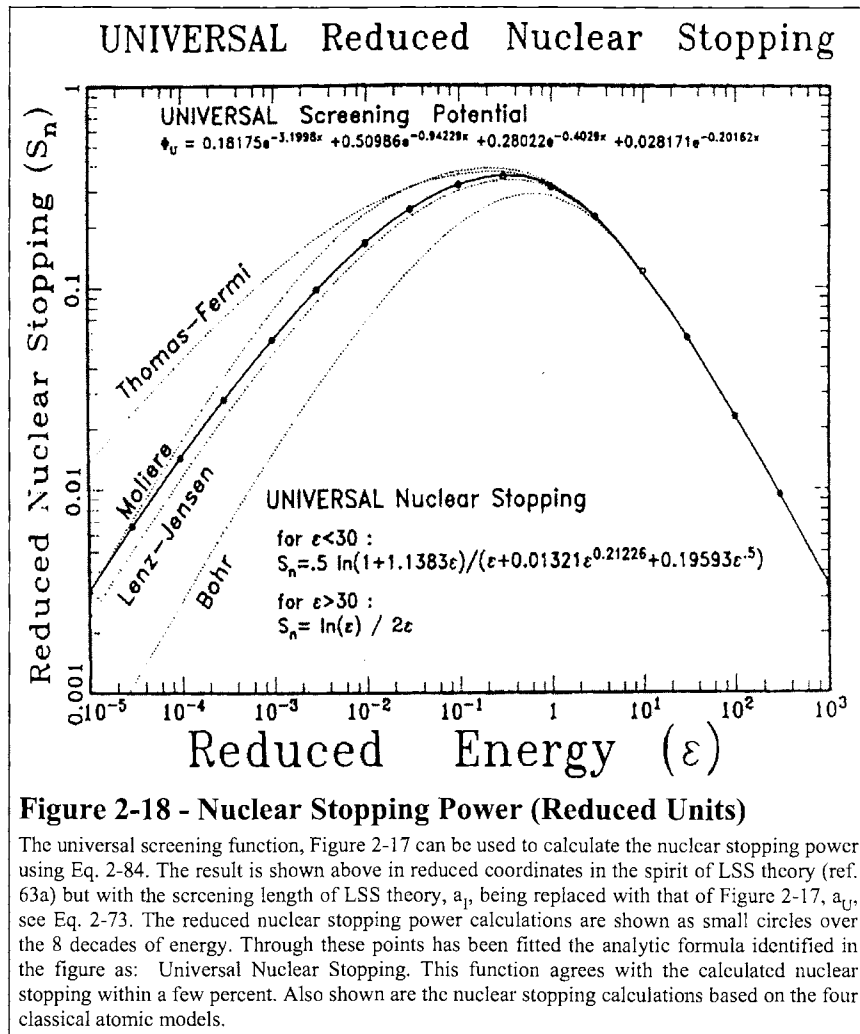


Figure 2-18 - Nuclear Stopping Power (Reduced Units)

The universal screening function, Figure 2-17 can be used to calculate the nuclear stopping power using Eq. 2-84. The result is shown above in reduced coordinates in the spirit of LSS theory (ref. 63a) but with the screening length of LSS theory, a_s , being replaced with that of Figure 2-17, a_U , see Eq. 2-73. The reduced nuclear stopping power calculations are shown as small circles over the 8 decades of energy. Through these points has been fitted the analytic formula identified in the figure as: Universal Nuclear Stopping. This function agrees with the calculated nuclear stopping within a few percent. Also shown are the nuclear stopping calculations based on the four classical atomic models.

with the reduced energy, ε , being calculated as

$$\text{Eq. 2-88: } \varepsilon = \frac{32.53 M_2 E_0}{Z_1 Z_2 (M_1 + M_2) (Z_1^{23} + Z_2^{23})}$$

and the reduced nuclear stopping being calculated as :

$$\text{Eq. 2-89: For } \varepsilon \leq 30 : S_n(\varepsilon) = \frac{\ln(1 + 1.1383\varepsilon)}{2 [\varepsilon + .01321\varepsilon^{21226} + .19593\varepsilon^5]}$$

$$\text{Eq. 2-90: For } \varepsilon > 30 : S_n(\varepsilon) = \frac{\ln(\varepsilon)}{2\varepsilon}$$

Nuclear Straggling

The straggling of the nuclear energy loss, defined as $Q_n = \int_0^\infty T^2 d\sigma$, can be evaluated in the same way as the nuclear stopping above. However, the same variables which made $S_n(\varepsilon)$ a universal function, i. e. independent of Z_1, M_1, Z_2, M_2 and density, cannot make Q_n a universal function. In the case of Q_n , a factor γ , see Eq. 2-81, will remain in the final result. After solving for Q_n , we have derived the following fit for nuclear straggling using the universal interatomic potential :

$$\text{Eq. 2-91: } Q_n = \gamma W_n(\varepsilon)$$

$$\text{Eq. 2-92: where: } W_n = \frac{1}{4 + 0.197\varepsilon^{-1.7} + 6.584\varepsilon^{-1.0494}}$$

This analytic fit is depicted as a dotted line in Figure 2-19 together with the precise data points as obtained from solving the scattering integral, Eq. 2-79, for the new universal screening function. Q_n can be seen to approach a constant value at high energies similar to the behavior of the electronic straggling.

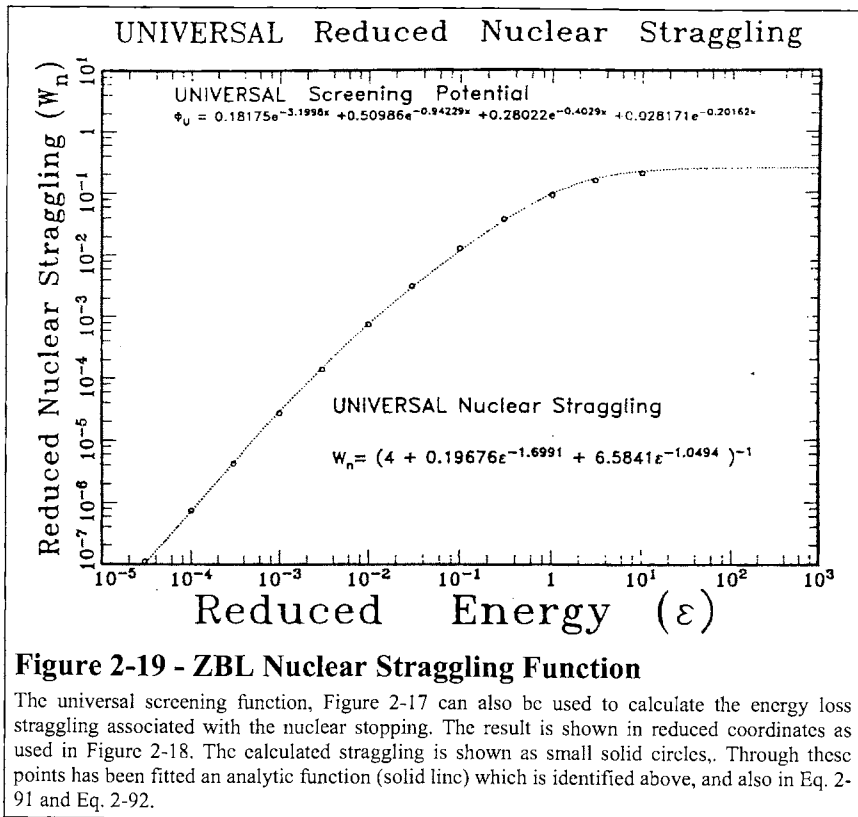


Figure 2-19 - ZBL Nuclear Straggling Function

The universal screening function, Figure 2-17 can also be used to calculate the energy loss straggling associated with the nuclear stopping. The result is shown in reduced coordinates as used in Figure 2-18. The calculated straggling is shown as small solid circles. Through these points has been fitted an analytic function (solid line) which is identified above, and also in Eq. 2-91 and Eq. 2-92.

Universal Scattering Formula

There are primarily two methods for calculating ion ranges in solids. One is to use Monte Carlo techniques and calculate each collision separately, while the other is to set up a differential transport equation and hope to be able to solve the mathematics. Each of these techniques has a long history and simplifying approximations enable them to be reasonably calculated. For both approaches, the major simplification is to replace the scattering integral, Eq. 2-77, with some analytic or numerical equivalent. We present next the most common scattering functions evaluated using the new universal interatomic potential described in this chapter.

The Monte-Carlo technique for calculating ion trajectories in solids originated in the early 1950's for the study of nuclear reaction products, especially as they occur in nuclear power reactors and in nuclear weapons. Late in that decade, experimental results began to show deviations from ion penetration calculations for amorphous targets. An example might be the range profile skewness

and deeply penetrating tail reported by Davies et al. (60d). This result led Robinson and Oen to construct a Monte-Carlo code for crystalline material and to the discovery by computer simulation (63c) what would later be called ion channeling (and which had been predicted 50 years before by Stark (12b)). Robinson and Oen greatly expanded the computer program to include effects such as target damage, sputtering and ion reflection, and this program, MARLOWE, became the first widely used Monte-Carlo program to calculate ion penetration phenomena (74c). This program used brute-force techniques to solve the scattering integral, Eq. 2-77, and hence was quite slow (and expensive) to operate. Authors in this field have long sought to simplify this integral and many analytic proposals have been proposed for limited situations (see review by Bohr, 48a). Two separate broad proposals have been presented by Lindhard et al. (68a) and Biersack and Haggmark (80d). Since simplification of the scattering integral is key to the creation of useful range calculations, the analytic equations proposed for its replacement have often been called the Magic Formula for scattering (68a, 80d).

One scattering formula which is often used in transport equations was developed by Lindhard, Nielsen and Scharff (68a). Their solution was to reduce the scattering to a single variable which they called "t" and which is proportional to *the energy transferred in a collision, T*, and the initial particle energy, E_0 :

$$\text{Eq. 2-93:} \quad t = \varepsilon T = \varepsilon^2 \sin^2(\Theta / 2) = T E_0 \left(\frac{M_1}{M_2} \right) \left(\frac{a}{2 Z_1 Z_2 e^2} \right)^2$$

Note that Θ is a function of two independent variables, ε and b . It can never be exactly replaced by a single variable. The differential scattering cross-section may be stated in the simple form

$$\text{Eq. 2-94:} \quad d\sigma = \left(\frac{-\pi a^2}{2} \right) \frac{f(t^{1/2})}{t^{3/2}} dt$$

where a is the classical screening length. This formula reduces the scattering from a 3 variable problem (normally the impact parameter, the particle energy and the scattering angle or transferred energy) to the single parameter t and a function of t called $f(t^{1/2})$. From this definition of t they show that the reduced nuclear stopping is simply:

$$\text{Eq. 2-95:} \quad S_n(\varepsilon) = \frac{1}{\varepsilon} \int_{-\infty}^{\infty} f(t^{1/2}) d(t^{1/2})$$

So the function $f(t^{1/2})$ contains the same information as the nuclear stopping cross-section. The authors evaluated $f(t^{1/2})$ for the case of Thomas-Fermi atoms, and for power-potentials. This latter potential can be any potential which is proportional to $1/r^s$ where r is the interatomic separation and s is the power. This form of potential yields simple scattering equations for several integer values of s , so it has been widely studied in atomic physics (see, for example, ref. 70c).

In order to obtain values of $f(t^{1/2})$ for an arbitrary potential such as our universal potential, one can solve the inverse of Eq. 2-95 and obtain:

$$\text{Eq. 2-96: } f(x) = \frac{d}{dx} [x S_n(x)]$$

where we have substituted x for $t^{1/2}$. We may then explicitly use for $S_n(x)$ our fitting formula, Eq. 2-85, to derive $f(x)$ as a function of x with a , b , c and d being the coefficients shown in Figure 2-18:

$$\text{Eq. 2-97: } f(x) = \frac{d}{dx} [x S_n(x)] = \frac{d}{dx} \left[\frac{x \ln(1+ax)}{2(x+bx^c+dx^{1/2})} \right]$$

$$\text{Eq. 2-98: } f(x) = \frac{\ln(A)}{2B} + \frac{ax}{2AB} - \frac{x \ln(A) [1+bcx^{c-1}+d/2x^{1/2}]}{2B^2}$$

where $A = (1+ax)$ and $B = (x^2 + bx^c + dx^{1/2})$.

This function is plotted in Figure 2-20 as small circles. It is possible to fit this kind of curve with a power-potential expansion (70c), but it has been shown that one can obtain only a 20% accuracy with this kind of fit (81b). A slightly more complex fit is the spline fit suggested by Littmark and Ziegler in (81b). They define

$$\text{Eq. 2-99: } f(x) = \lambda_i x^{1-2m(x)} \text{ for } x_i < x < x_{i+1}$$

$$\text{Eq. 2-100: where } \lambda_{i+1} = \lambda_i (x_{i+1})^{2mx(i+1)-mx(i)}$$

Now by specifying some simple function for m , the entire $f(x)$ function can be constructed. We use for m the expression:

$$\text{Eq. 2-101: } m(x) = 1 - \exp[-\exp \sum a_i (0.1 \ln x/x_i)^i]$$

where the coefficients a_i , λ_1 and $x_i = \varepsilon_i$ are shown in Figure 2-20. The fit averages better than 1% over the seventeen orders of magnitude of $t^{1/2}$!!! (This accuracy is extremely important and deserves 3 exclamation points.)

A second approach to simplifying the scattering integral was proposed by Biersack and Haggmark (80d). Their solution involves no approximations other than the validity of the scattering integral Eq. 2-77 or Eq. 2-79. They suggested that the center-of-mass scattering angle, Θ , has the following relation:

$$\text{Eq. 2-102: } \cos \frac{\Theta}{2} = \frac{B + R_C + \Delta}{R_0 + R_C}$$

The terms of Eq. 2-102 are defined as $B = p/a$, $R_C = \rho/a$, $R_0 = r_0/a$, and $\Delta = \delta/a$, with "a" being the screening length, and Δ is a correction term which is empirically fitted (80d). The term r_0 is the distance of closest approach defined as the solution of the scattering equation integrand denominator, Eq. 2-77 :

$$\text{Eq. 2-103: } \left(\frac{p}{r_0} \right)^2 + \frac{V(r_0)}{E_C} - 1 = 0$$

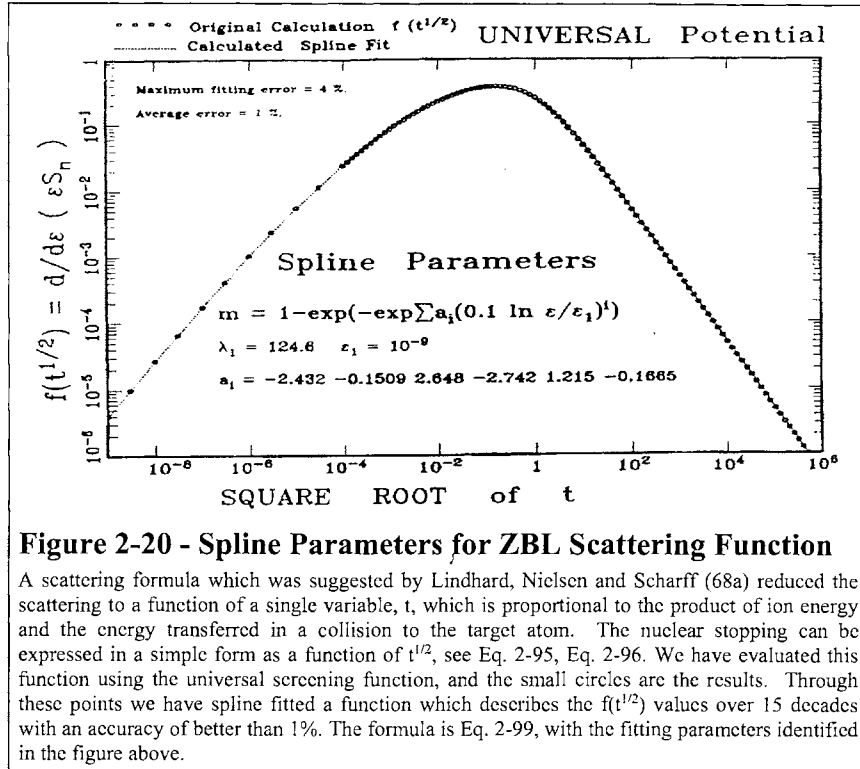


Figure 2-20 - Spline Parameters for ZBL Scattering Function

A scattering formula which was suggested by Lindhard, Nielsen and Scharff (68a) reduced the scattering to a function of a single variable, t , which is proportional to the product of ion energy and the energy transferred in a collision to the target atom. The nuclear stopping can be expressed in a simple form as a function of $t^{1/2}$, see Eq. 2-95, Eq. 2-96. We have evaluated this function using the universal screening function, and the small circles are the results. Through these points we have spline fitted a function which describes the $f(t^{1/2})$ values over 15 decades with an accuracy of better than 1%. The formula is Eq. 2-99, with the fitting parameters identified in the figure above.

with p being the impact parameter, V being the interatomic potential, and E_C being the center-of-mass energy.

The term ρ describes the radius of curvature of the two particles at the point of closest approach and is calculated from

$$\text{Eq. 2-104: } \rho = -2 [E_C - V(r_0)] / V'(r_0)$$

where $V'(r_0)$ is the spatial derivative of the interatomic potential at point r_0 (see 80d for details). All of these terms are straightforward to calculate.

Magic Formula For UNIVERSAL Potential

Lines use MAGIC coeff.: 0.0923 0.01162 0.007122 9.307 14.81
Average error = 2.1%

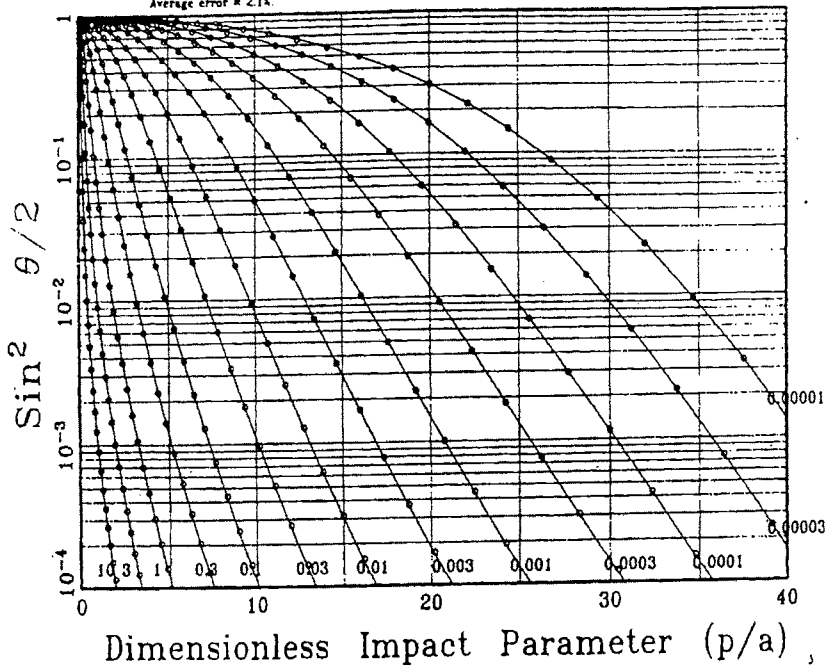


Figure 2-21 - Magic Formula Comparison to Full Calc. of Atomic Scattering

The scattering of two atoms can be reduced to a function of the collision energy and the impact parameter. The final scattering angle Θ can be calculated with the integral orbit Eq. 2-79. A greatly simplified analytic formula was proposed by Biersack and Haggmark (80d) which they called the Magic Formula for scattering. Shown above with small circles are the solutions of the complete orbit equation evaluated using the universal screening function of Figure 2-17. Each set of points is for a different reduced energy, ϵ , which is identified at the bottom of the figure as ranging from $\epsilon = .00001$ to $\epsilon = 10$. As shown above, for a constant impact parameter the angle of scatter increases as the collisional energy decreases.

Also shown as solid lines are the results of fitting the detailed scattering points with the Magic Formula, Eq. 2-102. This analytic expression fits the points with an average accuracy of about 2% over a wide range of impact parameters and collisional energies. The five fitting coefficients are shown at the top of the plot, and are the parameters C_1 to C_5 , Eq. 2-105.

The term Δ contains the interatomic scattering information and it is described as:

$$\text{Eq. 2-105: } \Delta = A (R - B) / (1 + G)$$

$$\text{with: } A = 2 \alpha \epsilon B^\beta$$

$$\alpha = 1 + C_1 / \epsilon^{1/2}$$

$$\beta = (C_2 + \epsilon^{1/2}) / (C_3 + \epsilon^{1/2})$$

$$\text{and } G = \gamma / [(1 + A^2)^{1/2} - A]$$

$$\gamma = (C_4 + \epsilon) / (C_5 + \epsilon)$$

where C_1 to C_5 being fitting coefficients to the interatomic potential selected. These terms were created in this form to yield Rutherford (unscreened) scattering in the high energy limit.

Does this work? Figure 2-21 shows a plot of the 3 variables of two particle scattering: The reduced impact parameter, p/a , the reduced energy, ϵ , and the final angle of scatter, Θ . We use $\sin^2(\Theta/2)$ for the ordinate as this is directly proportional to the energy transferred during the collision (see Eq. 2-75).

The small circles in Figure 2-21 are values of $\sin^2(\Theta/2)$ calculated with the *full scattering integral*, Eq. 2-77, with the Universal potentials. The solid lines are calculations of $\sin^2(\Theta/2)$ using the Biersack-Hagmark scattering Magic Formula (Eq. 2-102 to Eq. 2-105) with the fitting constants as shown in Figure 2-21. Over the 7 decades of ϵ , as shown, the average fit is 2%!

We have shown in this chapter that a large collection of interatomic potentials can be fit with a universal screening function. This has been used to create (a) a universal nuclear stopping power, (b) a scattering formula based on Lindhard's function of $f(t^{1/2})$, and (c) a scattering formula based on Biersack's 5-coefficient Magic formula.

APPENDIX TO CHAPTER

Accuracy of Universal Interatomic Potentials

Direct evaluation of the interatomic potential calculations presented in Chapter 2 is difficult because the extraction of a potential from atom scattering experiments involves the modeling of the collision which may introduce distortions. The accuracy of the universal potential described in this chapter will be briefly reviewed by comparing it to a variety of evidence to minimize the problem of distortion by the necessary modeling of the experiment.

One recent experiment involved the glancing angle scattering of low energy Ar ions from a cleaned single-crystal surface of Cu (74h, 82k, 82l). The ions were brought in at angles of 4° - 13° to the surface at energies of 20-35 keV. The scattered ions were analyzed with a narrow aperture electrostatic detector. From the 2-dimensional scattering array the data was reduced to find the necessary interatomic potential to reproduce the experimental data. Figure 2-22 shows their results as a shaded bar, and with the solid line showing the previously described *universal potential* calculated with Eq. 2-74. The agreement is very good.

The second type of experiment which can be related to interatomic potentials is that of atom scattering from noble gases. This type of scattering has a vast literature, and typical results are shown in Figure (2-22) for He-He and He-Ar scattering. From the spectrum of ions scattered from gases it is possible to extract the needed interatomic potentials. The shaded areas in Figure 2-24 indicate the experimental error. The two solid lines through the data are our results for each of the collisional pairs. For reference, the Moliere and Bohr potentials are also shown. Similar results are shown in Figure 2-24 where the actual scattering potential is shown as a function of interatomic separation. The importance of this plot is to illustrate that the universal potential is valid for noble gas scattering to potential energies well below 1 eV. Also shown is a calculation called a "universal Born-Mayer" potential by Andersen and Sigmund.

Another test of our calculation is to compare the results with theoretical calculations which were much more complex and included more effects. Figure 2-25 and Figure 2-26 compare four such calculations for several interatomic potentials. The triangles called "SCF ab initio" refer to a complex self-consistent field calculation by Sabelli, et al. (79f). The circles refer to a calculation performed as described in this chapter, using solid-state Al charge distributions (see Appendix of [84a]). The squares refer to a similar calculation using Hartree-Fock isolated atom charge distributions (77c), and the solid line is a simple analytic function proposed by Biersack and Ziegler (82f).

All curves show remarkable agreement.

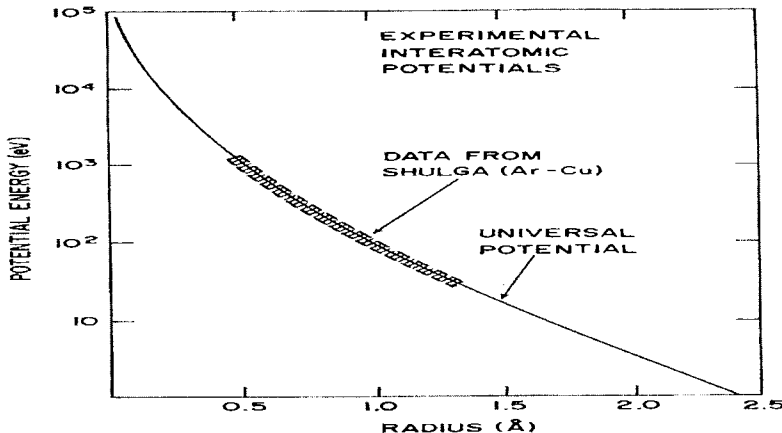


Figure 2-22 - Ar Scattering from Cu Target'

An experiment was performed to analyze the glancing angle scattering of low energy Ar ions from a cleaned single-crystal of Cu surface (82l, 82k). The scattering data was reduced to the interatomic potential shown. The shaded bar indicates the experimental values.

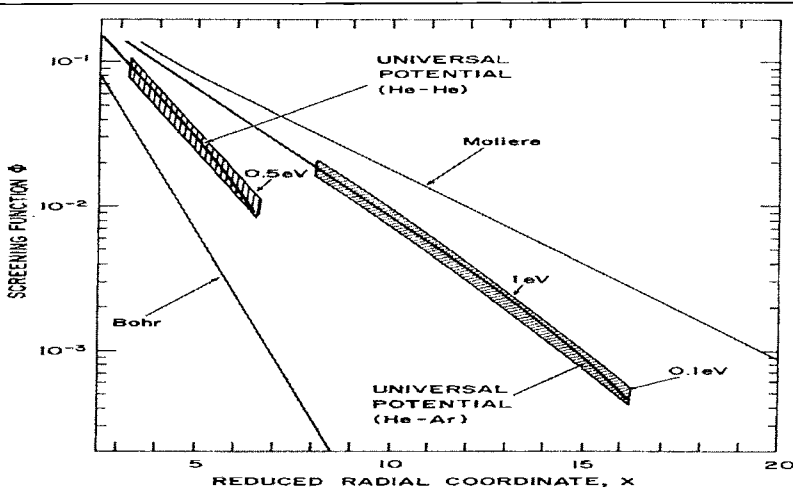


Figure 2-23 - Noble Gas Scattering from Noble Gases

The scattering of energetic noble gas ions from noble gas targets also gives information about interatomic potentials. The shaded areas show the interatomic potentials which best describe the scattering of He from He, and He from Ar. The solid lines through the data were calculated from the individual interatomic potentials obtained for He-He and He-Ar, in the previously described Free Electron Gas (FEG) model, see Eq. 2-41 and Eq. 2-42.

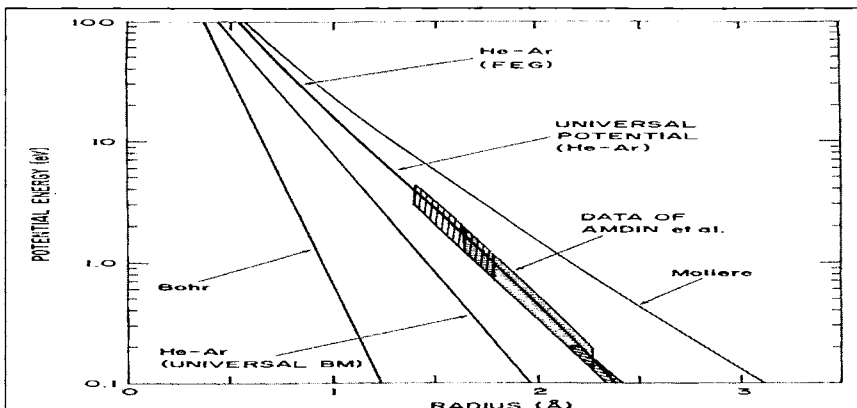


Figure 2-24 - Noble Gas Scattering from Noble Gases

The same data of Figure 2-23 is replotted as the actual interatomic potential in units of eV, versus the interatomic separation in Angstroms. This plot shows that for this collisional pair of rare gas atoms the universal potential is valid below 1 eV. This result may not be expected for atoms with non-closed electronic shells. The "universal Born-Mayer" potential follows a suggestion of Andersen and Sigmund.

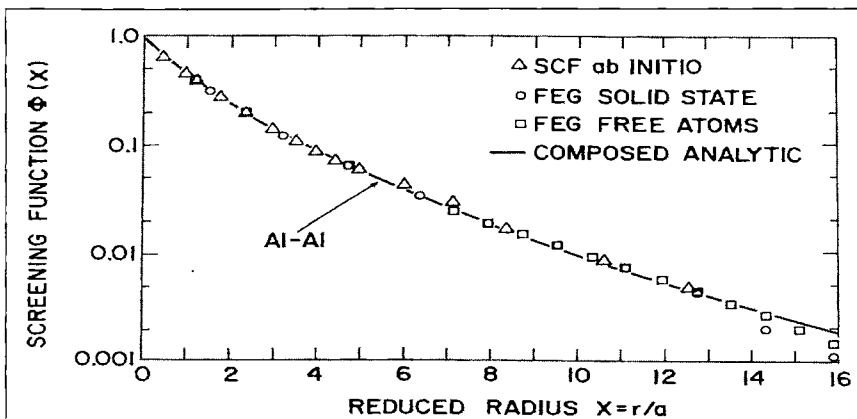


Figure 2-25 - Various Theoretical Interatomic Potentials

The results of calculating interatomic screening functions using various theoretical approaches. The diamonds are from a complex self-consistent-field (SCF) approach (79f); the circles are from calculations described in this chapter using the solid-state charge distributions for Al shown in the Appendix of [84a]; the squares are similar calculations using Hartree-Fock isolated-atom charge distributions; and the solid line is a simpler analytic expression (82f). The agreement appears satisfactory.

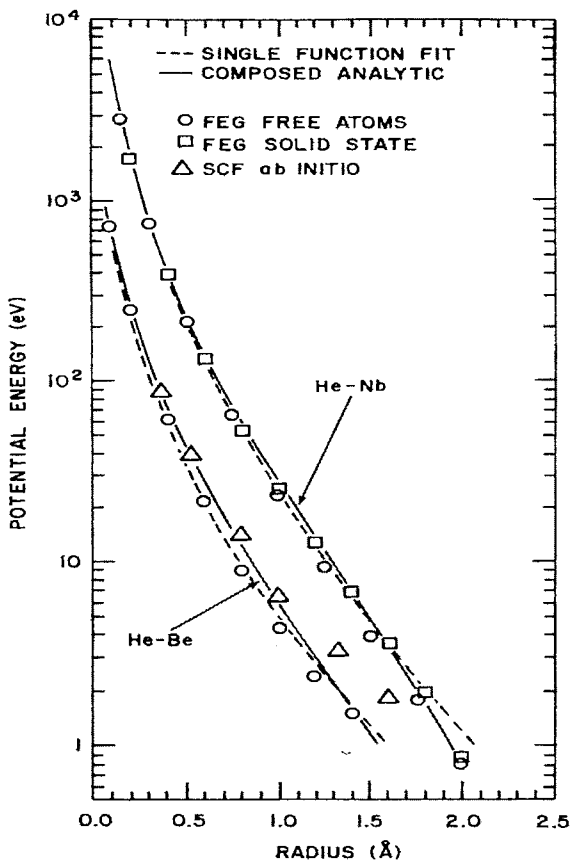


Figure 2-26 - Various Theoretical Interatomic Potentials

The results of calculating interatomic screening functions using various theoretical approaches. The diamonds are from a complex self-consistent-field (SCF) approach (79f); the circles are from calculations described in this chapter using the solid-state charge distributions for He, Be and Nb shown in the Appendix of [84a]; the squares are similar calculations using Hartree-Fock isolated-atom charge distributions; and the solid line is a simpler analytic expression (82f). The dashed lines depict the new universal potential. All show reasonable agreement.

CITATIONS TO CHAPTER 2

- 12b J. Stark, Z. f. Physik, 13, 973 (1912).
- 32b A. Sommerfeld, Z. f. Physik, 78, 283 (1932).
- 32c W. Lenz, Z. f. Physik, 77, 713 (1932); H. Jensen, Z. f. Physik, 77, 722 (1932).
- 32f W. Lenz, Z. f. Physik, 77, 722 (1932).
- 32g H. Jensen, Z. f. Physik, 77, 722 (1932).
- 40d N. Bohr, Phys. Rev., 58, 654 (1940).
- 41a N. Bohr, Phys. Rev., 59, 270 (1941).
- 47a G. Moliere, Z. f. Naturforschung, A2, 133 (1947).
- 47b E. Fenni and E. Teller, Phys. Rev., 72, 399 (1947).
- 47c G. Moliere, Z. f. Naturforschung, A2, 133 (1947).
- 48a N. Bohr, Mat. Fys. Medd. Dan. Vid. Selsk., 18, No. 8 (1948).
- 49a P. Gombas, "Die Statistische Theorie des Atoms und hirc Anwendungen," Springer-Verlag, Austria (1949).
- 57a O. B. Firsov, Zh. Eksp. Teor. Fiz., 32, 1464 (1957).
- 57b O. B. Firsov, Zh. Eksp. Teor. Fiz., 33, 696 (1957).
- 58a O. B. Firsov, Zh. Eksp. Teor. Fiz., 34, 447 (1958).
- 58b O. B. Firsov, JETP., 7, 308 (1958).
- 60d J. A. Davies, J. Friesen and J. D. McIntyre, Can. J. of Chem., 38, 1526 (1960).
- 63a J. Lindhard, M. Scharff and H. E. Schiott, Mat. Fys. Medd. Dan. Vid. Selsk., 33, No. 14 (1963).
- 63b U. Fano, Ann. Rev. Nucl. Sci., 13, 1 (1963).
- 63c L. C. Northcliffe, Ann. Rev. Nucl. Sci., 13, 67 (1963).
- 63d F. Herman and S. Skillmann, "Atomic Structure Calculations," Prentice-Hall (1963).
- 63e M. T. Robinson and O. S. Oen, Appl. Phys. Lett., 2, 30 (1963).
- 64c J. P. Biersack, Hahn-Meitner Report, HMI-B37 (1964).
- 67c P. T. Wedepohl, Proc. Phys. Soc., 92, 79 (1967)
- 67d T. L. Loucks, "Augmented Plane Wave Method", Benjamin Press, New York (1967).
- 68a J. Lindhard, V. Nielsen and M. Scharff, Mat. Fys. Medd. Dan. Vid. Selsk., 36, No. 10 (1968).
- 70c K. B. Winterbon, P. Sigmund and J. B. Sanders, Mat. Fys. Medd. Dan. Vid. Selsk., 37, No. 14 (1970).
- 70i V. I. Gaydaenko and V. K. Nikulin, Chem. Phys. Lett., 7, 360 (1970).
- 71a V. K. Nikulin, Zh. Tekh. Fiz., 41, 41 (1971) [Sov. Phys. - Tech. Phys. 16, 28 (1971)].
- 71b W. D. Wilson and C. L. Bisson, Phys. Rev., B3, 3984 (1971).
- 72h R. G. Gordon and Y. S. Kim, J. Chem. Phys., 56, 3122 (1972).
- 73c R. A. Johnson, J. Phys. F3, 295 (1973).
- 74d Y. S. Kim and R. G. Gordon, J. Chem. Phys., 60, 4323 (1974).
- 74c M. T. Robinson and I. M. Torrens, Phys. Rev., B9, 5008 (1974).
- 74h E. S. Mashkova and V. A. Molchanov, Rad. Eff., 23, 215 (1974).

- 76j N. W. Ashcroft and N. D. Mermin, "Solid State Physics", Holt, Rinehart and Winston Co., New York (1976).
- 77c W. D. Wilson, L. G. Haggmark and J. P. Biersack, Phys. Rev., 15B, 2458 (1977).
- 77f W. D. Wilson, L. G. Haggmark and J. P. Biersack, Phys. Rev., 15, 2458 (1977).
- 77j S. Datz, J. Gomez del Campo, P. F. Dittner, P. D. Miller and J. A. Biggerstaff, Phys. Rev. Lett., 38, 1145 (1977).
- 77l L. Meyer, M. Klein and R. Weddell, Phys. Stat. Sol., 83B, 451 (1977).
- 78d V. L. Moruzzi, J. F. Janak and A. R. Williams, "Calculated Electronic Properties of Metals", Pergamon Press (1978).
- 78c N. H. Sabelli, M. Kantor, R. Benedek and T. L. Gilbert, J. Chem. Phys., 68, 2767 (1978).
- 79f N. H. Sabelli, R. Benedek and T. L. Gilbert, Phys. Rev., A20, 677 (1979).
- 79g P. Loftager, F. Besenbacher, O. S. Jensen and V. S. Sorensen, Phys. Rev., A20, 1443 (1979).
- 80d J. P. Biersack and L. G. Haggmark, Nucl. Inst. and Meth., 174, 257 (1980).
- 81b U. Littmark and J. F. Ziegler, Phys. Rev., 23A, 64 (1981).
- 81h S. A. Cruz, L. T. Chadderton and J. C. Barthelat, Nucl. Inst. and Meth., 191, 479 (1981).
- 82f J. P. Biersack and J. F. Ziegler, Nucl. Inst. and Meth., 194, 93 (1982).
- 82i R. Ishiwari, N. Shiomi and N. Sakamoto, Phys. Rev., A25, 2524 (1982).
- 82k V. I. Shulga, Rad. Eff., 62, 237 (1982).
- 82l E. S. Mashkova, V. A. Molchanov and V. I. Shulga, Rad. Eff., 62, 107 (1982).
- 83a J. P. Biersack and P. Mertens, "Charge States and Dynamic Screening of Swift Ions in Solids," p 131, Oak Ridge Rpt. No. CONF-820131, Oak Ridge (1983).
- 83b W. N. Lennard, H. R. Andrews, I. V. Mitchell, D. Phillips and D. Ward, ibid, p 136 (1983).
- 83c H. Bichsel, Phys. Rev., A28, 1147 (1983).
- 84a J. F. Ziegler, J. P. Biersack, U. Littmark, "The Stopping and Range of Ions in Solids," vol. 1 of series "Stopping and Ranges of Ions in Matter," Pergamon Press, New York (1984).
- 85a D. J. O'Conner and J. P. Biersack, Nucl. Inst. and Meth., B15, 14-19 (1986).

3 Electronic Stopping of Ions

Chapter Abstract

In this section we shall review the energy loss of an ion to the electrons in the target. The chapter will first describe the simple case of a charged particle moving in a free electron gas, and the basic mechanisms of the interactions. The electronic structure of Hartree-Fock atoms in a solid is described, and how the local-density approximation allows these distributions to be used in ion stopping calculations. The charge state of heavy ions in solids is reviewed, and the concept of *effective charge* is presented. A description is made of how the effective charge of an ion changes with the local electron density in a solid. Finally, all these concepts are combined into the Brandt-Kitagawa theory of heavy ion stopping in solids. To apply this theory to solids, a description is made of how the screening length (described in detail in Chapter 2) of an ion varies with the Fermi velocity of the conduction electrons in a solid. All these concepts then are brought together in a description of the calculation of electronic stopping cross-sections for ions in solids.

Note: A recently published book reviews many recent developments in this field:
“Particle Penetration and Radiation Effects”, P. Sigmund, Springer Co. (2006). ISBN
:354 031 713 9.

Chapter Contents

Electronic Stopping of Ions	1
Introduction	1
Energy Loss of Energetic Protons in Solids	3
<i>Interaction of a Particle with a Free Electron Gas</i>	3
<i>Local Density Approximation in Stopping Theory</i>	7
<i>The Charge State of a Hydrogen Ion</i>	10
Experimental Hydrogen and Helium Ion Stopping	11
<i>Proton Stopping: Theory and Experiment</i>	16
The Electronic Stopping of Heavy Ions	20
<i>Electronic Stopping: Low Velocity Heavy Ions</i>	20
<i>Electronic Stopping: High Velocity Heavy Ions</i>	24
<i>Electronic Stopping: Medium Velocity Heavy Ions</i>	26
Empirical Electronic Stopping Cross-sections	31
Summary of Calculation of Stopping Powers	38
Chapter 3 – Citations	39

Introduction

The total stopping cross-section of ions in solids can be divided into two parts: the energy transferred by the ion to the target electrons (called electronic stopping or inelastic energy loss) and to the target nuclei (called nuclear stopping or elastic energy loss). The nuclear stopping component is usually considered separately because the heavy recoiling target nucleus can be assumed to be unconnected to its lattice during the passage of the ion, and the elastic recoil energy which is transferred to it can be treated simply as being due to the elastic scattering of two heavy screened particles (see Chapter 2: *Nuclear Stopping Cross-Sections*).

Separation of the energy loss of the ion into these two separate components ignores the possible correlation between hard nuclear collisions and large inelastic losses due to electronic excitation. It is felt that this correlation probably is not significant when many collisions are averaged, as when an ion penetrates a solid, but is of importance for single scattering studies (79g), and for very thin targets (83a, 83b).

The nature of the electronic energy loss is quite complex since both the ion and the target constantly change during the passage of the ion:

- a) The charge state of the ion continually changes depending on its velocity and the electronic density of the target.
- b) The target electrons polarize in front and around the ion, changing the local target electron density. The ion charge density also polarizes and changes its shape.
- c) As the ion penetrates the electron cloud of a target atom, its electrons are subjected to Pauli promotion since its fully occupied electron shells merge with the shells of fully occupied target atom shells.
- d) Band-gap effects in semiconductors reduce the available excitation levels which are open for its electrons, reducing the absorption of energy from the ion.

This chapter will describe the calculation of energy loss of an ion to the electrons of a solid in two sections:

- (1) *The energy loss of light ions in solids.* This section will review the classic theories of the energy transfer by a charged particle to the electrons of a solid. The discussion will review both the interaction of a charged particle with the localized electrons of an atom (which determines the quantal excitation of atomic electrons), and the interaction of a charged particle with an electron plasma (which determines collective excitations). A discussion will be made about the use of the local density approximation to extend these theories from particle interactions with isolated atoms and plasmas to particle interactions with electrons in real solids. A review will be made about the charge state of an energetic proton in a solid. Next, the charge state of He ions is considered and the dependence on the He ion's velocity, the target atomic number and the target's Fermi velocity. Finally, theoretical calculations are compared to extensive experimental data.
- (2) *The energy loss of heavy ions in solids.* The concept of an '**effective charge**' is reviewed with emphasis on scaling proton stopping powers to those of much heavier ions. This approach is shown to predict accurately the energy loss of high velocity heavy ions. A review is made about the theory of the energy loss of low velocity heavy ions in solids, and velocity proportional stopping is discussed. For intermediate velocity heavy ions, the work of Brandt and Kitagawa is discussed and is shown to adequately bridge the gap between low and high velocities.

Finally the above sections are combined to create an overall framework to calculate the energy loss of an ion to the electrons of a solid. This calculation is compared to thousands of experimental data and is shown to be accurate to about 10%.

Energy Loss of Energetic Protons in Solids

Interaction of a Particle with a Free Electron Gas

Both Thomson (12a) and Darwin (12c) treated energy loss as the energy transferred by a moving charged particle to a free electron. Since such a collision has an infinite energy-loss cross-section without some shielding to limit the distant interactions, they were both led into the problem of specifying maximum impact parameters based on atomic electron densities. Bohr based his study of electronic stopping cross sections on a model which considered the target electrons as a collection of harmonic oscillators whose frequency was determined by optical absorption data (13a). He argued, in contrast to the earlier work, that a natural energy-loss cross-section cut-off occurs with a limiting collision time, p/v , being equal to the atomic orbital time, $1/\nu$, where p is the impact parameter of a particle of velocity, v , on a harmonic oscillator of frequency, ν . For longer collision times the interaction becomes adiabatic and no energy is transferred from the ion to the target electrons.

During the next decade several attempts were made to bring quantum-mechanics into this problem, and it was finally done by Bethe (30a). This work was extended to relativistic particles by Bethe (32a) and Moller (32d), and then further expanded by Bethe and Bloch. What is sometimes called the Bethe-Bloch theory (30a, 31a, 32abcd, 33ab) considers a particle interacting with the electrons of an isolated atom of electronic harmonic oscillators. This approach solved the charged-particle/atom energy-loss problem quantum mechanically in the first Born approximation. The atomic nature of various target elements is concentrated into a single number representing the mean excitation of the atomic electrons of that element. The results of the earlier Bohr work differed significantly from the results of Bethe and this led several authors to comment on the discrepancy (31a, 33a, 33b). Bloch found that the Bohr distant collisions theory was quantum-mechanically correct as the mean energy loss averaged over all electronic transitions. Bloch's solution for the close-collision energy loss differed from that of Bohr and Bethe. Bohr had assumed for close collisions that the atomic electron was free, and Bethe had represented such collisions with plane waves. Bloch showed that the Bohr classical solution was valid for hard close collisions while the Bethe solution was valid for weak scattering. Bloch then provided a solution which reduced to the Bohr solution for hard collisions and almost reduced to the Bohr solution for weak collisions. The terms "hard" and "weak" refer to the amount of energy transferred, and are not well defined.

These original studies required that the incident particle velocity be much greater than that of the electrons bound in the atoms. Later extensions of the Bethe-Bloch theory attempted to find semi-empirical ways to correct it for energetic inner-shell atomic electrons (see, for example, 72c).

For details of the Bethe-Bloch stopping theory there are extensive review articles, e.g. (62b, 63b, 78h, and 80c). We shall use the Bethe-Bloch approach only in extending our calculations to relativistic ion velocities. This book will mostly concentrate on low energy non-relativistic stopping theory (energies below 10 MeV/amu) and it will not repeat these reviews.

After this work in the 1930's the next major step in electronic stopping theory was the consideration of the target as a collection of interacting electrons, i.e. a plasma, and to consider the energy loss to collective effects such as dynamic polarization and energy loss to plasmons. The classic papers to treat the target electrons as a plasma were by Fermi (40c) and Fermi and Teller (47b). These papers begin with Maxwell's equations and establish some estimates of the polarization of the target electronic medium. They consider the problems of binding energies, the dispersion of the electron oscillators and damping constants on collective motion. One result is that typical energy loss per unit distance, dE/dx , for slow particles is proportional to the ion velocity and the cube root of the electronic density of the medium,

$$\text{Eq. 3-1: } \frac{dE}{dx} \sim v \rho^{1/3}$$

where v is the particle velocity and ρ is the electron density.

Electronic interactions of a particle with a plasma were then extensively treated by Lindhard (54a), Neufeld and Ritchie (55a) and Fano (56c). We review primarily the results of Lindhard who presented generalized methods to treat the response of a free electron gas to a perturbation and present Lindhard's explicit function for the interaction.

The Lindhard treatment is a many-body self-consistent treatment of an electron gas responding to a perturbation by a charged particle. It naturally includes the polarization of the electrons by the charged particle and the resultant charge screening and the plasma density fluctuations. It treats smoothly both individual electron excitation and collective plasmon excitations without separate 'distant' and 'close' collision processes. Finally, when used with the local-density-approximation it can be directly applied to any target and, for example, the effects of chemical bonding or crystal structure on stopping powers can be treated. Lindhard's approach to the interaction of a particle with a free electron gas makes the following assumptions:

- The free electron gas consists of electrons at zero temperature (single electrons are described by plane waves) on a fixed uniform positive background with overall charge neutrality.
- The initial electron gas is of uniform density.
- The interaction of the charged particle is a perturbation on the electron gas.
- All particles are non-relativistic.

The electronic stopping of a charged particle in the local density approximation may be stated as:

$$\text{Eq. 3-2: } S_e = \int I(v, \rho) Z_1^2 \rho dx^3$$

where S_e is the electronic stopping cross-section; I is the stopping interaction function of a particle of unit charge with velocity, V , in a free electron gas of density ρ , Z_1 is the charge of the incident particle, ρ is the electronic density of the target, and the integral is performed over each volume element, dx^3 , of the target. (We use this form of stopping equation because it expands simply to the form that will be needed for heavy ions). The electronic density of a target atom is normalized so that its atomic number $Z_2 = \int \rho dx^3$ with the integration over the atomic volume. Each of the three components of Eq. 3-2 will be discussed below.

With these assumptions, Lindhard derived the interaction function, I , of Eq. 3-2 as:

$$\text{Eq. 3-3: } I = \frac{4\pi e^4}{m v^2} \cdot \frac{i}{\pi \omega_0^2} \int_0^\infty \frac{dk}{k} \int_{-kv}^{kv} \omega d\omega \left[\frac{1}{\epsilon^L(k, \omega)} - 1 \right]$$

where the longitudinal dielectric constant, ϵ^L , is derived to be

$$\text{Eq. 3-4: } \epsilon^L = 1 + \frac{2m^2\omega_0^2}{\hbar^2 k^2} \sum_n \frac{f(E_n)}{N} \left[\frac{1}{k^2 + 2\vec{k} \cdot \vec{k}_n - \frac{2m(\omega - i\delta)}{\hbar}} + \frac{1}{k^2 - 2\vec{k} \cdot \vec{k}_n + \frac{2m(\omega - i\delta)}{\hbar}} \right]$$

where e and m are the charge and mass of the electron; ω_0 is the classic plasma frequency defined as $\omega_0^2 = 4\pi e^2 \rho / m$; E_n is the energy and k_n the wave vector of the electron in the n 'th state; $f(E_n)$ is the distribution function and is an even function of k_n , and δ is a small damping factor. Simple polynomial fits to a numeric evaluation of Eq. 3-4 can be found in Ref. 79d.

The physical properties of Lindhard's particle-plasma interaction theory can be shown in several ways. Figure 3-1 shows the interaction term, I , of Eq. 3-3 and Eq. 3-4, versus a free electron gas density. Each curve has a horizontal slowly-changing section at low electron densities where the ion is going much faster than the mean electron velocity. Each curve bends down where the ion velocity becomes equal to the Fermi velocity, V_F , of the free electron gas, defined as

$$\text{Eq. 3-5: } V_F = \left(\frac{\hbar}{m} \right) (3\pi^2 \rho)^{1/3}$$

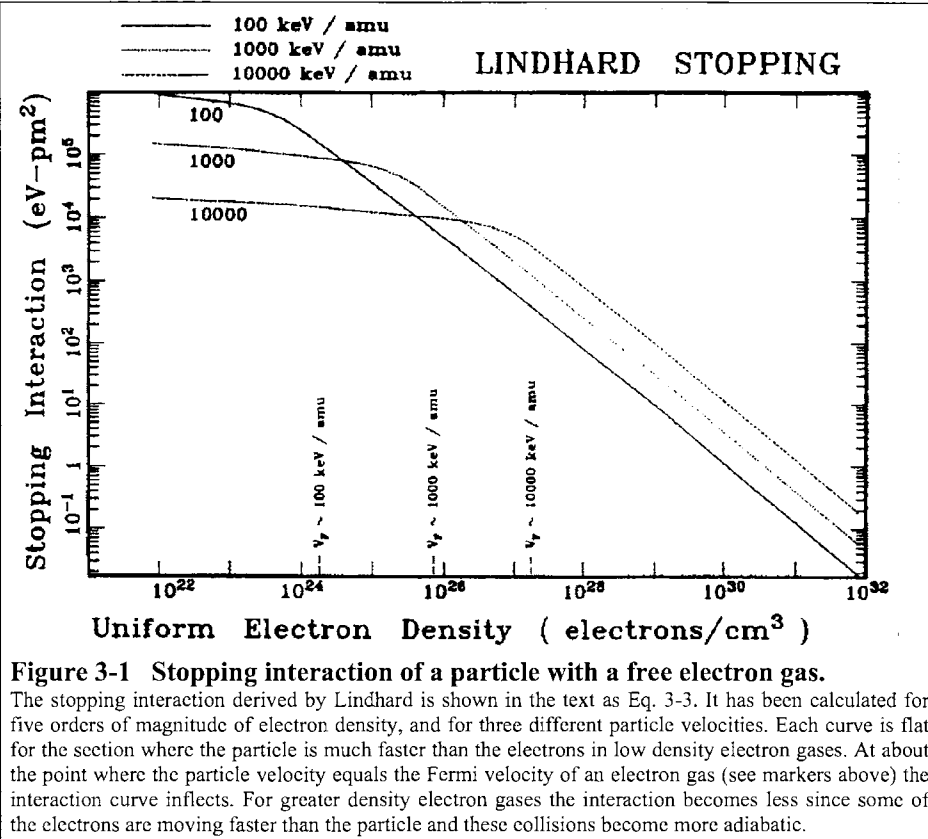


Figure 3-1 Stopping interaction of a particle with a free electron gas.

The stopping interaction derived by Lindhard is shown in the text as Eq. 3-3. It has been calculated for five orders of magnitude of electron density, and for three different particle velocities. Each curve is flat for the section where the particle is much faster than the electrons in low density electron gases. At about the point where the particle velocity equals the Fermi velocity of an electron gas (see markers above) the interaction curve inflects. For greater density electron gases the interaction becomes less since some of the electrons are moving faster than the particle and these collisions become more adiabatic.

For example, in Figure 3-1 the top curve is for particles with velocity of 100 keV/amu = 4.4×10^8 cm/sec. The Fermi velocity for an electron density of $10^{24}/\text{cm}^3$ is about 3.5×10^8 cm/sec, which is where the curve is inflecting. At higher electron densities, some of the electrons of the free electron gas can respond adiabatically because of their higher velocities and the interaction is reduced. For any single electron density there is a maximum interaction strength which occurs for particles with a velocity about equal to the electron Fermi velocity.

In Figure 3-2 is shown $I\rho$, the interaction term, I , times the electron charge density, ρ . If the particle has a unit charge, this plot shows the differential energy loss per unit path length, i.e. the stopping power, in units of eV/nm (energy loss per unit distance), for a particle in a uniform free electron gas. This figure shows how stopping power is dominated not by the local electron density, but by the interaction strength term shown in Figure 3-1 which depends on the ion velocity.

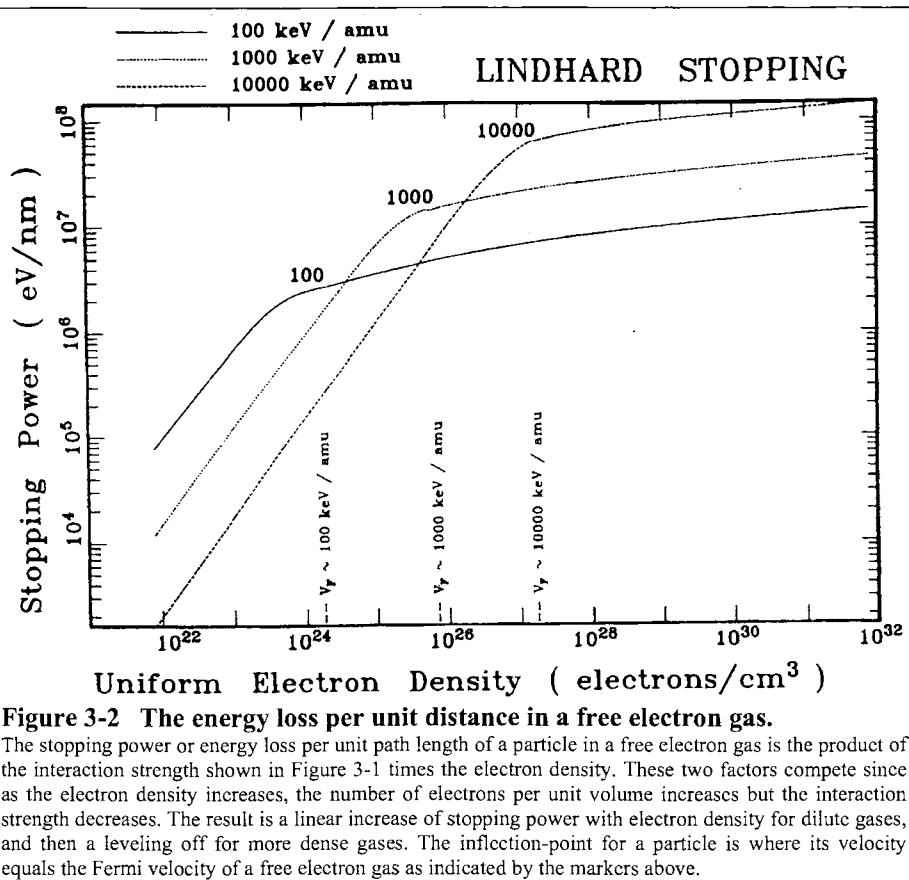


Figure 3-2 The energy loss per unit distance in a free electron gas.

The stopping power or energy loss per unit path length of a particle in a free electron gas is the product of the interaction strength shown in Figure 3-1 times the electron density. These two factors compete since as the electron density increases, the number of electrons per unit volume increases but the interaction strength decreases. The result is a linear increase of stopping power with electron density for dilute gases, and then a leveling off for more dense gases. The inflection-point for a particle is where its velocity equals the Fermi velocity of a free electron gas as indicated by the markers above.

Local Density Approximation in Stopping Theory

The theoretical electronic energy loss of a proton in a solid (in contrast to a free electron gas) is calculated using the local-density approximation. In essence, this approximation assumes that each volume element of the solid is an independent plasma. The stopping power is calculated for a particle in a plasma for each volume element's density, and the final stopping power is computed by averaging over these values, weighted by their distribution in the solid. Referring to Eq. 3-2:

$$\text{Eq. 3-6: } S_e = \int I(v, \rho) (Z_1^*(v))^2 \rho \, dx^3$$

where I is the interaction of the particle with velocity, V , in a plasma of density, ρ . The charge of the ion, Z_1^* , has an asterisk to indicate that this may be a value different from the atomic number because the ion may be only partially stripped of electrons. By integrating over the volume, dx^3 , we weigh each density interaction by the probability of that density occurring in the solid.

An extended comment might be made to explain the local-density-approximation to those completely unfamiliar with it. This method is widely used to evaluate the theoretical mean response of a solid to a perturbation. For our application, we consider the solid to be an electronic plasma with fluctuations in density. We first calculate the interaction (energy loss) of an energetic particle immersed in a uniform plasma sea with the same electronic density as any single volume element of the solid. A basic assumption is now made that the averaged interaction of a single particle with a uniform plasma is *identical* to the averaged interaction of a single volume element of plasma with a particle whose spatial location is uniformly probable. This equivalence allows the evaluation of the mean interaction of a single particle with a single volume of element plasma. This process is then repeated for the interaction of the particle with every volume element of the solid target to obtain the mean interaction of the particle with the solid.

Two of the more important assumptions in using this approach with Lindhard stopping theory for energy loss calculations are:

- The electron density in the target varies slowly with position.
- Available electron energy levels and transition strengths of the atoms of the solid are identical to those in a free electron gas.

The basic physics of applying the local density approximation to stopping theory may be seen in plots of the integrand of the stopping cross-section, Eq. 3-2, as evaluated for atomic targets, see Figure 3-3 to Figure 3-5. These plots show three curves which link the various parts of the stopping process. Figure 3-3 shows various shapes of the charge density of Cu with the Thomas-Fermi atom shown as a dashed line, the isolated atom Hartree-Fock atom shown as a dotted line and the solid-state Cu atom shown as a solid line. (See Chapter 2 for a review of how these various atomic models were developed). The plots use for an ordinate the factor $4\pi r^2 \rho$, where ρ is the electron density. With this factor, the area under the curve equals 29, the atomic number of Cu. Clearly the Thomas-Fermi atom has no shell-structure but is a reasonable average value. The isolated atom Hartree-Fock curve shows a pronounced shell structure but it has a long tail extending out many Angstroms since it is not confined. Finally, the solid-state structure of each individual atom is contained within 1.4 Å, with the electrons from 1.2-1.4 Å being averaged over the various bonding angles in the Cu face-centered-cubic crystal.

Figure 3-4 shows as a dotted line the same solid-state Cu distribution as a dotted line as shown in Figure 3-3. It shows as a dashed line the value of the particle-plasma interaction term, I , of Eq. 3-3 and Eq. 3-4 and of Figure 3-1. For each radius, the density of the Cu atom is taken and the equivalent I is calculated as

indicated in Figure 3-1. Since Figure 3-4 specifies that the ion has a velocity of 10000 keV/amu (about 20 times the Bohr velocity) it is moving much faster than most of the electrons in the solid, and so its interaction is relatively independent of the electron velocity. In Figure 3-1 the density of electrons in Cu is mostly on the flat section of the curve labeled 10,000 keV. (Note: the Bohr velocity, ~25 keV/u, is the nominal velocity of conduction electrons.)

Finally, the term ρI is plotted as a solid line in Figure 3-4. The area under this curve is the integral of Eq. 3-2 and hence is the stopping cross-section of a moving charged particle in Cu. This solid line shows how the energy loss is distributed among the various Cu electrons with all but the innermost electrons absorbing energy about proportional to their density.

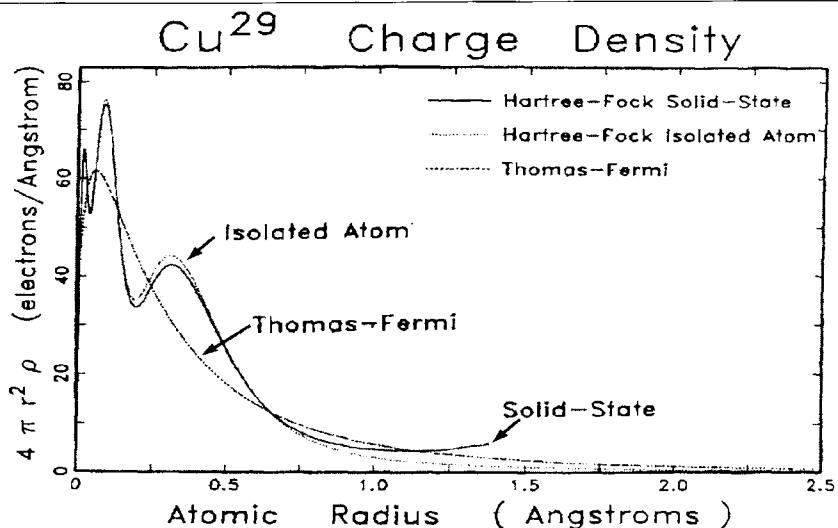


Figure 3-3 Various atomic charge densities.

The description of atoms in solids has progressed from a Thomas-Fermi description (1932-1955) to Hartree-Fock isolated atoms (1957-1974) to complete Hartree-Fock descriptions of atoms in solids (1976-1982). The Thomas-Fermi atom had no shell structure (curve with no bumps), but it allowed analytic solutions to the complex problems of stopping and range theory, see for example the LSS theory (62a). The use of Hartree-Fock atoms which are not simply expressed has led to full numeric treatment of the interaction of particles with matter.

In contrast, Figure 3-5 shows the same set of curves except they are evaluated for a low velocity particle of 100 keV/amu (about twice the Bohr velocity). The copper density curve (dotted line) is identical to that of Figure 3-3. The dashed interaction curve is quite different from that of Figure 3-4 for the particle is now at a velocity which is large only when compared to the low density outermost electrons of Cu atoms. For the inner electrons the interaction is almost adiabatic and there is little excitation. The solid line, ρI , is the integrand of the stopping power cross-section and it is clear that the outer shell electrons, about 20% of the total electrons, absorb almost 90% of the energy loss. The inner k-shell electrons absorb almost no energy and one would anticipate that there would be almost no k-shell x-rays emitted from the Cu target.

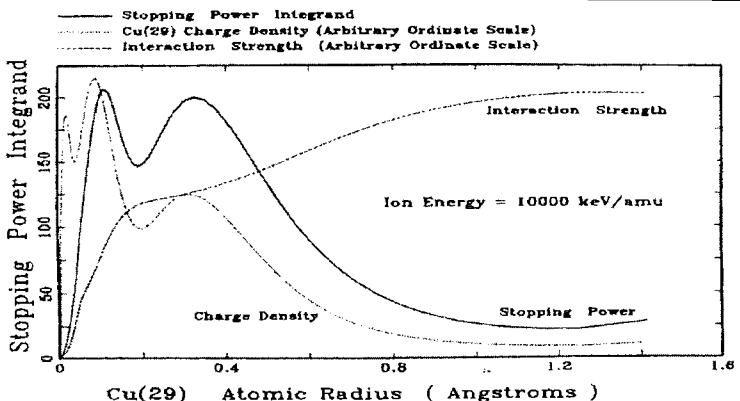


Figure 3-4 Interaction strength of high speed particle with copper atom.

The nature of the interaction of a high speed particle with a solid is illustrated by considering a target of copper (Cu). The dotted line is the curve of Figure 3-3. The dashed curve is the interaction strength, I , of a high velocity particle (10^4 keV/amu) with the charge distribution. It is small only for the inner k-shell electrons. The product I_p is the stopping cross-section, see Eq. 3-6. This product is shown as a solid line. It shows that the energy loss is evenly distributed across the Cu electrons except for the inner shell.

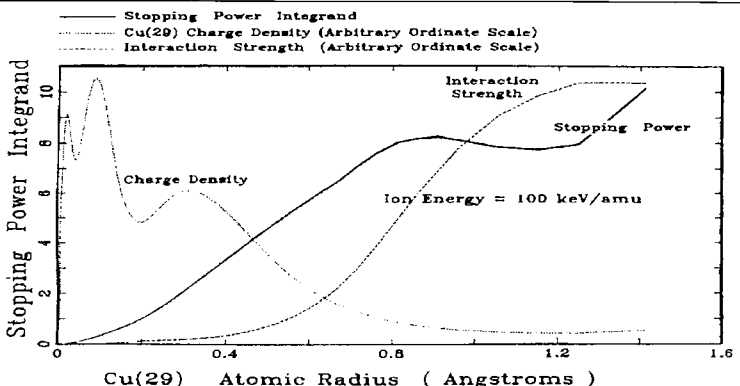


Figure 3-5 Interaction strength of slow speed particle with copper atom.

The interaction of a slow particle with copper. The dotted line is the electronic charge distribution of a Cu atom in a solid. The dashed curve is the interaction strength of the slow particle with this distribution. There is almost no interaction with the core electrons, and the interaction is almost exclusively with the conduction electrons. The solid line shows the stopping integrand, Eq. 3-6 and shows that the electronic energy transferred to either copper atom is mostly to the outer electrons. Since there is little energy transferred to either the K or L shells, it indicates there will be few x-rays produced during de-excitation of the atom.

The first attempt to evaluate electronic stopping cross-sections for protons in solids using the Lindhard stopping formalism and the local density approximation was by Bonderup who used Lenz-Jensen atoms

to represent the atoms in the solid (67a). This work was extended to isolated Hartree-Fock atoms by Rousseau et al. (70b) and to actual solid-state charge distributions by Ziegler (78a).

The Charge State of a Hydrogen Ion

To calculate the stopping of atomic hydrogen ions (i.e. protons) in solids (rather than in a gas of electrostatic particles) using Eq. 3-6, we now need to evaluate the effective charge, Z^* , of these ions in solids. As discussed below, this is a controversial and messy subject. The charge state of a proton in a solid is important for the basic stopping, Eq. 3-6, where the effective charge of the particle always acts to reduce its calculated stopping power relative to the stopping power of a bare nucleus. If a proton is always stripped of its electron then we might consider a proton penetrating a solid as the purest practical test of any stopping power theory of particles penetrating an electron plasma. This problem has been of concern since the 1930's, when it was found that heavy ion stopping powers scaled proportional to proton stopping powers (for identical velocities and targets).

For example, if a 100 MeV fission fragment (say an iron nucleus) had a known stopping power in aluminum and the proton stopping power for aluminum was known, then most of the iron stopping power curve could be predicted (as discussed later in this chapter). The question arose as to whether there was a lower velocity limit to this scaling. Proton stopping powers could be measured at very low velocities, but if the proton begins to have a partially bound electron at these low velocities then that might end the scaling proportionality. It was argued by some that it was unlikely that protons should have a bound electron at any velocity since the electronic orbital radius should be larger than the nearest atoms in the solid. This idea was countered by noting that because a bare proton may polarize the target electron-plasma, it still might have a virtual bound electron.

No one could propose a way to directly measure the charge state of protons in solids, so various secondary experiments were tried. One early work by Hall (50a) investigated the proton problem by looking at the charge states of low velocity protons exiting thin foils of Be, Al, Ag and Au. He found there to be no target dependence of the ratio of H^+/H^0 .

After several similar papers were published, Phillips reproduced much of this work with in-situ prepared targets and found significant differences in the H^+/H^0 ratio from freshly evaporated targets, and also that this ratio difference rapidly disappeared with time (58d). The conclusion was reached that unless 'fresh' surfaces were used, the measurements probably related more to surface contamination (H or C or O) than to the foils themselves.

A major review by Allison (58d) asserted that the studies of excited charge states only evaluated the influence of the final few atomic layers of the target surface and were useless as probes of the bulk material, and hence these measurements could not evaluate the charge states of protons within the bulk.

Brandt reviewed this subject of proton charge states in solids from both theoretical and experimental considerations (75I). He found no evidence that protons would have bound electrons in their passage through solids.

Ferrell and Ritchie (77I) calculated the charge state of light ions of low velocities in free electron gases using a variationally computed self-consistent potential approach. They found that He ions might bind an electron in metals, and that H ions could also do so in a dilute free electron gas. However, they state that their H ion argument neglected the influence of the positive nuclei (a free electron gas model assumes a uniform background of positive charge, not nuclear clumping of the positive charges) and other effects which might make the bound state of an electron to a proton impossible.

This tide of opinion that the H ions penetrating solids were always bare protons was suddenly objected to by Brandt et al. (78f) who analyzed experimental proton stopping powers in terms of velocity and energy criteria for electron stripping. They pointed out that for stopping theory, one is interested in an effective charge (not just the average number of bound electrons) and that polarization of the medium indicates that for velocities below about twice the Bohr velocity (100 keV/amu) a hydrogen projectile would have an effective charge less than one.

This opinion was reversed again by Brandt and other collaborators (81c, 81d, 82a) as they concluded a long series of experimental and theoretical advances to untangle the subject. They found that misinterpretation of heavy ion close-collision effects had made them conclude previously that it was necessary for the hydrogen projectile effective charge to be less than one at low velocities, but with a new, more complete theory (82a) their experimental evidence overwhelmingly showed that hydrogen ions were always protons with an effective charge equal to one.

Various other theoretical studies have also considered this subject with mixed conclusions (76l, 77n, 77o, 78i, 81m).

In this book we assume a proton in a solid always has a charge of +1.

Experimental Hydrogen and Helium Ion Stopping

The theory of heavy ion stopping, described later in this chapter, is greatly simplified when discussed as an extension of light ion stopping. This extension is sometimes called "scaling" which is defined as the formalism to calculate heavy ion stopping from the energy loss of light ions at the same velocity in the same medium. To achieve accurate heavy ion stopping cross-sections, it is essential to have a very reliable data-base of light-ion stopping powers.

When one surveys the experimental papers about light ion stopping powers it is immediately clear that there are more experimental stopping values for He ions than for any other ion. Further, the He ion values are more consistent than those for protons. The reason for this appears to be the development of He nuclear backscattering for material analysis during the 1970's (also known as RBS analysis), and this application required precise stopping powers.

In order to establish a reliable light ion stopping power base, it is very helpful to use the experimental measurements of both H and He ions in solids. To do this, we need to evaluate how to scale the He values into the corresponding H stopping powers. This technique is described in general with many plots in Vol. 3 of this series (78a).

We show in Figure 3-6 to Figure 3-7 the ratio of He to H experimental stopping powers in the same targets and at the same velocity, subdivided to see if the target Fermi velocity, or the target atomic number show deviations from a universal ratio which depends only on the ion's velocity. Note that V_F/V_0 refers to a solid's conduction electron velocity (V_F) relative to the classical Bohr velocity, V_0 .

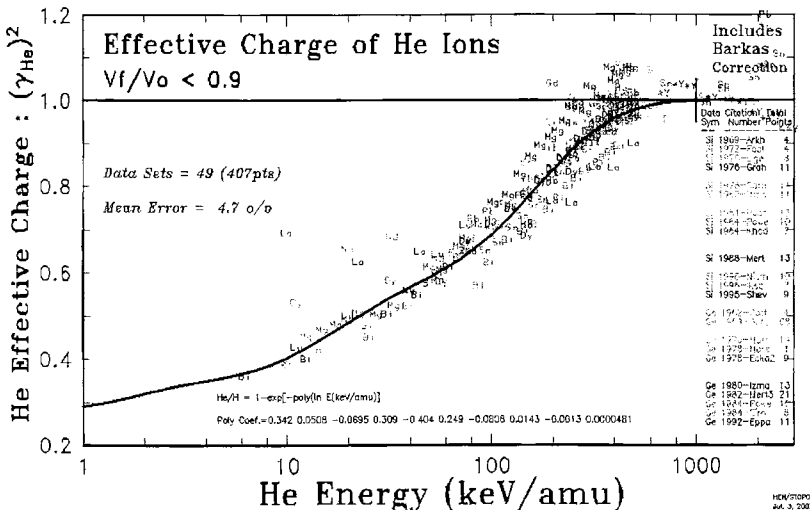


Figure 3-6 He fractional effective charges for low Fermi-velocity solids

The fractional effective charge of He ions is evaluated by comparing He stopping powers with H stopping in the same target at the same velocity, see Eq. 3-10. The purpose of this and the next 4 Figures is to evaluate if there are any major dependence of He/H stopping ratios on either the target Fermi velocity or its atomic number. If no dependence is found, then the H and He experimental data will be merged to form a very large data-base of experimental stopping powers.

The solid curve in the figure is the averaged He effective charge value from the analysis of thousands of experimental data. The curve's formula is described in Eq. 3-11, with coefficients as indicated in the figure. The data points are for He stopping only in targets with low Fermi velocities, $0 \leq V_F/V_0 \leq 0.9$, such as the rare earths, $Z_2 = 58 - 70$, and the heavy metals, $Z_2 = 81 - 83$.

It is convenient for later discussions to show the ratio of He to H stopping powers in a reduced form. We define as $\gamma = \text{fractional effective charge of an ion}$:

$$\text{Eq. 3-7: } Z_1^*(V, Z_2) = Z_1 \gamma(V, Z_2)$$

where Z_1^* is the effective charge of an ion of atomic number, Z_1 , at velocity, V , and in target, Z_2 . Hence γ will depend on the ion velocity and the type of target. Using Eq. 3-6, we can equate the ratio of S_{he} (He stopping,) to S_{H} (proton stopping) at the same velocity and in the same target as:

$$\text{Eq. 3-8: } \frac{S_{\text{He}}(V, Z_2)}{S_{\text{H}}(V, Z_2)} = \frac{\int (Z_{\text{He}}^*)^2 1\rho dV}{\int (Z_{\text{H}}^*)^2 1\rho dV}$$

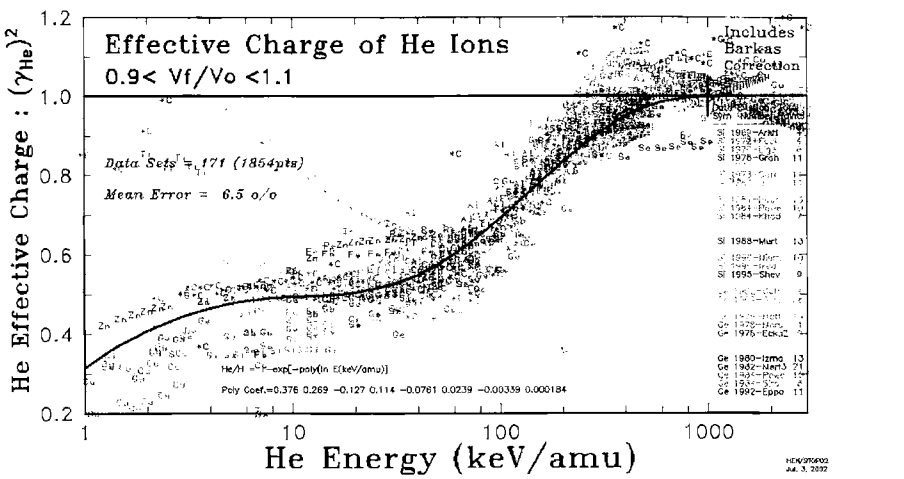


Figure 3-7

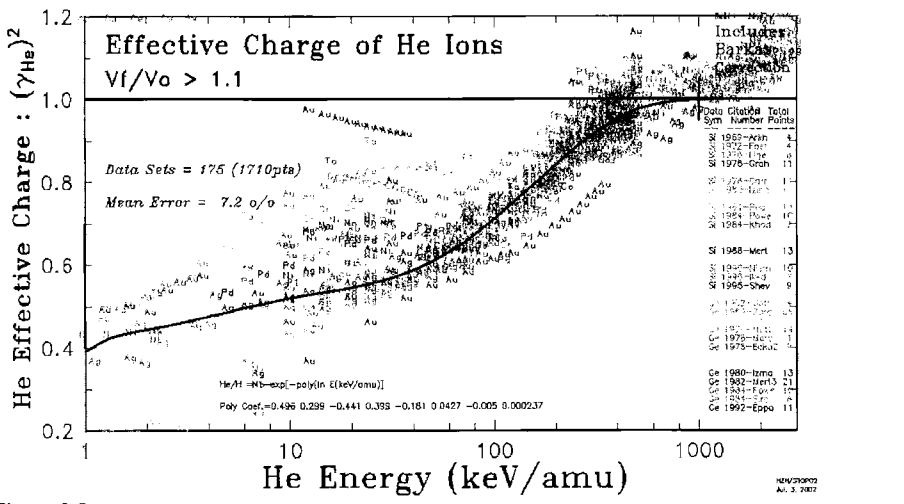


Figure 3-8 :

Fractional effective charge of He ions in high Fermi-velocity solids

The fractional effective charge of He ions is shown in Figure 3-7, above, for solid targets such as Al, Si, Ni, Cu and Sn. The lower figure (Figure 3-8) is for solids with high Fermi velocities such as Cr, Pd, Ag, Pt and Au. In both of these plots the distributions of experimental data are randomly scattered about the empirical line. The solid line is calculated using Eq. 3-11, with coefficients as indicated in the figure.

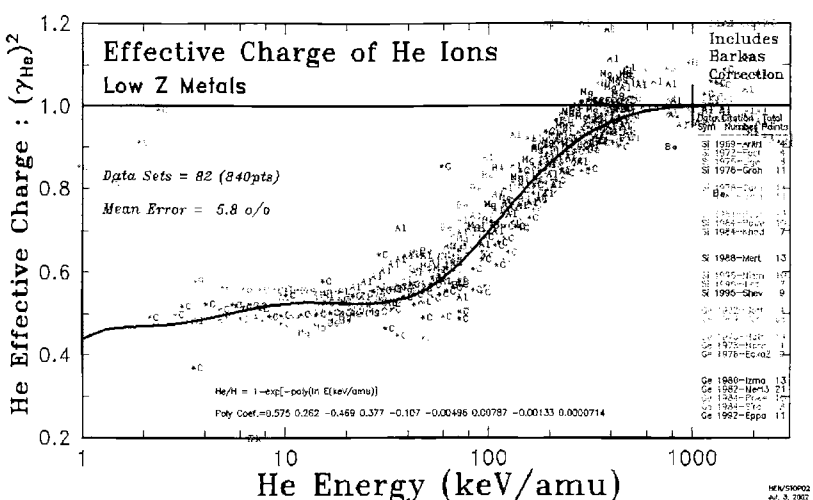


Figure 3-9

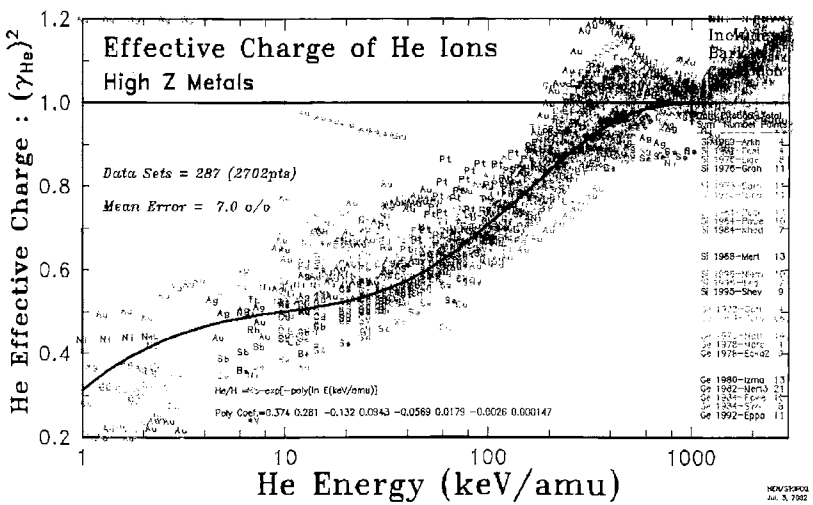


Figure 3-10

Fractional effective charge of He ions for various Metals.

The fractional effective charge of He ions is shown in Figure 3-9, above, for low atomic number solid targets, $Z_2 \leq 14$. Figure 3-10, below, shows data for solid targets with atomic numbers above 14. The distribution of data is randomly scattered about the empirical line. The solid line is calculated using Eq. 3-11, with coefficients as indicated in the figure.

As noted before, these equations and plots make the assumption that the proton is fully stripped of any orbiting electron at all velocities. This is an important assumption, usually justified by noting that the 1-s orbit of an electron about a proton (forming a H atom) has a diameter larger than the typical inter-atomic spacing of solids. Hence such an orbiting electron can not survive as an H atom penetrates a solid, and only a moving proton is observed.

Assuming the effective ion charge is independent of the target (this assumption is analyzed below), we use Eq. 3-7 to find:

$$\text{Eq. 3-9:} \quad \frac{S_{\text{He}}}{S_{\text{H}}} = \frac{(\gamma_{\text{He}} Z_{\text{He}})^2}{(\gamma_{\text{H}} Z_{\text{H}})^2}$$

$$\text{Eq. 3-10:} \quad \text{Therefore:} \quad \gamma_{\text{He}}^2 = \frac{S_{\text{He}}}{2^2 S_{\text{H}}}$$

where we have assumed in Eq. 3-10 that the fractional effective charge of H ions, γ_{H} , is always unity as discussed in the preceding section of this chapter. With this definition of γ_{He} , it is a function which must be equal to unity at very high velocities where the ion is completely stripped of its electrons, and perhaps decreases to zero at zero ion velocity where the ion may be neutral (it could be argued that the zero velocity value could be 1/2 as noted in the preceding sections). This function will be discussed in more detail later concerning the effective charge of heavy ions (and was also discussed in Chapter 1). Empirically, γ_{He} may be fitted with an expansion of the form:

$$\text{Eq. 3-11:} \quad \gamma_{\text{He}}^2 = 1 - \exp \left[- \sum_0^5 a_i \ln(E)^i \right]$$

where a_i are fitting constants. Using Eq. 3-10 and fitting all available experimental H and He stopping powers, we find for a_i the fitting coefficients shown in Figure 3-9 to Figure 3-10. This form of the fractional effective charge for He ions is shown as solid lines in these Figures..

The major assumption in the derivation of γ_{He} in Eq. 3-10 is that the ion effective charge does not depend on the target material. This is evaluated in Figure 3-6 to Figure 3-8 with regard to the Fermi velocity of the target, and in Figure 3-9 and Figure 3-10 concerning the target atomic number.

Figure 3-6 shows the results for targets with low Fermi velocities such as the rare earths, $Z_2 = 58-70$, and the heavy metals, $Z_2 = 81-83$. (The Fermi velocity is always indicated in units of the Bohr velocity, V_0). The data is sparse but there is reasonable agreement to the generalized curve for γ_{He}^2 .

The comparison for solids with Fermi velocities from $0.9 \leq V_F/V_0 \leq 1$. is shown in Figure 3-7. This band of solids contains the most popular materials for stopping measurements: Al, Si, Ni, Cu and Sn. Again the agreement between the data and the fitted curve is good.

The ratio for dense solids with high density interstitial electrons such as Cr, Pd, Ag, Pt and Au is shown in Figure 3-8. For low velocity ions, these materials might be expected to have the greatest polarization since their interstitial electrons are at higher relative velocities. But the results of Figure 3-8 show no significant deviation from those of Figure 3-6 and Figure 3-7.

Another variation might occur due to the atomic number of the target. Early experimental work found that low energy stopping powers were normally proportional to the ion's velocity, but for light targets ($Z_2 \leq 14$) the electronic stopping, S_e , was less than velocity proportional. That is, for $Z_2 > 14$, then $S_e \approx E^{1/2}$, but for $Z_2 \leq 14$ then it was proportional to $E^{0.45}$ (see, for example, references 65b and 65c).

We plot in Figure 3-9 the values of γ_{He}^2 for targets with atomic number from 3-14, and in Figure 3-10, the targets with atomic numbers above 14. Again we see only the normal scatter about the average effective charge line.

Proton Stopping: Theory and Experiment

The extended arguments above are presented to show the accuracy of converting He stopping powers to equivalent H stopping powers. With the combined data-base of experimental H and He stopping values, we can now examine an extensive test of the calculation of the electronic stopping of protons in solids using Eq. 3-2 to Eq. 3-4.

We show in Figure 3-11 to Figure 3-14 representative examples of the theoretical stopping of protons in solids. The solid line in each curve is the stopping power calculated from first principles using Eq. 3-2 to Eq. 3-4. The dotted line indicates the final empirical proton stopping power which is used in the stopping and range computer programs described later. The data shown with "H" are experimental data points, most of which are identified in Volume 3 of our early books on stopping and ranges (77a). The data labeled "He" are helium stopping data, reduced using Eq. 3-10 and Eq. 3-11:

$$\text{Eq. 3-12: } S_H = S_{He} / (2 \gamma_{He})^2$$

All the curves indicate that the theoretical calculation is very good for high velocities ($> 10^3$ keV/amu). Further, each theory curve has its peak at about the right energy. But there is a systematic deviation between the data and the theory below the peak. This means that the theoretical calculation is an accurate guide for higher energy H or He ions, but below 1 MeV/amu some correction is necessary in order to obtain proton stopping powers for elements without any experimental data. Note that this correction generally increases stopping powers which indicates that the deviation is not due to the effective charge of the ion because this number cannot physically exceed unity. All the theoretical curves shown assume the proton is fully stripped at all energies.

An overview of the deviation between the experimental and theoretical proton stopping powers is obtained by plotting the "fractional effective charge", γ^2 , which was discussed in Eq. 3-7 and, if one accurately knows the theoretical stopping of a fully stripped ion, it can be experimentally determined by

$$\text{Eq. 3-13: } \gamma^2 = S_{\text{exp}} / S_{\text{theory}}$$

as a function of the target's atomic number for a fixed ion velocity. Figure 3-15 and Figure 3-16 show all existing data for H- and He-ions at 250 keV/amu and 70 keV/amu. Data points which are considered as accurate are shown with an "H" symbol for hydrogen ions and with an "He" for Helium ions.

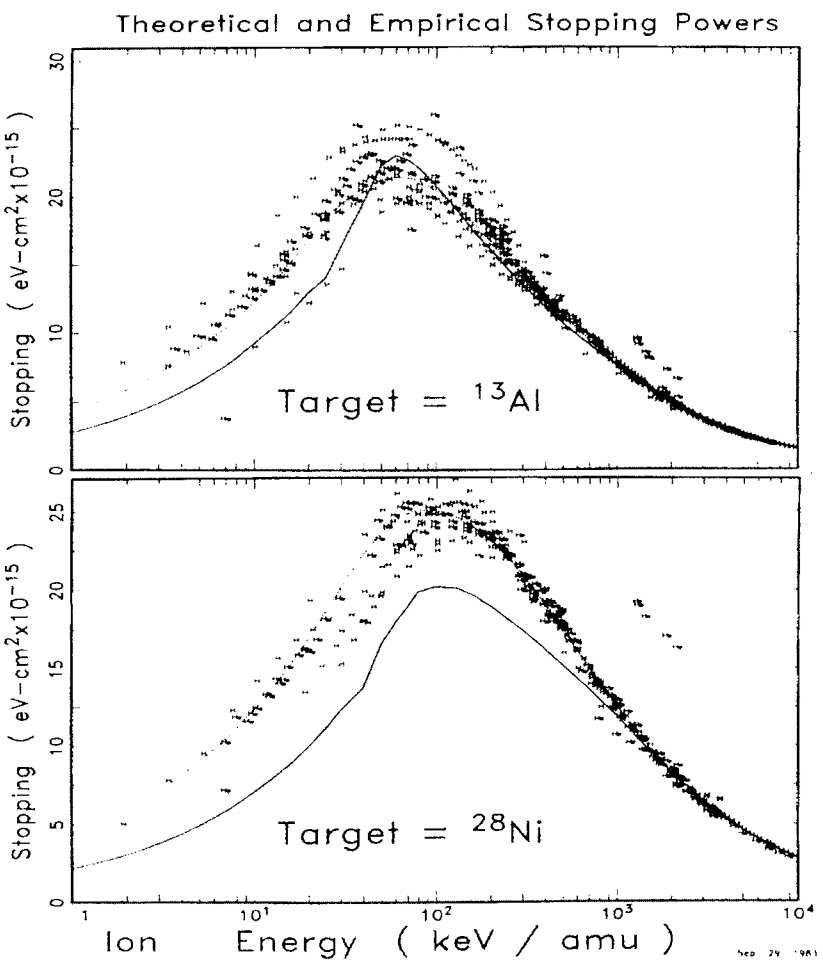


Figure 3-11 – Aluminum Target

Figure 3-12 – Nickel Target

Theoretical proton stopping powers and experimental data

The stopping cross-sections for protons in solids are shown both experimentally and theoretically. The data points indicated by "H" are proton stopping values, and those indicated by "He" are helium data reduced using the He effective charge of Figure 3-7 to Figure 3-9 using Eq. 3-11 and Eq. 3-12. The solid line is the calculation using Lindhard stopping and the local density approximation. The dotted curve is the final empirical curve discussed at the end of this chapter. The theoretical curve shows a peak at the same energy as the data, but it deviates from the data below 1 MeV/amu.

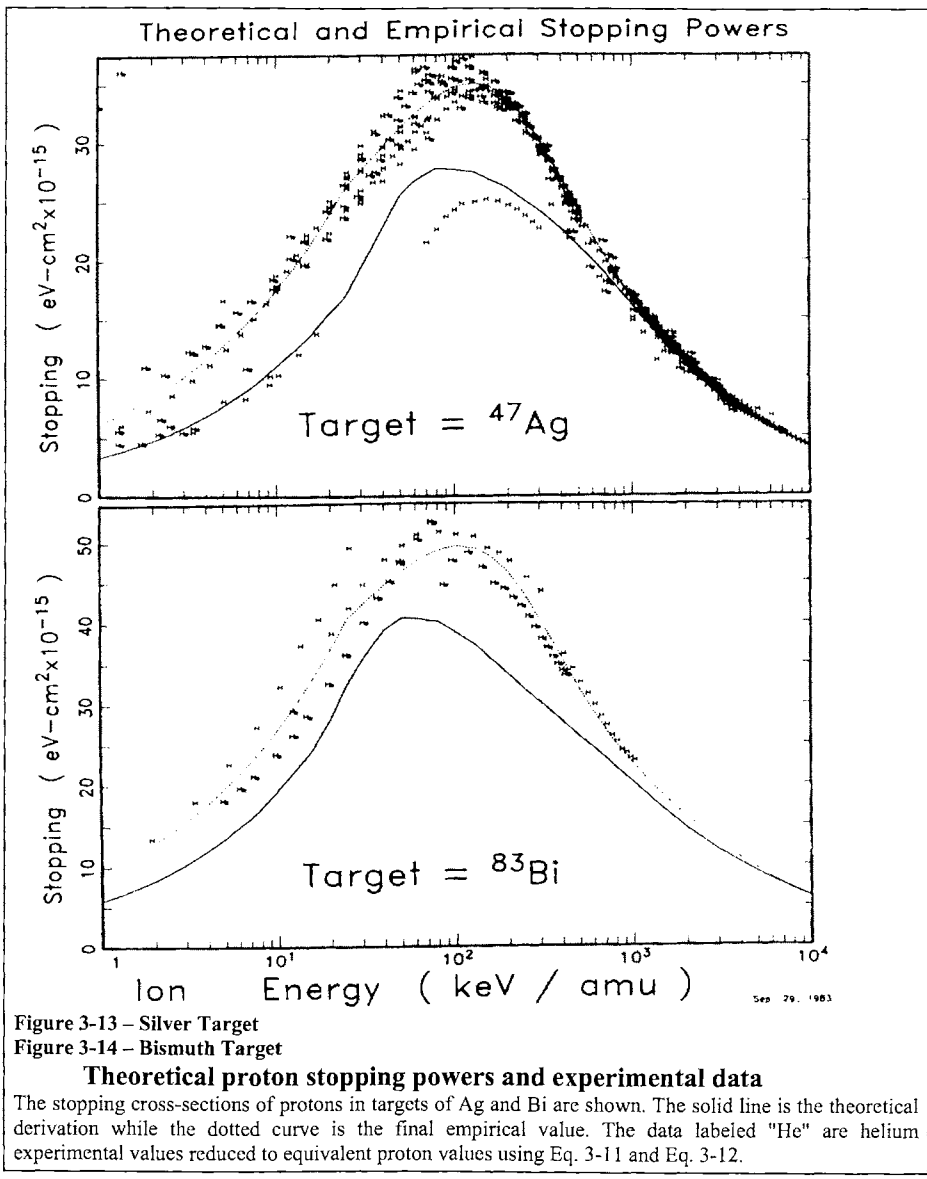


Figure 3-13 – Silver Target

Figure 3-14 – Bismuth Target

Theoretical proton stopping powers and experimental data

The stopping cross-sections of protons in targets of Ag and Bi are shown. The solid line is the theoretical derivation while the dotted curve is the final empirical value. The data labeled "He" are helium experimental values reduced to equivalent proton values using Eq. 3-11 and Eq. 3-12.

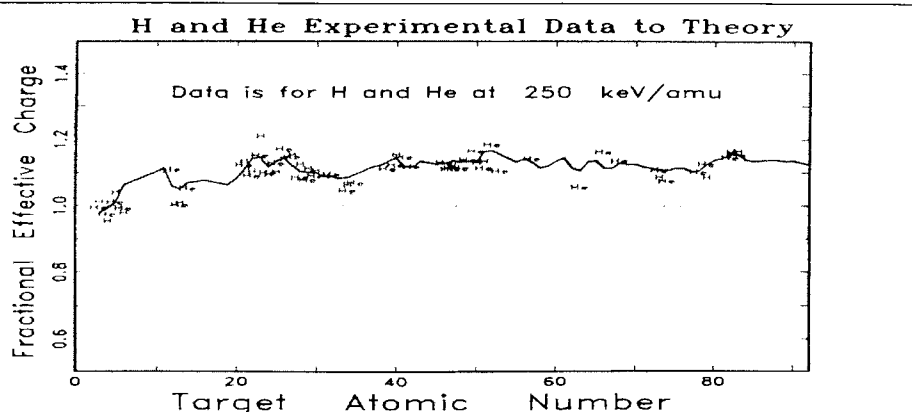


Figure 3-15 Fractional effective charge (250 keV/amu) vs. target atomic number

The interpolation procedure for finding proton stopping powers in targets with little experimental data. The plot is for an ion velocity of 250 keV/amu and shows the ratio of experimental to theoretical stopping powers as found from plots such as shown in Figure 3-11 to Figure 3-13 for single targets. Values for He ions are also shown and assume the He effective charge discussed previously in order to obtain equivalent H stopping powers. Through these points is drawn a line for interpolation to solids with little experimental data at this energy. The line is not smooth because experimental data may exist at nearby energies for a given solid and these are given more importance than the interpolation from nearby atomic numbers.

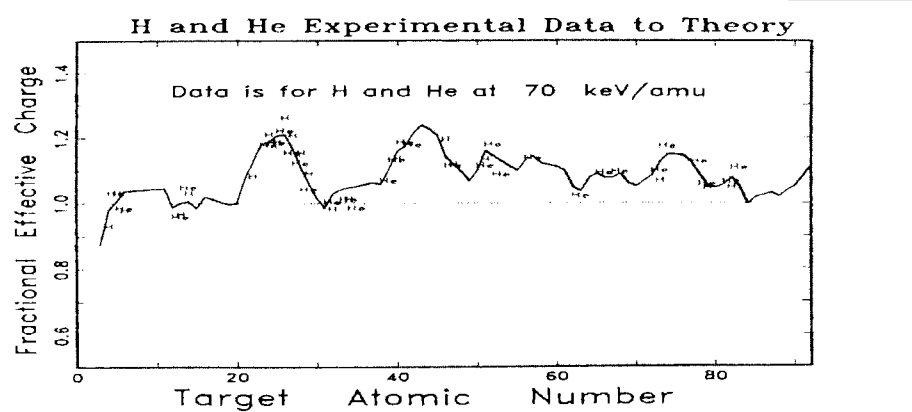


Figure 3-16 Fractional effective charge at (75 keV/amu) vs. target

The interpolation procedure for protons of velocity 75 keV/amu is similar to that in Figure 3-15. After the interpolation curves are found at various energies from 25 keV/amu to 1000 keV/amu, a final smoothing must be done to create smooth stopping curves as a function of energy. Hence a final stopping curve for protons in a solid with little data, e.g. Hg, is found by interpolating in two-parameters: both from neighboring atomic numbers and also from curves at other energies.

It is outside the intentions of this book to give reasons or explanations for the indicated deviations from stopping theory. Merely we want to demonstrate that the previously described theory gives a good basis for stopping power calculations, reducing the problem to the description of a residual 10-20% effects as shown in Figure 3-15 and Figure 3-16.

The determination of this small correction must be a smooth function of the target's atomic number as shown in Figure 3-15 and Figure 3-16 and also a smooth function of the ion velocity, as seen in Figure 3-11 to Figure 3-14. This two-dimensional smoothing problem has been solved as described in Vol. 4 (78a) of our series of books, and the final adopted "effective charge", γ , is shown in Figure 3-15 and Figure 3-16 as a solid curve. (Note: this proton "effective charge" is more accurately an empirical correction factor to theoretical proton stopping powers, but we retain the "effective charge" name to have a uniform formalism for all ions). Examples of the stopping powers evaluated on the basis of this γ (indicating also the energy dependence) is shown in Figure 3-11 to Figure 3-14 as a dotted line. By means of the proton stopping power theory described in the previous sections, and the effective charge, γ_H , and γ_{He} which are determined on the basis of all existing experimental data for H and He ions, we are now able to evaluate (interpolate) stopping powers for these lightest ions in any pure elemental target.

The Electronic Stopping of Heavy Ions

We have completed the discussion of the electronic energy loss of the very light ions, H and He. The energy loss of heavy ions to the electrons of a solid will be presented in three steps:

1. The stopping of very low velocity ions ($V_1 < V_F$) where we shall show that the energy loss is generally proportional to the ion's velocity.
2. The stopping of high velocity ions ($V_1 > 3V_F$) where we can scale proton stopping powers to equivalent heavy ion stopping using Thomas-Fermi scaling rules.
3. The use of more complex theory to bridge the low and high velocity regions ($V_F < V_1 < 3V_F$).

Since the Fermi velocity, V_F , of metals is about equal to the Bohr velocity, V_0 , the three velocity intervals described above will be approximately (1) < 25 keV/amu, (2) > 200 keV/amu and (3) 25-200 keV/amu.

Electronic Stopping: Low Velocity Heavy Ions

We are concerned here with heavy ions with ion velocities, V_1 , less than the Fermi velocity, V_F , of the material they are traversing. Since the Fermi velocities of solids usually falls between 0.7 to 1.3 V_0 , the ion velocity corresponds to less than 30 keV/amu. Here the majority of target electrons move much faster than the ion and collisions with the ion are mostly adiabatic without direct energy loss.

Firsov proposed a semi-classical model to evaluate this low velocity energy loss (59a). He considered two isolated atoms colliding with their undistorted electronic spheres penetrating each other. Firsov estimated the effective cross-sections of various inelastic processes as a function of the relative collisional velocity of the two atoms and the impact parameter of the collision. This was done by considering a plane located

in the center between the two nuclei, and the capture and loss of electrons was defined by the flux of electrons through this plane. Since the two atoms have a relative velocity, V_{Rel} , any captured electron must be accelerated up to this velocity and the ion loses a small energy proportional to this velocity. Firsov used Thomas-Fermi atoms to obtain electron distributions of the atoms and found that the electronic stopping cross-section would increase proportional to the heavy ion velocity.

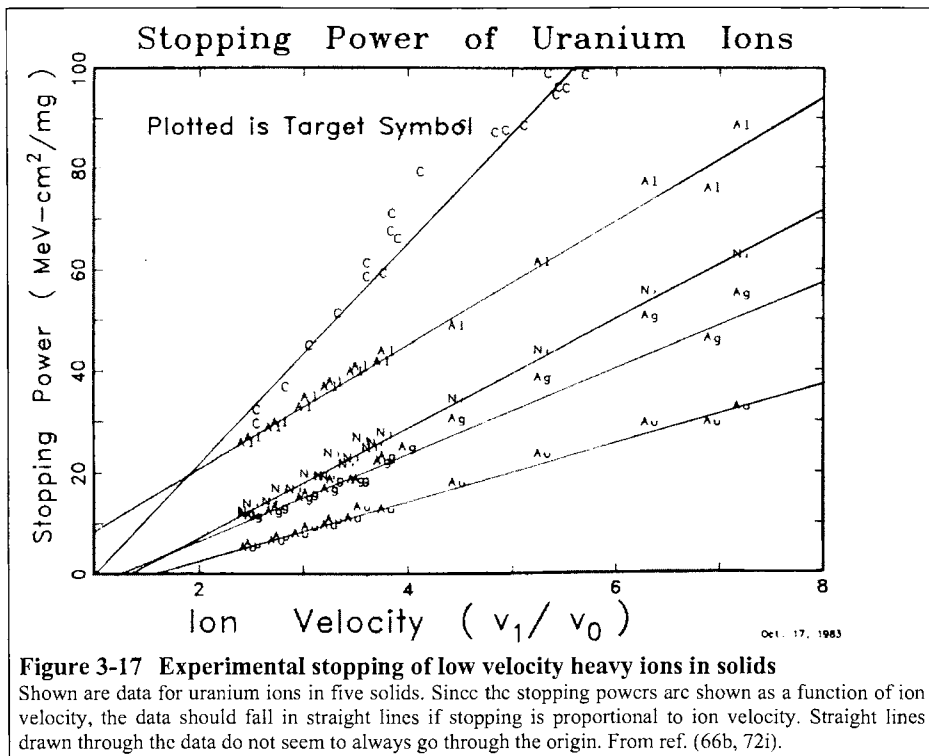


Figure 3-17 Experimental stopping of low velocity heavy ions in solids

Shown are data for uranium ions in five solids. Since the stopping powers are shown as a function of ion velocity, the data should fall in straight lines if stopping is proportional to ion velocity. Straight lines drawn through the data do not seem to always go through the origin. From ref. (66b, 72i).

Lindhard and Scharff also considered the problem of low velocity stopping, but used a model of a slow heavy ion in a uniform electron gas (61b, 63a). Relative to the ion, the electrons have a slight drift velocity. During a collision with the ion, a net energy is transferred which is proportional to this velocity. Hence, although Lindhard considered a more dynamic interaction between the target electrons and the ion, a velocity proportional energy loss was found which was similar to that found using the geometric model of Firsov.

These theoretical models have been the basis of many later calculations which have introduced more accurate Hartree atoms into the interactions (see, for example, 68c, 76d, 77m and 80g), but the preponderance of this work still yields velocity proportional stopping cross-sections.

Experimentally, there is general agreement with the prediction that the stopping cross-sections of low velocity heavy ions is velocity proportional. Extensive studies are presented in Refs. 65b, 66b, 68d, 72i

and 80a. There are two residual problems. First, although the stopping may be proportional to velocity, if a straight line is drawn through the data it may not go through the origin, see Figure (3-17). This non-zero intercept has been studied extensively over the last decade and, rather than being factual, it may be due to a breakdown of experimental technique (83a, 83b). For the measurement of low velocity stopping powers the experimentalist must use very thin foils, sometimes less than $0.1 \mu\text{m}$ in thickness. If the energy loss of an ion in a target is measured not as a function of the ion velocity but as a function of target foil thickness, that data may also not go through the origin, see Figure 3-18.

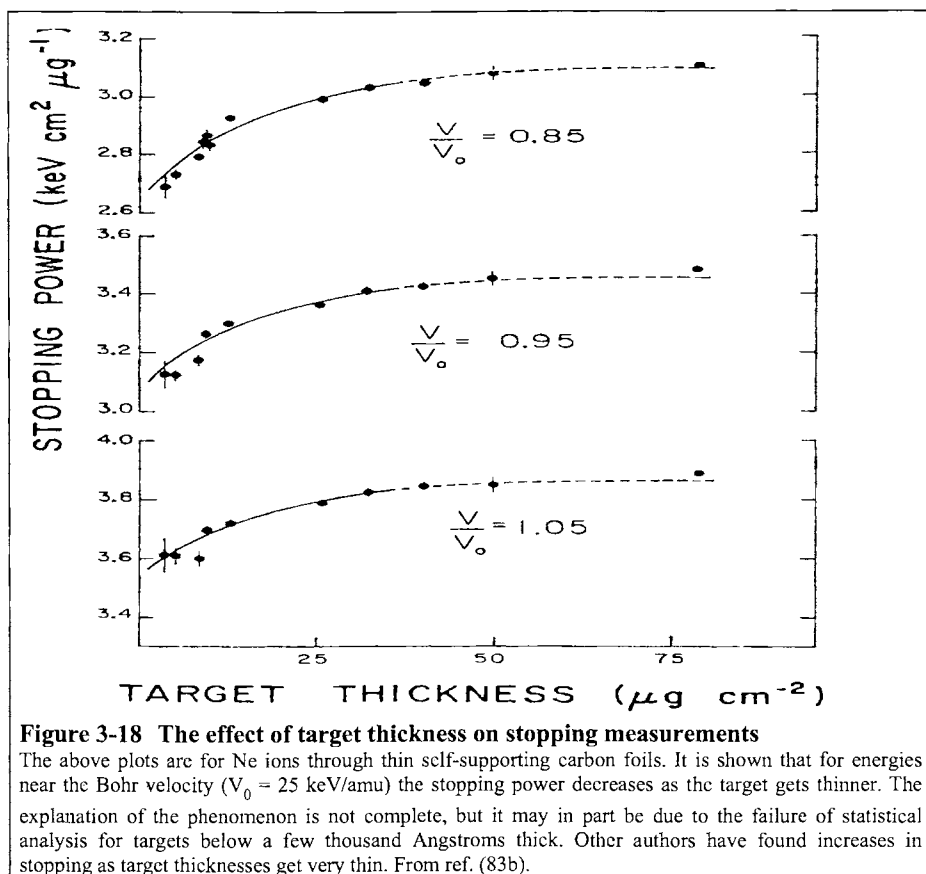


Figure 3-18 The effect of target thickness on stopping measurements

The above plots are for Ne ions through thin self-supporting carbon foils. It is shown that for energies near the Bohr velocity ($V_0 = 25 \text{ keV/amu}$) the stopping power decreases as the target gets thinner. The explanation of the phenomenon is not complete, but it may in part be due to the failure of statistical analysis for targets below a few thousand Angstroms thick. Other authors have found increases in stopping as target thicknesses get very thin. From ref. (83b).

The explanation of this phenomenon is believed to be that the statistical nature of the stopping process is breaking down with ion transmission through the very thin foils. With only a few collisions contributing to the energy loss, correlations between the nuclear and electronic stopping may make the experiment inappropriate for an evaluation of general energy loss theory. Such an experiment may be more like ion scattering in a gas target which gives experimental energy loss values which are sometimes quite different from the values found for similar solid targets (63f).

A second problem to velocity proportional energy loss theory is that for a few elemental targets there is clearly a different low velocity dependence. One example is for the semiconductors silicon and germanium. For metal targets the low velocity energy loss is primarily caused by the conduction band electrons which may be accurately described by a free electron gas. But the band-gap in the semiconductors clearly makes these targets different from metals in their theoretical electromagnetic response (60b, 70g).

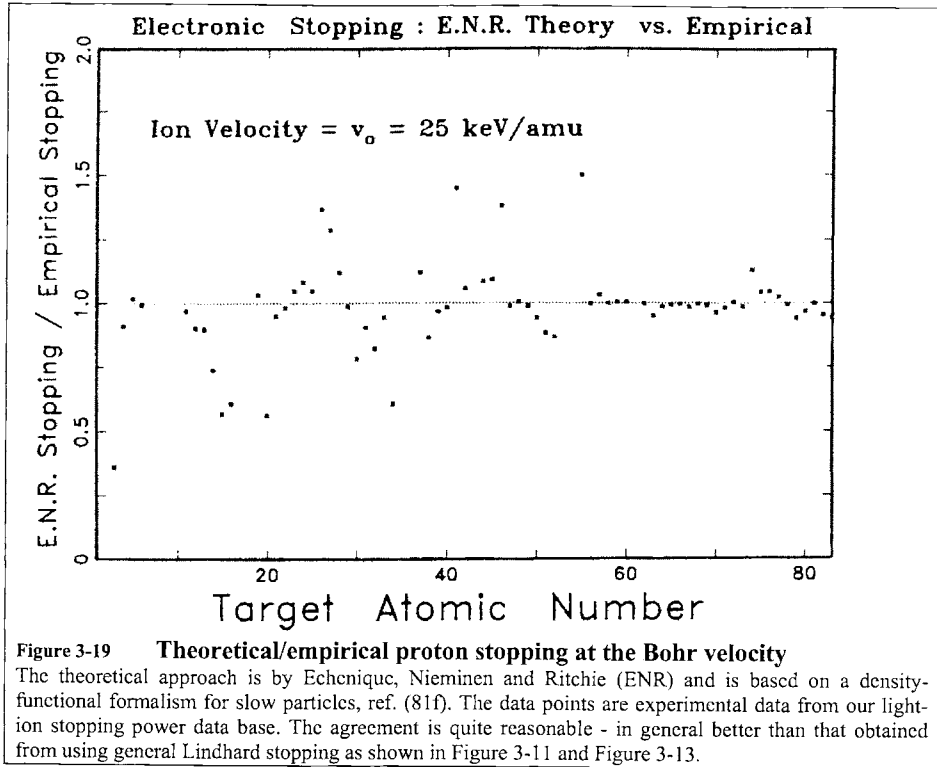
One might expect anomalously lower energy loss to materials with a band gap since there are fewer low-energy excitation levels available. Extensive analysis of experimental low velocity stopping powers in Si and Ge leads to the conclusion that stopping goes as $S_c \propto V^{0.7}$ in these narrow band-gap materials for ions with atomic number less than 19. For heavier ions the data is too sparse to draw any conclusion.

Similar behavior is experimentally found for stopping in carbon foils, $S_c \propto V^{0.7}$, but in this case the data is rather erratic. Very thin carbon foils are usually formed by evaporation techniques, and the foils are very absorbent of gases and water vapor (up to 30 atomic percent). Since experiments rarely report any efforts to avoid or remove such contaminations it is not clear that such low velocity measurements are meaningful.

A final minor exception to velocity proportional energy loss is the extensive evaluation of low energy proton stopping powers (77a) which found that a statistical analysis of hundreds of data points led to a low velocity stopping of protons $S_c \propto V^{0.9}$ rather than just a straight proportionality.

In summary, both theoretically and experimentally, one would expect very low energy heavy ions to have a velocity proportional energy loss in solids. If the material has a bandgap, this energy loss proportionality will be reduced.

A remaining question concerns the constant of proportionality if stopping depends directly on velocity. One study of this by Echenique, Nieminen and Ritchie (ENR) considers a density functional calculation of the stopping of slow particles in a free electron gas (81f). We have used the ENR approach with solid state charge distributions to calculate the stopping of particles in solids at the Bohr velocity, 25 keV/amu. We show in Figure 3-19 the ratio of an ENR calculation to the empirical values for all solids. The agreement is quite reasonable, usually within 25%. The empirical values at V_0 are based mostly on experimental data, and on the Brandt-Kitagawa theory to be discussed later, but for several groups of targets we have used the ENR approach for guidance (for example, $Z_2 = 57$ through 72 in Figure 3-19).



Electronic Stopping: High Velocity Heavy Ions

One broad empirical rule for the calculation of fast heavy ions in solids is to relate such stopping to the equivalent proton stopping powers. This is called *the heavy-ion scaling rule* and has the form:

$$\text{Eq. 3-14: } \frac{S_{HI}(V_1, Z_2)}{S_H(V_2, Z_2)} = \frac{S_{HI}(V_1, Z_2)}{S_{HI}(V_2, Z_2)}$$

This rule states that the electronic stopping of heavy ions, S_{HI} , at two velocities is directly proportional to the stopping of protons, S_H , at the same velocities and in the same material. S_H , in this relationship, is the stopping power per unit ion charge. It should be noted that this widely quoted rule is only valid for velocities over which there is little change in the heavy ion effective charge, $V_1 \gg V_F$.

The previous discussion about He to H stopping which led to Eq. 3-8 indicates this relationship between heavy ion stopping and proton stopping can be made simpler:

$$\text{Eq. 3-15: } S_{HI} = S_H (Z_{HI})^2 = S_H Z_{HI}^2 \gamma^2$$

where Z_{HI} is the atomic number of the heavy ion and γ is its fractional effective charge. This effective charge term can be estimated from Thomas-Fermi atomic theory, which may be applicable in the region where Thomas-Fermi atoms approximate Hartree-Fock atoms, i.e. where $0.3 \leq \gamma \leq 0.8$.

Eq. 3-16 :

The basic scaling relationships in a Thomas-Fermi atom are:

Charge density	$\equiv \rho \propto Z^2$
Electron binding energy	$\equiv E_b \propto Z^{7/3}$
Binding energy per electron	$\equiv e_b \propto Z^{4/3}$
Electron velocity	$\equiv V_e \propto Z^{2/3}$

where Z is the nuclear charge of the Thomas-Fermi atom.

As discussed in the historical summary of this book, scaling laws for heavy ion stopping powers received considerable attention in 1938-41 because of interest in nuclear fission experiments. Lamb suggested that the electron binding energy of the ion would be the primary parameter in determining γ , (40b), while Bohr suggested that the electron velocity would be critical (40d, 41a). Later evidence supported the Bohr view that one might consider the heavy ion to be stripped of all electrons whose classical orbital velocities are less than the ion velocity, which was expressed as the *Bohr relation*: $\gamma = V_1/(V_0 Z_1^{2/3})$ for moderate ion velocities. This Bohr concept was set in a more general form by Northcliffe (60c) as:

$$\text{Eq. 3-17: } \gamma^2 = 1 - \exp[-V_1 / (V_0 Z_1^{2/3})]$$

where Z_1 is the ion atomic number and V_1 is its velocity, which is compared to the Bohr velocity, V_0 . The $Z_1^{2/3}$ of Eq. 3-17 comes from the Thomas-Fermi atom relationships shown in Eq. 3-16, for the velocities of electrons in heavy ions. Eq. 3-17 has been shown to be valid over the region where the Thomas-Fermi atom approximates heavy ions; $0.3 \leq \gamma \leq 0.8$. This relationship has been supported by dozens of authors, see for example 65a, 66b, 68d, 72i and 77h. A typical parameterization of this Bohr/Northcliffe relationship is found in 77h:

$$\text{Eq. 3-18: } \gamma^2 = 1 - \exp[-0.92V_1 / (V_0 Z_1^{2/3})]$$

The accuracy of this equation is shown by plotting it versus experimental reduced heavy ion stopping powers defined using Eq. 3-15:

$$\text{Eq. 3-19: } \gamma^2 = \frac{S_{\text{HI}}}{Z_{\text{HI}}^2 S_H}$$

where S_H is the equivalent proton stopping power. An example is shown in Figure 3-20 with over 1000 data points from 127 heavy ion/target combinations for ion velocities $V_1 > 3V_0$. The accuracy of the fit is about 10%, which is as accurate as the experiments themselves.

The simple Thomas-Fermi picture is valid for a great range of heavy ion stopping. Volume 5 of this series (80a) analyzed Eq. 3-18 in detail and found that the stopping proportionality was valid for $3 \leq (V_1/V_0) \leq 100$. Below a relative velocity of $3V_0$ the Thomas-Fermi atom no longer represents the almost-neutral heavy ion, and the simple physics of the Bohr's stripping model becomes inadequate as discussed in the next section. For very high velocities, relativistic effects become important.

Electronic Stopping: Medium Velocity Heavy Ions

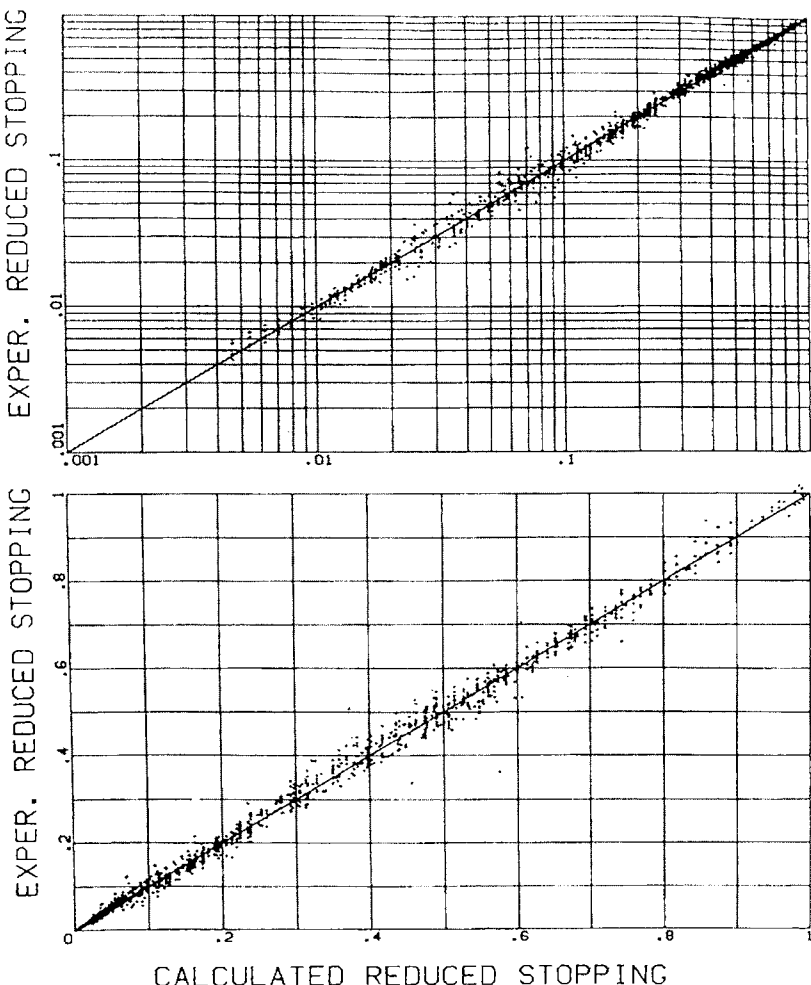
For the energy loss of medium velocity heavy ions in an electronic plasma we have constructed a model based on the ideas of Kreussler, Varelas and Brandt (81c) and Brandt and Kitagawa (82a), which we shall call the BK theory. The physical assumptions which differ from our previous discussions of particle and proton electronic stopping are:

- a) The charge state of the ion is determined approximately by assuming all electrons are stripped which have velocities less than the relative velocity between the ion and Fermi velocity of the electrons in the solid.
- b) For distant collisions (i.e. interactions with target electrons outside the ion's diameter) standard stopping theory holds with the ion having an effective charge determined by (a) above.
- c) For close collisions (i.e. with electrons which penetrate the ion's electronic shells) the energy loss increases because there is less shielding of the ion's nucleus. A comprehensive treatment is made of the reduced shielding and the increased energy loss with first order perturbation theory.
- d) The effective charge of an ion is based on its charge state in a solid, assumption (a) above, with an additional term to account for the increased interaction of close collisions, assumptions (c) above.

We shall briefly review the physics of this approach without detailing the mathematical derivations which are to be found in (81c) and (82a).

The first major concept is to calculate the stripping of the heavy ion not by comparing the ion's electron velocities to the ion velocity as suggested by Bohr, but to compare them to the relative velocity between the ion and the electronic velocity of the medium. For ion velocities, V_1 , much greater than the electron velocities of the medium the two stripping concepts are similar and hence the previously discussed scaling laws, Eq. 3-14, will hold.

For lower velocities, $1 \leq (V_1/V_0) \leq 5$, the ion velocity approaches the Fermi velocity of a solid, V_F , and the target inner-shell electrons can no longer be excited and the energy loss is mostly due to the conduction electrons. In the local density approximation (discussed at the beginning of this chapter) this is illustrated in Figure 3-4 and Figure 3-5.



CALCULATED REDUCED STOPPING

Figure 3-20 Experimental data versus calculated stopping powers

Experimental verification of Thomas-Fermi scaling of electronic stopping powers for high velocities, $V_1 > 3V_0$. The ordinate of each point is an experimental stopping power reduced to an effective charge by dividing by the equivalent proton stopping power and Z_1^2 , see Eq. 3-19. The abscissa is the Thomas-Fermi charge state of the ion which assumes all electrons are stripped which and have a velocity less than the ion velocity, see Eq. 3-18. In Thomas-Fermi atoms the electron velocity is proportional to $V_0 Z_1^{2/3}$. This excellent agreement between theory and experiment is only valid for ions with velocities $V_1 > 3V_0$.

The relative velocity, V_{rel} , of the ion to the velocity of the conduction electrons, V_e , in a solid is defined as

$$\text{Eq. 3-20:} \quad V_{\text{rel}} \equiv \langle \left| \vec{V}_i - \vec{V}_e \right| \rangle$$

which yields after averaging over all directions of electron motion (see ref. 82a):

$$\text{Eq. 3-21:} \quad V_{\text{rel}} = \frac{V_e}{6} \frac{(V_i/V_e + 1)^3 - |V_i/V_e - 1|^3}{V_i/V_e}$$

If we assume the conduction electrons are a free electron gas, in the ground state, i.e. occupy all velocities between 0 and V_F , we obtain by integration for

$$V_i > V_F :$$

$$\text{Eq. 3-22:} \quad V_{\text{rel}} = V_i \left(1 + \frac{V_F^2}{5 V_i^2} \right)$$

and for $V_i < V_F$:

$$\text{Eq. 3-23:} \quad V_{\text{rel}} = \frac{3}{4} V_F \left(1 + \frac{2 V_i^2}{3 V_F^2} - \frac{V_i^4}{15 V_F^4} \right)$$

Thus the relative velocity, and hence the final degree of ionization of the ion now depends only on the ion velocity, V_i , and the target Fermi velocity, V_F . The explicit relation between these two quantities will be discussed later. Once the charge state of the ion is known, it is necessary to establish its electronic charge distribution, and its diameter, based on its degree of ionization. This diameter will be used to separate the close and distant collisions of assumptions (b) and (c) above. The ionized atom electronic distribution can be found using the simple Bohr atomic electron density distribution

$$\text{Eq. 3-24:} \quad \rho(r) \propto e^{-r/r}$$

which can be extended to include a screening length, Λ , and can be properly normalized by using:

$$\text{Eq. 3-25:} \quad \rho(r) = \frac{N}{4 \pi \Lambda^3} \left(\frac{\Lambda}{r} \right) \exp(-r/\Lambda)$$

where N is the number of electrons remaining on the ion of atomic number, Z_i . The fractional ionization, q , is therefore $(Z_i - N)/Z_i$. (Note that an *ion's fractional ionization*, q , is different from the *ion's effective charge*, γ , which will be derived later.) The *screening length*, Λ , describes the dimensional changes to the electronic distribution as the degree of ionization changes. It is determined by assuming the variational conditions that for any degree of ionization :

$$\text{Eq. 3-26: } \frac{\delta E}{\delta \Lambda} = 0 \quad \text{and} \quad \left. \frac{\delta E}{\delta N} \right|_{N=Z_1} = 0$$

The first term states that for any value of N , Λ will be determined as a minimum energy configuration. The second term states that the neutral atom has the lowest energy of any degree of ionization. The total energy of the ion, E , is defined as

$$\text{Eq. 3-27: } E = E_{ne} + E_{kin} + E_{ee}$$

where E_{ne} is the nucleus-electron interaction which, with the atomic model of Eq. 3-25, is

$$\text{Eq. 3-28: } E_{ne} = -Z_1 N e^2 / \Lambda$$

Similarly, E_{kin} , the kinetic energy of the electrons, and E_{ee} , the electron-electron energy, have the simple forms

$$\text{Eq. 3-29: } E_{kin} = a N^{5/3} e^2 / \Lambda^2$$

$$\text{Eq. 3-30: } \text{and} \quad E_{ee} = N^2 e^2 / 4 \Lambda$$

Where “ a_0 ” = Bohr Radius = 0.529\AA , and “ a ” was determined to have a length of about $1/4\text{\AA} = a_0/2$. Eq. 3-27 is therefore completely described and, solving Eq. 3-26, we determine for the ion screening length (i.e. its spatial extent):

$$\text{Eq. 3-31: } \Lambda = \frac{2a_0 N^{2/3} a}{Z_1 \left[1 - \frac{N}{7Z_1} \right]} = \frac{2a_0 (1-q)^{2/3} a}{Z_1^{1/3} \left[1 - \frac{1-q}{7} \right]}$$

The authors of the BK theory (82a) discuss that this analytic derivation of the screening length of an ion is not limited by their choice of an exponential electron distribution, Eq. 3-24. Their result is shown to be virtually identical to numerical results based on Lenz-Jensen atoms for all values of ionization.

Brandt later suggested (82j) this evaluation of the ion's screening length would be significantly improved if a separate calculation be done for an ion's k-shell electrons. He suggested $\Lambda = 3a_0 / 2Z_1$, for ions with a single electron, and $\Lambda = 3a_0/(2Z_1 - 0.6)$ for a complete k-shell. This correction is supported by our study as will be discussed later.

With the electronic distribution of the ion now defined for all levels of ionization by Eq. 3-25 and Eq. 3-31, the next step is to calculate the electronic stopping using effective charge theory by adding together the energy loss in distant collisions, which involves target electrons that see a charge, $q Z_1$, and the energy loss to the electrons of the medium which penetrate the ion's diameter and feel increased nuclear interaction. Using perturbation theory, for heavy ions the BK theory produces the simple expression for the effective charge of an ion, γ :

$$\text{Eq. 3-32: } \gamma = q + c(1 - q) \ln [1 + (2 \Lambda V_F / (a_0 V_0))^2]$$

where q is the fractional ionization, $q = 1 - N/Z_1$, and N is the number of electrons still bound to the ion of atomic number Z_1 . The only undefined quantity is the constant, c , which is estimated to be about $1/2$ and weakly dependent on the target. We have found from extensive data analysis of the stopping cross-sections of the same ion in many targets that the best approximation is $c \approx (V_0/V_F)/2$, and so the effective charge of the ion is:

$$\text{Eq. 3-33:} \quad \gamma = q + (1 - q) \frac{(V_0 / V_F)^2}{2} \ln[1 + (2 \Delta V_F / (a_0 V_0))^2]$$

where q is the degree of ionization of the ion, and γ is its fractional effective charge. The first term, q , is the effective charge for distant collisions, i.e. for target electrons which do not penetrate the ion's electronic volume. For all degrees of ionization some electrons of the target will penetrate the ion's electronic cloud and increase the energy loss and this is the second term in Eq. 3-33. The sum of these two is the fractional effective charge, γ . The final consideration in evaluating the electronic stopping of heavy ions is how to evaluate the ion's degree of ionization, q , which will depend on the ion's velocity and the target material. We discussed earlier that q will depend on V_{rel} , the relative velocity of the ion to the target electrons, with $V_{\text{rel}} = \langle |\vec{V}_1 - \vec{V}_e| \rangle$, where V_1 is the ion velocity and V_e is the target electron velocity. From equations Eq. 3-20 to Eq. 3-23 we can derive the relation (82a) :

For $V_1 \geq V_F$:

$$\text{Eq. 3-34:} \quad V_{\text{rel}} = V_1 \left(1 + \frac{V_F^2}{5 V_1^2} \right)$$

For $V_1 < V_F$:

$$\text{Eq. 3-35:} \quad V_{\text{rel}} = \frac{3 V_F}{4} \left[1 + \left(\frac{2 V_1^2}{3 V_F^2} \right) - \frac{1}{15} \left(\frac{V_1}{V_F} \right)^4 \right]$$

We omitted an explicit relationship between q and V_{rel} when we discussed this subject before because it is a somewhat unfinished part of the published theory. If we argue that we can use the Bohr stripping criteria (based on Thomas-Fermi atoms) and upgrade it to strip all electrons whose relative velocity, V_{rel}/V_0 , is less than unity then:

$$\text{Eq. 3-36:} \quad q \sim \frac{V_{\text{rel}}}{V_0 Z_1^{2/3}}$$

Brandt said that this simple expression could be refined in a manner similar to his earlier work (75i) evaluating the Bohr stripping relation in which he numerically evaluated the Thomas-Fermi electronic distribution in order to predict more accurately the effective charge of an ion. This previous work still based ion stripping on the ion's electron velocities relative to the absolute velocity of the ion and did not consider any dependence on the electron velocities in the target. Brandt later suggested his comments on the Bohr stripping criterion could be extended to relative velocities (81d), but he did not derive a new expression before his sudden death.

We have extended the BK theory, and use in our treatment the expressions for Bohr stripping as revised by Northcliffe (3-16), and have changed the definition of the relative velocity from V_1 / V_0 to V_{rel} / V_0 :

$$\text{Eq. 3-37:} \quad q = 1 - \exp \left(\frac{-c V_{\text{rel}}}{V_0 Z_1^{2/3}} \right)$$

where "c" is a constant and V_{rel} is calculated using Eq. 3-34 or Eq. 3-35. The constant, c, should be about unity, and a first estimate would be to use directly the value found previously for high velocity heavy ions, $c = 0.92$, as discussed in Eq. 3-17. This would make the ionization level of heavy ions to be:

$$\text{Eq. 3-38:} \quad q = 1 - \exp \left(\frac{-0.92 V_{\text{rel}}}{V_0 Z_1^{2/3}} \right)$$

The accuracy of the above approach is shown in Figure 3-21 for several thousand heavy ion stopping powers. The plot shows heavy ion stopping power measurements, S_{HI} , reduced to obtain the corresponding effective charge by using Eq. 3-19: $\gamma^2 = S_{\text{HI}} / (Z_1^2 S_{\text{H}})$, where Z_1 is the ion atomic number and S_{H} is the equivalent proton stopping power. We then can invert Eq. 3-33 to solve for the ionization fraction, q , from the effective charge, γ . The abscissa is what might be called the "effective ion velocity" relative to the target electron velocity. The solid curve is the universal ionization fraction of ions, q , Eq. 3-38. The fit between the theoretical and experimental values is remarkably good, showing a data spread not much different from experimental error. The only problem occurs for very low ionization fractions, $q < 0.5$, where the data clearly does not follow the curve to the origin. This low value of ionization is where the ion is moving slowly through the solid, slower than some of the target electrons, and it is almost neutral. The problem probably lies in the approximations of BK theory, especially the application of perturbation theory to a situation to which it is clearly inappropriate. The outer shell of the ion contains the slowest electrons, and the stripping of these must be done using a more detailed approach. But a significant point is that the data of the slowest ions in Figure 3-21 do not disperse. They stay grouped about a tight common pattern which intersects the abscissa at about 0.1 effective ion velocity.

As discussed in the next section, Figure 3-21 provides the limits to the applicability of BK theory to calculating stopping cross-sections. The closely packed data may be fitted to obtain an empirical relationship for the ionization fraction of an ion as a function of its effective velocity. This relationship will be valid down to an effective velocity of about 0.1.

Empirical Electronic Stopping Cross-sections

This section will discuss how the preceding sections are merged together to form a unified approach to calculating electronic stopping cross-sections.

We have discussed how the energy loss of H and He ions in solids can be accurately predicted. For velocities above 200 keV/amu the Lindhard stopping theory, evaluated in the local density approximation with solid state charge distributions for the target, can accurately predict proton stopping cross-sections, see Figure 3-11 to Figure 3-14. For velocities in the interval of 25 - 200 keV/amu the theoretical predictions must be adjusted to fit the proton stopping data, but these corrections appear to slowly change with target element or ion velocity, see Figure 3-15 and Figure 3-16, and the lengthy discussion in Vol. 4 of the series (78a). This correction is probably accurate to better than 10%. Below 25 keV/amu there is little consistent data for protons, but the extensive analysis done in Vol. 3 of this series (77a) yielded on

energy dependence of $S_c \propto E_0^{-0.45}$ for protons, which is very close to the velocity proportional stopping of many theoretical predictions. The only exception is for targets of Be, B and C where the energy dependence found in experiments is $S_c \propto E_0^{-0.25}$. Proton stopping powers have been evaluated using the above approach, and then fitted with coefficients to form a data base of proton stopping cross-sections.

The comparisons between H and He stopping powers shown in Figure 3-6 to Figure 3-10 indicates that direct scaling between these two ions is independent of target element and so He stopping powers are obtained using Eq. 3-10 with S_H calculated using the proton data base and with the effective charge of He described by Eq. 3-11.

Finally, for solid targets for which there is little experimental data, an interpolation procedure is used as is shown in Figure 3-15 and Figure 3-16. This completes the data-base of H and He stopping powers.

For heavier ions the electronic stopping cross-sections for ion velocities above 200 keV/amu are accurately predicted by Thomas-Fermi scaling rules, see Figure 3-20. This result is also the same as predicted by BK theory for high velocity heavy ions. The BK theory may be used to predict stopping powers down to velocities where the ion stopping becomes velocity proportional. By inspecting Figure 3-21 we may estimate the lower velocity limit of the BK theory. This figure shows experimental stopping data reduced to a coordinate system in which the stopping of all ions in all targets at all energies should lie on a single line if the BK theory is accurate. The abscissa is the "Effective Ion Velocity", y_r , defined as

$$\text{Eq. 3-39:} \quad y_r \equiv \frac{V_{\text{rel}}}{V_0 Z_i^{2/3}}$$

where V_{rel} is the ion velocity relative to the target electron velocity as defined Eq. 3-34 and Eq. 3-35, V_0 is the Bohr velocity, and Z_i is the ion's atomic number. The ordinate is the "Ionization Fraction" of the ion, q , which is found by solving Eq. 3-33 for q with the fractional effective charge, γ , being defined by Eq. 3-19.

Figure 3-21 therefore shows that for ions $10 < Z_i < 92$ there is a tight bunching of the data down to an effective ion velocity $y_r \sim 0.1$. We have proposed that the relationship between y_r and q can be described using Thomas-Fermi theory by Eq. 3-38 and thus is shown in the figure as a solid line. This approach appears to be valid for $y_r > 0.3$. If we actually wished to fit the data, an even more accurate relation between y_r and q can be determined to be:

$$\text{Eq. 3-40:} \quad q = 1 - \exp[-0.95(y_r - 0.07)]$$

which fits the data for $y_r > 0.1$. Whichever approach is used, the stopping cross-section is calculated using Eq. 3-15 with the ion effective charge, γ , described by Eq. 3-33 with the ion's charge state, q , being described by one of the above approaches.

Our empirical approach to obtaining heavy ion stopping cross-sections is slightly more complicated than the approach described above because we have used numerical (computer) techniques to adjust the theoretical concepts to better agree with the data. Essentially, we have solved for two quantities, q and Λ (the ion's charge state and screening length), by simultaneously considering a data base of over 10,000 experimental heavy ion stopping powers. We have restricted the solution so that q vs. y_r is still a single curve for all ions, and that Λ vs. $q Z_i^{1/3}$ has a similar shape for all ions.

The Ionization Level of Ions in Solids

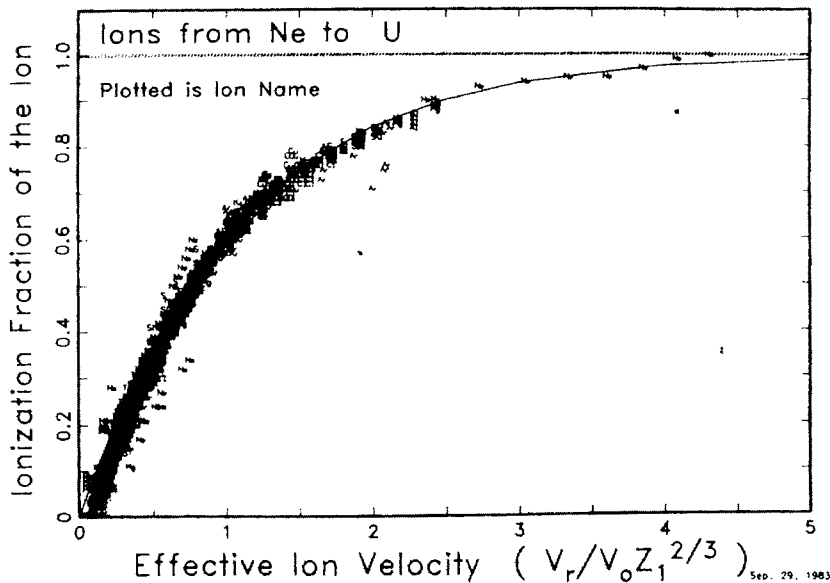


Figure 3-21 The ionization level of heavy ions in solids

The ionization level of heavy ions in solids, evaluated using the Brandt and Kitagawa (BK) formalism. The abscissa is called the ion's *effective velocity* and it combines the Thomas-Fermi stripping criteria, Figure 3-20, with Brandt's proposal that electrons are stripped whose velocity is less than the relative velocity, V_{rel} , between the ion and the solids Fermi velocity. The ordinate is the fraction of charge remaining on the ion as determined by reducing experimental data to an effective charge using Eq. 3-19 and then solving for the ionization level using Eq. 3-33. The solid line is the Northcliffe-Bohr estimate, Eq. 3-38. The agreement is remarkably good, deviating only at the lowest effective velocities where the ion is almost neutral.

This restriction was made so that a simple computer code could be constructed which would calculate the stopping of all ions in all targets. Our final results for the shape of the q and Λ curves may not be theoretically important for these are not independent variables (see, Eq. 3-31) and in the simultaneous solution for these quantities some non-physical distortions may appear. That is, if an experimental stopping cross-section is greater than a predicted value, the predicted value may be increased by increasing either the function q vs. y_r or the function Λ vs. $q Z^{1/3}$. When one does a multi-variate error minimization, the numerical solutions we found had a broad minimum in which the two functions were compensating with one increasing while the other decreased. It would be possible to further restrict the solution so that, for example, Λ vs. $q Z^{1/3}$ was close to the BK theory values, but then the q vs. y_r curve does not go through the origin as shown in Figure 3-21. Similarly, if q vs. y_r is forced through the origin, then some values of Λ became negative and clearly non-physical.

The final empirical plot of ionization versus effective velocity is shown in Figure 3-22, which has a data spread about a factor of two tighter than that of Figure 3-21. To minimize computational time for later stopping programs the empirical curve of q vs. y_r is expressed in the expansion:

$$\text{Eq. 3-41: } q = 1 - \exp [0.803 y_r^{0.3} - 1.3167 y_r^{0.6} - 0.38157 y_r - .008983 y_r^2]$$

which is valid for $y_r \geq 0.13$ (below which there is little data). This curve is shown as a solid line in Figure 3-22.

The assumptions of the BK theory make it applicable to heavy ions. The numerical reduction of all the stopping data enabled the finding of a screening length shape which was also applicable to light ions, $Z_1 = 3$ to 9. An evaluation of the accuracy of this fit for light ions is shown in Figure 3-23.

For the ion screening length, we find a similar shape for all ions, and a typical curve is shown in Figure 3-24 for nitrogen ions. This plot shows how the screening length of nitrogen ions changes with its level of ionization, with zero ionization being a neutral atom and $q = 1.0$ for a completely stripped high velocity ion. The curve shows a small bump for $0.7 < q < 1.0$ which is the enhanced k-shell screening radius discussed in the BK theory (see also Ref. (82j)). The scattered points show experimental stopping data with the target material identified, with each datum reduced to a value of Λ by inverting the BK stopping equations to solve for Λ with the stopping cross-section known. The solid curve is our approximation of the final numerical results, which describe the shape of Λ and it has been simplified into four straight line segments for ease of calculation. After the final minimization procedure to determine q and Λ was completed, a small amplitude adjustment was given to Λ for those ions with a great deal of data. This adjustment was a single numerical factor for each ion which corrects the size of Λ for that specific ion. The values are plotted in Figure 3-25.

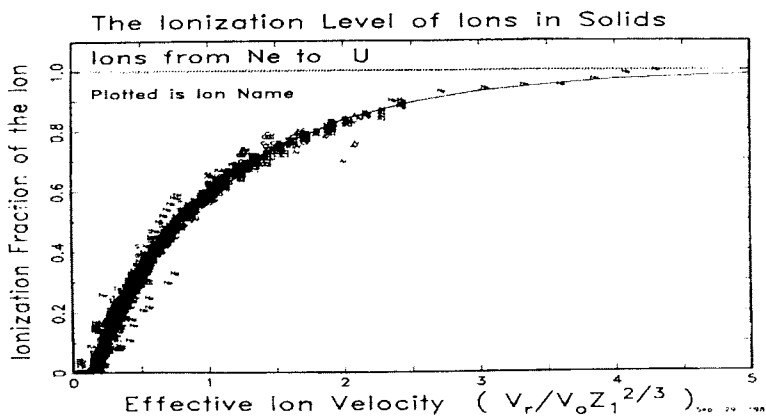


Figure 3-22 Ionization fraction of an ion versus its effective charge

Empirical relation between the ionization fraction of an ion, q , and its effective velocity for heavy ions, Ne to U. A computer technique was used to find a common shape of the ions' screening length, Λ , and also a new relationship of ionization fraction versus effective ion velocity. The data have a scatter about a factor of two better than the pure theory approach shown in Figure 3-21. The solid line is the empirical curve described by Eq. 3-41 and is valid for effective velocities above 0.13.

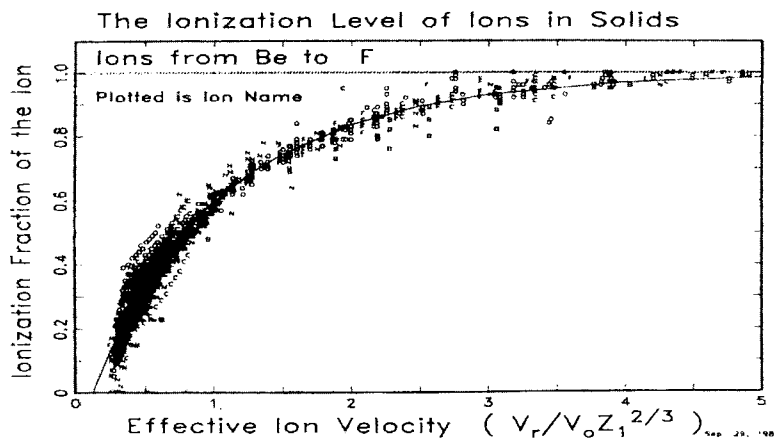


Figure 3-23 Ion ionization fraction versus ion velocity

The empirical relation between the ionization fraction of an ion, q , and its effective charge for light ions, Be to F. Although the BK theory is not applicable to light ions, the empirical construction of screening lengths for these ions allows their stopping powers to be calculated using the same formalism as that for heavy ions. The scatter of the data is mostly due to experimental scatter.

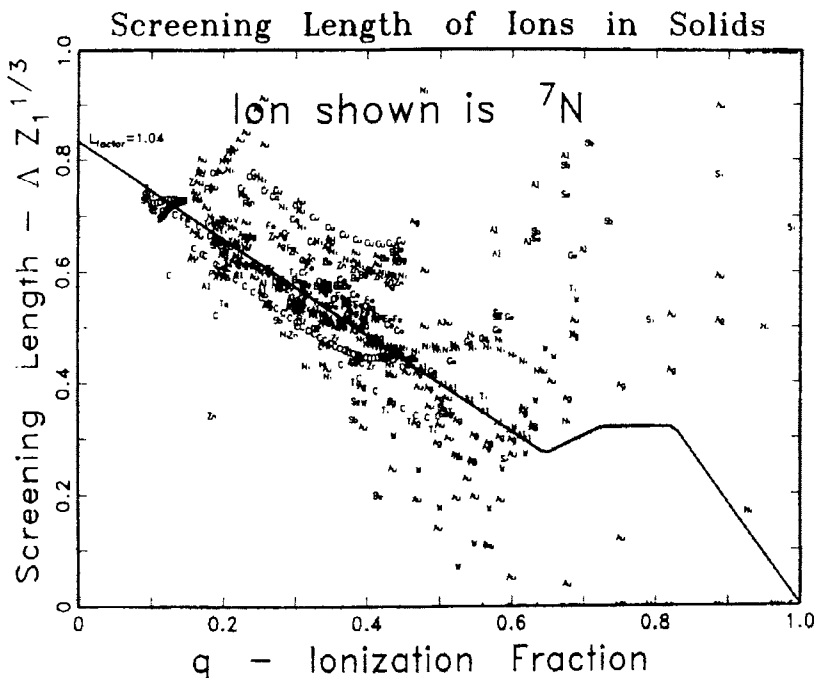


Figure 3-24 The screening length of nitrogen ions in solids.

The experimental data is reduced in a manner similar to that of Figure 3-21 to Figure 3-23 except the screening length, λ , is solved for rather than the ionization fraction. The ionization fraction is calculated using Eq. 3-41. The solid curve is the empirical screening length for nitrogen. It is a function which smoothly changes with the ion's atomic number and has no shell structure except for the inner-shell bump as suggested by Brandt. The smooth curve is corrected slightly for nitrogen ions by using the factor 1.04 (see Figure 3-25). The screening length of an ion has little influence on the stopping power of highly stripped ions so above an ionization fraction of about 0.7 the scatter of data has little meaning, and above 0.8 most of the data no longer falls within the limits of the plot (even though the stopping power is calculated to better than 5%).

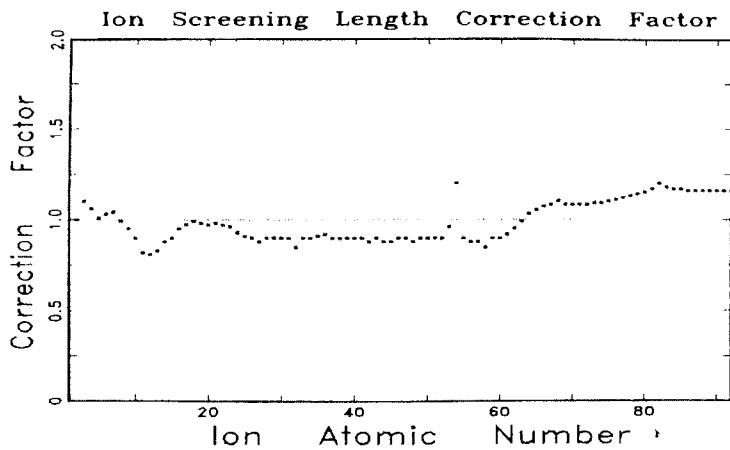


Figure 3-25 Empirical ion screening length correction factor

A smoothly changing empirical screening length was found for all ions. A slight correction factor was then found for individual ions using experimental data. The plot shows the correction factors used for various ions. Correction factors for ions without data were interpolated. The anomalous correction factor for Xe, $Z_1 = 54$, is due to the very wide scatter of experimental data and may be erroneous.

The reason these values deviate from unity is that the search for a similar shape for the Λ curve gave equal weight to each data point. About a third of the experimental stopping data occurs for the light ions $3 < Z_1 < 8$ and these dominate the mean amplitude of Λ . The final amplitude correction then adjusts changes in the amplitude of Λ to the atomic number of the ion. The correction slowly changes with Z_1 making interpolation possible. The reason for the unusual point for xenon ions, $Z_1 = 54$, is due to a very wide distribution of sparse experimental data.

The stopping cross-sections for very low velocity heavy ions is assumed to be proportional to the ion velocity for velocities below about $V_0/Z_1^{2/3} = (25 \text{ keV/amu}) / Z_1^{2/3}$. Actually, three tests are made to determine the point of cross-over from low-velocity stopping to medium-velocity stopping based on BK-theory. Velocity proportional stopping is used for ion velocities below any of three criteria: (a) if the effective ion velocity, $y_r < 0.13$, (b) if $y_r < Z_1^{2/3}$ or (c) if $y_r < V_{rel}/Z_1^{2/3}$. The first criteria results from the lower limit of validity of the q vs. y_r curve, see Figure 3-21. The second two limits come from the lower limits of the BK theory expansions which we use in the calculation. If any of these three conditions are met then the stopping cross-section at that cross-over velocity is determined and the stopping is assumed to be proportional to the ion velocity for slower ions. As discussed previously, for light ions, $3 < Z_1 < 19$, in semiconductor targets, $Z_2 = 6, 14$ or 32 , the low energy stopping cross-section has less than velocity proportional dependence, $S_c \sim V^{0.75}$.

Summary of Calculation of Stopping Powers

1. For H ions, we directly use coefficients from a table to obtain H stopping cross-sections in each element. For H energies below 25 keV/amu, $S_e \propto V^{0.9}$ except for $Z_2 \leq 6$ where $S_e \propto V^{0.5}$.
2. For He ions, we multiply the stopping for protons at the same velocity by the He effective charge at that velocity, $S_{He} = S_H (Z_{He} \gamma_{He})^2$, see Eq. 3-11. For energies below 1 keV/amu, $S_{He} \propto V^{1.0}$.
3. For heavy ions, we scale proton stopping powers using Brandt-Kitagawa theory (82a). The calculation of heavy ion ($Z_i > 2$) electronic stopping takes the following steps:
 - a) The relative velocity of the ion, V_{rel} , is calculated with Eq. 3-34 or Eq. 3-35 which depend only on the ion velocity, V_i , and the target Fermi velocity, V_F .
 - b) The fractional ionization of the ion, q , is calculated with Eq. 3-41.
 - c) The screening length of the ion, Λ , is calculated as a function of the ions charge state, see Eq. 3-31.
 - d) The effective charge, γ , of the ion is then calculated with Eq. 3-33.
 - e) The final stopping power is then found using Eq. 3-15 : $S_{HI} = S_H (Z_{HI} \gamma)^2 = S_H Z_{HI}^{-2} \gamma^2$, where S_H is the proton equivalent stopping power.
4. For very low velocity ions, $V_i < V_F / Z_i^{2/3}$, we use velocity proportional stopping except for $Z_i \sim < 19$ in semiconductor band-gap targets ($Z_2 = 6, 14$ or 32) where we use $S_e \propto V^{0.75}$.

The major assumptions of our approach to calculating electronic stopping powers which were discussed in this chapter are:

- The electron density in the target varies slowly with position.
 - Available electron energy levels and transition strengths of the atoms of the solid are described by those in a free electron gas.
 - Target band-gap effects can be accounted for by choosing appropriate (virtual) Fermi velocity.
 - The degree of ionization of the ion depends only on the velocity of the ion relative to the Fermi velocity of the target.
 - For distant collisions the electronic energy loss is described by Lindhard's free electron gas theory incorporated into a local-density-approximation for the particle-solid interaction.
 - For close collisions the electronic energy loss for heavy ion is corrected by Brandt and Kitagawa theory.
-

Chapter 3 – Citations

- 12a J. J. Thomson, Phil. Mag., 6-23, 449 (1912).
12c C. G. Darwin, Phil. Mag., 23, 901 (1912).
13a N. Bohr, Phil. Mag., 25, 10 (1913).
30 a H. A. Bethe, Ann. Physik, 5, 325 (1930).
31a N. F. Mott, Proc. Camb. Phil. Soc., 27, 553 (1931).
32a H. A. Bethe, Z. f. Physik, 76, 293 (1932).
32b A. Sommerfeld, Z. f. Physik, 78, 283 (1932).
32c W. Lenz, Z. f. Physik, 77, 713 (1932); H. Jensen, Z. f. Physik, 77, 722 (1932).
32d C. Moller, Ann. Physik, 14, 531 (1932).
33a F. Bloch, Ann. Physik, 16, 287 (1933).
33b F. Bloch, Z. f. Physik, 81, 363 (1933).
40c E. Fermi, Phys. Rev., 57, 485 (1940).
40d N. Bohr, Phys. Rev., 58, 654 (1940).
41a N. Bohr, Phys. Rev., 59, 270 (1941).
47b E. Fermi and E. Teller, Phys. Rev., 72, 399 (1947).
50a T. Hall, Phys. Rev. 79, 504 (1950).
54a J. Lindhard, Mat. Fys. Medd. Dan. Vid. Selsk., 28, No. 8 (1954).
55a J. Neufeld and R. H. Ritchie, Phys. Rev., 98, 1632 (1955); ibid. 99, 1125 (1955).
56c U. Fano, Phys. Rev., 103, 1202 (1956).
58d S. K. Allison, Rev. Mod. Phys., 30, 1137 (1958).
59a O. B. Firsov, Zh. Eksp. Teor. Fiz., (Transl.: Sov. Phys. JETP, 9, 1076 (1959)).
60b R. M. Sternheimer, Phys. Rev., 117, 485 (1960).
61b J. Lindhard and M. Scharff, Phys. Rev., 124, 128 (1961).
62b J. D. Jackson, "Classical Electrodynamics," Chapt. 13, Wiley, New York (1962, 1975).
63a J. Lindhard, M. Scharff and H. E. Schiott, Mat. Fys. Medd. Dan. Vid. Selsk., 33, No. 14 (1963).
63b U. Fano, Ann. Rev. Nucl. Sci., 13, 1 (1963).
63f W. Meckback and S. K. Allison, Phys. Rev., 132, 294 (1963).
65a W. Booth and I. S. Grant, Nucl. Phys., 63, 481 (1965).
65b J. H. Ormrod, J. R. MacDonald and H. E. Duckworth, Can. J. Phys., 43, 275 (1965).
66b C. D. Moak and M. D. Brown, Phys. Rev., 149, 244 (1966).
67a E. Bonderup, Kgl. Danske Vid. Sels. Mat. Fys. Medd., 35, No. 17 (1967).
68d T. E. Pierce and M. Blann, Phys. Rev., 173, 390 (1968).
68e K. B. Winterbon, Can. J. Phys., 46, 2479 (1968).
70b C. C. Rousseau, W. K. Chu and D. Powers, Phys. Rev., A4, 1066 (1970).
70g W. Brandt and J. Reinheimer, Phys. Rev., 2B, 3104 (1970).
70i V. I. Gaydaenko and V. K. Nikulin, Chem. Phys. Lett., 7, 360 (1970).
72i M. D. Brown and C. D. Moak, Phys. Rev., B6, 90 (1972).
72l P. C. Gehlen, J. R. Beeler jr. and R. I. Jaffee, "Interatomic Potentials and Simulation of Lattice Defects", Plenum Press, New York, (1972).
75i W. Brandt, "Atomic Collisions in Solids", Plenum Press, 1, 261 (1975).
75l L. F. Shampine and M. K. Gordon, "Computer Solutions to Differential Equations", W. H. Freeman Inc., San Francisco (1975).
76d B. M. Latta and P. J. Scanlon, Nucl. Inst. and Meth., 132, 133 (1976).

- 76l C. O. Amblanth, U. von Barth, Z. P. Popovic and M. J. Scott, Phys. Rev., 14B, 2250 (1976).
- 77b H. H. Andersen, "Bibliography and Index of Experimental Range and Stopping Power Data", vol. 2 of series "Stopping and Ranges of Ions in Matter," Pergamon Press, New York (1977).
- 77a H. H. Andersen and J. F. Ziegler, "Hydrogen Stopping Powers and Ranges in All Elements.", vol. 3 of series "Stopping and Ranges of Ions in Matter," Pergamon Press, New York (1977).
- 77h J. F. Ziegler, Appl. Phys. Lett., 31, 544 (1977).
- 77l L. Meyer, M. Klein and R. Wedell, Phys. Stat. Sol., 83B, 451 (1977).
- 77m D. J. Land, J. G. Brennan, D. G. Simons and M. D. Brown, Phys. Rev., A16, 492 (1977).
- 77n M. C. Cross, Phys. Rev., 15, 602 (1977).
- 77o E. Zaremba, L. M. Sander, H. B. Shore and J. H. Rose, J. Phys., F7, 1763 (1977).
- 78a J. F. Ziegler, "Helium Stopping Powers and Ranges in All Elements," vol. 4 of series "Stopping and Ranges of Ions in Matter," Pergamon Press, New York (1978).
- 78f B. S. Yarlogadda, J. E. Robinson and W. Brandt, Phys. Rev., 17B, 3473 (1978).
- 78h M. Inokuti, Y. Itikawa and J. E. Turner, Rev. Mod. Phys., 50, 23 (1978).
- 78i J. Arponen and E. Pajanne, J. Phys., C12, 3013 (1978).
- 79d G. J. Iafrate and J. F. Ziegler, Jour. Appl. Phys., 50, 5579 (1979) plus errata available from the authors.
- 79g P. Loftager, F. Besenbacher, O. S. Jensen and V. S. Sorensen, Phys. Rev., A20, 1443 (1979).
- 80a J. F. Ziegler, "Handbook of Stopping Cross Sections for Energetic Ions in All Elements," vol. 5 of series "Stopping and Ranges of Ions in Matter," Pergamon Press, New York (1980).
- 80e S. P. Ahlen, Rev. Mod. Phys., 52, 121 (1980).
- 80g S. A. Cruz, C. Vargas and D. K. Brice, Nucl. Inst. and Meth., 170, 208 (1980).
- 81c S. Kreussler, C. Varelas and W. Brandt, Phys., Rev., 23B, 82 (1981).
- 81d A. Mann and W. Brandt, Phys. Rev., 24, 4999 (1981). Note: Figure 3 of this paper can not be reproduced. It contains serious computational errors. The conclusions based on the figure must be considered unproven.
- 81f P. M. Echenique, R. M. Nieminen and R. H. Ritchie, Sol. Stat. Comm., 37, 779 (1981).
- 81m F. Guinea, F. Flores and P. M. Echenique, Phys. Ref. Lett., 47, 604 (1981).
- 82a W. Brandt and M. Kitagawa, Phys. Rev., 25B, 5631 (1982).
- 82j W. Brandt, Nucl. Inst. and Meth., 194, 13 (1982). Note that figure 4 of this paper contains a serious error and that the He ion data, if plotted correctly, fails to fall with the heavy ion data.
- 83a J. P. Biersack and P. Mertens, "Charge States and Dynamic Screening of Swift Ions in Solids," p 131, Oak Ridge Rpt. No. CONF-820131, Oak Ridge (1983).
- 83b W. N. Lennard, H. R. Andrews, I. V. Mitchell, D. Phillips and D. Ward, ibid, p 136 (1983).
- 04a P. Sigmund, "*Stopping of Heavy Ions. A Theoretical Approach*", Vol. 204, Springer Tracts of Modern Physics
- 06a P. Sigmund, "*Particle Penetration and Radiation Effects*", Springer Co. (2006). ISBN :354 031 713 9.
-

4. Stopping of Energetic Light Ions

ABSTRACT

The formalism for calculating the stopping of energetic light ions, H, He and Li at energies above 1 MeV/u, has advanced to the point that stopping powers may now be calculated with an accuracy of a few percent for all elemental materials. Although the subject has been of interest for a century, only recently have the final required corrections been understood and evaluated. The theory of energetic ion stopping is reviewed with emphasis on those aspects that pertain to the calculation of accurate stopping powers. This chapter duplicates some of Chapter 3, and extends the concepts to high velocity particles.

Table of Contents¹

4. STOPPING OF ENERGETIC LIGHT IONS	4-1
HISTORICAL REVIEW	4-2
THE BETHE-BLOCH EQUATION	4-3
<i>Variations of the Bethe-Bloch Equation</i>	4-6
<i>Low Velocity Limit of the Bethe-Bloch Theory: Particle Neutralization</i>	4-8
THE PRIMARY STOPPING NUMBER, L_0	4-9
<i>Shell Corrections, C/Z₂</i>	4-11
Shell Corrections using Hydrogenic Wave Functions	4-12
Shell Corrections using the Local Density Approximation	4-13
Empirical Summed Shell and Ionization Corrections	4-14
<i>Comparison of Two Types of Shell Correction Calculations</i>	4-18
<i>Density Effect Correction to L_0, δ/2</i>	4-20
THE BARKAS-ANDERSEN CORRECTION, L_1	4-22
<i>The Barkas-Andersen Effect from Charge Sign Considerations</i>	4-22
<i>The Barkas-Andersen Effect from Charge Magnitude Considerations</i>	4-24
<i>Theoretical Barkas-Andersen-Effect Calculations</i>	4-25
<i>Unified Barkas-Andersen Correction Factor</i>	4-26
<i>Empirical Barkas-Andersen Correction Term</i>	4-28
THE BLOCH CORRECTION, L_2	4-33
RELATIVE MAGNITUDE OF BETHE-BLOCH CORRECTIONS	4-34
THE ACCURACY OF CURRENT STOPPING THEORY	4-36
APPENDIX	4-39
. <i>Stopping Powers using the Local Density Approximation</i>	4-39
. <i>Lindhard Stopping in a Free Electron Gas</i>	4-39
. <i>Stopping Calculations using Local Density Approximation</i>	4-42
CHAPTER 4 - REFERENCES	4-46

¹ [Taken in part from: J F. Ziegler, J. Appl. Phys / Rev. Appl. Phys., **85**, 1249-1272 (1999)]

HISTORICAL REVIEW

Soon after the discovery of energetic particle emission from radioactive materials, there was interest in how these corpuscles were slowed down in traversing matter. From her work in 1898-1899, Marie Curie stated the hypothesis that "les rayons alpha sont des projectiles matériels susceptibles de perdre de leur vitesse en traversant la matière."¹ Many scientists immediately realized that since these particles could penetrate thin films, such experiments might finally unravel the secrets of the atom. Early attempts to create a particle energy loss theory were inconclusive for there was not yet an accurate proposed model of the atom. The theoretical treatment for the scattering of two point charges was derived by J. J. Thomson in his classic book on electricity.² Much of the traditional particle energy-loss symbolism can be traced to this book which introduced a comprehensive treatment for classical Coulombic scattering between energetic charged particles. This work, however, did not attempt to calculate actual stopping powers.

Enough experimental evidence of radioactive particle interactions with matter was collected in the next decade to make stopping power theory one of the central concerns of those attempting to develop an atomic model. In 1909, Geiger and Marsden were studying the penetration of alpha-particles through thin foils, and the spread of the trajectories after emerging from the back side.³ They reported that about 0.01% of the heavy alpha-particles were scattered backwards from the target, and from an analysis of the data statistics such backscattered events had to be from isolated single collisions. Two years later, Rutherford was able to demonstrate theoretically that the backscattering was indeed due to a single event, and by analyzing this and electron scattering data he was able to first calculate that the *nucleus* of Al atoms must have a mass of about 22 and platinum would have a mass of 138.⁴ J. J. Thomson, director of the prestigious Cavendish Laboratory, and Niels Bohr, a fresh post-doctoral scientist who had left the Cavendish lab for Rutherford's Manchester Laboratory, published almost simultaneously an analysis of the stopping of charged particles by matter.⁵ These papers illustrate much of their divergent ideas on the model of an atom. Thomson incredibly ignored the alpha-particle backscattering measurements of Geiger³ and the Rutherford heavy-particle scattering theory⁴ which emphasized the atomic positive charge must be concentrated within the atom. But the nuclear atom with a heavy positively-charged core was the basis of Bohr's ideas.^{6,7} Bohr's early work is instructive because for the first time a unified theory of stopping was attempted, and we can see in this and in similar works the essential problems of stopping theory:

- How does an energetic charged particle (a point charge) lose energy to the quantized electron plasma of a solid (inelastic energy loss)?
- How do you incorporate into this interaction simultaneous distortion of the electron plasma caused by the particle (target polarization)?
- How can you extend the point charge-plasma interaction to that for a finite moving atom in a plasma?
- How do you estimate the degree of ionization of the moving atom and describe its electrons when it is both ionized and within an electron plasma?
- How do you calculate the screened Coulomb scattering of the moving atom with each heavy target nucleus it passes?
- How do you include relativistic corrections to all of the above?

This is a brief list of the major problems encountered, and scientific interest shifts back and forth between them over the decades because of external scientific tidal forces such as (a) the development of quantum scattering in the nineteen twenties, (b) the study of nuclear fission in the

thirties and forties, (c) the study of nuclear physics in the fifties, (d) the technological applications of ion implantation for material modification in the sixties, and the use of ion beams in material analysis and in radiation oncology in the seventies. This ebb and flow of interest continues because of the recurrent importance of the problem, and the difficulty of calculating the penetration of energetic atoms in solids from first principles. We briefly review some of the historical milestones in this field below.

One of Bohr's original conclusions was that the energy loss of ions passing through matter could be divided into two components: nuclear stopping (energy loss to the medium's atomic positive cores) and electronic stopping (energy loss to the medium's light electrons). Bohr, in his first papers, correctly deduced that the electronic stopping would be far greater than the nuclear stopping for energetic light ions such as are emitted by radioactive sources. This conclusion was based on recoil kinematics considering only the relative masses and abundance of the target electrons and nuclei. Bohr further introduced atomic structure into stopping theory by giving target electrons the orbital frequencies obtained from optical spectra and calculating the energy transferred to such harmonic oscillators. He noted that the experimentally reported stopping powers for heavy atom targets indicated that many electrons in these targets must be more tightly bound than the optical data suggested. He also realized that his accounting of the energy loss process was seriously limited by a lack of knowledge of the charge state of the ion inside the matter, i.e., its effective charge in its interaction with the target medium.

A major advance in understanding stopping powers came 20 years later when Bethe⁸⁹ and Bloch¹⁰¹¹ restated the problems from the perspective of quantum mechanics, and derived in the Born approximation the fundamental equations for the stopping of very fast particles in a quantized medium. This theoretical approach remains the basic method for evaluating the energy loss of light particles with velocities above 1 MeV/amu.

THE BETHE-BLOCH EQUATION

The stopping of high velocity light ions in matter usually assumes two major simplifications in stopping theory: (1) the ion is moving much faster than the target electrons and is fully stripped of its electrons, and (2) the ion is much heavier than the target electrons. In general, this paper will treat light ions (H, He and Li) with energies between 1 MeV/u to 10 GeV/u. Considerations of partial ion neutralization at lower velocities establishes the lower energy limit (see details in the section *Low Velocity Limits*), while the upper energy limit is constrained by the lack of experimental data.

Extended reviews of the early concepts of Bohr, Bethe and Bloch, with significant additions using quantum-mechanical perturbation treatments, have been written by Fano¹²⁻¹⁶, Inokuti¹⁷, Bichsel¹⁸, Sigmund¹⁹, Jackson²⁰ and Ahlen²¹.

Relativistic quantum mechanics allows quite different approaches to analyze the transfer of energy from the particle to the medium, and the results of using various theoretical procedures are sometimes difficult to compare. All attempts to create tables of high energy ion stopping powers have required normalization of the theory to experimental data to obtain accurate values (see books by Fano²², Northcliffe²³, Janni²⁴, Andersen²⁵, Ziegler²⁶ and the ICRU²⁷).

Bohr's early work evaluated the classical stopping of a fast heavy charged particle to an electron bound in a harmonic potential.^{6,7} This early work was extended by others who applied quantum mechanics to particle energy loss - of note was the early work by Henderson in 1922, who considered the energy loss by a particle to an atom with quantized electrons, but ignored distant interactions or any collective excitation of the electronic medium of the target.²⁸ Gaunt, in 1927, applied a quantum mechanical treatment to the perturbation of atomic electrons by a charged

particle.²⁹ Unfortunately, Gaunt made an error in one approximation that led to the wrong formula for the particle's energy loss.³⁰ Bethe presented the first complete solution to high velocity stopping using the first Born approximation where the entire physical system is considered quantized.⁸ Then Moller³¹ and Bethe⁹ extended these ideas by including relativistic corrections.

The following theoretical review will assume the following symbols:

Z_1	=	Particle atomic number
M_1	=	Particle mass (u)
E	=	Particle energy
v	=	Particle velocity
v_0	=	The Bohr velocity = $e^2/h = 25 \text{ keV/u}$
b	=	Impact parameter of particle to a target electron
Z_2	=	Target atomic number
M_2	=	Target atomic weight (u)
N	=	Density of target atoms per unit volume
e	=	Charge of an electron
m_e	=	Mass of an electron
c	=	Velocity of light
β	=	Relative particle velocity, v/c

Certain primary assumptions pertain to all theories described. The particle is assumed to interact with the target only through electromagnetic forces. Any energy loss to nuclear reactions between the particle and the target nuclei are ignored. For high velocities, Bethe showed that the ratio of the energy loss by the particle to the target electrons was greater than the loss to the heavier target nuclei by at least $M_2/m_e Z_2$.⁸ Less than 0.1% of the energy loss of high velocity particles is to the target nuclei (ignoring nuclear reactions). Hence we shall not evaluate the energy loss between the particle and the target nuclei.

With the above assumptions, we can reduce the energy loss problem to one which considers only the energy loss by the high velocity particle to the atomic electrons, which are bound to infinitely heavy nuclei.

There are two basic approaches used to evaluate a particle's energy loss to target electrons. These are the Bohr approach, which is dependent on the impact parameter between the particle's trajectory and the target nucleus, and the Bethe approach which depends on momentum transfer from the particle to the target electrons. Bethe's approach was necessary since quantum mechanics prohibits a particle with a well defined momentum having a spatially localized position. Hence Bohr's concept of an impact parameter (defined in 1913, before quantum mechanics was developed) could not be directly upgraded to wave mechanics. There was no quantized solution to close collisions if one attempted to use the Bohr impact parameter concepts.

Briefly, the highlights of the Bethe-Bloch theory are described below. The reader is referred to the lengthy tutorials cited in the first paragraph of this paper for extended derivations.

The classical Bohr approach considers a heavy charged particle of charge, $Z_1 e$, moving at a velocity, v , passing near a light electron of charge, e , and mass, m , at an impact parameter, b . (See Chapter 2 for extended details of binary collisions and these parameters.) The transverse momentum impulse, Δp , to the light electron is:

$$\text{Eq. 4-1} \quad \Delta p = \int_{-\infty}^{\infty} e \bar{E}(t) dt = \frac{2Z_1 e^2}{bv}$$

where \bar{E} is the transverse electrical field. The energy transferred is then:

$$\text{Eq. 4-2} \quad \Delta E = \frac{(\Delta p)^2}{2m} = \frac{2Z_1^2 e^4}{mv^2} \left(\frac{1}{b^2} \right)$$

This expression assumes that the electron does not move much relative to the impact parameter, b . To obtain the stopping power, S , this transferred energy must be integrated over all possible impact parameters, b . Assuming the target is made of atoms of atomic number, Z_2 , the energy loss per target atom is :

$$\text{Eq. 4-3} \quad S = 2\pi Z_2 \int \Delta E(b) b db$$

$$\text{Eq. 4-4} \quad = 4\pi Z_2 \frac{Z_1^2 e^4}{mv^2} \int_0^{\infty} \frac{1}{b^2} b db$$

The integral of this expression diverges as $b \rightarrow 0$, so it is necessary to argue a minimum impact parameter, b_{\min} . If the electron mass is assumed to be very much smaller than the mass of the incident particle, the electron will recoil strongly for very small impact parameters. Noting that the maximum energy transfer is for a head-on collision, we may use Rutherford two-particle elastic scattering to estimate the closest distance of approach for a head-on collision. This gives a minimum distance of $b_{\min} \sim Z_1 e^2 / mv^2$.

The integral also becomes undefined for $b_{\max} \rightarrow \infty$. This can be made tractable by noting that, for distant collisions, if the interaction is long compared to the orbiting frequency of an electron, the collision will become adiabatic and no energy will be transferred. This suggests a cutoff when the collision time becomes longer than the orbital frequency, $b_{\max} \sim v/\omega$, where ω is the orbital frequency.

Inserting these values for b_{\min} and b_{\max} , the energy loss becomes:

$$\text{Eq. 4-5} \quad \frac{dE}{dx} = 4\pi Z_2 \frac{Z_1^2 e^4}{mv^2} \ln \left(\frac{mv^3}{Z_1 e^2 \omega} \right)$$

The relativistic form of this equation is made by equating the particle's energy, $E = \gamma M_1 c^2$, where $\gamma = 1/(1-\beta^2)^{1/2}$ and $\beta = v/c$. This expands $b_{\max} \sim \gamma v/\omega$, and $b_{\min} \sim Z_1 c^2 / \gamma m v^2$ and the integral becomes:

$$\text{Eq. 4-6} \quad \frac{dE}{dx} = \frac{4\pi Z_2 e^4}{mv^2} Z_1^2 \ln \left(\frac{\gamma^2 m v^3}{Z_1 e^2 \omega} \right)$$

Bohr used this expression to form the basis of his evaluation of the energy loss of a heavy particle to a medium of harmonically bound electrons.⁶

Bloch evaluated the differences between the classical (Bohr) and quantum-mechanical (Bethe) approaches for particles with velocities much larger than the target electrons. He showed that Bohr's approach was valid also in the quantum mechanics of a bound electron if the energy transferred was assumed to be the mean energy loss, summed over all possible atomic transitions. However, Bloch needed to assume the dipole approximation (impact parameter >> orbit diameter) to avoid the localization problem discussed above.

Bloch then analyzed the problem of close collisions. He did not assume, as Bethe had done, that it was valid to consider the electrons to be plane waves in the center of momentum frame. Instead, he confined the electrons to the interior of a cylinder, which then introduced transverse momentum components that interfere with one another under the forces of the electromagnetic interaction. This led to quite different momentum transfers than for the case of Bethe's plane wave scattering.

Bloch then showed that for low momentum transfers, his cylinder confinement radius would be large enough to permit the use of Bethe's plane-wave approach, and so for these collisions the Bethe approach was correct. Further, for large momentum transfers, the wave packets would scatter classically, and hence the Bohr approach would be valid. Thus Bloch found the bridging formulation between the classical Bohr impact-parameter approach, and the quantized Bethe momentum transfer approach to energy loss. Unfortunately, Bloch made a small error in estimating one scattering cross-section, and his final formula as presented in original the paper contains an error.

The original Bethe-Bloch relativistic stopping formula, S may be stated as:

$$\text{Eq. 4-7} \quad S = \frac{4\pi e^4 Z_2}{m_e v^2} Z_1^2 \left[\ln \frac{2mv^2}{\langle I \rangle} - \ln(1-\beta^2) - \beta^2 + \Psi(Z_1) \right]$$

where $\langle I \rangle$ is the averaged excitation potential per electron, and is defined as

$$\text{Eq. 4-8} \quad \ln \langle I \rangle = \sum f_n \ln E_n$$

where the logarithm of the mean ionization potential, $\ln \langle I \rangle$, can be expanded as the dipole oscillator strength for the n th energy level:

$$\text{Eq. 4-9} \quad f_n = \frac{2mE_n}{\hbar^2 Z_2} \left| \sum_j \left\langle n \left| x_j \right| 0 \right\rangle \right|^2$$

Normalization for this sum rule is that $\sum f_n = 1$.

The final term, $\Psi(Z_1)$ in Eq. 4-7, is a small term which contains Bloch's error so that the Bloch result does not reduce to the Bethe result for the limit $Z_1\alpha/\beta \rightarrow 0$, where $\alpha =$ the fine structure constant, $c^2/\hbar c = 1/137$.

Variations of the Bethe-Bloch Equation

The theoretical studies of the energy loss of high velocity particles have been active for almost a century. The earliest works which are still quoted are those by J. J. Thomson - 1903, 1912³², E. Rutherford - 1911³³ and N. Bohr - 1913³⁴. There are many traditions, practices and nomenclature that may make the field difficult to understand. Below we review some of the most widely used conventions.

Fano published various extensions of Bethe's and Bloch's work which summarized most of the theoretical work in the prior fifty years.¹²⁻¹⁵ The reader is referred to Fano's landmark review paper for a detailed derivation of many concepts and approximations.¹⁶

Fano's approach was to consider the momentum, q , transferred to a bound electron with an energy transfer, ΔE . Consider three regions for the energy transfer to an atomic electron at a distance, r , from the particle:

- For small ΔE , one assumes that $qr \ll \hbar$, so that the interaction between the particle and

electron reduces to dipole matrix elements.

2. For mid- ΔE (the definition of mid- ΔE is quite complex), one assumes that only the longitudinal electromagnetic terms of the interaction contribute to the momentum transfer.

3. For large ΔE , one assumes that the target electrons may be considered to be unbound, and the transfer can be reduced to standard two-particle relativistic interactions.

Assuming these approximations, Fano described a relativistic version of the Bethe-Bloch energy loss formula where two additional corrective terms are included, the **Shell Correction** term, C/Z_2 , and the **Density Effect** correction term, $\delta/2$ (these will be described in detail later):

$$\text{Eq. 4-10} \quad S = \frac{4\pi e^4 Z_2}{m_e v^2} Z_i^2 \left[\ln \frac{2mv^2}{\langle I \rangle} - \ln(1 - \beta^2) - \beta^2 - \frac{C}{Z_2} - \frac{\delta}{2} \right]$$

which is usually simplified using the definitions:

$$\text{Eq. 4-11} \quad r_0 \equiv c^2/m_e c^2 \quad (\text{the Bohr "classical" electron radius})$$

$$f(\beta) \equiv \ln[2mc^2\beta^2/(I-\beta^2)] - \beta^2 \quad (\text{combining the relativistic terms})$$

$$\text{Eq. 4-12} \quad S = \frac{4\pi r_0^2 m_e c^2 Z_2}{\beta^2} Z_i^2 \left[f(\beta) - \ln \langle I \rangle - \frac{C}{Z_2} - \frac{\delta}{2} \right]$$

The prefactor constant to this equation can also be simplified, using the definition $\kappa \equiv 4\pi r_0^2 m_e c^2$. The pre-factor constants have the value, $4\pi r_0^2 m_e c^2 = 0.0005099$, for stopping in units of eV/(10^{15} atoms/cm²), which is about the energy loss per mono-layer in a solid. This pre-factor may be converted to stopping units of keV/(mg/cm²) by multiplying the above pre-factor by $(N_0/10^{21}M_2)$, where N_0 = Avagadro's number, 6.02213×10^{23} , and M_2 is the target atomic weight (u). Thus the stopping pre-factor, κ , is $0.3071/M_2$ for stopping units of keV/(mg/cm²), which is the energy loss per mg/cm² of the target transited.

There have been many corrections proposed to improve on Fano's theoretical approximations. Traditionally, this is done by expanding this equation in powers of Z_i , which can be used to add additional corrections to the ion and target interaction:

The Bethe-Bloch stopping power formula is commonly expressed as:

$$\text{Eq. 4-13} \quad S = \frac{\kappa Z_2}{\beta^2} Z_i^2 [L_0(\beta) + Z_1 L_1(\beta) + Z_1^2 L_2(\beta) \dots]$$

where the term, L_0 , contains all the correction factors of the Fano formulation, Eq. 4-12, and extra higher order terms are added, $L_1, L_2 \dots$, which will be discussed below.

The term in the brackets of Eq. 4-13 is defined as the **Stopping Number**, $L(\beta)$, and this expansion will contain all the corrections to the basic two-particle energy loss process.

$$\text{Eq. 4-14} \quad L(\beta) \equiv L_0(\beta) + Z_1 L_1(\beta) + Z_1^2 L_2(\beta) \dots$$

This reduces the Bethe-Bloch formula to its simplest notation:

$$\text{Eq. 4-15} \quad S = \frac{\kappa Z_2}{\beta^2} Z_i^2 L(\beta)$$

The second term of the stopping number expansion, L_1 , is usually called the **Barkas-Andersen**

Correction or the Z_i^3 **Correction**, and the third term, L_2 , is called the **Bloch Correction** or the Z_i^4 **Correction**. Note that only the stopping number term L_1 contains an odd power of Z_i , and hence would be sensitive to the sign of the particle's charge (positive or negative). The implications of this are discussed in the later section on the Barkas-Andersen effect.

Rigorously, the name "Barkas-Andersen Correction" should apply to the sum of all odd-power terms of Z_i in Eq. 4-13 because it is based in part on the stopping differences between particles with opposite charge signs (+ or -). But since this term is historically used only for the factor $L_1 Z_i$, we shall continue this practice.

Low Velocity Limit of the Bethe-Bloch Theory: Particle Neutralization

The above discussion concerns the evaluation of the energy loss by a heavy charged particle to target electrons. However, at low velocities, the particle may capture electrons from the target and partially neutralize its nuclear charge. The Bethe-Bloch equation, in all its forms, requires a constant particle charge. Thus a lower limit to its applicability is necessary. Estimating the degree of particle neutralization has a long theoretical history. Various approaches may be understood by looking at the basic scaling relationships of the Thomas-Fermi atom:

Eq. 4-16

Charge density	$\equiv \rho \propto Z^2$
Electron binding energy	$\equiv E_b \propto Z^{7/3}$
Binding energy / electron	$\equiv e_b \propto Z^{4/3}$
Electron velocity	$\equiv v_e \propto Z^{2/3}$

Historically, scaling laws for heavy ions first received considerable attention in 1938-41 because of interest in nuclear fission experiments. It was recognized that a theory of stopping powers and ranges required both understanding the stopping due to the large charge-state of fission fragments, and also an understanding of neutralization of the particles from captured electrons. Lamb suggested that the particle's electron binding energies would be the primary influence in determining the degree of ionization of the fission fragments in matter,³⁵ while Bohr suggested that the electron orbital velocities would be the critical parameter.^{36,37} Later evidence supported the Bohr view that one could estimate the particle's charge neutralization by assuming it to be stripped of all electrons whose classical orbital velocities were less than the ion velocity. This Bohr concept was later set in explicit form by Northcliffe as:³⁸

$$\text{Eq. 4-17} \quad \frac{Z_i^*}{Z_i} = 1 - \exp \left[\frac{-v_i}{v_0 Z_i^{2/3}} \right]$$

where Z_i^* is the statistical net charge on the partially neutralized ion. At high velocities, $Z_i^*/Z_i = 1$ when the ion is fully stripped. This expression is useful in the analysis of heavy ion stopping data, but it is not considered accurate for low mass ions. As an example, Eq. 4-17 would indicate that protons could be expected to be 99% stripped at 529 keV, and 99.9% stripped at 1191 keV. For He ions these energies are 840 and 1890 keV. Various experiments with light ions indicate that these energics are too high (there has been extensive discussions of whether protons are ever partially neutralized while in motion, since its electron's orbital diameter would be greater than the mean distance between atoms in most solids).

The term *statistical net charge* (or *effective charge*) is sometimes defined as the charge state required to reduce calculated Bethe-Bloch stopping to agree with experimental stopping values.

The implication is that it accounts for the partial neutralization of some of the ions, or it compensates for polarization of the target electrons. Clearly, a proton cannot have a charge of 0.9 units. But, measured low velocity proton stopping powers, averaged over many protons, may be reduced to that calculated for a particle with this effective charge due to partial neutralization of some of the protons. However, a more reasonable interpretation is that the Bethe-Bloch theory is being used beyond its limits, and that this term is just a fitting parameter.

The problem of partial particle neutralization indicates the difficulty of a clear definition of where "high velocity" particle stopping starts, and when it can be assumed that the particle's nuclear charge is unshielded by orbital electrons. For light ions, H and He, the Bethe-Bloch theory is usually assumed to hold for energies above 1 MeV/amu.²⁷

THE PRIMARY STOPPING NUMBER, L_0

The stopping number term, L_0 , contains the largest corrections to the basic high-energy stopping power formula. Fano expressed it theoretically as:

$$Eq. 4-18 \quad L_0 = \frac{1}{2} \ln \left(\frac{2m_e c^2 \beta^2 \Delta E_{\max}}{1 - \beta^2} \right) - \beta^2 - \frac{C}{Z_2} - \ln \langle I \rangle - \frac{\delta}{2}$$

where C/Z_2 is the *shell correction* for the target atom, $\langle I \rangle$ is the *mean ionization energy* of the target atom, and $\delta/2$ is the *density effect* correction. These three terms correct for:

C/Z_2 - This *shell correction* term corrects the assumption that the ion velocity is much larger than the target electron velocity. The term is usually calculated by detailed accounting of the particle's interaction with each electronic orbit in various elements. This term contributes up to a 6% correction to stopping powers, and will be discussed in considerable detail later.

$\ln \langle I \rangle$ This *mean ionization* term corrects for the quantum mechanical energy levels available for transfer of energy to target electrons. It can also be used to correct for any band-gap in solids and also target phase changes (e.g. stopping differences in targets of water in liquid or vapor states). This term will be discussed in detail later.

$\delta/2$ - This *density effect* term corrects for polarization effects in the target, which reduces the stopping power since the ion's electromagnetic fields may not be at the assumed free-space values, but reduced by the dielectric constant of the target medium.

The term ΔE_{\max} , in Eq. 4-18, is the largest possible energy loss in a single collision, and can be defined as:²⁷

$$Eq. 4-19 \quad \Delta E_{\max} = \left(\frac{2m_e c^2 \beta^2}{1 - \beta^2} \right) \left(1 + \frac{2m_e}{M_i (1 - \beta^2)^{1/2}} + \left(\frac{m_e}{M_i} \right)^2 \right)^{-1}$$

The magnitude the right-hand correction term to ΔE_{\max} is quite small, and it is usually set to unity. In is shown the effect on calculated stopping powers by considering the full term, Eq. 4-19, and using on the abbreviated term,

$$Eq. 4-20 \quad \Delta E_{\max} \approx \left(\frac{2m_e c^2 \beta^2}{1 - \beta^2} \right)$$

The full term, Eq. 4-19, adds a correction which is always below 0.1%, and usually is contributes about 0.01%, which is beyond the accuracy of other corrective terms. So we shall use the abbreviated form for ΔE_{\max} . See Figure 4-1.

Note that for non-relativistic energies,

$$\text{Eq. 4-21} \quad \Delta E_{\max} \approx \left(\frac{2m_e c^2 \beta^2}{1 - \beta^2} \right) \approx 2m_e v^2$$

The term ΔE_{\min} is also sometimes used to restrict energy loss processes, which might occur with band-gap materials or insulators. Eq. 4-19 may be considered as the theoretical form of L_0 , since the term ΔE_{\min} is derived by considerations of the target medium.

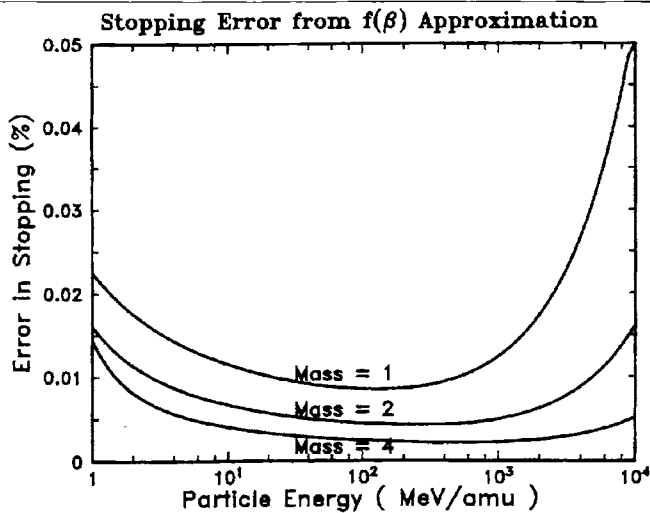


Figure 4-1 Evaluation of the term, ΔE_{\max} , on Stopping Powers

The traditional derivation of the first stopping number term, L_0 , includes a term which indicates the largest possible energy loss in a single collision with a free electron, Eq. 4-19. This plot shows the error introduced to calculated stopping powers by approximating this term with the simpler form, Eq. 4-20, $\Delta E_{\max} = (2m_e c^2 \beta^2 / 1 - \beta^2)$. The full term adds a stopping correction which is always below 0.1% in effect, and usually is about 0.01%, which is far greater accuracy than other terms. So we shall use the abbreviated approximate form for ΔE_{\max} hereafter.

By substituting Eq. 4-21 into Eq. 4-18, the stopping number term, L_0 , is converted to an equivalent form that is widely used for the analysis of experimental data:

$$\text{Eq. 4-22} \quad L_0 = \ln \left(\frac{2m_e c^2 \beta^2}{1 - \beta^2} \right) - \beta^2 - \frac{C}{Z_2} - \ln < I > - \frac{\delta}{2}$$

which is commonly simplified with the definition:

$$\text{Eq. 4-11} \quad f(\beta) \equiv \ln [2mc^2 \beta^2 / (1 - \beta^2)] - \beta^2$$

to obtain:

Eq. 4-23

$$L_0 = f(\beta) - \frac{C}{Z_2} - \ln <1> - \frac{\delta}{2}$$

With this equation, and using the Bethe-Bloch equation, Eq. 4-13, experimental data may be directly compared to theoretical evaluations of L_0 .

Shell Corrections, C/Z_2

Shell corrections constitute a large correction to proton stopping powers in the energy range of 1-100 MeV, with a maximum correction of about 6%. It corrects the Bethe-Bloch theory requirement that the particle's velocity is far greater than the bound electron velocity. As a particle velocity decreases from relativistic energies, the particle-electron collisions need to be considered with detailed evaluation of each target electron's orbital bonding in order to obtain accurate stopping powers.

Shell corrections have been calculated using various approximations. As we shall show, these all produce approximately the same curves and are effective in correcting stopping powers. The two most common approaches to calculate non-relativistic shell corrections are:

Hydrogenic Wave Functions - This HWF approach considers the particle interacting with individual target atom electrons which are described by hydrogenic wave functions.

Local Density Approximation - This LDA approach considers a particle interacting with a free electron gas (FEG) of various densities. The shell correction is extracted by assuming the target to be a linear superposition of FEG corrections based on their weighted densities in the target.

An early example of the results of these approaches is shown in Figure 4-2.

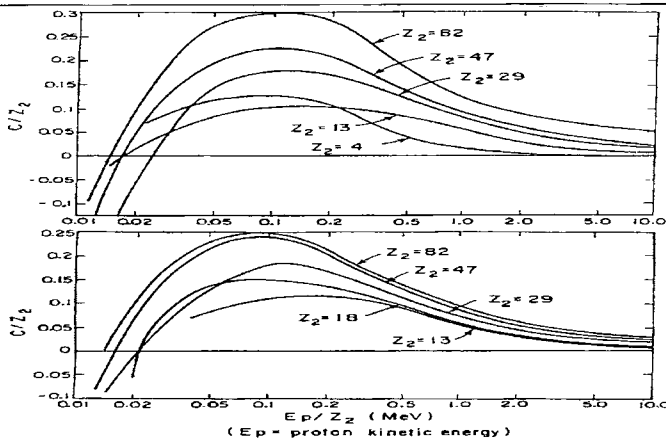


Figure 4-2 Early Shell Corrections to High Velocity Stopping (1963)

The basic stopping power formula for high velocity particles assumes that the particle is moving much faster than the target electrons. The term "Shell Correction" is given to factors which correct for interactions in which this assumption may not be accurate, for example for interactions with inner-shell electrons. In the upper set of curves are calculations of LDA shell corrections extracted from stopping interactions (from Fano in 1963 [12]). The lower curves come from shell corrections based on interactions between a particle with hydrogenic electrons representing various target atom shells (from Bichsel in 1972 [46]). Both methods yield similar curves.

There is no comprehensive theory of shell corrections which includes full relativistic interactions between the particle and the target, so this aspect of shell corrections will not be reviewed. Further, all target electrons are considered to be in quiescent orbits, unperturbed by nearby electrons which are also absorbing energy from the particle (the binary collision approximation).

Shell Corrections using Hydrogenic Wave Functions

Many authors have contributed to the theoretical definition of non-relativistic shell corrections using hydrogenic wave functions, see discussions by Bohr (39), Walske (40,41), Khandelwal (42), and Fano (16). This approach assumes that the shell correction is the sum of contributions from each target atom electron, without correlation. Early corrections were published for the k-shells by Walske (1952)⁴⁰ and Khandelwal (1968)⁴², for the l-shell by Walske (1956)⁴¹, Bichsel (1967)⁴³ and Khandelwal (1968)⁴², and for the m-shell by Khandelwal and Merzbacher (1966)⁴⁴.

The most widely used shell corrections of this type are those by Bichsel using the hydrogenic wave function approach.⁴⁵⁻⁴⁸ Examples of his work are shown in Figure 4-3.

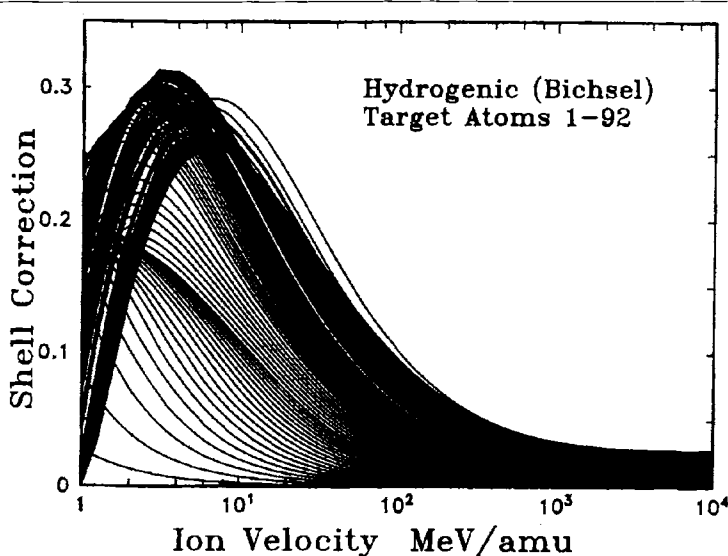


Figure 4-3 Bichsel Hydrogenic Shell Corrections

Shown are Bichsel's shell corrections based on hydrogenic wave functions, published after twenty years of refinements.⁴⁵⁻⁴⁸ The theoretical concepts contain several parameters which depend on experimental data for accuracy. The curves go from that for hydrogen targets (lowest curve) to uranium (furthest right curve). The shell corrections show a smooth and gradual change of shape, with the only small abrupt changes occurring when new shells are incorporated into the calculation.

The primary problem of this type of shell correction is that it is dependent on experimental stopping powers of unknown accuracy. Further, when the author extracts the shell correction, its magnitude depends on the other stopping corrections which have been used to reduce the stopping data. For example, the Barkas-Andersen correction at 1 MeV/amu has about a 10% effect on

stopping. However, the magnitude of this effect was not well determined before about 1990. Tabulations of hydrogenic shell corrections such as quoted in ICRU-37⁶² depended on a Barkas-Andersen correction factor which was about a factor of two in error. Thus the shell corrections, which were fit using parameters extracted from experimental data, would also be in error.

Shell Corrections using the Local Density Approximation

In contrast to the hydrogenic-electron approach, shell corrections may also be calculated without any free parameters, and hence their accuracy is fixed. The local density approximation (LDA) may be used to obtain shell corrections, as first indicated by Fano. This method calculates the stopping of a particle in an electronic medium, and then extracts the shell corrections by inverting the Bethe-Bloch equation, Eq. 4-13, expanding L_0 , and solving for the shell correction.¹⁶ This inversion is shown below, with the calculated stopping of the particle indicated by the term, S_{calc} (to distinguish it from S_{exp} which will be used later):

$$\text{Eq. 4-24} \quad \frac{C}{Z_2} = f(\beta) - \ln < I > - \frac{\beta^2 S_{\text{calc}}}{\kappa Z_2 Z_1^2} - \frac{\delta}{2} + Z_1 L_1 + Z_1^2 L_2$$

Examples of obtaining shell corrections using this method requires the calculation of stopping powers, S , using a different method, and then using Eq. 4-24 to extract shell corrections. Since calculations of stopping powers using the local density approximation does not use explicit shell corrections, the use of Eq. 4-24 allows these values to be directly compared to those calculated using hydrogenic wave functions.

The first attempt to evaluate electronic stopping cross-sections for protons in solids using the Lindhard stopping formalism and the local density approximation was by Bonderup who used Lenz-Jensen atoms to represent the atoms in the solid.⁴⁹ This work was extended to isolated Hartree-Fock atoms by Rousseau et al.⁴⁹ and to actual solid-state charge distributions by Ziegler.²⁶

The LDA approach assumes that the gradient of electron densities in the target is small, and that the response of any volume element of the target is independent of other elements. The first assumption can be made tractable by using very small volume elements, but any error introduced by the second assumption is difficult to evaluate. Note that the LDA approach can not directly evaluate the effects of many basic solid state parameters such as band gaps and surfaces.

Note that Eq. 4-24 requires the knowledge of the mean ionization potential, $< I >$. The theoretical calculation of the mean ionization potential has a long history, for it is a straight-forward calculation which may be done with almost any theoretical atom. Bonderup used the estimate that $< I > = 11.4 Z_2$ (eV), and then solved for the shell correction term, C/Z_2 .

There have been many other calculations of $< I >$. Summaries of these calculations may be found in reviews such as by Fano²², Ziegler⁵⁰, Ahlen²¹ or the ICRU²⁷. In the local density approximation, the value of $< I >$ may be calculated using :^{51,88,89,52}

$$\text{Eq. 4-25} \quad \ln < I > = \frac{1}{Z_2} \int_V \ln(\chi \hbar \omega_0) \rho dV$$

Where Z_2 is the target atom atomic number, ω_0 is the classical plasma frequency, $\omega_0 = (4 \pi \rho e^2 / m)^{1/2}$, and χ is a constant of the order of 1 and has been estimated by various theorists to be between 1 and 1.5. Shown in Figure 4-4 are shell corrections calculated using the above formalism with Hartree-Fock solid-state charge distributions. One primary difference between this approach and using hydrogenic wave functions is the LDA approach is an *ab initio* calculation, without any free parameters.

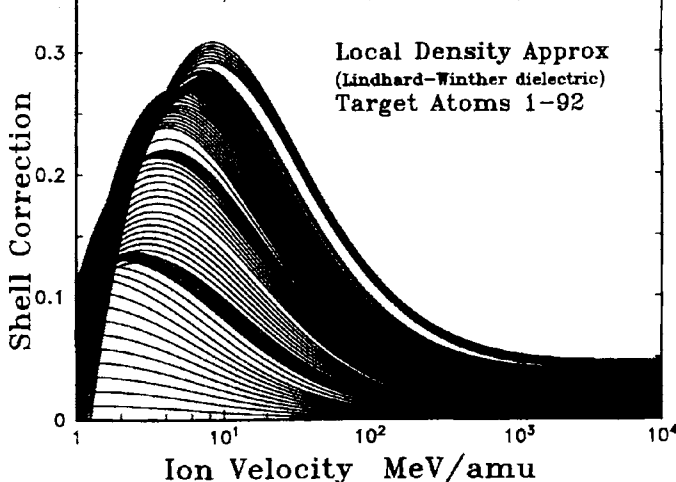


Figure 4-4 Lindhard Winther LDA Shell Corrections

Shown are shell corrections by Ziegler, based on Lindhard Winther's theory of particle stopping in a free electron gas, with the local density approximation (LDA) being used to generate shell corrections. This calculation is *ab initio*, without free parameters. The curves go from that for hydrogen targets (lowest curve) to uranium (highest curve). The shell corrections show a smooth and gradual change of shape, with the only small abrupt changes occurring when new shells are incorporated into the calculation. Although this calculation is based on totally different assumptions as those based hydrogenic atoms, the results are quite similar.

Empirical Summed Shell and Ionization Corrections

Fano suggested²² that the calculation of the mean ionization potential, and the shell correction, could properly be linked as a single term which could be evaluated directly from experimental stopping data, S_{exp} , by rearranging Eq. 4-24:

$$\text{Eq. 4-26} \quad \ln <I> + \frac{C}{Z_2} = f(\beta) - \left[\frac{S_{\text{exp}} \beta^2}{\kappa Z_2 Z_1^2} \right] - \frac{\delta}{2} + Z_1 L_1 + Z_1^2 L_2$$

where S_{exp} is the experimentally measured electronic stopping power. This approach has the advantage of isolating the two factors in the Bethe-Bloch equation which require extensive theoretical models, i.e. the mean ionization potential, $<I>$, and the shell correction, C/Z_2 . Using this equation, experimental data may be shown in reduced form and compared to theoretical calculations.

The importance of this approach is for the interpolation of stopping powers to targets with little experimental data. If the summed terms could be directly obtained from experimental data, then these can be used to interpolate for stopping powers of similar targets without experimental data. This technique was first used by Ziegler to extract the summed correction terms in order to normalize stopping calculations for targets without data, or to extrapolate to energies without experimental data.⁵⁰

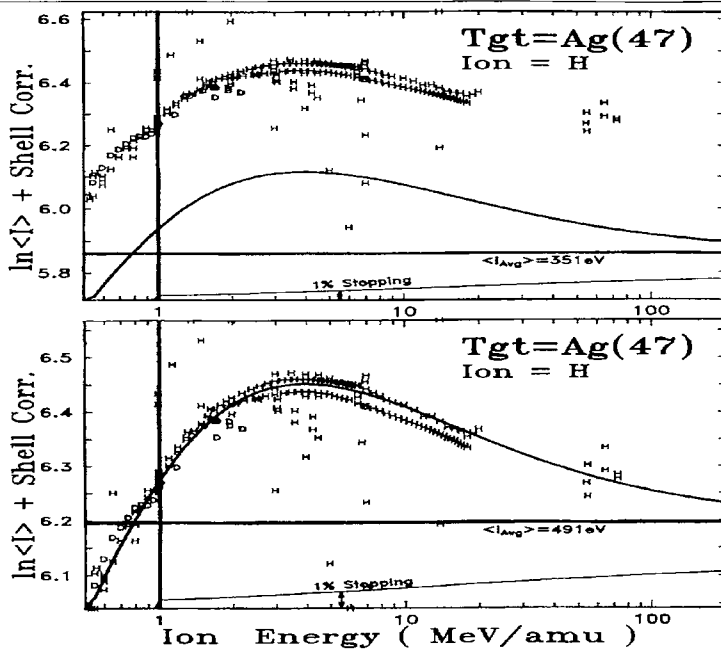


Figure 4-5 Determining ($\ln\langle I \rangle + \text{Shell Corrections}$) for Ag(47)

The upper figure shows experimental data for the stopping of H ions in a target of silver, Ag(47), from 26 papers. The data has been reduced using Eq. 4-26, so the plot indicates the summed terms of $\ln\langle I \rangle + C/Z_2$ as a function of ion energy, MeV/u. The curved line shows the summed corrections, while the straight line indicates the calculated value of $\langle I \rangle = 351$ eV, using Eq. 4-25. The value of $\langle I \rangle$ can be empirically determined by moving the curve vertically until it fits the data. The lower figure shows the summed corrections adjusted by increasing the fitted value of $\langle I \rangle$ to 491 eV from the original 351 eV. The theoretical curve agrees well with the data, and can be used to extrapolate to higher energies with confidence.

An example of this is shown in Figure 4-5 for stopping data for H ions in silver, Ag(47). The data has been reduced using Eq. 4-26, so the plot indicates the summed terms of $\ln\langle I \rangle + C/Z_2$ as a function of ion energy, MeV/u. The curved line shows the theoretical summed corrections, while the straight line indicates the calculated value of $\langle I \rangle = 351$ eV, which was determined using Eq. 4-25. The value of $\langle I \rangle$ can be empirically determined by moving the curve vertically until it fits the data. The lower figure shows the summed corrections adjusted by increasing the value of $\langle I \rangle$ to 491 eV from the original 351 eV. The theoretical curve agrees well with the data, and can be used to extrapolate to higher energies with confidence.

The amount that these terms modify the basic Bethe-Bloch stopping power is indicated by the line called "1 % Stopping" in Figure 4-5 . The gap between this line and the thick $\langle I \rangle$ line indicates a 1% change in stopping power. At 10 MeV/u, the shell correction modifies the stopping power by about 6%, while at 100 MeV/u the correction is 1%.

If one wishes to include ions heavier than protons, corrections have to be made for the Barkas-

Andersen effect (the Z_i^3 effect) and for possible neutralization of the particle. These corrections, discussed later, have been applied to the He data. Note on the right of both plots is a tabulation of the sources for all the plotted data, with the number of data points above 4 MeV from each citation. A total of 25 experimental papers have been published on the stopping of H in Ag at high energy, with a total of 105 data points above 4 MeV.

With the good agreement between the theoretical curve and the data, the curve in Figure 4-5 may be used to extrapolate the stopping of H in Ag to higher energies where there is no data.

Similar data and theoretical curves are shown in Figure 4-6 for H ions stopping in Au. The fit to the data allows one to predict that the stopping power is accurate to about 1% over the energy of the experimental data. For higher energies, the effect of the shell corrections becomes less important (note the divergence of the "1 % Stopping" curve) so this accuracy probably remains at 1%.

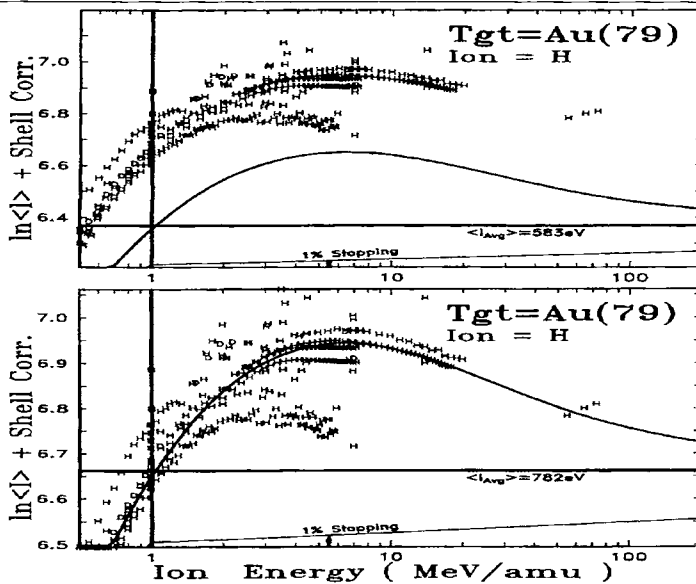


Figure 4-6 Determining ($\ln\langle I \rangle + \text{Shell Corrections}$) for Au(79)

The upper figure shows experimental data for the stopping of H ions in a target of gold, from a total of 26 papers, in a manner similar to that in Figure 4-5. The data has been reduced using Eq. 4-26, so the plot indicates the summed terms of $\ln\langle I \rangle + C/Z_2$ as a function of ion energy, MeV/u. The curved line shows the summed corrections, while the straight line indicates the calculated value of $\langle I \rangle = 583 \text{ eV}$, Eq. 4-25.

The value of $\langle I \rangle$ can be empirically determined by moving the curve vertically until it fits the data. The lower figure shows the summed corrections adjusted by increasing the fitted value of $\langle I \rangle$ to 782 eV from the original 583 eV. The theoretical curve agrees well with the data, and can be used to extrapolate to higher energies with confidence.

If needed, it is possible to include experimental data from heavier ions than H in order to establish an empirical value of $\langle I \rangle$. Figure 4-7 shows experimental data for the stopping of both H and He ions in a target of tantalum, upper figure, and in aluminum, lower figure. The helium data has also

been reduced using Eq. 4-26, so the 4x increase in stopping over protons is removed, and the plot indicates the summed terms of $\ln\langle I \rangle + C/Z_2$ as a function of ion energy, MeV/u.

If one wishes to include ions heavier than protons, corrections have to be made for the Barkas-Andersen effect (the Z_1^3 effect) and for possible neutralization of the particle. These corrections, discussed later, have been applied to the He data.

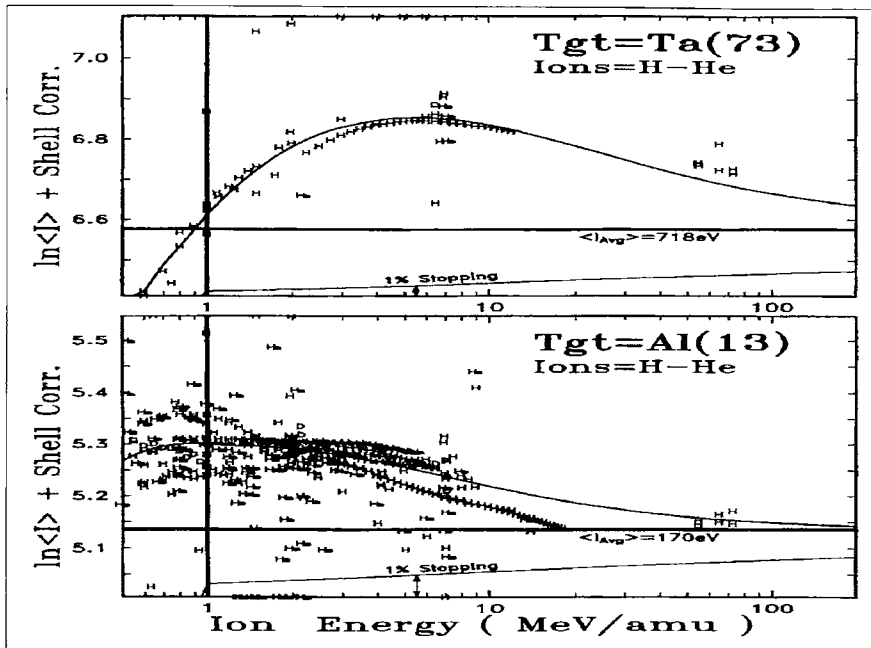


Figure 4-7 Using both H and He data Corrections to Ta(73) and Al(13)

If needed, it is possible to include experimental data from heavier ions than H in order to establish an empirical value of $\langle I \rangle$. The figures shows experimental data for the stopping of both H and He ions in a target of tantalum, upper figure, and in aluminum, lower figure, in a manner similar to that in Figure 4-5 . The data has been reduced using Eq. 4-26, so the plot indicates the summed terms of $\ln\langle I \rangle + C/Z_2$ as a function of ion energy, MeV/u.

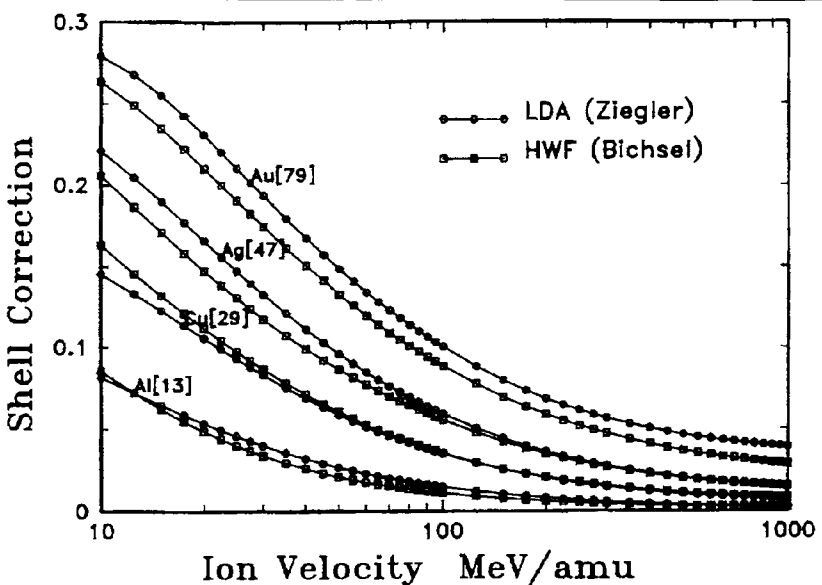


Figure 4-8 Comparison of Shell Corrections

Shown are shell corrections for typical atoms. One set is based on Bichsel's hydrogenic wave function calculations (line with squares) and one set is based on the local density approximation (line with circles). Above 10 MeV, there is not a significant difference between the two calculations. Slight offsets, such as appear in the pair of curves for Au targets, may be compensated by adjusting the mean ionization potential, $\langle I \rangle$, for that target. In practice, using one shell correction theory rather than the other results in less than 0.5% changes in stopping powers for energies above 10 MeV.

Comparison of Two Types of Shell Correction Calculations

The two basic methods of calculating shell corrections has been briefly discussed above. They are not easy to compare from fundamental considerations, since the hydrogenic wave function approach uses parameterized functions based on experimental stopping data, while the LDA approach is *ab initio*, using realistic solid state charge distributions. The differences between the two results may be illustrated by comparing them with each other, and to experimental data.

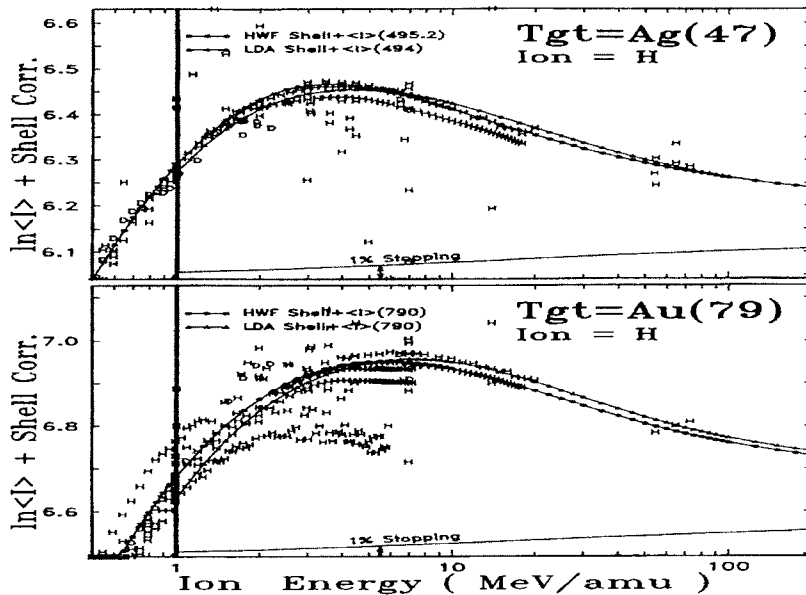


Figure 4-9 Which Shell Correction is Best? Stopping in Ag(47) and Au(79)

The differences between the two basic methods of calculating shell corrections is rather small- any differences will affect stopping powers by only a few percent. Shown above is the summed ($C/Z_2 + \ln\langle I \rangle$) terms for both Bichsel's hydrogenic wave function (HWF) calculations, and Ziegler's LDA calculation based on the Lindhard-Winther formalism. Proton stopping data is reduced using Eq. 4-26. Typical data is usually quoted as accurate to better than 1%, however the data scatter is greater than that. It is difficult to determine which curve more accurately fits the data. The hydrogenic shell correction indicates a higher correction for lower energies, and a lower correction for mid energies.

Shown in Figure 4-8 are representative examples of the shell corrections for four elements using both approaches. The difference between these shell corrections for the energies above 10 MeV/u amounts to, at most, about 0.5% in stopping power. Considering the completely different formalism upon which each is based, this is remarkable agreement.

Shown in Figure 4-9 and Figure 4-10 are several examples comparing the two types of shell corrections with experimental data. All of these plots illustrate that although there are differences in the two shell corrections, it is difficult from the existing experimental data to determine which is more accurate.

Figure 4-9 shows two plots for experimental stopping in silver and gold. In both cases, the experimental stopping is reduced by using the Bethe-Bloch equation, Eq. 4-26, to extract the correction terms, $\ln\langle I \rangle + C/Z_2$. At the bottom of each plot is a line marked "1% Stopping" which indicates the shell magnitude which affect the stopping power by 1%. Two significant points emerge from these plots: (1) The scatter of data (several percent in stopping) is far greater than the estimated experimental accuracy of individual papers (which typically are quoted as accurate to

~0.2%), and (2) because of the wide scatter in data, neither calculated shell correction curve is obviously more accurate.

Figure 4-10 shows similar data and shell corrections for targets of Cu and Al. For the Cu target, the hydrogenic shell corrections fit the low energy data better, but completely miss the high energy data points. Conversely, the LDA shell corrections appear to deviate from the data below 4 MeV/amu.

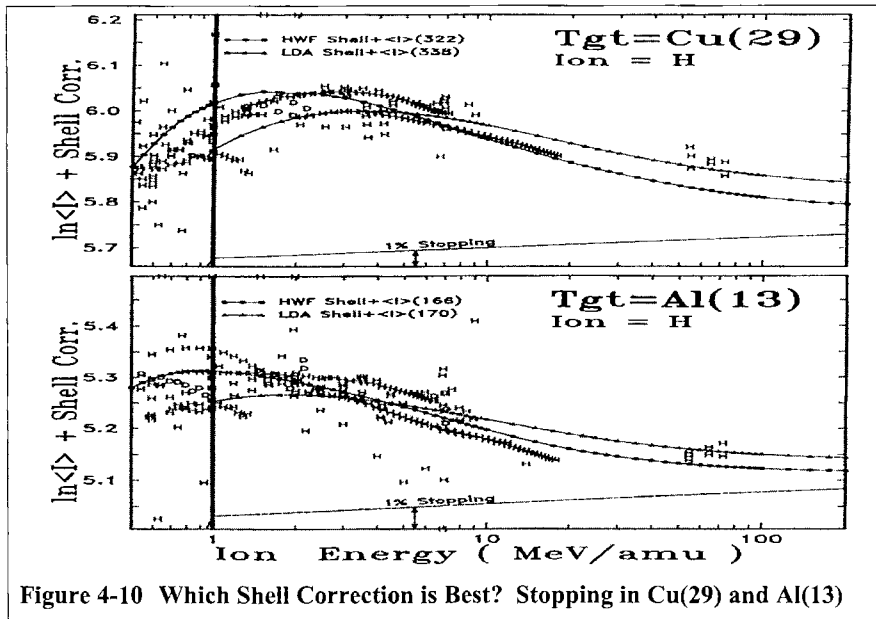


Figure 4-10 Which Shell Correction is Best? Stopping in Cu(29) and Al(13)

The differences between the two basic methods of calculating shell corrections is rather small. Shown above is the summed ($C/Z_2 + \ln<|I>$) terms for both Bichsel's hydrogenic wave function (HWF) calculations, and Ziegler's LDA calculation based on the Lindhard-Winther formalism. The upper curve is for a target of Cu(29) and the lower target is Al(13). Proton stopping data is reduced using Eq. 4-26. Typical data is usually quoted as accurate to better than 1%, however the data scatter is greater than that. It is difficult to determine which curve more accurately fits the data. For example, in the upper Cu(29) plot, at high energy the HWF curve fits the 70 MeV data well, but then has less accuracy for low energies, 1-3 MeV/u. The reverse is true for the LDA shell correction.

Density Effect Correction to $L_0, \delta/2$

When a very high energy relativistic particle passes into a solid, its energy loss has been found to be slightly less than predicted using the relativistic form of the Bethe-Bloch equation, Eq. 4-12. The divergence between theory and stopping data was found to increase at higher energies and in denser media. As an example, for protons at 1000 MeV in photographic emulsion, the measured proton stopping power was less than predicted by about 1%. At higher energies, e.g. 8 GeV, the difference reached 7% for emulsion, and 8% for stopping in the more dense graphite. This

phenomenon is called *the density effect*. It only becomes important when the kinetic energy of the particle exceeds its rest mass ($M_{\text{proton}} = 938 \text{ MeV}$).

The density effect correction was first treated theoretically by Swann⁵³ and Fermi.⁵⁴ Expansions on these original ideas have been made by Bohr³⁹, Sternheimer^{55,56,57} and Crispin and Fowler.⁵⁸

The original work of Bethe and Bloch ignored the dielectric properties of the medium. Fermi first discussed how these properties might be included into the general Bethe-Bloch formalism. Basically, in dense media the dielectric polarization of the material alters the particle's fields from their free-space values to those characteristic of the macroscopic fields in the dielectric. Since this approach implies that macroscopic fields are modified, it is usually assumed that there is little effect on close collisions since these usually are considered to be an interaction between the particle and a single electron in a harmonic potential. As usual, there is a problem in defining the impact parameter distance between close and distant collisions, but this is less important in the density effect correction because the impact parameter for distant collisions may be considered to be much larger than atomic dimensions without impacting the magnitude of the effect.

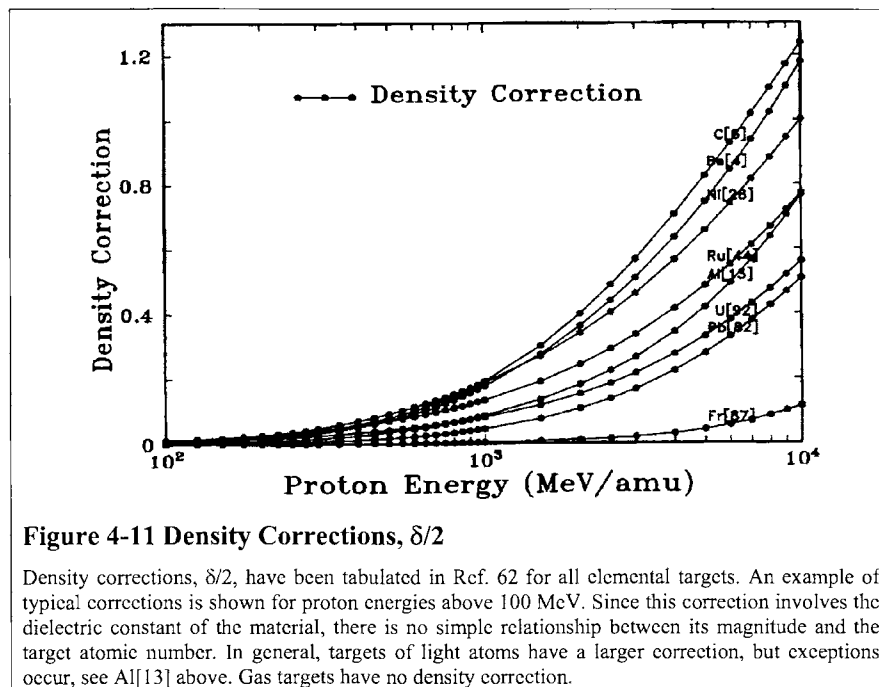


Figure 4-11 Density Corrections, $\delta/2$

Density corrections, $\delta/2$, have been tabulated in Ref. 62 for all elemental targets. An example of typical corrections is shown for proton energies above 100 MeV. Since this correction involves the dielectric constant of the material, there is no simple relationship between its magnitude and the target atomic number. In general, targets of light atoms have a larger correction, but exceptions occur, see Al[13] above. Gas targets have no density correction.

There is no simple algorithm for the density effect, because the dielectric response of the target material is required input in addition to the normal parameters about the particle and target. Shown in Figure 4-11 is an example of typical density corrections.

For tables of predictions of the density effect in many common high-energy physics materials, see Inokuti and Smith (59), Ashley (60), Bichsel (61), and ICRU report #37 (62).

THE BARKAS-ANDERSEN CORRECTION, L_1

The basic stopping equation for high velocity particles was shown as:

$$\text{Eq. 4-15} \quad S = \frac{\kappa Z_2}{\beta^2} Z_1^2 L(\beta)$$

where the variable L , called the *Stopping Number*, was defined to include the correction factors to the stopping equation for high velocity particles. Traditionally, it has been defined as an expansion in powers of the atomic number of the particle:

$$L(\beta) = L_0(\beta) + Z_1 L_1(\beta) + Z_1^2 L_2(\beta) \dots$$

In general, these terms have decreasing significance in determining the stopping powers of ions. To illustrate their relative contribution, consider the case of 10 MeV protons in silver, Ag(47) - the terms will contribute: $L_0 \approx 98.8\%$, $Z_1 L_1 \approx 1.1\%$, $Z_1^2 L_2 \approx 0.1\%$. However, there are special situations in which the higher-order terms become more significant.

Much of the work on the higher order terms, L_1 and L_2 , has been stimulated by two remarkable kinds of experimental evidence which highlighted inaccuracies in the Bethe-Bloch equation:

1. The discovery of different ranges for particles at the same velocity and in the same target, whose only difference was that one had a positive charge and the other had a negative charge. Since the Bethe-Bloch equation, Eq. 4-15 above, shows only a stopping dependence on Z_1^2 , there should be no difference in the stopping power of positive particles when compared to those of equivalent negative particles.
2. The discovery of errors in the scaling of stopping powers for particles at the same velocity and in the same target, whose only difference was their amount of charge. According to the Bethe-Bloch equation, Eq. 4-15, a particle with charge +2 should have four times the stopping of a similar particle with charge +1. However, the stopping of +2 charged particles was discovered to exceed 4x that of an equivalent +1 charged particle

Both of these experimental results will be discussed below, with some emphasis on the historical path leading to an understanding of how these remarkably different experiments led to a single explanation and solution. This final resolution concerns a correction to the basic Bethe-Bloch assumption that the initial distribution of target electrons are uniformly distributed about quiescent atoms. However, a positive charge will pull these target electrons towards it as it approaches, increasing the local electron density, while a negative charge will repel them. For the case of similar negative and positive particles, example (1) above, this polarization of the target will cause positive particles to pass through a slightly higher density of target electrons, increasing its energy loss relative to that of a negatively charged particle. At high velocities this effect may become negligible, since the target electrons do not have time to move, but near the maximum of the energy loss of light particles, about 1 MeV/amu, this effect becomes apparent. In the case of particles with different charges, example (2) above, a higher charged particle will pass through a slightly higher density of target electrons compared to the singly charged particle, increasing its stopping above what might be expected.

The Barkas-Andersen Effect from Charge Sign Considerations

The Barkas Correction, $Z_1 L_1$, was named after Walter Barkas, who discovered in 1956 a difference in the ranges of positive and negative pions in photographic emulsion, and showed that the range of

negative pions was longer than that of positive pions.⁶³ This range difference was small, about 0.36%, but Barkas measured it with great precision and established the clear unexpected difference. The explanation of this difference was later suggested by Barkas as being caused by a correction to the first-order Born approximation of the Bethe-Bloch equation. Positive projectiles tend to pull electrons towards its trajectory, while negative particles tend to repel them. The early experimental work by Barkas and others has been reviewed by Heckman.⁶⁴ A later paper by H. H. Andersen et al. (1969) evaluated the stopping of protons, deuterons and alpha particles in metals.⁶⁵ They showed that there was a distinct difference in stopping for high velocity particles that couldn't be accounted for by traditional Bethe-Bloch formalism, and that it was necessary to include a Z_1^3 term. This is the same conclusion that would be reached by analysis of the earlier Barkas effect experiments. Sigmund has suggested that the traditional name for the "**Barkas Effect**", be called the "**Barkas-Andersen Effect**" since Andersen's work was much clearer in suggesting the cause of the variations observed. We agree with this, and have used the "**Barkas-Andersen Effect**" for the Z_1^3 term in the Bethe-Bloch formalism for high velocity stopping.

This work prompted a series of papers by Ashley et al. from 1972-74.^{66,67,68} These papers presented a non-relativistic stopping power correction based on a harmonic oscillator approach. The authors assumed that close collisions would not be significant in the L_1 correction, and presented results for a correction to distant collision events. They assumed a target electron in a harmonic oscillator potential, which for small displacements varied the force on the electron. This was a correction to the original approach of Bohr who assumed that the force on the electron was independent of small displacements.⁶ The Ashley correction led to a term in Z_1^3 for the energy transfer to distant collisions. They suggested for the high velocity limit a form:

$$\text{Eq. 4-27} \quad Z_1 L_1 = \frac{3\pi Z_1 e^2 \omega}{2mv^3} \ln \left(\frac{v}{1.7\omega a_\omega} \right)$$

where v is the velocity of the particle, ω is the free electron gas plasma frequency, and a_ω is lower limit of the impact parameter for the distant collisions. This high velocity limit is for $v_1 \gg \omega a_\omega$. The authors refined this approximation over several papers, and produced a useful parameterized form:

$$\text{Eq. 4-28} \quad Z_1 L_1 = \frac{Z_1 F_{ab} (b/x^{1/2})}{Z_2^{1/2} x^{3/2}}$$

where $x = (\beta \alpha)^2 / Z_2$ and $b = \chi \eta Z_2^{1/6}$

The term χ is a free-electron-gas parameter which corrects for binding forces, and has a value of about $2^{1/2}$. This expression includes a tabulated function, F_{ab} , included in the final paper.

Soon after Ashley's first paper, Jackson and McCarthy suggested a different minimum impact parameter, $a_m = (\hbar 2m\omega)^{1/2}$.⁶⁹ Hill and Merzbacher performed a similar quantal calculation, but expanded the electron's harmonic potential to second order.⁷⁰

Lindhard reviewed these approaches, and suggested that the omission of close collisions from the above studies was wrong, and that these effects would be about as great as the distant collisions.⁷¹ The final correction would be almost twice what had been previously estimated. This suggestion of Lindhard was later supported by experiments measuring the stopping of p- (anti-protons) in silicon.⁷²

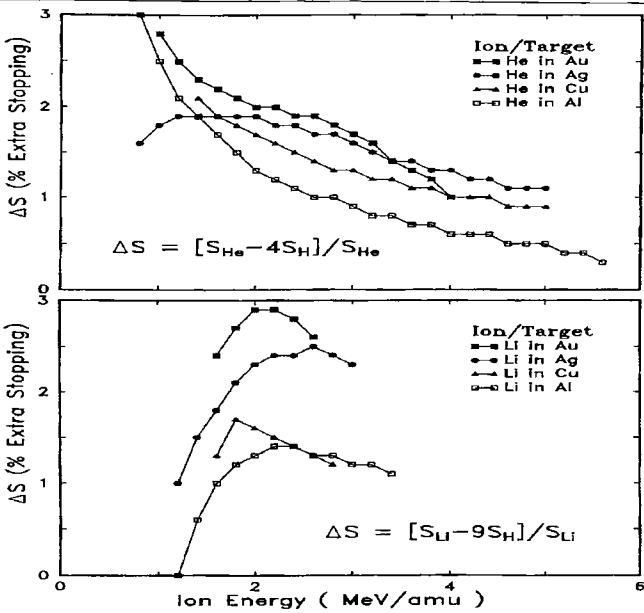


Figure 4-12 Excess Stopping for He and Li Ions

The figure comes from the stopping data of Andersen et al. for H, He and Li ions in targets of Al, Cu, Ag and Au.⁷³ The data was taken with the same targets, at identical ion velocities, in order to investigate deviations from the Bethe-Bloch equation which indicates that stopping should be proportional to Z_i^2 . The plot shows the excess stopping, in %, above this level. He stopping, S_{He} , exceeds four times the H stopping, $4S_H$, by up to 3%. The Li ions have extra stopping over $9S_H$ by up to 3%.

The Barkas-Andersen Effect from Charge Magnitude Considerations

A series of experiments by H. H. Andersen et al. added a different perspective to understanding higher order terms of the Bethe-Bloch equation. They reported accurate measurements of the stopping of H, He and Li particles at the same velocity in the same targets.⁷³ From the Bethe-Bloch equation, one expects that the stopping of particles of different atomic number would scale as Z_i^2 (the mass of the particle is assumed to be far larger than that of an absorbing electron, so the mass difference between particles was assumed to have negligible effect). Andersen found that the ratio of stopping exceeded Z_i^2 scaling by a few percent, see Figure 4-12. This plot shows the extra stopping of the heavier ions using the relation:

$$\text{Eq. 4-29} \quad \Delta S = [S_{Zi} - Z_i^2 S_H] / S_{Zi}$$

where S_H is the stopping power of Hydrogen ions, and S_{Zi} is the stopping of He or Li ions at the same velocity in the same target. The extra stopping, ΔS , reaches 3%. The excess stopping increases slightly with target atomic number. The experimental data has several peculiarities. The He in Au curve shows a distinctly different slope than the approximate 1/E decrease of the other He stopping curves. One He curve (Ag target) and all the Li curves show a peak in the excess

stopping, while the others show no peak.

Andersen et al. suggested that their experimental stopping powers for H, He and Li (covering the energy range of 0.8-7.2 MeV/u) could be fit by using complex Barkas-Andersen + Bloch terms (the Bloch correction will be discussed in the next section):

$$\text{Eq. 4-30} \quad Z_1^2 L_2 \text{ (Bloch term)} = -1.6 (Z_1 v_0 / v)^2$$

$$\text{Eq. 4-31} \quad Z_1 L_1 \text{ (Barkas-Andersen term)} = L_0 \frac{Z_1}{Z_2^{1/2}} \left[\frac{2.68}{V^2} (1 - 0.264 \ln V) \right]$$

$$V \equiv (v / v_0 Z_2^{1/3})$$

where Z_1 is the particle charge, v is the particle velocity and v_0 is the Bohr velocity (25 keV/u) and Z_2 is the target atomic number. Note that the Barkas-Andersen term depends on L_0 , the basic stopping number which includes shell corrections and the mean ionization potential of the target. These proposed correction terms are not clean expansion terms relative to the particle's charge, which was the original assumption in the expansion of the Bethe-Bloch equation into stopping numbers dependent on integer powers of the particle charge.

Bichsel approached the problem of the Barkas-Andersen Correction by a limited empirical approach.^{27,48,53} He started with a variation of the Ashley equation, Eq. 4-27, and used only Andersen's experimental stopping data shown in Figure 4-12 to extract a simpler $Z_1 L_1$ correction expression than that shown in Eq. 4-30 and Eq. 4-31. His results were:

$$\text{Eq. 4-32} \quad Z_1 L_1 = Z_1 C / \beta^{2\alpha}$$

where C and α were constants which varied with various targets:

Target	C	α
Al (13)	.001050	0.80
Cu (29)	.002415	0.65
Ag (47)	.006812	0.45
Au (79)	.002833	0.60

This fit was limited to He ions over the narrow energy range of the experimental data, 1-6 MeV/u. The expression is asymptotically incorrect since it rapidly diverges for energies below 1 MeV/u.

Theoretical Barkas-Andersen-Effect Calculations

Mikkelsen, Sigmund, and Esbensen have used various theoretical approaches to evaluate the Barkas-Andersen correction term based on these concepts, see Figure 4-13 for an example for a silicon target. A model using a harmonic oscillator with an oscillator energy corresponding to the mean ionization potential of silicon, 165 eV, was first used to generate an explicit quantal evaluation of the Barkas-Andersen term.^{74,75} This calculation showed that the Lindhard suggestion, that there would be approximate equi-partition between energy losses to close and distant collisions⁷¹, was supported by the calculation. This study then extended the analysis to a model using a static electron gas, deriving a self-consistent polarization field for the medium, and again reached the conclusion that the Lindhard ideas were approximately correct.⁷⁶ The evaluation of the Barkas-Andersen correction term was also evaluated using the local-density-approximation (see Appendix) using a Lenz-Jensen model for the target atoms.⁷⁷ This work was further extended to find a complete solution using a time-dependent Schrodinger equation for the interaction between the particle and a target electron represented as a quantum harmonic oscillator.⁷⁸

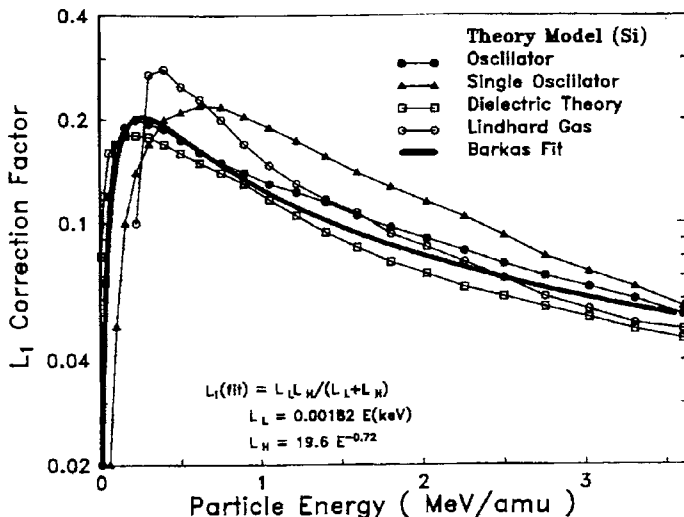


Figure 4-13 Theoretical evaluation of Barkas-Andersen Correction for Silicon

Shown are evaluations of the Barkas-Andersen effect using various models by Sigmund, Mikkelsen and Esbensen.⁷⁴⁻⁷⁹ The single oscillator model considers the target as an oscillator with a resonance frequency of I/\hbar , where I is the mean ionization energy or the target atoms. The oscillator model uses a spherical harmonic oscillator, with the Born series evaluated up to second order and preserving shell corrections in evaluating the Barkas-Andersen correction. The Lindhard gas model assumes the Lindhard interaction of a particle to an electron gas with a resonance frequency of I/\hbar .⁸⁷ The dielectric model considers the particle in a self-consistent polarized dense electron gas, and uses the local density model to evaluate the Barkas-Andersen correction.

The line in the figure called “**Barkas Fit**” is described in the text in the later section called **Empirical Barkas-Andersen Correction Term**.

All these approaches have been reviewed by Sigmund, who discussed many relevant approaches to stopping powers in the region where the Barkas-Andersen correction was significant.⁷⁹

Unified Barkas-Andersen Correction Factor

The Barkas-Andersen effect is caused by target electrons responding to the approaching particle, and slightly changing their orbits before any energy loss interaction occurs (called target polarization). At high energies (above $v_0 \approx 10$ MeV/u) the Barkas-Andersen effect becomes insignificant because the ion will be moving too fast to cause initial motion of the target electrons. At low energies, $\ll 1$ MeV/u, the Barkas-Andersen effect is difficult to isolate in experiments because of the onset of neutralization of the ion. That is, at low velocities (below $5 v_0 \approx 0.6$ MeV/u) the ion will begin to pick up electrons which will cause its charge to be partially shielded, causing any target polarization effects to be overshadowed by more dominant changes in the particle/target interaction. (Particle charge neutralization was discussed previously, see Eq. 4-17).

The experimental analysis of the Barkas-Andersen effect concerns ions with energies over the limited interval of about $5 - 20 v_0$ (0.6 - 10 MeV/u). In order to find a unified approach to the

Barkas-Andersen effect, one must convert all the relevant experimental and theoretical data to a common view.

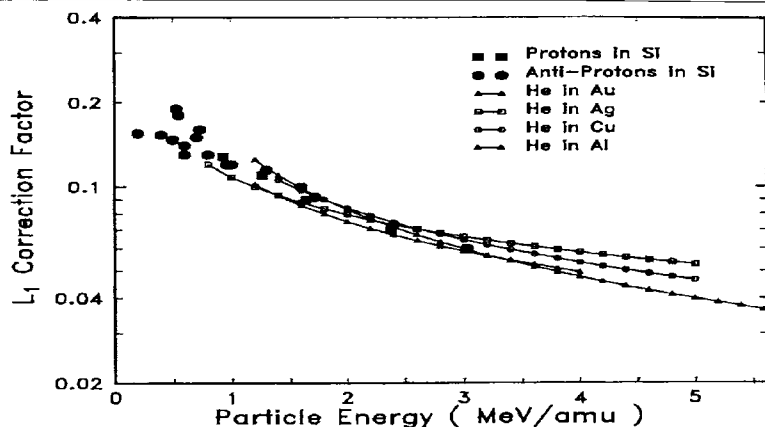


Figure 4-14 The L_1 Barkas-Andersen Correction Term for Andersen Stopping Data

The figure shows the data of Andersen et al. for He ions in targets of Al, Cu, Ag and Au (see Figure 4-12)⁷³. This plot shows the result of using this data to solve the Bethe-Bloch equation for $Z_1 L_1$ using Eq. 4-33. Although the original data shows a marked Z_2 effect, with the excess He stopping increasing with target atomic number, this effect is compensated by the shell corrections. The reduced data shows virtually no target effect in the $L_1 Z_1$ Barkas-Andersen term.

Also shown in this curve is precision stopping data for protons and anti-protons in silicon.^{72,80} The value of L_1 is positive for both particles, however the value of the stopping number term, $Z_1 L_1$, will be additive for protons, and subtractive for anti-protons.

Shown in Figure 4-14 is Andersen's He/H stopping data, illustrated in original form in Figure 4-12, but now reconfigured using Eq. 4-13 to extract values of L_1 . That is, Eq. 4-13 is inverted to solve for $Z_1 L_1$ as a function of the experimental stopping powers:

$$\text{Eq. 4-13} \quad S = \frac{\kappa Z_2}{\beta^2} Z_1^2 [L_0(\beta) + Z_1 L_1(\beta) + Z_2^2 L_2(\beta) \dots]$$

Inverting to solve for $Z_1 L_1$:

$$\text{Eq. 4-33} \quad Z_1 L_1(\beta) = \frac{S_{\text{exp}} \beta^2}{\kappa Z_2 Z_1^2} - L_0(\beta) - Z_1^2 L_2$$

The result is shown in Figure 4-14 for the four targets, Al, Cu, Ag and Au. Note that the Z_2 dependency noted in the original data has disappeared, since this has been accounted for by the L_0 shell corrections.

Also shown in Figure 4-14 are representative stopping results from precision measurements of protons and anti-protons in silicon, discussed before.^{72,80} These papers extracted the Barkas-Andersen correction directly by assuming it was proportional to exactly one-half the difference between proton and anti-proton stopping in the same target, at the same velocity. The Barkas-Andersen factor was determined by dividing this stopping difference by the Bethe-Bloch pre-

factor, shown above in Eq. 4-13. Remarkably, these results overlap the He results for four different targets, reinforcing the conclusion that the Barkas-Andersen term is independent of target atomic number.

Most important, Figure 4-14 shows that the two basic Barkas-Andersen effects described above are probably the same effect, seen in two different kinds of experiments. The proton/anti-proton stopping shows differences associated with the particle charge sign, while the He/H excess stopping shows differences from the basic Bethe-Bloch Z_1^2 stopping formalism. Both of these effects are caused by target electrons having time to polarize (move) in response to the incident charged particle. For the anti-proton data, $Z_1 = -1$, L_1 will be positive as shown but the value of $Z_1 L_1$ will be negative. Hence $Z_1 L_1$ for protons will contribute to the stopping (increasing its magnitude) while it will be subtracted from the anti-proton stopping. This may be viewed as an increased local electron density for the positive particle, and a decreased local electron density for the negative anti-protons.

To find an overall Barkas-Andersen correction factor, we combine three independent sources of Barkas-Andersen correction values: (1) the experimental stopping differences found for proton/anti-proton energy loss, see Figure 4-14, (2) the enhanced stopping of He particles over that expected by Bethe-Bloch Z_1^2 scaling, and (3) the theoretical modeling of Mikkelsen et al. based on polarization of the medium by incoming particles, see Figure 4-13. These values can be fitted using the simple expression:

$$\text{Eq. 4-34} \quad L_1 = S_L S_H / (S_L + S_H)$$

with $S_L = 0.00182 E$, and $S_H = 19.6 / E (\text{keV/u})^{0.72}$

where the particle energy units are keV/u. This formula is shown as a heavy solid line in both plots of Figure 4-15, which compares the fit to both experimental data (upper plot) and theoretical calculations (lower plot).

Note that Figure 4-12 also included data for Li ions, which were not used for this fitting of the Barkas-Andersen effect. The fall-off of the Li excess stopping powers below 2 MeV/amu may be due to partial neutralization of the Li ions. According to Eq. 4-17 Li ions begin to neutralize below 2.3 MeV/amu, $Z_1^* \leq 0.99 Z_1$. Although Eq. 4-17 has limited validity for light ions, it offers a cautionary indication that this data may be below the valid velocities for the Bethe-Bloch formalism. Hence this data was not used for fitting the Barkas-Andersen effect term.

Empirical Barkas-Andersen Correction Term

The above evaluation of the Barkas-Andersen correction may be extended using a larger database of experimental values. Experimental stopping powers may be reduced using Eq. 4-33 to extract the Barkas-Andersen correction for every element with data, see Figure 4-16 and Figure 4-17. These curves show the Barkas-Andersen effect is quite close to the one extracted from the analysis shown in Figure 4-15, however there is a distinct variation with target atomic number. The extracted Barkas-Andersen correction values may be empirically fit using the expression:

$$\text{Eq. 4-35} \quad Z_1 L_1 = \frac{L_{\text{low}} L_{\text{high}}}{L_{\text{low}} + L_{\text{high}}}$$

where: $L_{\text{low}} = .001 E$ and $L_{\text{high}} = (1.5/E^{0.4}) + 45000/Z_2 E^{1.6}$

with the energy, E , having units of keV/u.

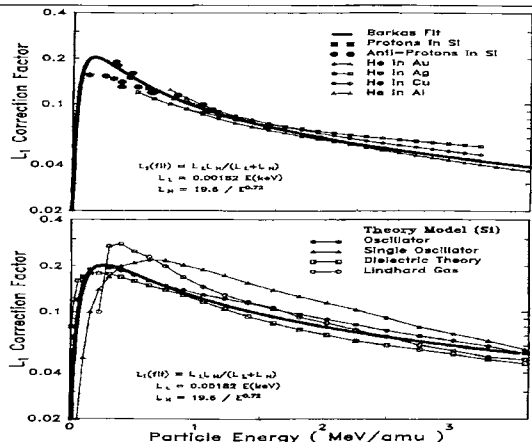


Figure 4-15 Preliminary Analytic function for Barkas-Andersen Correction

Shown is an analytic function which can be used to represent the Barkas-Andersen Correction, L_1 , in calculations of stopping powers. The upper plot shows how well this curve fits the experimental data of the proton/anti-proton stopping powers, and also the enhanced stopping powers for Hc ions over proton stopping. Since the maximum effect on stopping is about 3%, the fit is accurate to about 0.2%. The lower plot shows the same Barkas-Andersen correction with the four theoretical evaluations discussed in the text. These theoretical calculations were used for the low energy portion of the fitted Barkas-Andersen curve (<0.5 MeV/u).

This expression goes to zero for both low and high values of ion energy. Note that this empirical Barkas-Andersen correction term is dependent on the other terms used in Eq. 4-33, especially the shell correction. All empirical calculations of stopping powers are dependent on using self-consistent approximations. Since the shell corrections are not considered accurate below 1 MeV/u, this is also the limit of the above Barkas-Andersen correction. The plots show the extracted Barkas-Andersen term to lower energies in order to see the general trends.

Two final corroborative plots for this empirical Barkas-Andersen correction are shown in Figure 4-18. At the beginning of this discussion of the Barkas-Andersen effect, Figure 4-13 showed four theoretical calculations of the Barkas-Andersen correction for silicon targets. Shown in the upper part of Figure 4-18 is the empirical correction for silicon from Eq. 4-35, with the experimental data for H and Hc ions stopping from 15 papers (102 data points). The agreement is good.

Figure 4-18 shows in its lower plot the fit for Li ions in all solid targets. This shows important support for this Barkas-Andersen correction, $Z_1 L_1$, because of its very large contribution to the stopping of Li ions. For example, for 1 MeV/amu Li ions in Au, the Barkas-Andersen correction is 25% of the total stopping power. However, the scatter of data in the figure is quite small, such that the average stopping error is less than 4%.

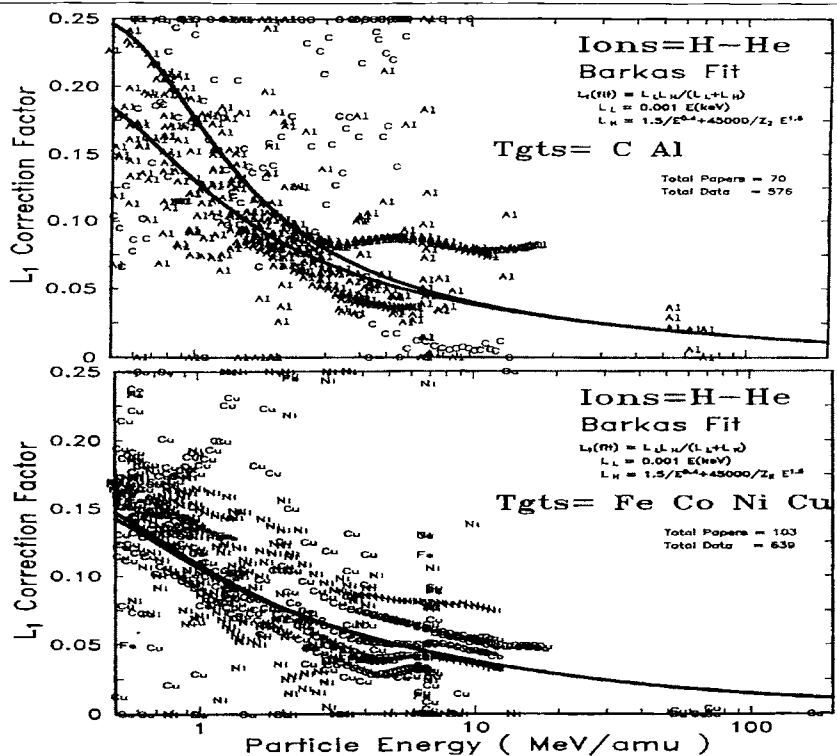


Figure 4-16 Barkas-Andersen Correction for C, Al, Fe, Co, Ni and Cu

Shown are the Barkas-Andersen correction terms to the Bethe-Bloch stopping equation extracted from experimental data using Eq. 4-33. The upper curve shows data from C and Al targets, while the bottom curve shows data from Fe, Co, Ni and Cu targets. Clearly, the data do not indicate a target-independent Barkas-Andersen correction value in the two plots. An empirical Barkas-Andersen correction expression, Eq. 4-35, is shown as a thick line in each plot. In the upper plot, for C and Al targets, the two lines are clearly separate, with the upper curve being for carbon targets. In the lower plot, the separate curves for the Barkas-Andersen correction for Fe, Co, Ni and Cu are too close to separate. Note that this empirical Barkas-Andersen correction is only valid when used with the other corrections used in Eq. 4-33, especially the shell correction term.

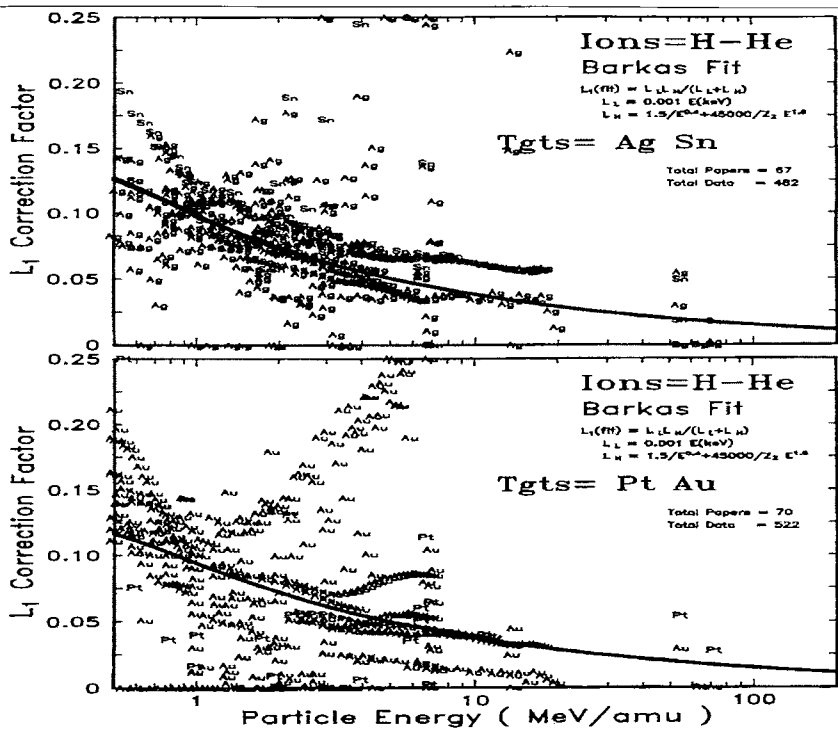


Figure 4-17 Barkas-Andersen Correction for Ag, Sn, Pt and Au

Shown are the Barkas-Andersen correction terms to the Bethe-Bloch stopping equation extracted from experimental data using Eq. 4-33. The upper curve shows data from Ag and Sn targets, while the bottom curve shows data from Pt and Au targets. Clearly, the data do not indicate the same Barkas-Andersen correction values as shown in Figure 4-14. An empirical Barkas-Andersen correction expression, Eq. 4-35, is shown as a thick line in each plot. Note that this empirical Barkas-Andersen correction is only valid when used with the other corrections used in Eq. 4-33, especially the shell correction term.

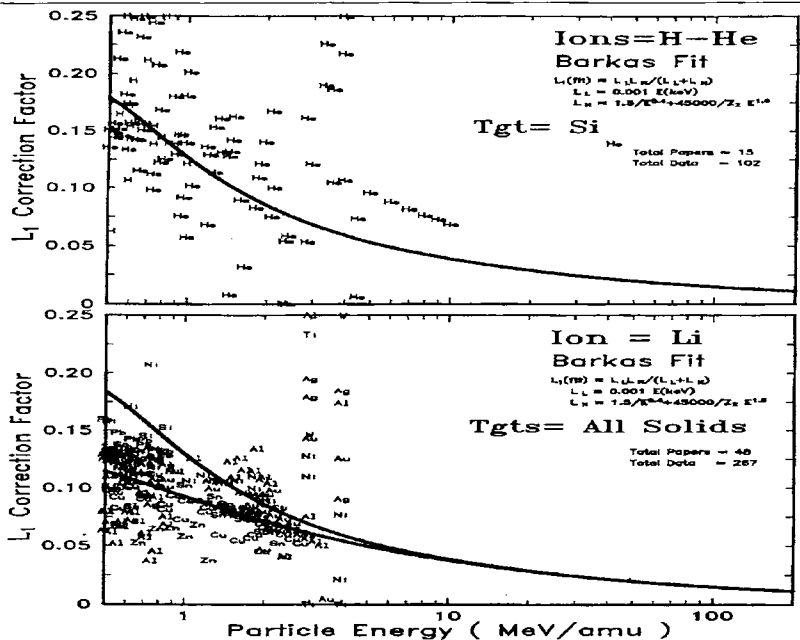


Figure 4-18 - Barkas-Andersen Correction for Silicon Targets, and for Li Ions

The theoretical Barkas-Andersen corrections shown in Figure 4-13 were for a target of silicon. In order to evaluate the accuracy of the proposed empirical Barkas-Andersen correction, this term needs to be compared with the extensive experimental data for H and He ion stopping in silicon. The upper curve shows the correction for silicon, along with the experimental data from 24 citations. The agreement is well within the scatter of experimental data.

For Li ions, the Barkas-Andersen correction, $Z_1 L_1$, is a significant contribution to stopping. For Li in Au at 1 MeV/amu, this correction is 25% of the total stopping. Shown are all available experimental stopping powers for Li in solids, along with the Barkas-Andersen corrections for Al (upper thick curve) and Au (lower thick curve). If one omits the single result for Li in Al, Au, and Ag at 1 and 2 MeV/amu, then the remaining 15 papers show complete agreement with the proposed empirical correction term. Since this correction term is so large, 10-25%, and the fit results in a stopping accuracy of about 4%, this data corroborates the empirical Barkas-Andersen correction.

THE BLOCH CORRECTION, L_2

The basic stopping equation for high velocity particles, as traditionally formulated, was shown as:

$$\text{Eq. 4-15} \quad S = \frac{\kappa Z_2}{\beta^2} Z_1^2 L(\beta)$$

where the variable L , called the *Stopping Number*, was defined to include the correction factors to the stopping equation for high velocity particles. Traditionally, it is defined as

expansions of the particle's charge: $L(\beta) = L_0(\beta) + Z_1 L_1(\beta) + Z_1^2 L_2(\beta)$. This paper has explored the primary corrections contained in L_0 and L_1 , which may make significant changes to calculated stopping values. Now, we consider the smaller Bloch Correction, L_2 . As discussed in the *Introduction*, Bloch attempted in 1933 to understand the differences between classical and quantum-mechanical methods of approaching the problem of the stopping of a high velocity particle.¹⁰ He showed that Bohr's harmonic oscillator approach was valid quantum mechanically, within limits. Bloch separated the consideration of impact parameters into two regions. For small impact parameters, Bloch considered the interactions to be that of free particles, as Bohr had done. However, for larger impact parameters, he showed that higher-order terms were also necessary, in particular the Z_1^4 term. He estimated that this correction was of the order of :

$$\text{Eq. 4-36} \quad L_2 \propto \left(\frac{Z_1 \alpha}{\beta} \right)^2 \left(\frac{r_0^2}{2 b^2} \right) / \ln \left(\frac{r_0 v_1}{b v_0} \right)$$

where α = the fine structure constant, r_0 is the typical radius of a target atom, v_0 is the typical velocity of a target electron, and b is the impact parameter. This correction applies to the case where $b \gg r_0$. By combining this result with the close-collision solution, Bloch proposed:

$$\text{Eq. 4-37} \quad S = \frac{4\pi e^4 Z_2}{m_e v^2} Z_1^2 \left[\ln \frac{2mv^2}{<I>} - \frac{1}{2} \ln(1-\beta^2) - \frac{\beta^2}{2} + \psi(1) - \operatorname{Re} \psi \left(1 + \frac{i \alpha Z_1}{\beta} \right) \right]$$

where ψ is the logarithmic derivative of the gamma function, sometimes called the digamma function by inept mathematicians. This expression does not reduce to the Bethe-Bloch formula for very high velocities, $Z_1 \alpha / \beta \rightarrow 0$, because Bloch made a mistake in estimating the close-collision cross-section. Various studies have corrected the mistake, extended the Bloch approach, and made formulations which allow it to be approximated with simple expressions.^{K1-K2}

The difference between Bloch's expression above, and Bethe's original expression, may be formulated as a Taylor series based on even powers of Z_1 . The first term of this expansion is often considered to be an accurate estimate of the Bloch correction term, L_2 .⁷¹

Modern evaluations of the Bloch term have been reviewed by Sigmund.⁷⁹ He points out that the contribution of this term is negligible for low particle energies, i.e. below $2Z_1 e^2 / \hbar v$ (100 keV protons). As soon as this correction becomes noticeable, one should also expect higher order terms, e. g. the L_3 and L_4 terms, to begin to contribute. By ending the summation series of the total stopping number, L , at the Bloch term, $L_2 Z_1^2$, the result is either insignificant or possibly wrong. For light ions, the Bloch term clearly overestimates the even corrections near the peak of the stopping power curve.

From a practical viewpoint of calculating accurate stopping powers, Bichsel has proposed a simple

parameterization of the Bloch correction which accurately fits a wide range of high velocity stopping data:^{83,27}

$$\text{Eq. 4-38} \quad Z_1^2 L_2 = -y^2 [1.202 - y^2 (1.042 - 0.855 y^2 + 0.343 y^4)]$$

where : $y = Z_1 \alpha / \beta \quad (\alpha=1/137)$

For low velocities, the value of $Z_1^2 L_2 \rightarrow -0.58 - \ln(y)$, and thus the Bloch correction provides the transition to the classical stopping power formula of Bohr. For high velocities, i.e. $y \rightarrow 0$, $Z_1^2 L_2 \rightarrow -1.2 y^2$. As will be shown in the next section, this term is usually quite small.

This expression is derived in conjunction with Bichsel's calculation of the other stopping numbers, especially his expressions for the shell correction, the mean ionization potential, and the Barkas-Andersen correction, L1. However, since this Bloch correction term is usually quite small, the Bichsel approach is quite useful in practice.

RELATIVE MAGNITUDE OF BETHE-BLOCH CORRECTIONS

It is important to put the various stopping numbers into perspective, in order to evaluate their relative importance. Reviewing, the basic Bethe-Bloch stopping equation is:

$$\text{Eq. 4-15} \quad S = \frac{\kappa Z_2}{\beta^2} Z_1^2 L(\beta)$$

where $\kappa = 4\pi r_0^2 m_e c^2 = 0.0005099$ for stopping in units of keV/(10¹⁵ atoms/cm²), and $\kappa = 0.3071/M_2(u)$ for stopping units of keV/(mg/cm²). The variable L, called the *Stopping Number*, was defined to include the correction factors to the stopping equation for high velocity particles. Traditionally, it is defined as expansions of the particle's charge: $L(\beta) = L_0(\beta) + Z_1 L_1(\beta) + Z_1^2 L_2(\beta)$. In review of the previous discussions, the stopping of high velocity ions may be expressed using

$$\text{Eq. 4-39} \quad L_0 = \ln \left(\frac{2m_e c^2 \beta^2}{1-\beta^2} \right) - \beta^2 - \frac{C}{Z_2} - \ln < I > - \frac{\delta}{2}$$

which can be evaluated with: $\beta^2 = (v/c)^2 = 1 - 1/[1+E(\text{keV})/931494 M_1(u)]^2$ and the definition: $f(\beta) = \ln[2mc^2\beta^2/(1-\beta^2)] - \beta^2$ to obtain:

$$\text{Eq. 4-23} \quad L_0 = f(\beta) - \frac{C}{Z_2} (\text{shell}) - \ln < I > - \frac{\delta}{2} (\text{density})$$

The Barkas-Andersen correction term, $Z_1 L_1$, may be estimated using

$$\text{Eq. 4-35} \quad Z_1 L_1 = \frac{L_{\text{low}} L_{\text{high}}}{L_{\text{low}} + L_{\text{high}}}$$

where: $L_{\text{low}} = .001 E$ and $L_{\text{high}} = (1.5/E^{0.4}) + 45000/Z_2 E^{1.6}$, with energy units in keV/u.

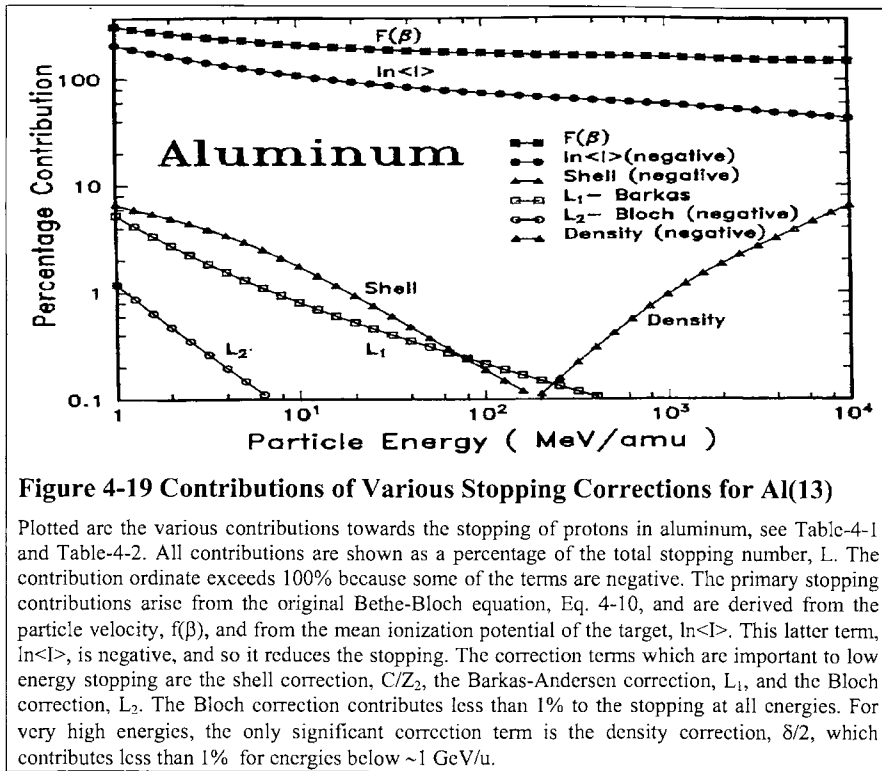


Figure 4-19 Contributions of Various Stopping Corrections for Al(13)

Plotted are the various contributions towards the stopping of protons in aluminum, see Table-4-1 and Table-4-2. All contributions are shown as a percentage of the total stopping number, L . The contribution ordinate exceeds 100% because some of the terms are negative. The primary stopping contributions arise from the original Bethe-Bloch equation, Eq. 4-10, and are derived from the particle velocity, $f(\beta)$, and from the mean ionization potential of the target, $\ln\langle I \rangle$. This latter term, $\ln\langle I \rangle$, is negative, and so it reduces the stopping. The correction terms which are important to low energy stopping are the shell correction, C/Z_2 , the Barkas-Andersen correction, L_1 , and the Bloch correction, L_2 . The Bloch correction contributes less than 1% to the stopping at all energies. For very high energies, the only significant correction term is the density correction, $\delta/2$, which contributes less than 1% for energies below ~ 1 GeV/u.

For the Bloch correction term, Bichsel's simple parameterization of the Bloch correction is useful for this small correction term:^{27,84}

$$Z_i^2 L_2 = -y^2 [1.202 - y^2 (1.042 - 0.855 y^2 + 0.343 y^4)]$$

$$\text{where } y = Z_i \alpha / \beta, \quad (\alpha = 1/137) \quad \text{Eq. 4-38}$$

Which gives the final stopping equation, tabulated below.

$$S = \frac{\kappa Z_2}{\beta^2} Z_i^2 \left\{ \left[f(\beta) - \frac{C}{Z_2} - \ln\langle I \rangle - \frac{\delta}{2} \right] + Z_i L_1 (\text{Barkas}) + Z_i^2 L_2^2 (\text{Bloch}) \right\}$$

Consider the case of protons in aluminum at energies from 1 - 10,000 MeV. From the equations above, we can calculate the importance of each of the stopping number terms, see Figure 4-19 and Table-4-1. The relative importance of each term is shown below as the percent contribution of each towards the total stopping number, L . Values for $f(\beta)$, the shell correction, and $\ln\langle I \rangle$ are shown also, although they are part of L_0 . Note that $f(\beta)$ is positive, while the shell correction and $\ln\langle I \rangle$ are negative terms, see Figure 4-19 and Table-4-2. Note that both the $Z_i L_1$ and the $Z_i^2 L_2$ corrections

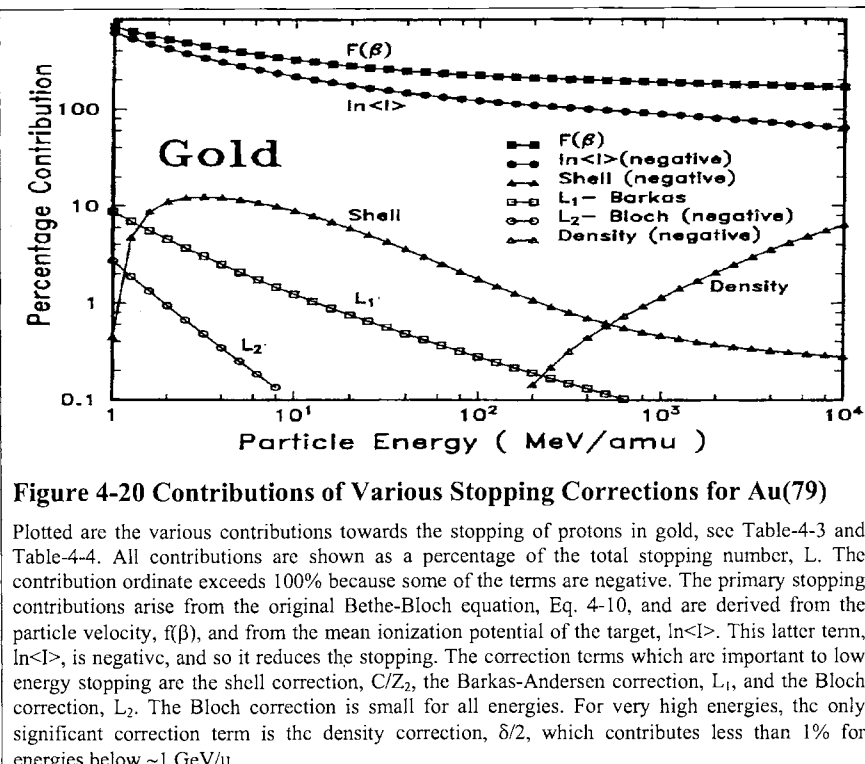


Figure 4-20 Contributions of Various Stopping Corrections for Au(79)

Plotted are the various contributions towards the stopping of protons in gold, see Table-4-3 and Table-4-4. All contributions are shown as a percentage of the total stopping number, L . The contribution ordinate exceeds 100% because some of the terms are negative. The primary stopping contributions arise from the original Bethe-Bloch equation, Eq. 4-10, and are derived from the particle velocity, $f(\beta)$, and from the mean ionization potential of the target, $\ln\langle I \rangle$. This latter term, $\ln\langle I \rangle$, is negative, and so it reduces the stopping. The correction terms which are important to low energy stopping are the shell correction, C/Z_2 , the Barkas-Andersen correction, L_1 , and the Bloch correction, L_2 . The Bloch correction is small for all energies. For very high energies, the only significant correction term is the density correction, $\delta/2$, which contributes less than 1% for energies below ~ 1 GeV/u.

for an aluminum target contribute less than 1% for all energies above 10 MeV.

Considering the case of protons in gold at energies from 1 - 10,000 MeV. From the equations above, we can calculate the importance of each of the stopping number terms, see Figure 4-20 and Table-4-3.

The relative importance of each term is shown below as the percent contribution of each towards the total stopping number, L . Values for $f(\beta)$, the shell correction, and $\ln\langle I \rangle$ are shown also, although they are part of L_0 . Note that $f(\beta)$ is positive, while the shell correction and $\ln\langle I \rangle$ are negative terms, see Figure 4-20 and Table-4-4 (in Appendix to this chapter).

Both the $Z_1 L_1$ and the $Z_1^2 L_2$ corrections for a gold target contribute less than 1% for all energies above 15 MeV/u.

THE ACCURACY OF CURRENT STOPPING THEORY

A natural question might concern the accuracy of modern stopping theory for predicting the energy loss of ions in matter. However, this question is specious in that there is no unified pure theoretical approach, but only a linear summation of parts as illustrated in Figure 4-19 and . The shell corrections, the Barkas-Andersen correction and the density correction as presented in Figure 4-19 and Figure 4-20 are theoretical concepts corrected to fit experimental data.

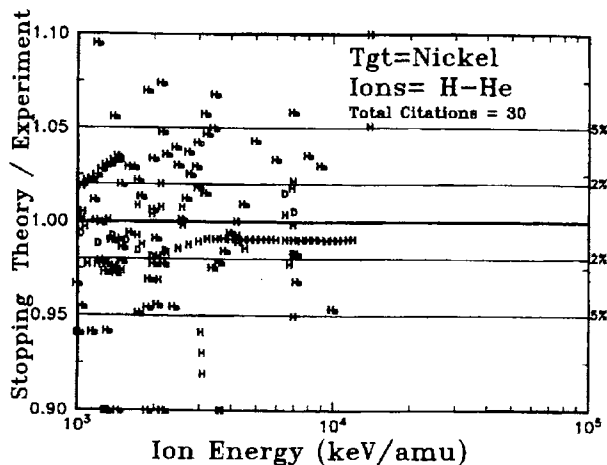


Figure 4-21 Calculation Accuracy for stopping of H and He ions in nickel.

The accuracy of calculations of the stopping of H and He ions in nickel is shown relative to the experimental data reported from 30 papers. Most of the experimental values lie within 3% of the calculated values. It is not clear whether this spread of values is due to experimental error (most papers claim an accuracy of 1% or better), or whether this may be a real variation in stopping in nickel metals prepared in different ways creating differences in grain size and orientation.

The question of the theoretical accuracy might instead be phrased: "How accurately may stopping powers be calculated?" Figure 4-21 show *experimental/calculated* values for the stopping of H and He ions in nickel targets.

There is a significant spread of experimental data beyond the 1% accuracy typically claimed by the experimentalists. For nickel targets, data from 30 papers shows agreement only to about $\pm 3\%$. However, this spread may be partly real and not experimental error. Studies have shown that metal films prepared by different methods (rolling, evaporation, sputtering, etc.) may have significantly different texture, which is defined as the degree to which the crystalline grains are aligned along a common axis.⁸⁵ That is, the crystalline grains are not randomly oriented, but have partial properties of a single-crystal. Such texture can promote ion channeling which can both increase and decrease stopping powers depending on the orientation of the ion beam to the target texture. Hence, some of the observed variation in stopping powers may actually be "real", i. e. due to structural differences in the targets and not just due to experimental errors.

A more critical evaluation of the accuracy of the Bethe-Bloch stopping calculation is to consider Li ions. The Barkas-Andersen correction for Li ions contributes Z_1 greater stopping (3x) than for protons, see Eq. 4-13, and the smaller Bloch correction is Z_1^2 greater (9x). Figure 4-19 and Figure 4-20 indicated that the Barkas-Andersen correction would contribute about 10% of the proton total stopping at 1 MeV/u. For Li ions, this increases to about 25% of the total stopping, and this term begins to dominate the correction terms.

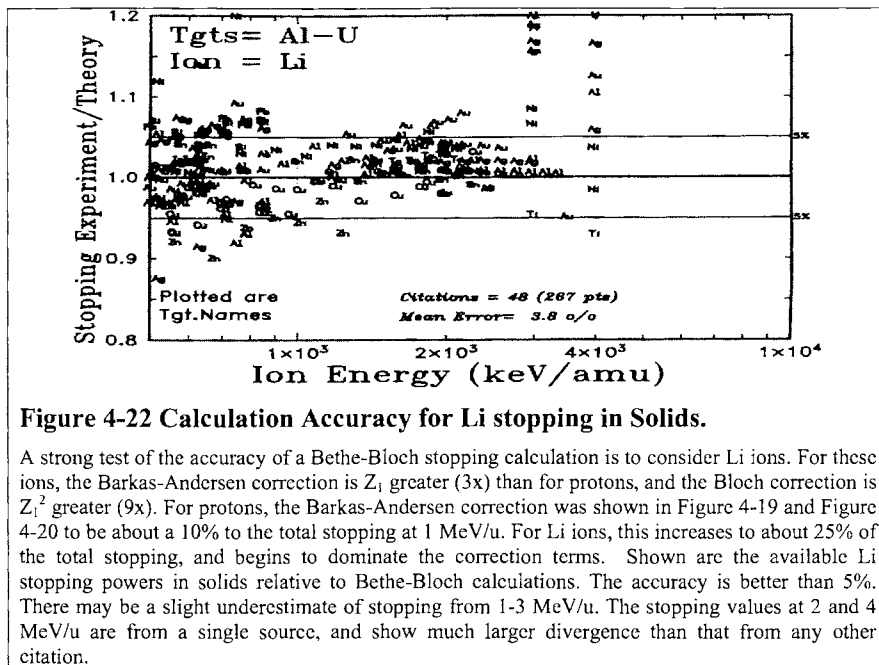


Figure 4-22 Calculation Accuracy for Li stopping in Solids.

A strong test of the accuracy of a Bethe-Bloch stopping calculation is to consider Li ions. For these ions, the Barkas-Andersen correction is Z_i greater (3x) than for protons, and the Bloch correction is Z_i^2 greater (9x). For protons, the Barkas-Andersen correction was shown in Figure 4-19 and Figure 4-20 to be about a 10% to the total stopping at 1 MeV/u. For Li ions, this increases to about 25% of the total stopping, and begins to dominate the correction terms. Shown are the available Li stopping powers in solids relative to Bethe-Bloch calculations. The accuracy is better than 5%. There may be a slight underestimate of stopping from 1-3 MeV/u. The stopping values at 2 and 4 MeV/u are from a single source, and show much larger divergence than that from any other citation.

Shown in Figure 4-22 are the available Li stopping powers in solids relative to Bethe-Bloch calculations. There may be a slight underestimate of Li stopping at 1-3 MeV/u but the general accuracy is better than 5%.

The stopping values at 2 and 4 MeV/u are from a single source, and show much larger divergence than that from any other citation. Excluding these data, the calculation agrees with the data from the other 46 different papers to about 2%.

APPENDIX

. Stopping Powers using the Local Density Approximation

. Lindhard Stopping in a Free Electron Gas

Fundamental electronic interactions of a particle with a plasma have been extensively treated by Lindhard⁸⁷, Neufeld and Ritchie⁸⁸ and Fano¹⁵. We review primarily the results of Lindhard who presented generalized methods to treat the response of a free electron gas to a perturbation and present Lindhard's explicit function for the interaction.

Lindhard, in 1954, developed the first comprehensive study of the energy loss of a particle to a free electron gas (FEG).⁸⁷ Using the first Born approximation, he found a complete solution which included polarization of the medium by the particle's fields. Later, Lindhard and Winther developed analytic expansions for this energy loss.⁸⁸ These expressions were then used by Bonderup for the first calculation of stopping powers using the Lindhard formalism.⁸⁹ Bonderup calculated the energy loss of a particle in a FEG at various densities. He then assumed a Lens-Jensen model for a target atom, and calculated stopping powers based upon using the Local Density Approximation (LDA) as discussed below.

Local Density Approximation solutions to solid-state problems are widely used because they are usually simple to evaluate, and are quite accurate for some problems.

The Lindhard treatment is a many-body self-consistent treatment of an electron gas responding to a perturbation by a charged particle. It naturally includes the polarization of the electrons by the charged particle and the resultant charge screening and the plasma density fluctuations. It treats smoothly both individual electron excitation and collective plasmon excitations without separate 'distant' and 'close' collision processes. Finally, when used with the local-density-approximation it can be directly applied to any target and, for example, the effects of chemical bonding or crystal structure on stopping powers can be treated. Lindhard's approach to the interaction of a particle with a free electron gas makes the following assumptions:

- The free electron gas consists of electrons at zero temperature (single electrons are described by plane waves) on a fixed uniform positive background with overall charge neutrality.
- The initial electron gas is of uniform density.
- The interaction of the charged particle is a small perturbation on the electron gas.
- All particles are non-relativistic.

The electronic stopping of a charged particle in the local density approximation may be stated as:

$$\text{Eq. 4-40} \quad S_e = \int I(v, \rho) Z_1^2 \rho d^3x$$

where S_e is the electronic stopping cross-section; I is the stopping interaction function of a particle of unit charge with velocity, v , in a free electron gas of density ρ , Z_1 is the charge of the particle, ρ is the electronic density of the target, and the integral is performed over each volume element, d^3x , of the target. (We use this form of a stopping equation because it expands simply to the form that will be needed for heavy ions). The electronic density of a target atom is normalized so that its atomic number $Z_2 = \int \rho d^3x$ with the integration over the atomic volume. Each of the three components of Eq. 4-40 will be discussed below.

With these assumptions, Lindhard derived the interaction function, I, as:

$$\text{Eq. 4-41} \quad I = \frac{4\pi e^4}{mv^2} \cdot \frac{i}{\pi\omega_0^2} \int_0^\infty \frac{dk}{k} \int_{kv}^\infty \omega d\omega \left[\frac{1}{\varepsilon^L(k, \omega)} - 1 \right]$$

where the longitudinal dielectric constant, ε^L , is derived to be

$$\text{Eq. 4-42} \quad \varepsilon^L = 1 + \frac{2m^2\omega_0^2}{\hbar^2 k^2} \quad x \downarrow$$

$$x \sum_n \frac{f(E_n)}{N} \left[\frac{1}{k^2 + 2\vec{k} \cdot \vec{k}_n - \frac{2m(\omega - i\delta)}{\hbar}} + \frac{1}{k^2 - 2\vec{k} \cdot \vec{k}_n + \frac{2m(\omega - i\delta)}{\hbar}} \right]$$

where e and m are the charge and mass of the electron; ω_0 is the classic plasma frequency defined as $\omega_0^2 = 4\pi e^2 \rho / m$; E_n is the energy and k_n the wave vector of the electron in the n 'th state; $f(E_n)$ is the distribution function and is an even function of k_n , and δ is a small damping factor. Simple polynomial fits to a numeric evaluation of Eq. 4-41 can be found in Ref. 90.

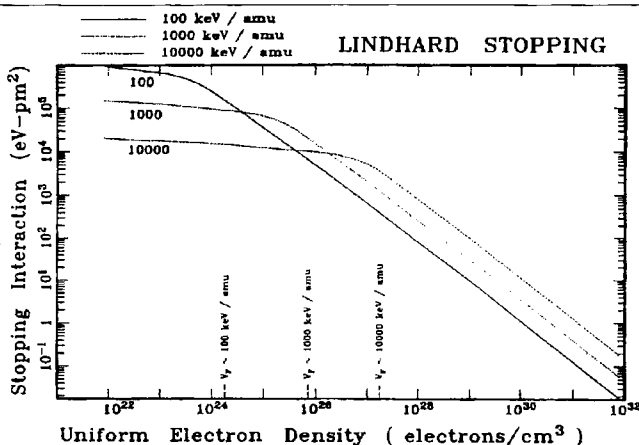


Figure 4-23 Stopping interaction of a particle with a free electron gas.

The stopping interaction derived by Lindhard is shown in the text as Eq. 4-41. It has been calculated for five orders of magnitude of electron density, and for three different particle velocities. Each curve is flat for the section where the particle is much faster than the electrons in low density electron gases. At about the point where the particle velocity equals the Fermi velocity of an electron gas (see arrows above) the interaction curve inflects. For greater density electron gases the interaction becomes less since some of the electrons are moving faster than the particle and these collisions become more adiabatic.

The physical properties of Lindhard's particle-plasma interaction theory can be shown in several ways. In Figure 4-23 is shown the interaction term, I, of Eq. 4-41 and Eq. 4-42, versus a free electron gas density. Each curve has a horizontal slowly-changing section at low electron densities

where the ion is going much faster than the mean electron velocity. Each curve bends down where the ion velocity becomes equal to the Fermi velocity, v_F , of the free electron gas, defined as

$$\text{Eq. 4-43} \quad v_F = \left(\frac{\hbar}{m} \right) (3\pi^2 \rho)^{1/3}$$

For example, in Figure 4-23 the top curve is for particles with velocity of 100 keV/u = 4.4 x

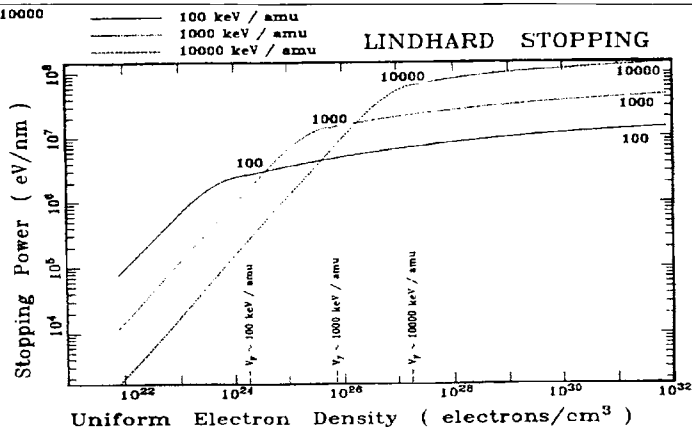


Figure 4-24 The energy loss per unit distance in a free electron gas.

The stopping power or energy loss per unit path length of a particle in a free electron gas is the product of the interaction strength shown in Figure 4-23 times the electron density. These two factors compete since as the electron density increases, the number of electrons per unit volume increases but the interaction strength decreases. The result is a linear increase of stopping power with electron density for dilute gases, and then a leveling off for more dense gases. The inflection-point for a particle is where its velocity equals the Fermi velocity of a free electron gas as indicated by the arrows above.

10^8 cm/sec. The Fermi velocity for an electron density of $10^{24}/\text{cm}^3$ is about 3.5×10^8 cm/sec, which is where the curve is inflecting. For low velocities, $v < v_F$, there are mostly binary encounters between the projectile and the target electrons, with a maximum energy transfer of $\Delta E_{\max} = m_e v_i (v_i + v_e)$. The inflection of the curve with increasing electron density, when $v \sim v_F$, is due to two effects: the projectile can no longer ($v < 1.3 v_F$) excite a plasmon, and the electrons at the center of the Fermi sphere can not gain sufficient momentum in a collision to have their final states outside of the Fermi sphere. At higher electron densities, plasmons of the free electron gas can respond adiabatically, reducing energy transfer. For any single electron density there is an inflection of interaction strength which occurs for particles with a velocity about equal to the electron Fermi velocity.

In Figure 4-24 is shown I_p , the interaction term, I , times the electron charge density, ρ . If the particle has a unit charge, this plot shows the differential energy loss per unit path length, i.e. the stopping power, in units of eV/cm, for a particle in a uniform free electron gas. This figure shows how stopping power is dominated not only by the local electron density, but also by the interaction strength term shown in Figure 4-24 which depends on the ion velocity.

Stopping Calculations using Local Density Approximation

The electronic energy loss of a proton in a solid (in contrast to a free electron gas) can be calculated using the above approach. In essence, this approximation assumes that each volume element of the solid is an independent plasma. The stopping power is calculated for

a particle in a plasma of each volume element's density, and the final stopping power is computed by averaging over these values, weighted by their distribution in the solid. Referring to Eq. 4-40:

$$\text{Eq. 4-44} \quad S_e = \int I(v, \rho) (Z_1^*(v))^2 \rho \, dx^3$$

where I is the interaction of the particle with velocity, v , in a plasma of density, ρ . The charge of the projectile, Z_1^* , has an asterisk to indicate this may be a value different from the atomic number because the ion may not be fully stripped. By integrating over the volume, dx^3 , we weigh each density interaction by the probability of that density occurring in the solid.

An extended comment might be made to explain the local-density-approximation to those completely unfamiliar with it. This is a widely used method to evaluate the theoretical mean response of a solid to a perturbation. For our application, we consider the solid to be an electronic plasma with fluctuations in density. We first calculate the interaction (energy loss) of an energetic particle immersed in a uniform plasma sea with the same electronic density as any single volume element of the solid. A basic assumption is now made that the averaged interaction of a single particle with a uniform plasma is *identical* to the averaged interaction of a single volume element of plasma with a particle whose spatial location is uniformly probable.

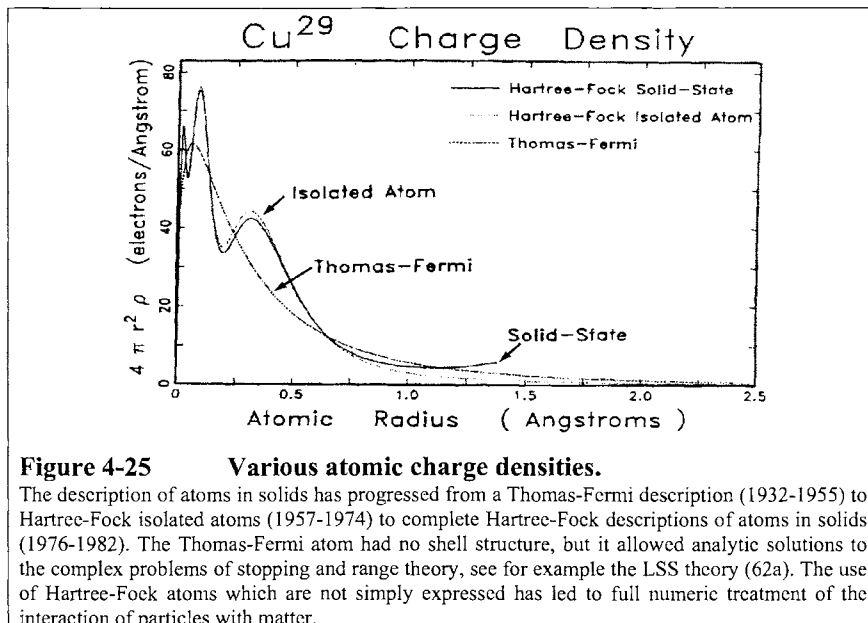


Figure 4-25 Various atomic charge densities.

The description of atoms in solids has progressed from a Thomas-Fermi description (1932-1955) to Hartree-Fock isolated atoms (1957-1974) to complete Hartree-Fock descriptions of atoms in solids (1976-1982). The Thomas-Fermi atom had no shell structure, but it allowed analytic solutions to the complex problems of stopping and range theory, see for example the LSS theory (62a). The use of Hartree-Fock atoms which are not simply expressed has led to full numeric treatment of the interaction of particles with matter.

This equivalence allows the evaluation of the mean interaction of a single particle with a single

volume of element plasma. This process is then repeated for the interaction of the particle with every volume element of the solid target to obtain the mean interaction of the particle with the solid.

Two of the more important assumptions in using this approach with Lindhard stopping theory for energy loss calculations are:

- The electron density in the target varies slowly with position.
- Available electron energy levels and transition strengths of the atoms of the solid are identical to those in a free electron gas.

The basic physics of applying the local density approximation to stopping powers in solids may be seen in plots of the integrand of the stopping cross-section, Eq. 4-40, as evaluated for atomic targets, see Figure 4-26 to Figure 4-27. These plots show three curves which link the various parts of the stopping process.

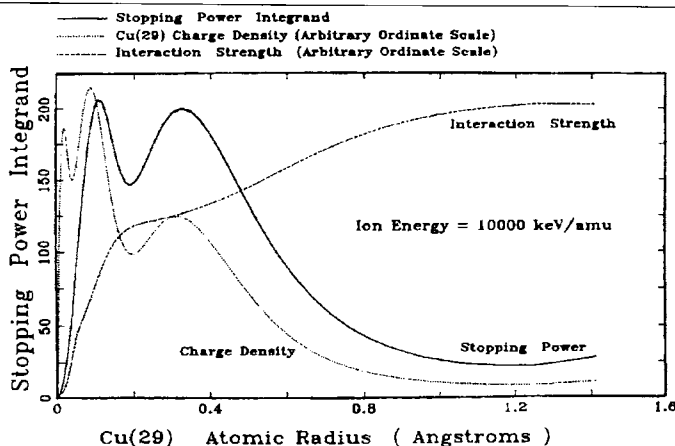


Figure 4-26 Interaction strength of high speed particle with copper atom.

The nature of the interaction of a high speed particle with a solid is illustrated by considering a target of copper (Cu). The dotted line is the charge distribution of a Cu atom in a solid, see Figure 4-25. The dashed curve is the interaction strength, I , of a high velocity particle (10^4 keV/u) with the charge distribution. It is small only for the inner k -shell electrons. The product I_p is the stopping cross-section, Eq. 4-44. This product is shown a solid line. It shows that the energy loss is evenly distributed across the Cu electrons except for the inner shell.

Figure 4-25 shows various shapes of the charge density of Cu with the Thomas-Fermi atom shown as a dashed line, the isolated atom Hartree-Fock atom shown as a dotted line and the solid-state Cu atom shown as a solid line. The plots use for an ordinate the factor $4\pi r^2 \rho$, where ρ is the electron density. With this factor, the area under the curve equals 29, the atomic number of Cu. Clearly the Thomas-Fermi atom has no shell-structure but is a reasonable average value. The isolated atom Hartree-Fock curve shows a pronounced shell structure but it has a long tail extending out many Angstroms since it is not confined. Finally, the solid-state structure of each individual atom is contained within 1.4 Å, with the electrons from 1.2-1.4 Å being averaged over the Wigner-Seitz cell of the Cu face-centered-cubic crystal.

Figure 4-26 shows as a dotted line the same solid-state Cu distribution as shown Figure 4-25. It shows as a dashed line the value of the particle-plasma interaction term, I , of Eq. 4-41 and Eq. 4-42 and of Figure 4-23. For each radius, the density of the Cu atom is taken and the equivalent I is calculated as indicated in Figure 4-23. Since Figure 4-26 specifies that the ion has a velocity of 10000 keV/u (about 20 times the Bohr velocity) it is moving much faster than most of the electrons in the solid, and so its interaction is relatively independent of the electron velocity. In the density of electrons in Cu is mostly on the flat section of the curve labeled 10000 keV.

Finally, the term ρI is plotted as a solid line in Figure 4-26. The area under this curve is the integral of Eq. 4-40 and hence is the stopping cross-section of a moving charged particle in Cu. This solid line shows how the energy loss is distributed among the various Cu electrons with all but the innermost electrons absorbing energy about proportional to their density.

In contrast, Figure 4-27 shows the same set of curves except they are evaluated for a low

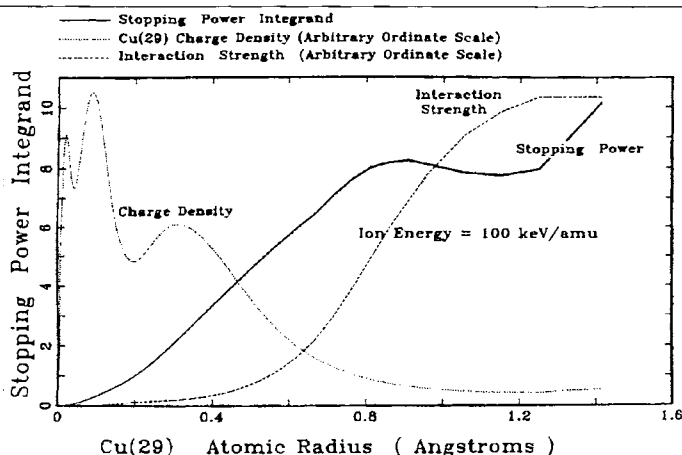


Figure 4-27 Interaction strength of slow speed particle with copper atom.

The interaction of a slow particle with copper. The dotted line is the electronic charge distribution of a Cu atom in a solid. The dashed curve is the interaction strength of the slow particle with this distribution. There is almost no interaction with the core electrons, and the interaction is almost exclusively with the conduction electrons. The solid line shows the stopping integrand, Eq. 4-44 and shows that the electronic energy transferred to either copper atom is mostly to the outer electrons. Since there is little energy transferred to either the K or L shells, it indicates there will be few x-rays produced during de-excitation of the atom.

velocity particle of 100 keV/u (about twice the Bohr velocity). The copper density curve (dotted line) is identical to that of Figure 4-25. The dashed interaction curve is quite different from that of Figure 4-26 for the particle is now at a velocity which is large only when compared to the low density outermost electrons of Cu atoms. For the high density electrons the interaction is almost adiabatic and there is little excitation. The solid line, ρI , is the integrand of the stopping power cross-section and it is clear that the outer shell electrons, about 20% of the total electrons, absorb almost 90% of the energy loss. The inner k-shell electrons absorb almost no energy and one would anticipate that there would be almost no k-shell x-rays emitted from the Cu target.

Table-4-1
Stopping Powers for Protons in Aluminum, Al(13)

Proton Energy (MeV)	Stopping Power MeV/g-cm ²	L Stopping Number	L ₀	f(β)	Shell+ ln<I>	δ/2 Density Corr.	L ₁ Barkas Corr.	L ₂ Bloch Corr.
1	172.7	2.483	2.382	7.684	- 5.301	- 0.00001	0.1301	-0.0294
5	57.1	4.078	4.031	9.287	- 5.256	- 0.00003	0.0533	-0.0060
10	33.79	4.789	4.753	9.972	- 5.219	- 0.00008	0.0389	-0.0030
50	9.582	6.383	6.364	11.52	- 5.16	- 0.00085	0.0198	-0.0006
100	5.67	7.022	7.007	12.16	- 5.149	- 0.00273	0.0150	-0.0003
1,000	1.746	9.034	9.029	14.25	- 5.138	- 0.08686	0.0059	-0.0000
10,000	1.764	11.84	11.84	17.74	- 5.138	- 0.7688	0.0023	-0.0000

Table-4-2
Percent contribution towards Stopping Number L

Proton Energy (MeV)	L ₀	f(β)	Shell+ ln<I>	δ/2 Density Corr.	L ₁ Barkas Corr.	L ₂ Bloch Corr.
1	95.95	309.5	- 207	- 0.0004	5.239	-1.187
5	98.84	227.7	- 126.1	- 0.0007	1.308	-0.1479
10	99.25	208.2	- 107.3	- 0.0016	0.8124	-0.0632
50	99.7	180.5	- 80.48	- 0.0133	0.3116	-0.0101
100	99.79	173.2	- 73.15	- 0.0388	0.2141	-0.0049
1,000	99.93	157.8	- 56.85	- 0.9614	0.0661	-0.001
10,000	99.98	149.9	- 43.39	- 6.495	0.0201	-0.000

Table-4-3
Stopping Powers for Protons in Gold, Au(79)

Proton Energy (MeV)	Stopping Power MeV/g-cm ²	L Stopping Number	L ₀	f(β)	Shell+ ln<I>	δ/2 Density Corr.	L ₁ Barkas Corr.	L ₂ Bloch Corr.
1	63.58	1.098	1.03	7.68	- 6.65	- 0.0000	0.0939	-0.0294
5	27.87	2.391	2.34	9.28	- 6.94	- 0.0001	0.0499	-0.0060
10	18.06	3.074	3.03	9.97	- 6.933	- 0.0002	0.03776	-0.0030
50	5.923	4.74	4.72	11.5	- 6.803	- 0.0010	0.0198	-0.0006
100	3.639	5.415	5.4	12.1	- 6.756	- 0.0025	0.015	-0.0003
1,000	1.203	7.478	7.47	14.2	- 6.696	- 0.0856	0.0059	-0.0000
10,000	1.289	10.39	10.3	17.7	- 6.691	- 0.6642	0.0023	-0.0000

Table-4-4
Protons into Gold: Percent contribution towards Stopping Number L

Proton Energy (MeV)	L ₀	f(β)	Shell+ ln<I>	δ/2 Density Corr.	L ₁ Barkas Corr.	L ₂ Bloch Corr.
1	94.1	699.	- 606.7	- 0.0000	8.555	-2.683
5	98.1	388.	- 278.9	- 0.0033	2.087	-0.2523
10	98.87	324.4	- 217	- 0.0052	1.229	-0.0991
50	99.6	243.1	- 140.7	- 0.0204	0.4177	-0.0136
100	99.73	224.5	- 123.1	- 0.0465	0.2771	-0.0064
1,000	99.92	190.6	- 89.12	- 1.145	0.0798	-0.0011
10,000	99.98	170.8	- 64.15	- 6.393	0.0228	-0.0006

CHAPTER 4 - REFERENCES

- 1 Mme. Pierre Curie, Comptes Rendus, 130, 76 (1900).
- 2 J. J. Thomson, "Conduction of Electricity through Gases", Cambridge University Press (1903).
- 3 H. Gieger and E. Marsden, Proc. Roy. Soc., 82, 495 (1909).
- 4 E. Rutherford, Phil. Mag., 21, 212 (1911); ibid. 21, 699 (1911).
- 5 J. J. Thomson, Phil. Mag., 6-23, 449 (1912).
- 6 N. Bohr, Phil. Mag., 25, 10 (1913).
- 7 N. Bohr, Phil. Mag., 30, 581 (1915).
- 8 H. Bethe, Ann. Physik, 5, 325 (1930).
- 9 H. Bethe, Z. Phys., 76, 293 (1932).
- 10 F. Bloch, Ann. Phys., 16, 285 (1933).
- 11 F. Bloch, Z. Phys., 81, 363 (1933).
- 12 U. Fano, Ann. Rev. Nucl. Sci., 13, 1 (1963). This extended work is based on earlier papers;); U. Fano, Phys. Rev.
- 13 U. Fano, Phys. Rev., 72, 26 (1947).
- 14 U. Fano, Phys. Rev., 102, 385 (1956).
- 15 U. Fano, Phys. Rev., 103, 1202 (1956).
- 16 U. Fano, Ann. Rev. Nucl. Sci., 13, 67 (1963). This paper can also be found in reference 22, included as Appendix A.
- 17 M. Inokuti, Rev. Mod. Phys., 43, 297 (1971)
- 18 H. Bichsel, Amer. Inst. of Physics Handbook, McGraw-Hill, New York, 8-142 (1972).
- 19 P. Sigmund, Radiation Damage Processes in Materials, C. duPuy, cd., Noordhoff, Leiden, 3 (1975).
- 20 J. D. Jackson, Classical Electrodynamics, 2nd Ed., Wiley, New York, Chap. 13, 15 (1975).
- 21 S. P. Ahlen, Rev. Mod. Phys., vol. 52, 121 (1980).
- 22 U. Fano, Chr., Studies in Penetration of Charged Particles in Matter, Nucl. Sci. Rpt., 39, U. S. National Academy of Sciences, Washington, 1-338 (1964).
- 23 L. C. Northcliffe and R. F. Schilling, Nucl. Data Tables, 7, 233-463 (1970).
- 24 J. F. Janni, Atom. Data and Nucl. Data Tables, vol. 27, (1982). Two volumes.
- 25 H. H. Andersen and J. F. Ziegler, Hydrogen Stopping Powers and Ranges in All Elements, Pergamon, New York (1977).
- 26 J. F. Ziegler, Helium Stopping Powers and Ranges in All Elemental Matter, Pergamon, New York (1977).
- 27 ICRU-49, H. O. Wyckoff (ICRU Scientific Counsellor), "Stopping Powers and Ranges for Protons and Alpha Particles", Intl. Comm. on Rad. Units, Bethesda, MD (1993).
- 28 G. H. Henderson, Phil. Mag., vol. 44, 680 (1922).
- 29 I. A. Gaunt, Proc. Camb. Phil. Soc., vol. 23, 732 (1927).
- 30 N. F. Mott, Proc. Camb. Phil. Soc., vol. 27, 553 (1931).
- 31 C. Moller, Ann. Physik, vol. 14, 531 (1932).
- 32 J. J. Thomson, "Conduction of Electricity Through Gases", Cambridge University Press, (1903). J. J. Thomson, Phil. Mag., 6-23, 449 (1912).
- 33 E. Rutherford, Phil. Mag., 21, 212 (1911); ibid 21, 699 (1911).
- 34 N. Bohr, Phil. Mag., 25, 10 (1913).
- 35 W. E. Lamb, Phys. Rev., 58, 696 (1940).
- 36 N. Bohr, Phys. Rev., 58, 654 (1940).
- 37 N. Bohr, Phys. Rev., 59, 279 (1941).

- 38 L. C. Northcliffe, Phys. Rev., 120, 1744 (1960).
39 N. Bohr, Kgl. Dansk. Vid. Scl., Mat.-Fys. Medd., 18, 1 (1948).
40 M. C. Walske, Phys. Rev., 88, 1283 (1952), and Phys. Rev., 101, 940 (1956).
41 M. C. Walske, Phys. Rev., 101, 940 (1956).
42 G. S. Khandelwal, Nucl. Phys., A116, 97 (1968).
43 H. Bichsel, Univ. of Calif. Rpt. USC-136-120.
44 G. S. Khandelwal and E. Merzbacher, Phys. Rev., 144, 349 (1966).
45 H. Bichsel, Studies in Penetration of Charged Particles in Matter, U. S. Natl. Acad. Sci., Pub. 1133, 17-38 (1964).
46 H. Bichsel, Amer. Inst. Phys. Handbook, McGraw Hill, New York, 8-142 (1972).
47 H. Bichsel, Phys. Rev. A, 28, 1147 (1983).
48 H. Bichsel, Phys. Rev. A, 46, 5761 (1992). Includes citations to numerous prior calculations.
49 C. C. Rousseau, W. K. Chu and D. Powers, Phys. Rev., A4, 1066 (1970).
50 J. F. Ziegler, "Handbook of Stopping Cross-Sections for Energetic Ions in All Elements", Pergamon Press (1980).
51 J. Lindhard and M. Scharff, Mat. Fys. Medd. Dan. Vid. Selsk., 27, No. 15 (1952).
52 W. K. Chu and D. Powers, Phys. Lett., 40A, 23 (1972).
53 W. F. G. Swann, J. Franklin Inst., 226, 598 (1938).
54 E. Fermi, Phys. Rev., 57, 485 (1940),
55 R. M. Sternheimer, Phys. Rev., 117, 485 (1960).
56 R. M. Sternheimer, Phys. Rev., 145, 247 (1966).
57 R. M. Sternheimer, S. M. Seltzer and M. J. Berger, Phys. Rev., B26, 6067 (1982).
58 A. Crispin and G. N. Fowler, Rev. Mod. Phys., 42, 290 (1970).
59 M. Inokuti and D. Y. Smith, Phys. Rev., B25, 61 (1982).
60 J. C. Ashley, Radiat. Res., 89, 32 (1982).
61 H. Bichsel, Rev. Mod. Phys., 60, 663 (1988).
62 ICRU Report #37, H. O. Wyckoff (ICRU Scientific Counsellor), "Stopping Powers for Electrons and Positrons", Intl. Comm. on Rad. Units, Bethesda, MD (1984).
63 W. H. Barkas, W. Birnbaum and F. M. Smith, Phys. Rev., 101, 778 (1956). See also the later paper: W. H. Barkas, N. J. Dyer and H. H. Heckmann, Phys. Rev. Lett., 11, 26 (1963).
64 H. H. Heckman, "Penetration of Charged Particles in Matter", U.S. National Academy of Science Report # 1133, Washington, D.C., 41 (1970).
65 H. H. Andersen, H. Simonsen and J. Serensen, "An Experimental Investigation of Charge-Dependent Deviations for the Bethe Stopping Power Formula", Nucl. Phys., A125, 171-175.
66 J. C. Ashley, R. H. Ritchie and W. Brandt, Phys. Rev., B5, 2393 (1972).
67 J. C. Ashley, R. H. Ritchie and W. Brandt, Phys. Rev., A8, 2404 (1973)
68 J. C. Ashley, V. E. Anderson, R. H. Ritchie and W. Brandt, National Auxiliary Publication Service, New York.
69 J. D. Jackson and R. L. McCarthy, Phys. Rev., B6, 4131 (1972).
70 K. W. Hill and E. Merzbacher, Phys. Rev., A9, 156 (1974).
71 J. Lindhard, Nucl. Inst. Methods, 132, 1 (1976).
72 R. Medenwaldt, S. P. Moller, E. Uggerhoj, T. Worm, P. Hvelplund, H. Knudsen and K. Eksner, Nucl. Inst. Methods, B58, 1 (1991), and Phys. Rev. Lett., A155, 155 (1991)..
73 H. H. Andersen, J. F. Bak, H. Knudsen, P. Moller-Petersen and B. R. Nielsen, "Physics of Ionized Gases", Navinsek (ed.), J. Stefan Institute, Ljubljana, 221 (1976). H. H. Andersen, J. F. Bak, H. Knudsen, and B. R. Nielsen, Phys. Rev., A16, 1929 (1977). H. H. Andersen,

- 74 Physica Scripta, 28, 268 (1983).
 75 H. H. Mikkelsen and P. Sigmund, Phys. Rev., A40, 101 (1989).
 76 H. H. Mikkelsen and E. H. Mortensen, Nucl. Inst. Methods, B48, 39 (1990).
 77 H. Esbensen and P. Sigmund, Ann. Physics, 201, 152 (1990). See also: H. Esbensen, Ph.
 78 D. Thesis, Odense University, Denmark (1991).
 79 H. H. Mikkelsen, H. Exbensen and P. Sigmund, Nucl. Inst. Methods, B48, 8 (1990).
 80 H. H. Mikkelsen and H. Flyvbjerg, Phys. Rev., A45, 3025 (1992).
 81 P. Sigmund, Nucl. Inst. Methods, B85, 541 (1994).
 82 L. H. Andersen, P. Hvilstedt, H. Knudsen, S. P. Moller, J. O. P. Pedersen, E. Uggerhoj,
 83 K. Elsener and E. Morenzoni, Phys. Rev. Lett., 62, 1731 (1989).
 84 H. Bichsel and L. E. Porter, Phys. Rev., A25, 2499 (1982).
 85 H. H. Andersen, J. F. Bak, H. Knudsen and B. R. Nielsen, Phys. Rev., A16, 1929 (1977).
 86 H. Bichsel, Phys. Rev., A41, 3642 (1990).
 87 H. Bichsel, Phys. Rev., A41, 3642 (1990).
 88 H. H. Andersen, K. N. Tu and J. F. Ziegler, Nucl. Inst. Methods, 149, 247-251 (1978).
 89 J. Neufeld and R. H. Ritchie, Phys. Rev., 98, 1632 (1955).
 90 J. Lindhard, Mat. Fys. Medd. Dan. Vid. Selsk., 28, No. 8 (1954).
 91 J. Lindhard and A. Winther, Mat. Fys. Medd. Dan. Vid. Selsk., 34, No. 4 (1964).
 92 E. Bonderup, Mat. Fys. Medd. Dan. Vid. Selsk., 35, No. 17 (1967).
 93 G. J. Iafrate and J. F. Ziegler, J. Appl. Phys., 50, 5579 (1979) plus errata available from the
 authors.

5 - Stopping of Ions in Compounds and Gases

5 - Stopping of Ions in Compounds and Gases	5-1
Early Experimental Studies	5-1
Examples of Compound Corrections	5-6
Calculation of Core and Bond Stopping Corrections	5-12
Bragg's Rule and Heavy Target Elements	5-17
Examples of Stopping Correction for Compounds	5-17
<i>Stopping Correction for a target of Ethylene</i>	5-17
<i>Stopping Correction for a target of Polystyrene</i>	5-19
Details and Limitations - Core and Bond Theory	5-21
The Phase Correction (Gas/Solid) to Stopping.....	5-21
Chapter Citations	5-22

Soon after the discovery of energetic particle emission from radioactive materials, there was interest about how these corpuscles were slowed down while transversing matter. In 1900 Marie Curie stated: "*Les rayons alpha sont des projectiles matériels susceptibles de perdre de leur vitesse en traversant la matière.*" [00a] Scientists realized that since these particles could penetrate thin films, experiments measuring their energy loss and scatter might finally unravel the secrets of the atom. Bragg and Kleeman started to conduct such experiments with a radium source in 1903, but were unable to find many types of thin films, since there were no "goldbeaters" in Australia. So they studied the energy loss of alpha particles in hydrocarbon gases such as methyl bromide and methyl iodide to find out how alpha stopping depended on the atomic weight of the target. They analyzed the stopping contribution of hydrogen and carbon atoms in various hydrocarbon target gases by a subtraction of the stopping powers in equivalent pure carbon and hydrogen targets. From their analysis in 1905, comes **Bragg's Rule** which states that the stopping of a compound may be estimated by the linear combination of the stopping powers of individual elements.[05a]

This rule was long thought to be reasonably accurate, and the measured stopping of ions in compounds usually deviated less than 20% from that predicted by Bragg's Rule. The accuracy of Bragg's Rule is limited because the energy loss to the electrons in any material depends on the detailed orbital and excitation structure of the matter, and any differences between elemental materials and the same atoms in compounds will cause Bragg's Rule to become inaccurate. Further, any bonding changes may also alter the charge state of the ion, thus changing the strength of its interaction with the target medium.

Early Experimental Studies

Detailed experimental studies of Bragg's Rule started in the 1960s, and some wide discrepancies were found from simple additivity of stopping powers. See Figure 5-1 for an example of H and C non-additivity in simple hydrocarbons.[74a] In this figure, the stopping in various hydrocarbons is taken for pairs of compounds, and the relative contribution of H and C is extracted (solving two equations with two unknowns). It is found that the relative stopping contribution of H and C differs by almost a factor of two over the range of compounds. Similar work studied more complex hydrocarbons but instead of adding H and C bonds, they added extra hydrocarbon molecules. In this study, they found that by adding molecules to hydrocarbon strings, stopping linearity returned.[80a] See Figure 5-2. Adding new molecules just scaled the stopping by the extra number

of atoms. These results showed that atomic bonding had large effects on stopping powers of simple molecules while extra agglomeration of molecules had a small stopping effect.

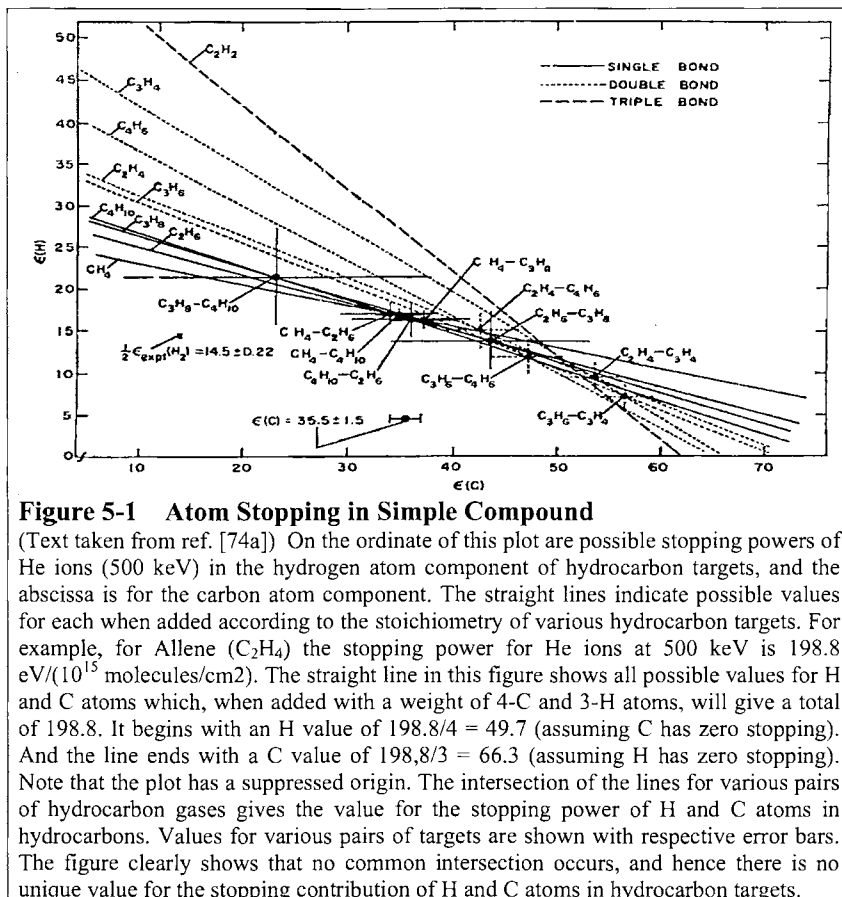


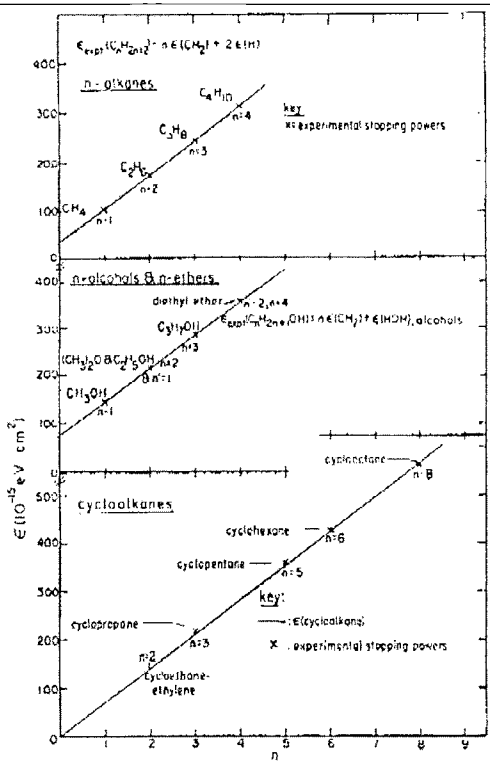
Figure 5-1 Atom Stopping in Simple Compound

(Text taken from ref. [74a]) On the ordinate of this plot are possible stopping powers of He ions (500 keV) in the hydrogen atom component of hydrocarbon targets, and the abscissa is for the carbon atom component. The straight lines indicate possible values for each when added according to the stoichiometry of various hydrocarbon targets. For example, for Allene (C_2H_4) the stopping power for He ions at 500 keV is $198.8 \text{ eV}/(10^{15} \text{ molecules/cm}^2)$. The straight line in this figure shows all possible values for H and C atoms which, when added with a weight of 4-C and 3-H atoms, will give a total of 198.8. It begins with an H value of $198.8/4 = 49.7$ (assuming C has zero stopping). And the line ends with a C value of $198.8/3 = 66.3$ (assuming H has zero stopping). Note that the plot has a suppressed origin. The intersection of the lines for various pairs of hydrocarbon gases gives the value for the stopping power of H and C atoms in hydrocarbons. Values for various pairs of targets are shown with respective error bars. The figure clearly shows that no common intersection occurs, and hence there is no unique value for the stopping contribution of H and C atoms in hydrocarbon targets.

Since these early experiments, theorists have shown that extensive calculations can predict the stopping of light ions (usually protons) in hydrocarbon compounds. Much of this work has been based on a seminal paper by Peter Sigmund that developed methods to account for detailed internal motion within a medium.[82a] This theory allows for arbitrary electronic configurations in the target. Sabin and collaborators used this approach to calculate stopping powers for protons in hydrocarbons with good success.[87x] Sabin's calculation follows what is sometimes called the **Köln Core and Bond (CAB)** approach which is discussed in detail below.

Figure 5-2 Molecular Stopping in Large Compounds

(Text taken from Ref. [80a]) When simple modules are added to hydrocarbon compounds, a linearity has been found in molecular stopping powers. For example, the basic form of alcohol is methanol, CH_3OH , and higher forms of alcohol are formed by inserting modules of CH_2 between the first CH_3 and the final OH groups. The abscissa of this plot shows the number of modules of CH_2 added to basic alkane in the upper figure, to basic alcohol in the middle figure, and to basic cycloalkane in the lower figure. The linearity of the stopping power increase with each additional module of CH_2 implies that each module adds an increment of stopping, and since the slopes of the three lines for the three chemical families are the same, the incremental addition to stopping is independent of the molecule. The stopping of ions in alcohols up to $\text{CH}_3(\text{CH}_2)_{10}\text{OH}$ has been studied and linearity of better than 1% has been observed for the additional CH_2 groups for both He and Li ion stopping power.



We are not going to review the complex theoretical work on stopping in compounds. Our interest is to try to find a simple way to estimate the changes that compounds introduce to the use of Bragg's Rule to generate stopping powers of compounds. For the general user of SRIM, with only a minimal knowledge of the physics of stopping theory, we need a simple method to estimate bonding corrections to stopping.

The Core and Bond (**CAB**) approach suggested that stopping powers in compounds can be predicted using the superposition of stopping by atomic "cores" and then adding the stopping due to the bonding electrons.[83a] The core stopping would simply follow Bragg's Rule for the atoms of the compound, where we linearly add the stopping from each of the atoms in the compounds. The chemical bonds of the compound would then contain the necessary stopping correction. They would be evaluated depending on the simple chemical nature of the compound. For example, for hydrocarbons, carbon in C-C, C=C and C=t=C structures would have different bonding contributions (C=C indicates a double-bond structure and C=t=C is a triple bond). The contribution to stopping by a carbon atom in a C=C bond is almost twice that of a carbon atom single-bond state. And a carbon atom in a triple-bond state contributes even greater stopping powers. See Table 5-1

(below). By merely specifying the bonding of the atoms in the compound, for example, SRIM can then generate a stopping correction required for the compound with this bonding arrangement.

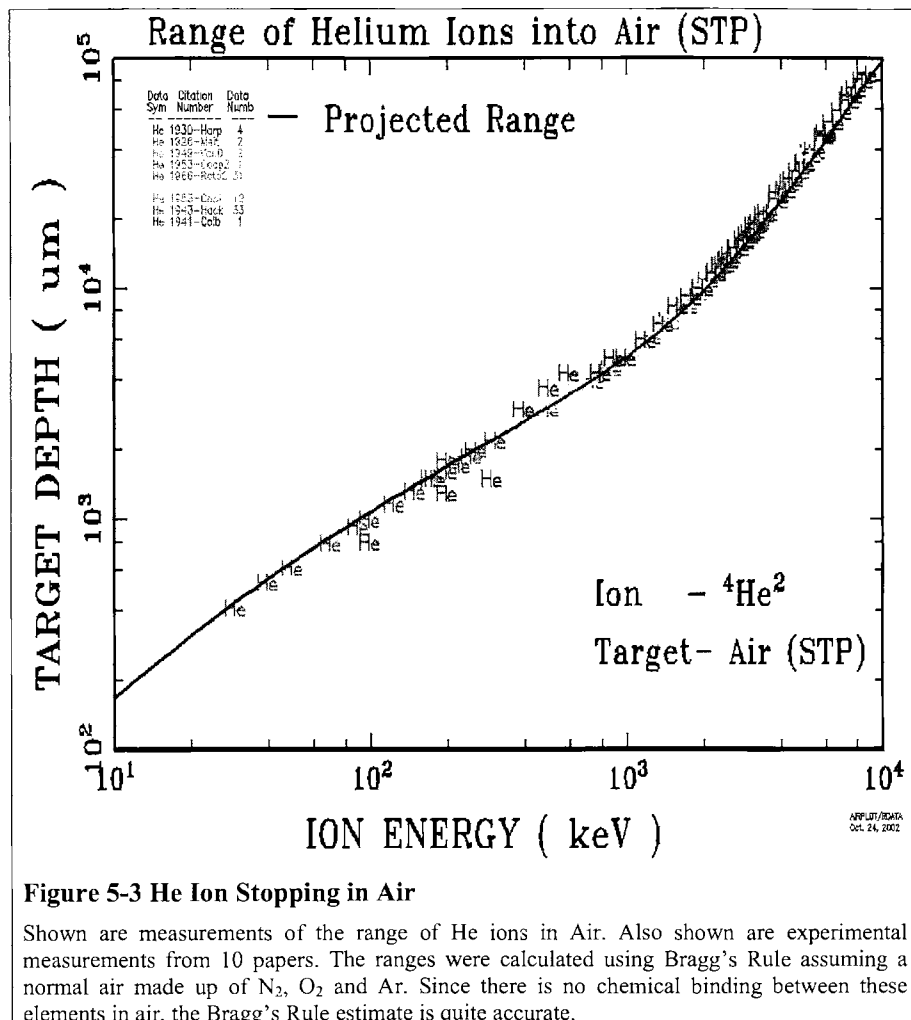
Table 5-1 Original published table of Core and Bonds Values [80x]

TABLE 3			
CORE and BOND Stopping Values			
The following are the stopping powers associated with various cores and bonds using stopping units of $eV/10^5 atoms/cm^2$. These values are for protons at 125 keV.			
Stopping due to atomic CORES :			
Target Atom	Stopping Power		
H	0.000		
C	6.145		
N	5.859		
O	5.446		
F	5.431		
S	32.735		
Cl	28.795		
Stopping due to atomic BONDS :			
Hydrogen Bonds	Carbon Bonds	Other Bonds	
(H-H)	9.590	(N=N)	20.380
(H-C)	7.224	(N-O)	15.795
(H-N)	8.244	(O=O)	21.290
(H-O)	8.758	(S-H)	4.844
		(S-C)	1.617
		(S-F)	8.132
" ≡ " indicates triple bonds.			

SRIM uses this approach to generate corrections between Bragg's Rule and compounds containing the common elements in compounds: H, C, N, O, F, S and Cl. These light atoms have the largest bonding effect on stopping powers. Heavier atoms are assumed not to contribute anomalously to stopping because of their bonds (*discussed later*). When you use SRIM, you have the option to use the **Compound Dictionary** which contains the chemical bonding information for about 250 common compounds. The compounds with corrections are shown with a Star symbol next to the name. When these compounds are selected, SRIM shows the chemical bonding diagram and calculates the best stopping correction. The correction is a variation from unity (1.0 = no correction). Notice that carbon atoms have almost a 4x variation in stopping power from single bonds to triple bonds. This large change indicates the importance of making some sort of correction for the stopping of ions in compounds.

The CAB approach that SRIM uses has been tested on more than 100 compounds, from 162 experiments (*discussed later*). SRIM correctly predicts the stopping of H and He ions in compounds with an accuracy of better than 2% at the peak of the stopping curve, ~125 keV/u.

You can introduce other compounds to SRIM by adding to the Compound Dictionary. You need to edit the file ..\Data\COMPOUND.dat. Instructions are at the top of the file, and included are more than 250 examples to guide you in creating your own compounds. SRIM will use your chemical bonding information to calculate the stopping correction. SRIM can only calculate bonding corrections for the seven elements: H, C, N, O, F, S and Cl. Any other elements will be assumed to have the same stopping as in their elemental form.



Examples of Compound Corrections

As an example of where Bragg's Rule works well without correction, consider the range of He ions into air. Air is a mixture of N₂, O₂ and Ar, all elements which are gaseous in their normal state. So the combined stopping powers would be expected to be quite close to Bragg's Rule. Figure 5-3 shows calculated and experimental range of He ions in air. The citations of the plotted data are listed in the SRIM website¹. These citations date back 100 years since energetic alpha particles were available since the discovery of radioactivity. The solid line is the SRIM calculation for AIR, which uses just the Bragg additivity of ion stopping in N(76%), O(23%) and Ar(1%).

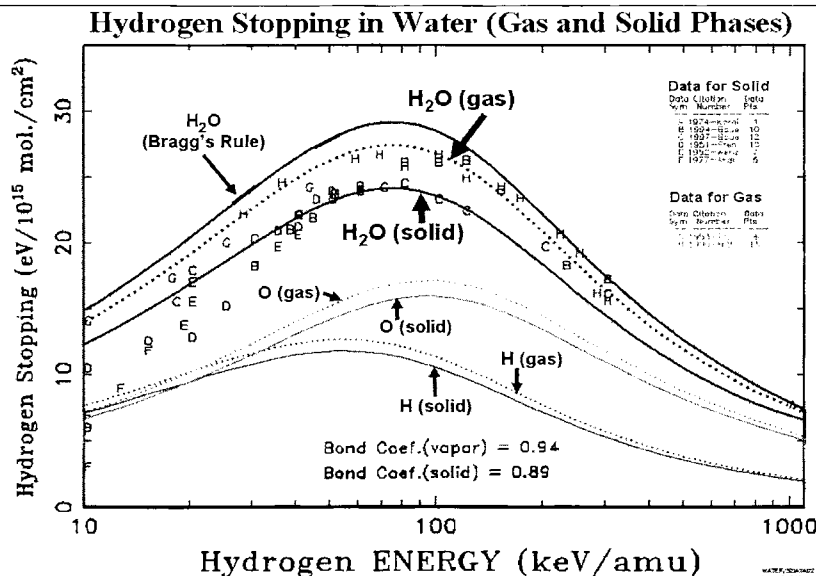


Figure 5-4 H Ion Stopping in Solid and Vapor Phases of Water

Shown are measurements of the range of H ions in Water in both vapor and liquid phases. This plot shows a clear "phase effect" in which the stopping power of protons varies depending whether the same target is in liquid phase or solid phase. From such experiments comes the "Phase Correction" for ion stopping powers. See the extended caption of Figure 5-5 for details of the various curves.²

An example of where Bragg's Rule fails is for water. Hydrogen undergoes a very large change in structure when it is in most compounds. Typically, hydrogen's stopping changes by up to 30% in compounds, but since its contribution to total stopping is small, its bonding may be a small change to the total stopping. Also, there is a phase change for solid water (ice) since stopping powers for H and O are most commonly measured in gaseous state, and we need stopping powers for both water vapor and water solid (ice). Figure 5-4 shows the stopping of protons in water using simple additivity (labeled **Bragg's Rule**), and with the corrections from the Compound Dictionary. The

¹ - www.srim.org/SRIM/Compounds/Citations/Air-He.pdf

² NOTE: All plots in this Chapter can be found on the website: [www.srim.org/SRIM/ Compounds](http://www.srim.org/SRIM/Compounds) Since these plots are in color, the various curves are easy to distinguish.

data is rather erratic, but the general trends are clear. The citations of the plotted data are in the file "Water".³

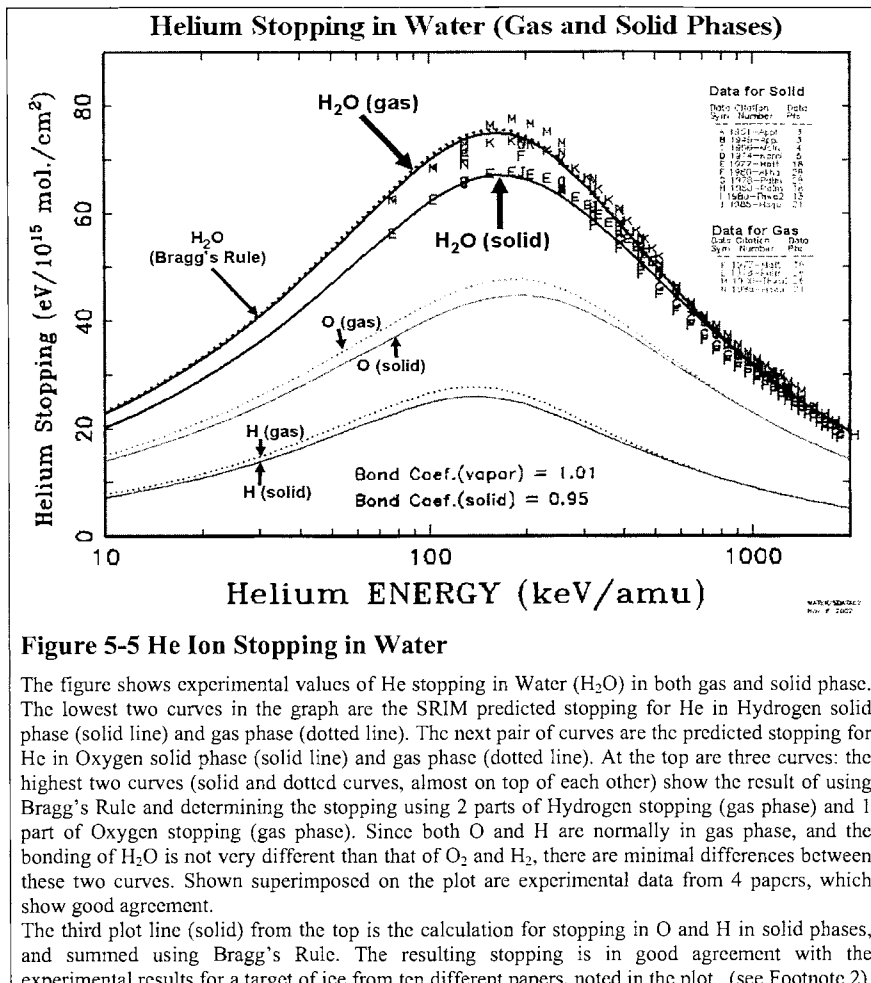


Figure 5-5 He Ion Stopping in Water

The figure shows experimental values of He stopping in Water (H_2O) in both gas and solid phase. The lowest two curves in the graph are the SRIM predicted stopping for He in Hydrogen solid phase (solid line) and gas phase (dotted line). The next pair of curves are the predicted stopping for He in Oxygen solid phase (solid line) and gas phase (dotted line). At the top are three curves: the highest two curves (solid and dotted curves, almost on top of each other) show the result of using Bragg's Rule and determining the stopping using 2 parts of Hydrogen stopping (gas phase) and 1 part of Oxygen stopping (gas phase). Since both O and H are normally in gas phase, and the bonding of H_2O is not very different than that of O_2 and H_2 , there are minimal differences between these two curves. Shown superimposed on the plot are experimental data from 4 papers, which show good agreement.

The third plot line (solid) from the top is the calculation for stopping in O and H in solid phases, and summed using Bragg's Rule. The resulting stopping is in good agreement with the experimental results for a target of ice from ten different papers, noted in the plot. (see Footnote 2)

Figure 5-5 shows a similar plot for He ions into water. This data is more consistent than that for H ions, above, and it also clearly shows the "phase effect" for water in gaseous phase and for water in solid phase. All the solid lines are SRIM calculations for H, O or H_2O in either gaseous or solid state. The citations for the plotted data are also found in Footnote 3.

³ <http://www.srim.org/SRIM/Compounds/Citations/Water.pdf>

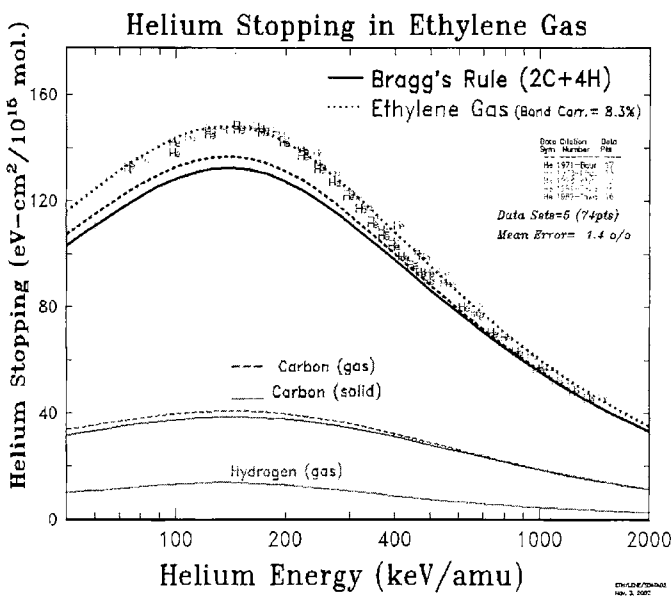


Figure 5-6 The Stopping of Helium Ions in Ethylene Gas

The figure shows experimental values of He stopping in Ethylene Gas. The lowest curve is the SRIM predicted stopping for He in Hydrogen gas. The next pair of curves are the predicted stopping for He in Carbon (solid) as a solid line and the corrected stopping for He ions in Carbon in gas phase. The bonding correction value used is, +8.3%, see also Table 5-7.

At the top are three curves. The lowest (solid line) is the result of using Bragg's Rule and determining the stopping using 2 parts of Carbon stopping (solid phase) and 4 parts of Hydrogen stopping (gas phase). The original Bragg's Rule does not suggest corrections for the target phase. Just above this solid line is a dotted line, which results from using a modified Bragg's Rule in which the stopping of He in Carbon (gas phase) is included in the calculation for stopping in C_2H_4 . Finally, the upper-most curve includes a bonding correction for the bond-states of C_2H_4 (gas phase) amounting to +8.3%. When both the target phase (+4%) and the bonding corrections (+8.3%) are included, the resulting stopping is in good agreement with the experimental results of 5 different papers, noted in the plot. The mean error of the fit is 1.4% to a total of 74 experimental data points.

An example of a large correction is the 12% stopping correction necessary for Ethylene, C_2H_4 . Shown in Figure 5-6, "He into Ethylene Gas" is the stopping of He ions into Ethylene showing the Bragg's Rule stopping estimate for (2 Carbon) + (4 Hydrogen) atoms (black curve). These values are clearly too small. There are two corrections that must be made. The stopping of He in Carbon assumes a solid-phase target. The stopping in gas-phases usually increases the stopping. Shown in the curve is the stopping due to a carbon solid (solid line) and carbon in gas phase (dashed line). Then we must consider the bonding effects. The ethylene molecule contains 4 H-C single bonds, and a C=C double bond. From the discussion above, the C=C bond adds significantly to the

stopping power near the peak of the stopping. SRIM calculates that this increase is 8.3%. So the two corrections make the total adjustment to the stopping to be about 12%, and it brings the calculation into reasonably accurate agreement with the data. The citations of the plotted data are listed on the website.⁴

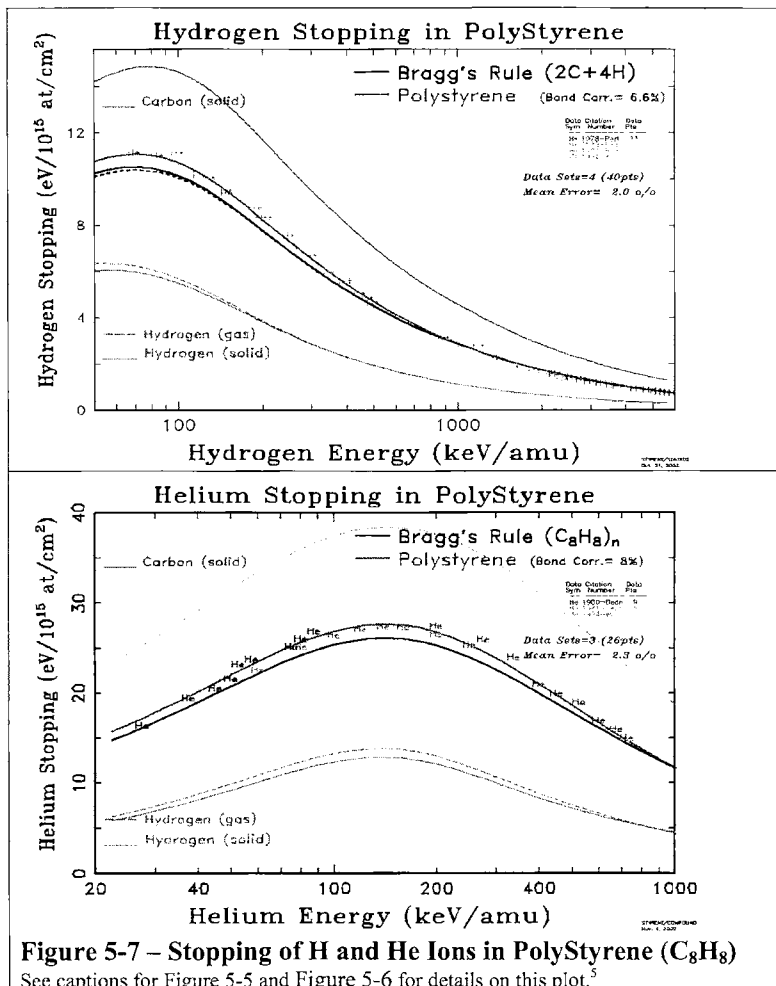


Figure 5-7 – Stopping of H and He Ions in PolyStyrene (C_8H_8)

See captions for Figure 5-5 and Figure 5-6 for details on this plot.⁵

⁴ <http://www.srim.org/SRIM/Compounds.htm#Ethylene> Citations

⁵ NOTE: All plots in this Chapter can be found on the website [www.srim.org/SRIM/ Compounds](http://www.srim.org/SRIM/Compounds). Since these plots are in color, the various curves are easy to distinguish.

Another similar example of a large correction is that necessary for a target of Polystyrene, C_8H_8 . Shown in Figure 5-7 are two plots: "H into Styrene" and "He into Styrene". These are the stopping of H and He ions into Polystyrene. They show the Bragg's Rule stopping estimate for (8 Carbon) + (8 Hydrogen) atoms (black curve). This estimate is too small. There are two corrections that must be made. The stopping of ions in Hydrogen measures a gas-phase target. **The stopping in gas-phases has higher stopping than for solid phase** (see discussion at end of the chapter). Shown in the curve is the stopping due to hydrogen in gas phase (dashed green line) and hydrogen solid (solid green line). Then we must consider the bonding effect correction. The Polystyrene molecule contains 8 H-C single bonds, 6 C-C single bonds, and 3 C=C double bonds (see the molecular structure in SRIM's *Compound Dictionary*). From the discussion above, the C=C bond adds significantly to the stopping power near the peak of the stopping. SRIM calculates that the bonding correction is +6.6%. In this case, the two corrections work opposite to each other. The phase-change correction for hydrogen (gas \rightarrow solid) reduces the stopping, while the bond correction increases the stopping. The total adjustment to the stopping is about 6%, and it brings the calculation into reasonably accurate agreement with the data for both H and He ions. The citations of the plotted data are listed on the website:⁶

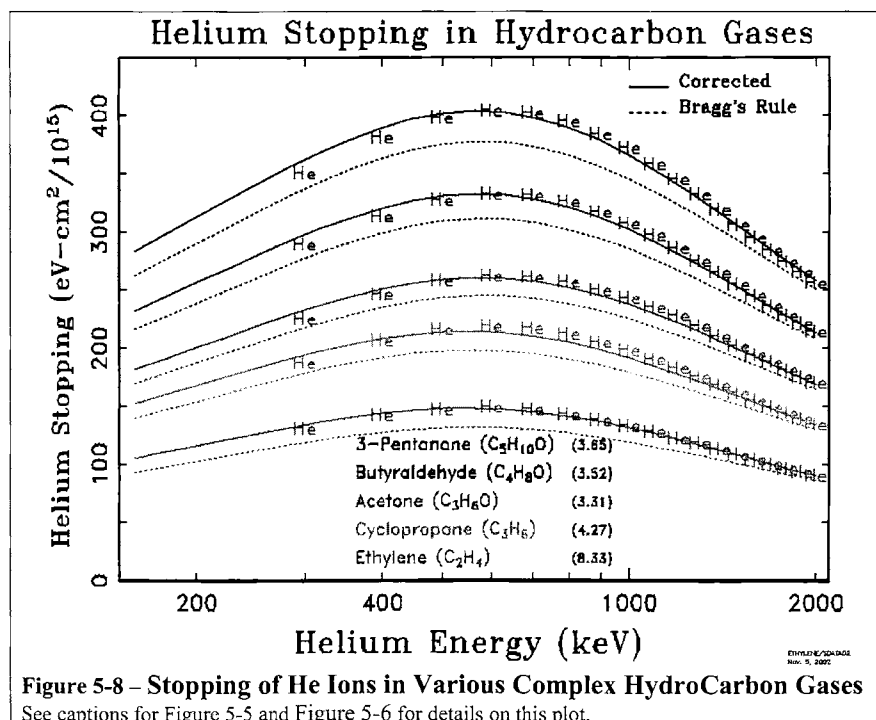


Figure 5-8 – Stopping of He Ions in Various Complex HydroCarbon Gases
See captions for Figure 5-5 and Figure 5-6 for details on this plot.

Another example shows the stopping of He into Hydrocarbon Gases. A wide variety of gases are shown, ranging from the simple molecule, C_2H_4 (ethylene) to the very complex

⁶ <http://www.srim.org/SRIM/Compounds.htm#Polystyrene>

molecule $C_5H_{10}O$ (3-pentanone). In all cases a significant correction is required to go from the simple Bragg's Rule of additivity to the corrected curves. The corrections involve a phase change for the carbon atoms (from solid to gas phase) and bonding corrections which range from 3.3% to 8.3%. All of the data is from the papers of D. Powers (Baylor Univ., USA) [80a]

For ions heavier than He, experimental data is sparse. Typical experimental data are for Li ions in Polymer Solids such as polyimide, formvar and polysulfone, see Figure 5-9. These compounds are complex and the SRIM calculations are shown only with the necessary phase correction for converting H, N and O stopping powers to equivalent solid phase stopping. Compounds such as these may show a range of stoichiometries. For example, Formvar is normally quoted as being $C_5H_8O_2$, while the authors quote their target as $C_{5.56}H_{7.7}O_2$. Since this formulation is from the manufacturer, it is used for the SRIM calculation. But such non-integer stoichiometries prevent the use of any Core and Bond (CAB) corrections.

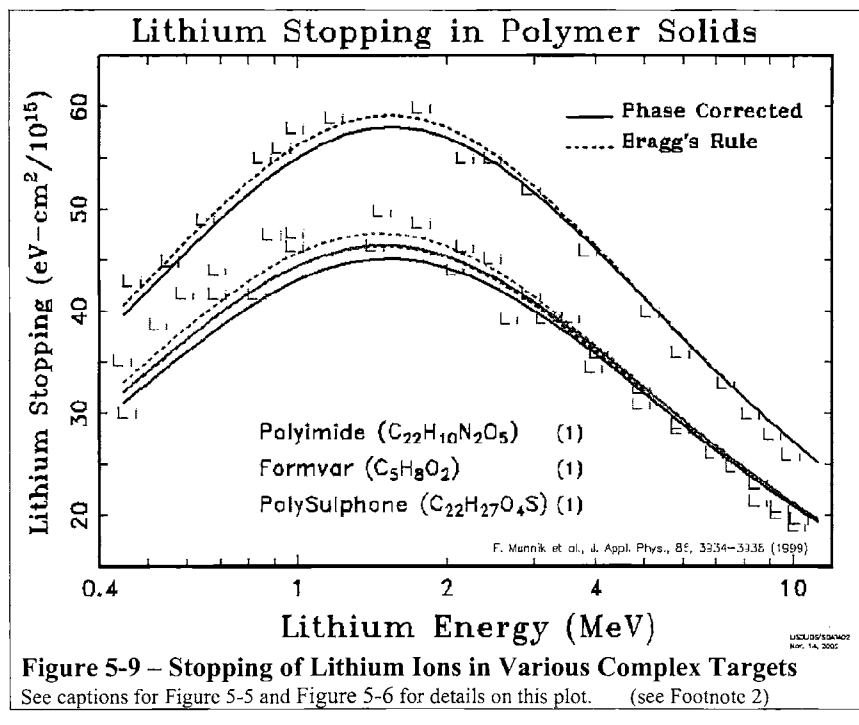


Figure 5-9 – Stopping of Lithium Ions in Various Complex Targets
See captions for Figure 5-5 and Figure 5-6 for details on this plot. (see Footnote 2)

Calculation of Core and Bond Stopping Corrections

There have been more than 400 papers which discuss methods of calculating the stopping of ions in compounds.⁷ Many recent papers are rather rigorous and apply molecular orbital calculations to single compound systems. Our interest is to find an accurate solution which can be used for any ion / compound situation with limited input from the user. The most basic information is still necessary: the chemical nature and the phase state of the compound. From this rudimentary information, SRIM then estimates the corrections needed to produce stopping which is accurate to a few percent.

The method which is used is called the Core and Bond (CAB) approach, which was first proposed by a group at the University of Cologne (Köln, Germany)[75m and later 83j]. They proposed approaching the problem by reducing each target atom to two parts: the core electrons which are unperturbed by bonding, and the bonding electrons. An example would be for carbon atoms, with a core of the nucleus and the inner shell electrons, and then separate outer shell contributions depending on how the carbon was bound into the compound.

The problem is to determine the Core and Bond values for common elements. The Core stopping contributions would simply follow Bragg's Rule for the atoms of the compound, which suggests a linear addition of the stopping from each of the elements in the compound. The chemical bonds of the compound would then contain a correction to this basic stopping. The bonds would be evaluated depending on the simple chemical nature of the compound. For example, for hydrocarbons, carbon in C-C, C=C and C≡C structures would have different bonding contributions (C=C indicates a double-bond structure and C≡C is a triple bond). The contribution to stopping by a carbon atom in a C=C bond is almost twice that of a carbon atom single-bond state. And a carbon atom in a triple-bond state contributes even greater stopping powers. By merely specifying the bonding of the atoms in the compound, for example, SRIM can then generate a stopping correction required for the compound with this bonding arrangement.

The Core and Bond (CAB) values may be determined by analyzing the stopping of ions over a great number of targets, and solving for the contribution from the Cores and the Bonds. We use the stopping of light ions, H, He and Li, in 162 different stopping experiments. The compounds contained 30 different elements. We will assume that for the targets with 12 heavy elements, the stopping is dominated by the non-bonding electrons (discussion below). But 114 of these compounds contained only light elements, and their stopping is significantly altered by their bonding. The light elements we consider are: H, C, N, O, F, S and Cl. For each of these elements there is a core contribution, and a separate bonding contribution. The bonds which appear in the 114 compounds with only light elements that we studied are shown in Table 5-2:

⁷ <http://www.srim.org/SRIM/Compounds.htm#Citations for Compounds>

Table 5-2 Core and Bonds which were evaluated.

Hydrogen Bonds	Carbon Bonds	Other Bonds
H-H	C-C	N≡N
H-C	C=C	N-O
H-N	C≡C	O=O
H-O	C-N	S-H
H-S	C-O	S-C
	C=O	
	C-F	
	C-Cl	

where "-" denotes a single bond, "=" denotes a double bond and "≡" denotes a triple bond. These 18 bonds are considered unknown parameters. The scaling of ion stopping from a H ion to a He ion to a Li ion are also considered unknowns. Finally the stopping effect of the phase-state of the target is another unknown parameter. This gives a total of (7 cores) + (18 bonds) + (3 ions) + (2 phase states) = 30 parameters that will be extracted from the data of 114 experiments (more than 1,500 data points). For H in targets, we assume there is no core (only one electron is available) and all its stopping is in the bonding electron. For the other elements, each possible bond is considered separately.

It is clear that we have an "over-defined" problem, in which there are many more equations than the number of unknowns, and this improves the accuracy of the solutions. The solving of the multiple equations was done in a standard iterative method for over-defined problems.

The limitations of this approach should be mentioned.

- The most important limitation might be that of the target band-gap. Experiments on insulating targets dominate the experimental results that we use. For compounds which are conducting, there might be an error with the suggested stopping correction. It might be too low. Theoretically, band gap materials are expected to have lower stopping powers than equivalent conductors because the small energy transfers to target electrons are not available in insulators. It is not clear what the magnitude of this effect is, but about 50 papers have discussed the stopping of ions in metals and their oxides, e.g. targets of Fe, Fe_2O_3 and Fe_3O_4 . These experiments evaluated similar materials with and without band-gaps. No significant differences were found that could be attributed to the band-gap. Measurements have also been made of the stopping of H and He ions into ice (solid water) with various dopings of salt (NaCl). No change of energy loss was observed for up to 6 orders of magnitude change in resistivity of the ice.
- The scaling of ion stopping from H to He to Li is assumed to be independent of target material. This assumption has been evaluated with 27 targets which have been measured for two of the three ions (at the same ion velocity) and 6 of these targets have been measured for all three ions (see listings in Table 2). In all cases, the stopping scaled identically within 4%. That is, for H (125 keV) and He (500 keV) and Li (875 keV) the scaling of stopping powers was 1 : 2.7 : 4.7 for the 27 targets (average error

was <4%). (For those unfamiliar with stopping theory, the primary parameter for the scaling of stopping powers is the ion velocity, which reduces to scaling in units of keV/amu.)

- The light elements of He and Ne are missing from the above list of target bonding atoms. No comparative experiments have been done on the stopping into He in solid / gas phases. However studies of stopping into targets of Ne and Ar have been conducted in both gas and solid form. These papers show no significant difference between the stopping in gas and solid phases. It appears that the van der Waals forces which hold noble gases together in frozen form, are too weak to effect the energy loss of ions. Of particular note is the extensive work done in the paper: F. Besenbacher, J. Bottiger, O. Graversen, J. Hanse and H. Sorensen, "Stopping Power of Solid Argon for Helium Ions", Nucl. Inst. Methods, 188, 657-667 (1981).
- The light target atoms of Li, Be and B are missing from the list of bonding atoms. This is a serious defect. The number of papers that have looked at compounds which contain significant amounts of these three elements is too limited to allow their evaluation. Target atoms of these three elements are considered by SRIM to have no bonding correction, which is clearly not true. But without experimental data, there is no reliable way to evaluate the contribution of their bonds in compounds.

Table 5-3 shows the compounds used for the extraction of Core and Bond parameters. For further details on CAB fitting see reference [83a] G. Both, R. Krotz, K. Lohman and W. Neuwirth, Phys. Rev., A28, 3212 (1983).

Table 5-3 Compounds used to extract Bonding Contributions

Compound	Formula	Ions	Compound	Formula	Ions
Acetaldehyde	C ₂ H ₄ O	He	Ethylene	C ₂ H ₄	H, He, Li
Acetic Acid	CH ₃ COOH	Li	Ethylene oxide	C ₂ H ₄ O	He
Acetone	C ₃ H ₆ O	He, Li	Ethylene sulfide	C ₂ H ₄ S	He
Acetylene	C ₂ H ₂	H, He	Formic Acid	HCOOH	Li
Alcohol, methyl-	CH ₃ OH	He, Li	Glycerol	C ₃ H ₈ O ₃	Li
Alcohol, ethyl-	C ₂ H ₅ OH	He, Li	Hydrogen Sulfide	SH ₂	He
Alcohol, propyl-	C ₃ H ₇ OH	He, Li	Methane	CH ₄	H, He
Alcohol, undecanol-	C ₁₁ H ₂₃ OH		Methane, chloro-trifluoro-	CClF ₃	He
Allene	C ₃ H ₄	He	Methane, dichloro-difluoro	CCl ₂ F ₂	He
Aluminum oxide	Al ₂ O ₃	H, He, Li	Methane, dichloro-fluoro-	CHCl ₂ F	He
Ammonia	NH ₃	H	2-Methyl, 1,3-butadiene	C ₅ H ₈	Li
Anthracene	C ₁₄ H ₁₀	H	Methyl sulfide	(CH ₃) ₂ S	He
Benzene	C ₆ H ₆	H, He, Li	Nickel oxide	Ni ₂ O ₃	H, He
Bicyclo[2.2.1]hepta2,5diene	C ₇ H ₈	Li	Nitrous oxide	N ₂ O	H, He
Butane	C ₄ H ₁₀	He	Octanoic acid	C ₇ H ₁₅ COOH	Li

1,30Butadiene	C ₄ H ₆	He	n-Pentane	C ₅ H ₁₂	Li
2-Butanone	C ₄ H ₈ O	He	N-Pentadecane	C ₁₅ H ₃₂	Li
Butyraldehyde	C ₄ H ₈ O	He	1,5-Pantanediol	C ₅ H ₁₂ O ₂	Li
Carbon tetrachloride	CCl ₄	He	3-Pantanone	C ₅ H ₁₀ O	He, Li
Carbon tetrafluoride	CF ₄	He	1-Pentene	C ₅ H ₁₀	Li
1-Chlorobutane	C ₄ H ₉ Cl	Li	Phenylacetylene	C ₈ H ₆	He
1-Chlorohehexadecane	C ₁₆ H ₃₃ Cl	Li	Polyethylene	(CH ₂) _n	H
1-Chlorohexane	C ₆ H ₁₃ Cl	Li	Polypropylene	(C ₃ H ₈) _n	H
2-Chloro-2-methylpropane	C ₄ H ₉ Cl	Li	Polystyrene	(C ₈ H ₈) _n	H, He
1-Chloropropane	C ₃ H ₇ Cl	Li	Propane	C ₃ H ₈	H, He
1,3,5-Cyclo-hcptatricne	C ₇ H ₈	Li	1,3-Propanediol	C ₃ H ₆ O ₂	Li
1,3-Cyclo-hexadicne	C ₆ H ₈	He	2-Propanol	C ₃ H ₇ NH ₂	Li
Cyclohexane	C ₆ H ₁₂	He, Li	Propylamine	C ₃ H ₇ NH ₂	Li
Cyclohexanone	C ₆ H ₁₀ O	He	Propylene	C ₃ H ₆	H, He
Cyclohexene	C ₆ H ₁₀	He, Li	Propylene oxide	C ₃ H ₆ O	He
Cyclooctane	C ₈ H ₁₆	He, Li	Propylene sulfide	C ₃ H ₆ S	He
Cyclopentane	C ₅ H ₁₀	He, Li	Silicon dioxide	SiO ₂	H, He, Li
Cyclopentene	C ₅ H ₈	He, Li	Thiophene	C ₄ H ₄ S	He
Cyclopropane	C ₃ H ₆	H, He	Toluene	C ₇ H ₈	He, Li
n-Decane	C ₁₀ H ₂₂	Li	Trimethylcne sulfide	C ₃ H ₆ S	He
1,2-Difluorethane	C ₂ H ₄ F ₂	He, Li	Water (solid)	H ₂ O	H, He, Li
p-Dioxane	C ₄ H ₈ O ₂	He	Water (gas)	H ₂ O	H, He, Li
Ethane	C ₂ H ₆	He	Hydrogen (gas)	H ₂	H, He
1,2-Ethanediol	(CH ₂ OH) ₂	Li	Nitrogen (gas)	N ₂	H, He
Ethane hexafluoride-	C ₂ F ₆	He	Oxygen (gas)	O ₂	H, He
Ethane hexafluoride	C ₂ F ₆	He	Graphite	C ₆	H, He
Ether, dimethyl-	C ₂ H ₆ O	He			
Ether, vinyl-methyl-	C ₃ H ₁₀ O	He			
Ether, diethyl-	C ₄ H ₁₀ O	He, Li			

The simultaneous fitting of ion stopping in all of these compounds yielded the following Bonding Corrections, see Table 5-4. The corrections are for H, He and Li ions at 125 keV/amu (about the peak of their stopping power curve) and all strengths are normalized to the C-C bond. The evaluations were done at several ion velocities, both higher and lower than 125 keV/amu, and the relative magnitude of the bonds changed. The spread of the relative effects was significantly reduced for higher ion energies. For lower energies, the spread of relative strengths slightly increased, but not by very much.

Table 5-4 The Relative Strength of Bonds in Compounds (C-C = 1.0)

Hydrogen Bonds	Relative Strength	Carbon Bonds	Relative Strength	Other Bonds	Relative Strength
H-H	2.44	C-C	1.00	N≡N	5.17
H-C	1.83	C=C	2.49	N-O	4.01
H-N	2.09	C≡C	3.81	O=O	5.40
H-O	2.22	C-N	1.29	S-H	1.23
H-S	1.23	C-O	15.7	S-C	0.41
		C=O	3.53		
		C-F	2.79		
		C-Cl	0.94		

The relative strength of the target atom "cores" were also extracted, see Table 5-5. The contribution of the hydrogen core was set to zero because its only electron is used in bonding. All core strengths are shown relative to carbon. The core contribution to stopping was found to be relatively independent of the ion velocity, in contrast to the contribution of bonding, above.

Table 5-5 Relative Strength of Atomic Cores (Table 4)

Target Atom	Relative Core Strength
Hydrogen	0.000
Carbon	1.000
Nitrogen	0.93
Oxygen	0.89
Fluorine	0.88
Sulphur	5.33
Chlorine	4.69

Bragg's Rule and Heavy Target Elements

We have concentrated on the analysis of the stopping of ions in compounds made up of light elements. For compounds with heavier atoms, many experiments have shown that deviations from Bragg's Rule disappear. Table 5-6 shows representative examples of ion stopping in various compounds containing heavy elements. None show significant deviations from Bragg's Rule. The citations for these measurements are tabulated in the [Compound Citation](#) webpage.⁸ Many articles with similar results were reviewed in the 1980s.⁹

Table 5-6 Bragg's Rule Accuracy in Heavy Compounds

Compound	Deviation from Bragg's Rule	Compound	Deviation from Bragg's Rule	Compound	Deviation from Bragg's Rule
Al_2O_3	< 1%	HfSi_2	< 2%	Si_3N_4	< 2%
Au-Ag alloys	< 1%	NbC	< 2%	Ta_2O_5	< 1%
Au-Cu alloys	< 2%	NbN	< 2%	TiO_2	< 1 %
BaCl_2	< 2%	Nb_2O_5	< 1%	W_2N_3	< 2%
BaF_2	< 2%	RhSi	< 2%	WO_3	< 2%
Fe_2O_3	< 1%	SiC	< 2%	ZnO	< 1%
Fe_3O_4	< 1%				

For compounds which contain elements with atomic numbers greater than 12, it is possible to combine the CAB approach with Bragg's Rule. The CAB approach can be used for the small atomic number cores and bonds, and these can be combined with the normal stopping contribution of the other components of the compound.

Examples of Stopping Correction for Compounds

Stopping Correction for a target of Ethylene

When you use SRIM, you are given the option of using the *Compound Dictionary*. This menu lists over 350 compounds, and provides stopping corrections for a great number of them. Table 5-7 shows a typical example for Ethylene, C_2H_4 , which has a total stopping correction of 12%. Below in Table 5-7 is the SRIM *Compound Dictionary* window for Ethylene. The Bonding Correction is 8.33%. Next in the figure is the density for Ethylene in gas phase, and the chemical formula and the bonding information in schematic form. The figure then shows the composition of Ethylene in both atomic percent and mass percent. The term "Core Stopping" is the same as in Table 5-5 above, but in different units. Finally, at the bottom the bonding information is listed. There are four (H-C) single bonds,

8 <http://www.srim.org/SRIM/Compounds.htm#Citations for Compounds>

9 See: D. I. Thwaites, Nucl. Inst. Methods, B12, 84 (1985); D. I. Thwaites, Nucl. Inst. Methods, B27, 293 (1987).

and one (C=C) double bond. The effect of these cores and bonds is to make an 8.3% correction. SRIM also makes an automatic correction for the phase change for carbon in the target if the "Gas Phase" box is checked in SRIM (we are assuming gaseous Ethylene in this example). The gas-phase correction is about 4% for carbon. This makes the total correction to be 12%.

Previously shown in Figure 5-6 is the stopping of He ions into Ethylene and indicating the Bragg's Rule stopping estimate for (2 Carbon) + (4 Hydrogen) atoms (black curve). These values are clearly too small. The above two corrections need to be applied. The stopping of He in Carbon assumes a solid-phase target. The stopping in gas-phases increases the stopping. Shown in the curve is the stopping due to carbon solid (solid line) and carbon in gas phase (dashed line). Then we must consider the bonding effects. The ethylene molecule contains 4 H-C single bonds and a C=C double bond. From the discussion above, the C=C bond adds significantly to the stopping power near the peak of the stopping. SRIM calculates that this increase is 8.3%. So the two corrections make the total adjustment to the stopping to be about 12%, and it brings the calculation into reasonably accurate agreement with the data in Figure 5-6.

Note that various versions of SRIM may have different correction factors. SRIM is constantly being upgraded, and corrections are included without notice. The above corrections are valid for SRIM-2000 and later.

Table 5-7 SRIM Compound Stopping Correction

Below is an example of what SRIM displays when a compound is selected from the Compound Dictionary. The upper section indicates the stopping correction applied for low velocity light ions depending on the phase of the Ethylene target. The next section indicates the density (gas phase) and the chemical composition, and a crude picture of the molecular bonding. The next section lists the Ethylene composition and the Core and Bond contribution of each of the various components.

Ethylene					
Stopping Correction for Target Chemistry					
Solid Target = +10.79%					
Gas Target = +8.31%					
Density = 0.00125 g/cm ³					
Chemical Formula					
$\begin{array}{c} & \text{H} & \text{H} \\ & & \\ \text{C} & == & \text{C} \\ / \quad \backslash & & / \quad \backslash \\ \text{C} & \text{H} & \text{H} \\ 2 \quad 4 & \text{H} & \text{H} \end{array}$					
----- TARGET COMPOSITION -----					
Atom Name	Atom Numb	Number Atoms	Atom Mass	Core %	Stopping
H	1	4.00	14.37	0.00	
C	6	2.00	85.63	6.21	
-TARGET BONDS (per molecule)-					
Bond Type	Bond Number	Stopping			
(H-C)	4	7.438			
(C=C)	1	10.023			

Stopping Correction for a target of Polystyrene

Another example of a large correction is that necessary for a target of Polystyrene, C₈H₈. Shown below is the **Compound Dictionary** entry in SRIM for Polystyrene (which is also identified by the tag - ICRU #226). This compound will have two corrections, one to convert stopping in H (gas) to stopping in H (solid). This will tend to decrease the stopping power. The second correction will be for the bonding of the compound, which will increase the stopping. The result will be a net increase of about 6%. The chemical form of Polystyrene is rather complex since it contains 8 (H-C) bonds, 6 (C-C) bonds and 3 (C=C) bonds. Note that the density of Polystyrene is quite variable, and you must be careful that your target density is correctly entered.

Shown in Figure 5-10 and Figure 5-11 are the stopping of H and He ions into Polystyrene. They show the Bragg's Rule stopping estimate for (8 Carbon) + (8 Hydrogen) atoms (central solid curve). These values are too small. There are two corrections that must be made. The stopping of ions in Hydrogen assumes a gas-phase target. The stopping in gas-phases has higher stopping than for solid phase. Shown in the curve is the stopping due to hydrogen in gas phase (dashed line) and hydrogen solid (solid line). Then we must consider the bonding effects. The Polystyrene molecule contains 8 H-C single bonds, 6 C-C single bonds, and 3 C=C double bonds (see the molecular structure in SRIM's **Compound Dictionary**). From the discussion above, the C=C bond adds significantly to the stopping power near the peak of the stopping. SRIM calculates that the bonding correction is +6.6%. In this case, the two corrections work opposite to each other. The phase-change correction for hydrogen reduces the stopping, while the bond correction increases the stopping. The total adjustment to the stopping is about 6%, and it brings the calculation into reasonably accurate agreement with the data for both H and He ions.

Table 5-8 SRIM Compound Stopping Correction

Polystyrene (ICRU-226)					
Stopping Correction for Target Chemistry					
Solid Target = +8.59%					
Gas Target = +0.99%					
<hr/>					
Density = 1.06 g/cm ³					
Chemical Formula					
H - C / \					
C - C //					
8 8 n C - C H - C - H					
H H H					
Density ranges from 0.98 to 1.075 g/cm ³ .					
<hr/> TARGET COMPOSITION <hr/>					
Atom Name	Atom Numb	Number Atoms	Atom Mass %	Core Stopping	
H	1	8.00	7.74	0.00	
C	6	8.00	92.26	6.21	
<hr/> TARGET BONDS (per molecule)-					
Bond Type	Number	Stopping			
(H-C)	8	7.438			
(C-C)	6	3.964			
(C=C)	3	10.023			

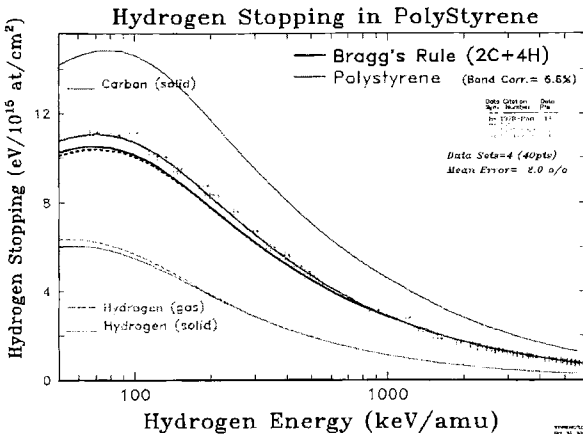


Figure 5-10 – The stopping of Hydrogen Ions in Polystyrene

Polystyrene is made up of C_8H_8 and is a solid. Bragg's Rule requires the inclusion of stopping in both C and H as solids, but there has never been a measurement of proton stopping in solid H. So a stopping correction is made to correct for the phase change for H, and also for the new bonding in the polystyrene. This difference can be seen in the difference between the middle curves. For these 3 middle curves: the middle solid line is H(gas)+C(solid); the lower dashed line is H(solid)+C(solid); the upper solid line H(solid)+C(solid)+Chemical Correction.¹⁰

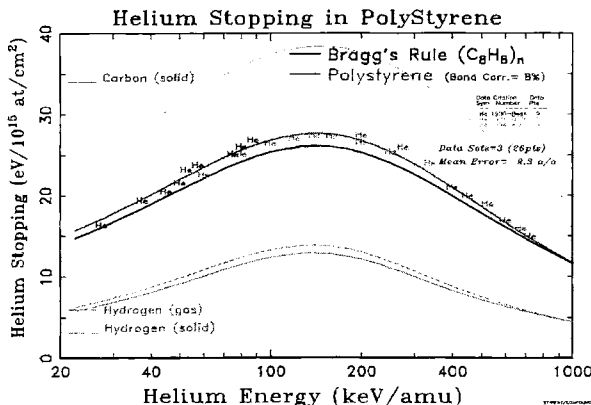


Figure 5-11 The stopping of Helium Ions in Polystyrene

¹⁰ NOTE: All plots in this Chapter can be found on the website www.srim.org/SRIM/Compounds Since these web plots are in color, the various curves are easy to distinguish.

The same comments as for Figure 5-10 apply.

Details and Limitations - Core and Bond Theory

Details of how SRIM calculates the bonding correction to stopping can be found in the paper: J. F. Ziegler and J. M. Manoyan, Nucl. Inst. Methods, B35, 215-228 (1988). This paper also discusses the limitations of this theory.

The Phase Correction (Gas/Solid) to Stopping

The **Phase Correction** to stopping is a correction applied to stopping in targets of gases vs. solids. This phase correction is extracted at the same time that the bonding corrections are found, see the section on: **Calculation of Core and Bond Stopping Corrections**. To calculate this correction theoretically is one of the most difficult challenges of stopping theory. There are three primary effects:

- (1) The ion's equilibrium charge state in a target depends on successive collisions. Initial collisions with the target electrons may only partially excite one of the ion's electrons, and if a succeeding collision occurs before it relaxes to a lower state, the stripping of this electron requires less energy. Because the target atoms in a solid are so close together, the ion's charge state will be higher in a solid than in a gas.
- (2) As the ion penetrates the solid, it polarizes the target electrons, especially those in the conduction band. This polarization pulls target electrons towards the incoming ion, and increases the local target electron density around the ion. This increase in density increases the ion/electron interactions.
- (3) However, the same target electron polarization effect as noted in (2) also shields the ion from interacting with the much more plentiful distant electrons, and hence reduces the ion/target electron interaction with these distant electrons.

Thus there are two interactions, (1) and (2) which increase the strength of ion/target interactions and stopping powers, and one interaction, (3), that decreases it. In general, the third interaction overrides the other two, especially for conductors, which generates this rule for low velocity ions: **The stopping in target gases is usually higher than the stopping in equivalent target solids**. This has been demonstrated by measuring the stopping in targets such as zinc in both metal and gas phases, and the stopping is always higher in the gas phase. A similar conclusion is reached by measuring the stopping of protons (1^+) and anti-protons (1^-) in metals. The protons will induce polarization, and hence be shielded from interactions with distant electrons, while the anti-protons will push target electrons away and have a higher interaction with distant target electrons. The anti-protons always have higher stopping powers. Not enough research has been done on insulating targets to make any conclusion about their phase effect.

The Gas/ Solid correction disappears for higher velocity ions with energies above 2 MeV/u. But at lower velocities the effect can be quite large – almost a 2 times change in stopping because of the Phase Effect near the Bohr velocity, 25 keV/u.

See, for example, citations 93c, 88y, 97g.

Chapter Citations

- 00a Mme. Pierre Curie, C. R. Acad. Sci., 130, (1900), 76.
- 05a W. H. Bragg and R. Kleeman, Philos. Mag., 10, (1905), 318.
- 13a N. Bohr, Phil. Mag. 25 (1913) 10, *ibidem* 30 (1915) 581.
- 33a F. Bloch, Z. Phys. 81 (1933) 363.
- 64a U. Fano, in *Studies in Penetration of Charged Particles in Matter*, Nucl. Sci. Series, No 39 (National Academy of Sciences-National Research Council, Washington D.C., 1964)
- 70a L.C. Northcliffe and R.F. Schilling, Nucl. Data Tables A7 (1970) 233.
- 73y D. Powers, A.S. Lodhi, W.K. Lin and H.L. Cox jr., Thin Sol. Films 19 (1973) 205.
- 74a A. S. Lodhi and D. Powers, Phys. Rev., A10, 2131 (1974).
- 75x W. Neuwirth, W. Pietsch, K. Richter and U. Hauser, Z. Physik A 275 (1975).
- 77a H.H. Andersen and J.F. Ziegler, in Stopping and Ranges of Ions in Matter, edited by J.F. Ziegler (Pergamon, New York, 1977).
- 77y E.K.L. Chau, R.B. Brown, A.S. Lodhi, D. Powers, S. Matteson, and S.R. Eisenbarth, Phys. Rev. A16 (1977) 1407.
- 77z S. Matteson, D. Powers, and E.K.L. Chau, Phys. Rev. A15 (1977) 856..
- 78y E.K.L. Chau, D. Powers, A.S. Lodhi, and R.B. Brown, J. Appl. Phys. 49 (1978) 2346.
- 78x W. Neuwirth, W. Pietsch and R. Kreutz, Nucl. Instr. Meth. 149 /1978) 105.
- 80a D. Powers, Acc. Chem. Res., 13, 433 (1980).
- 80x R. Kreutz, W. Neuwirth and W. Pietsch, Phys. Rev. A22 (1980) 2606.
- 81a P.M. Echenique, R. Nieminen, and R. H. Ritchie, Solid State Commun. 37 (1981) 779.
- 81b F. Besenbacher, J. Bottiger, O. Graversen, J. Hanse and H. Sorensen, "Stopping Power of Solid Argon for Helium Ions", Nucl. Inst. Methods, 188, 657-667 (1981).
- 82x J.F. Janni, Atomic Data and Nucl. Data Tab. 27 (1983) 585.
- 82a P. Sigmund, Phys. Rev. A26 (1982) 2497.
- 83a G. Both, R. Krotz, K. Lohmer and W. Neuwirth, Phys. Rev. A 28 (1983) 3212.
- 83b H. Geissel, Y. Laichter, W.F.W. Schneider and P. Armbruster, Phys. Lett. 99A (1983) 77.
- 83j G. Both, R. Krotz, K. Lohman and W. Neuwirth, Phys. Rev., A28, 3212 (1983)
- 83q D.I. Thwaites, Radiat. Res. 95 (1983) 495.
- 84a *Stopping Powers for Electrons and Positrons*, ICRU Report No. 37 (International Commission on Radiation Units and Measurements, Bethesda MD, 1984).
- 85q D.I. Thwaites, Nucl. Instr. Meth. B12 (1985) 84.
- 85a J.F. Ziegler, J.P. Biersack and U. Littmark, The Stopping and Range of Ions in Solids, vol. I (Pergamon, New York, 1985).
- 86a P.M. Echenique, R.M. Nieminen, J.C. Ashley and R.H. Ritchie, Phys. Rev. A33 (1986) 897.
- 87y G. Reiter, H. Baumgart, N. Kniest, E. Pfaff and G. Clausnitzer, Nucl. Instr. Meth. B27 (1987) 280.
- 87x J.R. Sabin and J. Oddershede, Nucl. Instr. Meth. B27 (1987) 280.
- 87q D.I. Thwaites, Nucl. Instr. Meth. B27 (1987) 293.
- 88x J.F. Ziegler and J.M. Manoyan, Nucl. Instr. Meth. B35 (1988) 215.

- 88y Ch. Eppacher and D. Semrad, Nucl. Instrum. and Methods B35, 109 (1988).
- 89a J.Oddershede and J.R.Sabin, Nucl. Instr. Meth. B42 (1989) 7.
- 89x J.R.Sabin and J.Oddershede, Phys. Rev. A39 (1989) 1033.
- 90a L.E. Porter and Hong Lin, J. Appl. Phys. 67 (1990) 6613.
- 91a R. Golser and D. Semrad, Phys. Rev. Lett. 66 (1991) 1831.
- 91b J.Lindhard, private communication, 1991.
- 92a A. Arnau, M. Peñalba, P.M. Echenique and F. Flores, Nucl. Instr. Meth. B69 (1992) 102.
- 92x P.Bauer, F.Kastner, A.Arnaud, A.Salin, P.D.Fainstein, V.H.Ponce and P.M.Echenique, Phys. Rev. Lett., 69 (1992) 1137.
- 92b P. Bauer, W. Rössler and P. Mertens, Nucl.Instr. and Meth. B69 (1992) 46.
- 92x H. Bichsel and T. Hiraoka, Nucl. Instr. Meth. B66 (1992) 345.
- 92q D.I. Thwaites, Nucl. Instr. Meth. B69 (1992) 53.
- 93a A. Schiefermueller, R. Golser, R. Stohl, and D. Semrad, Energy loss of hydrogen projectiles in gases, Phys. Rev. A 48 (1993) 4467.
- 93b *Stopping Powers and Ranges for Protons and Alpha Particles*, ICRU Report No. 49 (International Commission on Radiation Units and Measurements, Bethesda MD, 1993).
- 93c J.M.Pitarke, R.H.Rithchie and P.M.Echenique, Nucl. Instrum. Methods B79, 209 (1993).
- 94a A. Arnau, P. Bauer, F. Kastner, A. Salin, V.H. Ponce, P.D. Fainstein and P.M. Echenique, Phys. Rev. B, Phys. Rev. B49 (1994) 6470.
- 96a R. Golser, D. Semrad and F. Aumayr, Phys. Rev. Lett. 76 (1996) 3104.
- 96b J. Lindhard and A. Sørensen, Phys. Rev. A53, 1996.
- 97x P.Bauer, R.Golser, F.Aumayr, D.Semrad, A.Arnaud, E.Zarate, and R.Diez-Muiño, Nucl. Instr. Meth. B125 (1997) 102.
- 97a K.Eder, D.Semrad, P.Bauer, R.Golser, P.Maier-Komor, F.Aumayr, M.Peñalba, A.Arnaud and P.M. Echenique, Phys. Rev. Lett. 79 (1997) 4112.
- 97b Sigmund PRA56 (97) 3781.
- 97g S.P. Moller et al., Phys. Rev. A56, 2830 (1997).
- 98a A. Arnau, chapter 4 in this book
- 99x P.Bauer, R.Golser, D.Semrad, P.Maier-Komor, F.Aumayr and A.Arnaud, submitted to Nucl. Instr. Meth. B.

6 - ION STRAGGLING IN MATTER

CHAPTER SUMMARY

Straggling can be defined as the variation of energy loss or range of ions in matter. As in stopping powers, the straggling is usually divided into electronic and nuclear straggling. Both of these kinds of straggling are significant effects. Straggling is made quite complex by the variation of charge-state of the ion as it penetrates into matter. Since the experimental study of straggling is far less extensive than for stopping powers, straggling calculations are also less accurate. There are hundreds of theoretical papers on straggling, and this chapter will only attempt to review the primary theories which are widely cited.

Chapter Contents

6 - Ion Straggling in Matter	6-1
CHAPTER SUMMARY.....	6-1
INTRODUCTION	6-1
Energy Transfer from a Projectile to a Target Charge.....	6-2
Two Particle Straggling (Classical Bohr Straggling).....	6-5
ELECTRONIC STRAGGLING AND HIGHER MOMENTS.....	6-6
Bohr Straggling of Electronic Stopping (1940)	6-6
Landau Calculations of Electronic Straggling (1944).....	6-6
Vavilov Calculations of Electronic Straggling (1957).....	6-7
Advanced Calculations of Vavilov Straggling	6-10
NUCLEAR STRAGGLING AND HIGHER MOMENTS.....	6-10
Introduction to Nuclear Straggling	6-10
Calculation of Nuclear Straggling	6-13
Analytic Solutions and Approximations	6-16
COMMENTS	6-19
CHAPTER 6 - CITATIONS.....	6-20

INTRODUCTION

In SRIM, straggling refers to the distribution of energy loss about an average value. The term *Straggling* is used by many scientists in a loose way to indicate this general energy-loss distribution, and we shall, at times, use it generically. However, *Straggling* also has a precise statistical meaning as the second moment of the energy loss distribution from the mean. The third moment of this distribution is called its *Skewness*, and the fourth moment is called the distribution *Kurtosis*. These statistical terms of the moments of the energy loss distribution will be defined later in this chapter.

The simplest approach to understanding straggling is to understand high-velocity straggling of a point charge in matter which consists of independent charges. This subject was partially presented in Chapter 2, *Nuclear Stopping*, and is summarized below. This energy loss is then used as a basis for the case of electronic energy loss straggling (energy loss the target electrons) and for the case of nuclear energy loss straggling (energy loss to the target nuclei).

Note that two significant contributions to ion straggling are not discussed in this chapter: target surface roughness (and possibly target porosity), and changes in the charge state of the ion as it transits the target. See *Comments* at the end of this chapter.

Energy Transfer from a Projectile to a Target Charge

The energy transferred during the screened Coulomb collision of two charges, one in motion and one initially stationary, will be described as a function of two variables, the projectile atom's initial energy, E, and its impact parameter, p. These are identified in Figure 6-1, with p being defined as the projected offset of the original path of Z_1 from Z_2 . If these two variables are known, then the scattering angle in the CM system, Θ , can be determined as:

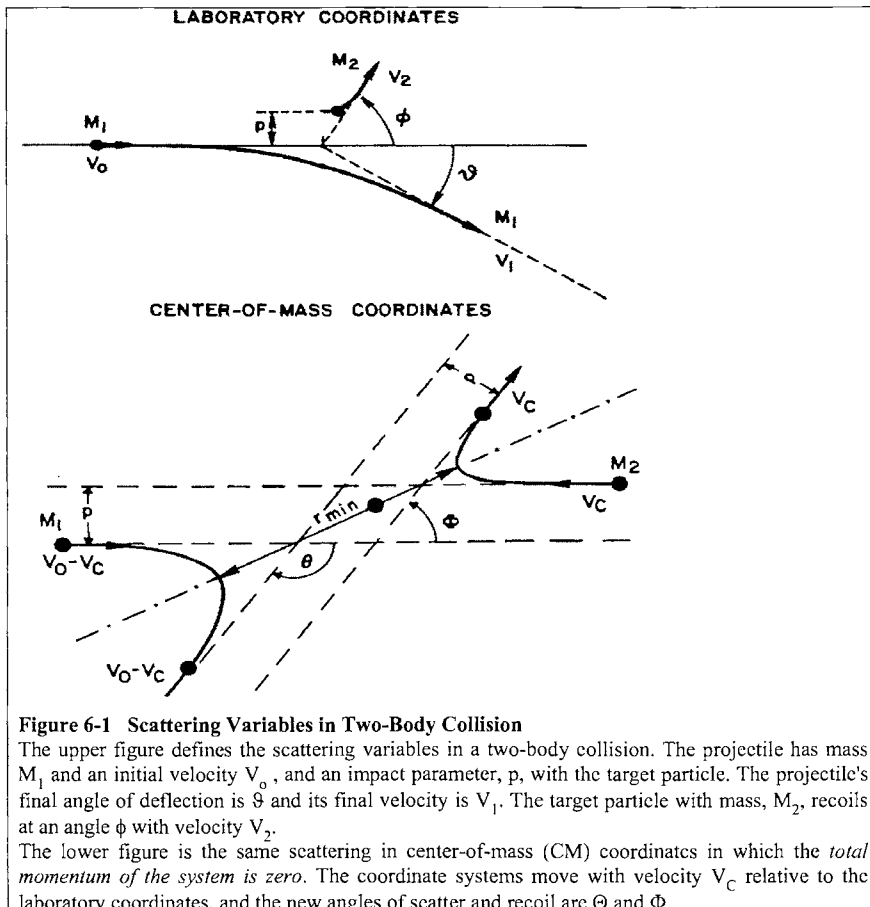


Figure 6-1 Scattering Variables in Two-Body Collision

The upper figure defines the scattering variables in a two-body collision. The projectile has mass M_1 and an initial velocity V_o , and an impact parameter, p , with the target particle. The projectile's final angle of deflection is θ and its final velocity is V_1 . The target particle with mass, M_2 , recoils at an angle ϕ with velocity V_2 .

The lower figure is the same scattering in center-of-mass (CM) coordinates in which the *total momentum of the system is zero*. The coordinate systems move with velocity V_c relative to the laboratory coordinates, and the new angles of scatter and recoil are Θ and Φ .

$$\text{Eq. 6-1: } \Theta = \pi - 2 \int_{r_{\min}}^{\infty} \frac{p dr}{r^2 \left[1 - \frac{V(r)}{E_c} - \frac{p^2}{r^2} \right]^{1/2}}$$

E_c is the center-of-mass energy defined

$$\text{Eq. 6-2: } E_c = E_0 M_2 / (M_1 + M_2).$$

and r_{\min} is the distance of closest approach during the collision, see Figure 6-1. This equation allows us to evaluate the final angle of scatter, Θ , in terms of the initial CM energy, E_c , the potential, $V(r)$, and the impact parameter, p .

The energy transfer, T , to the target atom can be determined from conservation of energy and momentum, as was shown in the derivation of the general orbit equation,

$$\text{Eq. 6-3: } T = \frac{2}{M_2} \left(V_0 M_c \sin \frac{\Theta}{2} \right)^2 = \frac{4 E_c M_c}{M_2} \sin^2 \frac{\Theta}{2} = \frac{4 E_0 M_1 M_2}{(M_1 + M_2)^2} \sin^2 \frac{\Theta}{2}$$

where M_1 and M_2 are the masses of charges, Z_1 and Z_2 , and where Θ is the projectile's scattering angle in center-of-mass coordinates, which is related to the lab frame by:

$$\text{Eq. 6-4: } \vartheta = \tan^{-1} |\sin \Theta / (\cos \Theta + M_1/M_2)|$$

where ϑ is the laboratory final deflection angle of the projectile, see Figure 6-1 and Figure 6-2.

Eq. 6-1 is the general solution for a particle in a spherically symmetric central force field and the difficult problem of two atom scattering has been reduced to this simple form. The energy transferred to the target atom is now a function p and E , and is found by inserting the solution of Eq. 6-1 into Eq. 6-3.

In order to solve Eq. 6-1 in an universal way, especially in a way that is independent of the ion-target combination, we use the substitutions: $x = r/a$, $b = p/a$, and $\varepsilon = E_c / (Z_1 Z_2 e^2 / a)$ and obtain:

$$\text{Eq. 6-5: } \Theta = \pi - 2 \int_{x_0}^{\infty} \frac{b dx}{x^2 \left[1 - \frac{\Phi(x)}{x\varepsilon} - \frac{b^2}{x^2} \right]^{1/2}}$$

where we have also replaced the inter-atomic potential with the previously discussed screening function $V = (Z_1 Z_2 e^2 / r) \Phi(r/a)$, see Chapter 2. Now Eq. 6-5 allows the calculation of the final scattering angle with the new parameters ε and b , and the individual atomic variables, Z_1 , Z_2 , M_1 and M_2 have been eliminated (see further comments on this derivation in references (57a,b, 63a, and 64c)).

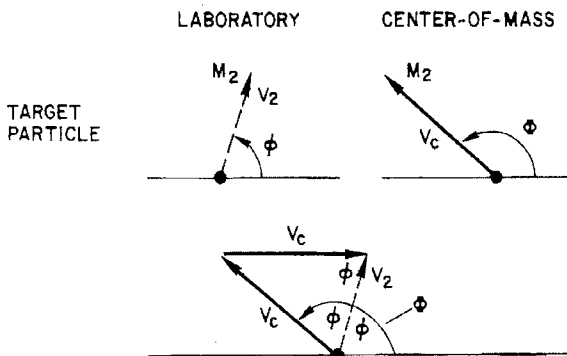


Figure 6-2 - Center-of-Mass Coordinates

Angular conversion of center-of-mass coordinates to laboratory coordinates for the target particle. The upper two figures show the final particle vectors in both systems. The two systems are related since the CM system moves laterally with velocity, V_C , as defined by equations 2-5 and 2-6 (see Chapter 2) to make the total momentum of the CM system to be zero.

The lower figure then relates the final target velocity, V_2 in the Lab and V_C in CM, by the lateral vector V_C which is their difference. Since the triangle is isosceles, $\Phi = 2\phi$, which is independent of the particle masses and velocities.

For energy loss by simple Coulombic scattering, the energy loss for 2-particle scattering, S_2 , is, proportional to:

$$\text{Eq. 6-6: } S_2(E) \equiv \int_0^{\infty} T d\sigma = \int_0^{\infty} T(E, p) 2\pi p dp = 2\pi\gamma E \int_0^{\infty} \sin^2 \frac{\Theta}{2} p dp$$

The integration's upper limit must be limited, and it can be easily truncated for atoms in a solid to the sum of the two atomic radii, p_{\max} , beyond which the inter-atomic potential and energy transfer, T , are zero. We now define a CM to lab transformation unit, γ , which will be used below :

$$\text{Eq. 6-7: } \gamma \equiv 4 M_1 M_2 / (M_1 + M_2)^2$$

In order to show clearly the results of using classical charge distributions and also those using solid state distributions, it is easiest to again plot the 2-particle stopping power in reduced units in which a single curve describes all combinations of classical atom-atom collisions. Lindhard et al. have discussed at length the calculation of nuclear stopping using Thomas-Fermi atoms (63a, 68a). They suggested a reduced coordinate system for 2-particle stopping which we will extend to our new calculations. Using the formalism, similar to that of Lindhard, we define:

$$\text{Eq. 6-8: } S_2(\epsilon) = \frac{\epsilon}{\pi a_u^2 \gamma E} S_n(E)$$

where S_2 indicates the stopping in a two-particle collision, and where ϵ is a *reduced energy* which is defined as:

$$\text{Eq. 6-9: } \varepsilon = a_U M_2 E / Z_1 Z_2 e^2 (M_1 + M_2)$$

and a_U is the universal screening length discussed in Chapter 2.

Eq. 6-1 defines 2-particle stopping in physical units, and Eq. 6-8 to Eq. 6-9 converts it to LSS reduced units [63a], which is usually defined for $\varepsilon > 30$:

$$\text{Eq. 6-10: For } \varepsilon > 30 : S_2(\varepsilon) = \frac{\ln(\varepsilon)}{2\varepsilon}$$

Two Particle Straggling (Classical Bohr Straggling)

The study of particle straggling begins with deriving Bohr Straggling, which is the straggling between a moving charged particle and a stationary charged particle, in the limit of non-relativistic Coulomb Interactions. Straggling attempts to indicate the distribution of particle energy loss about a mean value, and it is usually considered as a series of moments. The units of straggling are $[(\text{energy loss})^2 / \text{distance}]$. The concepts presented below about straggling may not seem intuitive since they involve a long tradition of statistical notations.

The straggling of the 2-particle energy loss is defined as $Q_2 \equiv \langle T^2 \rangle / \langle \Delta x \rangle$, where T is the energy loss to the stationary particle, which will vary with impact parameter, and Δx is the distance traveled by the projectile. By integrating over all impact parameters, one may obtain the mean of the energy-loss squared, $\langle T^2 \rangle$. Note that $\langle T^2 \rangle = (\int^\infty T^2 d\sigma) / \sigma$, where sigma is the geometric cross-section, defined as $d\sigma = 2\pi p dp$, with p being the impact parameter. The notation, Q_2 , is used because this is the second moment of the energy loss between the two particles. It can be evaluated in the same way as the 2-particle stopping discussed above, by using:

$$\text{Eq. 6-3} \quad T = \frac{4E_0 M_1 M_2}{(M_1 + M_2)^2} \sin^2 \frac{\Theta}{2}$$

and inserting the definition defined above in Eq. 6-7

$$\text{Eq. 6-7} \quad \gamma \equiv 4 M_1 M_2 / (M_1 + M_2)^2$$

we obtain:

$$\text{Eq. 6-11} \quad T^2 = \gamma^2 E_0^2 \sin^2 \frac{\Theta}{2}$$

Inserting this into $\langle T^2 \rangle = (\int^\infty T^2 d\sigma) / \sigma$, and converting the cross-section to geometric units, $d\sigma = 2\pi p dp$, reduces to:

$$\text{Eq. 6-12} \quad \langle T^2 \rangle = 2\pi \gamma^2 E_0^2 \int_0^\infty \sin^4 \frac{\Theta}{2} p dp / \sigma$$

The term σ is the total cross-section, defined by the limits of the integral, $2\pi p_{\max}$, discussed below. This equation will lead to the Bohr Formula for straggling when the Coulomb Potential is inserted to solve for $\sin^2 \Theta/2$ using Eq. 6-1. The Coulomb potential for two point charged particles is

$$\text{Eq. 6-13} \quad V(r) = Z_1 Z_2 e^2 / r$$

which, when inserted into Eq. 6-1 yields:

$$\text{Eq. 6-14} \quad \sin^2 \Theta/2 = 1 / [1 + (2 \varepsilon p)^2].$$

Inserting Eq. 6-14 into Eq. 6-12 gives

$$\text{Eq. 6-15} \quad \langle T^2 \rangle = \pi \gamma Z_1^2 e^4 M_1 / (M_2 \sigma) \quad (\text{units are energy}^2)$$

yielding the increase in (energy loss)² / path length, Q_2 , for the two-particle collision:

$$\text{Eq. 6-16} \quad Q_2 \equiv \langle T^2 \rangle / \langle \Delta x \rangle = \pi \gamma Z_1^2 e^4 M_1 / (\langle \Delta x \rangle M_2 \sigma).$$

ELECTRONIC STRAGGLING AND HIGHER MOMENTS

Bohr Straggling of Electronic Stopping (1940)

The above ideas were outlined by Bohr in 1940 [40d]. He then extended this formalism to the ion/electron energy loss case. He found that the term $\gamma M_1/M_2$ is approximately 4 for straggling due only to target electrons, in which $M_1 \gg M_2$. Assuming a target with atomic density, N , atoms/cm³, with Z_2 electrons/atom, then the mean distance between collisions is $\langle \Delta x \rangle = 1/N\sigma$. From Eq. 6-16 we obtain the final equation:

Bohr Electronic Straggling

$$\text{Eq. 6-17} \quad Q_2 = 4 \pi e^4 Z_1^2 Z_2 N \Delta x$$

This formula may be corrected for relativistic effects by defining $\beta^2 = v^2/c^2$, and following standard corrections to the Rutherford scattering formula (84a). This gives a relativistic Bohr straggling as:

$$\text{Eq. 6-18} \quad Q_2 = 4 \pi Z_1^2 Z_2 e^4 N \Delta x (1 - \beta^2/2) / (1 - \beta^2)$$

This is the formula used in TRIM (see Chapter 7) and PRAL (see Chapter 10), programs in the SRIM package to generate electronic straggling at high particle velocities.

Landau Calculations of Electronic Straggling (1944)

After Bohr [40d] had established Eq. 6-18, the solution for straggling of high energy particles, the next significant paper on straggling was published by Landau [44a]. This paper used relativistic scattering laws and contained more than straggling: *Landau's result showed for the first time that his more detailed calculation resulted in a skewed distribution of energy loss, with a considerable tail towards higher energy losses.* This straggling calculation is limited to high velocity light ions. His work yielded the result for the energy loss distribution, f , for an ion passing through a target with thickness, Δx :

$$\text{Eq. 6-19} \quad f(\Delta E, \Delta x) = \frac{1}{\pi \xi} \int_0^{\infty} e^{-\frac{\pi y}{2}} \cos[y \ln(y + \lambda(\kappa, \xi))] dy$$

where the parameters λ , κ and ξ are defined below.

$$\text{Eq. 6-20} \quad \lambda = \frac{\Delta E - \overline{\Delta E}}{\xi} - (1 - \Gamma) - \beta^2 - \ln \kappa$$

where $\Gamma = 0.577216$ (Euler's Number), with the mean energy loss over the pathlength, Δx , being

$$\text{Eq. 6-21} \quad \overline{\Delta E} = S_e \Delta x$$

where S_e is the electronic stopping power using Bethe's formula (see chapter 4). ΔE is distributed about the mean energy loss, $\overline{\Delta E}$. The other parameters in Landau's result are:

$$\text{Eq. 6-22} \quad \xi = 0.30058 \frac{m_0}{v^2} \frac{Z_2}{A} \Delta x$$

where m_0 is the mass of the electron, v is the ion velocity, Z_2 is the atomic number of the target atoms, and A is the target atom mass. Finally, he defines

$$\text{Eq. 6-23} \quad \kappa = \frac{\xi}{T_{\max}}$$

where T_{\max} is a complicated term to evaluate. T_{\max} is defined as the maximum energy which can be transferred to a free electron in a single collision. This parameter is evaluated to be:

$$\text{Eq. 6-24} \quad T_{\max} = 0.30058 \frac{m_0 v^2}{1 - \beta^2} \left[1 + \frac{2 m_0}{M_1 (1 - \beta^2)} + \left(\frac{m_0}{M_1} \right)^2 \right]^{-1}$$

where $\beta = v / c$. One may approximate the brackets of Eq. 6-24 with unity for non-relativistic energies ($v \ll c$, $\beta \ll 1$) and for projectiles which are much heavier than the electrons, i. e. any ion ($M_1 \gg m_0$). This approximation was also used by Vavilov which is discussed next.

Note that very approximately, ξ is a measure of the mean energy loss over the distance Δx , whereas t and the parameter κ is a rough measure of the number of collisions occurring over the distance Δx .

The Landau distribution contains more than the straggling of the particles in matter; it also includes higher moments with a quite skewed distribution of mean energy loss.

Vavilov Calculations of Electronic Straggling (1957)

Landau's work, Eq. 6-19 - Eq. 6-24, was the basis of a much more elaborate calculation by Vavilov [57d]. This paper assumes the Landau solution for the limiting case of $\kappa \ll 1$ (one or

very few collisions). For the other limit, $\kappa \gg 1$ (very many collisions), the distribution becomes Gaussian as predicted by Bohr (above).

Vavilov started with the exact integro-differential transport equation:

$$\text{Eq. 6-25} \quad \frac{\partial f(\Delta E, \Delta x)}{\partial x} = \int_0^T w(E) f(\Delta E - E, \Delta x) dE - f(\Delta E, \Delta x) \int_0^{T_{\max}} w(E) dE$$

Where $T = \Delta E$, if $\Delta E < T_{\max}$, and $T = T_{\max}$ if $\Delta E > T_{\max}$. The function $w(E)$ is the energy transferred to the target electrons in a single collision event:

$$\text{Eq. 6-26} \quad w(E) = \frac{\xi}{\Delta x} \frac{1 - \beta^2}{E^2} \frac{E / T_{\max}}{} \quad \text{for } E \leq T_{\max}$$

and

$$\text{Eq. 6-27} \quad w(E) = 0 \quad \text{for } E > T_{\max}.$$

Vavilov stated that he followed the example of Landau in solving the transport equation in the Laplace transformed space (whatever that means), where one obtains an analytic solution for the expression $f(\Delta E, \Delta x)$. Then, his harder problem was the inverse Laplace transform back to real space by an integration along a path parallel to the imaginary axis, but avoiding the origin. This transformation could not be done analytically without approximations. Vavilov needed some novel approximations which did not affect the main features of his calculation. He found the following analytic result:

$$\text{Eq. 6-28} \quad f(\Delta E, \Delta x) dE = \frac{1}{\xi} \varphi_v(\lambda_v, \kappa, \beta^2) d\lambda_v$$

with

$$\text{Eq. 6-29} \quad \lambda_v = \frac{\Delta E - \overline{\Delta E}}{T_{\max}} - \kappa(1 - \gamma + \beta^2)$$

and

$$\text{Eq. 6-30} \quad \varphi_v = \frac{\kappa}{\pi} e^{\kappa(1 + \beta^2)} \int_0^\infty e^{\kappa f_1} \cos(\lambda_v y + \kappa f_2) dy$$

where the functions f_1 and f_2 are defined by:

$$\text{Eq. 6-31} \quad f_1(y) = \beta^2 [\ln y + \underline{Ci}(y)] - \cos y - y \underline{Si}(y)$$

and

$$\text{Eq. 6-32} \quad f_2(y) = y [\ln y + \underline{Ci}(y)] + \sin y + \beta^2 \underline{Si}(y)$$

and the special functions \underline{Ci} and \underline{Si} are the cosine and sine integral functions respectively.

This final result embraces all previously published energy loss distributions (Bohr and Landau). In the limit of very few collisions, where $\kappa \rightarrow 0$, the Vavilov formula, Eq. 6-28, approaches the "Landau Distribution" with the Landau parameter defined as:

$$\text{Eq. 6-33} \quad \lambda = \frac{\lambda_v}{\kappa} - \ln \kappa = \frac{\Delta E - \overline{\Delta E}}{\xi} - (1 - \gamma) - \beta^2 - \ln x.$$

In the limit of very many collisions, where $\kappa \rightarrow \infty$, the Vavilov distribution becomes a Gaussian distribution:

$$\text{Eq. 6-34} \quad f(\Delta E, \Delta x) = \frac{1}{\xi \sqrt{\frac{2\pi}{\kappa}(1 - \beta^2/2)}} \exp\left\{-\frac{(\Delta E - \overline{\Delta E})^2}{2\xi^2(1 - \beta^2/2)/\kappa}\right\}.$$

This distribution is centered about the mean energy loss, $\overline{\Delta E}$, with a standard deviation, σ , in a Gaussian form:

$$\text{Eq. 6-35} \quad \sigma = \xi \sqrt{\frac{2(1 - \beta^2/2)}{\kappa}}$$

The Vavilov distributions were widely discussed, and led to precise experimental verification. Gooding and Eisberg [57e] measured the distribution of the energy loss of high velocity protons, 32 MeV, in argon gas, $\Delta x \approx 10$ cm at about one atmosphere. Their results confirmed Vavilov's predictions, and are shown in Figure 6-3.

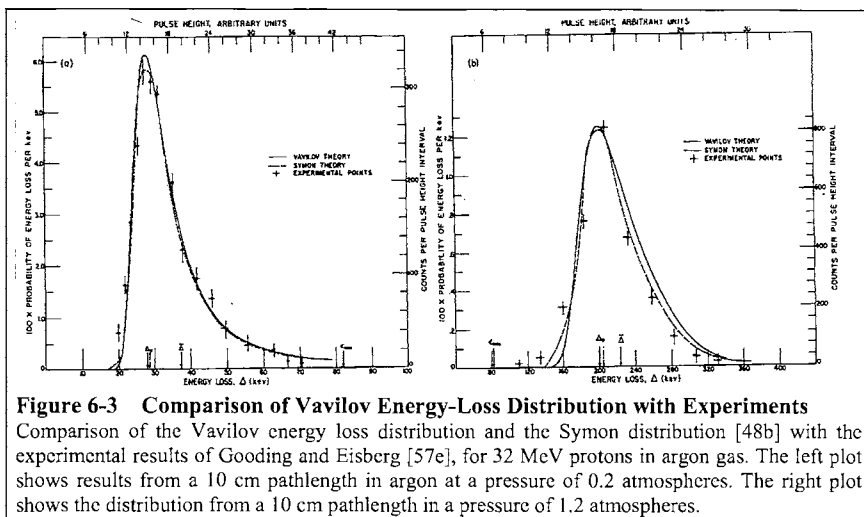


Figure 6-3 Comparison of Vavilov Energy-Loss Distribution with Experiments

Comparison of the Vavilov energy loss distribution and the Symon distribution [48b] with the experimental results of Gooding and Eisberg [57e], for 32 MeV protons in argon gas. The left plot shows results from a 10 cm pathlength in argon at a pressure of 0.2 atmospheres. The right plot shows the distribution from a 10 cm pathlength in a pressure of 1.2 atmospheres.

Advanced Calculations of Vavilov Straggling

The Vavilov straggling theory has led to several computer evaluations which produced accessible tables. Of note was the work of Seltzer and Berger (64d), who evaluated the Vavilov functions for protons, kaons, pions and muons and producing tables of the Vavilov parameters $\xi/\Delta x$ and $\kappa/\Delta x$. They compare these results to Gooding and Eisberg [57e]. They also evaluate the Vavilov distribution for $\kappa = 0.01 - 10$ and produce convenient tables. At $\kappa = 10$ they indicate its minor deviations from a perfect Gaussian.

Tschaler [68f, 68g] used a transport equation similar to that of Landau and Vavilov. He made predictions of the higher moments of the energy loss distributions for high energy light particles. In particular, he showed distributions for particles with very large energy losses such as 49 MeV protons being slowed to 5 MeV in aluminum. These distributions were almost Gaussian with small Skewness. He compared his results with the experimental results of Raju (65a), and found excellent agreement. However, he knew the experimental results before he published his calculations.

All these calculations apply to high energy light projectiles. At low velocities, Firsov gave a useful prediction [59a]. He stated that below the Fermi velocity (25 keV/amu) the straggling can be estimated to be proportional to the projectile energy up to the intersection with the Bohr straggling. That is, up to the point where its value reaches the Bohr value. **Both the TRIM program (Ch. 7-9) and the PRAL program (Ch 10) introduce electronic straggling by using Firsov straggling for low energies and Bohr straggling for higher ion energies.**

NUCLEAR STRAGGLING AND HIGHER MOMENTS

Introduction to Nuclear Straggling

In TRIM computer simulations for the slowing down of energetic ions, or in other types of range calculations, we may follow energetic ions from their initial energy down to a final energy, E_f , of 5 to 10 eV. The lower limit for applying classical mechanics (as we do in this chapter) can be defined as when the particle wavelength exceeds the atomic spacing of the solid. However, a more conservative limit would be about 0.1 Å, since this is about the spacing between atomic shells. For light ions such as protons, this would equate to an energy of about 7.6 eV. Below this energy, classical mechanics would not be valid and a quantum-mechanical treatment would be necessary. So for this chapter, we shall assume a minimum energy which gives the ion a wavelength $< 0.1 \text{ \AA}$.

The classical treatment uses a potential, $V(r)$, and the concept of an impact parameter p . A simple way to start is to use the universal potential, defined in chapter 2, $V = \Phi(x) Z_1 Z_2 e^2 / r$, where x is defined as $x = r / a$, with

$$\text{Eq. 6-36} \quad a = .8853 a_0 / (Z_1^{0.23} + Z_2^{0.23})$$

and the screening function, Φ , may be fitted with the function found in chapter 2:

$$\text{Eq. 6-37} \quad \Phi(x) = 0.1818 \exp(-3.2x) + .5099 \exp(-.9423x) + .2802 \exp(-.4028x) \\ + .02817 \exp(-.2016x).$$

By using the universal potential in the binary collision, the collision may be considered to begin at a distance "a", the screening length, in front of the target nucleus. The collision ends at a distance "a" beyond the nucleus. This gives a collision diameter of $2a$. Considering the most critical case of protons moving in hydrogen, this distance becomes about 1 Å with a de Broglie wavelength of 0.1

Å. Since the particle wavelength is much smaller than the collision distance, this is a conservative approach to applying classical mechanics to the collision calculation.

These last two definitions for "a" and $\Phi(x)$ are valid for any pair of two atoms, Z_1 , Z_2 . The resulting potential was developed by Ziegler - Biersack - Littmark [84a], and checked for 522 randomly chosen Z_1 and Z_2 . All these potentials were found to be in good agreement within a standard deviation of ~18% in all cases. The 522 screening functions were calculated by Thomas-Fermi statistical methods, summing up the kinetic electron energies, the potential electron energies, and the exchange energies of the overlapping electron clouds of the two solid state electron distributions (each obtained from a single atom Hartree - Fock - Slater solid state calculation).

The calculational methods were similar to the previous calculation by Wilson - Haggmark - Biersack [77c]. The tight grouping of all 522 potentials could only be achieved by the choice of the Z dependence given in Eq. 6-36. These equations are the only ones which are applicable to all ion-target pairs of the entire periodic table; for this reason they could be called "universal". [84a]

The best agreement of all 522 potentials could be achieved when they were compared at small distances - i.e. up to distances where the potential had dropped down to 2 eV. At larger separations the pair potentials show strong individual variations, and may even become attractive. But larger separations need a completely different treatment by molecular orbital theory. This treatment would require a different approach, and is beyond our present scope. The distance has been calculated for the 92 homo-nuclear collisions (ion atom = target atom). Defining r_2 as the distance between two homo-nuclear atoms when the inter-atomic potential is 2 eV, the potential can be expressed as:

$$\text{Eq. 6-38} \quad V(r_2) = \Phi(r_2/a_{ii}) \frac{(Z_i e)^2}{r_2} = 2 \text{ eV}$$

with $a_{ii} = 0.8853 a_0 / (2 Z_i^{23})$ (sec Eq. 6-36). Below the value of r_2 , the binary inter-atomic potentials can be used. The numerical results of Eq. 6-38 are depicted in Figure 6-4.

Similar to the above "universal" screening function is the "composed analytic" potential by Biersack and Ziegler [82f] which treats the kinetic and potential energies in a different way than the exchange energy. It needs two types of functions which are scaled differently for each Z_1 and Z_2 which may come closer to the individual potentials, but needs an input of two differently scaling functions - not one "universal" function as in Eq. 6-37 above. The next higher step in complexity would be to provide all the possible individual pair potentials, i.e. $92 \times 91 = 8372$ pairs.

It is instructive to compare the above assumptions with the ideas of Bohr, which he summarized brilliantly in his 1948 publication [48a]. Bohr always followed the developments of quantum mechanics related to atomic collisions very closely. His paper is still referenced by many researchers in the field of stopping powers and ranges. Definitions which are still used frequently are the "collision diameter"

$$\text{Eq. 6-39} \quad D = (2 Z_1 Z_2 e^2) / (M_0 v^2)$$

with $M_0 = M_1 M_2 / (M_1 + M_2)$ (the reduced mass), and the variable, K, defined as

$$\text{Eq. 6-40} \quad K = D / \lambda = \frac{2 Z_1 Z_2 e^2}{\hbar v},$$

where λ is the de Broglie wave length divided by 2π (note that K is independent of the masses involved) and v is the particle velocity. The limits of validity of classical mechanics vs. quantum

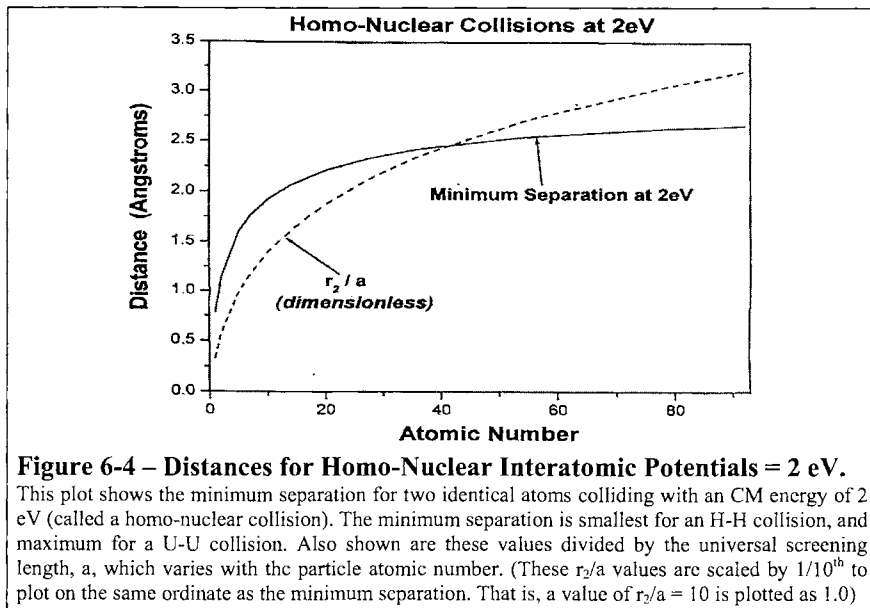


Figure 6-4 – Distances for Homo-Nuclear Interatomic Potentials = 2 eV.

This plot shows the minimum separation for two identical atoms colliding with a CM energy of 2 eV (called a homo-nuclear collision). The minimum separation is smallest for an H-H collision, and maximum for a U-U collision. Also shown are these values divided by the universal screening length, a , which varies with the particle atomic number. (These r_2/a values are scaled by $1/10^{\text{th}}$ to plot on the same ordinate as the minimum separation. That is, a value of $r_2/a = 10$ is plotted as 1.0)

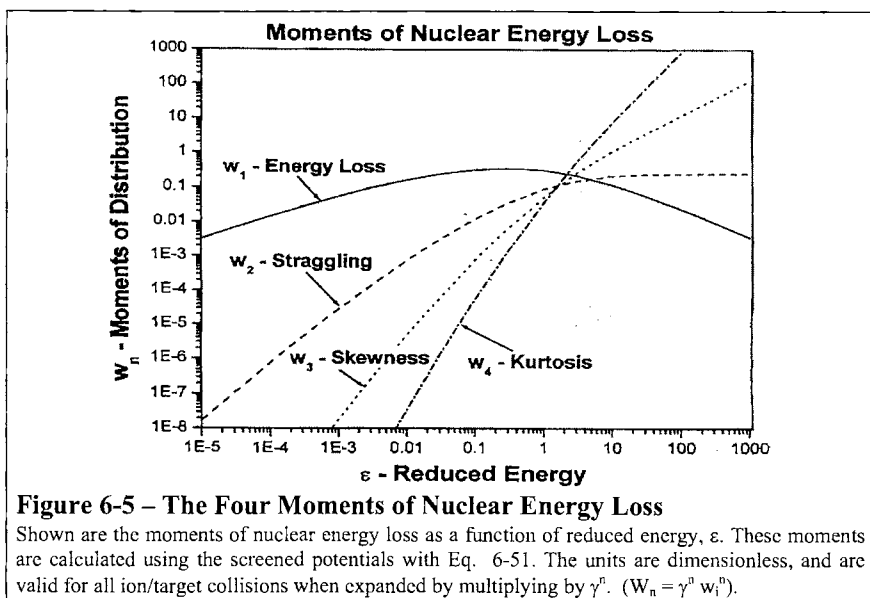


Figure 6-5 – The Four Moments of Nuclear Energy Loss

Shown are the moments of nuclear energy loss as a function of reduced energy, ϵ . These moments are calculated using the screened potentials with Eq. 6-51. The units are dimensionless, and are valid for all ion/target collisions when expanded by multiplying by γ^n . ($W_n = \gamma^n w_i^n$).

where λ is the Broglie wave length divided by 2π (note that K is independent of the masses involved) and v is the particle velocity. The limits of validity of classical mechanics vs. quantum mechanics, were of much concern to Bohr. His criterion, $K \gg 1$, for the validity of classical mechanics is completely consistent with the limits discussed at the beginning of the discussion of this section.

Calculation of Nuclear Straggling

In a nuclear collision the projectile gets deflected and some momentum is transferred to the target atom assumed to be at rest before the collision. The energy loss of the projectile is calculated from classical mechanics (non-relativistic) and is:

$$\text{Eq. 6-41} \quad T = \gamma E_c \sin^2(\Theta/2)$$

where $\gamma = 4 M_1 M_2 / (M_1 + M_2)^2$ is a factor which is always ≤ 1 , but may vary over two orders of magnitude. Θ is the angle of scatter in the center-of-mass system. It can be shown that it depends on exactly two independent variables: one, which is the energy in the center-of-mass system expressed in units of $Z_1 Z_2 e^2 / a$, and the other the impact parameter P in units of a , the screening length. Both of these variables are apparently dimensionless and represent the easiest way to describe a binary collision in classical mechanics:

$$\text{Eq. 6-42} \quad \varepsilon = \frac{E_c}{Z_1 Z_2 e^2 / a}$$

and

$$\text{Eq. 6-43} \quad \mathbf{b} = \mathbf{p} / a.$$

As a general rule which always holds true (for any arbitrary potential), it should be remembered that the scattering process can be described by two and only two variables: for example ε and b : $\Theta = \Theta(\varepsilon, b)$. There are, however, special classes of potentials, where the two variables can be combined into one.

In power potentials of the type, $V = c r^{-n}$, the scattering process can be described by one combined variable εb^n . The only such potential verified in nature is the pure Coulomb interaction, where everything can be expressed as a function of the product εb , e.g. $\sin^2(\Theta/2) = 1 / [1 + (2 \varepsilon b)^2]$. The other potential of this class was provided by the Sommerfeld [32b] solution to the Thomas-Fermi statistical atom which yielded an r^4 potential at large separations. The use of this potential was later abandoned, because the Moliere [47a] approximation was found to be more realistic than the more precise solution of the Thomas-Fermi equation. This fact may sound strange that the approximation was more accurate than the exact solution, and this result was possibly serendipity.

Before attempting to obtain precise energy transfers, we need at first to obtain the precise scattering angles $\Theta(\varepsilon, b)$ by determining the full orbital integrals. For this purpose we first have to calculate the distance of closest approach, $x_{min} = r_{min} / a$, in the center of mass system, and then perform the orbital integral from this point to infinity. We use an iterative method to calculate the distance of closest approach to a precision of 8 digits. As this precision is obtained by setting the denominator of the integrand equal to zero, we have to integrate from a point where the integrand exhibits a pole (denominator=zero) up to infinity (over an infinite distance). One can avoid

problems in numerical integration by performing the transformation $x = x_{min} / (1-u^2)$, which can be solved by allowing the integral to be integrated from 0 to 1 over a new variable u .

To obtain the changes of energy loss, or its moments per path length, $d(T^n) / dx$, we need to get the average $\langle T^n \rangle$ and divide this by the mean free flight pass, $\langle \lambda \rangle = 1/N\sigma$. In averaging over all possible collisions, we assume an amorphous target, where all impact parameters occur at random with probabilities proportional to their cross-sections, $d\sigma$, which are proportional to $d(b^2) = 2b db$.

The quantities dT^n / dx , $n = 1, 2, 3, 4$, can be obtained in a universal way, valid for all Z_1, Z_2 combinations, when we convert the energies and the impact parameters to the dimensionless new parameters, ε and b according to Eq. 6-42 and Eq. 6-43. Then we get:

$$\text{Eq. 6-44} \quad \langle T^n \rangle = \frac{\gamma E_c^n \int_0^\infty \sin^{2n} \frac{\Theta}{2} 2\pi p dp}{\pi p_{max}^2}$$

Due to the exponentially decreasing screening function, there might be difficulties with the upper limit of integration of $\sin^2(\Theta/2)$. However, the value of $\sin^2(\Theta/2)$ drops sharply below 10^{-8} at a finite value of the impact parameter, $p = p_{max}$, where the integration stops. Hence we replace the integration to infinity with p_{max} , defined as the impact parameter where the value of $\sin^2(\Theta/2) < 10^{-8}$. Hence:

$$\text{Eq. 6-45} \quad \langle T^n \rangle = \frac{\gamma E_c^n \int_0^{p_{max}} \sin^{2n} \frac{\Theta}{2} 2\pi p dp}{\pi p_{max}^2}$$

and using the substitution of $b = p/a$, described in Eq. 6-43, we obtain:

$$\text{Eq. 6-46} \quad \langle T^n \rangle = \frac{\left(\frac{\gamma Z_1 Z_2 e^2}{a} \right)^n \varepsilon^n a^2 \int_0^{b_{max}} \sin^{2n} \frac{\Theta}{2} 2\pi b db}{\left(\pi p_{max}^2 \right)}$$

and

$$\text{Eq. 6-47} \quad \langle \lambda \rangle = \frac{1}{N \sigma} = \frac{1}{N \pi p_{max}^2}.$$

The total cross-sections, $\sigma = \pi p_{max}^2$, vary with ε , but they cancel for any given energy. Then we obtain the desired result:

$$\text{Eq. 6-48} \quad \frac{dT^n}{dx} = \left(\frac{\gamma Z_1 Z_2 e^2}{a} \right)^n a^2 N \cdot \varepsilon^n \int_0^{b_{max}} \sin^{2n} \frac{\Theta}{2} 2b db$$

or

$$\text{Eq. 6-49} \quad \frac{1}{a^2 N} \frac{dT^n}{dx} = \left(\frac{\gamma Z_1 Z_2 e^2}{a} \right)^n \cdot \varepsilon^n \int_0^{b_{\max}} \sin^{2n} \frac{\Theta}{2} 2b db.$$

This leads to the definitions:

$$\text{Eq. 6-50} \quad W_n = \frac{d T^n}{a^2 N dx} = \left(\frac{\gamma Z_1 Z_2 e^2}{a} \right)^n w_n$$

where

$$\text{Eq. 6-51} \quad w_n = \varepsilon^n \int_0^{b_{\max}} \sin^{2n} \frac{\Theta}{2} 2b db, \text{ where } n = 1, 2, 3, 4.$$

This definition is universal, i. e. independent of Z_1, Z_2, M_1 and M_2 . The calculation of the moments of nuclear energy losses then requires the evaluation of w_n . The $\sin^2(\Theta/2)$ values drop sharply below the 10^{-8} level at a finite value of $b = b_{\max}$, where the integration stops.

These four moments of the nuclear energy loss are shown in Figure 6-5. It may be noticed that the higher moments span many orders of magnitude.

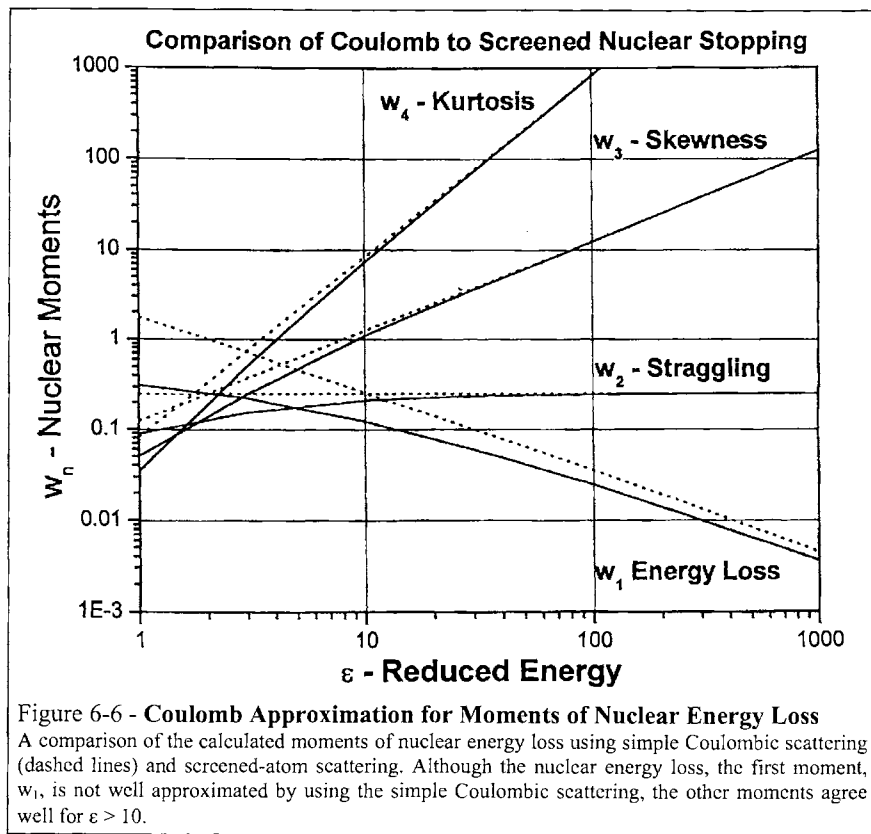
The variables in the denominator of Eq. 6-50 can also be combined into one dimensionless variable:

$$\text{Eq. 6-52} \quad \xi = N a^2 x$$

to get the universal final result

$$\text{Eq. 6-53} \quad W_n = \frac{dT^n}{d\xi} = \left(\frac{\gamma Z_1 Z_2 e^2}{a} \right)^n \cdot w_n$$

with the units of $(eV)^n$.



Analytic Solutions and Approximations

As mentioned before, the Coulomb interaction is a realistic potential which leads to analytic formulations. For the Coulomb potential, $V = Z_1 Z_2 e^2 / r$, we can define $\epsilon \equiv E_c / (Z_1 Z_2 e^2 / a)$ and $b \equiv r / a$ with any arbitrary a (which cancels regardless). This potential can be used with Eq. 6-5 to obtain the analytic scattering law

$$\text{Eq. 6-54} \quad \sin^2\left(\frac{\Theta}{2}\right) = \frac{1}{1 + (2\epsilon b)^2}.$$

Using this simple relation, the integrations leading to w_n can be done using Eq. 6-51 or Eq. 6-53. The integrals are:

$$\text{Eq. 6-55} \quad w_n = \varepsilon^n \int_0^{b_{\max}} \sin^{2n} \left(\frac{\Theta(\varepsilon, b)}{2} \right) 2b db, \quad n = 1, 2, 3, 4$$

which may be expanded to give the final analytic descriptions for the special case of Coulomb Interactions (no atomic screening):

Straggling from Coulomb Interactions

$$\text{Eq. 6-56} \quad w_1 = \frac{\log(1+X)}{4\varepsilon} \quad (\text{Nuclear Energy Loss})$$

$$\text{Eq. 6-57} \quad w_2 = \frac{1}{4} \left(1 - \frac{1}{(1+X)} \right) \quad (\text{Nuclear Straggling})$$

$$\text{Eq. 6-58} \quad w_3 = \frac{1}{8} \varepsilon \left(1 - \frac{1}{(1+X)^2} \right) \quad (\text{Skewness of Energy Loss})$$

$$\text{Eq. 6-59} \quad w_4 = \frac{1}{12} \varepsilon^2 \left(1 - \frac{1}{(1+X)^3} \right) \quad (\text{Kurtosis of Energy Loss})$$

where $X = (2\varepsilon b_{\max})^2$. It is clear from these formulas that all higher moments, $n = 2, 3, 4$, converge rapidly with increasing εb_{\max} values, while only the first moment, the stopping power, behaves exceptionally. Increasing b_{\max} will result in the value of w_1 (nuclear energy loss) for any given ε to increase and become divergent. In other words, an unscreened Coulomb interaction without cut-off or some kind of screening has no defined stopping power.

If we use the same cut-off values as previously used in the exact calculation (the maximum impact parameter b_{\max} , where $\sin^2(\Theta/2) < 10^{-8}$), then we obtain reasonable results by applying the above set of formulas. Of course, they yield higher values for w_n than the exact data calculated before, which used the correctly screened Coulomb potential. For an easy inspection, the results of the pure Coulomb interaction, Eq. 6-56 - Eq. 6-59, are given together with the exact values of w_1, w_2, w_3 and w_4 , for comparison in Table 6-1

Table 6-1 Comparison of analytic results for pure Coulomb interaction and exact data for realistically screened potential.

ε	b_{\max}	\underline{W}_1 (Coul)	\underline{W}_1 (exact)	\underline{W}_2 (Coul)	\underline{W}_2 (exact)	\underline{W}_3 (Coul)	\underline{W}_3 (exact)	\underline{W}_4 (Coul)	\underline{W}_4 (exact)
1	17	1.763	0.3118	0.2497	0.0895	.1249	.0503	.0833	.0348
3	13	0.726	0.2236	0.2499	0.1547	.375	.2492	0.75	.509
10	8.5	0.257	0.1226	0.2499	0.2123	1.25	1.0927	8.33	7.33
30	7	0.1007	0.0598	0.2499	0.2373	3.75	3.5916	75.	71.95
100	6	.03545	0.0247	0.2500	0.2468	12.5	12.376	833	826
300	5	.01334	0.0099	0.2500	0.25	37.5	37.5	7500	7500
1000	4	.00449	0.0036	0.25000	0.25	125.	125.	83333	83333

The behavior at large energies provides a helpful guide for analytic approximations. They determine principally which asymptotic behavior must be approached at high energies. The

functions given below are examples of such fits. They deviate less than 9% (relative error) over the span of variation of $w_4(\epsilon)$ between 10^{-18} and 10^{-5} (this corresponds to a variation of $\epsilon = 10^{-5}$ up to $\epsilon = 1000$). The errors are even less for the lower moments w_3 and w_2 , and the largest deviations occur in the lowest part, at $\epsilon = 10^{-5}$. These fits are fairly good in consideration of the 18% uncertainty of the potentials. The exact solutions may be simply calculated using the following fits to the exact solutions:

Straggling from Screened Interactions

$$\text{Eq. 6-60} \quad w_1 = \frac{0.5 \log(1 + 1.1383 \epsilon)}{\epsilon + 0.1321 \epsilon^{21226} + .19593 \epsilon^{0.5}} \quad (\text{Nuclear Energy Loss})$$

$$\text{Eq. 6-61} \quad w_2 = \frac{1}{4 + .197 \epsilon_1 + 6.584 \epsilon_2} \quad (\text{Nuclear Straggling})$$

$$\text{Eq. 6-62} \quad w_3 = \frac{\epsilon}{8 + 0.28 \epsilon_1 + 10.7 \epsilon_2} \quad (\text{Skewness of Energy Loss})$$

$$\text{Eq. 6-63} \quad w_4 = \frac{\epsilon^2}{12 + 0.37 \epsilon_1 + 16.4 \epsilon_2} \quad (\text{Kurtosis of Energy Loss})$$

with $\epsilon_1 = \epsilon^{1.6991}$ and $\epsilon_2 = \epsilon^{1.0494}$. These two values were intentionally kept fixed (for any one energy) to facilitate fast calculations of all higher energy loss moments. The analytic formulas for fitting the theoretical results were first developed by Biersack[64c] and later used in [77c] and [84a]. The formulas for w_1 and w_2 were taken from ref [84a], where the universal potential was used for the first time.

COMMENTS

The electronic energy loss distribution of ions transiting a target is quite complex, and it has been described well only for energetic light ions. There are hundreds of papers on straggling, and this chapter has only attempted to review the primary theories which are widely discussed.

A major contribution to straggling comes from physical aspects of the target, especially target roughness, and possible target porosity. Further, solid targets may contain crystallites which may be partially aligned (*target texture*) and cause the ion to channel.

A major contribution to heavy ion straggling is the change in charge state of the ion as it goes into and through the target. The distribution of charge states about a mean value can significantly widen the straggling of the ions. And since this distribution changes with the ion velocity, the final energy loss distribution may vary significantly from that predicted from the light-ion theories discussed in this chapter. For further discussions of this, see the extended work of Sigmund, refs. [94a], [94b], [95a], [97a], [98a] and [98b].

The moments of the nuclear energy loss distributions were calculated for a single two-particle collision. This should be understood clearly. The assumptions made were that a broad beam might hit the target atom, i.e. with all possible impact parameters occurring at random. One can imagine an experiment which averages 1.5 collisions. Then one must apply the Poisson distribution for the following number of collisions: In 22% of the time there is no energy loss at all, in 33% of the time a one single encounter, in 25% two successive encounters, in 12.5% three encounters etc. Thus one obtains the final distribution by leaving the original distribution (a delta function at the original energy) unchanged with the probability of 22%, then adding the single collision distribution with 33%, the double collision distribution (two convolutions) with 25%, the triple collision (three times convoluted) with 12.5% etc. (Notice that all probability distributions are normalized.) This procedure would yield the whole theoretically expected distribution. Of course, such a result must be convoluted with the resolution function of the experiment. Such multiple overlays of distribution functions are handled numerically on a computer without any special difficulty.

Electronic energy loss spectra are easy to measure: if the theory requires a random target then fine-grained poly-crystalline solids or gas cells will be adequate to measure an energy loss spectrum. Not so for a nuclear energy loss spectrum. Here, the energy transferred is inevitably related to momentum transfer to the target atoms, and hence changes in the direction of the projectile trajectory. This means that during the slowing down process, the ion may significantly change direction and the distribution becomes two-dimensional, varying both the energy of the ion and its trajectory. This means that nuclear energy loss distributions must contain both full energy loss and angular distributions. To date, this kind of experiment has not been conducted.

Especially important are errors included in experimental results which are performed with high-resolution spectrometers. These experiments normally include only very small exit solid-angles, and exclude particles with larger scattering angles, and perhaps the multiple-scattered ions.

These limitations of experimental distributions are discussed in detail in [88a] and in a lengthy review in [93a].

CHAPTER 6 - CITATIONS

- 32b A. Sommerfeld, Z. f. Physik, 78, 283 (1932).
- 40d N. Bohr, Phys. Rev., 58, 654 (1940).
- 44a L. Landau, J. Exp. Phys. USSR, 8, 201 (1944).
- 47a G. Moliere, Z. f. Naturforschung, A2, 133 (1947).
- 48a N. Bohr, Mat. Fys. Medd. Dan. Vid. Selsk., 18, No. 8 (1948).
- 48b K. R. Symon, PhD Thesis, Harvard University (1948). Unpublished.
- 57a O. B. Firsov, Zh. Eksp. Teor. Fiz., 32, 1464 (1957).
- 57b O. B. Firsov, Zh. Eksp. Teor. Fiz., 33, 696 (1957).
- 57d P. V. Vavilov, Zh. Eksp. Teor. Fiz., 32, 320 (1957). English translation in JETP, 5, 749 (1957).
- 57e T. J. Gooding and R. M. Eisberg, Phys. Rev., 105, 357 (1957).
- 59a O. B. Firsov, Soviet Phys., JETP, 9, 1076 (1959).
- 63a J. Lindhard, M. Scharff and H. E. Schiott, Mat. Fys. Medd. Dan. Vid. Selsk., 33, No. 14 (1963).
- 64c J. P. Biersack, Hahn-Meitner Report, HMI-B37 (1964).
- 64d S. M. Seltzer and M. J. Berger, pp 187-203, "Studies in Penetration of Charged Particles in Matter", U. S. National Acad. Sci., Nucl. Sci. Rpt. 39, ed. by U. Fano.
- 65a M. R. Raju, Ph. D. Thesis, Univ. California Report #16613 (1965), unpublished.
- 68a J. Lindhard, V. Nielsen and M. Scharff, Mat. Fys. Medd. Dan. Vid. Selsk., 36, No. 10 (1968).
- 68e K. B. Winterbon, Can. J. Phys., 46, 2479 (1968).
- 68f C. Tschalar, Nucl. Inst. Methods, 61, 141-156 (1968).
- 68g C. Tschalar, Nucl. Inst. Methods, 64, 237-243 (1968).
- 77c W. D. Wilson, L. G. Haggmark and J. P. Biersack, Phys. Rev., 15B, 2458 (1977).
- 82f J. P. Biersack and J. F. Ziegler, Nucl. Inst. and Meth., 194, 93 (1982).
- 84a J. F. Ziegler, J. P. Biersack, U. Littmark, "The Stopping and Range of Ions in Solids," vol. 1 of series "Stopping and Ranges of Ions in Matter," Pergamon Press, New York (1984).
- 88a J. P. Biersack, Nucl. Inst. Methods, B35, 205-214 (1988).
- 93a ICRU Report #49, "Stopping Powers and Ranges for Protons and Alpha Particles", 1993. See pages 82-105 for a length discussion of experimental methods and their limitations.
- 94a P. Sigmund, Phys. Rev. A, 50, 3197-3201 (1994).
- 94b A. N. Narmann and P. Sigmund, Phys. Rev. A, 49, 4709-4715 (1994).
- 95a P. Sigmund and A. N. Narmann, Laser and Part. Beams, 13, 281-292 (1995).
- 97a L. Glazov and P. Sigmund, Nucl. Inst. Methods, B125, 110-115 (1997).
- 98a P. Sigmund, Nucl. Inst. Methods, 135B, 1-15 (1998).
- 98b P. Sigmund and L. Glazov, Nucl. Inst. Methods, B136-138 (1998).

7 - TRIM: SCIENTIFIC BACKGROUND

TRANSPORT OF IONS IN MATTER

CHAPTER SUMMARY

TRIM is Monte Carlo computer program that calculates the interactions of energetic ions with amorphous targets. This program has been called TRIM (transport of ions in matter) for more than 30 years. The program uses several physical approximations to obtain high computer efficiency, while still maintaining accuracy. The two most important approximations are (a) using an analytic formula for determining atom-atom collisions (see section *The Magic Formula: Atom-Atom Collisions*) and (b) using the concept of a *Free-Flight-Path* between collisions, so that only significant collisions are evaluated (see section *The Free Flight Path*). This chapter provides the scientific and mathematical background to TRIM, and the next two chapters provides help in setting up TRIM calculations and understanding the output files and plots.

Chapter Contents

7 -TRIM: Scientific Background	7-1
CHAPTER SUMMARY	7-1
INTRODUCTION	7-2
THE MAGIC FORMULA: ATOM-ATOM SCATTERING	7-3
Fitting the Magic Formula Parameter : Δ	7-5
Interatomic Potentials for the Magic Formula	7-6
Nuclear Energy Loss and Angular Deflection.....	7-7
THE FREE FLIGHT PATH BETWEEN COLLISIONS.....	7-8
Free Flight Path for High Energy Ions	7-8
Free Flight Path for Low Energy Ions and Target Recoils.....	7-10
Using the Impulse Approximation for the Free Flight Path.....	7-14
Electronic Energy Loss Limits on Free Flight Path	7-17
COMPARISON OF CALCULATION AND EXPERIMENTS	7-18
Definition of Range Moments: Straggling, Skewness and Kurtosis	7-19
ELECTRONIC STRAGGLING IN TRIM	7-24
THE CALCULATION OF TARGET DAMAGE	7-26
The Kinchin-Pease Model for Vacancy Production	7-27
EVALUATION OF SPUTTERING IN TRIM	7-28
Summary of Radiation Damage Calculations.....	7-32
LAYERED TARGET STRUCTURES, SURFACES	7-33
SELECTION OF TARGET ATOMS IN COMPOUNDS	7-33
RANDOM NUMBER SEED –	7-35
CHAPTER 7 - CITATIONS.....	7-35

INTRODUCTION

This chapter presumes that the reader is somewhat familiar with the tutorial presentations of Chapters 2 and 3 on the physics and mathematics of ion-atom nuclear and electronic interactions. The presentation here will take highlights from these chapters in order to develop the concepts of the Magic Formula and the Free Flight Path.

The computer simulation of the slowing down and scattering of energetic ions in materials has been used in studies of ion implantation, radiation damage, sputtering, and the reflection and transmission of ions. The Monte Carlo method as applied in simulation techniques has a number of distinct advantages over analytical formulations based on transport theory. It allows more rigorous treatment of elastic scattering, explicit consideration of surfaces and interfaces, and easy determination of energy and angular distributions. The major limitation of this method is that it is inherently a time consuming calculation. Thus there is often a conflict between computer time and desired statistical precision. In the Monte Carlo computer program presented here, we attempt to alleviate this problem by using techniques which reduce computer time by at least two orders of magnitude while at the same time sacrificing little accuracy. In using TRIM, the user has the option to override the approximations and make a full detailed Monte Carlo calculation.

Several ion transport procedures based on the Monte Carlo method have been reported, see for example, Refs. (63e, 74e, 72j, 80b, 81b). Aside from considering crystalline or amorphous targets, their major differences lie in their treatment of elastic or nuclear scattering. Only Oen, Robinson and co-workers treat this scattering in a precise manner by numerically evaluating the classical scattering integral for realistic interatomic potentials. Other authors base their scattering formalisms on either the momentum approximation extended to large angles or on fitted, truncated Coulomb potentials to obtain analytical representations of the scattering integral. Since energetic ions undergo many collisions in the process of slowing down, the method used to evaluate the scattering integral is of critical importance in terms of its relative computer efficiency. Therefore, we have made use of a new analytical scheme which very accurately reproduces scattering integral results for realistic potentials.

As with other simulation programs, TRIM follows a large number of individual ion or particle "histories" in a target. Each history begins with a given ion energy, position, and direction. The particle is assumed to change direction as a result of binary nuclear collisions and move in straight free-flight-paths between collisions. The energy is reduced as a result of nuclear and electronic (inelastic) energy losses, and a history is terminated either when the energy drops below a pre-specified value or when the particle's position is outside the target. The target is considered amorphous with atoms at random locations, and thus the directional properties of the crystal lattice are ignored. This method is applicable to a wide range of incident energies from approximately 0.1 keV/u to several MeV/u, depending on the masses involved. The lower limit is due to the inclusion of binary collisions only, while the upper limit results from the omission of nuclear reactions and of relativistic effects. The efficiency for dealing with high energy particles has been increased by introducing an energy dependent *free-flight-path*. Thus a particle's free flight path between collisions is longer at high energies and is steadily reduced in the course of slowing down.

The nuclear and electronic energy losses or stopping powers are assumed to be independent. Thus, particles lose energy in discrete amounts in nuclear collisions and lose energy continuously from electronic interactions. For low energies, where nuclear scattering and energy loss are particularly important, the program utilizes the above mentioned analytic scheme based on a

solid-state interatomic potential as described in Chapter 2. The electronic energy loss of ion has been described in Chapters 3-5.

The formalism incorporated into the computer programs is applicable to all ion-target combinations, and the program provides information on ion range and damage characteristics as well as reflection and transmission properties of planar targets. Some results of representative calculations are presented later in this chapter and are compared with experimental data and other calculations.

THE MAGIC FORMULA: ATOM-ATOM SCATTERING

TRIM uses an analytic formula for the evaluation of atom-atom scattering. This technique, developed by J. P. Biersack and collaborators over a 10 year period, is called the *Magic Formula*, because it increases computing speed by up to 50x over other methods. This section will briefly review the details of the Magic Formula (see ref. 77c, 77r and 80d for full details). The development of the Magic Formula, Eq. 7-8, is briefly reviewed, and the parameterization of this formula, Eq. 7-10 to Eq. 7-12, are not derived here because the form of these equations resulted mostly in "what works" rather than from a direct analytic path.

Figure 7-1 depicts the scattering, through an angle Θ in the center-of-mass (CM) system, of an incident particle of mass M_1 and kinetic energy E by an initially stationary particle of mass M_2 for a repulsive interaction potential. Superimposed upon the orbits of the two particles is what we call the "scattering triangle". This triangle is comprised of the known or easily calculated quantities: p (impact parameter), r_0 (distance of closest approach), ρ_1 , ρ_2 (radii of curvature of the trajectories at closest approach), and the usually small "correction terms," δ_1 and δ_2 . From the scattering triangle shown in Figure 7-1, one can immediately define the cosine of Θ (note: some authors use the lower case theta: θ) to be:

$$\text{Eq. 7-1: } \cos\left(\frac{\Theta}{2}\right) = \frac{\rho + p + \delta}{\rho + r_0} \text{ with } \rho \equiv \rho_1 + \rho_2 \text{ and } \delta \equiv \delta_1 + \delta_2$$

The distance of closest approach, r_0 , was derived in detail in Chapter 2, and is obtained from the relation :

$$\text{Eq. 7-2: } 1 - \frac{V(r_0)}{E_c} - \left(\frac{p}{r_0} \right)^2 = 0$$

where $E_C = E / (1 + M_1/M_2)$ is the energy available in the CM system and $V(r)$ the interaction potential between the incident ion and the target atom. Eq. 7-2 can be solved by Newton's method in 2 or 3 iterative steps to an accuracy of better than 0.1% (Newton's method is discussed in most books on applied mathematics. See refs. 69b, 71e and 75l). The radius of curvature in the CM system is obtained by expressing the two-body scattering using the centrifugal force, f_c , of the CM system (this scattering formalism was originally developed by Harrison et al. (69c)). For particle velocities, V_1 and V_2 , in the CM system we obtain :

$$\text{Eq. 7-3: } \rho = \rho_1 + \rho_2 = (M_1 V_1^2 + M_2 V_2^2) / f_c$$

where the kinetic energy and force may be expressed in terms of E_C and $V(r)$ to yield:

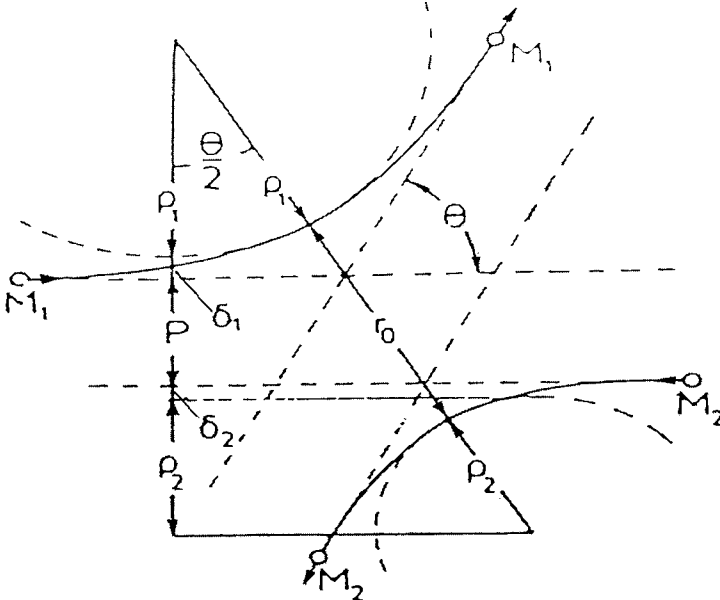


Figure 7-1 - Particle trajectories in the CM system.

The particle trajectories in the CM system with superimposed "scattering triangle", comprised of impact parameter, p , distance of closest approach, r_0 , radii of curvature ρ_1 , and ρ_2 , (curvature of the trajectories at closest approach), and the small correction terms, δ_1 and δ_2 . From this construction the CM deflection angle, Θ , can be obtained. See chapter 2 for more details.

$$\text{Eq. 7-4:} \quad p = \frac{2 [E_C - V(r_0)]}{-V'(r_0)}$$

where $V'(r_0)$ is the spatial derivative of the potential evaluated at r_0 .

It is convenient here to express the CM energy, E_C , in units of $Z_1 Z_2 e^2 / a$, with the lengths in units of the *screening length*, a , which was discussed in extended detail in Chapter 2. We introduce the dimensionless “*reduced energy*”, ε , defined as:

$$\text{Eq. 7-5:} \quad \varepsilon \equiv \frac{a E_C}{Z_1 Z_2 e^2}$$

where Z_1 and Z_2 are the *incident particle and target atomic numbers*, respectively, e is the *electronic charge*, and a is the *screening length*. We have chosen to use the “universal screening length” derived in Ref. 85a which is:

$$\text{Eq. 7-6: } a = \frac{0.8853 a_0}{(Z_1^{2/3} + Z_2^{2/3})}$$

where $a_0 = 0.529\text{\AA}$ is the Bohr radius (see Chapter 2 for more details of the derivation of Eq. 7-6). Expressing the various lengths in Eq. 7-1 in units of the screening length, a , we define :

$$\text{Eq. 7-7: } B \equiv p/a, \quad R_0 \equiv r_0/a, \quad R_C \equiv p/a, \quad \text{and} \quad \Delta \equiv \delta/a$$

so that Eq. 7-1 becomes

$$\text{Eq. 7-8: } \cos \frac{\Theta}{2} = \frac{B + R_C + \Delta}{R_0 + R_C} \quad (\text{The } \textit{MAGIC} \text{ Formula})$$

The above formula for $\cos \Theta/2$, and hence for determining the angle of scatter of both the ion and the recoil, and also the transferred energy during the collision, was developed by Biersack (77c, 80d) who called it the *Magic Formula*, because it allowed for the first time a quick solution to the scattering problem with high precision, instead of having to do the complete evaluation of the scattering integral which was derived in Chapter 2. Note that Chapter 2 also showed that the final angle of scatter, Θ , could be determined from the initial CM energy, E_c , the potential, $V(r)$, and the impact parameter, p , in what is called the *General Orbit Equation*:

$$\text{Eq. 7-9: } \Theta = \pi - \int_{-\infty}^{\infty} \frac{p dr}{r^2 \left[1 - \frac{V(r)}{E_c} - \frac{p^2}{r^2} \right]^{1/2}}$$

The Magic Formula is at the heart of TRIM, for it allows an analytic solution to the scattering of the ion and target atom.

Fitting the Magic Formula Parameter : Δ

In the high energy limit, atomic collisions can be adequately described using the unscreened Coulomb interatomic potential, i.e., Rutherford scattering. Therefore, a formula for Δ (defined in Eq. 7-7 and the main “correction” term using in the Magic Formula) should asymptotically approach the Rutherford result as ϵ becomes large. We will first derive a formula for Δ for Rutherford scattering, and then expand it with parameters so that it will smoothly fit scattering results for slower ions in screened Coulomb potentials. (A screened Coulomb potential occurs in atoms where the positive central point-charge is progressively screened by orbital electrons until, at one atomic radius, the potential goes to zero. A screened Coulomb collision is the scattering of two atoms responding to each other’s screened potential.) This expansion took many years to develop and tune so that suitable constants could be obtained which could be used with a wide variety of atomic potentials. The final form was the expression:

$$\text{Eq. 7-10: } \Delta = A \frac{R_0 - B}{1 + G}$$

with

$$\text{Eq. 7-11: } A = 2 \alpha \varepsilon B^\beta \quad \text{and} \quad G = \gamma [(1 + A^2)^{1/2} - A]^{-1}$$

where

$$\text{Eq. 7-12: } \alpha = 1 + C_1 \varepsilon^{-1/2}, \quad \beta = \frac{C_2 + \varepsilon^{1/2}}{C_3 + \varepsilon^{1/2}}, \quad \text{and} \quad \gamma = \frac{C_4 + \varepsilon}{C_5 + \varepsilon}$$

and $C_1 - C_5$ are the fitting parameters to be determined for the screened potential of interest. Eq. 7-10 is not a unique expression for Δ , but it was found in the fitting procedure that this form, containing the factor $(R_0 - B)$, gave the best fit and the most stable result. As ε becomes sufficiently large, α , β and γ approach unity and Eq. 7-8 reproduces Rutherford scattering, as is desired. (See ref. 77c, 77f and 80d for details.)

Interatomic Potentials for the Magic Formula

As noted in Chapter 2, *Interatomic Potentials* are the net potentials between two colliding screened atoms as their electrons clouds merge. It contains a lot of quantum mechanics and is complicated. Since the nucleus carries almost all the atoms mass, the two atoms can be considered as massive point charges in their joint interatomic potentials. As noted in Eq. 7-4, the evaluation of ρ requires the evaluation of an interatomic potential at r_0 , and also its differential at that point. We have adopted the universal potential derived in Chapter 2 for general nuclear scattering in TRIM. This potential is given by

$$\text{Eq. 7-13: } V(R) = \frac{Z_1 Z_2 e^2}{a R} \Phi(R)$$

where R is the reduced interatomic separation, $R = r/a$ and $\Phi(R)$ is either the universal screening function shown in Chapter 2, Fig. 2-17, or specific interatomic potentials between the two atoms.

We have tabulated the solutions of the classical scattering integral for the universal potential for a wide range of *reduced energy*, ε , and *reduced impact parameter*, b , values, see Fig. 2-21. These tables include R_0 as well as $\sin^2(\Theta/2)$. Using these tables, the parameters necessary for Eq. 7-10 to Eq. 7-12 can be found by minimizing in the least-squares sense the deviation between the fitted and the tabulated $\sin^2(\Theta/2)$ values. This quantity was selected for use in the fitting procedure because the nuclear energy loss is proportional to $\sin^2(\Theta/2)$.

Table 4-1 gives the values determined for the five parameters indicated in Eq. 7-12 for various potentials which have been used in the TRIM program up until 2008. After this date, TRIM uses

Table 4-1 Values for constants in Eq. 7-12 for various potentials

Coefficient	Moliere	Kr-C Spec	Universal
C_1	0.6743	0.7887	0.99229
C_2	0.009611	0.01166	0.011615
C_3	0.005175	0.006913	0.007122
C_4	10.00	17.16	9.3066
C_5	6.314	10.79	14.813

specific interatomic potentials for the two atoms involved in the collision.

Figure 2-21, in Chapter 2, evaluated the Magic Formula over nine orders of magnitude of collisional energies. And showed $\sin^2(\Theta/2)$ as a function of the *impact parameter*, b , for various values of ϵ . In the figure, the solid lines are based on the formulation presented here, whereas the circled points represent the tabulated exact values using a full orbital scattering calculation.

In Fig. 2-21, it is difficult to perceive the differences between the points calculated from the integral orbit equation, Eq. 7-9, and the curves generated using the Magic Formula, but discrepancies as large as 5% exist. However, discrepancies this large are the exception rather than the rule. Detailed examination indicates most differences are 2% or less and the mean deviation is 2.1%. This quality of the agreement between the fitted results and the detailed calculations over at least 9 orders of magnitude in ϵ is considered quite satisfactory, and since it asymptotically approaches the proper limit for large ϵ , this provides some justification for the detailed five-parameter formulation that has been used to achieve these results.

Even though the above formalism for nuclear scattering has built-in validity for large values of ϵ , it is more efficient to base the calculations directly on the Coulomb potential for higher energies, $\epsilon > 10$. For the Coulomb potential, $\sin^2(\Theta/2)$ is simply related to ϵ and b by the following expression:

$$\text{Eq. 7-14:} \quad \sin^2(\Theta/2) = 1 / [1 + (2\epsilon b)^2]$$

At $\epsilon = 10$ and small impact parameters, where $\sin^2(\Theta/2)$ is large, the results for the Coulomb and Moliere potentials are quite similar. There exists marked differences only for small values of $\sin^2(\Theta/2)$ where the energy loss and angular deflection are small. For example, consider the case near $b = 0.4$ where the ratio of the Coulomb to Moliere values of $\sin^2(\Theta/2)$ is 1.5. For equal mass atoms, the incident atom would lose $\sim 1.5\%$ of its energy using the Coulomb potential rather than 1% with the Moliere potential. At higher values of ϵ these types of differences become less, and therefore the use of the Coulomb potential for $\epsilon > 10$ should perturb results of calculations only slightly while significantly reducing the computing time. In TRIM, the analytic expression in Eq. 7-14 includes the electronic screening effect near the nucleus (varying from an r^{-1} through an $r^{-1.5}$ to an r^2 potential). This reduces the above mentioned differences to about the level of the magic formula, Eq. 7-8. This final correction for $\epsilon > 10$ is:

$$\text{Eq. 7-15} \quad \sin^2(\Theta/2) = 1 / [1 + (1+b(1+b))(2\epsilon b)^2]$$

Nuclear Energy Loss and Angular Deflection

As discussed at length in Chapter 2, the nuclear energy loss or *energy transfer*, T , to the target atom in a single collision is proportional to $\sin^2(\Theta/2)$ and is given by the following relationship:

$$\text{Eq. 7-16:} \quad T = \frac{4 M_1 M_2}{(M_1 + M_2)^2} E \sin^2 \frac{\Theta}{2}$$

The above formalism for nuclear scattering provides the *scattering angle*, Θ , in the CM system. The *laboratory scattering angle*, ϑ , is given by the following relationship:

$$\text{Eq. 7-17:} \quad \vartheta = \arctan \{ \sin \Theta / [\cos \Theta + (M_1/M_2)] \}$$

After the collision, the azimuthal scattering angle, ϕ , for both the incident atom and the recoiling atom is randomly selected using the relation

$$\text{Eq. 7-18:} \quad \phi = 2\pi R_n,$$

where R_n is a random number uniformly distributed between 0 and 1. In actual calculations, the particles are followed with reference to a fixed axis, chosen to be normal to the target surface. The angle, α , with respect to this axis is determined after each collision. The cosine of this angle, after the i^{th} collision, is given by:

$$\text{Eq. 7-19:} \quad \cos \alpha_i = \cos \alpha_{i-1} \cos \theta_i + \sin \alpha_{i-1} \sin \theta_i \cos \phi_i.$$

Similarly the directional cosines with respect to the other Cartesian coordinates (lateral directions) are determined for following the particle trajectories in three-dimensional space.

THE FREE FLIGHT PATH BETWEEN COLLISIONS

In TRIM, CPU calculation time is reduced by omitting the calculation of collisions which transfer "negligible" amounts of energy and cause "negligible" deflection angles in the ion's trajectory. This skipping of minor collisions can save a great deal of time: for example, for protons at 10 MeV in various materials more than a thousand monolayers may be skipped between each calculated collision of the ion with a target atom. When the ion skips over many monolayers, such quantities as electronic energy loss are still spread properly into these layers since this requires little CPU time. The purpose of this section is to discuss what the term *negligible* means in the context of calculating the free-flight path of the ion between calculated collisions.

Free Flight Path for High Energy Ions

At high energies, $\epsilon \gg 10$, only a few of the many collisions in the target cause significant deflections from the straight path of flight. Even over distances, L , large compared to the interatomic distance in a solid, a noticeable deflection ($\theta > 1^\circ$) is a rare event, and it is connected with a very small impact parameter. TRIM sets up criteria for a minimum energy transfer (to be discussed later) and calculates the maximum distance the ion can jump (without collisions) until there must be one significant collision. The free-flight-path (FFP) is not a constant length, for once the maximum jump distance is estimated, this length is reduced by a random number (ranging from 0-1) to distribute the probability of the collision to somewhere randomly within the jump length.

The smallest impact parameter over the path length L is found in the following way: The probability, $W_1(p)\delta p$, for finding a target atom at a radial impact distance between p and $p + \delta p$ is:

$$\text{Eq. 7-20:} \quad W_1(p)\delta p = N L 2\pi p \delta p$$

where N is the atomic density of the target. The probability for not finding another atom closer than p , i.e., between 0 and p , is

$$\text{Eq. 7-21:} \quad W_2(p) = \exp(-N L \pi p^2)$$

Hence the probability for finding the closest target atom between p and $p + \delta p$, i.e. finding an atom there, provided no other atom is closer, becomes the product:

$$\text{Eq. 7-22: } W(p) \delta p = W_2(p) W_1(p) \delta p = \exp(-N L \pi p^2) N L 2 \pi p \delta p$$

This probability distribution leads to the impact parameter determination

$$\text{Eq. 7-23: } p = [-\ln(R_n)/\pi N L]$$

Which includes a random number, R_n , which is evenly distributed between 0 and 1.

For high energies, the *free flight path length*, L , is chosen such that the mean angular deflection per path length L remains about constant :

$$\text{Eq. 7-24: } \frac{M_2}{M_1} \frac{\Delta E_n}{E} = \frac{M_2}{M_1} \frac{L S_n(E)}{E} = \text{constant}$$

according to what are sometimes called the Bohr [48a] and Williams [39a, 40c] Rules. Introducing this analytic expression for the Universal nuclear stopping power, S_n , for the universal potential (see Fig. 2-18) and choosing the constant in Eq. 7-24 to yield, for example, an average deflection of about 5° per path interval L ; we obtain from Eq. 7-24:

$$\text{Eq. 7-25: } L = \frac{0.02 [1 + (M_1 + M_2)]^2 \varepsilon^2 + 0.1 \varepsilon^{1.38}}{4\pi a^2 N \ln(1 + \varepsilon)}$$

By choosing the free flight path (FFP) in this way, one is assured that $L(E)$ is always short compared to the mean distance between large angle deflections ($9 > 10^\circ$). Therefore, it does not matter where such a deflection occurs within each L -interval, and TRIM places the collision at each interval's end. Normally, deflection angles are small and account for the "multiple scattering" which gradually changes the direction of the ion's motion. In addition, a second independent check is performed on the path length, L , in order to ensure that the electronic energy loss does not exceed 5% of the ion energy. In cases where this could happen (e.g., high energy light particles), the path length L is reduced accordingly.

For low energies, where (using Eq. 7-25) the FFP, L , becomes less than the target's interatomic distance, $N^{1/3}$, the approximate *mean atomic separation*, $N^{1/3}$, is used for L instead of (4-22). In this case, however, the impact parameter has to be chosen according to

$$\text{Eq. 7-26: } W(p) \delta p = \begin{cases} 2\pi N^{2/3} p \delta p & \text{for } p < \pi^{-1/2} N^{-1/3} \\ 0 & \text{for } p > \pi^{-1/2} N^{-1/3} \end{cases}$$

since now only one atom is assumed in the volume element of length $N^{-1/3}$ and base area of $N^{-2/3}$. This procedure maintains the atomic density in the target without correlating the lateral positions of successive target atoms (TRIM neglects any lattice structure). This assumption, Eq. 7-26, leads to the determination of impact parameters :

$$\text{Eq. 7-27: } p = [R_n / (\pi N^{2/3})]^{1/2}$$

With the impact parameter selections, Eq. 7-23 and Eq. 7-27, a discontinuity in the treatment is created at the transition from the "high energy" to the "low energy" part of slowing down of the ion. To evaluate the importance of this effect, we have performed hundreds of ion/solid calculations over many orders of energy. No difference of more than 1% could be found in the results when using the prescribed FFP procedure or when using a minimum value for the next collision, the interatomic target spacing, $L = N^{-1/3}$, throughout the slowing down process. When using TRIM, the user is always given to choice to omit using the Free Flight Path.

Also, another check was performed on using a realistic distribution of L values, e.g. between $d/\sqrt{2}$ and $d/2$ in an f.c.c. lattice, rather than the fixed value $L = N^{-1/3}$ ($= d / 2^{2/3}$ for f.c.c. lattices) where d denotes the lattice constant. However, no difference in the results could be detected, and the fixed value was chosen for best efficiency in succeeding tests.

At very low energies, e.g., He^+ ($< 200\text{eV}$) incident on Cu, the FFP of the ion becomes less than the distance to the next target atom, since the next deflection point of the ion trajectory lies in front of the target's center. This can sometimes be visualized by assuming hard sphere collisions. Indeed, comparative tests showed that the hard sphere approximation yields a sufficiently accurate estimate for this effect. Therefore, at low energies, the path value is changed to $L = [N^{-1/3} - p \tan(\Theta/2)]$ to account for the path-length reduction. (In the literature this offset is connected to the *time-integral*, τ , which is given by an integral expression similar to the scattering integral.) At higher energies, however, this offset becomes small and here it is set to zero in TRIM.

Free Flight Path for Low Energy Ions and Target Recoils

The path length extension as described in the previous section was successfully applied for the motion of the incident particles at high energies, e.g., for predicting the projected ranges, transmission or reflection of ions (complete distributions in space or in energy and angle, respectively). For the transport of recoiling target atoms, which are responsible for recoil implantation and mixing, damage and sputtering of the target material, additional requirements must be placed on the choice of the maximum impact parameters and hence on the mean free flight path, in order to ensure that all energy transfers, T , above a given threshold, T_{\min} , are fully accounted for even at very low energies. Such thresholds should be well below the *displacement energy*, E_d , of a target atom in the solid, or the *surface binding energy*, E_s , in the case of sputtering. In these studies we are not only concerned about including all scattering angles down to a very low value, but also about the absolute amount of the energy transfer, T , to the target atom, which imposes another quite different requirement on the choice of the *maximum impact parameter*, p_{\max} .

In this case we adhere to our previously used rule of assuming one target atom in cylinder of volume N^{-1} :

$$\text{Eq. 7-28:} \quad \pi (p_{\max})^2 \cdot L = N^{-1}$$

where ion's *path length*, L , is now connected to the impact parameter, p_{\max} . Instead of determining the flight path, L , by the methods described in the last section we now predetermine the *maximum impact parameter*, p_{\max} , in such a way as to obtain the required *minimum transferred energy*, T_{\min} , and then calculate L from Eq. 7-28. This procedure ensures (i) that the correct minimum path length is used, and (ii) that all displacements (or sputtered atoms) are fully accounted for. This method also has the advantage of automatically extending the free flight path, L , at higher energies and thus saving computer time.

In calculations of sputtering or damage production, we have to treat the low energies quite precisely. In collision cascades, for example, we have to follow the recoils through several generations until their energies typically reach $E_s = 3\text{-}6 \text{ eV}$ or $E_d = 15\text{-}30 \text{ eV}$. At such low energies the atomic collisions behave like hard spheres, strongly interacting even at separations of $2\text{-}3 \text{\AA}$. (The hard sphere behavior is a consequence of the exponential decay of realistic potentials, which drop off more steeply than any power potential). We therefore allow the maximum impact parameter to increase at low energies up to two Seitz-Wigner radii, i.e. about 3\AA . This large p_{\max} in turn results in rather small free flight paths between collisions, which may become as low as 0.5\AA according to Eq. 7-28.

The actual functional dependence of $p_{\max}(\epsilon; T_{\min}, Z_1, Z_2, M_1, M_2)$ is rather difficult to obtain, but it can be fitted numerically in the form of a close upper limit which ensures being always on the safe side but not unnecessarily wasting computer time (T_{\min} is usually chosen between 1 and 5 eV). As an example, the shape of such functions, computed precisely for minimum transferred energies of 30 eV and 0.0413 eV for He and Al impinging on Al, are depicted in Figure 7-2 and Figure 7-3; more examples can be found in ref. (82m). Figure 7-2 and Figure 7-3 indicate that in cases of equal masses, e.g. Al recoils moving in Al, the maximum impact parameter indeed reaches values of $p_{\max} = 25 \cdot a = 3.15 \text{\AA}$. It may also be seen from Figure 7-2 and Figure 7-3 that for bad mass mismatches, e.g. for He ions in Al, about half that value suffices, and hence a four times larger flight path, L, is then used according to Eq. 7-28.

A final question is whether a small minimum transferred energy also ensures that all the scattering angles down to a few degrees are fully accounted for. Unfortunately, the answer is *No*, which means that both criteria, the one of the last section on small angles and the new one on small transferred energies, have both to be checked independently in order to get the defect production or sputtering correctly calculated, and also to obtain a geometrically precise ion trajectory. This can be shown in the following example. Assume for simplicity that the scattering angles are below 15° , then we may write :

$$\text{Eq. 7-29:} \quad T = \gamma E \sin^2(\Theta/2) \approx \gamma E \Theta^2 / 4$$

From this equation we obtain $\Theta_{\min} = (4 T_{\min} / \gamma E)^{1/2}$ which must be converted in order to get the *deflection angle in the lab system*, ϑ_{\min} :

$$\text{Eq. 7-30:} \quad \vartheta_{\min} = \Theta_{\min} / (1 + M_1 / M_2) = (M_2 T_{\min} / M_1 E)^{1/2}$$

In the example of a 50 keV Al^+ -Al self-bombardment, and studying the sputtering process with a surface binding energy, $E_s = 3.36 \text{ eV}$, Eq. 7-29 leads to $\vartheta_{\min} = (3.36/50000)^{1/2} = 0.0082 \text{ rad} = 0.47^\circ$, which is a small lower angular limit for obtaining correct ion trajectories. On the other hand, asking for defect production ($E_d = 16 \text{ eV}$) by ${}^4\text{He}(2.5 \text{ keV})$ impinging on ${}^{27}\text{Al}$, we would obtain $\vartheta_{\min} = [(27 \cdot 16)/(4 \cdot 2500)]^{1/2} = 0.208 \text{ rad} = 12^\circ$, which is already an intolerably large minimum scattering angle for following the ion trajectories with good precision. We therefore must conclude that both checks on the minimum transferred energy and on the minimum scattering angle have to be carried out separately and the larger of the two impact parameters corresponding to the smaller of the two free path lengths has to be chosen. For multi-atomic targets, the above checks are carried out individually for each target atom species, and the largest p_{\max} is then chosen in the TRIM program.

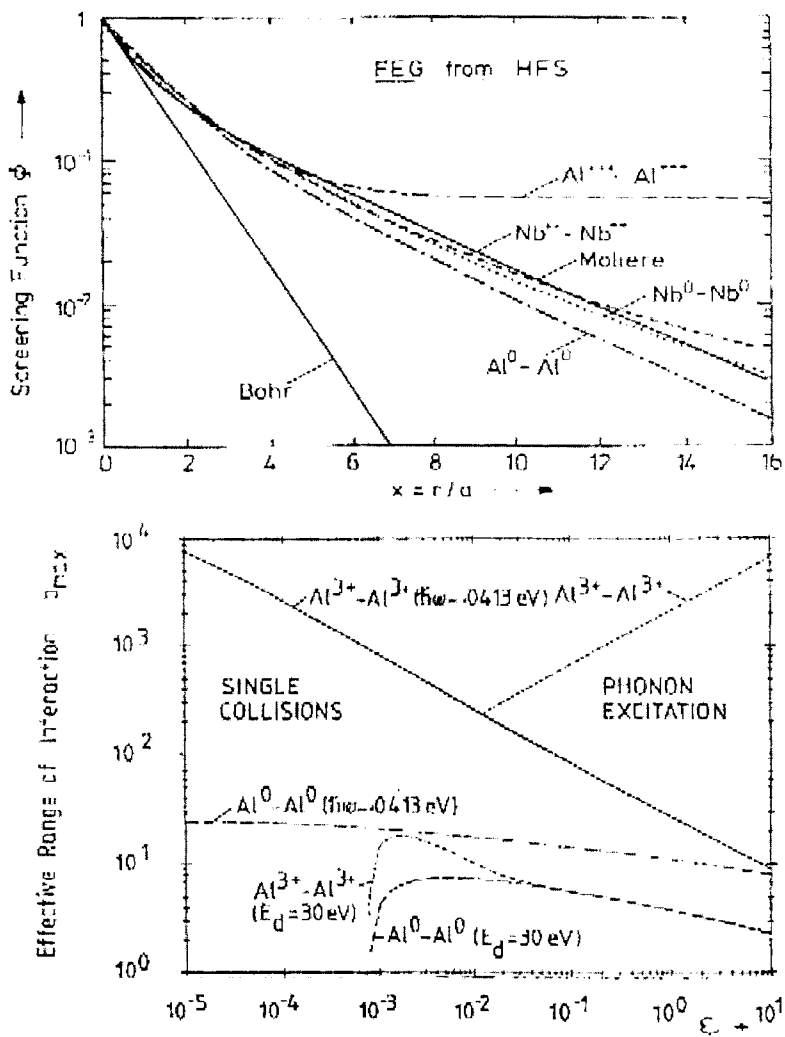


Figure 7-2 - Calculations of Effects of Impact Parameter b_{\max} for $\text{Al} \rightarrow \text{Al}$

The impact parameters b_{\max} ($b_{\max} = p_{\max}/a$) which correspond to the smallest transferred energies, $\hbar\omega = 0.0413 \text{ eV}$ (phonon excitation), and $E_d = 30 \text{ eV}$ (displacement energy in Al_2O_3) for the above given potentials. (A) In the case of Al in Al, b_{\max} may become as large as 25, corresponding to $p_{\max} = 3.15 \text{ \AA}$, while for the poorer mass match of He Al, (Figure 7-2), b_{\max} is half of that value.

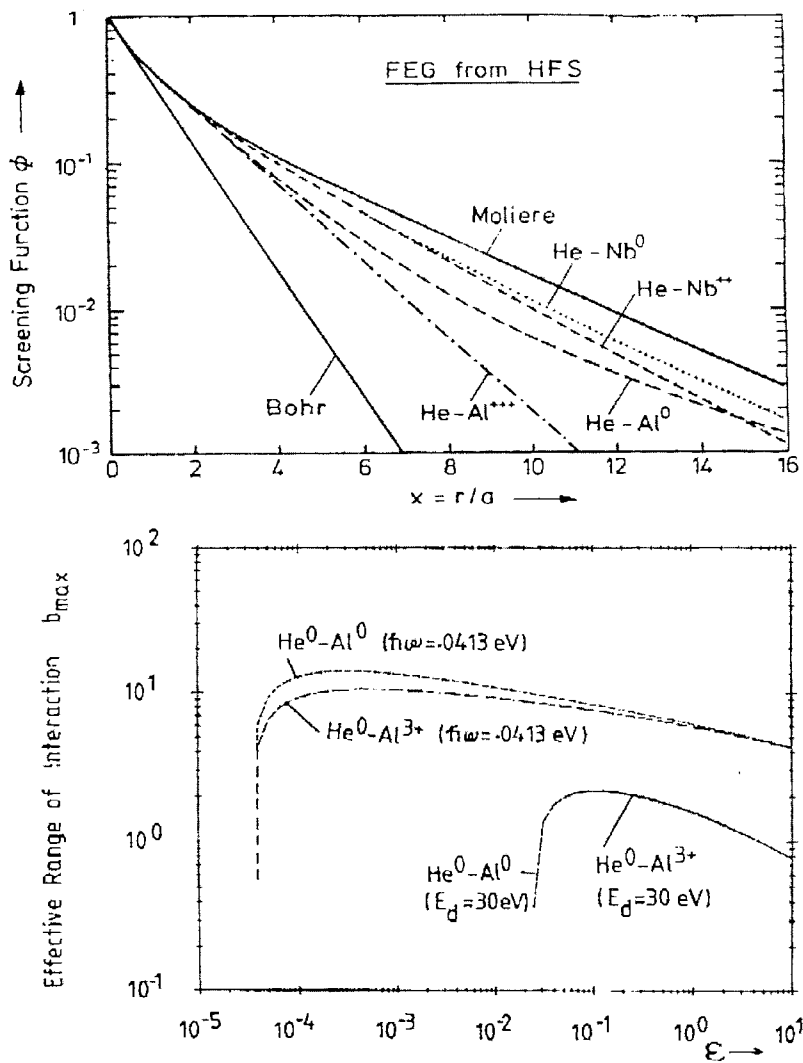


Figure 7-3 - Calculations of Effects of Impact Parameter b_{\max} for $\text{He} \rightarrow \text{Al}$

The impact parameters b_{\max} which correspond to the smallest transferred energies $\hbar\omega = 0.0413 \text{ eV}$ (phonon excitation), and $E_d = 30 \text{ eV}$ (displacement energy in Al_2O_3) for the above given potentials. For the case of $\text{He} \rightarrow \text{Al}$, which has a poorer mass match than for $\text{Al} \rightarrow \text{Al}$, b_{\max} is half of the value for $\text{Al} \rightarrow \text{Al}$ shown in Figure 7-2.

The ideas behind the impact parameter selection in a more general form are best understood from Figure 7-4 which shows the (universal) curve of $b(\epsilon)$ for a fixed small angle, here $\Theta = 6.3^\circ$ in the center-of mass system, and the various curves "1" through "4" for transferring a fixed amount of energy to the target atoms. The left curve (label "1") may be considered as an example of defect production ($T_{\min} \approx E_d \approx 25$ eV) in the case of Au recoils moving in an Au target. The right hand curve (label "4") could be an example of sputtering of Al by H_c^+ ions ($T_{\min} = E_S = 3.4$ eV). It is obvious from this picture that at high energies p_{\max} , and hence the free flight path, L , is determined by the minimum energy transfer, while at low energies the minimum deflection angles are the more stringent criteria. The curves of Figure 7-4 are based on the new universal potential (see Chapter 2).

In TRIM, increased efficiency can be obtained by scaling all collisions which transfer negligible amounts of energy and cause negligible deflection angles in the ion trajectory. ***The definition of "negligible" is assumed in TRIM to be any random quantity (non-cumulative) which has less than 0.1% effect on the final results.*** A random quantity would be a small angle collision which deflects the ion less than 0.1° (for example, for 10 MeV protons in silicon, a thousand monolayers will not sum to a deflection of the proton of 0.1°). If several of these collisions are correctly grouped into a single collision, then the particle's trajectory remains within the framework of a Monte-Carlo calculation. Some similar events may be cumulative, and non-random, and care must be made to include every one of these. An example would be a collision near the target surface, where every collision must be treated in detail to correctly evaluate surface events such as sputtering or backscattering of the incident ion.

When conditions permit (especially when the ion is not near the surface or any target interface), TRIM evaluates a *Free Flight Path*, L , over which the ion jumps between calculated collisions. The electronic energy loss is still distributed over this jump, but all intermediate collisions are grouped into one final collision, which is non-negligible. We define such a collision as one which transfers a predefined *minimum energy transfer*, T_{\min} , below which any energy transfer is considered negligible. One way to define this energy would be to restrict collisions to only those which can transfer more than the displacement energy, E_d , which is the minimum energy required to make a target atom recoil into the target (E_d is declared by the TRIM user). Typical values of E_d range from 10 - 30 eV.

Note: As discussed later, when the ion's position is such that the Free Flight Path will jump over a target interface, or the target's surface or bottom, then this FFP jump is truncated to a random distance less than the trajectory distance to this nearest edge. These jumps get increasingly limited, until the final jump over the edge is made in monolayer steps.

Using the Impulse Approximation for the Free Flight Path

The method of calculating L is straightforward if we use the traditional *Impulse Approximation*, which is applicable whenever $T \ll E$, or using Eq. 7-16, the scattering occurs with $\sin^2 \Theta/2 \ll 1$.

The impulse approximation has been studied extensively by Leibfried (65e), who concluded that $\sin^2 \Theta/2$ could be reduced, for Coulomb collisions, to a simple relationship with the impact parameter of the collision (see chapter 2, Figures 2-1 to 2-3, for a schematic of the two-body collision with impact parameter, p . The dimensionless impact parameter $b = p/a$, where a is the screening constant):

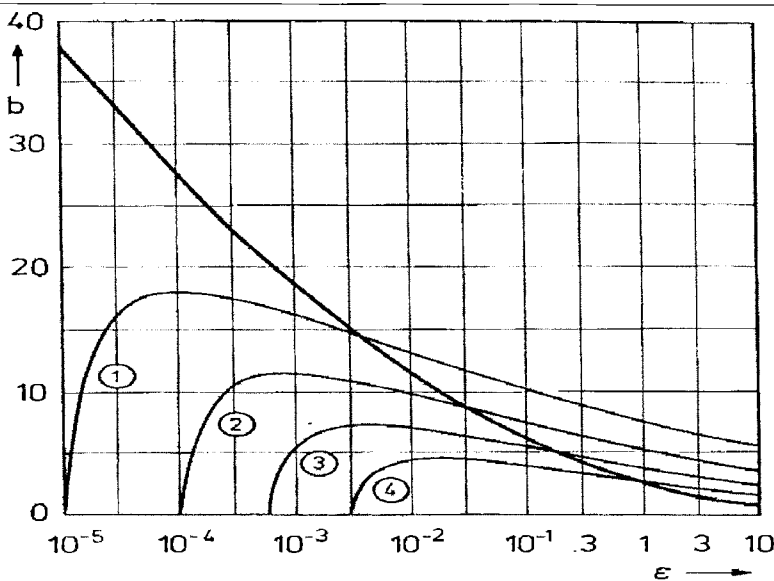


Figure 7-4 - Universal Curves of the Impact Parameter, b_{\max} .

Universal curves of the impact parameter, $b = p/a$, versus the dimensionless energy, ε . The heavy solid line represents a constant deflection angle, here 6.3° , for obtaining precise ion trajectories. It is also roughly the limit of validity of the impulse approximation. Curves 1 through 4 represent the $b(\varepsilon)$ values which correspond to fixed energy transfers T . Curve 1 could be taken as an example of choosing b_{\max} for sputtering Al by He ($T_{\min} = E_s = 3.4$ eV), while curve 4 would correspond to damage production by Au recoils moving in an Au target ($T_{\min} = E_d = 25$ eV). These curves are based on the Universal potential described in Chapter 2.

$$\text{Eq. 7-31:} \quad \sin^2 \Theta/2 = f(b) / (2b\varepsilon)$$

where ε is the reduced energy in units of $Z_1 Z_2 e^2/a$, see Eq. 7-5. The function $f(b)$ depends on the details of the central potential of the collision. For a given energy transfer, for example $T = E_d$, and using Eq. 7-29, we have:

$$\text{Eq. 7-32:} \quad E_{\min} = \gamma E \sin^2 (\Theta/2)$$

and hence

$$\text{Eq. 7-33:} \quad \sin (\Theta_{\min}/2) = (E_{\min} / \gamma E)^{1/2} = f(b_{\max}) / 2\varepsilon b_{\max}$$

Converting both E_{\min} and E , the ion energy, into dimensionless ε values by using the same conversion factors, we obtain

$$\text{Eq. 7-34:} \quad (\varepsilon_{\min} / \gamma \varepsilon)^{1/2} = f(b_{\max}) / 2\varepsilon b_{\max}$$

or

$$\text{Eq. 7-35: } (\varepsilon \varepsilon_{\min} / \gamma)^{1/2} = f(b_{\max}) / 2b_{\max}$$

We now solve for b_{\max} by inverting this equation using a function, F :

$$\text{Eq. 7-36: } b_{\max} = F(\xi) \quad \text{where } \xi = (\varepsilon \varepsilon_{\min} / \gamma)^{1/2}$$

This solution has been studied extensively and a rough approximation for the Universal potential, discussed earlier in Chapter 2, can be obtained by using the expression:

$$\text{Eq. 7-37: } b_{\max} = \xi + \xi^{0.5} + 0.125 \xi^{0.1}$$

This is the equation which is used in TRIM to calculate the maximum free-flight path of the ion between calculated collisions based on energy-transfer considerations. Since this expression is essential in understanding TRIM's free flight path, it is worth restating from a different perspective. For any given *energy transfer*, T, then Eq. 7-29 and Eq. 7-31 may be expanded to evaluate the required collision values (see derivation in Chapter 2) :

$$\text{Eq. 7-38: } T = \frac{2}{M_2} \left(V_0 M_c \sin \frac{\Theta}{2} \right)^2 = \frac{4 E_c M_c \sin^2 \frac{\Theta}{2}}{M_2} = \frac{4 E_0 M_1 M_2 \sin^2 \frac{\Theta}{2}}{(M_1 + M_2)^2}$$

where the ion values are E_0 , V_0 , Z_1 and M_1 , the target atom values are Z_2 and M_2 , and the center-of-mass values are M_c , E_c and Θ . For a *minimum energy transfer*, T_{\min} , we can extend Eq. 7-31 to:

$$\text{Eq. 7-39: } \sin^2(\Theta_{\min} / 2) = f(b_{\max}) / 2 b_{\max} \varepsilon$$

where b_{\max} is the *maximum impact parameter* to result in a *minimum scattering angle*, Θ_{\min} , and hence a *minimum energy transfer*, T_{\min} . This isolates b_{\max} on the right side of the equation, and we need now to invert Eq. 7-39 to solve for the maximum b_{\max} which can give the minimum energy transfer, T_{\min} . This can not be done analytically, but we have numerically evaluated it using Eq. 7-38 and Eq. 7-39 with the Universal potential, Φ_U , derived in Chapter 2, to the following expansion:

$$\text{Eq. 7-40: } b_{\max} \equiv p_{\max}/a = [\xi + \xi^{0.5} + 0.125\xi^{0.1}]^{-1}$$

where we define :

$$\text{Eq. 7-41: } \xi \equiv (\varepsilon \varepsilon_{\min} / \gamma)^{1/2} \quad \text{with } \gamma \equiv 4 M_1 M_2 / (M_1 + M_2)^2$$

with ε and ε_{\min} being the ion energy, and minimum energy, reduced using Eq. 7-5.

So the Free Flight Path, L, used in TRIM, for random collisions, is made such that the total mean energy transfer of all intermediate collisions is less than T_{\min} .

Electronic Energy Loss Limits on Free Flight Path

In the high energy region, the inelastic or electronic energy loss is treated independent of the nuclear energy loss, as in all other ion transport theories and models. Neglecting impact parameter dependence and straggling at high energies, we relate the electronic energy loss to the distance traveled between collisions, L, by :

$$\text{Eq. 7-42:} \quad \Delta E_e = L N S_e(E)$$

where the *electronic stopping cross section*, $S_e(E)$, which was described in Chapters 3-5. At low energies, where the electronic stopping power becomes about proportional to the ion's velocity, one might consider the use of an electronic loss which is correlated with the impact parameter of each collision. Expressions for the electronic energy loss as a function of impact parameter, p, or of the distance of closest approach, r_0 , have been provided by Firsov [59c] and by Oen and Robinson [76n]. Firsov's derivation assumes about equal size of ion and target atom, and is therefore restricted in validity to

$$\text{Eq. 7-43:} \quad 1/4 < Z_1/Z_2 < 4, \\ \text{and}$$

$$\text{Eq. 7-44:} \quad \Delta E = \frac{4.3 \times 10^{-8} (Z_1 + Z_2)^{5/3} V}{[1 + 0.31 p (Z_1 + Z_2)^{1/3}]^5}$$

where the constant assumes physical units for velocity, V in cm/s, and the impact parameter, p in Å. Oen and Robinson have suggested a different correlation:

$$\text{Eq. 7-45:} \quad \Delta E = \frac{0.045 k \sqrt{E}}{\pi a^2} \exp(-0.3 r_0/a)$$

where $k\sqrt{E}$ is the electronic stopping cross section in the low energy regime, and the fore-factor is chosen such that at higher energies, when $r_0 \rightarrow p$, the full electronic stopping is retrieved.

Eq. 7-45 has been made available as an option in the TRIM program. We prefer Oen's and Robinson's formalism for the following reasons: (1) it has no restrictions in the Z_1/Z_2 ratio, (2) it accounts for the real ion trajectory by considering a closest approach of r_0 rather than p, and (3) it was found to yield approximately the right amount of total electronic straggling, as compared to current theoretical predictions. Applying this option to low energy light ions, the most drastic changes are seen in the path-length distribution, e.g. for 8 keV protons in a gold target, the total path length is increased nearly 50%, and the path length straggling is increased about five times. However, the physically observable distributions, e.g. projected ranges or backscattered particles, undergo only minor (< 15%) changes. For heavy ions these effects become completely negligible, as the slowing down becomes dominated by nuclear stopping. At very high energies, however, the electronic straggling reaches rather high values (the Bohr plateau [48a]) and effects the projected range distribution in a drastic way, as will be discussed in a later section on high energy particles.

COMPARISON OF CALCULATION AND EXPERIMENTS

To demonstrate the applicability and reliability of TRIM, a number of representative calculations have been performed. We have tried to select cases which have some intrinsic interest, and, in addition, have been studied previously, either experimentally or by extended computational methods. Helium and lithium ion beams interacting with metals have been a field of basic research interest as well as an applied field in nuclear-fusion research. Since reliable measurements of He and Li depth profiles are available, we show in Figure 7-5 such range distributions in comparison with TRIM predictions. The TRIM results are typically depicted in the form of a histogram; the full lines are obtained by convoluting these TRIM results with the reported experimental resolution; and they represent our expectation for the experimental outcome, which was then added in the form of points [82n, 82o].

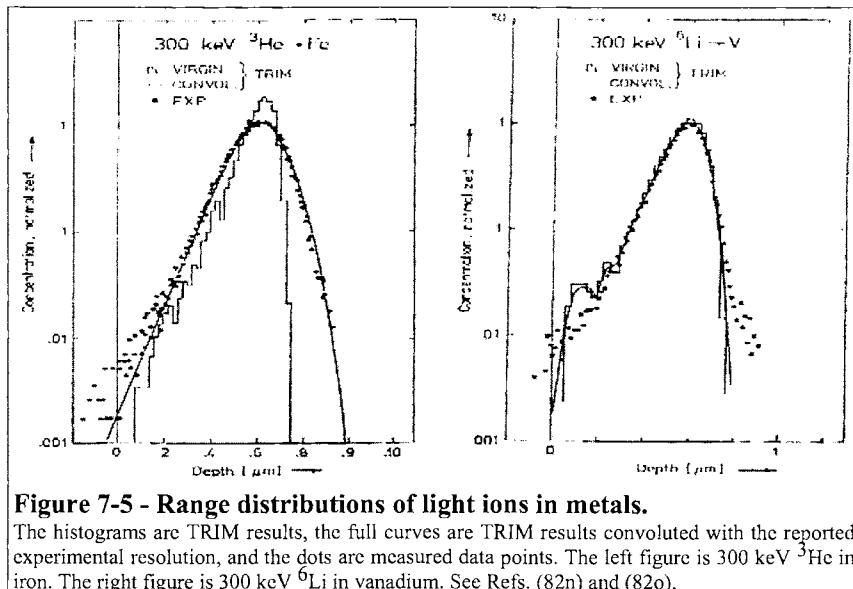


Figure 7-5 - Range distributions of light ions in metals.

The histograms are TRIM results, the full curves are TRIM results convoluted with the reported experimental resolution, and the dots are measured data points. The left figure is 300 keV ${}^3\text{He}$ in iron. The right figure is 300 keV ${}^6\text{Li}$ in vanadium. See Refs. (82n) and (82o).

The next figure on He ranges in Cu, Figure 7-6, shows the range moments of TRIM calculations as compared to predictions of the Littmark transport theory (see ref. 85a) using similar potentials and electronic stopping powers [81b]. The differences at lower energies are mainly due to the fact that the free surface is taken into account in TRIM, while the solutions of transport theory only considered the slowing down in an infinite medium. The *third moment, skewness* $\equiv \gamma$, and the *fourth moment, kurtosis* $\equiv \beta$, are results from TRIM. The skewness is seen to change sign because of surface influences, while the kurtosis (peakedness) remains close to 3 at lower energies, as in the case of a Gaussian distribution.

"*Straggling*" is a word which is used in ion implantation in several ways, and care should be taken to determine the author's definition. Sometimes it is a synonym for variance and sometimes it is defined as the square root of the variance. In other cases an author, such as Winterbon, uses

normalized definitions such as: Straggling = $\langle \Delta x_i^2 \rangle / \langle x \rangle^2$. We use the common statistical definition that straggling is the square root of the variance:

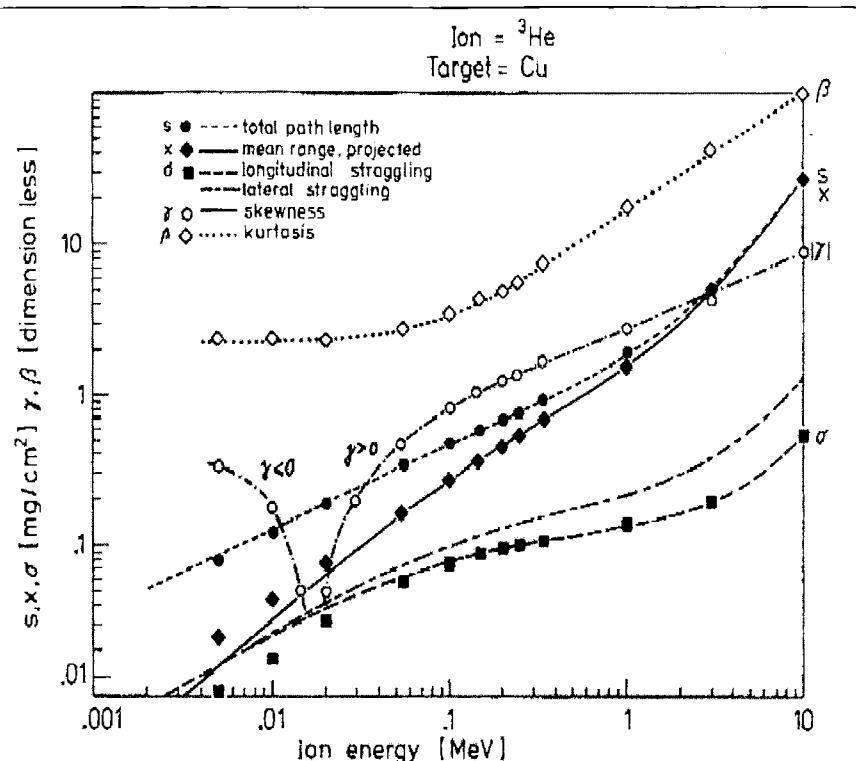


Figure 7-6 - ${}^3\text{He}$ ions implanted into copper

For the case of ${}^3\text{He}$ ions implanted into copper, two theoretical approaches are compared: an analytic transport calculation (solid lines), and TRIM, for the range, straggling, and the third and fourth moments of the final ion distribution. Total range (sometimes called total path length), s , shows perfect agreement. Projected range, x , and range straggling, σ_x , show at low energies the expected influence of the target surface which may be neglected in transport theory. The skewness (third moment), γ changes from positive to negative as soon as the distribution is no longer affected by the surface. Both skewness, γ , and kurtosis, β , reach very high values above 1 MeV.

Definition of Range Moments: Straggling, Skewness and Kurtosis

The various moments of the range distribution of ions in a target are discussed in great detail in Chapter 6. Summarizing, assuming the x-axis is perpendicular to the target surface, and the y and z axes are normal to this, then after N atoms

$$\text{Mean Projected Range} \quad = \quad R_p = \sum_i x_i / N \quad = \quad \langle x \rangle$$

$$\begin{aligned}\text{Lateral Projected Range} &\equiv R_y = \sum_i |y_i| / N = <|y|> \\ \text{Radial Range} &\equiv R_r = \sum_i (y_i^2 + z_i^2)^{1/2} / N\end{aligned}$$

Where x_i is the projected range of ion "i" on the x-axis, i.e. the perpendicular distance from the surface to the end of an ion's track; $\sum_i x_i$ = sum of the ion ranges; $\sum_i x_i / N$ = the mean projected range of N ions; and $<x>$ = the mean projected range of all ions. The transverse coordinate "y" is treated the same, except the distance is taken in the XY plane. The mean projected lateral range is zero for a perpendicular beam, so the above lateral range definition averages the absolute values to provide other information on the first moment of the radial spread. The mean radial range assumes cylindrical symmetry of the ion distribution.

"Variance" is the second moment of the range distribution, and below are several identical definitions using various common notations.

$$\text{Straggling} \equiv \sigma = [(\sum_i x_i^2) / N - R_p^2]^{1/2} = <(\Delta x_i)^2>^{1/2} .$$

$$\text{Radial Straggling} \equiv \sigma_r = [\sum_i (y_i^2 + z_i^2) / N - R_r^2]^{1/2} = <(\Delta r_i)^2>^{1/2} .$$

We define lateral straggling in the same way as range straggling above. (Lateral coordinates are sometimes called *Transverse* coordinates.) For a normally incident beam we can assume cylindrical symmetry of the range distribution, so the mean lateral projected range is zero (i.e. $R_y = 0$). Further, we average the Y and Z projected ranges to increase statistical accuracy:

$$\text{Lateral Straggling} \equiv \sigma_y = [\sum_i ((|y_i| + |z_i|)/2)^2 / N]^{1/2} .$$

$$\text{Skewness} \equiv \gamma = <\Delta x^3> / <\Delta x^2>^{3/2} ,$$

$$= \sum_i (x_i - R_p)^3 / (N\sigma^3) ,$$

$$= \sum_i [x_i^3 - 3R_p x_i^2 + 3R_p^2 x_i - R_p^3] / (N\sigma^3) .$$

$$\text{Kurtosis} \equiv \beta = <\Delta x^4> / <\Delta x^2>^2 ,$$

$$= \sum_i (x_i - R_p)^4 / (N\sigma^4) ,$$

$$= \sum_i [x_i^4 - 4R_p x_i^3 + 6R_p^2 x_i^2 - 4R_p^3 x_i + R_p^4] / (N\sigma^4) .$$

TRIM uses the last variations shown above for the calculation of skewness and kurtosis.

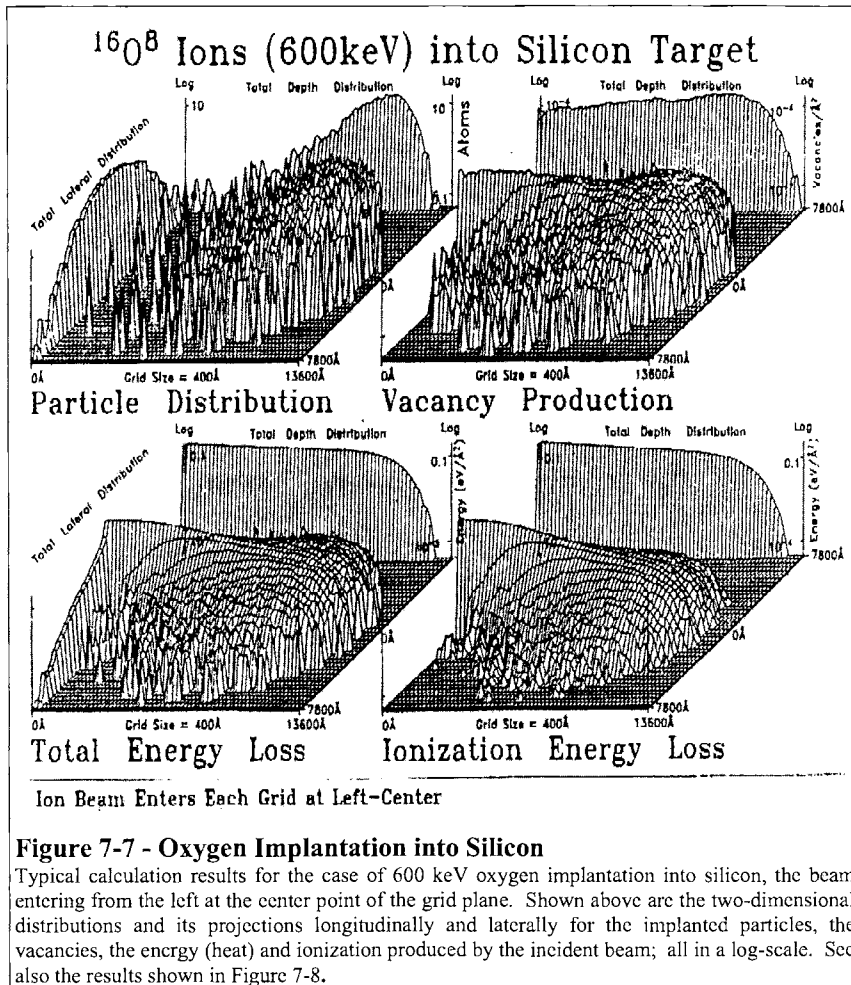
Significant deviations from a Gaussian are seen to occur at high energies, where both the (negative) skewness and the peakedness (kurtosis) reach very large values. The physical reasons for this behavior will be discussed in the next section on high energy implants.

In Figure 7-7 and Figure 7-8, we show the case of oxygen implantation into silicon, which is a method for introducing insulating layers into semiconductor structures.

Figure 7-7 shows the implantation profiles longitudinally, laterally and in a two-dimensional projection. The longitudinal distribution has the typical negative skewness, while the lateral profile looks like a parabola in the logarithmic plot, which corresponds to a Gaussian curve. The two-dimensional distribution depicts the typical sharp cut-off at the deep end, which has an envelope shaped like an umbrella (the beam enters from the left into the center of the ground plane). The other parts of

Figure 7-7 show the damage introduced by the beam ("vacancies"), the heat production ("total energy loss"), and the amount of ionization which in many insulating and semiconducting materials also produces defects. It should be noticed that both lateral and longitudinal

distributions of these three quantities are quite different from the (oxygen) particle distribution, and far from being Gaussian. They appear rather triangular laterally (e.g. see the projection on the left hand side of "total energy loss"), and nearly constant over most of the depth between the surface and the (projected) particle range. Figure 7-8 shows the same quantities as before, but in a linear scale, and with the special feature of a homogeneous beam entering into a partly masked target. In these linear plots, one can clearly observe that mainly the oxygen implant and the vacancies spill over into the shadowed region. The total energy deposition and ionization remain more sharply defined by the mask.



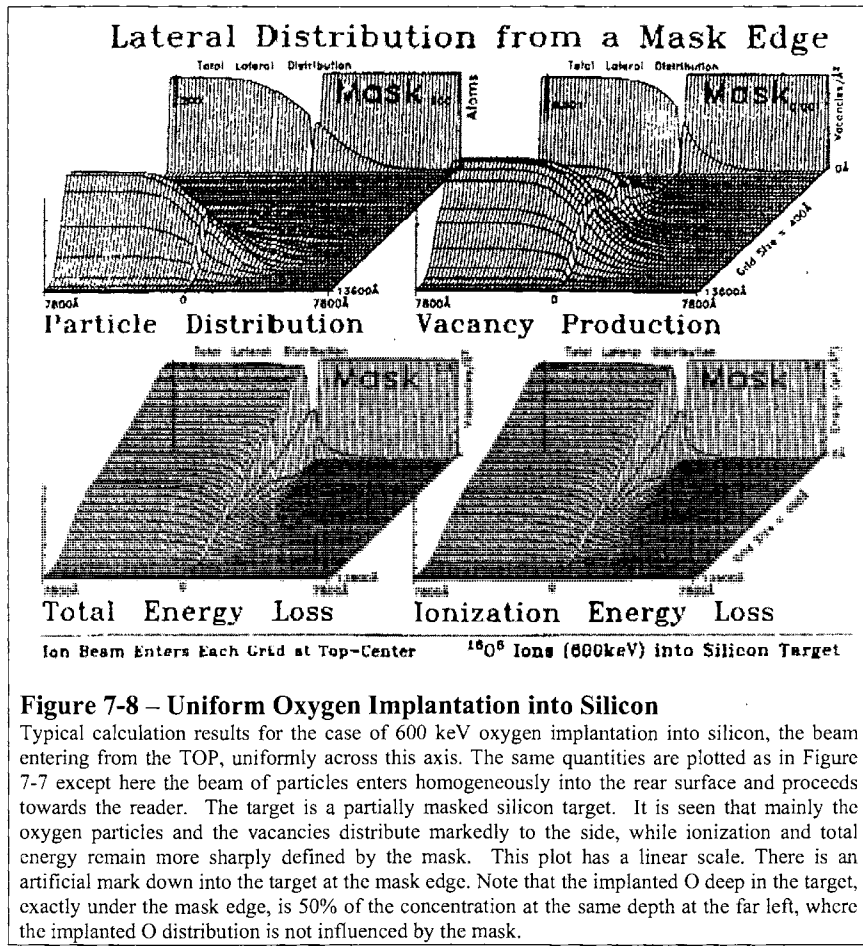
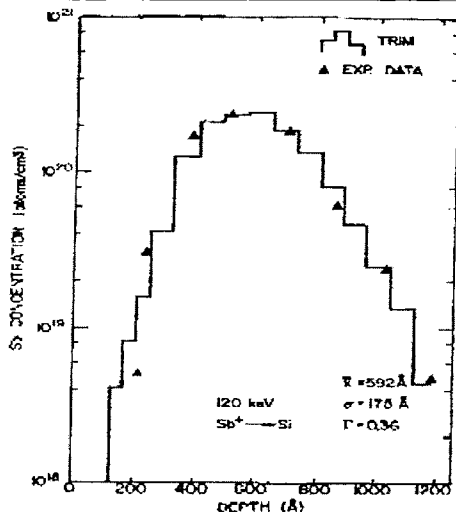


Figure 7-8 – Uniform Oxygen Implantation into Silicon

Typical calculation results for the case of 600 keV oxygen implantation into silicon, the beam entering from the TOP, uniformly across this axis. The same quantities are plotted as in Figure 7-7 except here the beam of particles enters homogeneously into the rear surface and proceeds towards the reader. The target is a partially masked silicon target. It is seen that mainly the oxygen particles and the vacancies distribute markedly to the side, while ionization and total energy remain more sharply defined by the mask. This plot has a linear scale. There is an artificial mark down into the target at the mask edge. Note that the implanted O deep in the target, exactly under the mask edge, is 50% of the concentration at the same depth at the far left, where the implanted O distribution is not influenced by the mask.

Examples of heavy ion depth profiles are shown in Figure 7-9 for the cases of Sb and Bi implants into silicon (both 120 keV) [68i, 82p]. The experimental data points are depicted in the figure together with the TRIM histogram. These profiles are skewed towards the right side, $\gamma > 0$, in contrast to light ion implants. The physical reason lies in the fact that the heavy ions are mainly slowed down by collisional encounters (nuclear energy loss), and some of the ions have a good chance for traveling nearly straight ahead without severe encounters, thus causing the tail at the deep side of the profile.



$^{209}\text{Bi}^{83}$ Ions (120keV) into Silicon Target

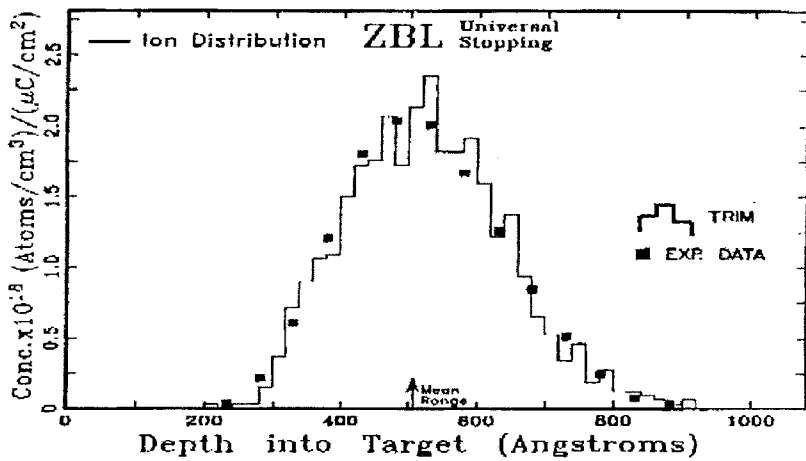


Figure 7-9 - Heavy Ion Implantation Profiles into Silicon

Depth profiles of 120 keV heavy ion implants in silicon. The plots show with histograms the TRIM predictions. The upper figure shows with triangles the high resolution experimental data on Sb implantation distributions, see Ref. (68). The lower figure shows with squares the high resolution experimental data of a Bi implantation, see Ref. (82p). These profiles are somewhat skewed towards the right side, $\gamma > 0$, in contrast to light ion implants.

ELECTRONIC STRAGGLING IN TRIM

Range distributions of high energy particles, e.g. 10-100 MeV light ions, can exhibit strange features, such as very large third and fourth moments indicating drastic deviations from a Gaussian distribution. The example shown in Figure 7-10 indicates the typical large (negative) skewness and high peakedness (kurtosis), which may not be reliably predicted by analytical theories. In order to treat such cases in a Monte-Carlo program, a number of special effects have to be considered: (1) relativistic effects will influence the stopping powers, (2) the electronic straggling becomes of high relative importance, and (3) nuclear interactions may occur. Each effect shall be discussed individually in the following paragraphs.

The most important stopping mechanism at these energies is the electronic energy loss. We have to use relativistic corrections, which change the Bethe-Bloch formula to:

$$\text{Eq. 7-46: } S_e = \frac{4 \pi Z_2 N Z_1^2 e^4}{m_0 c^2} \beta \cdot \ln \left[\frac{2 m_0 c^2}{Z_2 I_0 (\beta - 1)} \right]$$

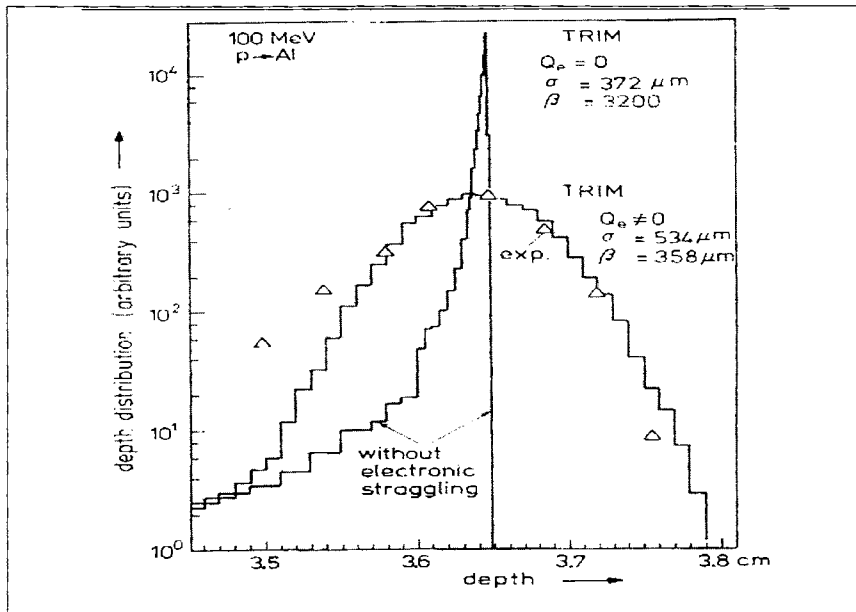


Figure 7-10 - Very High Energy Implant into Aluminum

100 MeV proton projected range in aluminum. The extremely skew and peaked function was obtained with TRIM using no electronic straggling. The peakedness and skewness were reduced (skewness = -10, peakedness = 358) when electronic straggling was included in TRIM. The experimental data [65d] shown as triangles show agreement with the latter TRIM curve for the right half of the plot, while TRIM is in error in the left side (see text for explanation).

where m_0 is the electron rest mass, c is the speed of light, and $\beta \equiv c^2 / V^2$, V is the speed of the ion. Eq. 7-46 is not for ultra-relativistic ions, but suffices for energies up to several thousand MeV/amu. It reproduces the well known minimum in electronic stopping at about 2 GeV/amu.

Another important effect is due to electronic straggling, which somewhat reduces the sharp peakedness (kurtosis) of the depth profile that results from the nearly straightforward motion of the high energy ions, shown in Figure 7-10. The electronic straggling, Q_e , increases roughly proportional to E at low energies (Bonderup and Hvidplund [71c]) to finally reach a high constant level (the Bohr straggling, [48a]). In the TRIM program, the electronic straggling for high energies is accordingly described by the minimum of two expressions :

$$\text{Eq. 7-47: } Q_e = \text{Minimum of} \left\{ \frac{4\pi Z_1^2 e^4 Z_2 N(\beta - .5) / [\beta - 1]}{(Z_1 + Z_2)^{8/3} E(\text{keV}) N / [3.2 M_1]} \right.$$

where the Bohr straggling has been corrected for relativistic effects.

The calculation of range distributions for high energy ions creates little problem with computer time, since most of the particles move nearly straightforward, with very little chance of large angle scattering. The probability of being deflected by more than 5° is rather small during most of the slowing down process (say, down to about 1 MeV/amu) so that the free flight path (FFP) concept comes to its full advantage. The computer time increases only by small fractions when increasing the energy by large factors (above 1 MeV/amu). Also, time consuming calculations of low energy ions, which are below the displacement energy threshold for damage, can be avoided by using a cut-off energy, E_f , chosen in proper accordance with the width of the depth bins of the output distribution. In conclusion, the high energy version of TRIM is particularly fast, while still maintaining all relevant features.

Despite the possibility of nuclear encounters, the most of ions, which move on in a forward direction, are slowed down by "normal" processes, i.e. electronic energy loss and (small angle) Rutherford scattering. Only those particles which undergo large angle, even backward scattering, may "feel" nuclear forces, as their distance of closest approach may become less than 10^{-12} cm. In this case, not only the scattering cross section will deviate drastically from Rutherford scattering, but also the particle may disappear completely, being absorbed into the target nucleus and causing a nuclear reaction.

TRIM does not incorporate individual nuclear properties and possible nuclear reactions for high energy ions. TRIM can only predict the range distribution consisting of particles which have slowed down in a "normal" way. The peak distribution and the deep tail may be accurately calculated. However, the tail extending from the peak towards the surface, and the backscattered fraction of particles are normally effected by nuclear processes (elastic and inelastic scattering), and this (small) ion fraction is therefore not predicted reliably at very high ion energies, $>> 1 \text{ MeV/u}$.

Figure 7-10 and Figure 7-11 show the special features of high energy range profiles, such as the significant skewness and peakedness, which make the profiles differ very much from a Gaussian shape. The electronic straggling is seen to effect the distribution at 2.5 MeV/u (10 MeV He⁺, Figure 7-11), while at 100 MeV/u it is of utmost importance for understanding the range straggling (100 MeV protons, Figure 7-10) and errors show in the TRIM distribution towards the surface because of nuclear reactions which were not included in the calculation.

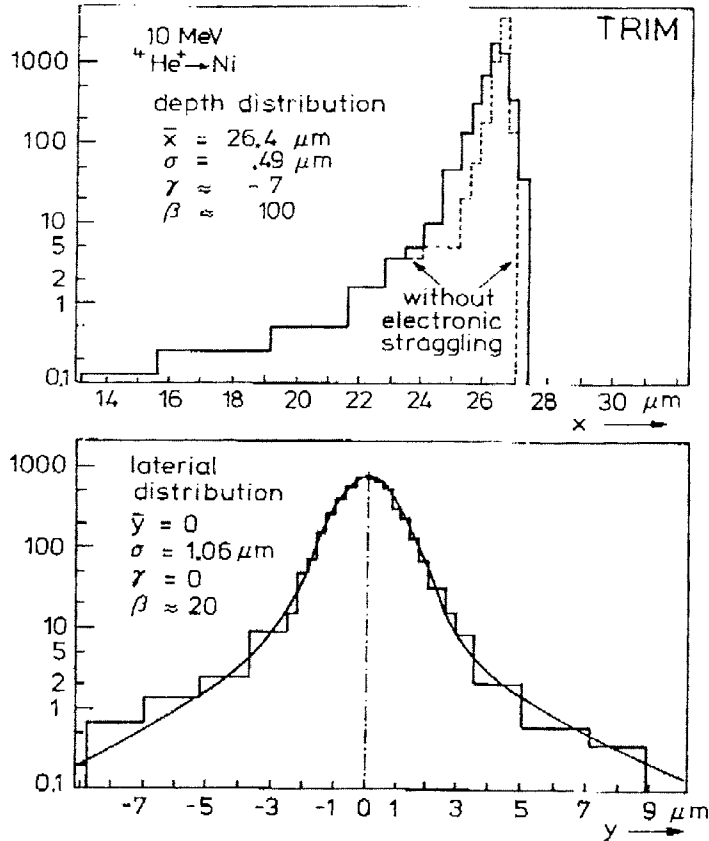


Figure 7-11 - High Energy Implant into Aluminum

The 10 MeV He depth profile in aluminum shows in the upper curve the effects of electronic straggling on the calculation of the ion range distribution. The lateral profile of this distribution is shown in the lower figure. It exhibits a Gaussian central peak for those particles which did not scatter by large angles at high energies, while the flat shoulders are caused by the small fraction of ions which suffered one or two severe collisions with large deflection angles.

THE CALCULATION OF TARGET DAMAGE

The calculation of cascades, target displacements, replacement collisions, etc. uses terminology that has been in use for a century, and the definitions of the terms are quite precise.

Assume an incident atom has atomic number Z_1 , and energy E . It has a collision within the target with an atom of atomic number Z_2 . After the collision, the incident ion has energy E_1 and the struck atom has energy E_2 . Previously specified for the target are energies E_d , the displacement

energy, E_b , the binding energy of a lattice atom to its site, and E_f , the final energy of a moving atom, below which it is considered to be stopped.

A **displacement** occurs if $E_2 > E_d$ (the hit atom is given enough energy to leave the site). A **vacancy** occurs if both $E_1 > E_d$ and $E_2 > E_d$ (both atoms have enough energy to leave the site). Both atoms then become moving atoms of the cascade. The energy, E_2 , of atom Z_2 is reduced by E_b before it has another collision. If $E_2 < E_d$, then the struck atom does not have enough energy to leave the site and it will vibrate back to its original site releasing E_2 as **phonons**.

If $E_1 < E_d$ and $E_2 > E_d$ and $Z_1 = Z_2$, then the incoming atom will remain at the site and the collision is called a **replacement collision** with E_1 released as **phonons**. The atom in the lattice site remains the same atom by exchange. This type of collision is common in single element targets with large recoil cascades. If $E_1 < E_d$ and $E_2 > E_d$ and $Z_1 \neq Z_2$, then Z_1 becomes a stopped **interstitial** atom.

Finally, if $E_1 < E_d$ and $E_2 < E_d$, then Z_1 becomes an **interstitial** and $E_1 + E_2$ is released as **phonons**. If your target has several different elements in it, and each has a different displacement energy, then E_d will change for each atom of the cascade hitting different target atoms.

Briefly, the basic relations of the above are:

$$\text{Eq. 7-48: Displacements} = \text{Vacancies} + \text{Replacement Collisions}$$

and:

$$\text{Eq. 7-49: Vacancies} = \text{Interstitials} + (\text{Atoms which leave target volume})$$

For those using the TRIM "quick" calculation of target damage, TRIM uses the Kinchin-Pease analytic solution for target damage as modified by two later authors. A brief description of this method is given below.

The Kinchin-Pease Model for Vacancy Production

In the TRIM program, the energy transferred to a target atom is analyzed further to yield such results as (i) ionization by recoiling atoms in a cascade, (ii) damage energy and number of vacancies produced in a collision cascade, and (iii) damage energy and number of sub-threshold collisions in the cascade which transfer energies less than E_d , where knock-on atoms cannot permanently escape their lattice site and their energy ends up in lattice vibrations (phonons).

Most users of TRIM are interested in target damage, but do not want to spend the hours required to fully calculate all cascades. Analytic approximations have been developed which allow accurate evaluation of target damage (they usually achieve a result within a factor of two of the full cascade evaluation). The main problem with these kinds of solutions is that they do not determine the spatial extension of the damage after the first recoil is initiated (called the *prime recoil*), since the full cascade progression is not calculated. Hence all the calculated damage is dumped into the point of the initial collision, and can lead to a poor representation of the distribution of the target damage.

TRIM uses the theory originally proposed by Kinchin and Pease (55c) and Lindhard et al. (63g) as extended by Robinson et al. (70j). From this theory the *defect producing energy*, E_V , is obtained from the *transferred energy*, T , of the recoil by taking into account electronic losses:

$$\text{Eq. 7-50:} \quad E_V = \frac{T}{1 + k_d g(\varepsilon_d)}$$

where the electronic losses are governed by

$$\text{Eq. 7-51:} \quad k_d = 0.1334 Z_2^{2/3} M_2^{-1/2}$$

and

$$\text{Eq. 7-52:} \quad g(\varepsilon_d) = \varepsilon_d + 0.40244 \varepsilon_d^{3/4} + 34008 \varepsilon_d^{1/6}$$

where

$$\text{Eq. 7-53:} \quad \varepsilon_d = 0.01014 Z_2^{7/3} T.$$

From the transferred energy, E_V , the number of displacements is calculated by the well known "modified Kinchin-Pease" model [69a, 74g]

$$\text{Eq. 7-54:} \quad v = 1, \text{if: } E_D < E < 2.5 E_D$$

and

$$\text{Eq. 7-55:} \quad v = \frac{0.8 E_v}{2 E_D}, \text{if: } E_v > 2.5 E_D$$

Thus the number of vacancies per depth interval are calculated and provided as standard output of the TRIM program.

EVALUATION OF SPUTTERING IN TRIM

Sputtering is the removal of near-surface atoms from the target. When a cascade gives a target atom an energy greater than the "surface binding energy" of that target, the atom may be sputtered. To actually be sputtered, the atom's energy normal to the surface must still be above the surface binding energy when it crosses the plane of the surface. The sputtering of a surface is described by a "Sputtering Yield", which is defined as the mean number of sputtered target atoms per incident ion. If the target is made of several elements, there is a separate sputtering yield for each element. Discussions of the physical concepts of sputtering have been presented by Kinchin and Pease (55c), Sigmund (69a) and Robinson (74c and 74g).

The sputtering yield is very sensitive to the Surface Binding Energy, E_b , which you input to the calculation. Be aware that for real surfaces, this changes under bombardment due to surface roughness, and also changes due to surface stoichiometry for compounds. Further, sputtering involves mostly the upper monolayer of the target. For targets such as Ni, or

heavier, the electronic energy loss of a target atom moving through the last monolayer is of the order of the surface binding energy, so even monolayer roughness will change the sputtering yield.

The surface binding energy of an atom to a surface is known only for a few materials, but it is common to use the heat of sublimation as an estimate. Typical values are: Ni (4.46 eV), Cu (3.52 eV), Pd (3.91 eV), Ag (2.97 eV), Pt (5.86 eV) and Au (3.80 eV). Values will be suggested when you set up the TRIM calculation.

To calculate sputtering effects, the incident ions and the recoil atoms are followed throughout their slowing-down process in three-dimensional motion until their energy falls below a predetermined energy; usually about 2 eV.

TRIM can follow the knock-on atoms created by the incident ion. The primary knock-on atom gets the label $i = 1$, the secondary knock-on is $i = 2$, etc. TRIM follows the newly created knock-on atom, say with label $i + 1$, and stores the information of the last particle with label i ($i = 0$ would be the ion itself). If that atom leaves the surface as a sputtered particle, TRIM returns to the previous recoil atom with label i . If, however, the recoil is followed through further collisions and a new recoil is created, now with label $i + 2$, this will be treated first. The complete data set of a recoil atom contains the following information: atomic species, created by an inward or outward moving ion, primary knock-on atom (PKA) or secondary knock-on (SKA), depth of origin, present energy, present position, and present direction of motion (the last two in a 3-dimensional space). If a recoil atom has moved into a position $x < 0$, i.e. outside of the surface, it is considered as a candidate for sputtering. After reducing its energy component normal to the surface by the action of the planar surface potential, i.e. subtracting the surface binding energy E_s , it will either be found to be reflected back onto the surface (add-on atoms trapped but unable to penetrate due to the repulsive forces of the target atoms), or it will leave the surface with the reduced energy and refracted emission angle as a sputtered particle, which is registered with its relevant data (species, PKA or SKA, resulting from incident or reflected ion, its energy and angles, depth of origin, etc.) for the final output of the TRIM plots and data files.

Some examples of applying TRIM are given in the following figures. Figure 7-12 shows sputtering yields for He^+ impinging on nickel. In this case of an ion lighter than the target atoms, one can most easily recognize the various mechanisms. For example, near the low energy threshold, sputtering is only possible if the He ion is backscattered from Ni atoms and then - on its way back through the surface - knocks out a Ni surface atom (curve $Y_{\text{OUT,SKA}}$ or $Y_{\text{OUT,TKA}}$). On the other hand, at high energies, most sputtering is seen to result from cascades created by the incident ion (curve $Y_{\text{IN,SKA}}$). Figure 7-13 gives a comparison of TRIM results with experimental data on the sputtering of nickel. It should be noticed that the TRIM calculation yields the realistic decrease of sputtering yield towards lower energies (the *threshold effect*).

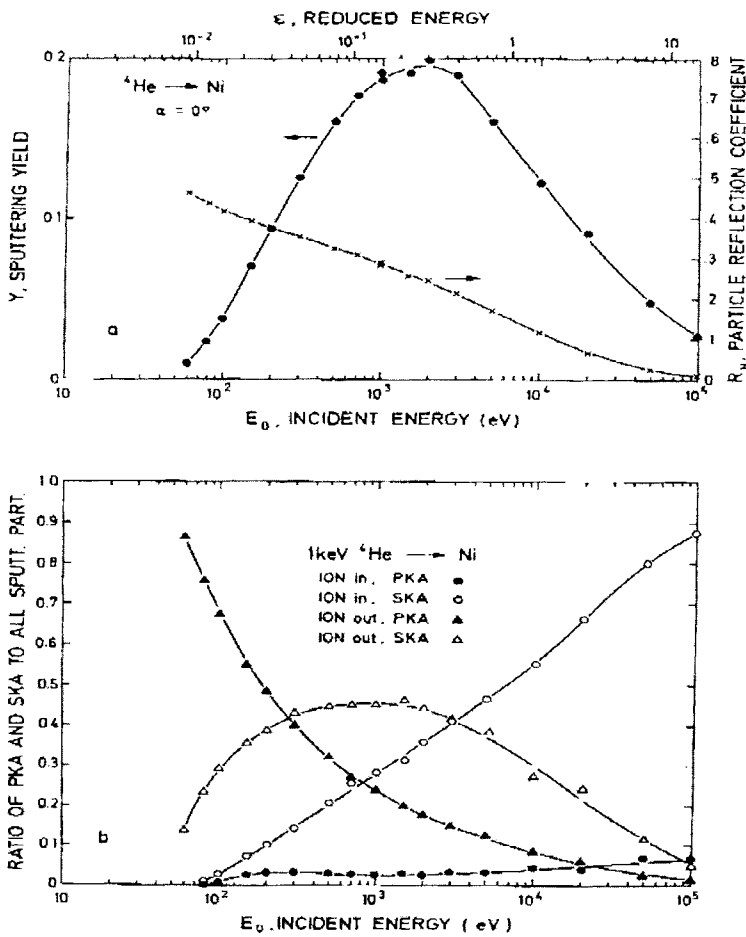


Figure 7-12 - Sputtering of Nickel by He Ions

Sputtering yield and its various components as a function of energy. At low energies, particularly near the threshold, most sputtering is seen to result from reflected He ions "ION out, PKA" and "ION out, SKA" denote sputtering yields due to reflected ions, primary or secondary knock-on atoms, respectively). At higher energies the incident ions cause large collision cascades, which emit mainly secondary knock-on atoms "ION in, PKA" and "ION in, SKA" denote fractions sputtered by incident ions, primary or secondary knock-on atoms, respectively).

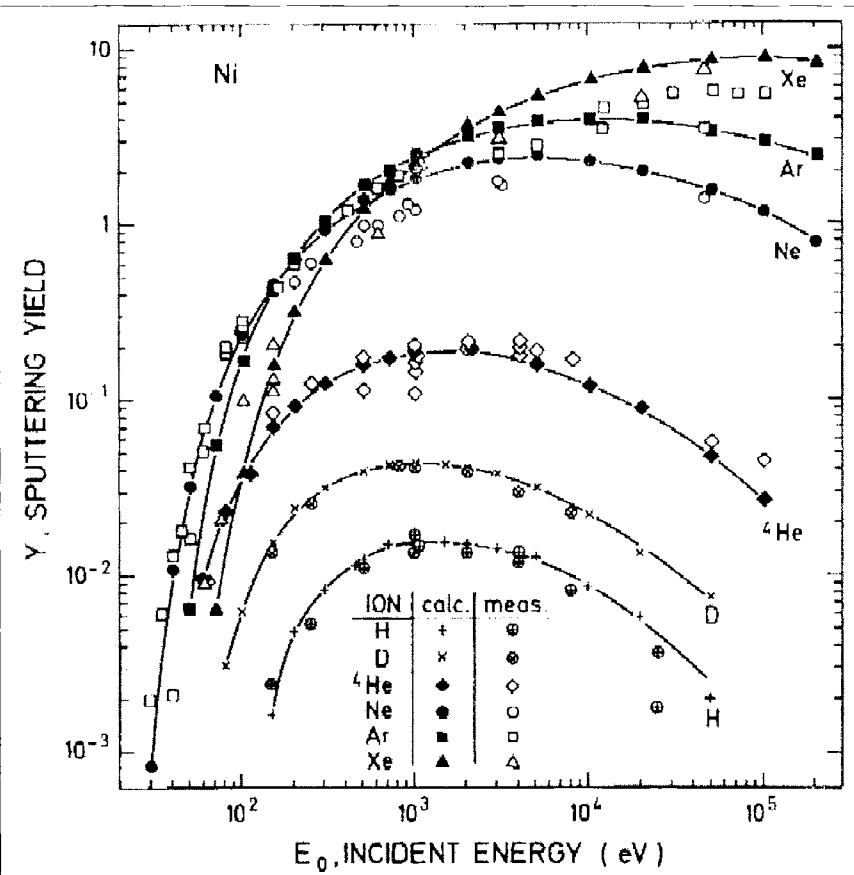


Figure 7-13 - Sputtering: Experiments vs. TRIM Yields

This plot compares TRIM calculations with experimental data for the sputter yield of various ions onto a nickel substrate. The agreement over the broad range of values is good.

Another comparison is shown in Figure 7-14: the angular dependence of sputtering yields at various ion energies as described in the figure caption. This would be a particularly difficult case for analytic transport theories, as the ion motion in the near-surface region is strongly effected by the presence of the free surface. One of the obvious features is the sharp peak in sputtering yield for high energy ions at glancing incidence, which is a result of the nearly straight ion trajectories proceeding close to the surface. On the other hand, at low energies the sputtering peak vanishes as the ions undergo large angle scattering which removes them rapidly from the surface region. In particular, backscattering increases as soon as the angle of incidence is varied from normal.

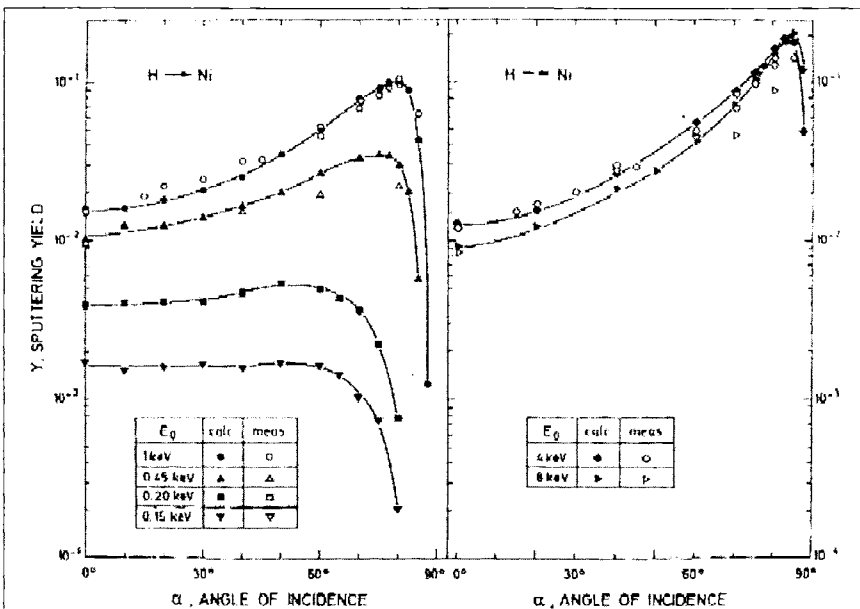


Figure 7-14 - Sputtering: Experiments vs. TRIM Yields

Above are shown sputtering results using TRIM calculations. The example shows the sputtering yield as a function of the incident angle for H ions onto a Nickel target. It is seen from these curves that for low energies the sputtering yield is nearly constant up to angles where backscattering causes significant losses of ions. This is due to large scattering angles and a rather wide-spread, diffuse motion of ions. In contrast to this, at high energies, the ion beam maintains its original direction along a nearly straight flight path, thus transferring only little energy near the surface, when normally incident, but transferring much energy close to the surface, when traveling at grazing incident angles nearly parallel to the surface. This explains the low yield at $\alpha \approx 0^\circ$, and the sharp peak around $\alpha \approx 80^\circ$. At more glancing angles, $\alpha \rightarrow 90^\circ$, the ions become mostly backscattered, with the sputtering yield dropping accordingly.

Summary of Radiation Damage Calculations

In the above section, we described the vacancy production by a modified Kinchin-Pease model applied to every recoil atom which received a transferred energy $T > E_d$, where E_d denotes the displacement energy of a lattice atom. The number of vacancies obtained by this procedure was then stored in the depth channel, where the primary knock-on atom (PKA) was created. In order to study the formation of vacancies, interstitials and replacement collisions in more detail, one has actually to follow the individual recoils through a number of collisions and generations until their energy has dropped below E_d . This way, the spatial distribution of the defects is obtained, showing often a transport of recoils (and energy) over far distances. Particularly for ion masses larger than or equal to the target atom mass, $M_1 > M_2$, the recoils may move further than the incident ion. The transport of energy could not be obtained as precisely with the semi-analytical

procedures of transport theory. one of the main reasons is that the Lindhard-Nielsen-Scharff cross-section approximation, $\delta \sigma (t^{1/2})$, breaks down at these low energies.

In TRIM, the recoils are followed through many generations (as in the sputtering case, see last section) until their energy has dropped below the displacement energy E_d . Any knock-on atom receiving more energy than E_d is considered to leave its lattice position and to create a vacancy. Thereafter, a second check is performed in order to determine whether the incident particle (the ion itself or a previous recoil) is left with enough energy to move on; if its energy - after the collision - is below E_d , then it is considered to remain within the recombination volume and finally combine with the vacancy, this way annihilating the previously created vacancy and registering now as a "replacement" collision. By this process a large fraction of the vacancies may disappear (at times up to 20%) mainly by target-target collisions at low energies. The ion-target collisions account only for a very small fraction (usually less than a percent) of all replacement collisions. If a moving particle (ion or recoil) is not ending up in a replacement collision before being slowed down to an energy less than E_d , then it will be recorded as an "interstitial" atom.

LAYERED TARGET STRUCTURES, SURFACES

In a Monte-Carlo simulation of ion transport no difficulties arise when taking into account any free surfaces or interfaces - in contrast to analytic treatments of most solutions to transport equations. Therefore, TRIM is set up to incorporate various layers of different materials, e.g. an SiO_2 or WSi_2 layer on top of silicon bulk material, as well as front and rear surfaces. The way to handle this is straightforward: after the ion (or recoil) has moved its mean free flight path along its new direction into the *position*, x , y , z , two random numbers are called to determine the *impact parameter*, p , and the *azimuthal angle*, ϕ . The position of the target atom is calculated and checked as to whether it is located inside one of the layers or in front or behind the target. In the latter case, no target atom is encountered and the ion (or recoil) moves on with no deflection or nuclear energy loss, becoming a candidate for a reflected or transmitted ion (or a sputtered particle, respectively). Otherwise, if a new target layer is encountered, a target atom of this layer is selected as the next collision partner.

SELECTION OF TARGET ATOMS IN COMPOUNDS

The selection of the target atoms is performed in the TRIM code by random numbers, assuming the probabilities of encounters being proportional to their stoichiometric abundance, e.g. oxygen is encountered twice as frequent as silicon in an SiO_2 target. This is by no means trivial, and actually it was a matter of some concern whether lighter atoms should have a smaller cross section than heavier ones, thus favoring collisions with the heavier components beyond their stoichiometric fraction. TRIM lets the potentials take care of the situation without imposing any arbitrary cut-offs for lighter atoms as compared to heavier ones. This means that TRIM allows interactions at equally large impact parameters for all target atoms, but expect, for example, at a given large impact parameter that a light target atom with a lower interaction potential will cause only minimal deflection and lower energy transfer as compared to a heavier component. This concept is supported by the fact that the atomic radii and also the range of interaction as calculated from overlapping solid state HFS atoms are by no means smaller for light atoms than for heavy ones (see, for example, discussions in Chapter 2 of this book). The difference between

light and heavy target atoms turns out to lie in the magnitude of the potential, but not in the range of interaction.

An example of particle and damage distributions in a layered and multi-component structure is shown in Figure 7-15. Here, 200 keV boron ions are followed through a 2000 Å layer of tungsten on top of SiO_2 . The number of stopped ions, as well as the vacancies produced, are seen to be much denser in the heavy layer of W than in the light and low density SiO_2 . Particularly in the tungsten layer, large scattering angles occur frequently and the lateral resolution behind a mask edge would be very poor (lower part of Figure 7-15).

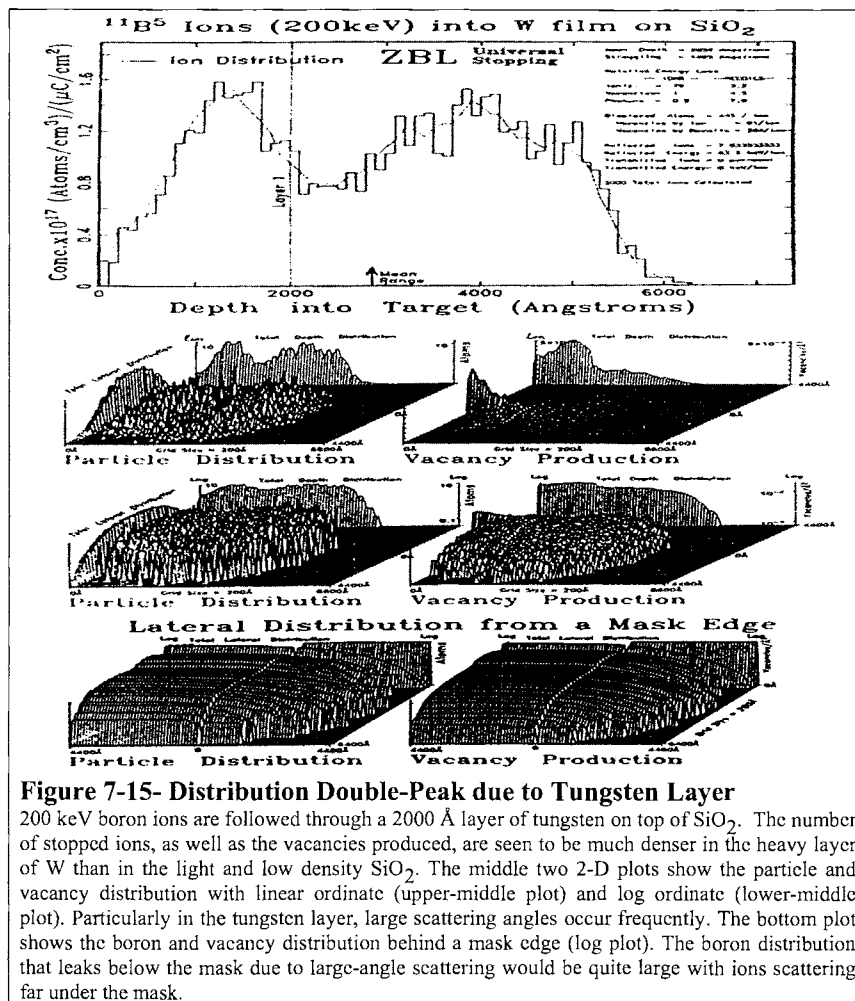


Figure 7-15- Distribution Double-Peak due to Tungsten Layer

200 keV boron ions are followed through a 2000 Å layer of tungsten on top of SiO_2 . The number of stopped ions, as well as the vacancies produced, are seen to be much denser in the heavy layer of W than in the light and low density SiO_2 . The middle two 2-D plots show the particle and vacancy distribution with linear ordinate (upper-middle plot) and log ordinate (lower-middle plot). Particularly in the tungsten layer, large scattering angles occur frequently. The bottom plot shows the boron and vacancy distribution behind a mask edge (log plot). The boron distribution that leaks below the mask due to large-angle scattering would be quite large with ions scattering far under the mask.

RANDOM NUMBER SEED —

TRIM will always produce identical calculations (with the same input setup) unless this number is changed. You may input any integer number from 0 - 999999999. The default is set at **716381** which is an almost mystical number in random number theory, and is better than any other number that you will come up with (see Fishman & Moore, S.I.A.M.- J.S.C., vol. 7, 24 (1986)). However, if you want to have three similar but different calculations, then changing the seed from 1 to 2 to 3 will do nicely. The actual random number generator in TRIM is adapted from: P. L'Ecuyer, C.A.C.M., vol. 31, 742-749, 774-776 (1988), "An Efficient and Portable Combined Random Number Generator". At the bottom-right of the TRIM calculation window is a counter of the number of random-numbers used. For calculations with large recoils, this number grows rapidly and may exceed 2^{31} for less than 1000 ions.

CHAPTER 7 - CITATIONS

- 48a N. Bohr, Mat. Fys. Medd. Dan. Vid. Selsk., **18**, No. 8 (1948).
55c Kinchin and R. S. Pease, Rep. Prog. Phys., **18**, 1 (1955).
57a O. B. Firsov, Zh. Eksp. Teor. Fiz., **32**, 1464 (1957).
57b O. B. Firsov, Zh. Eksp. Teor. Fiz., **33**, 696 (1957).
58a O. B. Firsov, Zh. Eksp. Teor. Fiz., **34**, 447 (1958).
58b O. B. Firsov, JETP., **7**, 308 (1958).
59a O. B. Firsov, Zh. Eksp. Teor. Fiz., (Transl.: Sov. Phys. JETP, **9**, 1076 (1959)).
63e M. T. Robinson and O. S. Oen, Appl. Phys. Lett., **2**, 30 (1963).
63g J. Lindhard, V. Nicisen, M. Scharff and P. V. Thomsen, Dansk Videnskab. Mat.-Fys. Medd., **33**, no. 10 (1963).
65d P. M. Porter and R. B. Moore, Can. J. Phys., **43**, 1904 (1965).
68i B. L. Crowder, J. Electrochem. Soc., **46**, 455 (1968).
69a P. Sigmund, Rad. Eff., **1**, 15 (1969).
70j M. T. Robinson, "Nuclear Fission Reactors", British Nuclear Energy Society, London, 364 (1970).
71b W. D. Wilson and C. L. Bisson, Phys. Rev., **B3**, 3984 (1971).
71c E. Bonderup and P. Hvelplund, Phys. Rev., **A4**, 562 (1971).
74c M. T. Robinson and I. M. Torrens, Phys. Rev., **B9**, 5008 (1974).
74g M. J. Norgett, M. T. Robinson and I. M. Torrens, Nucl. Eng. Design, **33**, 50 (1974).
72i M. D. Brown and C. D. Moak, Phys. Rev., **B6**, 90 (1972).
72j K. Guttner, H. Ewald and H. Schmidt, Rad. Eff., **13**, 111 (1972).
74c M. T. Robinson and I. M. Torrens, Phys. Rev., **B9**, 5008 (1974).
74g M. J. Norgett, M. T. Robinson and I. M. Torrens, Nucl. Eng. Design, **33**, 50 (1974).
76n O. S. Oen and M. T. Robinson, Nucl. Inst. Meth., **132**, 647 (1976).
81b U. Littmark and J. F. Ziegler, Phys. Rev., **23A**, 64 (1981).
82b J. P. Biersack and J. F. Ziegler, "Ion Implantation Techniques," Springer-Verlag, p. 122 (1982).
82m J. P. Biersack and M. Stadele, Rad. Eff., **64**, 51 (1982).
82n D. Fink, J. P. Biersack, K. Tjan and V. K. Cheng, Nucl. Inst. and Meth., **194**, 105 (1982).
82o J. F. Janni, Atomic Data and Nucl. Data Tables, **27**, No. 2-5, 1 (1982).
82p D. J. O'Connor, Nucl. Inst. and Meth., **196**, 493 (1982).

- 82q J. P. Biersack, Z. f. Physik, **A-95**, 305 (1982).
- 82r P. Mertens and Th. Krist, Nucl. Inst. and Meth., **194**, 57 (1982).
- 84a J. F. Ziegler, J. P. Biersack, U. Littmark, "The Stopping and Range of Ions in Solids," vol. **1** of series "Stopping and Ranges of Ions in Matter," Pergamon Press, New York (1984).
- 84b J. P. Biersack and W. Eckstein, Appl. Phys., **A34**, 73 (1984).
- 86g D. J. O'Connor and J. P. Biersack, Nucl. Inst. and Meth., **B15**, 14 (1986).
- 88i W. Eckstein and M. Hou, Nucl. Inst. and Meth., **B31**, 386 (1988).
- 90b A. Arnau, M. Penalba, P. M. Echenique, F. Flores and R. H. Ritchie, Phys. Rev. Lett., **65**, 1024 (1990).
- 90j A. H. Sorensen, Nucl. Inst. and Meth., **B48**, 10 (1990).
- 91g W. Eckstein, "Computer Simulation of Ion-Solid Interactions", Springer-Verlag, Berlin (1991).

8 - TRIM – SETUP AND INPUT *

TRANSPORT OF IONS IN MATTER

TRIM is Monte Carlo computer program that calculates the interactions of energetic ions with amorphous targets. The specific science and mathematics behind the program were summarized in Chapter 7. This chapter reviews the use of TRIM to evaluate many different kinds of calculations. Most of this chapter may also be found in the Help menus included in the TRIM program. See also Chapter 9, TRIM Output Files, for an explanation of the various TRIM output plots and files.

8 - TRIM - INPUT/SETUP	8-1
Introduction	8-2
TRIM Setup Window.....	8-2
Types of TRIM Calculation (Menu in upper-right corner)	8-3
• Ion Distribution and Quick Calculation of Damage	8-3
• Detailed Calculation with Full Damage Cascades.....	8-3
• Monolayer Collision Steps	8-4
• Calculation of Surface Sputtering.....	8-4
• Neutron / Electron / Photon Cascades.....	8-4
• Various Ion Energy / Angle / Positions.....	8-4
• Special Multi-Layer Biological Targets.....	8-4
Ion Name, Mass, Energy	8-4
Target Description.....	8-6
Damage Energies of Target Atoms	8-6
Calculation Parameters	8-7
“Viewing Window” for Data and Plotting	8-7
Output Disk Files.....	8-8
Scientific Terms used in TRIM.....	8-9
Physics of Recoil Cascades.....	8-9
Physics of Sputtering.....	8-10
The Stopping of Ions in Compounds	8-11
Stopping Powers for Ions in Gases	8-12
Special Applications of TRIM.....	8-13
Adding Multiple Ions/ Energies/Angles to Same Calculation	8-13
Using file TRIM.DAT to make Complex TRIM Calculations	8-14
Calculating Plasma Ions Hitting a Solid (TRIM.DAT).....	8-14
Simulating a Receding Surface from Sputtering (TRIM.DAT).....	8-14
Simulating Reactor Radiation Damage in Metals (TRIM.DAT)	8-14
Radiation Damage from Neutrons/Electrons/Photons (TRIM.DAT).....	8-16
Special Setup for Multi-Layered Biological Targets.....	8-18
How to Obtain 3-D plots of the Ion’s Electronic Energy Loss	8-19

* Note: This text is from Chapter 8 of the SRIM textbook (2008):

“SRIM – The Stopping and Range of Ions in Matter”

How to use TRIM for Isotopically Enriched Targets	8-20
Straggling in Ion Energy Reducers (Energy Degraders)	8-20
Getting High-Resolution Collision Data from TRIM	8-22
Evaluating the Details of "Ion Mixing" Experiments	8-22
Using TRIM for Mixed Gas/Solid Targets	8-22
Datafile of Complete Ion Trajectories through a Target	8-23
TRIM - Common Questions and Solutions	8-24
What are "Projected Range" and "Radial Range" Distributions ?	8-24
What is Straggling, Skewness and Kurtosis ?	8-25
What Causes Anomalous Peaks and Dips at Layer Edges ?	8-26
Running TRIM in Batch mode: TRIM.IN.....	8-27
Changing TRIM Plot Colors (TRIM.cfg)	8-31
Changing The Maximum Size of Recoil Cascades (TRIM.cfg).....	8-31
Incorporating SRIM into Other Software (SRIM Module)	8-32
Using "SR Module" to generate customized tables of Stopping and Range.	8-33
Calculation Individual Atom-Atom Nuclear Stopping Powers.....	8-34
Citations for Chapter 8.....	8-35

Introduction

TRIM is a group of programs which calculate the stopping and range of ions (10 eV - 2 GeV/amu) into matter using a quantum mechanical treatment of ion-atom collisions (this manual refers to the moving atom as an "*ion*", and all target atoms as "*atoms*"). This calculation is made very efficient by the use of statistical algorithms which allow the ion to make jumps between calculated collisions and then averaging the collision results over the intervening gap. During the collisions, the ion and atom have a screened Coulomb collision, including exchange and correlation interactions between the overlapping electron shells. The ion has long range interactions creating electron excitations and plasmons within the target. These are described by including a description of the target's collective electronic structure and interatomic bond structure when the calculation is setup (tables of nominal values are supplied). The charge state of the ion within the target is described using the concept of effective charge, which includes a velocity dependent charge state and long range screening due to the collective electron sea of the target. A full description of the calculation is found in Chapter 7.

TRIM will accept complex targets made of compound materials with up to eight layers, each of different materials. It will calculate both the final 3D distribution of the ions and also all kinetic phenomena associated with the ion's energy loss: target damage, sputtering, ionization, and phonon production. All target atom cascades in the target can be followed in detail. The programs are made so they can be interrupted at any time, and then resumed later. Plots of the calculation may be saved, and displayed when needed.

TRIM Setup Window

TRIM is contained in the programs called SRIM (The Stopping and Range of Ions in Matter). It can be accessed from its Title page by pressing the button marked TRIM. The easiest way to understand TRIM is to try one of the demonstration calculations. These have been selected to illustrate many of the variations available in TRIM. In the Setup Window, Figure 8-1, see button: **TRIM Demo**.

The TRIM Tutorials are especially recommended to understand how to setup TRIM (see Chapter 11 and also www.SRIM.org). These tutorials will explain in detail each of the required TRIM inputs.

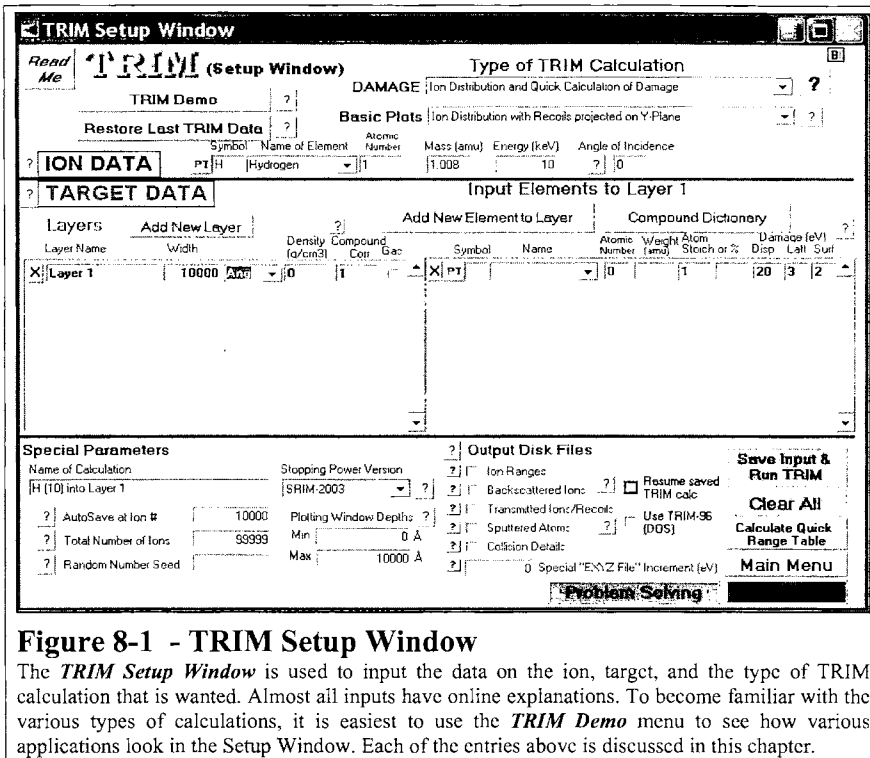


Figure 8-1 - TRIM Setup Window

The **TRIM Setup Window** is used to input the data on the ion, target, and the type of TRIM calculation that is wanted. Almost all inputs have online explanations. To become familiar with the various types of calculations, it is easiest to use the **TRIM Demo** menu to see how various applications look in the Setup Window. Each of the entries above is discussed in this chapter.

Types of TRIM Calculation (Menu in upper-right corner)

- **Ion Distribution and Quick Calculation of Damage** - This option should be used if you don't care about details of target damage or sputtering. The damage calculated with this option will be the quick statistical estimates based on the Kinchin-Pease formalism (see section *Physics of Recoil Cascades* for details about target damage). The following data will be calculated correctly: Final distribution of ions in the target, Ionization energy loss by the ion into the target, Energy transferred to recoil atoms, Backscattered Ions and Transmitted Ions. You will get identical ion range results as when you use the *Full Damage Cascade* option below, since the random number generator for the ions is separate from that used for the recoils. This is useful to compare calculations.
- **Detailed Calculation with Full Damage Cascades** - This option follows every recoiling atom until its energy drops below the lowest displacement energy of any target atom. Hence all collisional damage to the target is analyzed. The one exception is for very rare massive cascades which exceed 20,000 atoms. At this point TRIM runs out of memory, and an error

message is posted indicating that the limit of 20,000 recoiling atoms in a single cascade has been exceeded. The calculation continues after the message is posted. This error can be eliminated using the datafile: ..\Data\TRIM.cfg. See the later section in this chapter on “*Changing Maximum Size of Recoil Cascades (TRIM.cfg)*”

- **Monolayer Collision Steps** - This calculation requires TRIM to make the ion have a collision in each monolayer of the target. This omits any use of the **Free Flight Path**, described in Chapter 7, and every collision will be calculated without any approximations. The results of using this option will ultimately give the same averaged quantities such as mean range, ionization, damage, etc., but the calculation will take far longer to execute. This type of calculation is essential for special applications such as sputtering (below) and to generate data on every possible collision in the file **COLLISION.txt** (see Chapter 9 for more details).
 - **Calculation of Surface Sputtering** - This calculation requires TRIM to make the ion have a collision in each monolayer of the target, which is essential for an accurate calculation of ion sputtering. Special plots are available to aid in understanding the special physics of sputtering. They allow you to analyze the effect of small variations on the Surface Binding Energy on the sputtering yield. This parameter is at the heart of sputtering, and its value is sometimes difficult to estimate. TRIM provides a table of Heat of Sublimation values, which are the normal starting values in estimating the surface binding energy of a target (see file ..\Data\ATOMDATA). There is no significant difference in choosing this item over the previous selection above. (Details are found in the later section in this chapter called “*The Physics of Sputtering*”).
 - **Neutron / Electron / Photon Cascades** - This option is used to calculate only the damage cascades in a target. It uses as input the file **TRIM.DAT** which contains the kinetic information about atoms which start recoil cascades. The file **TRIM.DAT** is generated by some other program which calculates the energy transferred to target atoms by either neutrons, electrons or photons. Then TRIM takes this external information and calculates the damage done to the target from recoil cascades. This is explained in the special TRIM application section “*Radiation Damage from Neutrons / Electrons / Photons*”. If you select this option, you will get a sub-menu which requests which kind of damage calculation you wish to make.
 - **Various Ion Energy / Angle / Positions** - This option allows the calculation of TRIM with ions starting at various energies, or with varying trajectory angles to the target surface, or starting at various depths in the target. There are a wide range of applications which require the ability to vary these ion parameters, and they are discussed in the section “*Ions starting with various Energy / Angle / Position*”. Typical are calculations of ions from a diffuse plasma, or for a target with a receding surface due to rapid sputtering, or reactor radiation damage to metals. This option requires the file **TRIM.DAT** for the initial ion energy, trajectory and starting position. If you select this option, you will get a sub-menu which requests which kind of damage calculation you wish to make.
 - **Special Multi-Layer Biological Targets** - TRIM allows the calculation of complex biological targets with up to eight layers using standard ICRU and ICRP target designations. This setup is special, and if you want this calculation you should read the section on *Special Setup for Multi-Layer Biological Targets*, later in this manual.
-
-

Ion Name, Mass, Energy

- Enter the ion name, e.g. O for oxygen or He for helium (TRIM ignores the case of the letters). It is usually convenient to press **PT**, see Figure 8-2, to obtain a Periodic Table of Elements, and just click on the element. For the ion mass, TRIM suggests the mass of the most abundant isotope (not the natural weight). These values are shown in the Periodic Table as MAI (Most Abundant Isotope). However, you may enter any mass (units = amu). For the ion energy, enter

any value (units = keV). TRIM will accept any values from 10 eV to 10 GeV/amu. One should be cautioned that TRIM does not include any nuclear reaction analysis, so that ions with energies above about 5 MeV/amu may have inelastic energy losses which are not included in its calculation.

Periodic Table of the Elements																																	
14		Si		Nat. Wgt. = 28.086		Density = 2.3212 g/cm ³		Atom Dens. = 4.977E+22 at/cm ³		MAI Mass=28		Heat Subl. = 4.7 eV		MAI Wgt.= 27.977		Fermi Vel. = 0.974 V ₀																	
IA																																	
Silicon																																	
								IIIIB		IVB		VB		VIIB		VIIIB																	
								B		C		N		O		F																	
								Al		Si		P		S		Cl																	
								Ga		Ge		As		Se		Br																	
								Ru		Y		Zr		Nb		Mo																	
								Tc		Ru		Rh		Pd		Ag																	
								Cd		In		Sn		Sb		Te																	
								Cs		Ba		La		Hf		Ta																	
								W		Re		Os		Ir		Pt																	
								Au		Hg		Tl		Pb		Bi																	
								Fr		Ra		Ac																					
Close		Ce		Pr		Nd		Pm		Sm		Eu		Gd		Tb																	
		Th		Pa		U																											
Click to select an element																																	
Wgt./Mass = amu Densities = Solid Phase																																	

Figure 8-2 – Periodic Table of Elements

The TRIM Setup window provides the user with a Periodic Table of Elements for the ion and target atoms. An element is selected the button **PT** and then clicking on an element. Also provided are the default parameters for that element. MAI is the most abundant isotope, which is typically the isotope used for the ion. The Heat of Sublimation is the default value for the surface binding energy of a solid (used for sputtering) and the Fermi Velocity, V_0 , is used to calculate the stopping power in that element, given in units of $V_0 \sim 1.3 \times 10^6$ m/s.

- **PROBLEM NOTE:** To setup TRIM, you have to declare in Windows that your Regional Setting is “English (United States)”, which uses a period as a decimal point. This is explained in the ReadMe file in the SRIM root directory (which helps correct initial SRIM installation errors). Basically, you must do the following:
 - Open “My Computer”
 - Open “Control Panel”
 - Open “Regional Settings”.
 - Set your Regional Settings to “English (United States)”.
 - You can now check that the decimal point is now a period by selecting the Tab called “Number”. It should show a period for the “Decimal Symbol”.
 - Close the Regional Settings window.
 - ***It is NOT necessary to restart your computer.***
 - When you complete using TRIM, you can reset your Regional Settings without restarting your computer.
- **Angle of Incidence of Ion** - This varies the angle of incidence of the ion with respect to the target surface. Normally, the ion is perpendicular to the target surface, along the X-axis at an angle defined as 0°. This angle may be changed to any angle from 0 - 89.9°. The change in ion direction is assumed to be in the XY plane.

Target Description

- **Solid or Gas Target** - TRIM treats gas targets different from solid targets. You must declare your target phase here. If your target has mixed gas and solid layers, then you need to read the later section "*Using TRIM with Mixed Gas / Solid Targets*". Targets containing normal gases such as oxygen, in solid form such as in a quartz target, should be declared as solids. The interaction of ions with atoms in solid phase is treated differently than for those atoms in gases. See Chapter 5.
- **Target Elements** - Input the various elements which make up your target, in the same way that you input your ion, e.g. Si = silicon. The same Periodic Table of Elements is available using the button , see Figure 8-2. Using this table, you will see the default values used for each target element. You may enter up to twelve target elements per layer. One special application of TRIM is to follow the mixing of layers by ion beams which create cascades. If, for example, you wish to follow silicon atoms from a surface layer of SiO_2 mixing into a silicon substrate, you can specify the target element Si twice, once for the surface layer and once for the substrate. TRIM will keep the two Si atoms separate, and you will be able to distinguish one from the other in the various analytic plots.
- **Table of Compounds** - TRIM has an encyclopedia of common compounds available for simple single-layer targets. In the TRIM Setup window, by pressing  these tables are accessed. In addition to the compound stoichiometries, this table provides typical densities and also bonding information. For many light compounds, especially hydrocarbons, this bonding information is later used to make significant corrections to the stopping powers. When you use this table, you will be able to skip over most of the target input steps. See Chapter 5 for special considerations when you have a compound target.
- **Layer Depths and Stoichiometry** - Once you have entered your list of target elements, you will build up your target layers (up to eight layers). Enter the first target thickness. The default units are Angstroms, however you may also use units of microns, millimeters, meters or kilometers by using the drop-down menu of units. For each layer, you will enter the amount of each element in that layer. TRIM normalizes this input, so you may use any units. For example, for a target of SiO_2 you may use any of the following: Si(1) O(2); Si(100) O(200); Si(33) O(67); etc.
- **Layer Density** - Each layer must have a density (units = g/cm³). TRIM will guess at densities, using a mixture of elemental target densities weighted by their relative stoichiometry. However, you should be careful to check that the density is reasonable. ***The final TRIM distributions will scale with target density, so any errors in density will directly transcribe into errors in ranges, etc.***
- **Layer Name** - Each layer is described on the plots and in all the data files using the name you input here. You can use simple names such as Silicon, or SiO_2 , or more detailed descriptive names such as Si(33)-Ge(67).

You can have TRIM print subscripts and superscripts for layer names on the plots by using the special commands \$ (superscript) and @ (subscript). The name $\text{SiO}@2$ will print on the screen as SiO_2 . If you use one of these in the middle of a layer name, then you can return the lettering to normal size using a “_” character. For example, “Fe@2_O@3” will create “ Fe_2O_3 ” for that layer name.

Damage Energies of Target Atoms

On the far right of the target data are three entries for: *Damage (eV)* / *Disp.*, *Latt.*, *Surf*. These are the values for the target atoms *Displacement Energy*, *Lattice Binding Energy*, and *Surface Binding*

Energy. These quantities were discussed in detail in chapter 7 on TRIM Theory. TRIM provides default values for every element.

- **Displacement Energy** - This is the energy that a recoil needs to overcome the target's lattice forces and to move more than one atomic spacing away from its original site. If the recoiling atom does not move more than one lattice spacing, it is assumed that it will hop back into its original site and give up its recoil energy into phonons. Typical values are about 15 eV for semiconductors and 25 eV for metals. For fragile materials like polymers, a value as low as 2 - 5 eV may be more accurate. For users who understand the physics of displacements, individual energies may be input for each of the different target atoms. For targets with several layers containing the same element, for example SiO₂ on Si, you may use different displacement energies for Si atoms in the two layers.
- **Surface Binding Energy** - If you are interested in sputtering, then this parameter is key to the sputtering yield (number of target atoms leaving the target surface). This is the energy that target atoms must overcome to leave the surface of the target (units = eV). Note that this is not the traditional chemical binding energy for surface atoms, for it includes all surface non-linearities such as those produced by radiation damage, surface relaxation, surface roughness, etc. Typically, the Heat of Sublimation is a good estimate of this energy. For single element targets, TRIM will default to a table of energies for each element. This value can be viewed using the Periodic Table of Elements using the button **PT**, which will also show the values for nearby elements. During a specialized sputtering calculation, special plots are available on the Menu of Plots to show you what effect small changes of the surface binding energy will have on sputtering yield.
- **Lattice Binding Energy** - This is the energy that every recoiling target atoms loses when it leaves its lattice site and recoils in the target. Typically it is about 1 - 3 eV, but values are not known for most compounds. This energy is assumed to go into phonons. The lattice binding energy is, unfortunately, also significant in calculating sputtering yield. Changing the binding energy from 1 to 3 eV may lower the sputtering yield by up to 2x (see section on "*The Physics of Sputtering*").

Calculation Parameters

"Viewing Window" for Data and Plotting – Although TRIM uses the entire target depth to generate averages such as projected range, vacancies per ion, etc., it is possible to enlarge one portion of the target for detailed analysis. This is TRIM's **Viewing Window**. For thick targets, this is an important consideration. The depth window allows TRIM to expand a small depth region in the target for fine detail. For example, in the TRIM Demo called "He (5 MeV) in a Gas Ionization Detector" the target is 50mm deep. However, the **Viewing Window** is set at 40mm-50mm, allowing more detailed analysis of the end-of-range of the He ions for both the plots and the datafiles. TRIM divides this window into 100 equal-depth bins and stores in them the averaged data for the calculation, for example the energy loss to ionization and the final ion ranges. As another example, in the DEMO section of the TRIM Setup Window, one selection is for 10 MeV H into Be, which has a range of almost 8 mm. For this DEMO, the depth window is set at 7.99 - 8.00 mm. This allows you to see on the plot the detailed collisions at just the final end of each ion's path, and also to have the final collision details in depth segments of 0.1 μm. The **Viewing Window** is set in the TRIM Setup Window, under "*Plotting Window Depths*". The default is zero, which means TRIM will use the total target depth for its stored data. If you input a Depth Window that results in bins smaller than a single atomic monolayer, you will be given a warning that this was requested (e.g. a depth window of 100 Å will make data-bins of 1 Å, less than any target monolayer). Requesting a window depth less than 100 monolayers may result in distortions near the layer edges. TRIM defines a monolayer as the inverse cube root of the atomic density of a layer, $N^{-1/3}$, where the

density, N, has units of atoms/cm³. Hence silicon, with a density of 5×10^{22} atoms/cm³, has a layer thickness of $(5 \times 10^{22})^{-1/3} = 2.7 \text{ \AA}$.

- **Number of Ions** - This allows you to set the number of ions which will be calculated. The number can go up to 9999999 ions (which has been requested by several strange users). Normally, you select the default (99999) and interrupt TRIM when it has adequate statistics. Some users wish to stop after a selected number of ions so that different TRIM calculations may be directly compared. If you repeat a TRIM calculation, every ion will be identical to that of a previous calculation unless you change the random number seed (discussed below). If you complete a calculation (finish all ions requested) you can continue this calculation by using the button *Resume Saved TRIM Calc.* Then increase the total number of ions to be calculated.
 - **Automatic Saving of Calculations** - Since some TRIM calculations may take days, this allows TRIM to automatically save itself at intervals. You may change this number during the calculation. It may range from 1 - 32000.
 - **Random Number Seed** - TRIM will always produce identical calculations (with the same input setup) unless this number is changed. You may input any integer number from 0 - 999999999. The default is set at **716381** which is an almost mystical number in random number theory, and is better than any other number that you will come up with (see Fishman & Moore, S.I.A.M.- J.S.C., vol. 7, 24 (1986)). However, if you want to have three similar but different calculations, then changing the seed from 1 to 2 to 3 will do nicely. The actual random number generator in TRIM is adapted from: P. L'Ecuyer, C.A.C.M., vol. 31, 742-749, 774-776 (1988), "An Efficient and Portable Combined Random Number Generator". At the bottom-right of the TRIM calculation window is a counter of the number of random-numbers used. For calculations with large recoils, this number grows rapidly and may exceed 2^{31} for less than 1000 ions.
-

Output Disk Files

All of TRIM output files may be declared either from the TRIM Setup window, or requested during the calculation. The advantage of declaring these files in the Setup window is that they start recording from the first ion. These files are explained in much more detail in Chapter 9, TRIM Output Files, and they will be briefly noted here.

- **Backscattered / Transmitted / Sputtered Atoms** - This activates the datafiles for individual ion statistics so that the information about the kinetics of every ion Backscattered or Transmitted, or every target atom Transmitted or Sputtered, is recorded. These files may also be toggled on or off during the calculation by clearing the check-marks beside these requests in the TRIM Calculation window. See the section "*Files of Individual Ion or Recoil Atom Kinetics*" and Chapter 9.
 - **Recoil Collision File** - This activates the datafiles for every ion / atom collision which leads to a displaced atom. This file can get big quite fast and should be used carefully (1000 collisions will take up about 64 kB of disk space). In some cases with large cascades, a single ion will generate >1 MB of data). See section *Files of Individual Ion or Recoil Atom Kinetics*, and the extensive notes in Chapter 9.
-

Scientific Terms used in TRIM

Physics of Recoil Cascades

The easiest way to understand the TRIM cascades is to start TRIM and select various DEMO calculations. During the calculation, play with the various plots and files, to see what they do. Each plot and file has a *Help* file associated with it, to explain its details.

Following this, you may create a more detailed understanding of cascades by selecting one of the DEMO calculations and then checking the box called "*Collision Details*", which will store every ion/atom collision in a file called ".SRIM Outputs/COLLISION.txt" (see Chapter on **TRIM Outputs**). Note that during the TRIM calculation, you may stop this data collection by un-checking the *Collision Detail* box in the TRIM window. This file can get quite large, so for a first experiment try it only for a few minutes of calculation time. Then stop TRIM and edit the file **COLLISION.txt** in the SRIM directory using any text editor. You will see tables of each ion colliding with various atoms in the target, and the detailed results of any collision cascades. Only those collisions which produce at least one displacement are tabulated, so you may not have a record of every collision.

In the file **COLLISON.txt**, first the current ion energy and depth are given, and then the current rate of energy loss of the ion to the target electrons, i.e. the electronic stopping power, called "Se" in the table with units of eV/Angstrom. Then the target atom that is hit and starts a recoil cascade is identified, along with its recoil energy. Each cascade is then divided into displacement collisions, vacancy production, replacement collisions and interstitial atoms, as described below.

In the file, the number of Displacement collisions indicates how many target atoms were set in motion in the cascade with energies above their displacement energy (which you specified in the TRIM Setup window). The next item in the table is Target Vacancies. A vacancy is the hole left behind when a recoil atom moves from its original site. Next, the table shows Replacement collisions, which reduce the number of vacancies. If a moving atom strikes a stationary target atom and transfers more than its displacement energy to it, and the initial atom, after the collision, does not have enough energy to move onwards, and it is the same element as the atom it struck, then it just replaces that atom in the target and there is no vacancy created. Although this may sound complicated, this mechanism may reduce the total vacancies by up to 30%. The summation goes:

$$\text{Displacements} = \text{Vacancies} + \text{Replacement Collisions}$$

Finally, the table lists interstitial atoms. When a recoil atom stops, and is not a replacement atom, then it becomes an interstitial. These may be summed as:

$$\text{Vacancies} = \text{Interstitials} + (\text{Atoms which leave the target volume})$$

If a cascade atom leaves the target volume, it is no longer followed. That is, if it leaves the target front surface or the rear surface, it is noted and then discarded. TRIM will follow atoms indefinitely as they go sideways, even though they leave your screen. But if they go through either target surface they are discarded and not counted. So vacancies occur within the target, and the final resting place of a moving recoil atom can be some distance from its vacancy. If the recoil leaves the target, clearly the sum of interstitials will be less than the number of vacancies by the loss of that atom. Replacement collisions are not part of this equation because each replacement collision reduces the number of vacancies and the number of interstitials by one, leaving the equation in balance. Finally, an atom which comes to rest in the topmost monolayer of the target is

always assumed to be a lattice atom if it originated in that layer (i.e. it is neither a replacement nor an interstitial atom).

The calculation of cascades, target displacements, replacement collisions, etc. makes certain assumptions which are defined explicitly below:

Assume an incident atom has atomic number Z_1 , and energy E . It has a collision within the target with an atom of atomic number Z_2 . After the collision, the incident ion has energy E_1 and the struck atom has energy E_2 . Previously specified for the target are energies E_d , the displacement energy, E_b , the binding energy of a lattice atom to its site, and E_f , the final energy of a moving atom, below which it is considered to be stopped.

A **displacement** occurs if $E_2 > E_d$ (the hit atom is given enough energy to leave the site). A **vacancy** occurs if both $E_1 > E_d$ and $E_2 > E_d$ (both atoms have enough energy to leave the site). Both atoms then become moving atoms of the cascade. The energy, E_2 , of atom Z_2 is reduced by E_b before it has another collision. If $E_2 < E_d$, then the struck atom does not have enough energy and it will vibrate back to its original site, releasing E_2 as **phonons**.

If $E_1 < E_d$ and $E_2 > E_d$ and $Z_1 = Z_2$, then the incoming atom will remain at the site and the collision is called a **replacement collision** with E_1 released as **phonons**. The atom in the lattice site remains the same atom by exchange. This type of collision is common in single element targets with large recoil cascades. If $E_1 < E_d$ and $E_2 > E_d$ and $Z_1 \neq Z_2$, then Z_1 becomes a stopped **interstitial** atom.

Finally, if $E_1 < E_d$ and $E_2 < E_d$, then Z_1 becomes an **interstitial** and $E_1 + E_2$ is released as **phonons**. If a target has several different elements in it, and each has a different displacement energy, then E_d will change for each atom of the cascade hitting different target atoms.

For those using the TRIM "quick" calculation of target damage, TRIM uses the Kinchin-Pease analytic solution for target damage as modified by two later authors. Typical output is shown in the Chapter 9 on **TRIM Outputs**. The following references would also help in understanding its formalism:

-
1. Kinchin and R. S. Pease, Rep. Prog. Phys., vol. 18, 1 (1955).
 2. P. Sigmund, Rad. Eff., vol. 1, 15 (1969).
 3. M. J. Norgett, M. T. Robinson and I. M. Torrens, Nucl. Eng. Design, vol. 33, 50 (1974).
-

Physics of Sputtering

Sputtering is the removal of near-surface atoms from the target. When a cascade gives a target atom an energy greater than the "surface binding energy" of that target, the atom may be sputtered. To actually be sputtered, the atom's energy normal to the surface must still be above the surface binding energy when it crosses the plane of the surface. The sputtering of a surface is described by a "Sputtering Yield", which is defined as the mean number of sputtered target atoms per incident ion. If the target is made of several elements, there is a separate sputtering yield for each element.

The surface binding energy (SBE) of an atom to a surface is known only for a few materials, but it is common to use the heat of sublimation as an estimate. Typical values are: Ni (4.46 eV), Cu (3.52 eV), Pd (3.91 eV), Ag (2.97 eV), Pt (5.86 eV) and Au (3.80 eV). Values will be suggested when you set up the TRIM calculation.

One may calculate sputtering by setting up a normal TRIM calculation with *Full Damage Cascades*. By asking for the data file SPUTTER.txt, a description will be made of each sputtercd atom. This request can be made either in the TRIM setup program or during the TRIM Calculation.

Only the cascades which reach back to the target surface are important to sputtering, so it is usually adequate to use only a thin target to simulate sputtering. For heavy ions, e.g. heavier than 20 amu, a target thickness of 40 Å to 50 Å is usually adequate. Using a very thin target reduces the time spent calculating cascades which will not contribute to sputtering. For light ions, e.g. He, it will be necessary to use thicker targets, as much as 300 - 500 Å, since these ions may backscatter from deeper in the target and cause sputtering as they exit from the target surface. The target depth needed for a calculation may be estimated by running several quick cases and seeing for which target depth the sputtering yield remains constant.

For cascades within the target at very low energy (which is a major contributor to sputtering) we use the hard-sphere model for scattering as described in J. P. Biersack and W. Eckstein, *Appl. Phys.*, A34, 73-94 (1984). See figure 3 of this paper, for example.

A final word of caution about Sputtering Yields. The sputtering yield is very sensitive to the surface binding energy (SBE) which you input to the calculation. Be aware that for real surfaces, this changes under bombardment due to surface roughness, and also changes due to surface stoichiometry for compounds. Further, sputtering involves mostly the upper monolayer of the target. For targets such as Ni, or heavier, the electronic energy loss of a target atom moving through the last monolayer is of the order of the surface binding energy, so even monolayer roughness will change the sputtering yield.

The sensitivity of sputtering yield to surface binding energy may be displayed during the calculation by using the plotting menu of *Integral Sputtering* and *Differential Sputtering*.

The Stopping of Ions in Compounds

(See Chapter 5 for an extended discussion of this subject)

A large dictionary of COMPOUNDS has been integrated into the SRIM setup programs. The stopping of ions in compounds is executed using the formalism described in "*The Stopping of Ions in Compounds*", by J. F. Ziegler and J. M. Manoyan, published in Nuclear Instruments and Methods, Vol. B35, 215-228 (1989). The dictionary of compounds can be accessed from the programs by pressing "*Compound Dictionary*".

About 300+ compounds are described in the SRIM Compound Dictionary. You may add other compounds by editing the file *..Data/COMPOUND.DAT*. At the top of this file are instructions about how the dictionary is constructed, and then the dictionary shows its 300+ examples. You will need to know not only the composition of the compound, but also the chemical bonding state of the light elements such as H, C, N, and O. It is easiest to find a compound in the dictionary which closely resembles your new compound, and just alter the parts of this definition.

For a review of the stopping of H and He in compounds, see the review in the report: ICRU Report #49 (ISBN 0-913394-47-5), International Commission on Radiation Units and Measurements, 7910 Woodmont Ave., Bethesda, MD, 20814, USA. Note that the values quoted in this reference as being from *TRIM* or *Ziegler* are from 1977, and are not representative of current SRIM values.

Stopping Powers for Ions in Gases

(See Chapter 5 for an extended discussion of this subject)

TRIM calculates special stopping powers for ions in gas targets of H, He, N, O, Ne, Ar, Kr and Xe. Any gas targets of elements other than those in the above list are treated as solids. This does not mean that the target phase-state is not important. For example, measurements of the stopping of H in Zn, comparing stopping in gas and solid phases, shows 50% stopping differences for ion energies below 100 keV (see references below).

The difference in the ion stopping of gases vs. solids is primarily due to three effects. In a solid, especially a metal, the electrons may form a continuous cloud of mobile conduction electrons which can interact with the ion collectively. Also, the ion will interact with successive atoms very quickly, and excitations of its own electrons may not relax before a subsequent collision. Finally, the ion's polarization of the target electrons will shield the ion from having distant collisions (the polarization effectively decreases the ion's charge state for distant collisions).. In general, the stopping of ions in a solid is lower than for the equivalent gas target (measured by transiting the same number of atoms/cm³) because of the shielding of the ion by the polarized electrons in the solid. Experiments have shown that both the stopping of ions, and the ion charge state, will vary with gas pressure

The difference between the stopping of ions in gas versus solid targets of H, He, N, O, Ne, Ar, Kr and Xe is only important at low ion velocities. For ions above 200 keV/amu, their stopping powers in solid and gas targets of the same element differ by less than 10%. Below this energy, the difference may reach almost a factor of two. See reference below (Z & M) as to how TRIM treats the differences.

If you ask TRIM for the stopping of ions in gases of compounds, e. g. CO₂, it will use gaseous stopping powers for O (which is in the above gas list) and stopping powers for gaseous C. If you ask for stopping in solid targets of CO₂, you will get stopping for solid C and for solid O added together. If you use the *Table of Compounds*, you can select CO₂ from the table and obtain chemical binding corrections to the stopping of both C and O (see section "*The Stopping of Ions in Compounds*".)

For heavy ions, Li - U, there is little data about stopping differences between solids and gases. For these ions, TRIM assumes similar phase differences as for H and He ions in the same targets.

The stopping of ions in gases is very dependent on the gas pressure. One may find stopping differences of more than a factor of two for pressures other than STP (0° C, 760 mm). This difference is especially true for gas densities greater than STP, i.e. several atmospheres. TRIM always assumes a gas target is at STP.

- The phase effect (gas vs. solid target) on stopping powers is of long interest, and one might begin a study of this subject with the excellent ancient paper: W. McChabach and S. K. Allison, Phys. Rev. **132**, 294 (1963).
- There is no recent review paper which covers all of the above physics. For a discussion of current insights into the phase-effect on stopping powers of ions in materials, see P. Bauer, F. Kastner, A. Arnau, A. Salin, P. D. Fainstein, V. H. Ponce and P. M. Echenique, Phys. Rev Lett, **69**, 1137 (1992), or G. Schiowitz, Phys. Rev. **42A**, 296, (1990).
- For details of solid/gas calculations in TRIM, see J. F. Ziegler and J. M. Manoyan, Nuclear Inst. and Meth., **B35**, 215-228 (1989).

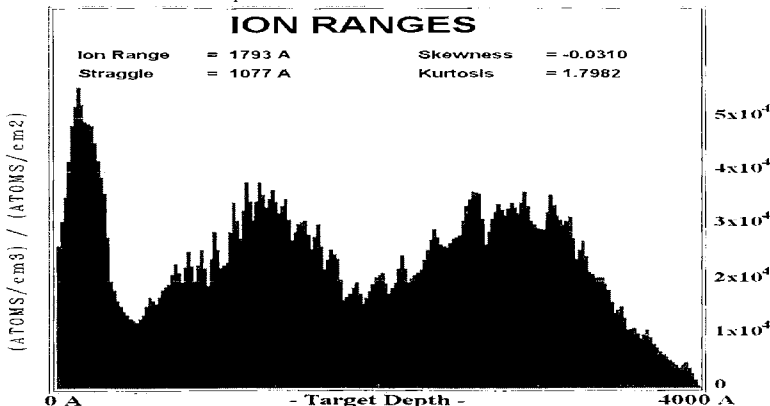
Special Applications of TRIM

Adding Multiple Ions/ Energies/Angles to Same Calculation

During the TRIM calculation, it is possible to merge multiple calculations into one set of datafiles. For example, in the semiconductor industry one might want to make a "triple well" structure, which is very common in CMOS integrated circuit processing. This might require two implants of boron at different energies and doses and one implant of indium into the silicon substrate. It may be that one of these implants is at an angle, 45°, to prevent a phenomenon called "side-wall shadowing". This kind of implant can be easily simulated using TRIM.

Assume that three implants are required at 80 keV, 30 keV and 5 keV, with the 5 keV Indium ion implant being at 45°. For convenience, assume that all three implants will have the same dose.

- Start the first calculation for Boron ions (80 keV) into a silicon (4000Å) target.
- When there are adequate statistics for the ion distribution, say at 1000 ions, press the button at the top of the TRIM Calculation window **Pause TRIM**.
- You can now look at the Ion Distribution plot to see if it is adequate. You will see a broad peak with a range of about 2600Å.
- Press the button **Change TRIM**. The Ion data window will turn yellow. Change the Ion Energy to 30 keV. Then Press **End Edit**.
- A window will pop up indicating that the Ion Data has changed. It will ask if you want to add to the existing calculation (YES) or restart the TRIM calculation (NO). Press the **YES** key.
- Press the **Continue** button to resume the TRIM calculation, with the boron ions now at 30 keV.
- After another set of ions, press **Pause TRIM**. You will see that the original deep peak has been modified with a shallower peak added at about 1700Å.
- Press the button **Change TRIM**. The Ion data window will turn yellow. Change the Ion to Indium (pressing the Ion button brings up the Periodic Table). Change the Ion Energy to 5 keV. Change the Ion Angle to 45. Then Press **End Edit**.
- A window will pop up indicating that the Ion Data has changed. It will ask if you want to add to the existing calculation (YES) or restart the TRIM calculation (NO). Press the **YES** key.
- Press the **Continue** button to resume the TRIM calculation, but with the Indium ions at 5 keV.
- After another group of ions, press **Pause TRIM**. You will see that the original two peaks have been modified with a shallower peak added at about 130Å.



Using file TRIM.DAT to make Complex TRIM Calculations

Calculating Plasma Ions Hitting a Solid (TRIM.DAT)

Simulating a Receding Surface from Sputtering (TRIM.DAT)

Simulating Reactor Radiation Damage in Metals (TRIM.DAT)

Sometimes users wish to consider incident ions with various energies, with various angles of incidence and possibly starting at various depths. For this application the data file, **TRIM.DAT**, is used, see Table 8-1 below. It can be used to simulate the ions from a plasma hitting a surface (various angles and energies), e.g. solar wind effects on planetary materials. It can be used to simulate a receding surface with subsequent ions starting at increasing depths, e.g. from ion sputtering effects. Or it can be used to simulate nuclear reaction processes, e.g. neutron induced alpha-particles created throughout reactor materials. Examples of the control file, TRIM.DAT, can be found in the SRIM directory: **../SRIM Tools**.

Note: See also the application (later in this chapter):

Radiation Damage from Neutrons/ Electrons/ Photons (TRIM.DAT)

The top of file **TRIM.DAT** contains 10 lines of comments, which are not used in the TRIM calculation. (Ignore the special fonts used in the Table for emphasis; the data file on the disk will be in simple ASCII format.) One of the data lines, as noted in the sample file, will be included as an identifying comment in all output files (named *.txt) which tabulates the statistics of each collision. This is the line: *Ar Plasma Ions into Si (1000A thick) (Energies 20-80 keV, Various Angles)*.

Table 8-1- TRIM.DAT - Sample File for Varying Energy/ Angle/ Depth

TRIM.DAT: TRIM - various Incident Ion Energies/Angles and Depths

- Comment:* Top 10 lines are user comments, with line #8 describing experiment.
Comment: Line #8 will be written into all TRIM output files (various files: *.txt).
Comment: Data Table line consist of: EventName(5 char.) + 8 numbers separated by spaces.
Comment: The Event Name consists of any 5 characters to identify that line.
Comment: Typical Data File is shown below, with a variety of numerical formats, all acceptable.
Comment: Note: cos(X) = 1 for normal incidence; cos(X) = -1 for back towards the target surface.

Ar Plasma Ions into Si (1000A thick) (Energies 20-80 keV, Various Angles)

Event Name	Atom Numb	Energy (eV)	Depth X (Å)	-Lateral-Position- Y (Å)	Z (Å)	Atom Direction Cos(X)	Cos(Y)	Cos(Z)
A-1	18	12345	0	0	0	1.00000	.000000	-.000000
abcde	18	54321	0	0	0	0.62344	-.295513	.003415
AA#1	18	1.31E4	123	0	-154	0.34234	-.336437	-.017437
C-3	18	123.55	1230	432	12.3E2	-0.23258	-.543453	.443483
AA-1	18	0.123E2	0	-10	-12	0.99998	.000012	-.000017

Table 8-1 shows the data format for several ions using various numerical styles to show how to specify numbers (all are acceptable). The numbers must be separated by spaces or commas. The first column, called *Event Name*, is a five character ID which will be displayed on the screen while that ion is active. Columns 2-3 show the ion atomic number and energy (eV). Column 4 indicates the depth (Å) in the target where the ion begins: (its x-axis coordinate). The depth must be a positive number. Columns 5-6 are the initial lateral position (Y and Z axis coordinate) of the ion

(Å). TRIM normally uses (0,0,0) as the starting coordinates of the ion. The ion's starting position is always randomly modified within an atomic diameter so that successive ions starting, for example, at (0,0,0) will not have the same impact parameter with a target surface atom. The incident angle of the ion is specified by its directional cosines, columns 7-9, with the x-axis corresponding to depth into the target. For normal incidence, the three directional cosines are: 1,0,0. Note that $\cos(X)$ is positive when the ion is going into the target, and negative when moving towards the target surface. The TRIM.DAT file may be up to 99999 lines long. If any illegal input values are discovered, an error message is displayed on the screen and that input line is skipped.

Important NOTE: TRIM expects that each line of TRIM.DAT ends with two ASCII symbols #13(CR) + #10(LF). These symbols date back to the teletype era, and mean: CR = Carriage Return, LF = Line Feed. All simple computer editors use this convention, but advanced programs like MS-Word do not. So if you get an error, especially "Illegal Data Line" then you probably need to try another editor to format the file TRIM.DAT.

A second requirement is that at the TRIM.DAT data, there must be an EOF character (EOF = End Of File). Most editors do this automatically and these characters are essential. **If you finish your calculation and suddenly get Error #62, then your data file is missing the EOF character.**

As an example, a file TRIM1.DAT is included in the SRIM directory: *../SRIM Tools*. This file contains data similar to that shown in the box above for Ar ions (20-80 keV) incident on a Si target (1000 Å thick) To illustrate various modes, this file starts the ions at different angles and at different depths in the target. To use this file to make a TRIM calculation, do the following:

- 1) Using Windows Explorer, copy *TRIM1.DAT* and paste it into a new file, *TRIM.DAT*. This will create the control file TRIM.DAT out of the above TRIM1.DAT demo file. Put this file into the root SRIM directory (which holds the program TRIM.exe).
- 2) Start SRIM normally. Select *TRIM Calculation*, which opens the *TRIM Setup* window.
- 3) In the DAMAGE menu window (upper right) you may specify either the 4th item (quick damage) or the 5th item (full cascade) in the list, "Varying Ion Energy/Angle/Position using TRIM.DAT". For this example use the 5th item, *Full Cascades*.
- 4) Enter the ion type, mass and energy for Ar ions at 80 keV. Note that you must use, for the ion energy, the maximum energy of ions which occurs in the TRIM.DAT file, column 3.
- 5) Specify for the first Target Atom the element Si .
- 6) Specify 1000 Angstroms for the depth of Layer #1.
- 7) Specify the stoichiometry as Si = 1 . (default).
- 8) Use the defaults to specify target density and description (2.32 g/cm² and Silicon).
- 9) Specify no other layers.
- 10) The rest of the questions of the TRIM setup program are optional.
- 11) Finally, press "Save Input & Run TRIM".
- 12) During the running of TRIM you will see in the top left of the plots the current ion Event Name from the table in TRIM.DAT. On the left side of the screen you will see the ion energy and position.
- 13) Run TRIM to completion, (a few seconds)
- 14) When TRIM reaches Ion #4, an **Error window** opens since this ion is declared in TRIM.DAT to start at 1130A while the target is only 1000A thick. This Error is included in this example to show how TRIM reacts to error in the input file. This error shows you the error messages associated with using TRIM.DAT.
- 15) After 5 ions, the calculation ends..

To run your own calculation, make up a new file TRIM.DAT, then follow the instructions above. You will have to specify your own ion and target. When you prepare the TRIM.DAT file be sure that your editor places CR+LF characters at the end of each line, and at the end of the file there is an EOF character (EOF = End Of File). These characters are essential. *If you finish your calculation and suddenly get Error #62, then your data file is missing the EOF character.*

This application of TRIM was suggested by: K. Bodek, PSI, Switzerland, F. Calvino, Barcelona, Spain and many others.

Radiation Damage from Neutrons/Electrons/Photons (TRIM.DAT)

TRIM can be used to calculate the recoil cascades in solids caused by neutrons, electrons or photons (which we will call NEP particles). These cases are treated identically, with TRIM evaluating only cascade damage without any incident particle damage.

One must first obtain another computer program for the transport of NEP particles through matter. Widely used codes are the "Integrated TIGER Series", (ITS code) for electrons and photons, or the "Monte Carlo Neutron Program" (MCNP code) for neutrons in matter. Both are available from the Radiation Shielding Information Center, Oak Ridge National Laboratory, P.O. Box 2008, Oak Ridge, TN, 37831-6362, USA, telephone: (01)-615-5746176, Fax: (01)-615-574-6182, Internet: <http://rsicc.ornl.gov>. The separate NEP transport programs are used to calculate where collisions are made in the target, and give the position, and recoil statistics for each collision atom. Then TRIM can be used to calculate the full target recoil cascade which occurs from each NEP collision atom.

A file called **TRIM.DAT** must be prepared by the user which specifies the parameters of each cascade. An example of **TRIM.DAT** is shown in Table 8-2 and included in SRIM as ..\SRIM Tools\TRIM2.DAT. TRIM calculates the cascades with an "invisible" incident particle. TRIM.DAT specifies each recoil atom and TRIM calculates its cascade.

Table 8-2 - TRIM.DAT - Sample File for Collision Cascades

TRIM.DAT : TRIM recoil cascade data file

- Comment: Top 10 lines are user comments, with line #8 describing experiment.
- Comment: Line #8 will be written into all TRIM output files (various files: *.txt).
- Comment: Data Table consists of: EventName(5 char.) + 9 numbers separated by spaces.
- Comment: The Event Name consists of any 5 characters to identify that line.
- Comment: Typical Data File is shown below, with a variety of numerical formats, all acceptable.
- Comment: Note: cos(X) = 1 for normal incidence; cos(X) = -1 for back towards the target surface.

Recoils from 1670000 eV electrons in SiO₂(1200A)+GaAs(10000A)

Event Name	Atom Numb	Energy (eV)	Depth X (Å)	-Lateral-Position- Y (Å)	Z (Å)	Atom Direction Cos(X)	Cos(Y)	Cos(Z)
A-1	8	59.2	322	24	12.34	0.99998	.000012	-.000017
C-3	33	1259.	10.02E3	432	12.3E2	-0.23258	-.543453	.443483
AA-1	8	98764	522	-24.3	-12	0.99998	.000012	-.000017
123C	14	1.56E4	2222	-33	-69	0.62344	-.295513	.003415
9875	33	7.31E4	3322	-82.9	154	0.34234	-.336437	-.017437
asd	6	0.98E5	0.882E2	-206	588	0.03754	.032936	-.334616

The top of file **TRIM.DAT** contains 10 lines of comments, which are not used in the TRIM calculation. (Ignore the special fonts used in the Table for emphasis; the data file on the disk is in simple ASCII format.) One of the data lines, as noted in the sample file, will be included as an identifying comment in the file **COLLISON.txt** which tabulates the statistics of each collision (This is the line: "Recoils from 1670000 eV electrons in SiO₂(1200 Å)+ GaAs(10000 Å)"). The important numerical data at the bottom of the file may be written in several different formats, such as 12345, 12.345E3, 0.12345E5, etc.

Table 8-2 shows the data for several recoils using various formats to show how to specify numbers. The numbers must be separated by spaces or commas. The first data column, *Event Name*, is a five character ID which will be displayed on the screen while that recoil is active. Columns 2-3 show the recoiling atom atomic number and energy (eV). Column 4 indicates the depth (Å) in the target where the recoil atom starts- this is the x-axis coordinate. The depth must be a positive number. Columns 5-6 are the initial lateral position of the atom (Å). The initial trajectory of the recoiling atom is specified by its directional cosines, columns 7-9, with the x-axis corresponding to depth into the target. For a recoil trajectory normal to the target surface, the three directional cosines would be: cos(X)=1, cos(Y)=0, cos (Z)=0. Note that cos(X) is positive when the ion is going into the target, and negative when moving towards the target surface. The TRIM.DAT file may be up to 99999 lines long. If any illegal input values are discovered, an error message is displayed on the screen and that input line is skipped.

The sample input data file shown in Table 8-2 is for 1.67 MeV electrons into a target of SiO₂ (1200 Å) on GaAs (10000 Å). If you wish to try TRIM using the sample data file, follow these steps:

- Using Windows Explorer, copy *TRIM2.DAT* and paste it into a new file, *TRIM.DAT* in the root SRIM directory. This will create the control file TRIM.DAT out of the above TRIM2.DAT demo file. The file must be in the same directory as **TRIM.exe**.
- Start TRIM normally and select *TRIM Calculation* to go to the TRIM Setup window.
- In the DAMAGE menu (upper right) specify either the 6^h item (quick damage) or the 7^h item (full cascade) in the list, "Damage cascades from neutrons, using *TRIM.DAT*". For this example, choose the 7^h item: "Damage Cascades from Neutrons, etc. (Full Cascades) using *TRIM.DAT*"
- For the ion Type and Mass use any values since **this data is not used**. For this calculation, there is no ion, only recoils. So in this example, for electron irradiation, you can still get the full target damage even though SRIM can not normally be used for beams of electrons.
- For the *Ion Energy*, specify the maximum energy which occurs in column 3 in *TRIM.DAT*. For the data shown in Table 8-2, you use 100 keV. This will assure that stopping powers are calculated for all recoils up to this energy.
- You will make a target with atoms of **Si**, **O**, **Ga** and **As** (You must specify every atom noted in column 2 of the TRIM.DAT file, and this atom must exist at the depth noted in column 4. Otherwise, you will get an error message on the screen, and this event will be omitted.)
- Specify that the target first layer with a depth of **1200** Å and containing **Si(1)+O(2)**. TRIM normalizes the stoichiometry so you may use any equivalent units such as **Si(33)+O(66)**. The second target layer has a layer depth of **10000** Å and is composed of **Ga(1)+ As(1)**. There is no third target layer.
- Finally, press "**Save Input & Run TRIM**".
- You may get a window asking if you want to generate the file **COLLISON.txt**. Answer "**No**"
- During the cascade calculation, on the screen you will see small isolated pockets of damage, with no intermediate ion tracks. The TRIM damage plots may be accessed normally at any

time. The cascade results will be stored in **COLLISON.txt** if you answered "Yes" in the above step. You may interrupt the calculation at any time, and continue it later (TRIM will start where it left off).

When you prepare the **TRIM.DAT** file be sure that your editor places CR+LF characters at the end of each line, and at the end of the file there is an EOF character (EOF = End Of File). Most editors do this automatically and these characters are essential. If you finish your calculation and suddenly get Error #62, then your data file is missing the EOF character.

NOTE: TRIM will assume that each *Event Name* data row in TRIM.DAT comes from a different incident particle, and hence its statistical averages will be in error for cases where a single particle may cause several recoils, e.g. for a high energy neutron may cause several *Event* data lines in TRIM.DAT. To correct for this counting error, take the calculated TRIM statistical averages and multiply by $(N_{\text{Events}}/N_{\text{Particles}})$. For example, if the TRIM.DAT file contains 100 events caused by 20 incident particles, then every average needs to be corrected by multiplying by $(100/20) = 5$. So if the TRIM output shows "*Vacancies/Ion = 10*" the corrected average value would be 50 Vacancies/Particle.

As with normal runs of TRIM, the calculation may be interrupted and saved at any time. When TRIM resumes, it will automatically skip cascades which have been previously calculated.

COLLISON.txt contains the data on every ion/target collision which exchanges enough energy to produce a vacancy (energy above the Displacement Energy). This file can get quite large. If the data file is turned off, then on again, further data may be appended to the old data. (See section on TRIM Execution and Commands in Chapter 9 on **TRIM Outputs**.)

The above instructions were suggested by R. Macaulay-Newcombe of McMaster Univ.; Canada; and M. Robbins, Univ. of West London, UK; and F. Calvino, Barcelona, Spain).

Special Setup for Multi-Layered Biological Targets

Use the *Compound Dictionary* in the TRIM setup window to use any of the standard ICRU or ICRP biological target specifications. See the following citations for "standard" compounds:

- International Commission on Radiation Units - Report ICRU- 33, "Radiation Quantities and Units", 1980, ICRU, Bethesda, MD, USA.
- International Commission on Radiation Units - Report ICRU- 37, "Stopping Powers for Electrons and Positrons", 1984, ICRU, Bethesda, MD, USA.
- International Commission on Radiation Units - Report ICRU- 49, "Stopping Powers and Ranges for Protons and Alpha Particles", 1993, ICRU, Bethesda, MD, USA.
- H.Q. Woodward and D. R. White, British J. of Radiology, vol. 59, 1209-1219 (1986).

An example of this type of calculation is included in the *Demo* examples available in the TRIM Setup window. If you wish to enlarge or change the *Table of Biological Targets*, you need to edit the file **../Data/COMPOUND.DAT** in the SRIM directory. This contains all the data of the biological targets. There are instructions at the top of the file which indicate the data format. In general, each target is described by a line of text, which is displayed in the table-of-contents during layer selection, and a line of data which describes the layer to the TRIM calculation. The table also contains the data for corrections to the ion stopping powers based on chemical binding information,

but this correction is beyond the scope of this manual. Please note that TRIM will accept targets made of up to 12 elements.

This application was suggested by Tammy Utteridge, Royal Adelaide Hospital, Australia, and Wayne Newhauser, PTB, Braunschweig, Germany.

How to Obtain 3-D plots of the Ion's Electronic Energy Loss

Some applications require the generation of three dimensional plots of the electronic energy loss of light ions. Examples of such applications are the use of ion beams for micro-lithography, or the use of ion beams in studying or altering biological samples. Below are the steps required to generate the required data. (Note that this procedure may be inaccurate for heavy ions which create significant recoil cascades, whose electron excitation is not included in the ion's electronic energy loss.)

- Setup your TRIM target in the usual way.
- Check the box for Collision Details (bottom of setup window).
- Continue with the TRIM setup program. When TRIM starts, you will be asked whether you wish to create a *New* file or *Append* to an old COLLISON.txt file. Specify *New*. Run TRIM for several ions. You will notice that the box called *Collision Details* is checked. You can start this file at any time during the TRIM calculation by checking this box, and stop it by unchecking it later.
- After several ions are completed, stop TRIM
- Now edit the datafile *../SRIM Outputs/COLLISON.txt*. A sample of this file is described in detail in the Chapter on **TRIM Outputs**. You will see a file like the one shown below:

Table 8-3 - 3-D plots of Electronic Energy Loss (COLLISON.txt)

TRIM Calc.= B(17 keV) ==> Tungsten(300A)

COLLISION HISTORY

NOTES: Only Ion Collisions which produce Displacements are tabulated.

Atom Sums and Averages are Incomplete if Recoil Cascades Leave Target.

Target DISPlacements = VACancies + REPLACEMENT Collisions.

Target VACancies = INTERstitial Atoms + (Atoms Leave Target Volume).

Ion	Energy	Depth	Lateral Dist(A)	Se	Atom Recoil	Tgt	Tgt	Tgt	Tgt		
Num	(keV)	(A)	Y Axis	Z Axis	(eV/A)	Hit	Enrg (eV)	DISP	VAC	REPLAC	INTER
1	16.00E+00	33E+00	1E-05	4E+00	15.84	W	83E+00	0	0	0	0
1	16.10E+00	49E+00	-3E-02	7E+00	15.86	W	57E+00	4	2	2	2
1	16.28E+00	65E+00	-6E+00	6E+00	15.93	W	94E+00	2	1	1	1
1	16.06E+00	111E+00	-12E+00	-8E+00	15.85	W	48E+00	4	1	3	1
1	15.00E+00	125E+00	-14E+00	-15E+00	15.32	W	114E+00	2	1	1	1

Data Omitted

This file shows the three-dimensional position of each major collision between the ion and the target atoms. It also shows in column six the instantaneous electronic stopping (rate of energy loss) of the ion to the target, Se, in units of eV/Å. If you need the three-dimensional electronic energy loss of the ion to the target, you now have all the necessary information. To obtain the energy deposited, calculate the path length between two successive collisions and multiply by the specific energy loss. For example, the distance between the first two collisions shown above is 16.3Å, with an energy loss of 15.86 eV/Å. This means the ion loses 258 eV into electronic excitations in this segment. If higher accuracy is needed, one can interpolate between the instantaneous energy loss values shown at each major collision point. Note that electronic stopping, col. 6, does not change

smoothly due to Monte Carlo straggling variations. The values of Se oscillate about a mean value because TRIM is applying straggling statistics to this parameter (see Chapter 7 on TRIM Theory). This application was suggested by Lidia Didenko, Univ. of Maryland.

How to use TRIM for Isotopically Enriched Targets

TRIM assumes that a target has the natural abundance of isotopes, e.g. that lithium is made up of 7.5% of Li⁶ and 92.5% of Li⁷. To use TRIM with isotopically enriched targets, it is necessary to follow the steps below (using the example of an enriched target with 90% Li⁶ and 10% Li⁷):

During the TRIM setup program, for the target atoms declare *Li* twice. Then declare the mass of one to be 6 with a stoich of 90, and the other with a mass of 7 and a stoich of 10. (For elements with more isotopes, you may specify the element up to twelve times, for up to twelve isotopes.)

Straggling in Ion Energy Reducers (Energy Degraders)

TRIM may be used to calculate the energy loss through foils or thick blocks of materials used to lower the energy of a beam of particles. This is often done for light ions, such as protons, to obtain lower energies quickly. For example, if one starts with a beam of monocenergetic protons at 158.6 MeV and introduces a block of plexiglas (called *perspex* in Europe, and Japan) 14.1 cm thick, the exiting beam of particles will be at 30 MeV. Degrader blocks made with light atoms can reduce particle energy with a minimum of straggle and little long term radioactivity (plexiglas is C₆H₄O₂).

Two problems occur in planning "energy degraders". First is the calculation of the proper block thickness, and second is the calculation of the final beam energy spread. Below we illustrate both calculations.

The calculation of the required degrader thickness consists of four basic steps. We illustrate these steps below using the example of protons being slowed by a block of plexiglas from an initial energy of 158.6 MeV to a final energy of 30 MeV.

- 1 Make a table of proton stopping in plexiglas by executing the program Table of Stopping and Range of Ions using the SRIM Title Menu. In the program, select a target of plexiglas in the Table of Compounds and then generate a stopping/range table for protons up to 160 MeV in plexiglas, with the stopping powers specified in units of MeV/min.
- 2 Using the table generated in (1), find the range of protons for the initial beam energy and estimate the depth at which the protons will be at 30 MeV by looking at the ranges and working backwards. For example, the table will show that 160 MeV protons have a range of 154.54mm in plexiglas, and 30 MeV protons will go 7.63mm. Hence your first guess for the thickness of plexiglas to reduce 160 MeV protons to 30 MeV will be 154.54 - 7.63 = 146.9 mm thick. Further, since the initial proton beam is not 160 MeV but 158.6 MeV, one interpolates the distance protons travel between 160 MeV to 158.6 MeV as 2.30 mm, so the initial block size for an incident 158.6 MeV beam will be 146.9 - 2.30 = 144.6 mm. Setup TRIM for protons in plexiglas at this thickness. Be sure to set the flag to store the energy spectrum of the *Transmitted Ions*, which will create the file TRANSMIT.txt that contains all the kinetic details about the transmitted ions.
- 3 Execute TRIM to get a file of transmitted ions. You now need to execute a program to analyze these results. SRIM includes a BASIC program, ..\SRIM Tools\TRANSMIT.BAS, which will analyze the transmitted particles which TRIM stores in the file TRANSMIT.txt. This program will give you both the mean final energy and the energy straggling of the transmitted protons.

- This program is written in BASIC so that you can look at the source code and modify it for your needs. (You can easily generate your own code, since the datafile is simple to read.)
- 4 Use the difference between your desired final energy (30 MeV) and mean final energy found in step 3 above, along with the stopping power tables, made in step 1 above, to estimate a new target thickness. For example, if the protons exit at 32 MeV and the stopping power for protons at 30 MeV is 2.16 MeV/mm, then you need $(2 \text{ MeV})/(2.16 \text{ MeV/mm}) = 0.92 \text{ mm}$ more plexiglas in the block to bring the beam down to 30 MeV. Use the TRIM setup program with "Restore Last TRIM Data" to make up a new plexiglas target with a width of 144.6 mm (initial estimate) + 0.92 mm (correction) = 145.52 mm. Loop through steps 2-4 until you come get as close as you want to the desired thickness.

The final energy straggle of the beam after it has passed through the energy reducing block is a mixture of two components: (1) the straggle introduced by random collisions in the degrader block and (2) the broadening of any incident beam energy straggle by the block (straggle is the spread of the ion beam energy spectrum). We calculate the straggle of the incident monoenergetic beam with the TRIM calculations above, steps 1-4, and we find, for example, a straggle of about 2.0 MeV when we degrade protons from 160 MeV to 30 MeV using plexiglas (this comes out of the analysis program TRANSMIT.BAS). To this broadening, we have to add the straggle due to expansion of the initial beam energy spread, which may be the dominant factor in the final energy width. Assuming that the incident beam is not monoenergetic, but has a spread of 1 MeV at 160 MeV, we will find that this spread expands to 3.6 MeV by the time the beam degrades to 30 MeV. This expansion occurs because of the non-linearity of stopping powers with particle energy as explained below.

Assume that the energy straggle of the incident beam is σ . We show below that the final energy straggle of the exiting beam, σ' , can be estimated as :

$$\sigma' = (S'/S) \sigma,$$

where S and S' are the stopping powers, dE/dx , in the degrader material at the initial and final beam energy.

Consider two particles of the incident beam with energies E_1 and E_2 , separated by the incident beam energy straggle, σ . The final energy straggle of these two particles, after transiting the energy-lowering block of material, is defined as $\sigma' = E'_1 - E'_2$, where E'_1 and E'_2 are the final energies of particles 1 and 2.

Considering the incident particles, assuming $E_1 > E_2$, then particle #1 will travel a short distance into the degrader block before its energy will be reduced to that of particle #2. This distance, x , is about $x = \sigma / S$, where S is the particle stopping power (dE/dx) at energy E. After particle #1 reaches depth x, then both particles #1 and #2 will transit through the block similarly until particle #1 reaches the end of the block. Particle #2 will still have more of the block to traverse, an amount $x' = \sigma' / S'$, where $\sigma' = E'_1 - E'_2$, the final energy difference between the two particles, and S' is the stopping power at the final beam energy, E' . But the block length is the same for both particles, so $x = x'$, and therefore $\sigma / S = \sigma' / S'$. This can be solved for the energy straggle, $\sigma' = (S'/S) \sigma$.

Note that several approximations are made in this argument, especially that $S(E_1) = S(E_2)$ and $S(E'_1) = S(E'_2)$, and that the total energy loss is much larger than the straggling, $(E - E') \gg \sigma$.

For an example, protons at 160 MeV in plexiglas have a stopping power of 0.593 MeV/mm and at 30 MeV have a stopping power of 2.157 MeV/mm. Assuming the initial beam straggle, σ , is 1

MeV, then the final beam energy straggle, $\sigma' = (1 \text{ MeV}) (2.157 \text{ MeV/mm}) / (.593 \text{ MeV/mm}) = 3.6 \text{ MeV}$.

The total beam spread through the energy-degrader block is the rms total value of two separate quantities : (1) the beam straggle through the block, 2.0 MeV, and (2) the beam energy broadening due to non-linear stopping powers, 3.6 MeV, which, when added in quadrature, gives a total straggle of 4.1 MeV .when protons at 160 MeV are degraded to 30 MeV.

The above comments come from Dr. Bernard Gottschalk, Harvard Cyclotron Laboratory, Harvard University, USA.

Getting High-Resolution Collision Data from TRIM

TRIM breaks the target into 100 equal-depth layers, each parallel to the surface. These layers are defined by the ***Viewing Window***, i.e. the depths that you see on your screen during the calculation. For example, if you try the DEMO (from the TRIM Setup window) of 10 MeV protons into Be, you will find that the target is defined down to 1000 μm , but the viewing screen is defined as the 800-900 μm depth in the target. The collision data (vacancies, displacements, ion ranges, etc.) are stored in 1 μm bins from 800 to 900 μm . You can get data in 1 μm bins for the whole 1000 μm target depth by repeating the calculation with different viewing windows, and saving each set of data files separately. That is, repeat the same calculation for viewing depths of 0-100 μm , 100-200 μm , etc., each time storing the data separately. When TRIM repeats a calculation, it calculates exactly the same ions which follow the same trajectories and which have the same collisions (unless you explicitly change the random-number seed in the TRIM setup program). So the data you collect in the ten calculations necessary to cover the 0-1000 μm total target thickness will smoothly go together, and you can get 1000 bins, with 1 μm resolution, after ten TRIM runs with the above example.

This suggestion was made by Sarah Clark, Princeton University, USA.

Evaluating the Details of “Ion Mixing” Experiments

TRIM is often used for studying the mixing of similar layers such as NiSi/SiO₂/Si. It is sometimes useful to try to identify which layer recoil atoms come from. You can specify different identical atoms for each layer, and TRIM will treat them separately. For the example, you can specify target atoms of **Ni**, **Si**, **Si**, **O** and **Si**. TRIM will treat these as separate atom types, and in plots or in text files they will be separately indexed.

If you wish to examine an interface closely, remember that you can isolate the interface using the ***Viewing Window*** option in TRIM, and blow up the interface region with monolayer resolution. As an example, assume your target is: NiSi (3000 Å) / SiO₂ (2000 Å) / Si (5000 Å). The total target is 10,000 Å thick. But you may specify the ***Viewing Window*** as 2800 Å to 5200 Å and thereby see the interface with twice the resolution. If you save data in the *.txt files (previously discussed) the data will now be grouped in 24 Å segments instead of 100 Å segments. Note that the TRIM averages (e.g. the range or straggling) are calculated precisely and are not limited by the data segments.

Using TRIM for Mixed Gas/Solid Targets

If you wish to calculate ion stopping in a mixed solid/gas target, for example alpha-particles transmitted through an ionization chamber, you must consider how TRIM stores collision data. TRIM is set up to store the averaged collision results in 100 bins. The bins are equally spaced in

depth, so if you have a thin window, say 10 μm of Al, then 100 mm of gas, then a final layer of 10 μm of Al, the TRIM output will be stored in about 1 mm bins. Since these bins are far bigger than the solid 10 μm windows, TRIM stores combined solid and gas collision data in the first and last bins.

There are 3 different ways to get accurate data for all parts of the target:

1. If you care only about the gas-cell part of the target, then set the *viewing window* only for the gas part of the target. TRIM will then set up its 100 bins for this gas layer only (the bins are defined by the viewing window, not by the total target width). In the above example, Al(10 μm) + Gas(100 mm) + Al(10 μm), your target thickness is 100.02 mm and your viewing window will start at .01 mm and end at 100.01 mm. (Note: TRIM does not use bins in its ion transport calculation, only to store averaged results.) The declaration of the “*Plotting Window Depths*”, also called the *Viewing Window*, is part of the TRIM Setup window. See Chapter 12, TRIM Tutorials, #4, for more details.
2. Use the detailed data supplied in the Individual Ion Datafiles. These are described in detail in Chapter 9, **TRIM Outputs**, which discusses all the possible TRIM datafiles. You can generate a file called COLLISON.txt, which contains all the data of every ion/atom collision, and then extract whatever data that you need. This file can be initiated either in the TRIM setup program by pressing “*Collision Details*” or checking this box during the TRIM calculation
3. Run TRIM for each section separately, e.g. the entrance foil, the gas cell and the exit foil. For each calculation, you will save a file of transmitted ions and use this as input data for the ions into the next layer. This is described in the section on *Ions starting with varying Energies, Angles and Depths*. After each calculation you must rename the collision data files, *.txt, so they are not written over by the next calculation.

Be sure to remember to declare any GAS portions of the target, so that it will be treated correctly as a gas (Chapter 5 discusses the differences in stopping in gases vs. solids).

(Discussion suggested by F. Calvino, Barcelona, Spain)

Datafile of Complete Ion Trajectories through a Target

It is possible to track an ion through the target, storing its position at various points of its path. Doing this for every collision is possible using the special output datafile called **COLLISION.txt**. TRIM has various filters for this file to keep it from overwhelming the user with its details. See Chapter 9 for details.

However, it is possible to track the 3-dimensional position of an ion at intervals through its path into the target. To do this, in the TRIM Setup window, at the bottom, is a selection called “**Special EXYZ File Increment (eV)**” This will generate a datafile of the ion position at specific energies: ..// **SRIM Outputs / EXYZ.txt**

There is an example of this command in the **DEMO** menu of this window. The Demo sets up Bi(500 keV) ions into silicon. It is set so that every time the ion loses 25 keV, an entry will be made into the file of the ion's position. That is, the ion's position is stored at energies of about 500 keV, 475 keV, 450 keV, 425 keV.

Table 8-4 shows a typical output of this DEMO calculation. The ion energies are not exactly at the 100 keV intervals because the energy losses of the ion occur in uneven steps. The position of the

ion at the nearest energy to each increment is used for the table.

Table 8-4 - Table of 3-D Position of Ion Trajectory in Target

SRIM-2006						
Ion Energy vs Position File						
AXIS DEFINITIONS: X=Depth, Y,Z= Lateral plane of target surface.						
(If beam enters target at an angle, this tilt is in Y direction)						
Shown are: Ion Number, Energy (keV), X, Y, Z Position						
CALCULATION DATA						
Ion Data: Name, Mass, Energy , Energy Interval						
Bi 208.98 500 keV 100 keV						
Ion Number	Energy (keV)	Depth (X) (Angstrom)	Y (Angstrom)	Z (Angstrom)	Energy Lost(eV)	Last Collision
0000001	5.0000E+05	0.0000E+00	0.0000E+00	0.0000E+00	0.0000E+00	
0000001	4.9990E+05	4.5634E+03	-7.9972E-01	1.8242E+00	1.8998E+05	
0000001	3.9991E+05	4.6482E+04	1.1253E+02	6.4566E+01	1.9992E+05	
0000001	2.9992E+05	9.6187E+04	1.1568E+02	-1.2677E+02	9.8713E+04	
0000001	2.0000E+05	1.5203E+05	-3.9668E+02	-8.1722E+02	6.6356E+04	
0000001	9.9985E+04	2.2324E+05	-7.8673E+02	-1.0863E+03	7.3526E+04	
0000002	5.0000E+05	0.0000E+00	0.0000E+00	0.0000E+00	1.2233E+00	
0000002	3.9979E+05	4.6043E+04	2.8184E+01	1.0037E+01	2.1920E+05	
0000002	2.9992E+05	9.5422E+04	1.6411E+02	-2.3177E+02	1.7898E+05	
0000002	1.9995E+05	1.5194E+05	-8.5354E+02	-5.0238E+02	6.6654E+04	
0000002	9.9942E+04	2.2295E+05	-1.8743E+03	-2.9341E+02	9.2119E+04	

TRIM - Common Questions and Solutions

What are "Projected Range" and "Radial Range" Distributions ?

The program assumes that there is cylindrical symmetry in the final ion distributions. The assumed cylindrical axis is perpendicular to the target surface at the point of ion impact. (If the initial ion beam is not normal to the target surface, then none of the following is valid.) The "radial" parameters refers to these cylindrical coordinates. The "projected" parameters assumes that an X-Y plane has been inserted through the axis, and the final ion distribution is projected onto this plane. This projection is identical to the view on the PC screen and marked as the "XY Plane" (X is the depth axis; the XZ plane is perpendicular to the XY plane).

The mean "lateral range" of the ions is zero in both the radial and projected definitions if there is cylindrical symmetry. So the lateral range in TRIM is defined as the mean absolute value of the lateral range. The "ion straggling" has its normal definition as the second moment of the distribution. The lateral projected parameters directly describe the final distribution under a mask edge as used in VLSI technology. Remember, the total ion concentration directly at a mask edge is one half of the concentration of a uniform implantation distribution.

What is Straggling, Skewness and Kurtosis ?

These words are names for statistical quantities related to the second, third and forth moments of the ion distribution. They are important because many VLSI modeling programs require these parameters to create analytic functions of ion implantation distributions. The use of these words in the ion implantation field is DIFFERENT from that in some statistics textbooks. In this field, we use mostly the definitions first proposed by B. Winterbon ("Ion Implantation Range and Energy Distributions", vol. 2, Plenum Press, 1975). For convenience, we define each moment below in several different standard notations. It is assumed below that the ion trajectory begins perpendicular to the target surface, co-linear to the x-axis, and the y-axis and z-axis are orthogonal in the target surface plane (during the TRIM calculation, the window "Collision Plots" controls four displays of the ion and recoil trajectories projected on the XY, XZ and the YZ planes).

$$\begin{aligned}\text{Mean Projected Range} &= R_p = \sum_i x_i / N = \langle x \rangle . \\ \text{Lateral Projected Range} &= R_y = \sum_i |y_i| / N = \langle |y| \rangle . \\ \text{Radial Range} &= R_r = \sum_i (y_i^2 + z_i^2)^{1/2} / N .\end{aligned}$$

Where x_i is the projected range of ion "i" on the x-axis, i.e. the perpendicular distance from the surface to the end of an ion's track; $\sum_i x_i$ = sum of the ion projected ranges; $\sum_i x_i / N$ = the mean projected range of N ions; and $\langle x \rangle$ = the mean projected range of all ions. The transverse coordinate "y" is treated the same, except the distance is taken in the XY plane. The mean projected lateral range is zero for a perpendicular beam, so the above lateral range definition averages the absolute values to provide other information on the first moment of the radial spread. The mean radial range assumes cylindrical symmetry of the ion distribution.

"Variance" is the second moment of the range distribution, and we show below several identical definitions using various common notations.

$$\begin{aligned}\text{Variance} &= \sum_i (x_i - R_p)^2 / N = \langle (x - R_p)^2 \rangle , \\ &= \sum_i \Delta x_i^2 / N = \langle (\Delta x_i)^2 \rangle , \\ &= \langle x^2 \rangle - \langle x \rangle^2 = (\sum_i x_i^2) / N - (R_p)^2 .\end{aligned}$$

Where $\sum_i \Delta x_i^2$ = sum of the square of the deviations of the ion ranges from the mean projected range with $\Delta x_i = (x_i - R_p)$.

"Straggling" is a word which is used in ion implantation in several ways, and care should be taken to determine the author's definition. Sometimes it is a synonym for variance and sometimes it is defined as the square root of the variance. In other cases an author, such as Winterbon, uses normalized definitions such as: Straggling = $\langle \Delta x_i^2 \rangle / \langle x \rangle^2$. We use the common definition that straggling is the square root of the variance:

$$\text{Straggling} \equiv \sigma = [(\sum_i x_i^2) / N - R_p^2]^{1/2} = \langle (\Delta x_i)^2 \rangle^{1/2} .$$

Radial

$$\text{Straggling} \equiv \sigma_r = [\sum_i (y_i^2 + z_i^2) / N - R_r^2]^{1/2} = \langle (\Delta r_i)^2 \rangle^{1/2} .$$

We define lateral straggling in the same way as range straggling above. (Lateral coordinates are sometimes called Transverse coordinates.) For a normally incident beam we can assume cylindrical symmetry of the range distribution, so the mean lateral projected range is zero (i.e. $R_y = 0$). Further, we average the Y and Z projected ranges to increase statistical accuracy:

Lateral

$$\text{Straggling} \equiv \sigma_y = [\sum_i ((|y_i| + |z_i|)/2)^2 / N]^{1/2} .$$

$$\begin{aligned}\text{Skewness} \equiv \gamma &= \langle \Delta x^3 \rangle / \langle \Delta x^2 \rangle^{3/2}, \\ &= \sum_i (x_i - R_p)^3 / (N\sigma^3), \\ &= \sum_i [x_i^3 - 3R_p x_i^2 + 3R_p^2 x_i - R_p^3] / (N\sigma^3) .\end{aligned}$$

$$\begin{aligned}\text{Kurtosis} \equiv \beta &= \langle \Delta x^4 \rangle / \langle \Delta x^2 \rangle^2, \\ &= \sum_i (x_i - R_p)^4 / (N\sigma^4), \\ &= \sum_i [x_i^4 - 4R_p x_i^3 + 6R_p^2 x_i^2 - 4R_p^3 x_i + R_p^4] / (N\sigma^4) .\end{aligned}$$

TRIM uses the last variations shown above for the calculation of skewness and kurtosis.

In the above TRIM definitions, the projected range and the straggling have dimensions of length, while the higher moments, skewness and kurtosis, are dimensionless. Note that we do NOT include backscattered or transmitted ions in our moment calculations, in contrast to some theorists. The skewness tells whether the peak is skewed towards the surface (negative values) or away from the surface (positive values). Another way of stating this is that negative skewness indicates that the most probable depth (the peak position) is greater than the mean depth, and positive values indicate the reverse. Kurtosis indicates the extent of the distribution tails, with a value of 3.0 indicating a Gaussian distribution. Since both the shallow and deep tails contribute, no simple rule indicates what variation from 3.0 means about the ion distribution. In general, values from 0 to 3 indicate abbreviated tails, and values above 3 indicate broad tails. The papers which most clearly discuss how to regenerate complete distributions from statistical moments are : K. B. Winterbon, A.E.C.L. Reports #4829 (1972) and #4832 (1972), and especially CRNL-1817 (1978), available from the Chalk River Nuclear Laboratory, Chalk River, Ontario, Canada, K0J-1J0.

What Causes Anomalous Peaks and Dips at Layer Edges ?

There are several reasons that small artifacts occur at layer edges, and these are all associated with inconsistencies between two parts of TRIM :

1. The TRIM "Viewing Window", which is the portion of the target displayed on the screen, is divided into 100 equal segments or bins. (Your target may be much larger than the data window, but only the collision data within the window is saved. The position of the data window within the target is set in the TRIM input program.)
2. Atoms in a target are not randomly spaced, even in amorphous targets. There is a minimum distance between atoms, and once a collision occurs the ion must travel at least one monolayer to reach the next atom. TRIM defines a monolayer as the inverse cube root of the atomic density of a layer, $N^{-1/3}$, where the density, N, has units of atoms/cm³. Hence silicon,

with a density of 5×10^{22} atoms/cm³, has a layer thickness of $(5 \times 10^{22})^{1/3} = 2.7$ Å. If your layer thickness is not a multiple of this monolayer thickness, there may be a small error at the bottom edge.

An accounting problem occurs when the ion jumps from one layer to another, and TRIM must decide where to place the collision data. Typically, the following conditions cause small problems

- If your target layers do not end exactly at a data bin edge, then that bin consists of two different materials, and TRIM will assume one or the other based on the current ion's trajectory at that bin. When you input a new target, you are warned of this problem if it occurs.
- If a data bin is less than one monolayer wide, then TRIM may not treat it accurately since calculation distances are never smaller than one monolayer. The same occurs to a lesser extent if a thin layer, say 20Å wide, is not an integral number of monolayers wide.
- Thin layers at the surface, or at the bottom of a target, may cause problems if ions leave the target. The point where the target ends is not clean if this layer is less than many monolayers thick, since TRIM works in monolayer steps, and the surface appears "smoother" to an ion moving almost parallel to the surface than to one moving perpendicular to the surface. Once the next ion step is found to be outside the target there are no further collisions. So inaccuracies of the order of one monolayer are probable. The special TRIM calculation for sputtering takes special precautions to prevent these errors from occurring at the target surface.

The small dips and peaks may extend more than one data bin at a layer's edge. TRIM runs efficiently because the ion can jump many monolayers between collisions, and the intermediate collisions are approximated. We suggest that you do not worry about small peaks and dips at layer edges, they are not worth the trouble to try to avoid, and just average the final curves.

Running TRIM in Batch mode: TRIM.IN

The input data file which controls the TRIM calculation is called TRIM.IN. It is normally created by the TRIM Setup window. Once you have set up a TRIM calculation, you may wish to only change a few parameters, e.g. the ion's energy and angle for simulation of an ion plasma bombarding a solid surface. You will need to run software which executes a few simple steps as in the following example.

- (1) Setup the first TRIM calculation with a fixed “Number of Total Ions” = 100 (as an example). This TRIM calculation must specify the highest energy that the ion will have in any subsequent calculation. Run the TRIM calculation until it completes all the ions.
- (2) Edit the file TRIM.IN in the SRIM root directory. Change the ion energy and angle. The new energy may not be larger than that of the initial calculation. Increase the total number of ions (line 3) from 100 to 200 to calculate for another 100 ions.
- (3) Edit the file TRIMAUTO in the SRIM root directory. Replace the “0” in the first line with a “2”. This will make TRIM run without any keyboard inputs until it reaches the end of the next calculation (Ions = 100 in this example). It will also add the next calculation results to the previous ones. There is an explanation of this procedure in the file TRIMAUTO.txt.
- (4) Execute the file TRIM.exe in the SRIM directory. This will run TRIM with the new setup (in this example with a changed ion energy and angle) and add the results to the old calculation results.
- (5) Continue with steps 2-4 until you have completed all various of ion energy and angle. TRIM will not require any keyboard inputs during the calculation, so by automating steps 2-4 you will make TRIM sum all the calculations into the standard files, and the plots will show the summed results.

Below are examples of TRIM.IN. Note that the datafile contains lines of comments (which are not

used). The comment lines are show in *Italics*, while the input data are shown in **Bold**. Only the **Bold** items are used by TRIM. The numerical data has free format, with almost all standard formats accepted (e.g. 99 or 99.00 or 99E0 or 0.99E2). This file is also described in detail in Chapter 9.

Table 8-5 - Datafile TRIM.IN for Au(100keV) into Lead(2000Å).

```

==> SRIM-2006.02 This file controls TRIM Calculations.
Ion: Z1 , M1, Energy (keV), Angle,Number,Bragg Corr.AutoSave Number.
79 197 100 0 99999 0 100
Cascades(l=No;2=Full;3=Spull;4-5=Ions;6-7=Neutrons), Random Number Seed, Reminders
2 0 0
Diskfiles (0=no,1=yes): Ranges, Backscatt, Transmit, Sputtered, Collisions, Special EXYZ.txt file
0 0 0
Target material : Number of Elements & Layers
"Au(100 keV) into Pb (3000 Vacancies/Ion)" 1 1
PlotType (0-5); Plot Depths: Xmin, Xmax(Ang.) [= 0 0 for Viewing Full Target]
1 0 0
Target Elements: Z Mass(amu)
Atom 1 = Pb = 82 208
Layer Layer Name / Width Density Pb(82)
Numb. Description (Ang) (g/cm3) Stoich
1 "Lead" 2000 1.14 1
Target layer phases (0=Solid, 1=Gas)
0
Target Compound Corrections (Bragg)
1
Individual target atom displacement energies (eV)
21
Individual target atom lattice binding energies (eV)
2.1
Individual target atom surface binding energies (eV)
3.1
Stopping Power Version (l=2006, 0=2006)
0

```

The above TRIM.IN is obtained by executing the TRIM Setup window, and selecting the DEMO for “Au (100 keV) in Pb”. In Table 8-5: Note: (This file is explained in much more detail in Ch. 9.)

- Lines 1 and 2 are comments
- Line 3 = the data for the ion, showing atomic number, mass (amu), energy (keV), incident angle to the surface (degrees), Bragg correction to stopping (0=none), and the Autosave number (save calculation after every 100 ions).
- Line 4 is a comment
- Line 5 = Type of calculation (full calculation of cascades), and the random seed number.
- Line 6 is a comment
- Line 7 = Automatic disk datafiles of individual ion data (0=no, 1=yes).
- Line 8 is a comment
- Line 9 = Target description (in quotes), number of elements and number of layers in target.
- Line 10 is a comment
- Line 11 = Plot display type for ion animation during calculation; Viewing window (Angstroms) for calculation (this window defines the 100 bins for the average ion collisional data; 0 0= show entire target).

- Line 14 is a comment
- Line 15+ = (first 14 characters are ignored) then target element atomic number and weight (amu). Target elements are listed until they reach the total number of elements in target as specified in Line 9. Then two lines of comments about target, then the target data: Layer number, Layer description (in quotes), Layer width (Å), Layer density (g/cm³), Stoichiometry of each target element. After all target layers are complete, the final data line specifies the target as 0=Solid, or 1=Gas.

Note that after comment Line 14, *Target Elements: Z, Mass (amu)*, the number of data lines varies with the number of target elements and the number of target layers. TRIM expects that the number of these lines will conform with the data stated in line 9, *Number of Elements & Layers*. See next two examples of TRIM.IN for the format.

- Last 10 lines = Stopping corrections for special bonding in compound targets. Target energies (eV) for lattice binding, surface binding and displacement (one displacement energy for each target element). Finally, optional selection of stopping powers to be used in TRIM. See Ch.9.

Table 8-6 - Datafile TRIM.IN for DEMO: Xe(100 keV) into Si/Pt/Si.

```
--> SRIM-2008.01 This file controls TRIM Calculations.
Ion: Z1 , M1, Energy (keV), Angle,Number,Bragg Corr,AutoSave Number.
      54   131   100      0  999999      0  10000
Cascades(1=No;2=Full;3=Sputt;4-5=Ions;6-7=Neutrons), Random Number Seed, Reminders
      2          0          0
Diskfiles (0=no,1=yes): Ranges, Backscatt, Transmit, Sputtered,
Collisions(1=Ion;2=Ion+Recoils), Special EXYZ.txt file
      0          0          0          0          0
Target material : Number of Elements & Layers
"Xe into Si/Pt/Si [Mixing a Marker]"    3    3
PlotType(0-5);Plot Depths: Xmin, Xmax(Ang.)
      0          300
Target Elements: Z   Mass (amu)
Atom 1 = Si =      14     28
Atom 2 = Pt =      78    195
Atom 3 = Si =      14     28
Layer   Layer Name  Width Density  Si(14)  Pt(78)  Si(14)
Numb.  Description  (Ang) (g/cm3)  Stoich  Stoich  Stoich
  1    "Silicon"    200    2.33     1       0       0
  2    "Platinum"   30     21.4     0       1       0
  3    "Silicon"    70     2.33     0       0       1
Target layer phases (0=Solid, 1=Gas)
  0   0   0
Target Compound Corrections (Bragg)
  1   1   1
Individual target atom displacement energies (eV)
  21   22   21
Individual target atom lattice binding energies (eV)
  2.1   2.2   2.1
Individual target atom surface binding energies (eV)
  3.1   3.2   3.1
Stopping Power Version (1=2008, 0=2003)
  1
```

The description of this TRIM.IN file is the same as the previous one, except that it has two different elements in the target with three layers. Note that there is a further explanation of TRIM.IN in Chapter 9, which contains more details.

Table 8-7 - Datafile TRIM.IN for Demo: H(50 MeV) into Biological Target

```
----- Input Data File for TRIM -----
Ion:Z1, M1, Energy (keV), Angle, Number, Bragg Corr, AutoSave Number.
    1 1.01      50000     00.0    99999    0.00      500
Cascades(1=No; 2=Full; 3=Sputt.; 4,5= Neutrons), Random Number Seed
                                1                      0
Diskfiles(0=no,1=yes) Ranges Backscatt Transmit Sputtered, Recoils
                                0          0          0          0          0
Target material :           Number of Elements & Layers
" H(50MeV) Irradiation of Thyroid"   12            5
Target Energies (eV): Binding, Surface, Individual Displacement
                    2.000  4.000 15 15 15 15 15 15 15 15 15 15 15 15 15
PlotType(0-5); Plot Depths: Xmin, Xmax(A) [=0 View Full Target]
                                1          000000  000000
Target Elements: Z      Mass (amu)
Atom 1 = H =      1      1.0080
Atom 2 = C =      6      12.011
Atom 3 = N =      7      14.007
Atom 4 = O =      8      15.999
Atom 5 = Na =     11     22.990
Atom 6 = Mg =     12     24.305
Atom 7 = P =      15     30.974
Atom 8 = S =      16     32.066
Atom 9 = Cl =     17     35.453
Atom10 = K =      19     39.098
Atom11 = Ca =     20     40.080
Atom12 = Fe =     26     55.847
Layer Layer Name or Width Density H( 1) C( 6) N( 7) O( 8) Na(11) Mg(12) P(15)
Numb. Description (A) (g/cm3) Stoich Stoich Stoich Stoich
1 "Skin-Human #3" 12000.E+03 1.090E+00 0.62744 0.08237 0.01654 0.27202 0.00054
2 "Adipose Tissue" 40000.E+03 9.200E-01 0.63482 0.28408 0.00306 0.07775 0.00012
3 "Skel. Muscle #2" 60000.E+03 1.050E+00 0.63169 0.07432 0.01515 0.27703 0.00000.
4 "Thyroid (W&W)" 14000.E+04 1.050E+00 0.63870 0.06133 0.01061 0.28826 0.00054
5 "Skel. Muscle #1" 20000.E+03 1.050E+00 0.63169 0.07432 0.01515 0.27703 0.00000
0 Target is a SOLID
NOTE : Data for atoms S, Cl, K, Ca and Fe omitted in target description
above. Also, final 12 lines of TRIM.IN are omitted. See Table 8-6. For a full
TRIM.IN datafile, run the DEMO included in the TRIM Setup window.
```

This TRIM.IN shows a most complicated target, with twelve elements in five layers. This is a special input for biological targets. The target description shown is truncated at the right edge: the datafile actually continues to include the stoichiometry of S, Cl, K, Ca and Fe atoms. If you wish to make up a manual input file, like the above, first generate this file with the standard TRIM Input window and use the TRIM.IN file which is generated as a template.

Changing TRIM Plot Colors (TRIM.cfg)

All of the TRIM plots and colors are set using the datafile: *..Data/TRIM.cfg*, see Table 8-8. Typical default settings are shown in this Table. If you change a TRIM color, e.g. using the color tables available in the TRIM Calculation window, then when you save TRIM these changes become the default values.

Table 8-8 -Datafile ..Data/TRIM.cfg (TRIM Plot Colors)

[Ion Colors - MOVE, STOP]
255 0
[12 Recoil Colors - MOVE, STOP]
1 6487906 837122
2 15982183 16417654
3 16744703 12519886
4 16777088 13814035
5 13159423 9673727
6 16760769 16711680
7 8421376 65280
8 6422724 12615935
9 8388736 16716287
10 4755857 8700353
11 9408399 12566463
12 255 0
[Distribution Plot Labels - SIZE, COLOR]
6 8388608
[4 Distribution Plot Colors]
255 8388608 65280 16776960
[Plot Background, Outer Box, Axes, Layer Lines, Layer Names]
16777215 255 0 0
Maximum number of secondary recoils (default=20000)
20000
Note: 100k recoils requires 2MB of memory, 1M recoils requires 35MB.

The colors are identified by standard PC color codes, which are too complicated to review here. For example, the plot of the Ion Color is RED (#255) when it has a collision, and BLACK (#000) for the point where it stops. The target recoil atoms are identified by numbers 1-12 in the next section of TRIM.cfg. However, to change colors, it is easiest to start a TRIM calculation, and then click on the button **Pause TRIM** at the top of the TRIM Calculation window. Then press **Change TRIM**. Expand the sub-window called **Target Data** and you will see bars of colors for each of the target elements. Click on any one, and you can select a new color from a color grid. Change as many colors as you want, and see how they look by pressing **Continue** and opening a plot. When you finally stop the TRIM calculation and save it, these new colors will be stored as the default recoil atom colors.

Changing The Maximum Size of Recoil Cascades (TRIM.cfg)

Using the datafile: *..Data/TRIM.cfg* (see Table 8-8) one can modify the maximum number of recoiling atoms in a detailed collision calculation. The default is 20,000, i.e. up to 20,000 recoils can be counted in a single recoil cascade. The ion may impact many atoms as it goes into the target. When it hits an atom and transfers a very large amount of energy, the recoiling atom may hit

thousands of other atoms before it stops. TRIM stores the data about each collision and each recoiling atom, until the prime recoil (the recoil that starts the cascade) is stopped. This storage of the kinetics of thousands of recoils takes a lot of computer memory, and so the default maximum is set at 20,000. However, this value can be increased. TRIM has been tested with a recoil cascade limit of 10,000,000 without any problems.

Incorporating SRIM into Other Software (SRIM Module)

"*SR Module.exe*" is a program that can run under the control of other programs that needs stopping powers and ranges. When it is executed, it reads a control file and then outputs a new file containing stopping powers and ranges. This output can then be used by the other programs. Since it has no user interface, it is invisible to the user.

SR-Module uses the same controls as the "*Tables of Stopping and Ranges*" which can be called from the SRIM Title Page. When "*Tables of Stopping and Ranges*" is run, the Setup program creates a file called "*SR.IN*" in the SRIM directory. It then calculates the requested stopping powers and ranges and places them in a separate file in the directory "*/SRIM Outputs*".

To use SR-Module, first look in the SRIM sub-directory ".../SR Module". You will find a program "*SR Module.exe*", and data files: *SCOEF03.dat*, *SNUC03.dat* and *VERSION*. The first two are datafiles for the stopping and range program and the third contains the current version of SRIM.

You will also find a copy of the control file "*SR.IN*". It contains information such as:

Table 8-9 - File SR.IN controlling Stopping and Range Tables

```
1  Stopping/Range Input Data (Number-format: Period=Decimal Point)
2  ---Output File Name
3  "Hydrogen in Water_Liquid"
4  ---Ion(Z), Ion Mass(u)
5      1      1.008
6  ---Target Data: (Solid=0, Gas=1), Density(g/cm3), Compound Corr.
7          0          1          1
8  ---Number of Target Elements
9      2
10 ---Target Elements: (Z), Target name, Stoich, Target Mass(u)
11           1 "Hydrogen"    2     1.008
12           8 "Oxygen"     "     1     15.999
13 ---Output Stopping Units (1-8)
14     5
15 ---Ion Energy : E-Min(keV), E-Max(keV)
16     10      10000
```

SR Module reads this file and generates a file called "Hydrogen in Water_Liquid" containing the stopping and range of H ions into water from 10 keV to 10 MeV. The lines of the above file are explained below:

- 1 Title line. Note that all numbers **MUST** use a period as a decimal point.
- 2 Comment describing the next input line.
- 3 Name of the Output File
- 4 Comment describing the next input line.
- 5 Ion Atomic Number and Mass

6 Comment describing the next input line.
7 Target Data: [Target is a solid or gas], [Target Density- g/cm3], [Compound Correction]
8 Comment describing the next input line.
9 Number of target atoms (up to 100)
10 Comment describing the next input line.
11 Tgt Atom #1: Atomic Number, Name, Atomic Mass
12 Tgt Atom #2: Atomic Number, Name, Atomic Mass
13 Comment describing the next input line.
14 Output Stopping Units (1-8) [see listing of units below]
15 Comment describing the next input line.
16 Ion Energy Range, keV, of output tables (2 numbers)

To understand the details of this file, go to the SRIM program "*Tables of Stopping and Ranges*" and read the various HELP files. Execute this SRIM program to calculate a new Table, and then exit and look at the file "*SR.IN*". You can copy this control file into the subdirectory "..*SR Module*" and then execute "*SR Module.exe*". You will find that it generates the same table, but with no input from the user. This new file will be saved into the current directory of "*SR Module.exe*".

In the input file, the next to last item is "Output Stopping Units (1-8)":

- (1) - eV / Angstrom
- (2) - keV / micron
- (3) - MeV / mm
- (4) - keV / (ug/cm2)
- (5) - MeV / (mg/cm2) = keV / (ug/cm2)
- (6) - keV / (mg/cm2) = eV / (ug/cm2) = MeV / (g/cm2)
- (7) - eV / (IE15 atoms/cm2)
- (8) - L.S.S. reduced units

Use the SRIM program to generate several Tables, and look at each of the "*SR.IN*" files. These will guide you to make new control *SR.IN* files.

LEGAL NOTICE:

The software described in this file "*SR Module.exe*" is covered by the same legal notice as SRIM. It may be freely copied and used for any non-commercial application. Its inclusion in any commercial software requires a license from SRIM.org. See the legal notice "*/Data/Legal.rif*" in the www.SRIM.org directory for full details.

Using "*SR Module*" to generate customized tables of Stopping and Range.

When you produce the Tables, you specify the starting and final ion energy, but you do not control the spacing of the energy increments. However, you can generate stopping powers for any list of energies using "*SR Module.exe*" by using the following change to the above "*SR.IN*" file.

Line 15: --Ion Energy : E-Min(keV), E-Max(keV)
Line 16: 0 0
Line 17: 1.02
Line 18: 2.55
Line 19: 3.98

**Line 20: 0
(Additional Lines Omitted)**

Line 16 used to contain the lowest and highest ion energies of SR.IN as shown in Table 8-9. Now it contains " 0 0 ". This indicates that the lines following this line will contain a list of specific energies. Enter your list of energies (up to 1000) and terminate the list with a " 0 " as shown above. The list shown above will generate a simple Output File that will look like:

```
Ion = Hydrogen , Mass = 1.008
Tgt = H + O (Solid), Density = 1 g/cm3
Stopping Units = MeV/(mg/cm2)
Energy(keV) S(Elec) S(Nuc)
1.020E+00 1.751E-01 3.921E-02
2.550E+00 2.694E-01 2.391E-02
3.980E+00 3.264E-01 1.681E-02
```

The top four lines of this output file allow a check of the input values. Then there is a list with three values on each line: [Energy (keV)], [Electronic Stopping Power], [Nuclear Stopping Power]. This file can then be read into another program which requires stopping powers for specific ion energies.

Calculation Individual Atom-Atom Nuclear Stopping Powers

The nuclear stopping powers of *SR Module* will be slightly different from those in the full tables since these are improved values which will be incorporated into SRIM. The Table *SNUC03.dat* contains individually calculated nuclear stopping powers for all possible combinations of ion/targets, i.e. it contains 92 x 92 individual nuclear stopping powers. The nuclear stopping used in SRIM is a scaled stopping power, often called "ZBL" in the literature. This approximation is quite good for the interaction of atoms of approximately the same mass. However, it is somewhat inaccurate for ion / target atoms with quite different masses, especially H or He ions. The values produced by the SR tables described above are quite good because they are specific for the ion/target atoms specified, and do not come from a "universal" formula.

LEGAL NOTICE:

The software described in this file "*SR Module.exe*" is covered by the same legal notice as SRIM. It may be freely copied and used for any non-commercial application. Its inclusion in any commercial software requires a license from SRIM.org. See the legal notice "*/Data/Legal.rtf*" in the www.SRIM.org directory for full details.

Citations for Chapter 8

1. Kinchin and R. S. Pease, Rep. Prog. Phys., vol. 18, 1 (1955).
2. W. Mechbach and S. K. Allison, Phys. Rev. **132**, 294 (1963).
3. P. Sigmund, Rad. Eff., vol. 1, 15 (1969).
4. J. B. Winterbon, A.E.C.L. Reports #4829 (1972) and #4832 (1972), and especially CRNL-1817 (1978), available from the Chalk River Nuclear Laboratory, Chalk River, Ontario, Canada, K0J-1J0.
5. M. J. Norgett, M. T. Robinson and I. M. Torrens, Nucl. Eng. Design, vol. 33, 50 (1974).
6. B. Winterbon ("Ion Implantation Range and Energy Distributions", vol. 2, Plenum Press, 1975).
7. International Commission on Radiation Units - Report ICRU- 33, "Radiation Quantities and Units", 1980, ICRU, Bethesda, MD, USA.
8. International Commission on Radiation Units - Report ICRU- 33, "Radiation Quantities and Units", 1980, ICRU, Bethesda, MD, USA.
9. International Commission on Radiation Units - Report ICRU- 37, "Stopping Powers for Electrons and Positrons", 1984, ICRU, Bethesda, MD, USA.
10. J. P. Biersack and W. Eckstein, Appl. Phys., A34, 73-94 (1984)
11. International Commission on Radiation Units - Report ICRU- 37, "Stopping Powers for Electrons and Positrons", 1984, ICRU, Bethesda, MD, USA.
12. H.Q. Woodward and D. R. White, British J. of Radiology, vol. 59, 1209-1219 (1986).
13. Fishman & Moore, S.I.A.M.- J.S.C., vol. 7, 24 (1986)).
14. H.Q. Woodward and D. R. White, British J. of Radiology, vol. 59, 1209-1219 (1986).
15. P. L'Ecuyer, C.A.C.M., vol. 31, 742-749, 774-776 (1988), "An Efficient and Portable Combined Random Number Generator".
16. "*The Stopping of Ions in Compounds*", by J. F. Ziegler and J. M. Manoyan, published in Nuclear Instruments and Methods, Vol. B35, 215-228 (1989).
17. J. F. Ziegler and J. M. Manoyan, Nuclear Inst. and Meth., **B35**, 215-228 (1989).
18. G. Schiwietz, Phys. Rev. **42A**, 296, (1990)
19. P. Bauer, F. Kastner, A. Arnaud, A. Salin, P. D. Fainstein, V. H. Ponce and P. M. Echenique, Phys. Rev Lett, **69**, 1137 (1992)
20. International Commission on Radiation Units - Report ICRU- 49, "Stopping Powers and Ranges for Protons and Alpha Particles", 1993, ICRU, Bethesda, MD, USA.
21. W. Mechbach and S. K. Allison, Phys. Rev. **132**, 294 (1963).
22. G. Schiwietz, Phys. Rev. **42A**, 296, (1990).
23. J. F. Ziegler and J. M. Manoyan, Nuclear Inst. and Meth., **B35**, 215-228 (1989).

9 - TRIM: Output Files *

The output of TRIM can be viewed in plots (while the calculation is proceeding) and also in detailed numerical files. The plots are especially useful to see if the calculation is proceeding as expected, but are usually limited in resolution. Most of the datafiles can be requested in the Setup Window for TRIM (menus at the bottom of the window) or can be requested during the calculation. All calculated averages are made over the entire calculation, regardless of when they are requested. That is, if you request a plot of ion ranges after the 100th ion, it will include all the previous ions. Other types of datafiles show details of each ion's interactions, and are started with the file is selected, and continues filing data on each following ion until the file is stopped. If you leave the plots or datafiles "live" during a calculation, they may significantly slow down TRIM.

Chapter Contents

9 - TRIM: Output Files	9-1
Brief Summary of TRIM Plots and Data Files	9-2
<i>Ion/Recoil Distribution Plots and Files:</i>	9-2
<i>Target Damage Plots and Files:</i>	9-3
<i>Full Calculation Details (Datafile COLLISON.txt)</i>	9-3
Ion / Target Example used for Chapter's Output Plots and Files	9-4
Ion Range Distribution and Recoil Atom Distributions.....	9-9
<i>3-Dimensional Ion Range Distributions</i>	9-13
<i>Datafile of Ion Trajectory and Energy in the Target</i>	9-14
<i>Lateral Ion Range Distribution</i>	9-15
<i>3-D plots of the Ion's Electronic Energy Loss</i>	9-17
Backscattered Ions	9-18
Transmitted Ions	9-20
Sputtered Target Atoms	9-21
Combined Tables of Backscattering, Transmitted and Sputtering	9-24
<i>Ion's Energy Loss to the Target Electrons</i>	9-25
<i>Ion's Energy Loss to the Target Phonons</i>	9-26
<i>Energy Loss to Vacancy Production / Replacement Collisions</i>	9-27
<i>Energy Loss from Ions – Energy Loss Absorbed by Target Atoms</i>	9-31
Details of the Ion-Atom Collision Kinetics.....	9-33
Physics of Recoil Cascades.....	9-33
<i>COLLISON.txt - Type "A"– Ions and Quick Estimate of Damage</i>	9-35
<i>COLLISON.txt - Type "B"– Ions and Recoil Atoms (no cascade data)</i>	9-36
<i>COLLISON.txt - Type "C"– Ions, Recoil Atoms and Cascades</i>	9-38
Special Commands for a TRIM Calculation.....	9-39
<i>Changing TRIM Parameters during the Calculation</i>	9-39
<i>Changing TRIM Plots and Colors (TRIM.cfg)</i>	9-40
<i>Making TRIM Animated Plots</i>	9-40
<i>TRIM "Help, FAQ and Scientific Explanations"</i>	9-41

* Note: This text is Chapter 9 of the SRIM textbook (2008):

"SRIM – The Stopping and Range of Ions in Matter"

Note that TRIM can be stopped during the calculation, and basic parameters may be changed. This allows the user to focus the calculation on a specific problem without having to start over. To change TRIM during a calculation, click on the button ***Pause TRIM*** at the top of the TRIM Calculation window. Then press ***Change TRIM***. All the parameters that can be changed will have a yellow background, and it includes almost all Setup parameters. Make changes in the parameters, or in the colors used for the plots (clicking on the colors in the Target Data window will bring up a color-chart to use). When you are done, press ***End Edit*** and then ***Continue***. This procedure allows the user to modify a TRIM calculation simply, or to superimpose several calculations.

Brief Summary of TRIM Plots and Data Files

Note: All TRIM output datafiles are found in the sub-directory: ..//SRIM Outputs

Ion/Recoil Distribution Plots and Files:

- ***Ion Distribution*** : Both Plots and Datafiles are available. The ***Ion Distribution*** plot shows the ion distribution for all ions stopped within the target viewing window. (The ***Viewing Window*** is explained in Chapter 8) and its four statistical moments: range, straggling, skewness and kurtosis (see Chapter 8 for definitions of these moments). These moments are calculated for the entire target (not just the viewing window). The plot ordinate units are $(\text{atoms}/\text{cm}^3)/(\text{atoms}/\text{cm}^2)$. When this plot is multiplied by the ion dose (some authors call it a *fluence*) in units of $(\text{atoms}/\text{cm}^3)$ the plot is directly converted to a target density $(\text{atoms}/\text{cm}^3)$. See Figure 9-2 for a sample plot, and Table 9-3 and Table 9-4 for sample datafiles.
- ***Ion/Recoil Distribution***: Both Plots and Datafiles are available. The ***Ion/Recoil Distribution*** shows both the ion distribution and all target atom redistributions within the target window. See Figure 9-3 for a sample plot, and Table 9-3 and Table 9-4 for sample datafiles.
- ***Ion Ranges 3D***: Only datafiles are available. Some special applications require detailed 3-D data on the final position of each ion. This is an ACTIVE file, that stores the final three dimensional position of every ion while the calculation is proceeding. A new data line is appended to this file after each ion is finished. No data is recorded until the “***Ion Ranges (3-D data)***” is pressed in the TRIM Calculation Window. Data is then recorded until this box is cleared, or when the calculation ends. See example in Table 9-5.
- ***Ion Trajectory and Energy - 3D***: A datafile may be made of the ion’s position at various energies as it penetrates into the target. See example in Table 9-6. Also included is the electronic energy loss of the ion at that point, and the energy transferred in its last collision. This file allows later plotting of each ion’s trajectory and also a 3D file of the electronic energy loss of each ion.
- ***Ion Lateral Distribution***. Both Plots and Datafiles are available. As the beam penetrates the target, it spreads out. This lateral spread is evaluated for its first and second moments (the same idea as for the 4 moments of the ion range). See Figure 9-5 for a sample plot, and Table 9-7 for a typical datafile.

Ion Backscattering and Transmission Files

- ***Ion Backscattering*** - Some ions might have a strong collision near the surface of the target and may be backscattered back out of the surface of the target. These ions and their kinetic data (final energy and trajectory) can be found in the file ***BACKSCAT.txt*** which is shown in Table 9-9. There is no plot for this data.
- ***Transmitted Ions*** - Some ions reach the bottom of the target and exit through this surface.

These ions, and their kinetic data (final energy and trajectory) can be found in the file **TRANSMIT.txt** which is shown in Table 9-10. There is no plot for this data.

Target Sputtering Files

Ions can cause large cascades of recoil atoms, and their motion may make some of the target recoils exit back through the target surface. These atoms that leave the target surface are called *sputtered atoms*. The number of these atoms may be quite large, and they are often described in a *sputtering yield*, which is defined as the number of atoms sputtered per incident ion. See Figure 9-6 and Figure 9-7. Heavy energetic ions in light targets may cause large sputtering yields- an example is shown in the TRIM Demo “*Se in GaAs*” where the sputtering yield is about 4 target atoms sputtered per incident ion. The value of the sputtering yield is shown in the TRIM Calculation window during the calculation. Files of the energy and trajectory of sputtered atoms can be generated by checking the box “Sputtered Atoms” in either the TRIM Setup window or the TRIM Calculation window. An example of the data file **SPUTTER.txt** file is shown in Table 9-11 and Table 9-12.

Target Damage Plots and Files:

TRIM is often used to gain an understanding of the changes to the target under bombardment by ions. TRIM can be used for detailed examination of this target damage, but it must be interpreted with knowledge of two major TRIM limitations: (a) There is no build-up of ions or damage in the target. Every ion is calculated with the assumption of *zero dose*, i. e. the target is perfect and previous ions have no effect on subsequent ions. (b) The target temperature is 0°K, and there are no thermal effects changing the distribution of ions (thermal diffusion) or affecting the target damage (thermal annealing). Several experiments have been reported at very low temperatures (15 - 40°K) which validate the TRIM results, but show that thermal effects can be quite substantial. For example, for a low dose of ions into crystalline silicon, more than 99% of the target damage may anneal at room temperature. See Chapters 7 and 8 for extended discussions of the various types of damage.

- **Ion's Energy Loss to Electrons in the Target** – Both Plots and Datafiles are available. When ions penetrate into the target, they interact immediately with the target electrons, both single electrons and collectively. This interaction is very complicated, and TRIM uses the physics described in Chapter 3. The energy loss to electrons is collected for the TRIM Viewing Window (in 100 channels of information) and can be accessed during the calculation by selecting the *Ionization Plot* button, or the *Ionization File* button. The term “Ionization” is often used as a synonym for energy loss to electrons. Examples are shown in Figure 9-8 and Table 9-14. See also the above discussion of Table 9-6.
- **Ion's Energy Loss to Phonons in the Target** – Both Plots and Datafiles are available. See Figure 9-9 and Table 9-15.
- **Production of Vacancies in the Target.** – Both Plots and Datafiles are available. See Figure 9-10 and Table 9-16.
- **Production of Replacement Collisions in the Target.** – Both Plots and Datafiles are available. See Figure 9-12 and Table 9-17.

Full Calculation Details (Datafile **COLLISON.txt**)

Almost every detail of the ion's penetration into the target can be put into a special datafile, ..**SRIM Outputs/COLLISON.txt**, for later examination. This kind of file has various filters available to allow only special details to be recorded. See the later discussion in this chapter on “*Details of the Ion-Atom Collision Kinetics*”.

To get the most detailed file on ion interactions and all the recoil cascades, in the TRIM Setup window select “*Monolayer Collision Step*” in the Damage menu in the upper-right corner. Then check “Collision Details” in the same TRIM Setup window, at the bottom. When a sub-menu comes up and asks if details of the Recoils should also be kept, answer “Yes”.

This selection will overwhelm you with data. For the only the first 5 ions of the ion/target used in this chapter for an example (see Figure 9-1), TRIM will generate 94,000 numbers concerning 12,000 collisions. TRIM provides various filters to help you to screen this data. For example, if you are mostly interested in sampling the ion’s impact on the target, change your TRIM Setup selection from “*Monolayer Collision Step*” to “*Detailed Calculation with Full Damage Cascades*”, and the output datafile drops by 10% to 11,000 collisions. This is because TRIM now uses the Free Flight Path assumption. To further filter the data, if you care mostly about how the ion affects the targets, and you can ignore the recoil cascades, then when you are in the TRIM Setup window, select “Collision Details” and when the sub-menu asks to store data about the recoils, answer “No”. This will reduce the **COLLISON.txt** output for the first 5 ions by 90%, down to about 1,100 collisions.

Ion / Target Example used for Chapter’s Output Plots and Files

In most of the following examples, the calculation will be one of the TRIM Demo Examples available from the TRIM Setup window. This Demo example is a beam of Boron at 200 keV, into a three layer target, see Figure 9-1.

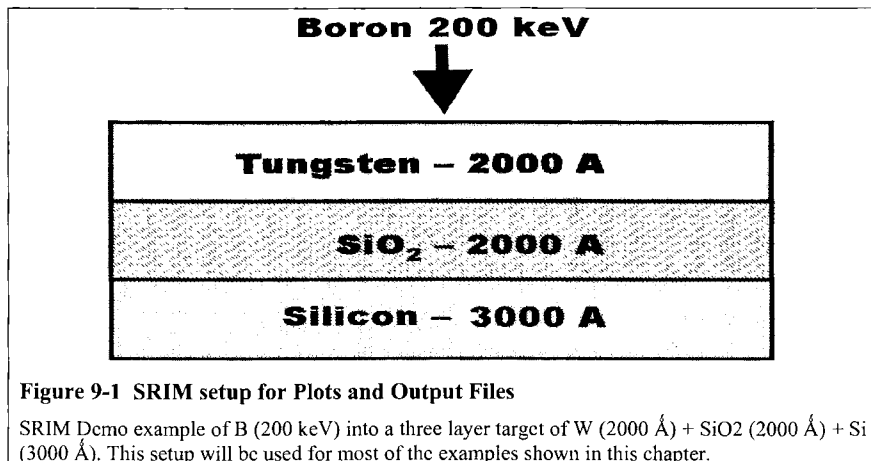


Figure 9-1 SRIM setup for Plots and Output Files

SRIM Demo example of B (200 keV) into a three layer target of W (2000 Å) + SiO₂ (2000 Å) + Si (3000 Å). This setup will be used for most of the examples shown in this chapter.

When you save plots or data files, it is often useful to save the datafile that contains all the details of the calculation. This file can be found in two places in the SRIM directory. The original TRIM Setup data is in the file TRIM.IN, located in the root SRIM direction, Table 9-1. The datafile TRIM.IN is also described in some detail in Chapter 8. Once you start a TRIM calculation, another version is at: **..SRIM Restore/TDATA.sav**, Table 9-2. This file contains all the details of the TRIM calculation, and will include any changes you made to the ion/target parameters during the calculation. This file is created when you stop TRIM and store the results for later use.

Table 9-1 – TRIM.IN contains the Setup parameters for TRIM

```

====> SRIM-2008.01 This file controls TRIM Calculations.
Ion: Z1 , M1, Energy (keV), Angle,Number,Bragg Corr,AutoSave Number.
      5       11      200      0     20000      0      5000
Cascades(1=No;2=Full;3=Sputt;4-5=Ions;6-7=Neutrons), Random Number Seed
                           2                               0
Diskfiles (0=no,1=yes): Ranges, Backscatt, Transmit, Sputtered,
    Collisions(1=Ion;2=Ion+Recoils), Special EXYZ.txt file
          0       0       0       1       0       0
Target material : Number of Elements & Layers
"B" into W/SiO2/Silicon (Double Peak)           "        4           3
PlotType (0-5); Plot Depths: Xmin, Xmax(A) [=0 0 for Viewing Full Target]
          1           0       300
Target Elements:   Z   Mass(amu)
Atom 1 = W =      74      183
Atom 2 = Si =     14       28
Atom 3 = O =       8       16
Atom 4 = Si =     14       28
Layer   Layer Name /   Width   Density   W(74)   Si(14)   O(8)   Si(14)
Numb.   Description   (Ang)   (g/cm3)   Stoich   Stoich   Stoich   Stoich
  1      "Tungsten"   2000    19.3      1        0        0        0
  2      "SiO@2"      2000    2.33      0       .333     .666      0
  3      "Silicon"    2000    2.32      0        0        0        1
Target layer phases (0=Solid, 1=Gas)
0 0 0
Target Compound Corrections (Bragg)
  1   1   1
Individual target atom displacement energies (eV)
  21   22   23   22
Individual target atom lattice binding energies (eV)
  2.1   2.2   2.3   2.2
Individual target atom surface binding energies (eV)
  3.1   3.2   3.3   3.2
Stopping Power Version (1=2006, 0=2006)
  0

```

Briefly, TRIM.IN's information is mostly in two-line increments. The first line of each pair is a text explanation and does not contain data, and it is followed by a data line which contains the data values.

The first line of TRIM.IN contains the version number of the SRIM software being used:

```
====> SRIM-2008.01 This file controls TRIM Calculations.
```

The 2nd and 3rd lines contain information about the ion (atomic number, mass, energy and incident angle to the target), the total ions to calculate (20,000), a term called “Bragg Corr” that is not used, and the AutoSave number (the TRIM calculation is automatically saved after this number of ions).

```
Ion: Z1 , M1, Energy (keV), Angle,Number,Bragg Corr,AutoSave Number.
      5       11      200      0     20000      0      5000
```

(Note: Several parameters in TRIM are “unused”, which means they are left-over from earlier TRIM versions and are kept as dummy variables so TRIM is compatible with other software.)

The next two lines contain parameters for the calculation: (a) the *Cascades* number declares the type of Damage Calculation (upper right menu of the TRIM Setup window), and (b) a random number seed (use zero to use the default value)

Cascades (1=No;2=Full;3=Sputt;4-5=Ions;6-7=Neutrons)	Random Number Seed
2	0

The next two lines contain instructions about any datafiles that should be created when TRIM starts (these datafiles are described in the menu at the bottom of the TRIM Setup window). Note that the explanation line is quite long and is duplicated here as two lines of text. In the data line, a "0" means no file, and a "1" asks that this file be created. The EXYZ parameter may be a number such as 1000 - see the section on this file later in this chapter.

Diskfiles (0=no,1=yes): Ranges, Backscatt, Transmit, Sputtered,
Collisions(1=Ion;2=Ion+Recoils), Special EXYZ.txt file
0 0 0 1 0 0

The next data line contains (a) a description of the calculation that will be included in every datafile that is produced by TRIM (must be in quotes), and (b) the number of elements in the target and the number of layers in the target. This latter information is necessary because the TRIM.IN file may have several lines of data depending on the number of elements and layers in the target.

Target material : Number of Elements & Layers
"B into W/SiO₂/Silicon (Double Peak)" 4 3

The next data line gives the type of initial plot that TRIM should display (use "0" for no plot), and the depths of the Viewing Window. This window can cover the entire target depth, or it can blow-up a small segment of the target so interactions may be seen with greater detail. To default the Viewing Window to the total target depth, you can use "0 0" as the depths.

PlotType (0-5); Plot Depths: Xmin, Xmax(A) [=0 0 for Viewing Full Target]
1 0 300

The next data lines defines the elements in the target. First is the chemical symbol, then the atomic number and finally the mass of each target atom. The number of lines must agree with the number of target elements declared above. The first 15 characters in each line are ignored (e.g. "Atom 1 = W = ") and are only included to make the file readable. Only the Z and Mass are used by TRIM. In this example, Si (Z=14) is included twice to allow separate analysis of their recoil distributions.

Target Elements: Z Mass (amu)
Atom 1 = W = 74 183
Atom 2 = Si = 14 28
Atom 3 = O = 8 16
Atom 4 = Si = 14 28

The next section describes each layer of the target. Note that the explanations takes up two lines of the TRIM.IN datafile. The "Layer Name" is a description (in quotes) that will appear in all the plots. In order to get subscripts use a "@" symbol as shown below for the SiO₂ layer. You can get a superscript by using the symbol "\$". If you use one of these in the middle of a layer name, then you can return the lettering to normal size using a "_" character. For example, "Fe@2_O@3" will create "Fe₂O₃" for that layer name. Following the layer name is the layer width (Å), the layer density (g/cm³), and the relative concentration of each of the elements in that layer of the target.

Layer Numb.	Layer Name / Description	Width (Ang)	Density (g/cm ³)	W(74) Stoich	Si(14) Stoich	O(8) Stoich	Si(14) Stoich
1	"Tungsten"	2000	19.3	1	0	0	0
2	"SiO ₂ "	2000	2.33	0	.333	.666	0
3	"Silicon"	2000	2.32	0	0	0	1

The next two lines give the phase state of the layers, i.e. whether each layer is a solid or a gas. This is used to calculate the stopping of the ions because, in general, gases have a higher stopping power than equivalent solids (see Chapter 5).

Target layer phases (0=Solid, 1=Gas)
0 0 0

The next two lines give any bonding corrections that need to be applied to the electronic stopping powers of the ion (see Chapter 5). A "1" means no special bonding correction.

Target Compound Corrections (Bragg)
1 1 1

The next section gives the damage parameters for the target layers. Each atom has a Displacement Energy, Binding Energy and Surface Binding Energy for each layer. All energies are in units of eV. If an atom does not appear in one layer, you can input "0" for the required energy. See Chapter 7, "TRIM Theory", for more details.

Individual target atom displacement energies (eV)
21 22 23 22
Individual target atom lattice binding energies (eV)
2.1 2.2 2.3 2.2
Individual target atom surface binding energies (eV)
3.1 3.2 3.3 3.2

The final input is a declaration of which version of SRIM's Stopping Powers to use. About every 5 years, the complete stopping theory of SRIM is revisited and all the experimental data of that period is added to the database. Any new ideas on stopping theory are also included. This results in new stopping power concepts, and variations in stopping powers from earlier versions of SRIM. The user is usually given the choice of using the new stopping powers, or an older version, for the first couple of years after a major change.

Stopping Power Version (1=2008, 0=2003)
1

A second file containing all the information of a TRIM calculation is found in:

./SRIM Restore/TDATA.sav, see Table 9-2.

This datafile is created when a TRIM calculation is interrupted, and includes data on the calculation in progress as well as any changes that the user has made to the TRIM parameters after the calculation has started. This file, Table 9-2, begins with the version number of SRIM, and the ID text that you gave to the calculation. It then relates the ion data: Atomic Number = 5 (boron), Mass = 11 amu, Energy = 200 keV, impacting at an angle of 0° to the target (perpendicular incidence).

The next item lists the current status of the calculation. This calculation was stopped at ion number 13,126 of a total of 99,999 requested ions. The calculation had an auto-save every 10,000 ions. This means that for a long calculation, after every 10,000 ions all the calculation is saved so if there is a computer failure, the calculation can be restarted at the point of this last save. The "Save Number" can have any value – it is part of your input in the TRIM Setup window. Finally, the calculation to date had zero transmitted ions (ions that went completely through the target) but there were 772 backscattered boron ions. The next lines start to record details at the instant the calculation was stopped. Most of this data is omitted in Table 9-2 to save space. This file is used when you press the button "*Resume Saved TRIM Calc*" in the SRIM Setup window. When this

button is selected, TRIM reads the data files of the last calculation, including *../SRIM Restore/TDATA.sav*, and can then resume the calculation from the point that it was last saved.

Table 9-2 -“*../SRIM Restore/TDATA.sav*” contains Restore data for TRIM

```
=====
          Saved DATA File for TRIM
          Changes will Modify Continued TRIM Calculations
=====

TRIM Version Number / Calculation Name
"SRIM-2008.01"      "B into W/SiO2/Silicon (Double Peak)      "
ION DATA:At.Numb, Mass(amu), Energy (keV) , Angle to Target
           5       11.0000  2.0000E+02    00.0
ION NUMB: Current, Total, AutoSave, Transmitted, Backscattered
        13126     99999   10000         0       772
=====

..... Calculation Data Omitted .....
===== TARGET MATERIAL =====
Layer # 1 - Tungsten
Layer # 1 - Bottom Depth=      2.E+03 A
Layer # 1- Density = 6.351E22 atoms/cm3 = 19.3 g/cm3
Layer # 1- W = 100 Atomic Percent = 50 Mass Percent
=====

Layer # 2 - SiO2
Layer # 2 - Bottom Depth=      4.E+03 A
Layer # 2- Density = 7.015E22 atoms/cm3 = 2.33 g/cm3
Layer # 2- Si = 33.3 Atomic Percent = 23.3 Mass Percent
Layer # 2- O = 66.6 Atomic Percent = 26.6 Mass Percent
=====

Layer # 3 - Silicon
Layer # 3 - Bottom Depth=      7.E+03 A
Layer # 3- Density = 4.989E22 atoms/cm3 = 2.32 g/cm3
Layer # 3- Si = 100 Atomic Percent = 50 Mass Percent
=====

Target energies for target atom = W
    Displacement = 21 eV, Binding = 2.1 eV, Surface = 3.1 eV
Target energies for target atom = Si
    Displacement = 22 eV, Binding = 2.2 eV, Surface = 3.2 eV
Target energies for target atom = O
    Displacement = 23 eV, Binding = 2.3 eV, Surface = 3.3 eV
=====

Depth Range of Tabulated Data= 000000.E+00 - 700000.E-02 Angstroms
=====

Total Ions calculated = 013126
Average Range      = 23697.E-01 Angstroms
Average Straggling = 13420.E-01 Angstroms
Average Vacancy/Ion = 94044.E-02
=====

Total Backscattered Ions= 772
```

Ion Range Distribution and Recoil Atom Distributions

Ion Distribution Plots

TRIM can determine the final distribution of ions that are directed into a complex target, like that shown in Figure 9-1. The calculation of the ion distribution can be also tabulated in a datafile on the computer, see Table 9-3 and Table 9-4. The target recoil atom distribution is also shown in Figure 9-3, and the numerical values are also found in Table 9-3 and Table 9-4. The plot and tables show the four moments of the final distribution (for definitions of the statistical terms: Range, Straggle, Skewness and Kurtosis, see Chapter 8 in the section "*TRIM Output: Straggling, Skewness and Kurtosis*").

During a TRIM calculation, when the *Ion Distribution "Plot"* box is checked, a range plot is created, Figure 9-2, showing the distribution of the ions in the target. This plot is updated after each ion. The continuous display of the plot slows down the calculation.

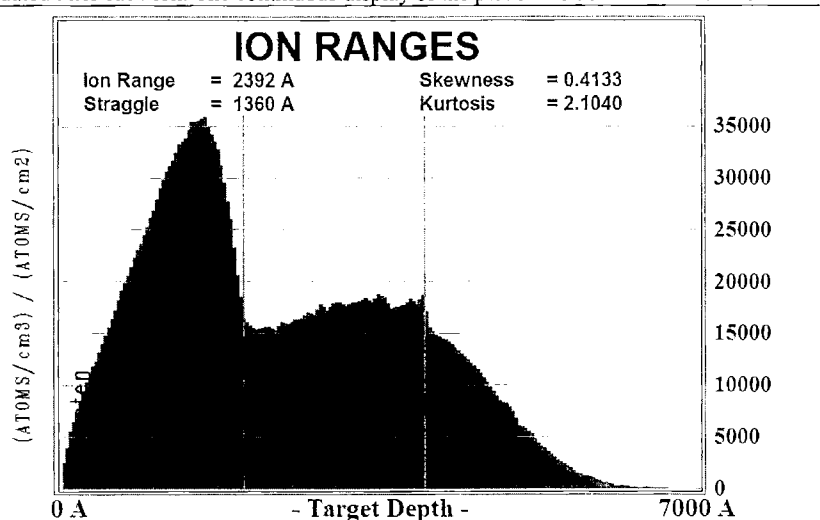


Figure 9-2 Plot of Ion Ranges

This plot is generated by requesting the plot "*Ion Distribution*" from the active TRIM screen. The example chosen is somewhat unusual in that the ion distribution forms a shallow peak, and then a broad peak deeper into the target. The plot ordinate has units: $(\text{Atoms}/\text{cm}^3)/(\text{Atoms}/\text{cm}^3)$. With these units, by multiplying by the ion dose (in units of Boron atoms/cm^3), the ordinate converts directly into a density distribution with units of $(\text{Boron atoms}/\text{cm}^3)$.

When the *Ion Distribution "File"* button is pressed, a datafile called RANGE.TXT is created (see example below in Table 9-3). This contains the range distribution (final depth) of the ions and all recoiling atoms in the TRIM plot window. The datafile RANGE.TXT is made once, when the button is pressed, and stores the result of the TRIM calculation up to that point in the calculation. (Note: A file which stores the final 3-D coordinates of every ion may be initiated using the separate

check-box called "Ion 3-D Ranges" This option is described later.)

The plot ordinate has units: $(\text{Atoms}/\text{cm}^3)/(\text{Atoms}/\text{cm}^2)$. With these units, by multiplying by the ion dose (in units of Boron atoms/cm²), the ordinate converts directly into a density distribution with units of (Boron atoms/cm³). The word *dose* is sometimes called *fluence*, and is also called the *areal density* of injected ions in units of atoms/cm².

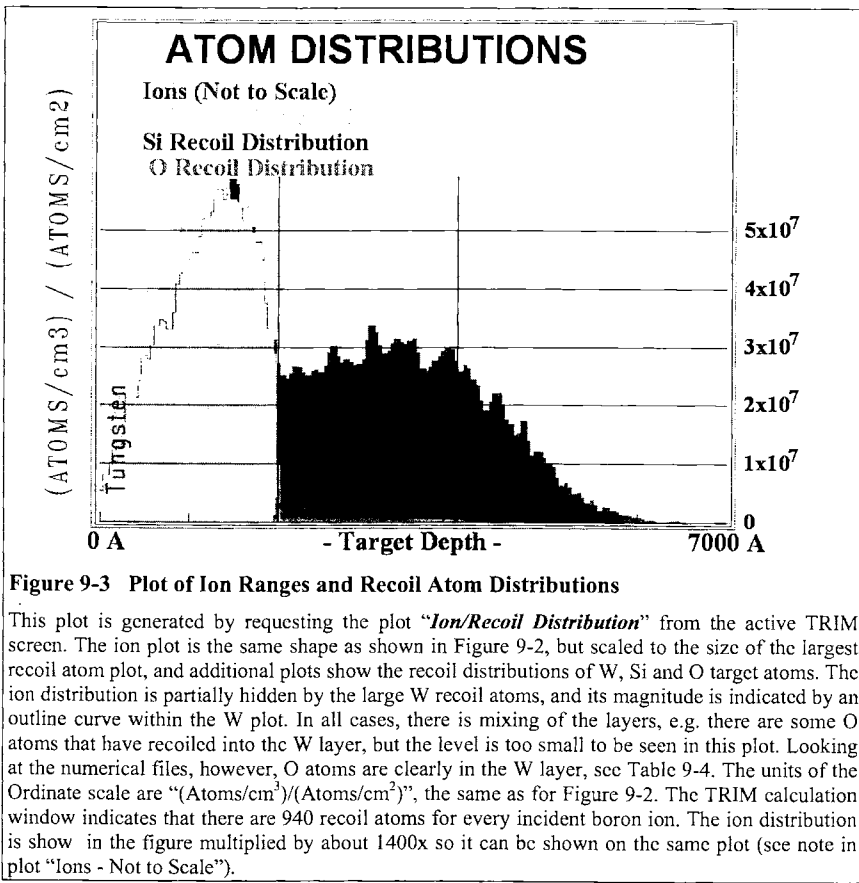


Figure 9-3 Plot of Ion Ranges and Recoil Atom Distributions

This plot is generated by requesting the plot "Ion/Recoil Distribution" from the active TRIM screen. The ion plot is the same shape as shown in Figure 9-2, but scaled to the size of the largest recoil atom plot, and additional plots show the recoil distributions of W, Si and O target atoms. The ion distribution is partially hidden by the large W recoil atoms, and its magnitude is indicated by an outline curve within the W plot. In all cases, there is mixing of the layers, e.g. there are some O atoms that have recoiled into the W layer, but the level is too small to be seen in this plot. Looking at the numerical files, however, O atoms are clearly in the W layer, see Table 9-4. The units of the Ordinate scale are " $(\text{Atoms}/\text{cm}^3)/(\text{Atoms}/\text{cm}^2)$ ", the same as for Figure 9-2. The TRIM calculation window indicates that there are 940 recoil atoms for every incident boron ion. The ion distribution is shown in the figure multiplied by about 1400x so it can be shown on the same plot (see note in plot "Ions - Not to Scale").

When the *Ion Distribution "File"* button is pressed during a TRIM calculation, a datafile called RANGE.TXT is created (see example below in Table 9-3). This file gives various statistical values for the distribution, including mean range, lateral range (width of the distribution), radial range (also width of the distribution using different statistics), straggling, skewness and kurtosis. All of these values are defined in Chapter 8, and also in the HELP beside the button in the TRIM window, and also at the HELP at the top of the TRIM Calculation window by clicking on the button "FAQs and Scientific Explanations". Look for the topic "Statistics of Range Distributions".

Table 9-3 shows the top part of the file ..**/SRIM Outputs/RANGE.txt**, which includes all the data on the ion and the target, as well as details about the calculation. For the case shown, a total of 13,073 ions were calculated, giving rather accurate ion and atom recoil distributions.

Table 9-3 - RANGE.TXT (File Header Information)

Below is the header at the top of the ..**/SRIM Outputs/RANGE.txt** file. It contains all the details of the ion, target and the calculation (e.g. a total of 13,073 ions had been calculated for this data).

```
===== B into W/SiO2/Silicon (Double Peak) =====
SRIM-2006.02
=====
ION and final RECOIL ATOM Distributions
See SRIM Outputs\TDATA.txt for calculation details
=====
See file : SRIM Outputs\TDATA.txt for details of calculation
Ion = B Energy = 200 keV
===== TARGET MATERIAL =====
Layer 1 : Tungsten
Layer Width=2.E+03A Layer #1- Density=6.351E22 atoms/cm3 = 19.3 g/cm3
Layer # 1- W = 100 Atomic Percent = 100 Mass Percent
Layer 2 : SiO@2
Layer Width=2.E+03A Layer #2- Density=7.015E22 atoms/cm3 = 2.33 g/cm3
Layer # 2- Si = 33.3 Atomic Percent = 46.6 Mass Percent
Layer # 2- O = 66.6 Atomic Percent = 53.3 Mass Percent
Layer 3 : Silicon
Layer Width=3.E+03A Layer #3- Density=4.989E22 atoms/cm3 = 2.32 g/cm3
Layer # 3- Si = 100 Atomic Percent = 100 Mass Percent
=====
Total Ions calculated =13073.00
Ion Average Range = 236.9E+01 A Straggling = 134.0E+01 A
Ion Lateral Range = 101.9E+01 A Straggling = 124.7E+01 A
Ion Radial Range = 160.0E+01 A Straggling = 743.3E+00 A
=====
Transmitted Ions =; Backscattered Ions =770
(These are not included in Skewness and Kurtosis below.)
Range Skewness = 000.3955 = [ $\Sigma (X-R_p)^3]/[N^*Straggle^3]$ 
Range Kurtosis = 002.1326 = [ $\Sigma (X-R_p)^4]/[N^*Straggle^4]$ 
---- Data Omitted from Table ----
```

Table 9-4 shows the bottom part of the file ..**/SRIM Outputs/RANGE.txt**. It shows the final numerical values for the ions and the recoiling target atoms. The table uses units: $(Atoms/cm^3)/(Atoms/cm^3)$. With these units, by multiplying by the ion dose (in units of Boron atoms/cm²), the ordinate converts directly into a density distribution with units of (Boron atoms/cm³). Note: the word **dose** is sometimes called **fluence**, and it is the **areal density of injected ions** usually in units of **Ions/cm²**.

Table 9-4 contains all the details of the final ion range distribution, and also the final distribution of recoiling target atoms. The table has exactly 100 rows. The target in the SRIM "viewing window" is divided into 100 sub-units. If the target window is 1000A deep, then each row

represents the atoms that end up in each 10Å of the target. For a 10,000Å target, each row would represent 100Å. For the below data, since the target is 7000Å thick, each row is 70Å deep.

It is possible to obtain high depth resolution for a thick target by changing the *viewing window* in the TRIM Setup window. The Viewing window does not have to coincide with the target thickness. For example, in one of the TRIM Demo calculations for “*He (5 MeV) in a Gas Ionization Detector*” the target is 50mm deep, but the viewing window is only the deepest 10mm, resulting in a range resolution of 0.1mm for tables like Table 9-4.

The plot ordinate has units: $(\text{Atoms}/\text{cm}^3)/(\text{Atoms}/\text{cm}^2)$. With these units, by multiplying by the ion dose (in units of Boron atoms/cm³), the ordinate converts directly into a density distribution with units of (Boron atoms/cm³).

Table 9-4 - RANGE.TXT (Ion and Recoil Atom Data Information)

---- Header Data Omitted from Table ----

Table Distribution Units are >>> $(\text{Atoms}/\text{cm}^3) / (\text{Atoms}/\text{cm}^2)$

DEPTH (Ang.)	B Ions	W Tgt. Atoms	Si Tgt. Atoms	O Tgt. Atoms
700100.E-04	1.7122E+03	2.0836E+07	0.0000E+00	0.0000E+00
140010.E-03	4.7086E+03	2.8225E+07	0.0000E+00	0.0000E+00
210010.E-03	7.1343E+03	2.9513E+07	0.0000E+00	0.0000E+00
280010.E-03	7.8477E+03	3.0463E+07	0.0000E+00	0.0000E+00
350010.E-03	1.2414E+04	3.3801E+07	0.0000E+00	0.0000E+00
420010.E-03	1.3555E+04	3.5089E+07	0.0000E+00	0.0000E+00
490010.E-03	1.1700E+04	3.7143E+07	0.0000E+00	0.0000E+00
560010.E-03	1.7978E+04	3.9666E+07	0.0000E+00	0.0000E+00
630010.E-03	1.6837E+04	4.0662E+07	0.0000E+00	0.0000E+00
700010.E-03	1.9263E+04	4.3655E+07	0.0000E+00	0.0000E+00
770010.E-03	2.2116E+04	4.6669E+07	0.0000E+00	0.0000E+00
840010.E-03	2.1403E+04	4.5595E+07	0.0000E+00	0.0000E+00
910010.E-03	2.5255E+04	4.9248E+07	0.0000E+00	0.0000E+00
980010.E-03	2.7538E+04	5.0160E+07	0.0000E+00	0.0000E+00
105001.E-02	2.6825E+04	5.3482E+07	0.0000E+00	0.0000E+00
112001.E-02	2.7966E+04	5.3743E+07	0.0000E+00	0.0000E+00
119001.E-02	3.0678E+04	5.4996E+07	0.0000E+00	0.0000E+00
126001.E-02	3.2104E+04	5.7872E+07	0.0000E+00	0.0000E+00
133001.E-02	3.2390E+04	5.7188E+07	0.0000E+00	0.0000E+00
140001.E-02	3.6528E+04	5.7631E+07	0.0000E+00	1.4269E+02
147001.E-02	3.3817E+04	5.8754E+07	0.0000E+00	0.0000E+00
154001.E-02	3.7955E+04	5.4198E+07	0.0000E+00	0.0000E+00
161001.E-02	3.5101E+04	5.5147E+07	0.0000E+00	0.0000E+00

---- Data Omitted from Table ----

3-Dimensional Ion Range Distributions

The previous section described how to obtain both ion and recoil atom distributions. Many applications require more elaborate 3-Dimensional (3-D) distributions, for example might be an analysis in the semiconductor technology of how implanted ions will spread under a mask edge.

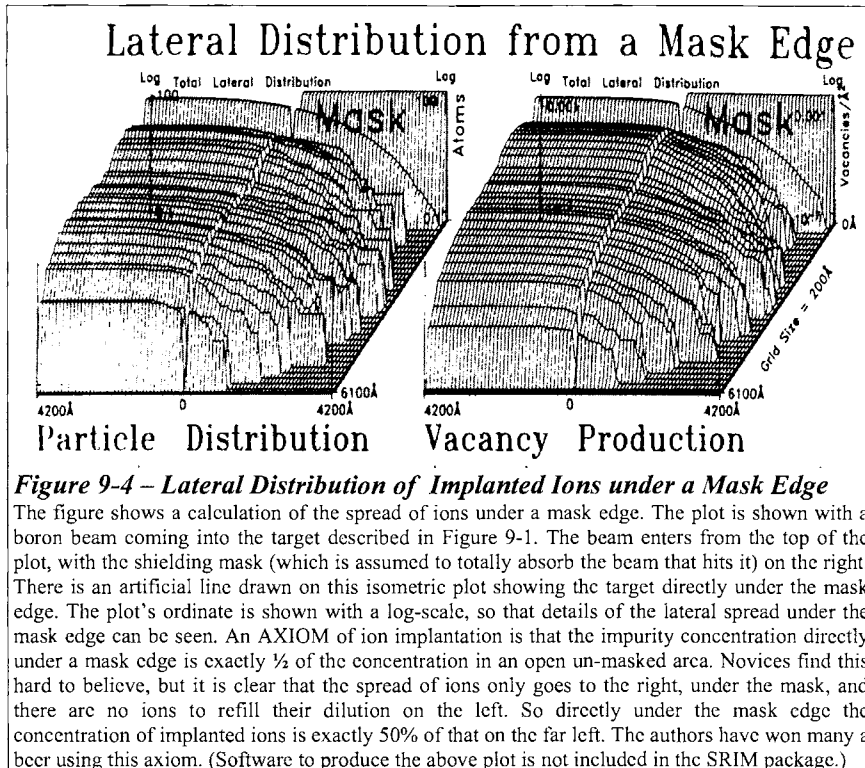


Figure 9-4 – Lateral Distribution of Implanted Ions under a Mask Edge

The figure shows a calculation of the spread of ions under a mask edge. The plot is shown with a boron beam coming into the target described in Figure 9-1. The beam enters from the top of the plot, with the shielding mask (which is assumed to totally absorb the beam that hits it) on the right. There is an artificial line drawn on this isometric plot showing the target directly under the mask edge. The plot's ordinate is shown with a log-scale, so that details of the lateral spread under the mask edge can be seen. An AXIOM of ion implantation is that the impurity concentration directly under a mask edge is exactly $\frac{1}{2}$ of the concentration in an open un-masked area. Novices find this hard to believe, but it is clear that the spread of ions only goes to the right, under the mask, and there are no ions to refill their dilution on the left. So directly under the mask edge the concentration of implanted ions is exactly 50% of that on the far left. The authors have won many a beer using this axiom. (Software to produce the above plot is not included in the SRIM package.)

A 3-D table of ion ranges (with full X,Y,Z coordinates of the final ion position) may be obtained by clicking on the box called “**3-D Ion Ranges**” in the TRIM Calculation window. This data is not stored unless this box is checked, so initiating it starts the storage of the final ion positions from the time the request is made. This datafile is called **..SRIM Outputs/RANGE_3D.txt**, and it will be appended for the remainder of the TRIM calculation until the check mark is removed by clicking on it again.

Shown in Table 9-5 is the table **..SRIM Outputs/RANGE_3D.txt** which contains the final positions of the ions in the target shown in Figure 9-1. Tabulated are ions number 13082-13094. At the top of RANGE_3D.TXT is a description of the calculation. Then the ions are tabulated with their X (depth), Y and Z (lateral) coordinates. Any ions which are backscattered or transmitted are not tabulated (note that backscattered ion #13089 is missing from the table). If the incident ion

beam is specified as at an angle to the target, this angle is in the X-Y plane. See details in Chapter 7 and 8.

This table can then be used to generate special 3-D plots such as shown in Table 9-4 using standard 3-D software (not included in SRIM).

Table 9-5 - RANGE_3D.TXT (Final 3D Ion Distribution)

===== SRIM Outputs\RANGE_3D.txt =====				
Ion = B (05) Ion Mass= 011.0000				
Energy = 2000000.E-04 keV				
Ion Angle to Surface = 00.0 degrees				
--- Header Data Omitted from Table (See Table 9-3) ---				
Ion Number	Depth (Angstrom)	X (Angstrom)	Lateral Y (Angstrom)	Lateral Z (Angstrom)
0013082	4.4202E+03	1.1992E+03	8.4194E+01	
0013083	2.5755E+03	2.2882E+03	4.9715E+02	
0013084	1.8796E+03	2.4276E+03	9.7905E+02	
0013085	4.1970E+03	5.9111E+02	-1.0712E+03	
0013086	3.7087E+03	-1.5715E+03	-2.3427E+03	
0013087	2.5107E+03	1.4551E+03	-4.4562E+02	
0013088	3.1975E+03	2.5150E+02	2.3512E+03	
0013090	3.0767E+03	1.1650E+02	-1.3126E+03	
0013091	1.4088E+03	-2.4023E+03	-1.2174E+02	
0013092	4.3233E+03	8.1428E+02	-3.8231E+02	
0013093	3.2774E+03	-1.3397E+03	6.3019E+02	
0013094	1.3404E+03	2.5045E+03	2.0818E+02	
---- Data Omitted from Table ----				

Datafile of Ion Trajectory and Energy in the Target

You can track the 3-dimensional position of an ion at intervals through its path into the target. To do this, in the TRIM Setup window, at the bottom, is a window called “**Special EXYZ File Increment (eV)**” For example, assuming an incident ion of 200 keV, if 10000 (eV) is entered as the EXYZ increment, the table will show the ion’s position at 10 keV increments, e.g. at 200 keV, 190 keV, 180 keV,.... The datafile of the ion position will be stored at these specific energies into: ..\SRIM Outputs / EXYZ.txt

An example of the datafile using this command is shown in Table 9-6 for the target of Figure 9-1. The EXYZ parameter is set for 10,000 eV (10 keV), which gives about 20 positions for each ion’s track. The ion energies are not exactly at the 10 keV intervals because the energy losses of the ion occur in uneven steps. The position of the ion at the nearest energy to each increment is used for the table. Note in column 6 is tabulated the electronic stopping power (eV/Å), and in column 7 is the energy lost (eV) to a target atom during the ion’s last ion/target atom collision.

It is possible to setup TRIM for another EXYZ file example using the TRIM Demo for Bi(500 keV) ions into silicon. This DEMO is set so that every time the ion loses 25 keV, an entry will be

made into the file of the Bi ion's position. That is, the ion's position is stored at energies of about 500 keV, 475 keV, 450 keV, 425 keV....

Table 9-6 - Table of 3-D Position of Ion Trajectory and Energy in Target

Ion Energy vs Position File						
<hr/>						
= AXIS DEFINITIONS: X=Depth, Y,Z= Lateral plane of target surface.=						
= (If beam enters target at an angle, this tilt is in Y direction)=						
= Shown are: Ion Number, Energy (keV), X, Y, Z Position =						
<hr/>						
CALCULATION DATA						
Ion Data: Name, Mass, Energy , Energy Interval						
B	11.00	200keV	10000eV			
<hr/>						
Ion Number	Energy (keV)	Depth (X) (Angstrom)	Y (Angstrom)	Z (Angstrom)	Electronic Stop. (eV/A)	Energy Lost to Last Recoil (eV)
0000001	2.0000E+02	0.0000E+00	0.0000E+00	0.0000E+00	7.1892E+01	0.0000E+00
0000001	1.8952E+02	1.5127E+02	-7.5751E-01	-1.0005E+00	7.0049E+01	2.2508E+00
0000001	1.7998E+02	2.7998E+02	1.0416E+00	-1.0838E+01	6.8356E+01	2.4354E-01
0000001	1.6847E+02	3.7142E+02	8.0857E+00	-1.9087E+01	6.6291E+01	3.7167E+00
0000001	1.5974E+02	4.7846E+02	2.4859E+01	-3.2319E+01	6.4704E+01	2.0871E+00
0000001	1.4987E+02	5.7549E+02	4.1584E+01	-4.8587E+01	6.2887E+01	5.2197E+01
0000001	1.3997E+02	8.1777E+02	6.6407E+01	-9.5390E+01	6.1027E+01	6.5079E+01
0000001	1.2475E+02	9.8262E+02	7.9988E+01	-1.2718E+02	5.8073E+01	7.0028E+03
0000001	1.1635E+02	1.0987E+03	-7.8480E+01	-1.8039E+02	5.6371E+01	6.4216E+00
0000001	1.0966E+02	1.1916E+03	-2.5511E+02	-2.0275E+02	5.4967E+01	7.1201E+00
<hr/>						
---- Data Omitted from Table ----						

Lateral Ion Range Distribution

The range of ions has been described above with regard to the final distribution as a function of depth below the target surface. For ion beams with perpendicular incidence to the target, the ion distribution will spread out with azimuthal symmetry. The spread of ions laterally can be conveniently summarized by using the averaging:

$$\text{Eq. 9-1} \quad \text{Lateral Range} \quad = \quad \sum_i |y_i| / N \quad = \quad <|y|>$$

$$\text{Eq. 9-2} \quad \text{Lateral Straggling} \quad = \quad [\sum_i ((|y_i| + |z_i|)/2)^2 / N]^{1/2}$$

$$\text{Eq. 9-3} \quad \text{Radial Range} \quad = \quad R_r = \sum_i (y_i^2 + z_i^2)^{1/2} / N$$

Where y_i is the final y-axis value of the ion, z_i is the final z-axis value of the ion, and N is the number of ions calculated. Thus the Lateral Range is merely the average final y-z displacement of the ions assuming a perpendicular incidence of the ion beam.

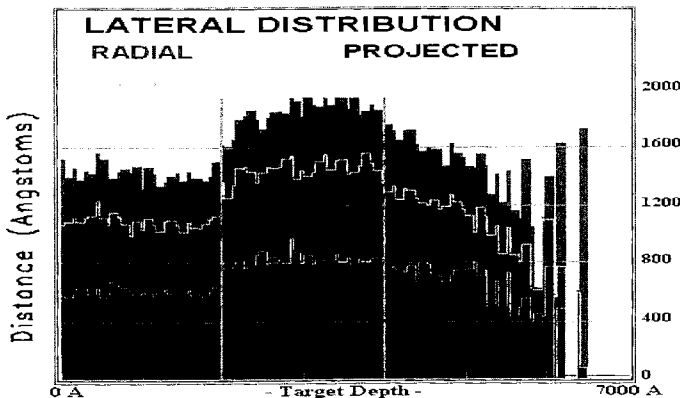


Figure 9-5 - Lateral Spread of Ions

The figure shows the lateral spread of the ions from the original ion axis. Both the first moment of the spread (solid plots) and the second moment, the straggle, of the spread (line plots) are shown. These plots are easier to see on the computer screen where each part is color coded.

The datafile, `../SRIM Outputs/LATERAL.txt`, and the plot summaries the lateral spread of ions within the target window.

- The plot is created when the TRIM Calculation window button “*Lateral Range*” Plot is pressed, and then this plot is updated after each later ion. The continuous display of the plot slows down the calculation.
- The datafile is created once, when the “*Lateral Range*” File button is pressed (see Table 9-7 below) The datafile summarizes the calculation to that point. Also included in this datafile are averages of both the Range, the Lateral Range and the Radial Range..
- The datafile also includes the extended note:

“NOTE : The Projected LATERAL Spread is based on a projection on a plane - just the way the XY or XZ displays look on the screen. The Lateral Projected Range is defined as the average of the absolute values of the projected lateral displacements from the X-axis. One use of this range: If a mask covers half of a target, the lateral range is the distance under the mask where the concentration drops to 25% (at the mask edge the concentration= 50% of the uniform value). The Radial Range is the mean radial displacement range from the X-axis assuming cylindrical symmetry.”

Table 9-7 - LATERAL.TXT (Ion Range Distribution)

===== B into W/SiO ₂ /Silicon (Double Peak) =====					
SRIM-2006.02					
===== LATERAL SPREAD OF IONS =====					
NOTE : The Projected LATERAL Spread is based on a projection on a plane- just the way the XY or XZ displays look on the screen. The Lateral Projected Range is defined as the average of the absolute values of the projected lateral displacements from the X-axis.					
One use of this range: If a mask covers half of a target, the lateral range is the distance under the mask where the concentration drops to 25% (at the mask edge the concentration= 50% of the uniform value).					
The Radial Range is the mean radial displacement range from the X-axis assuming cylindrical symmetry.					
=====					
Ion Average Range = 236972.E-02 A	Projected	LATERAL	Radial		
Ion Lateral Range = 101693.E-02 A	Straggling	RADIAL	Straggling		
Ion Radial Range = 159752.E-02 A	(Angstroms)	(Angstroms)	(Angstroms)	(Angstroms)	
=====					
TARGET	LATERAL	Projected	LATERAL	Radial	
DEPTH (A)	PROJ. RANGE	Straggling	RADIAL	Straggling	
	(Angstroms)	(Angstroms)	(Angstroms)	(Angstroms)	
7001000.E-05	86047569.E-05	10618028.E-04	15144395.E-04	57437670.E-05	
1400100.E-04	90123628.E-05	10804629.E-04	13958601.E-04	56282605.E-05	
2100100.E-04	92878883.E-05	11137749.E-04	14525209.E-04	59630276.E-05	
2800100.E-04	89000485.E-05	10831485.E-04	13759439.E-04	62767446.E-05	
3500100.E-04	91299021.E-05	11041263.E-04	14327649.E-04	62547777.E-05	
4200100.E-04	94310302.E-05	11228703.E-04	14184628.E-04	58636979.E-05	
4900100.E-04	10303406.E-04	12348963.E-04	15515912.E-04	62491014.E-05	
5600100.E-04	94818444.E-05	10952660.E-04	15095818.E-04	55719145.E-05	
---- Data Omitted from Table ----					

3-D plots of the Ion's Electronic Energy Loss

Some applications require the generation of three dimensional plots of the electronic energy loss of the ions. Examples of such applications are the use of ion beams for micro-lithography, or the use of ion beams in studying or altering biological samples. One method to do this was discussed before in "**Datafile of Ion Trajectory and Energy in the Target**", see Table 9-6. The steps below generate a more detailed datafile. (Note that this procedure may be inaccurate for heavy ions which create significant recoil cascades. The electronic energy loss of the recoils is omitted.)

- Setup your TRIM target in the usual way.
- Check the box for Collision Details (bottom of setup window).
- Continue with the TRIM setup program. When TRIM starts, you will be asked whether you wish to create a *New* file or *Append* to an old COLLISON.txt file. Specify *New*. Run TRIM for several ions. You will notice that the box called *Collision Details* is checked. You can start this file at any time during the TRIM calculation by checking this box, and stop it by unchecking it later.

- After several ions are completed, stop TRIM
- Now edit the file **COLLISON.txt**. You will see a file like the one shown below:

Table 9-8 - 3-D plots of Ion's Electronic Energy Loss (COLLISON.txt)

TRIM Calc.= B(17 keV) ==> Tungsten(300A)

COLLISION HISTORY

```
+-----+
| NOTES: Only Ion Collisions which produce Displacements are tabulated. |
| Atom Sums and Averages are Incomplete if Recoil Cascades Leave Target. |
| Target DISPlacements = VACancies + REPLACement Collisions.           |
| Target VACancies = INTERstitial Atoms + (Atoms Leave Target Volume). |
+-----+
|Ion| Energy | Depth |Lateral Dist(A)| Se |Atom|Recoil |Tgt |Tgt| Tgt | Tgt |
|Num| (keV) | (A) | |Y Axis |Z Axis |(eV/A)|Hit|Engy(eV)|DISP|VAC|REPLAC|INTER|
+-----+
| 1 |16.00E+00| 33E+00| 1E-05| 4E+00| 15.84| W | 83E+00| 0| 0| 0| 0|
| 1 |16.10E+00| 49E+00| -3E-02| 7E+00| 15.86| W | 57E+00| 4| 2| 2| 2|
| 1 |16.29E+00| 65E+00| -6E+00| 6E+00| 15.93| W | 94E+00| 2| 1| 1| 1|
| 1 |16.06E+00|111E+00|-12E+00|-8E+00| 15.85| W | 48E+00| 4| 1| 3| 1|
| 1 |15.00E+00|125E+00|-14E+00|-15E+00| 15.32| W | 114E+00| 2| 1| 1| 1|
+-----+
```

Data Omitted

This file shows the three-dimensional position of each major collision between the ion and the target atoms. It also shows in column six the instantaneous electronic energy loss of the ion to the target in units of eV/Å. If you need the three-dimensional electronic energy loss of the ion to the target, you now have all the necessary information. To obtain the energy deposited, calculate the path length between two successive collisions and multiply by the specific energy loss. For example, the distance between the first two collisions shown above is 16.3Å, with an energy loss of 15.86 eV/Å. This means the ion loses 258 eV into electronic excitations in this segment. If higher accuracy is needed, one can interpolate between the instantaneous energy loss values shown at each major collision point. Note that electronic stopping, col. 6, does not smoothly change due to Monte Carlo straggling variations.

NOTE that this table does not include the electronic energy loss of recoiling atoms- only that of the ions.

This application was suggested by Lidia Didenko, Univ. of Maryland.

Backscattered Ions

Backscattered ions are those which, after one or more target collisions, have a trajectory that exits the target back through its surface. The datafile **..//SRIM Outputs/BACKSCAT.txt** contains the kinetic data of Backscattered Ions. The datafile is opened when the **Backscattered Ions** selection is checked in the TRIM Setup window , or when the **Backscattered Ions** button is pressed in the TRIM Calculation window.

An example is shown in Table 9-9 for the target shown in Figure 9-1. The first 9 lines of BACKSCAT.txt describe the data in this file. Line #10 is a short description of the current calculation based on your input.

Table 9-9 - BACKSCAT.TXT (Backscattered Ions Kinetics)

SRIM-2006.02									
=	SRIM Outputs\BACKSCATSRIM Outputs\ : File of Backscattered Ions								
=	This file tabulates the kinetics of ions or atoms leaving the target.								
=	Column #1: S= Sputtered Atom, B= Backscattered Ion, T= Transmitted Ion.								
=	Col.#2: Ion Number, Col.#3: Z of atom leaving, Col.#4: Atom energy (eV)=								
=	Col.#5-7: Last location: X= Depth into target, Y,Z= Transverse axes.								
=	Col.#8-10: Cosines of final trajectory.								
=	*** This data file is in the same format as TRIM.DAT (see manual)								
=	TRIM Calc.= B(200 keV) ==> Tungsten+SiO ₂ +Silicon(7000 A)								
Ion	Atom	Energy	Depth	Lateral-Position	Atom	Direction			
Num	Numb	(eV)	X(A)	Y(A)	Z(A)	Cos(X)	Cos(Y)	Cos(Z)	
B	18	5	.15625E+05	-44030E-07	.3389E+03	.1930E+04	-.7723	-.2483	.5846
B	59	5	.73610E-04	-59772E-07	-.1148E+04	-.1856E+04	-.32106	-.8717	.3700
B	60	5	.30068E+05	-10512E-07	.6851E+03	-.8028E+03	-.77827	-.2837	.5601
B	90	5	.95421E+05	-20704E-06	.1986E+02	.4276E+03	-.87273	.0660	.4837
B	103	5	.31129E+05	-19596E-06	-.1222E+04	-.3741E+03	-.96821	.2025	-.1467
B	119	5	.94703E+05	-23078E-06	-.2757E+03	-.1914E+03	-.99243	.1175	.0355
B	127	5	.39248E+05	-14227E-06	-.1143E+04	.1261E+04	.92518	-.2322	.3001
B	135	5	.11210E+06	-10779E-06	-.2087E+03	.3356E+03	-.65032	-.4227	.6311
B	153	5	.56244E+05	-14285E-06	.3022E+03	.3440E+03	-.89376	.1925	.4050
B	154	5	.70127E+05	-10415E-06	.5957E+02	.1529E+04	-.78766	-.3408	.5132

---- Data Omitted from Table ----

For correct Display of this datafile, use Microsoft font "Courier New" or "MS-LineDraw". "Linedraw" is included in the SRIM software package. See the subdirectory: SRIM/Data/Linedraw.ttf

Lines #11 - 12 are descriptive headers to the columns of data. The first column in all the data fields in this table is the letter "B" which indicates that this is a backscattered ion. This letter is also used in the summary file TRIMOUT.dat (see Table 9-13) which includes entries from datafiles BACKSCAT.txt, TRANSMIT.txt and SPUTTER.txt. Next is the sequential ion number starting with #18 (ion numbers 1-17 are not backscattered and are omitted), followed by ion #59. Column #3 is the atomic number of the ion. Column #4 is the energy of the backscattered ion (eV) as it leaves the target. Column #5 is its position when it was declared *backscattered*. Since the target atoms are randomly placed within their lattice cells, this number will vary slightly from zero, but will always be in the upper monolayer of the target. Columns #6-7 are the lateral position of the ion when it exits the target. Columns #8-10 are the directional cosines of the trajectory of the backscattered ion. Note that cos(X) is always negative, since the x-axis measures depth into the target and this indicates a backwards trajectory.

Note that all the data files BACKSCAT.txt, TRANSMIT.txt and SPUTTER.txt (Table 9-9, Table 9-10 and Table 9-11) have the same format, and can be used as input for a subsequent TRIM calculation. This is necessary for some of the special applications discussed in Chapter 8, the TRIM Input chapter.

Transmitted Ions

The plot and the datafile `../SRIM Outputs/TRANSMIT.txt` contains the kinetic data of Transmitted Ions. It contains the kinetic data of Ions which leave the bottom of the target. The datafile is opened when the **Transmitted Ions** selection is checked in the TRIM Setup window, or when the **Transmitted Ions** button is pressed in the TRIM Calculation window.

Table 9-10 - TRANSMIT.TXT (Transmitted Ion Kinetics)

===== SRIM-2006.02 =====									
===== TRANSMIT.txt : File of Transmitted Ions =====									
= File tabulates the kinetics of ions or atoms leaving the target. =									
= Col. #1: S= Sputtered Atom, B= Backscattered Ion, T= Transmitted Ion. =									
= Col.#2: Ion Number, Col.#3: Z of atom leaving, Col.#4: Atom energy)=									
= Col.#5-7: Last location: X= Depth into target, Y,Z= Transverse axes=									
= Col.#8-10: Cosines of final trajectory. =									
= TRIM Calc.= B(300 keV) => Tungsten+SiO@2+Silicon(7000 Å) =====									
Ion	Atom	Energy	Depth	Lateral-Position	Atom	Direction			
Numb	Numb	(eV)	X(A)	Y(A)	Z(A)	Cos(X)	Cos(Y)	Cos(Z)	
T	1	5	.7838E+03	7000E-03	.3092E+03	.3348E+04	.8839	.2127	-.4164
T	7	5	.2891E+05	7001E-03	.6063E+03	-.1998E+04	.7350	.6451	-.2084
T	10	5	.1088E+05	7002E-03	.2308E+04	.6435E+03	.9840	-.1623	-.0728
T	11	5	.9959E+04	7002E-03	.2709E+04	-.4060E+04	.7797	.3948	-.4858
T	12	5	.1576E+05	7001E-03	.3100E+03	-.1407E+04	.9119	.1164	.3934
T	13	5	.1432E+05	7001E-03	.1441E+04	.1857E+04	.8282	.5170	.2161

---- Data Omitted from Table ----

For correct Display of this file, use Microsoft font “*Courier New*” or “*MS-LineDraw*”. “*Linedraw*” is included in the SRIM software package. See the subdirectory: SRIM/Data/Linedraw.ttf

NOTE: Table 9-10 was calculated with the target of Figure 9-1, however the boron ions were set at 300 keV, instead of 200 keV, in order to get some ions transmitted through the target.

The first 7 lines of TRANSMIT.TXT, Table 9-10, describe the data. Line #8 is a short description of the calculation based on your input. Lines #9 - 10 are descriptive headers to the data fields. Beginning in line #11 is the data. The first item in all these data fields is the letter "T" which indicates that this is a transmitted ion (this letter is also used in the summary file TRIMOUT.DAT (see Table 9-13) which includes entries from BACKSCAT.TXT, TRANSMIT.TXT and SPUTTER.TXT.) Next is the sequential ion number (ions number 2-6 are not transmitted). Column #3 is the atomic number of the ion. Column #4 is the energy of the transmitted ion (eV). Column #5 is its position when it was declared *transmitted*. Since the target atoms are randomly placed within their lattice cells, this number will vary slightly from the total target depth of 7000Å. Columns #6-7 are the lateral position of the ion when it exits the target. Columns #8-10 are the directional cosines of the trajectory of the backscattered ion. Note that cos(X) is always positive, since the x-axis measures depth into the target, and cos(x) = 1 would mean a perpendicular exit from the target.

Note that all the data files BACKSCAT.txt, TRANSMIT.txt and SPUTTER.txt (Table 9-9, Table 9-10 and Table 9-11) have the same format, and can be used as input for a subsequent TRIM

calculations. This is necessary for some of the special applications discussed in Chapter 8, the TRIM Manual.

Sputtered Target Atoms

The datafile `../SRIM Outputs/SPUTTER.txt` contains the kinetic data of Sputtered Target Atoms. The datafile is opened when the *Sputtered Atoms* selection is checked in the TRIM Setup window, or when the *Sputtered Atoms* button is pressed in the TRIM Calculation window.

In contrast to files for backscattered or transmitted ions, TRIM maintains a constant file of sputtered atoms and their energy. This is important because the target **Surface Binding Energy** (SBE) is used to determine if a recoiling target atom has enough energy to leave the solid, or whether it will be held in by the target's surface binding energy. These energies are not well known, and the plots allow the user to see what would be the effect of changing this value from that suggested. Among other problems in determining its value, the Surface Binding Energy will change as the target roughens after initial sputtering (its SBE would probably decrease), or materials like silicon crystal will become amorphous with extended bombardment, and the sputtering yield will change.

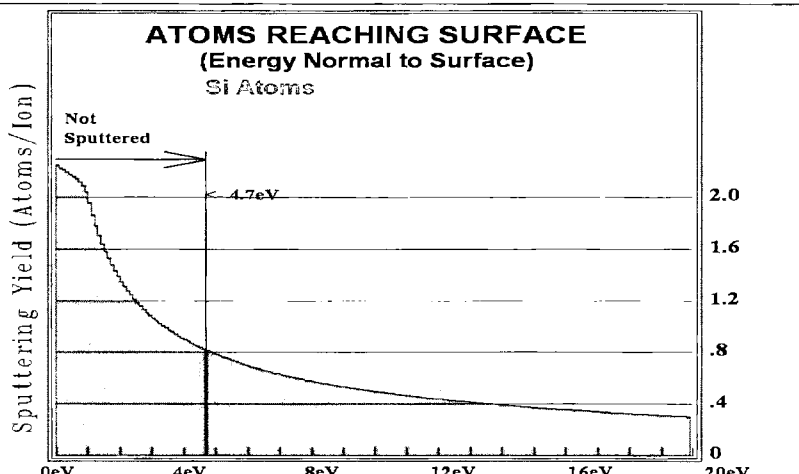


Figure 9-6 – Integral Plot of Sputtered Atoms

The plot shows the sputtering yield (atoms sputtered per incident ion) as a function of the final atom energy as it leaves the target. The SBE for W atoms was set for 3.2eV in the calculation. As shown, a great number of W atoms reached the surface without enough energy to be sputtered (the area to the left of the 3.2eV SBE). Since the SBE is not well known, this allows the user to estimate the error in using the value of 3.2 eV.

The sputtering plots can show either an Integral plot (Figure 9-6) or a Differential plot (Figure 9-7) of sputtered atom yield vs. energy. The surface binding energy for the first atom in the first layer is also indicated as a guide. The Integral plot is useful to estimate how many atoms reach the surface and do not have enough energy to leave it. The Differential plot gives an indication of how rapidly the sputtering yield will change with small changes of the SBE.

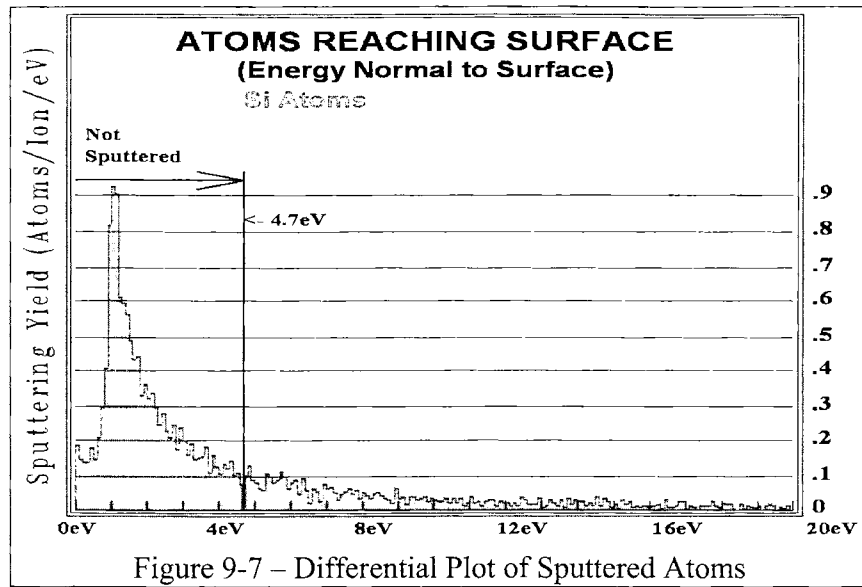


Figure 9-7 – Differential Plot of Sputtered Atoms

Also available is the datafile, **../SRIM Outputs/SPUTTER.txt**. The first lines of SPUTTER.TXT contain explanations of the table as well as details of the calculation, quite similar to those shown in Table 9-2 and Table 9-3. In addition, it contains the input values for the three target lattice energies, the Surface Binding Energy (SBE), the Displacement Energy (DE) and the Lattice Binding Energy (LBE), see Table 9-11.

Table 9-11 - SPUTTER.txt (Header File)

TRIM Calc.= B(200 keV) ==> Tungsten+SiO ₂ +Silicon(7000 Å)
Ion Data: Name, Mass, Energy (keV)
B 11. 200.
Displacement Energy of W = 21.0 eV
Latt.Binding Energy of W = 2.1 eV
SurfaceBind. Energy of W = 3.2 eV
Displacement Energy of Si = 22.0 eV
Latt.Binding Energy of Si = 2.2 eV
SurfaceBind. Energy of Si = 3.2 eV
Displacement Energy of O = 23.0 eV
Latt.Binding Energy of O = 2.3 eV
SurfaceBind. Energy of O = 3.3 eV

The bottom part of the *..SRIM Outputs/SPUTTER.txt* datafile is shown in Table 9-12. The format is the same as seen for the BACKSCAT.txt and the TRANSMIT.txt files, only the leading character at the left is an “S” instead of a “B” or a “T”. Note that ion numbers 1-3 sputter no atoms, and then #4 is responsible for nine sputtered target atoms. Then ion #6 sputters one atom, and the next 14 ions sputter none. There is additional sputtering with ions #21 and #60. Often there will be no sputtering, and then one ion is scattered with a near-surface trajectory and sputters a group of surface atoms.

Table 9-12 - SPUTTER.txt (Data File)

SPUTTERING CALCULATION							
CALCULATION DATA							
Ion Data:	Name,	Mass,	Energy (keV)				
B		11.	200.				
Displacement Energy of W =	21.00000	eV					
Latt. Binding Energy of W =	2.10000	eV					
SurfaceBind. Energy of W =	3.10000	eV					
Displacement Energy of Si =	22.00000	eV					
Latt. Binding Energy of Si =	2.20000	eV					
SurfaceBind. Energy of Si =	3.20000	eV					
Displacement Energy of O =	23.00000	eV					
Latt. Binding Energy of O =	2.30000	eV					
SurfaceBind. Energy of O =	3.30000	eV					

=This file tabulates the kinetics of ions or atoms leaving the target.							
=Column #1: S= Sputtered Atom, B= Backscattered Ion, T= Transmitted Ion.							
=Col. #2: Ion Number, Col. #3:Z of atom leaving, Col.#4:Atom energy (eV).							
=Col. #5-7:Last location: X=Depth into target, Y,Z= Transverse axes.							
=Col. #8-10: Cosines of final trajectory.							
= *** This data file is in the same format as TRIM.DAT							
===== TRIM Calc.= B(200 keV) ==> Tungsten+SiO ₂ @2+Silicon(7000 A) =====							
Ion	Atom	Energy	Depth	Lateral-Position	Atom	Direction	
Numb	Numb	(eV)	X(A)	Y(A)	Z(A)	Cos(X)	Cos(Y)
S	4	.4092E+02	0000E+00	.8122E+01	.4582E+01	-.9477	.0491
S	4	.3783E+02	0000E+00	.5972E+01	.2946E+01	-.4821	-.8085
S	4	.2115E+02	0000E+00	.3995E+01	.1648E+01	-.9992	-.0348
S	4	.1014E+02	0000E+00	-.7089E+00	.7400E+01	-.8854	-.1321
S	4	.1236E+02	0000E+00	-.1938E+01	.7513E+01	-.6098	-.6226
S	4	.1372E+02	0000E+00	-.9035E+00	.4104E+01	-.9383	-.1890
S	4	.1586E+02	0000E+00	-.6473E+00	.1077E+01	-.4759	-.3683
S	4	.3325E+02	0000E+00	.2464E+01	.5488E+00	-.9193	-.3805
S	4	.1151E+02	0000E+00	.1906E+01	.6609E+01	-.8518	.4732
S	6	.74	.1371E+02	0000E+00	.4263E+01	.1425E+01	-.8315
S	21	.74	.3334E+02	0000E+00	.7378E+00	.3956E+01	-.6313
S	21	.74	.1252E+02	0000E+00	-.1067E+01	.1999E+01	-.7440
S	60	.74	.5663E+01	0000E+00	.6389E+03	-.8752E+03	-.8163
----- Data Omitted from Table -----							

For correct Display of this file, use Microsoft font “Courier New” or “MS-LineDraw”. “Linedraw” is included in the SRIM software package. See the subdirectory: SRIM/Data/Linedraw.ttf

Combined Tables of Backscattering, Transmitted and Sputtering

TRIMOUT.TXT contains all the information of BACKSCAT.TXT, TRANSMIT.TXT and SPUTTER.TXT which are shown in Table 9-9 to Table 9-12. See explanations of these tables for details. TRIMOUT.TXT is generated automatically when you ask for any of the other output tables. It will only contain the data requested, e.g. if you request backscattered and sputtered data, the transmitted ion data will not be recorded.

Table 9-13 - TRIMOUT.TXT (Includes all of Table 9-9 to Table 9-11)

TRIMOUT.TXT: File of Transmitted / Backscattered / Sputtered Atoms									
This file tabulates the kinetics of ions or atoms leaving the target.									
Column #1: S= Sputtered Atom, B= Backscattered Ion, T= Transmitted Ion.									
Col. #2: Ion Number, Col. #3: Z of atom leaving, Col. #4: Atom energy (eV).									
Col. #5-7: Last location: X= Depth into target, Y,Z= Transverse axes.									
Col. #8-10: Cosines of final trajectory.									
*** This data file is in the same format as TRIM.DAT (see manual details)									
TRIM Calc.= B(200 keV) => Tungsten+SiO ₂ :Silicon(7000 Å)									

Ion Numb	Atom Numb	Energy (eV)	Depth	Lateral-Position			Atom Direction		
				X(A)	Y(A)	Z(A)	Cos(X)	Cos(Y)	Cos(Z)
T 1 5 .7838E+03 7000E-03 .3092E+03 .3348E+04 .8839 .2127 -.4164									
S 4 74 .4092E+02 0000E+00 .8122E+01 .4582E+01 -.9477 .0491 .3153									
S 4 74 .3783E+02 0000E+00 .5972E+01 .2946E+01 -.4821 -.8085 -.3372									
S 4 74 .2115E+02 0000E+00 .3995E+01 .1648E+01 -.9992 -.0348 -.0185									
S 4 74 .1014E+02 0000E+00 -.7089E+00 .7400E+01 -.8854 -.1321 .4455									
S 4 74 .1236E+02 0000E+00 -.1938E+01 .7513E+01 -.6098 -.6226 .4902									
S 4 74 .1372E+02 0000E+00 -.9035E+00 .4104E+01 -.9383 -.1890 .2894									
S 4 74 .1586E+02 0000E+00 -.6473E+00 .1077E+01 -.4759 -.3683 -.7986									
S 4 74 .3325E+02 0000E+00 .2464E+01 .5488E+00 -.9193 -.3805 -.0996									
S 4 74 .1151E+02 0000E+00 .1906E+01 -.6609E+01 -.8518 .4732 -.2246									
S 6 74 .1371E+02 0000E+00 .4263E+01 .1425B+01 -.8315 -.5131 .2124									
T 7 5 .2891E+05 7001E-03 .6063E+03 -.1998E+04 .7350 .6451 -.2084									
T 10 5 .1088E+05 7002E-03 .2308E+04 .6435E+03 .9840 -.1623 -.0728									
T 11 5 .9959E+04 7002E-03 .2709E+04 -.4060E+04 .7797 .3948 -.4858									
B 18 5 .1562E+05 -4403E-07 .3389E+03 .1930E+04 -.7723 -.2483 .5846									
S 21 74 .3334E+02 0000E+00 .7378E+00 .3956E+01 -.6313 .3118 -.7100									
S 21 74 .1252E+02 0000E+00 -.1067E+01 .1999E+01 -.7440 -.6290 -.2248									
B 59 5 .7361E+04 -5977E-07 -.1148E+04 -.1856E+04 -.3210 -.8717 .3700									
S 60 74 .5663E+01 0000E+00 .6389E+03 -.8752E+03 -.8163 -.1866 .5465									

---- Data Omitted from Table ----

For correct Display of this file, use Microsoft font "Courier New" or "MS-LineDraw". "Linedraw" is included in the SRIM software package. See the subdirectory: SRIM/Data/Linedraw.ttf

Note that every type of atom is covered here. There are 12 sputtered atoms, all of the target atom, tungsten (Z=74); there are 4 transmitted atoms, all of the incident ion, boron (Z=5); and there are 2 backscattered atoms, boron (Z=5). Since TRIM always assumes a zero-dose approximation (the incident ion does not pile up in the target), the sputtered and backscattered atoms always must be the same as the incident ion, and the sputtered atoms must always be a target atom.

Target Damage by the Ion

TRIM is often used to gain an understanding of the changes to the target under bombardment by ions. TRIM can be used for detailed examination of this target damage, but it must be interpreted with knowledge of two major TRIM limitations: (a) There is no build-up of ions or damage in the target. Every ion is calculated with the assumption of *zero dose*, i. e. the target is perfect and previous ions have no effect on subsequent ions. (b) The target temperature is 0°K, and there are no thermal effects changing the distribution of ions (thermal diffusion) or affecting the target damage (thermal annealing). Several experiments have been reported at very low temperatures (15-40°K) which validate the TRIM results, but show that thermal effects can be quite substantial. For example, for a low dose of boron ions into crystalline silicon, more than 99% of the target damage anneals at room temperature.

Full details of how TRIM calculates target damage is given in Chapter 7 and 8.

Ion's Energy Loss to the Target Electrons

The energy loss of ions to the target electrons is often called "Electronic Energy Loss" or "Ionization Losses". These terms are synonyms. Both Plots and Datafiles are available. When ions penetrate into the target, they interact immediately with the target electrons, both single electrons and collectively. This interaction is very complicated, and TRIM uses the physics described in Chapter 3 and Chapter 7. The energy loss to electrons is collected for the TRIM Viewing Window (in 100 channels of information) and can be accessed during the TRIM calculation by selecting the *Ionization Plot* button, or the *Ionization File* button

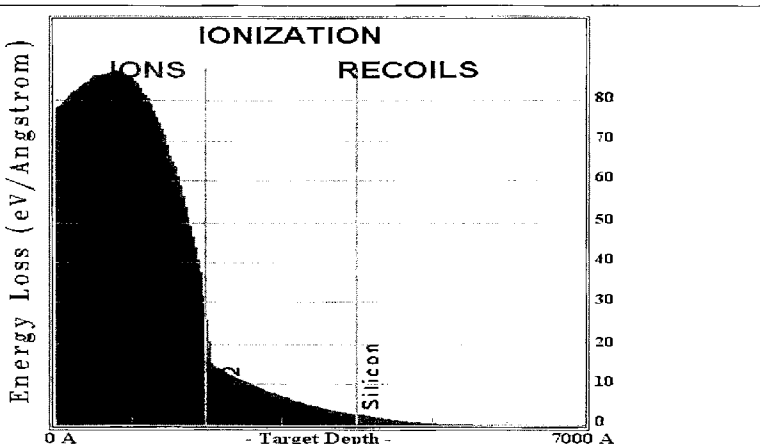


Figure 9-8 - Target Ionization (Energy Loss to Target Electrons)

The ion loses energy to the target electrons as shown in the plot in units of $eV/\text{\AA}$. This energy loss will cause target damage in insulators where the charge can build up until macroscopic damage may occur, e.g. cracking or delamination. Also shown is the electronic losses into the target caused by recoiling target atoms (dark curve). Since the recoiling atoms move relatively slowly, they have much less interaction with the faster moving target electrons

Table 9-14 - Datafile of Ionization Energy Loss in Target

--- Header Information omitted from Table ---

Total Ions calculated =003859.69
Ionization Units are >>> eV / Angstrom / Ion <<<

TARGET DEPTH (Ang)	IONIZ. by IONS	IONIZ. by RECOILS
700100.E-04	7770.18E-02	2116.60E-03
140010.E-03	7837.15E-02	2705.78E-03
210010.E-03	8014.79E-02	2966.79E-03
280010.E-03	8144.14E-02	2875.40E-03
350010.E-03	8216.98E-02	3197.69E-03
420010.E-03	8345.11E-02	3316.41E-03
490010.E-03	8418.28E-02	3501.37E-03
560010.E-03	8565.63E-02	3741.85E-03
630010.E-03	8562.24E-02	3874.91E-03
700010.E-03	8581.36E-02	4178.15E-03

--- Data Omitted from Table ---

The left hand column in all tables is the depth of the bottom of each bin. The tabulated event units are usually: eV/(Å-Ion). The Header of datafile IONIZ.txt, indicates the version of TRIM used, the details of the ion and target structure, various collision parameters, and the final averages for the calculation. This header is omitted from Table 9-14.

Note that the number of ions is not an integer (here 3859.69) since the calculation was stopped in mid-flight of ion #3860. All averages are calculated including this partial ion, i.e. the Ionization/Ion = (Total Ionization) / 3859.69.

Ion's Energy Loss to the Target Phonons

When the ion collides with a target nucleus, it imparts some recoil energy to this atom. We discussed in Chapter 8 the term **Displacement Energy**, which is the minimum amount of energy that must be transferred to the target atom to knock it out of its lattice site and far enough away so it doesn't immediately fall back into this lattice hole. If the transferred energy is less than the Displacement Energy, then it is assumed that the atom returns to its lattice site and its recoil energy is transferred into target phonons. See Chapter 8 for more details.

Typical values for Displacement Energies are about 15 eV for semiconductors and 25 - 40 eV for metals. For fragile materials like polymers, a value as low as 2 - 5 eV may be more accurate.

A plot of Energy Loss to the Target Phonons is shown in Figure 9-9. The datafile, ..SRIM Outputs/PHONON.txt, Table 9-15, stores the data of this plot as a datafile.

- The plot is created when the TRIM Calculation button “*Phonons*” is pressed, and then updated after each ion. The constant display of the plot slows down the calculation.

- In the plot, >90% of the phonons are produced by the recoiling atoms, while a thin line near the bottom of the plot indicates the phonons produced by the ion.

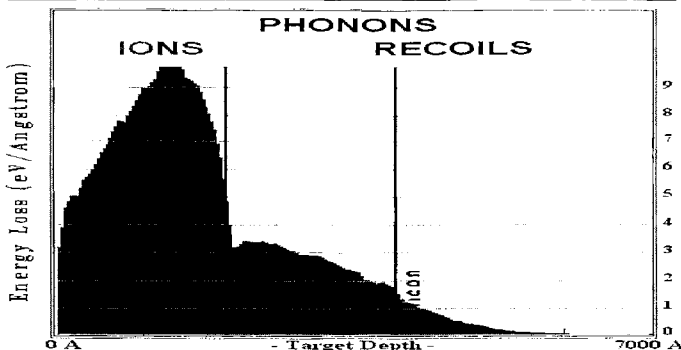


Figure 9-9 - Plot of Target Phonons

The plot shows the distribution of target phonons produced in the target.

Table 9-15 - PHONON.TXT (Energy Loss to Phonons)

<i>---- Header Information omitted from Table ----</i>		
Table Units are >>> Phonons / (Angstrom - Ion) <<<		
DEPTH (Ang.)	PHONONS by ION	PHONONS by RECOILS
700100.E-04	189790.E-06	314755.E-05
140010.E-03	209309.E-06	458183.E-05
210010.E-03	229019.E-06	500557.E-05
280010.E-03	250753.E-06	500532.E-05

---- Data Omitted from Table ----

Energy Loss to Vacancy Production / Replacement Collisions

The plot shown in Figure 9-10 and in the datafiles, *..SRIM Outputs/VACANCY.txt* and *..SRIM Outputs/NOVAC.txt*, tabulate the energy loss to the target producing vacancies and replacement collisions. Each target atom element is shown separately. The number of vacancies depends on the Displacement Energy assigned to each target atom. A **Displacement Energy** is the minimum amount of energy that must be transferred to the target atom to knock it out of its lattice site and far enough away so it doesn't immediately fall back into this lattice hole. If the transferred energy is less than the Displacement Energy, then the atom remains in its lattice site and we assume the energy is transferred into target phonons. If it is greater than the Displacement Energy, then the new recoil has this transferred energy, minus the **Binding Energy** of the atom to its lattice site

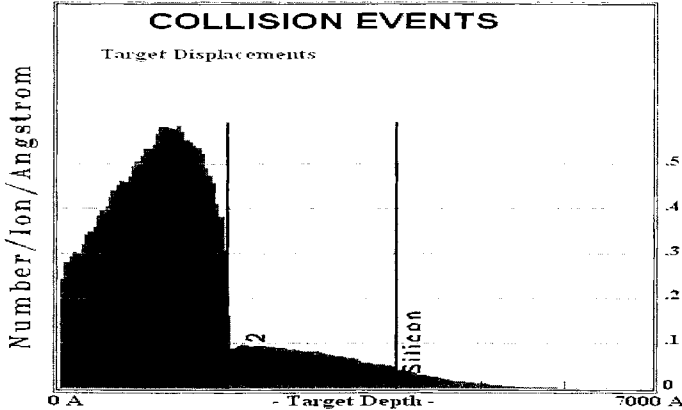


Figure 9-10 - Plot of Total Target Displacements

The plot shows the number of target atom displacements made by the incident ions. The plot includes both displacements made by the ion and by all the recoiling target atoms. These displacements will lead to either a target vacancy, or a replacement collision (see following two plots).

The above description has to be expanded for the special case of the displacement being caused not by the ion but by a recoiling target atom. If the recoiling atom knocks out a target atom, and the incoming atom does not have enough energy to go on, then it will fall into the lattice site emptied by the recoiling lattice atom. If the target atom and the recoiling target atom are the same element (which is natural since the recoiling atom probably originated in that same layer), then there is effectively no change in the target composition. For example, if an incoming recoiling W atom (110 eV) hits another W atom (with a displacement energy of 25 eV) and gives it 100 eV, the incoming ion will have only 10 eV left. This is below the displacement energy for W atoms in this layer, so it will merely replace the W atom that is knocked out. This is a **Replacement Collision**. Is this rare? No, it can be rather common, for in the target that we are using in this Chapter (see Figure 9-1), the calculation finds:

- **Total Ions calculated =13081**
- **Average Target Displacements = 1077 /Ion**
- **Average Target Vacancies = 940 /Ion**
- **Average Target Replacement Collisions = 137 /Ion**

So the ions and recoiling atoms create 1077 displacements/ion. Of these, 940 result in vacancies, and 137 result in Replacement Collisions. So Replacement Collisions are about 13% of the total displacements. See Chapters 7 and 8 for more details.

- The plot is created in the TRIM Calculation window, when the “Damage Events” Plot button is selected. The plot is created when the button is pressed, and then updated after each ion. The display of the plot slows down the calculation.

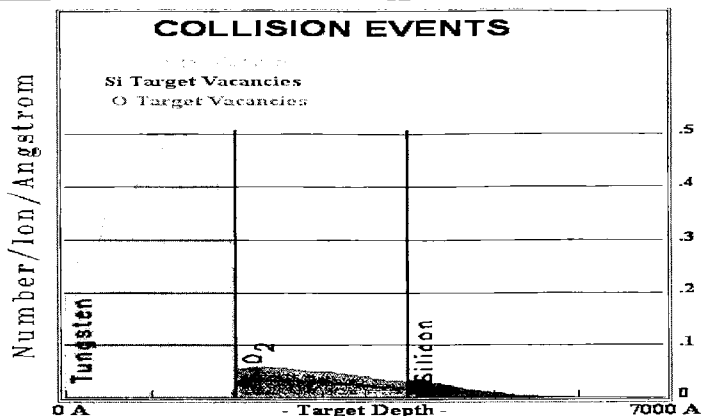


Figure 9-11 – Plot of Target Vacancies

The figure shows the plot of target vacancies, which are caused by displacements that transfer to a target atom an energy greater than that atom's Displacement Energy. Since vacancies can not migrate from the layer that contains that atom, in the upper layer are only W vacancies, and in the lower layer there are only Si vacancies. The middle layer contains two elements: Si and O, and there are two plots shown for each of types of vacancies (the plot of oxygen vacancies is a thin line).

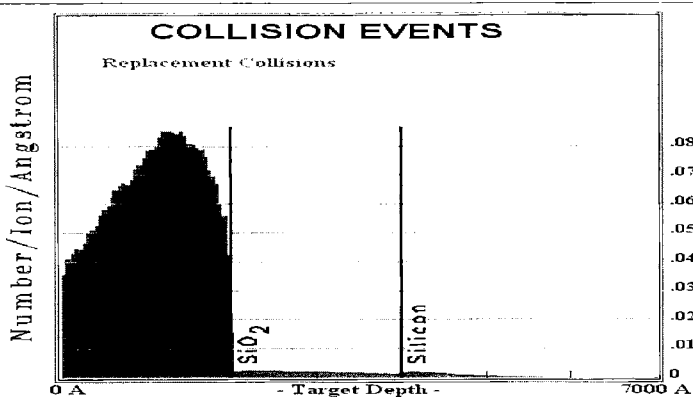


Figure 9-12 – Target Replacement Collisions

The figure shows the Replacement Collisions of the target. This is the special case where the target atom displacement is caused by a target atom of the same element, and after the collision takes place, the incoming atom does not have enough energy to leave the lattice site. Hence, it replaces the atom that it knocked out, and since it is the same elemental type, there is no change or damage to the target from this collision. Similar data for the other two layers shows a much smaller number of events in the SiO_2 and Si layers, and the datafile table has to be consulted for values.

Table 9-16 - ..\SRIM Outputs\VACANCY.txt (Vacancy Production)

Ion and Target VACANCY production

See file : SRIM Outputs\TDATA.txt for calculation data
Ion = B Energy = 200 keV

Total Ions calculated =13081.00

Total Target Vacancies = 940 /Ion

Total Target Displacements = 1077 /Ion

Total Target Replacement Collisions = 137 /Ion

!! NOTE : 2nd Column below is number of Primary Knock-Ons !!
(PKO are number of Target Atoms Recoiling from the Ion.)

Table Units are >>> Vacancies / (Angstrom - Ion) <<<

DEPTH (Ang.)	B Knock-Ons	W Vacancies	Si Vacancies	O Vacancies
700100.E-04	1198.08E-05	1744.28E-04	0000.00E+00	0000.00E+00
140010.E-03	1580.77E-05	2385.35E-04	0000.00E+00	0000.00E+00
210010.E-03	1714.74E-05	2599.64E-04	0000.00E+00	0000.00E+00
280010.E-03	1882.77E-05	2568.85E-04	0000.00E+00	0000.00E+00
350010.E-03	2068.05E-05	2860.98E-04	0000.00E+00	0000.00E+00
420010.E-03	2234.34E-05	2975.10E-04	0000.00E+00	0000.00E+00

The 2nd column of the datafile VACANCY.txt, Table 9-16, “B Knock-Ons” refer to vacancies directly caused by the incoming boron ion. All the other columns include both ion and recoil cascade induced vacancies.

Replacement collisions are a special type of collision in which the moving atom collides with an identical target atom, transfers an amount of energy greater than that atom's displacement energy, and does not have enough energy to move on out of the lattice site. Hence the original moving atom replaces the target atom, the target atom moves on, and since the two atoms are the same atomic species, there is no final damage. The two atoms exchange places, but since they are the same species there is no detectable change. See Chapters 7 and 8 for more details. Table 9-17 shows the Replacement Collisions which are stored in datafile: NOVAC.txt.

Table 9-17 - NOVAC.txt (Replacement Collisions)

<u>Replacement Collisions</u>	
--- Header Data Omitted ---	
===== TARGET MATERIAL =====	
<u>Layer 1 : Tungsten</u>	
Layer Width =	2.E+03 AAA ;
Layer # 1- Density =	6.351E22 atoms/cm ³ = 19.3 g/cm ³
Layer # 1- W = 100	Atomic Percent = 100 Mass Percent
<u>Layer 2 : SiO@2</u>	
Layer Width =	2.E+03 AAA ;
Layer # 2- Density =	7.015E22 atoms/cm ³ = 2.33 g/cm ³
Layer # 2- Si = 33.3	Atomic Percent = 46.6 Mass Percent
Layer # 2- O = 66.6	Atomic Percent = 53.3 Mass Percent
<u>Layer 3 : Silicon</u>	
Layer Width =	3.E+03 AAA ;
Layer # 3- Density =	4.989E22 atoms/cm ³ = 2.32 g/cm ³
Layer # 3- Si = 100	Atomic Percent = 100 Mass Percent
=====	
Total Ions calculated =	13081.00
Total Target Vacancies =	940 /Ion
Total Target Displacements =	1077 /Ion
Total Target Replacement Collisions =	137 /Ion
=====	
Table Units are >>> Number / (Angstrom _ Ion) <<<	
=====	
DEPTH (A)	Number
-----	-----
7001000.E-05	0000.029330
1400100.E-04	0000.040761
2100100.E-04	0000.044445
2800100.E-04	0000.043975
3500100.E-04	0000.048435
4200100.E-04	0000.050544
4900100.E-04	0000.053586
5600100.E-04	0000.057753
--- Data Omitted -----	

Energy Loss from Ions – Energy Loss Absorbed by Target Atoms

There are two plots available which can be used to summarize the ion's energy that goes into recoil cascades. They are generated in the TRIM Calculation window by selecting the Plot called "Energy to Recoils". This generates the two plots shown below.

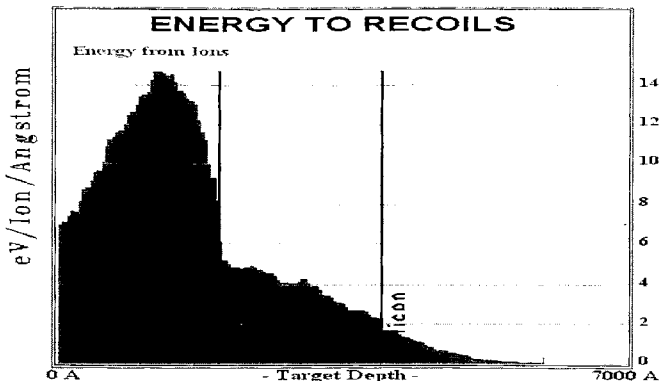


Figure 9-13 - Plot of the Energy Transferred from the Ion to Recoil Atoms

This plot shows the energy transferred from the ion to recoil atoms. The layer of tungsten atoms absorbs more recoil energy than the other two layers combined.

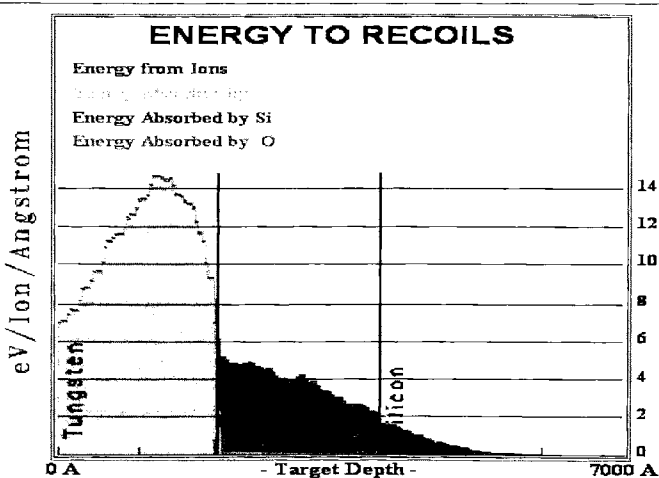


Figure 9-14 - Plot of the Energy Absorbed by the Various Target Atoms

This plot shows the amount of energy absorbed by the W, Si and O atoms of the target. It is identical to Figure 9-13 except for the middle compound layer, SiO_2 . The energy in this layer is separated into that absorbed by the Si atoms and that for the O atoms (lower two lines) which add up to the energy deposited by the ions (upper curve). This plot is color-coded when viewed in SRIM and is much easier to understand.

Details of the Ion-Atom Collision Kinetics

Physics of Recoil Cascades

The following comments come from the discussions of Target Damage in Chapters 7 and 8.

The easiest way to understand the TRIM cascades is to start TRIM and select various DEMO calculations. During the calculation, play with the various plots and files, to see what they do. Each plot and file has a *Help* file associated with it, to explain its details.

Following this, you may create a more detailed understanding of cascades by selecting one of the DEMO calculations and then checking the box called “*Collision Details*”, which will store every ion/atom collision in a file called “*...SRIM Outputs/COLLISION.txt*” (see Chapter on *TRIM Outputs*). Note that during the TRIM calculation, you may stop this data collection by un-checking the *Collision Detail* box in the TRIM window. This file can get quite large, so for a first experiment try it only for a few minutes of calculation time. Then stop TRIM and edit the file *COLLISON.txt* in the SRIM directory using any text editor. You will see tables of each ion colliding with various atoms in the target, and the detailed results of any collision cascades. Only those collisions which produce at least one displacement are tabulated, so you may not have a record of every collision.

In the file *COLLISON.txt*, first the current ion energy and depth are given, and then the current rate of energy loss of the ion to the target electrons, i.e. the electronic stopping power, called “Se” in the table with units of eV/Angstrom. Then the target atom that is hit and starts a recoil cascade is identified, along with its recoil energy. Each cascade is then divided into displacement collisions, vacancy production, replacement collisions and interstitial atoms, as described below.

In the file, the number of Displacement collisions indicates how many target atoms were set in motion in the cascade with energies above their displacement energy (which you specified in the TRIM Setup window). The next item in the table is Target Vacancies. A vacancy is the hole left behind when a recoil atom moves from its original site. Next, the table shows Replacement collisions, which reduce the number of vacancies. If a moving atom strikes a stationary target atom and transfers more than its displacement energy to it, and the initial atom, after the collision, does not have enough energy to move onwards, and it is the same element as the atom it struck, then it just replaces that atom in the target and there is no vacancy created. Although this may sound complicated, this mechanism may reduce the total vacancies by up to 30%. The summation goes:

$$\text{Displacements} = \text{Vacancies} + \text{Replacement Collisions}$$

Finally, the table lists interstitial atoms. When a recoil atom stops, and is not a replacement atom, then it becomes an interstitial. These may be summed as:

$$\text{Vacancies} = \text{Interstitials} + (\text{Atoms which leave the target volume})$$

If a cascade atom leaves the target volume, it is no longer followed. That is, if it leaves the target front surface or the rear surface, it is noted and then discarded. TRIM will follow atoms indefinitely as they go sideways, even though they leave your screen. But if they go through either target surface they are discarded and not counted. So vacancies occur within the target, and the final resting place of a moving recoil atom can be some distance from its vacancy. If the recoil leaves the target, clearly the sum of interstitials will be less than the number of vacancies by the

loss of that atom. Replacement collisions are not part of this equation because each replacement collision reduces the number of vacancies and the number of interstitials by one, leaving the equation in balance. Finally, an atom which comes to rest in the topmost monolayer of the target is always assumed to be a lattice atom if it originated in that layer (i.e. it is neither a replacement nor an interstitial atom).

The calculation of cascades, target displacements, replacement collisions, etc. makes certain assumptions which are defined explicitly below:

Assume an incident atom has atomic number Z_1 , and energy E . It has a collision within the target with an atom of atomic number Z_2 . After the collision, the incident ion has energy E_1 and the struck atom has energy E_2 . Previously specified for the target are energies E_d , the displacement energy, E_b , the binding energy of a lattice atom to its site, and E_f , the final energy of a moving atom, below which it is considered to be stopped.

A **displacement** occurs if $E_2 > E_d$ (the hit atom is given enough energy to leave the site). A **vacancy** occurs if both $E_1 > E_d$ and $E_2 > E_d$ (both atoms have enough energy to leave the site). Both atoms then become moving atoms of the cascade. The energy, E_2 , of atom Z_2 is reduced by E_b before it has another collision. If $E_2 < E_d$, then the struck atom does not have enough energy and it will vibrate back to its original site, releasing E_2 as **phonons**.

If $E_1 < E_d$ and $E_2 > E_d$ and $Z_1 = Z_2$, then the incoming atom will remain at the site and the collision is called a **replacement collision** with E_1 released as **phonons**. The atom in the lattice site remains the same atom by exchange. This type of collision is common in single element targets with large recoil cascades. If $E_1 < E_d$ and $E_2 > E_d$ and $Z_1 \neq Z_2$, then Z_1 becomes a stopped **interstitial** atom.

Finally, if $E_1 < E_d$ and $E_2 < E_d$, then Z_1 becomes an **interstitial** and $E_1 + E_2$ is released as **phonons**. If a target has several different elements in it, and each has a different displacement energy, then E_d will change for each atom of the cascade hitting different target atoms.

For those using the TRIM "quick" calculation of target damage, TRIM uses the Kinchin-Pease analytic solution for target damage as modified by two later authors. Typical output is shown in the Chapter 9 on **TRIM Outputs**. The following references would also help in understanding its formalism:

-
1. Kinchin and R. S. Pease, Rep. Prog. Phys., vol. 18, 1 (1955).
 2. P. Sigmund, Rad. Eff., vol. 1, 15 (1969).
 3. M. J. Norgett, M. T. Robinson and I. M. Torrens, Nucl. Eng. Design, vol. 33, 50 (1974).

COLLISON.TXT (Tabulated Detail of Collision Kinetics)

Some users need to know many more details about ions penetrating targets than is collected in the preceding plots and datafiles. For these users, it is possible to tabulate every detail of every collision between the ion and the target atoms, as well as every detail of every recoil cascade.

Details of the ion's penetration into the target can be put into a datafile, ***..SRIM Outputs/COLLISON.txt***, for later examination. To get the most detailed file, in the TRIM Setup window select "Monolayer Collision Step" in the Damage menu in the upper-right corner. Then

check “*Collision Details*” in the same Setup window, at the bottom. When a sub-menu comes up and asks if details of the Recoils should also be kept, answer “Yes”.

This selection will overwhelm you with data. For the first **5** ions of the ion/target used in this chapter for an example (see Figure 9-1), the datafile will contain 94,000 numbers concerning 12,000 collisions. TRIM provides various filters to help you to screen this data. For example, if you are mostly interested in sampling the ion’s impact on the target, change your TRIM Setup selection from “*Monolayer Collision Step*” to “*Detailed Calculation with Full Damage Cascades*”, and the output datafile drops by 10% to 11,000 collisions. This is because TRIM now uses the Free Flight Path assumption (see Ch. 8 and 9). To further filter the data, if you care mostly about how the ion affects the target, and you can ignore the recoil cascades, then when you are in the TRIM Setup window, select “*Collision Details*” and when the sub-menu asks to store data about the recoils, answer “No”. This will reduce the **COLLISON.txt** output for the first 5 ions another 90%, down to about 1,100 collisions.

The datafile **..SRIM Outputs/COLLISON.txt** contains the kinetic data of all Ion-Atom collisions. The datafile is opened when the *Collision Details* button is pressed either in the TRIM Setup window, or in the TRIM Calculation window. After this selection, data is added for every subsequent collision. Three types of files may be generated, which vary in the amount of detail stored:

- (A) For a "Quick Damage" calculation, the damage details for each ion are summarized. No recoils are included.
- (B) For a "Full Recoils" calculation, the details of every ion/atom collision which leads to a displacement are itemized.
- (C) For a "Full Recoils" calculation, the details of every ion/atom collision and also every recoil atom/atom collision are itemized.

Special Note

These files are the most complete data files in TRIM, since they contain every significant detail of the calculation. Type “A” does not contain every collision, since the Free Flight Path approximation allows large jumps of the ion over many monolayers of targets without intervening collisions. (See Chapter 7, TRIM Theory, on the concept of a Free Flight Path.) This approximation may be overridden by specifying “*Use Monolayer Steps*” in the setup window for TRIM (this selection is in the upper right corner of the TRIM Setup window).

The file **COLLISON.txt** can increase in size very rapidly and GigaBytes of data may be generated for just a few thousand heavy ions with high energies. It is best to try a short test of **COLLISON.txt** to estimate the rate at which datafiles are generated.

Each of the three types of **COLLISON.txt** (as noted above) will be considered separately. The output file contains a notation for the various approximations used so that you can tell the conditions that generated the file.

COLLISON.txt - Type "A"- Ions and Quick Estimate of Damage

This variation on **COLLISON.txt** will be called type “A”. This **COLLISON.txt** datafile will contain information on every ion/target collision which results in a recoil cascade. For the “Quick Damage” calculation, TRIM uses the Kinchin-Pease approximation to predict damage based on the ion, its energy at collision, the atom hit and the target matrix. It allows for the very rapid calculation of

damage, but may be in error by up to a factor of two.

This approximation can be chosen in the TRIM Setup window, or in the TRIM Calculation window. When the **Collision Details** button is chosen in either window, a sub-menu asks whether a new file should be generated, or to add onto an existing file. Note that you must separately choose “*Ion Distribution with Quick Calculation of Damage*” (upper right corner in TRIM Setup window) in order to complete the selection of a type **A** datafile.

Table 9-18 - COLLISON.TXT (with Kinchin-Pease Damage)

--- Datafile Header Deleted ---

Only Ion Collisions which produce Displacements are tabulated.
Sums and Averages are Incomplete if Recoil Cascades Leave Target
Target DISPlacements = VACancies + REPLACEMENT Collisions.
Target VACancies = INTERstitials + Sputtered + Transmitted Atoms
Recoil Atoms which end at the surface, are not counted

Ion Numb	Energy (keV)	Depth (Å)	Lateral Distance(A) Y Axis	Z Axis	Se (eV/Å)	Atom Hit	Recoil Energy(eV)	Target DISP.
001	19.44E+01	6556.E-03	-5879.E-04	7829.E-04	070.9	W	2692.E-03	001.000
001	18.79E+01	1108.E-02	-3462.E-03	2453.E-03	069.7	W	1391.E-02	002.372
001	18.30E+01	1983.E-02	-1796.E-02	-1620.E-03	068.9	W	9326.E-03	001.601
001	16.93E+01	3714.E-02	-3236.E-02	-5096.E-03	066.4	W	1346.E-02	002.297
001	16.46E+01	4553.E-02	-4331.E-02	1341.E-04	065.6	W	3279.E-03	001.000
001	16.46E+01	4972.E-02	-4685.E-02	5893.E-04	065.5	W	3610.E-02	006.046
001	15.87E+01	5387.E-02	-4707.E-02	-6262.E-03	064.5	W	3775.E-03	001.000
001	15.04E+01	7401.E-02	-6075.E-02	-4969.E-02	062.9	W	3549.E-02	005.947
001	13.69E+01	8856.E-02	-7700.E-02	-1139.E-01	060.4	W	4198.E-03	001.000

The datafile shown in Table 9-18 starts when ion #001 enters the target and has its first collision at a depth of 6.56Å when it has an energy of 194.4 keV. (Because of the Free Flight Path, there is not a collision in every target monolayer.) The Lateral Distance column shows a slight displacement from the original ion axis. The ion hits a W atom, and gives up 2.69 eV to this atom. It creates 1.0 target displacements. Note that other harder collisions in the table generate fractional displacements since the displacements are calculated using the Kinchen-Pease approximation. If you wish to make the ion interact with every monolayer of the target, then in the TRIM Setup window specify “*Use Monolayer Collision Steps*”.

Unlike the detailed damage and recoil data shown in the *COLLISON.txt* files type **B** and **C**, described below, for the Kinchen-Pease approximation there is only a single estimate of the target displacements produced. This calculation is made with the same random numbers as that of the more detailed tables of the “*Full Recoils*” calculation, so there is a direct correspondence in collisions. In general, Kinchen-Pease estimates more displacements than TRIM with full recoil cascades.

COLLISON.txt - Type "B"- Ions and Recoil Atoms (no cascade data)

This variation on *COLLISON.txt* will be called type “**B**”. This version of *COLLISON.txt* shows only those collisions which result in a recoiling target atom, i. e. only those collisions in which the ion transfers to the target atom an energy greater than its displacement energy (which was entered in the setup program). Additionally, this datafile contains additional information as noted below:

This approximation can be chosen in the TRIM Setup window, or in the TRIM Calculation window. When the ***Collision Details*** button is chosen in either window, a sub-menu asks whether a new file should include data for Recoil. Select “**No**” to generate this type **B** datafile. Note that you must separately choose “*Detailed Calculation with Full Damage Cascades*” or “*Use Monolayer Collision Steps*” (menu in the upper right corner in TRIM Setup window) in order to complete the selection of a type **B** datafile.

In the file below, ***Se (eV/Å)*** is the electronic stopping power of the ion in the target at its current energy. This energy is modified by including a straggling component (random variation) in the calculation, so that the actual ion electronic energy loss between specific collisions can not be directly obtained from this number. Because of mathematically required statistical fluctuations, the ion energy may actually increase between collisions (this sounds crazy, but it really is true).

Target ***Displacements, Vacancies, Replacement Collisions, and Interstitial Atoms*** were described previously in this chapter in the section **Physics of Recoil Cascades**. They are also described in Chapter 7 - **TRIM Theory**. These types of damage constitute the changes introduced into the target by each collision. Since data on recoils was not requested for a type **B** datafile, the final results of each collision cascade are given in four columns of target damage (number of displacements, vacancies, replacement collisions and interstitial atoms).

Table 9-19 - COLLISON.txt (Recoil Atoms without cascade data)

COLLISION HISTORY												
Ion Numb	Energy (keV)	Depth (Å)	Lateral Distance (Å) Y Axis	Lateral Distance (Å) Z Axis	Se (eV/A)	Atom Hit	Recoil Egy(eV)	Tgt DISP.	Tgt VAC.	Tgt REPL	Tgt INTER	
001	19.44E+01	65564.E-03	-5879.E-04	7829.E-04	0070.90	W	26922.E-03	002	001	001	002	
001	18.44E+01	15224.E-02	-7317.E-03	3660.E-03	0069.15	W	75609.E-03	006	005	001	006	
001	17.99E+01	31873.E-02	-2894.E-02	2599.E-02	0068.34	W	33106.E-02	011	010	001	011	
001	17.19E+01	39161.E-02	-4127.E-02	2706.E-02	0066.90	W	89507.E-03	005	003	002	005	
001	17.03E+01	43332.E-02	-4873.E-02	3179.E-02	0066.62	W	94263.E-03	006	006	000	006	
001	15.60E+01	62681.E-02	-1008.E-01	5174.E-02	0064.01	W	92898.E-03	004	002	002	004	
001	15.13E+01	71468.E-02	-1331.E-01	4748.E-02	0063.14	W	46885.E-03	003	003	000	003	
001	14.63E+01	75113.E-02	-1468.E-01	4719.E-02	0062.22	W	52406.E-03	003	003	000	003	

For correct Display of this file, use Microsoft font “*Courier New*” or “*MS-LineDraw*”. “*Linedraw*” is included in the SRIM software package. See the subdirectory: SRIM/Data/Linedraw.ttf

COLLISON.txt - Type "C"- Ions, Recoil Atoms and Cascades

This variation on *COLLISON.txt* will be called type "C". This version of *COLLISON.txt* includes all the ion/target collisions which result in a recoiling target atom, and also the history of what happens to that recoiling atom and also any atoms that recoil hits, i.e. the full details of the full recoil cascade.

Table 9-20 - COLLISON.txt (Full Recoil Cascades)

COLLISION HISTORY												
NOTES: Only Ion Collisions which produce Displacements are tabulated. Atom Sums and Averages are Incomplete if Recoil Cascades Leave Target. Target DISPlacements = VACancies + REPLACEMENT Collisions. Target VACancies = INTERstitials + Sputtered + Transmitted Atoms. Recoil Atoms which end at the surface, are not counted (see manual).												
Ion Numb	Energy (keV)	Depth (A)	Lateral Distance (A)	Se Y Axis	Atom Z Axis	Recoil (eV/A)	Hit	Tgt Egy(eV)	Tgt DISP.	Tgt VAC.	Tgt REPLAC.	INTER
001	9.4E+01	65564.E-03	-587.E-04	7829.E-04	0070.90	W	26922.E-03					<= New Cascade
Recoil Atom Energy(eV)		X (A)	Y (A)	Z (A)	Vac	Repl	Ion Numb					
00001	74	26922.E-03	65564.E-02	-5879.E-04	7829.E-04	1	00					<-Prime Recoil
00002	74	00000.E+00	6577.E-02	1880.E-03	1167.E-03	0	01					
00003	74	22058.E-03	6577.E-02	1880.E-03	1167.E-03	1	00					
Summary of Above Cascade =>												
001	18.4E+01	15224.E-02	-7317.E-03	3660.E-03	69.15	W	75609.E-03					= New Cascade
Recoil Atom Energy(eV)		X (A)	Y (A)	Z (A)	Vac	Repl	Ion Numb					
00001	74	75609.E-03	1522.E-01	-7317.E-03	3660.E-03	1	00					<-Prime Recoil
00002	74	33842.E-03	1517.E-01	-6850.E-03	-1038.E-03	1	00					
00003	74	27773.E-03	1504.E-01	-7967.E-03	-2840.E-03	1	00					
00004	74	24541.E-03	1483.E-01	-7860.E-03	-1394.E-03	1	00					
00005	74	26789.E-03	1527.E-01	-6710.E-03	1267.E-03	1	00					
00006	74	00000.E+00	1530.E-01	-8912.E-03	2419.E-03	0	01					
00007	74	23177.E-03	1530.E-01	-8912.E-03	2419.E-03	1	00					
Summary of Above Cascade =>												
001	17.99E+01	31873.E-02	-2894.E-02	2599.E-02	0068.34	W	33106.E-02					= New Cascade
Recoil Atom Energy(eV)		X (A)	Y (A)	Z (A)	Vac	Repl	Ion Numb					
00001	74	33106.E-02	3187.E-01	-2894.E-02	2599.E-02	1	00					<-Prime Recoil
00002	74	41182.E-03	3156.E-01	-2969.E-02	3458.E-02	1	00					
00003	74	24907.E-03	3168.E-01	-3053.E-02	3254.E-02	1	00					
00004	74	21368.E-03	3166.E-01	-3245.E-02	3414.E-02	1	00					
00005	74	51224.E-03	3171.E-01	-3061.E-02	3005.E-02	1	00					
00006	74	14846.E-02	3187.E-01	-3019.E-02	2816.E-02	1	00					
00007	74	98698.E-03	3187.E-01	-3254.E-02	2904.E-02	1	00					
00008	74	73706.E-03	3187.E-01	-3505.E-02	2896.E-02	1	00					
00009	74	67029.E-03	3187.E-01	-3289.E-02	3024.E-02	1	00					
00010	74	29954.E-03	3186.E-01	-3150.E-02	3232.E-02	1	00					
00011	74	00000.E+00	3185.E-01	-3174.E-02	2983.E-02	0	01					
00012	74	22731.E-03	3185.E-01	-3174.E-02	2983.E-02	1	00					
Summary of Above Cascade =>												
001	17.19E+01	39161.E-02	-4127.E-02	2706.E-02	0066.90	W	89507.E-03					= New Cascade
--- Data Omitted ---												

For correct Display of this file, use Microsoft font "Courier New" or "MS-LineDraw". "Linedraw" is included in the SRIM software package. See the subdirectory: SRIM/Data/Linedraw.ttf

Table 9-20 is quite complicated since it contains all the kinetic information about every ion collision, as well as the data for every recoil collision. One must be careful of using this type of file because strong recoil cascades may involve 10,000+ sub-collisions which can rapidly make the file unmanageable.

This approximation can be chosen in the TRIM Setup window, or in the TRIM Calculation window. When the **Collision Details** button is chosen in either window, a sub-menu asks whether a new file should include data for Recoil. Select "Yes" to generate this type **C** datafile. Note that you must separately choose "Detailed Calculation with Full Damage Cascades" or "Use Monolayer Collision Steps" (upper right corner in TRIM Setup window) in order to complete the selection of a type **C** datafile.

See the comments for **COLLISON.txt**, type "**B**", for details about most of this table. The additional information is for the recoil cascades.

Analysis of Table 9-20 - COLLISON.txt (Full Recoil Cascades)

The calculation shown did not demand monolayer collisions (where the ion impacts a target atom every monolayer). Hence, the Free Flight Path approximation (see Ch. 8 and 9) allowed the ion to jump 66Å into the target for its first collision which transfers 27eV, and this causes the recoil to start a 3 atom cascade. This cascade is shown in detail in the box between this collision and next ion collision. The first line in this box shows the primary recoil (identified with "<- Prime Recoil") and then the succeeding recoils. If some of these secondary recoils cause further recoils, the box gets complicated. But each recoil is followed until it reaches zero energy, and then the last recoil it caused is tracked, etc. until the first recoil caused by the prime recoil is tracked. For a monoatomic target, Displacements = Vacancies + Replacements = Replacements + Interstitials. For more details, see brief explanation called **Physics of Recoil Cascades** which was copied from Chapter 7. More details are in Chapters 7 and 8. Note that the "Final Summary" of each cascade showing the target damage is identical in type "**B**" and type "**C**" tables.

Special Commands for a TRIM Calculation

Changing TRIM Parameters during the Calculation

Note that TRIM can be stopped during the calculation, and basic parameters may be changed. This allows the user to focus the calculation on a specific problem without having to start over. To change TRIM during a calculation, click on the button **Pause TRIM** at the top of the TRIM Calculation window. Then press **Change TRIM**. All the parameters which can be changed will have a yellow background, and it includes almost all Setup parameters. Make changes in the parameters, or in the colors used for the plots (clicking on the colors in the Target Data window will bring up a color-chart to use). When you are done, press **End Edit** and then **Continue**. You will be asked if you wish to add the next calculation to the previous results, or restart TRIM.. This procedure allows the user to modify a TRIM calculation simply, or include ions of different energies or incident angles (for example) into one plot. See Chapter 8 for more details.

Changing TRIM Plots and Colors (TRIM.cfg)

All of the TRIM plots and colors are set using the datafile: *../Data/TRIM.cfg*, see Table 9-21. Typical default settings are shown in this Table. If you change TRIM colors, e.g. using the color tables available in the TRIM Calculation window, then when you save TRIM these changes become the default values.

Table 9-21 -Datafile ..Data/TRIM.cfg (TRIM Plots and Colors)

[Ion Colors - MOVE, STOP]		
255	0	
[12 Recoil Colors - MOVE, STOP]		
1	6487906	837122
2	15982183	16417654
3	16744703	12519886
4	16777088	13814035
5	13159423	9673727
6	16760769	16711680
7	8421376	65280
8	6422724	12615935
9	8388736	16716287
10	4755857	8700353
11	9408399	12566463
12	255	0
[Distribution Plot Labels - SIZE, COLOR]		
6	8388608	
[4 Distribution Plot Colors]		
255	8388608	65280 16776960
[Plot Background, Outer Box, Axes, Layer Lines, Layer Names]		
16777215	255	0 0 0
Maximum number of secondary recoils (default=20000)		
20000		
Note: 100k recoils requires 2MB of memory, 1M recoils requires 35MB.		

The colors are identified by standard PC color codes, which are too complicated to review here. For example, the Ion Color is RED (#255) when it has a collision, and BLACK (#000) for the point where it stops. The target recoil atoms are identified by numbers 1-12 in the next section of Table 9-21. However, it is easiest to start a TRIM calculation, and then click on the button **Pause TRIM** at the top of the TRIM Calculation window. Then press **Change TRIM**. Expand the sub-window called **Target Data** and you will see bars of color for each of the target elements. Click on any one, and you can select a new color from a color grid. Change as many colors as you want, and see how they look by pressing **Continue** and opening a plot. When you finally stop the TRIM calculation and save it, these new colors will be stored as the default recoil atom colors.

Making TRIM Animated Plots

Normally TRIM waits until the end of each ion's path before plotting the details of this trajectory on the TRIM plots. However, it is possible to plot each collision as it occurs. In the TRIM Calculation window, in the **ION** sub-window, there is a box called **SHOW LIVE DATA**. You may press this at any time, and a new window will pop up, and show the ion's position (x, y, z co-ordinates) its energy, and the energy transferred to any cascade that it makes. The data moves

rather fast, but a quick finger can hit **Pause** to stop the ion at any instant to see where it is and what size cascade it has made. This display slows down the calculation.

To end this display, click on **END LIVE DATA**, and after the current ion completes its path, the sub-window will close and the calculation will resume normally.

TRIM “Help, FAQ and Scientific Explanations”

At the top of the TRIM Calculation window is a tab called **Help, FAQ and Scientific Explanations**. Many of the concepts of TRIM are in this file, and it is useful to read explanations while the TRIM calculation proceeds. It also has **Help** files for common errors that might occur.

Among the available topics are:

- **The Scientific Background of TRIM**
 - Physics of Recoil Cascades
 - Physics of Sputtering
 - The Stopping of Ions in Compounds
 - Stopping Powers for Ions in Gases
- **Special Applications of TRIM**
 - 3-D Plots of Electronic Energy Loss
 - Isotopically Enriched Targets
 - Ion Energy Reducers (Energy Degraders)
 - Adding Together Sequential TRIM Calculations
 - High Resolution Collision Data
 - Ion Mixing Experiments
- **TRIM FAQ and Solutions**
 - Printing Problems
 - High Resolution Plots
 - Statistics of Range Distributions
 - Peaks and Dips at Layer Edges
 - Auto-TRIM (Running TRIM in Batch Mode)
- **Identification of TRIM Programs and Software**

10 - STOPPING AND RANGE TABLES

Chapter Summary

The program SRIM allows the immediate construction of *Ion Stopping and Range Tables* in any material, for a wide range of ion energies. This application is based on a program called PRAL, as described in this chapter.

PRAL = Projected Range Algorithm

Analytic solutions for ion ranges provide a quick efficient way to obtain tables of ion energy vs. range. Normally, this is done by elaborate and complex solutions to the differential Boltzmann Equation, as described in the well-known LSS theory (63a) or Littmark et al. (81b). PRAL was developed by J. P. Biersack as a much simpler approach which connects the ion's angular divergence directly to the nuclear energy loss (82b, 82q). PRAL has been evaluated by many users, and it provides good agreement with other more-elaborate theories and also precise experimental results on projected ranges. This chapter discusses the theoretical basis of PRAL, explaining its various approximations.

Chapter Contents

10 - Stopping and Range Tables	10-1
DIRECTIONAL SPREAD OF MOTION	10-1
ANGULAR SPREAD PARAMETER, τ , AND ENERGY LOSS.....	10-3
Calculation of the Mean Projected Range.....	10-4
Analytic Treatment of Heavy-Ion Ranges	10-5
Universal Algorithm for Projected Ranges	10-6
CALCULATIONS WITH HIGH PRECISION.....	10-12
Projected Ranges in Compound Materials.....	10-13
LIMITATIONS OF PRAL CALCULATIONS.....	10-15
UNIVERSAL NUCLEAR STOPPING POWERS.....	10-15
Nuclear Straggling	10-18
LIMITATIONS OF PRAL CALCULATIONS OF ION DISTRIBUTIONS.....	10-18
CHAPTER 10 - CITATIONS	10-20

DIRECTIONAL SPREAD OF MOTION

The projected range of an ion is its path length (distance of travel) projected onto a coordinate axis. For an ion normally incident to a solid, typically the projected range is its final depth. The total path length of the ion may be much longer, depending on the number of violent collisions it undergoes. The average projected range of ions can be broken into the summation of the mean projections of each path length element. This summation can be accomplished by calculating the mean directional cosine of the ion motion during the slowing-down process, i.e. we have to consider the distribution of the directions of ion motion as a function of the ion energy. The general picture is simply that with each collision with a target atom, the ion loses energy and at the same time changes direction, where the *nuclear energy loss*, T , (due to momentum transfer to the target atom) is directly related to the *center-of-mass deflection angle*, Θ , of the ion:

$$\text{Eq. 10-1: } T = \frac{4M_1 M_2 E}{(M_1 + M_2)^2} \sin^2 \frac{\Theta}{2}$$

where M_1 and M_2 denote the masses of ion and target atom, respectively. The derivation of this equation was explained in Chapter 2. Consequently, with increasing nuclear energy loss the ion will tend to deviate more and more from its original direction. We may represent the directions of ion motion by the *polar angle*, Ψ , and the *azimuthal angles*, θ , and depict them as points on the unit sphere, Figure 10-1a, with the initial direction of ion motion on the pole ($\Psi = 0$), corresponding to the x axis, along which we want to measure the projected range. As the direction of motion changes at random with each collision, with no correlation between successive deflections, the point on our directional sphere performs a random walk, like a Brownian motion, as indicated in Figure 10-1a. If we project the point of the unit sphere onto the x axis (polar axis), we obtain values between -1 and +1, corresponding to the directional cosine of the ion motion, Figure 10-1b.

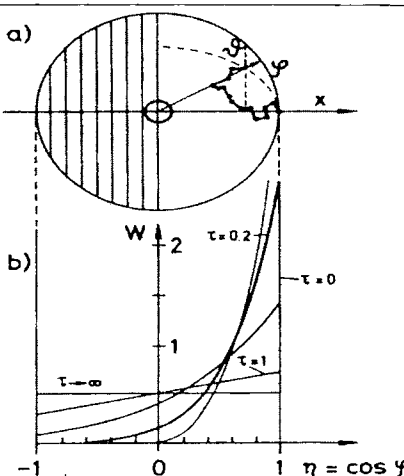


Figure 10-1 - Random Motion of Trajectory on Unit Sphere

Directional changes of ion motion are depicted as a Brownian motion on a unit sphere. Initially ($\tau \leq 1$), the ion motion is preferentially directed forward. Towards the end of the slowing-down process ($\tau \geq 1$), all directions become equally probable, resulting in a uniform distribution on the sphere (a) or in the directional cosines (b). In (b) intermediate distributions are also shown, according to the solution of Eq. 10-2.

If we now consider the *probability distribution function*, w , either of the polar angle Ψ or of the *directional cosine*, $\eta \equiv \cos \Psi$, we observe that (i) originally it is a delta function centered at $\Psi = 0$ or $\eta = 1$, (ii) the probability distribution then spreads out in a diffusion-like manner, while the ion slows down, until (iii) finally the ion has completely "forgotten" its initial direction, i.e. at the end of the trajectory, all directions of motion are equally probable. At this stage, the probability distribution is constant over the Ψ, θ sphere, and hence also constant over the range -1, +1 for η .

(slices indicated in Figure 10-1a have equal surface areas).

The qualitative picture can easily be converted into a more rigorous mathematical description: The stochastic motion on our unit sphere is governed by the diffusion equation:

$$\text{Eq. 10-2: } \frac{\partial w}{\partial \tau} = \frac{\partial}{\partial \eta} \left[(1-\eta^2) \frac{\partial w}{\partial \eta} \right]$$

where $\eta = \cos \Psi$, and τ is equivalent to Dt in ordinary diffusion. Solutions of this equation are readily obtained, and yield the curves shown in Figure 10-1b.

In assessing projected ranges, we actually need not know the distribution functions (η, τ) explicitly. For our purpose it is sufficient to find the average value of the directional cosine, $\bar{\eta}(\tau)$, which is obtained from Eq. 10-2, yielding the simple expression:

$$\text{Eq. 10-3: } \bar{\eta}(\tau) = \int_{-1}^{+1} \eta w(\eta, \tau) d\eta = \exp(-2\tau)$$

This result shows again - now in a quantitative way - how the initial forward motion, $\bar{\eta} = <\cos \Psi> = 1$, changes in the course of slowing down, i.e. with increasing τ , to the finally isotropic motion, $\bar{\eta} = <\cos \Psi> \rightarrow 0$, where no net forward motion but rather diffusional spread of the ions occurs. Forward motion, $\eta \geq 0$, and backward motion, $\eta \leq 0$, may become equally likely towards the end of the ion trajectory.

ANGULAR SPREAD PARAMETER, τ , AND ENERGY LOSS

We now show the relation between τ and the ion's nuclear energy loss. From the way τ was placed in the diffusion Eq. 10-2 or Eq. 10-3, τ is seen to correspond to Dt , or \sqrt{Dt} in ordinary space-time diffusion. In our case of a surface diffusion on the unit sphere, we may evaluate τ by using the two-dimensional Einstein relation:

$$\text{Eq. 10-4 } \delta \tau = \delta \phi^2 / 4$$

which is valid in the plane, and - to a good approximation - also in small surface regions of our unit sphere. $\delta \phi^2$ is the (mean) squared distance on the sphere connected to the increment $\delta \tau$ (or $D\delta t$). If in that interval a number, n , of collisions occurs, noting that in a random walk the squares of the distance are additive, we may write:

$$\text{Eq. 10-5 } \delta \tau = \frac{\delta \phi^2}{4} = \frac{1}{4} \sum_i^n \phi_i^2 \approx \frac{1}{4} \sum_i^n \frac{\Theta_i^2}{(1+M_1/M_2)} \approx \frac{1}{4} \frac{M_2 \sum T_i}{M_1 E}$$

Here the symbol " \approx " was used twice to indicate that small-angle approximations were used in both cases, (i) for converting the scattering lab angle, ϕ_i , into center-of-mass scattering angle, Θ_i , and (ii) to relate the scattering angle, Θ_i , to the transferred energy, T_i , according to Eq. 12-1.

Eq. 10-5 may be rewritten in the shorter form:

$$\text{Eq. 10-6: } \delta\tau = \frac{\mu \delta E_n}{4 E}$$

which most clearly indicates the natural connection between angular spread and nuclear energy loss δE_n , using the abbreviation: $\mu \equiv M_2/M_1$. Using the notation for *nuclear stopping*, $S_n(E)$, and for *total stopping powers*, $S_t(E)$, where the *projectile energy* is E , and its energy change is δE , one finally obtains:

$$\text{Eq. 10-7: } \delta\tau = -\frac{\mu S_n \delta E}{4 S_t E}, \quad \text{and} \quad \tau(E_0, E) = -\frac{\mu}{4} \int_{E_0}^E \frac{S_n dE}{S_t E}$$

where E_0 is the *initial energy of the ion*.

As mentioned above, our treatment has up to now been based on small-angle approximations corresponding to using only first terms of power series expansions which lead to $\delta\tau \approx \sum T_i \approx S_n$. Thus, τ depends up to now on $S_n(E)$ only, which of course contains no more information than a differential cross section depending only on a single variable, as in previous theories. In order to improve the precision beyond this level, one has to maintain higher terms of the various expansions in Eq. 10-5. For example, the last step in Eq. 10-5 :

$$\text{Eq. 10-8: } \frac{\Theta^2}{4} = \sin^2 \frac{\Theta}{2} + \frac{1}{3} \sin^4 \frac{\Theta}{2} + \frac{8}{45} \sin^6 \frac{\Theta}{2} + \dots$$

would lead - with Eq. 10-1 - to the terms $\sum T_i$, $\sum T_i^2$, $\sum T_i^3$ and finally to S_n , Q_n , and higher moments in nuclear energy loss. Clearly, the set of energy-loss moments contains the full information on the differential cross section.

Calculation of the Mean Projected Range

The *mean projected range*, \bar{x} , is now, by application of Eq. 10-3 and Eq. 10-7, directly accessible, as easily as the *total path length*, s :

$$\text{Eq. 10-9: } s = \int ds = \int_{E_0}^{E_0} \frac{dE}{S_t(E)}$$

$$\text{Eq. 10-10: } \bar{x} = \int <\cos\psi> ds = \int_{E_0}^{E_0} \frac{\exp[-2\tau(E_0, E)]}{S_t(E)} dE$$

Each *path length element*, s , of the ion trajectory is projected on the x axis by multiplying with the corresponding directional cosine. Although the mean projected range for ions of an energy E_0 may be calculated directly by first obtaining $\tau(E_0, E)$ through Eq. 10-7, and inserting this into Eq. 10-10, it should be mentioned that more practical methods for obtaining tables of \bar{x} vs. E will be developed.

Analytic Treatment of Heavy-Ion Ranges

For heavy ions of low energy, the nuclear stopping is the dominant slowing-down process. If we use $S_t \approx S_n$ in Eq. 10-7, we obtain:

$$\text{Eq. 10-11: } \tau = \frac{\mu}{4} \ln\left(\frac{E_0}{E}\right) .$$

and the mean projected range becomes, through Eq. 10-10 :

$$\text{Eq. 10-12: } \bar{x} = \int_{E_0}^{\infty} \frac{\exp(-2\tau)}{S_t} dE = \int_{E_0}^{\infty} \left(\frac{E}{E_0}\right)^{\mu/2} \frac{dE}{S_t(E)}$$

which, using the *path length*, $s(E)$, expands to:

$$\text{Eq. 10-13: } \bar{x} = \left(\frac{E}{E_0}\right)^{\mu/2} s(E) \Big|_0^{E_0} - \int_0^{E_0} \frac{\mu}{2E_0} \left(\frac{E}{E_0}\right)^{\mu/2-1} s(E) dE$$

We have applied partial integration in the last step. In this interim result, Eq. 10-13, the first term yields only $s(E_0)$, the total path length itself, while the second term indicates the reduction due to angular deviations from a straight forward flight path.

In the low-energy regime, stopping powers and ranges follow power laws over wide energy regions; e.g. it was shown in Ref. (77c) that the expression $de/dp = 1/2 \ln(1+\epsilon)/(\epsilon + Ae^B)$, with the parameter B made to give the best fit to realistic stopping powers ($0 < B < 1$). This expression leads for low energies, $\epsilon \ll 1$, to $de/dp \approx \epsilon^{1-B}/2A$, and hence to a total range $\approx (2A/B)\epsilon^B$, where B is about 1/2. If we use $s \approx E^B$ in Eq. 10-12 and Eq. 10-13, we obtain:

$$\text{Eq. 10-14: } \bar{x} = s(E_0) \frac{\mu s(E_0)}{2B + \mu} = \frac{s}{1 + \mu/2B}$$

Correspondingly, the second moment of the range distribution (range straggling) can be obtained through:

$$\text{Eq. 10-15: } \overline{x^2} = \frac{s^2}{1 + \mu/B}$$

which yields the variance of the projected range distribution:

$$\text{Eq. 10-16: } \sigma_x^2 \equiv \overline{x^2} - \bar{x}^2 = \frac{(\bar{x}\mu/2B)^2}{1 + \mu/B}$$

These simple expressions yield quite satisfactory results as compared with other more sophisticated calculations. An example is shown in Figure 10-2, where PRAL results (heavy lines) are compared

to solutions of the full transport equation (light lines) as obtained by Littmark and Ziegler (81b) and (84a).

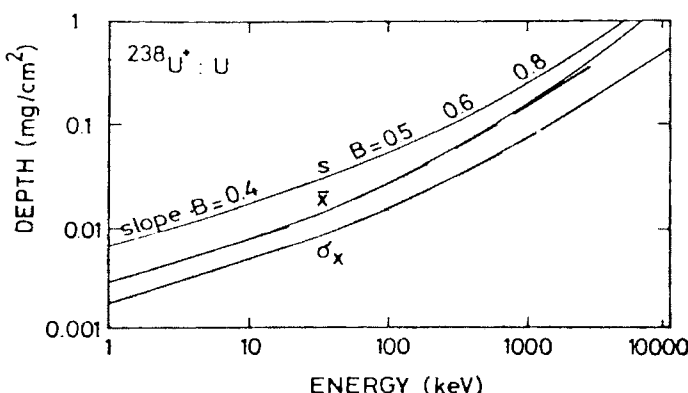


Figure 10-2 - Analytic Ranges for Heavy Ions

Simple analytical range predictions for heavy ions, where nuclear stopping is predominant: The expressions $s/x = 1 + \mu/2B$, and $\sigma/x = (1 + \mu/B)^{1/2} \mu/2B$, are applied to deduce x and σ from the total path length, $s(E)$. B is the slope of $s(E)$ in the log-log plot, and $\mu \equiv M_2/M_1$. The light lines are the results of the detailed transport theory of Littmark and Ziegler (81a and 84a), while the heavy lines are from PRAL, discussed in this chapter. They are in excellent agreement.

Universal Algorithm for Projected Ranges

In some cases, the user wants to apply arbitrarily chosen functions for $S_e(E)$ and $S_n(E)$, the electronic and nuclear stopping powers, other than the default ones of PRAL, or he has to deal with compound targets, containing more than one element. For such general calculations of projected ranges, the theory can be developed further to provide $\bar{x}(E + \Delta E)$ from a given $\bar{x}(E)$ in an iterative way, starting with $\bar{x}(0) = 0$. This is most easily accomplished by differentiating Eq. 10-10 with respect to E_0 , which appears once in the integral boundary and once in the function $\tau(E_0, E)$, thus yielding the following two terms:

$$\text{Eq. 10-17: } \frac{d\bar{x}}{dE_0} = \frac{\exp[-2\tau(E_0, E)]}{S_i(E_0)} + \int_{E_0}^{\infty} \frac{\partial \exp[-2\tau(E_0, E)]}{\partial E_0} \frac{dE}{S_i(E)}$$

From Eq. 10-7 for $\tau(E_0, E)$ one obtains $\tau(E_0, E_0) = 0$, and:

$$\text{Eq. 10-18: } \frac{\partial \tau}{\partial E_0} = \frac{\mu}{4} \frac{S_n(E_0)}{S_i(E_0) E_0}$$

which is used in Eq. 10-17 to yield:

$$\text{Eq. 10-19: } \frac{d\bar{x}}{dE_0} = \frac{1}{S_i(E_0)} - \frac{2\mu S_n(E_0)}{4S_i(E_0)E_0} \int_{E_0}^{\infty} \frac{\exp[-2\tau(E_0, E)]}{S_i(E)} dE$$

The last integral equals \bar{x} , according to Eq. 10-10, and hence we obtain :

$$\text{Eq. 10-20: } \frac{d\bar{x}}{dE_0} = \frac{1}{S_i} - \frac{\mu S_n}{2S_i E_0} \bar{x}$$

This is a linear differential equation for $\bar{x}(E_0)$ with the initial condition $\bar{x}(0) = 0$, which is easily solved by standard computer routines. This can be simplified even further by replacing \bar{x}/dE_0 by $[\bar{x}(E_0 + \Delta E_0) - \bar{x}(E_0)]/\Delta E_0$ to obtain for the range algorithm:

$$\text{Eq. 10-21: } \bar{x}(E_0 + \Delta E_0) = \bar{x}(E_0) + \left[1 - \frac{\mu S_n \bar{x}(E_0)}{2E_0} \right] \frac{\Delta E_0}{S_i}$$

This iteration has the advantage of using the least number of program steps and memory locations.

An example for applying Eq. 10-21 is shown in Figure 10-3 for the case of boron implantation in silicon, which has been experimentally studied. Besides the *projected range*, \bar{x} , the *projected range straggling*, σ_x , is now also accessible in experiment and theory, and is depicted in Figure 10-3 as well. In the present theoretical model, the *projected range variance*, σ_x^2 , is defined

$$\text{Eq. 10-22: } \sigma_x^2 = \bar{x}^2 - \bar{x}^2$$

and it is obtained through the following equations:

$$\text{Eq. 10-23: } \frac{d\bar{x}^2}{dE} = (\bar{x}^2 - \bar{x}^2) \frac{\mu S_n}{ES_i} + \frac{2\bar{x}}{S_i}$$

and

$$\text{Eq. 10-24: } \frac{d\bar{z}^2}{dE} = (\bar{x}^2 - \bar{z}^2) \frac{\mu S_n}{ES_i}$$

where \bar{z}^2 denotes the *lateral straggling*, measured along a Cartesian axis normal to the x axis. The *lateral straggling*, $\sigma_z^2 \equiv \bar{z}^2$, is here obtained as a by-product and is depicted as a dashed line in. The agreement of the present results with LSS results (75g) and with experiments (81o) is good, including σ_z values. Eq. 10-23 and Eq. 10-24 can be applied in various ways, e.g. summing the two equations yields a simpler equation:

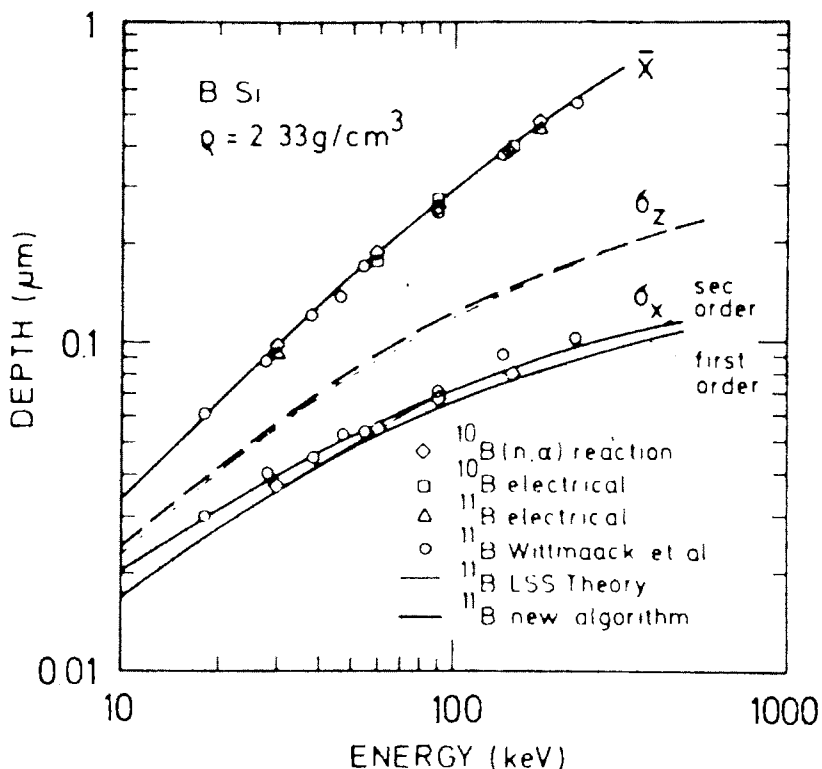


Figure 10-3- Comparison of PRAL with Experiments

Comparison of the present range algorithm with transport theory (75g) and precision measurements (81o), for boron ranges in silicon. Projected ranges, $x(E)$, from the LSS theory [63a], and from the present calculation to the first order or to a higher order, fall all on one line. Longitudinal Range Straggling $\equiv \sigma_x(E)$, and lateral range straggling $\equiv \sigma_z(E)$, are depicted by heavy lines (present predictions) and by light lines (LSS predictions). For electronic stopping, the standard value of $k = 1.59 k_{LS}$ was used.

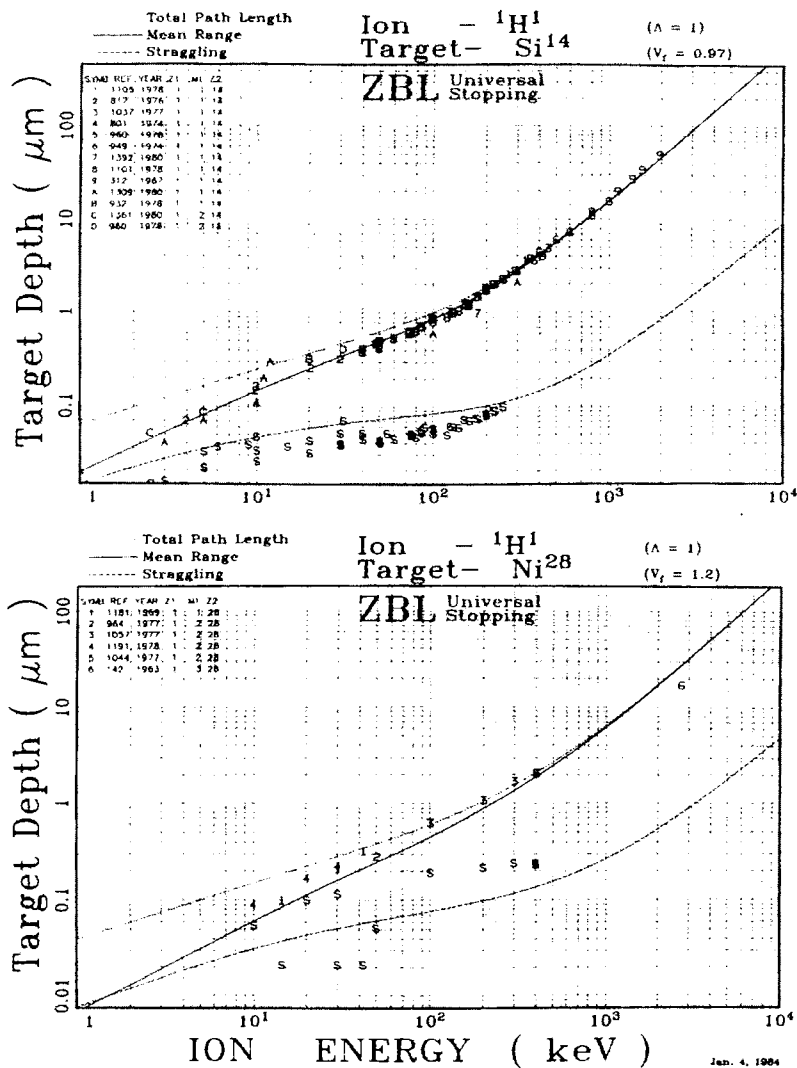


Figure 10-4 Comparison of PRAL Ranges and Straggling with Experiments

The plot shows PRAL calculations for H ions into targets of silicon and nickel. In both cases, the range calculation (solid line) is within the spread of experimental data. The range calculation (dotted line) is the range without nuclear scattering. The straggling calculation is somewhat high for the case of the silicon target, but within the wide scatter of experimental data for the nickel target.

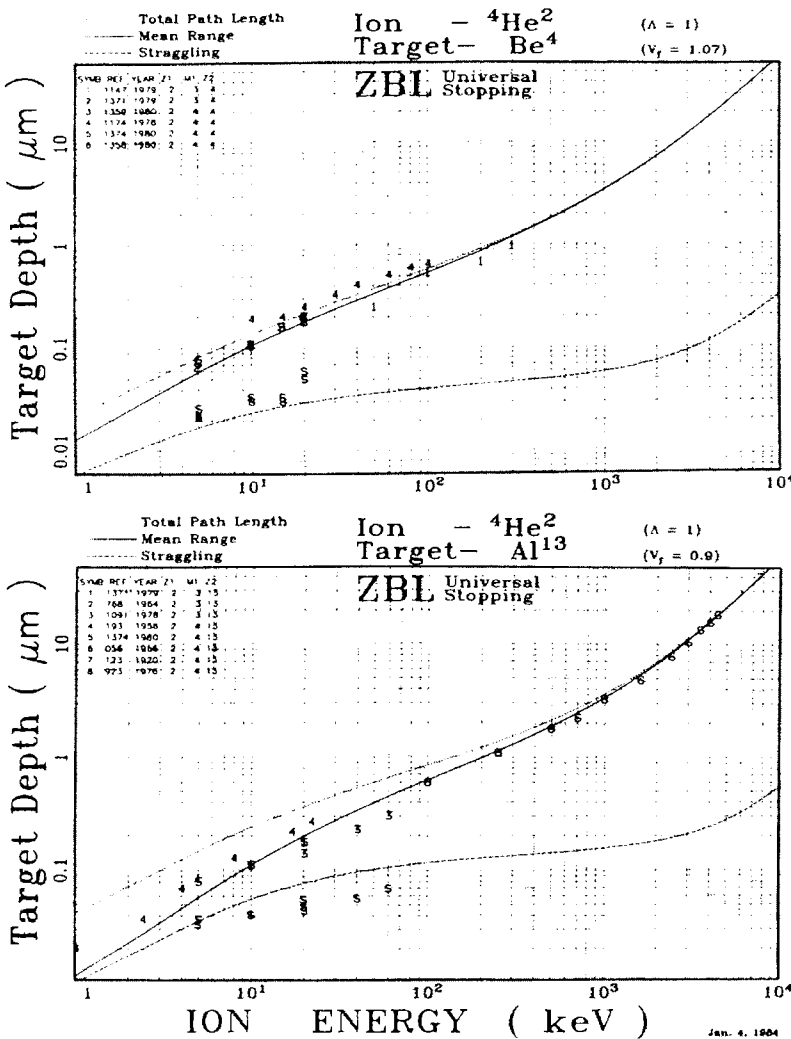


Figure 10-5 Comparison of PRAL Ranges and Straggling with Experiments

The plot shows PRAL calculations for He ions into targets of beryllium and aluminum. In both cases, the range calculation (solid line) is within the spread of experimental data. The range calculation (dotted line) is the range without nuclear scattering. The straggling calculation is somewhat high for both targets.

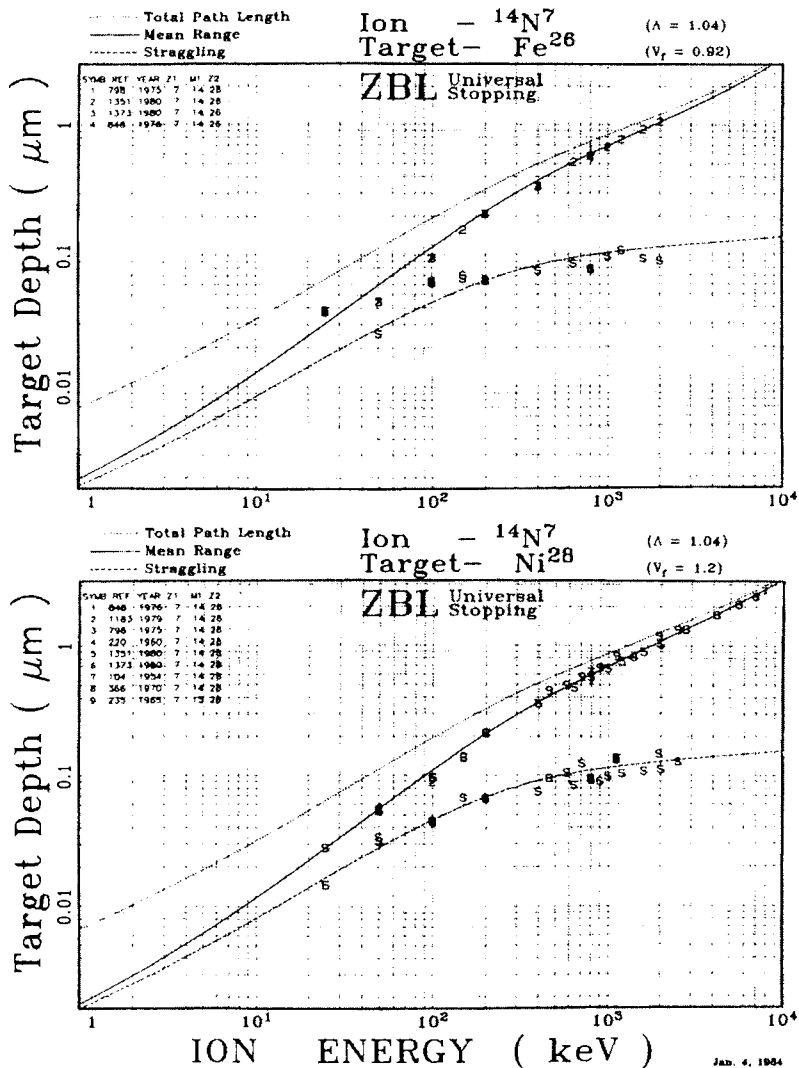


Figure 10-6 Comparison of PRAL Ranges and Straggling with Experiments

The plot shows PRAL calculations for heavy Nickel ions into targets of iron and nickel. In both cases, the range calculation (solid line) is within the spread of experimental data. The range calculation (dotted line) is the range without nuclear scattering. The straggling calculation is also quite good for both targets.

$$\text{Eq. 10-25: } \frac{d}{dE} \left(\overline{x^2} + \overline{z^2} \right) = \frac{2\overline{x}}{S_t}$$

which together with Eq. 10-24 leads to the following algorithm, using the notation :

$$\xi \equiv \overline{x^2} + \overline{z^2} :$$

$$\text{Eq. 10-26: } \xi(E + \Delta E) = \xi(E) + \frac{2\overline{x}(E)}{S_t E} \Delta E$$

and

$$\text{Eq. 10-27: } \overline{z^2}(E + \Delta E) = \overline{z^2}(E) + [\xi(E) - 2\overline{z^2}(E)] \frac{\mu S_n(E)}{ES_t(E)} \Delta E$$

Eq. 10-21, Eq. 10-26 and Eq. 10-27, in that sequence, provide an efficient method for calculating projected ranges and range straggling.

CALCULATIONS WITH HIGH PRECISION

In order to estimate the precision of our projected range predictions, we need to include higher terms of the expansions used in Eq. 10-4 and Eq. 10-5, and to determine their contributions. In these equations, the small angle approximations were used in all places, where the symbol " \approx " was placed instead of the equal sign. If all these approximations were developed to higher terms, then, besides T, also T^2 , T^3 , ... would enter the equations, leading finally to S_n , Q_n and higher energy loss moments in nuclear stopping. Including for example the second moment in nuclear energy loss, $Q_n = d(E_n^2)/dx$ (but still neglecting electronic energy loss straggling as in LSS range calculations where $Q_e=0$), our range equations (instead of Eq. 10-21, Eq. 10-26 and Eq. 10-27) would now be:

$$\text{Eq. 10-28: } \left(S_t - \frac{\mu Q_n}{2E} \right) \frac{d\overline{x}}{dE} = 1 - \left(\frac{\mu S_n}{2E} + \frac{\mu Q_n}{4E^2} \right) \overline{x}$$

$$\text{Eq. 10-29: } S_t \frac{d\xi}{dE} = 2\overline{x} \quad \text{and} \quad \xi = \overline{x^2 + z^2}$$

giving:

$$\text{Eq. 10-30: } \left(S_t - \frac{2\mu Q_n}{E} \right) \frac{d\overline{z^2}}{dE} = \left(\frac{-2\mu Q_n \overline{x}}{ES_t} \right) + \left(\frac{\mu S_n}{E} - \frac{(1-\mu)^2 Q_n}{4E^2} \right) \left(\xi + 2\overline{z^2} \right)$$

These equations are written in a differential form, as in the source reference (82q), and should be changed to finite differences, as Eq. 10-21, Eq. 10-26 and Eq. 10-27, for numerical solutions on the computer. This conversion requires a division by the forefactor of the differential quotient. In the previous equation and in the new Eq. 10-28 and Eq. 10-29, these factors, S_t or $(S_t -$

$0.5\mu Q_n/E$), are always positive and cause no problems. In dealing with Eq. 10-30, however, users reported difficulties, as the forefactor $(S_t - 2\mu Q_n/E)$ can become zero. In this case, one has to realize that Eq. 10-30 is no longer a differential equation but a simple algebraic equation which can be directly solved for the unknown, \bar{z}^2 , after inserting the already known quantities, \bar{x} and ξ , obtained through the two previous Eq. 10-28 and Eq. 10-29. Results of this set of equations for the mean projected range, \bar{x} , differ only slightly from the results obtained by the first order treatment. For example, differences of only a few percent were observed in \bar{x} . This good precision can best be understood by considering that at low energies $\bar{x} \propto E^B$ with $B \approx 1/2$ holds true, c.f. Figure 10-2, and that for the case $B=1/2$ the two terms in Eq. 10-28 containing $\mu Q_n/E$ cancel each other exactly. At higher energies, the $\mu Q_n/E$ terms become small enough to be neglected.

For the calculation of the second order range moments, \bar{x}^2 and \bar{z}^2 , it is more significant to take the Q_n terms into account, particularly for heavy ions at low energies, where nuclear stopping is the main slowing-down process. This is demonstrated in Figure 10-7 for the well documented case of Bi^+ implanted into silicon. While our first order treatment, Eq. 10-21, Eq. 10-26 and Eq. 10-27, reproduced the LSS results, see Figure 10-2, the newly included Q_n terms have the effect of increasing the *longitudinal range straggling*, σ_x^2 , at the cost of the *transverse straggling*, σ_z^2 . In light of precise experimental data, as depicted for example in Figure 10-7, the agreement between theory and experiments appear well improved with the inclusion of Q_n in Eq. 10-30, which may justify the use of this slightly more complex equation instead of Eq. 10-27.

Projected Ranges in Compound Materials

Although our present approach for calculating projected range moments is equivalent to solving the Boltzmann Equation, as shown in ref. (82q and 84a), it has one important advantage: the present derivations and equations are independent of the value of the mass ratio, $\mu = M_2/M_1$, be it large or small. Thus the range equations can be developed similarly for any target material composed of arbitrary constituents, i.e. atoms of any masses. The resulting equations are the same as Eq. 10-28, Eq. 10-29 and Eq. 10-30, except that now μS_n , μQ_n , and $(1-\mu)^2 Q_n$ have to be replaced by

$$\text{Eq. 10-31: } \langle \mu S_n \rangle = \sum_i \mu_i S_{n_i}$$

$$\text{Eq. 10-32: } \langle \mu Q_n \rangle = \sum_i \mu_i Q_{n_i}$$

$$\text{Eq. 10-33: } \langle (1-\mu)^2 Q_n \rangle = \sum_i (1-\mu_i)^2 Q_{n_i}$$

where the sums are taken over the number of different atomic species in the target. The target composition is implicitly accounted for, as in our notation S_n , Q_n , etc. are defined as energy loss, energy straggling etc. *per path length*, i.e. they include the atomic densities, N_i , as factors.

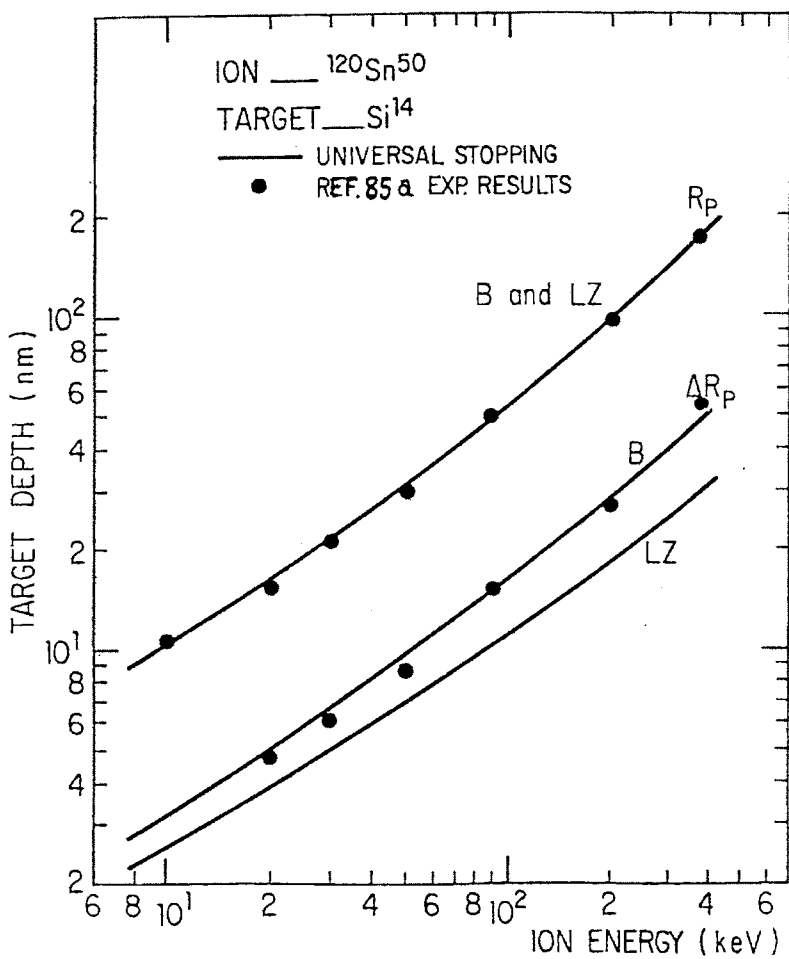


Figure 10-7 - Comparison of PRAL with More Detailed Theory

Comparison of PRAL (denoted "B") including Q_n terms (nuclear straggling) with precision experiments (85b) and highly detailed solutions (81a, 84a) of transport theory (denoted by "LZ") from [81b].

LIMITATIONS OF PRAL CALCULATIONS

Convenient analytic expressions for S_n , Q_n etc. exist. An example was shown in Chapter 2 of this book for the "universal" potential, and also in ref. (77c) for some other popular potentials.

Also, presently, for any arbitrary ion-target combination, the appropriate nuclear stopping expression, $S_n(c)$, and nuclear straggling expression, $Q_n(E)$, can be calculated by 3 coefficient pairs for each individual Z_1, Z_2 combination. See the software file "*../SR Module/HELP - SR Module.rtf*". Using this software, you can calculate individual atom-atom nuclear stopping.

Unfortunately, for the electronic energy losses, $S_e(E)$, there is no simple analytic expression for its corresponding straggling, $Q_e(E)$, except for the high energy limit, approximately above 1 MeV/u. For high energies, the Bohr values for $Q_e(E)$ have been shown by many authors to be quite accurate.

Hence, the conclusion is that PRAL is usually quite accurate in predicting ion ranges, but its estimates of range straggling is limited because of the lack of accurate analytic expressions for the straggling of the ion's energy loss.

UNIVERSAL NUCLEAR STOPPING POWERS

As noted above, PRAL needs nuclear stopping and straggling functions. This information is obtained through the use of the Universal interatomic potential as derived in Chapter 2. Below, the analytic evaluation of S_n (nuclear stopping) and Q_n (nuclear straggling) are summarized.

The energy lost by an ion per unit path length is defined as dE/dR . This is related to the nuclear stopping cross section, $S_n(E)$, by the relation $dE/dR = NS_n(E)$ where N = the atomic density of the target. The nuclear stopping power, $S_n(E)$, is the average energy transferred when summed over all impact parameters, so using:

$$\text{Eq. 10-34} \quad T = \frac{2}{M_2} \left(V_0 M_c \sin \frac{\Theta}{2} \right)^2 = \frac{4 E_c M_c}{M_2} \sin^2 \frac{\Theta}{2} = \frac{4 E_0 M_1 M_2}{(M_1 + M_2)^2} \sin^2 \frac{\Theta}{2}$$

We have:

$$\text{Eq. 10-35} \quad S_n(E) = \int_0^\infty T d\sigma = \int_0^\infty T(E, p) 2\pi p dp = 2\pi \gamma E \int_0^{p_{\max}} \sin^2 \frac{\Theta}{2} p dp$$

With the integration's upper limit being the sum of the two atomic radii, p_{\max} , beyond which the interatomic potential, and T , are zero. We now define a Center of Mass (CM) to Lab transformation unit, γ , which will be used below (this conversion has been discussed at length in Chapter 2):

$$\text{Eq. 10-36} \quad \gamma \equiv 4 M_1 M_2 / (M_1 + M_2)^2$$

In order to show clearly the results of using classical charge distributions and also those using solid state distributions, it is easiest to again plot the nuclear stopping in reduced units in which a single

curve describes all combinations of classical atom-atom collision. Lindhard et al. have discussed at length the calculation of nuclear stopping using Thomas-Fermi atoms (63a, 68a). They suggested a reduced coordinate system for nuclear stopping which we will extend to our new calculations. Using the formalism of Lindhard we define :

$$\text{Eq. 10-37: } S_n(\varepsilon) = \frac{\varepsilon}{\pi a_U^2 \gamma E_0} S_n(E)$$

where ε is a *reduced energy* introduced by Lindhard et al. (63a, 68a) defined as

$$\text{Eq. 10-38: } \varepsilon = a_U M_2 E_0 / Z_1 Z_2 e^2 (M_1 + M_2)$$

and a_U is the universal screening length, defined in Chapter 2 as:

$$\text{Eq. 10-39 } a_U = 0.8853 a_0 / (Z_1^{23} + Z_2^{23})$$

Eq. 10-35 defines nuclear stopping in physical units, and Eq. 10-37 - Eq. 10-38 converts it to LSS reduced units.

We show in Figure 10-8 the reduced nuclear stopping based on the four classical atom screening functions and for the universal screening function. The universal nuclear stopping is calculated by restating Eq. 10-35 in reduced units using the reduced impact parameter, $b = p/a_U$:

$$\text{Eq. 10-40 } S_n(\varepsilon) = \varepsilon \int_0^\infty \sin^2 \frac{\Theta}{2} d(b^2)$$

which is now independent of the chosen screening length, since Θ is a function of ε and b only (see Chapter 2 or ref. 68a or 77f for expansions of this equation).

The dotted lines in Figure 10-8 reproduce within a few percent the similar calculations of ref. 77f for the classical interatomic potentials and confirm the accuracy of our computer program. The small circles on the plot are solutions of Eq. 10-40 using the universal screening function, see Chapter 2. The solid line is an analytic expression fitted to the points with the form :

$$\text{Eq. 10-41: } S_n(\varepsilon) = \frac{\ln(1+a\varepsilon)}{2(\varepsilon+b\varepsilon^c+d\varepsilon^{1/2})}$$

where a , b , c and d are fitting coefficients as shown on the Figure 10-8. This equation does not have accurate high energy properties where nuclear stopping must become like Rutherford scattering. So for reduced energies, ε , above 30, it may be simplified to the unscreened form of nuclear stopping :

$$\text{Eq. 10-42: } S_n(\varepsilon) = (\ln \varepsilon) / 2 \varepsilon$$

UNIVERSAL Reduced Nuclear Stopping

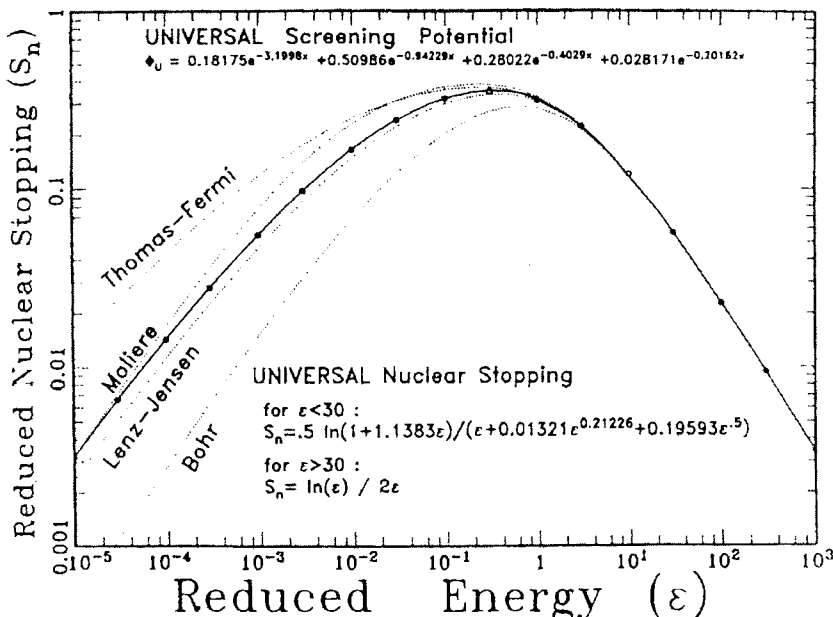


Figure 10-8 - Nuclear Stopping Power (Reduced Units)

The universal screening function can be used to calculate the nuclear stopping power using Eq. 10-40. The result is shown above in reduced coordinates in the spirit of LSS theory (ref. 63a) but with the screening length of LSS theory, a_1 , being replaced with that of a_0 , see Eq. 10-39. The reduced nuclear stopping power calculations are shown as small circles over the 8 decades of energy. Through these points has been fitted the analytic formula identified in the figure as: *Universal Nuclear Stopping*. This function agrees with the calculated nuclear stopping within a few percent. Also shown are the nuclear stopping calculations based on the four classical atomic models.

Figure 10-8 shows for all potentials the nuclear stopping is identical for $\epsilon > 10$. For lower values of epsilon the universal stopping curve falls between the Moliere and Lenz-Jensen curves.

For practical calculations, the universal nuclear stopping is

$$\text{Eq. 10-43: } S_n(E_0) = \frac{8.462 \times 10^{-15} Z_1 Z_2 M_1 S_n(\epsilon)}{(M_1 + M_2)(Z_1^{23} + Z_2^{23})} \text{ eV/(atom/cm}^2\text{)}$$

with the reduced energy, ϵ , being calculated as

$$\text{Eq. 10-44: } \epsilon = \frac{32.53 M_2 E_0}{Z_1 Z_2 (M_1 + M_2)(Z_1^{23} + Z_2^{23})}$$

and the reduced nuclear stopping being calculated as :

$$\text{Eq. 10-45: For } \varepsilon \leq 30 : S_n(\varepsilon) = \frac{\ln(1 + 1.1383\varepsilon)}{2[\varepsilon + .01321\varepsilon^{.21226} + .19593\varepsilon^{.5}]}$$

$$\text{Eq. 10-46: For } \varepsilon > 30 : S_n(\varepsilon) = \frac{\ln(\varepsilon)}{2\varepsilon}$$

Nuclear Straggling

The straggling of the nuclear energy loss, defined as $Q_n \equiv \int_0^\infty T^2 d\sigma$, can be evaluated in the same way as the nuclear stopping above. However, the same variables which made $S_n(\varepsilon)$ a universal function, i. e. independent of Z_1, M_1, Z_2, M_2 and density, cannot make Q_n a universal function. In the case of Q_n , a factor γ , see Eq. 10-36, will remain in the final result. After solving for Q_n , we have derived the following fit for nuclear straggling using the universal interatomic potential :

$$\text{Eq. 10-47: } Q_n = \gamma W_n(\varepsilon)$$

$$\text{Eq. 10-48: where: } W_n = \frac{1}{4+0.197\varepsilon^{-1.7} + 6.584\varepsilon^{-1.0494}}$$

This analytic fit is depicted as a dotted line in Figure 10-9 together with the precise data points as obtained from solving the scattering integral for the new universal screening function. Q_n can be seen to approach a constant value at high energies similar to the behavior of the electronic straggling.

LIMITATIONS OF PRAL CALCULATIONS OF ION DISTRIBUTIONS

Convenient analytic expressions for S_n , Q_n , etc. exist. An example was shown in Chapter 2 of this book for the "Universal" potential, and also in ref. (77c) for some other popular potentials.

Also, presently, for any arbitrary ion-target combination, the appropriate nuclear stopping expression, $S_n(\varepsilon)$, and nuclear straggling expression, $Q_n(\varepsilon)$, can be found in this book as determined by 3 coefficient pairs for each individual ion and target, Z_1 and Z_2 , combination.

Unfortunately, for the electronic energy losses, $S_e(E)$, there is no simple analytic expression for its corresponding straggling, $Q_e(E)$, except for the high energy limit, approximately above 1 MeV/u. For high energies, the Bohr values for $Q_e(E)$ have been shown by many authors to be quite accurate.

Hence, the conclusion is that PRAL is usually quite accurate in predicting ion ranges, but its estimates of range straggling is limited because of the lack of accurate analytic expressions for the straggling of the ion's energy loss.

UNIVERSAL Reduced Nuclear Straggling

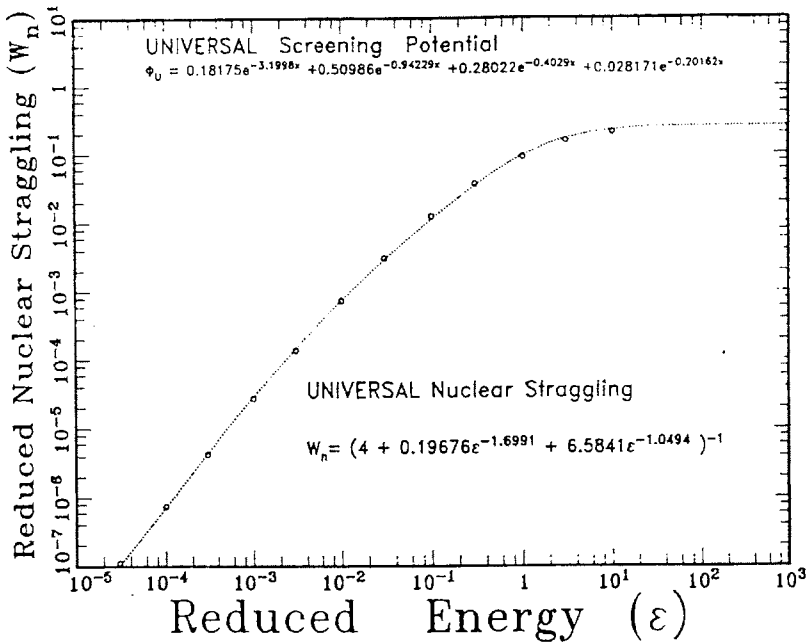


Figure 10-9 - ZBL Nuclear Straggling Function

The universal screening function, can also be used to calculate the energy loss straggling associated with the nuclear stopping. The result is shown in reduced coordinates as used in Figure 10-8. The calculated straggling is shown as small solid circles,. Through these points has been fitted an analytic function (solid line) which is identified above, and also in Eq. 10-47 and Eq. 10-48.

CHAPTER 10 - CITATIONS

- 63a J. Lindhard, M. Scharff and H. E. Schiott, Mat. Fys. Medd. Dan. Vid. Selsk., 33, No. 14 (1963).
- 68a J. Lindhard, V. Nielsen and M. Scharff, Mat. Fys. Medd. Dan. Vid. Selsk., 36, No. 10 (1968).
- 75g J. F. Gibbons, W. S. Johnson and S. W. Mylroie, "Projected Range Statistics: Semiconductors and Related Materials," 2nd Edition, Halsted Press, Stroudsbury, PA, USA (1975).
- 77c W. D. Wilson, L. G. Haggmark and J. P. Biersack, Phys. Rev., 15B, 2458 (1977).
- 77f W. D. Wilson, L. G. Haggmark and J. P. Biersack, Phys. Rev., 15, 2458 (1977).
- 77r J. P. Biersack and W. Kruger, "Ionenimplantation", by H. Ryssel and G. Ruge, B. G. Teubner Press, Stuttgart (1978).
- 80h H. Ryssel, G. Lang, J. P. Biersack, K. Muller and W. Kruger, IEEE Trans. Elec. Dev., ED-27, 58 (1980).
- 81b U. Littmark and J. F. Ziegler, Phys. Rev., 23A, 64 (1981).
- 81o F. Jahnle, H. Ryssel, G. Prinke, K. Hoffman, K. Muller, J. P. Biersack and R. Henkelman, Nucl. Inst and Meth., 182/183, 223 (1981).
- 82b J. P. Biersack and J. F. Ziegler, "Ion Implantation Techniques," Springer-Verlag, p. 122 (1982).
- 82q J. P. Biersack, Z. f. Physik, A-95, 305 (1982).
- 84a J. F. Ziegler, J. P. Biersack, U. Littmark, "The Stopping and Range of Ions in Solids," vol. 1 of series "Stopping and Ranges of Ions in Matter," Pergamon Press, New York (1984).
- 85a D. J. O'Conner and J. P. Biersack, Nucl. Inst. and Meth., B15, 14-19 (1986).

11 - SRIM Tutorials

The SRIM website contains several tutorials, all of which have been used by thousands of students, and upgraded with their comments. Each tutorial is constructed to take about 40 minutes (for English speaking students).

Many of the comments refer to colors in the TRIM plots, which can not be reproduced in this textbook. Tutorials with color graphics can be found at: www.SRIM.org. The tutorials are made to be executed with access to TRIM on a PC, which is necessary to follow many of the instructions of this chapter.

Chapter Contents

11 - SRIM Tutorials	11-1
Tutorial #1- Introduction to Ion Ranges, Doses and Damage.....	11-2
<i>Finding Ion and Energy to Use</i>	11-2
<i>Damage Production by Phosphorus ions at 190 keV</i>	11-3
<i>TRIM Calculation Results for Damage</i>	11-4
<i>Does the Phosphorus Create an Amorphous Layer ?</i>	11-7
Tutorial #2 – Target Mixing and Sputtering	11-8
<i>Interface Mixing and Sputtering</i>	11-8
<i>Target Mixing</i>	11-9
<i>Target Sputtering</i>	11-10
<i>Comments on Sputtering</i>	11-11
<i>SUMMARY : Mixing and Sputtering Calculation:</i>	11-14
<i>Example of datafile SPUTTER.txt</i>	11-14
Tutorial #3 – Building Complex Targets	11-15
<i>Mixed Gas/Solid Targets – Gas Ionization Chamber</i>	11-15
<i>Special Notes about the TRIM Setup Window</i>	11-20
Tutorial #4 - Calculations of Target Damage	11-21
<i>Scientific Background – “The Physics of Recoil Cascades”</i>	11-23
<i>Energy Loss to Ionization and Phonons</i>	11-25
<i>Damage Creation in the Target</i>	11-27
<i>Answers to Questions in this Tutorial:</i>	11-28

Tutorial #1- Introduction to Ion Ranges, Doses and Damage

This Tutorial will cover how to find the energy and dose of ions required to implant atoms into a target at a given depth and concentration. To illustrate this, we will assume that we wish to implant the n-well of a CMOS semiconductor device. The implanted ions should be an n-type dopant (implanted atom) in silicon and have a peak concentration depth (**projected range**) of about 250 nm (2500 Å) below the silicon surface. The peak dopant concentration should be 5×10^{18} atoms/cm³. Although this seems complicated (especially if you are not an electrical engineer) it merely asks that ions of elements phosphorus (P) or arsenic (As) or antimony (Sb) be directed into a silicon target to a certain depth and concentration (atoms of P, As and Sb are all n-type dopants to silicon).

As an additional limitation, we will assume that your implanter (accelerator) is limited to 200 keV. [Note: TRIM sometimes uses Å units because this is about the width of a monolayer of atoms in a solid. 10 Å = 1 nm. These units are common in assessing target microscopic damage.]

Questions :

- Which element will your use?
- What dose is required (ions/cm²)?
- Will your target be amorphous after the implant?

This set of questions will be the subject of this Tutorial. By the end, you will be able to answer these questions for any ion into any target material.

Finding Ion and Energy to Use

- Click on the **SRIM** icon on your desktop.
- Click on **Stopping and Range Tables** (S & R Tables)
 - First enter the ion. Start by clicking on the Help button **?** next to “ION”. Read the definitions and then close this window by pressing **CLOSE**.
 - In order to implant an n-well in silicon, you need to implant an impurity from column 5 of the Periodic Table. Typical dopants are Phosphorus (P), Arsenic (As) or Antimony (Sb). Start with the middle possibility: **Arsenic**. To enter an ion, use the **PT** button next to **Ion** in the window to bring up a chart of the elements. Select **As** as the ion.
 - The program will automatically fill in various boxes describing the ion. Note that this ion mass is not the average mass of arsenic, but the mass of the most abundant isotope, MAI. You can confirm this by activating the Periodic Table button, **PT**, which gives the various mass descriptions of arsenic.
 - Go down to **Target** in the window.. Click on this Help button, **?**.
 - Specify target = **Silicon** using the **PT** button to specify **Si**.
 - Note that this target mass is not the MAI mass, but the average natural weight of the element. You can confirm this by activating the Periodic Table button, **PT**, which gives the various mass descriptions of silicon. Press **Close** to close the window.

- The rest of the target table is blank, and not needed. The term “Stoich” is used for compound targets, for the stoichiometry of each of the elements of the compound.
- Press **Calculate Table**.
- Accept the suggested filename: “SRIM Outputs\Arsenic in Silicon”. This file is stored in the SRIM directory: **..\\SRIM Outputs** if you need to reference it again.

Look at the table. What is the energy needed to have a *Projected Range* (depth of the peak concentration) of 2500Å? (Answer - ~400 keV)

Ion	dE/dx	dE/dx	Proj.	Longit.	Lateral
Energy	Elec.	Nuclear	Range	Strag.	Strag
350.00 keV	1.876E+00	4.139E+00	2243 Å	557 Å	436 Å
375.00 keV	1.944E+00	4.049E+00	2404 Å	590 Å	462 Å
400.00 keV	2.013E+00	3.964E+00	2566 Å	622 Å	489 Å
450.00 keV	2.150E+00	3.804E+00	2892 Å	685 Å	542 Å
500.00 keV	2.285E+00	3.659E+00	3221 Å	746 Å	595 Å

- Conclusion: This is a higher energy than your 200 keV implanter can reach!
- Redo the Range Tables but calculate using **Phosphorus (P)** ions.
- Look at the new table. What is the energy needed to have a Range of 250nm?

Ion	dE/dx	dE/dx	Proj.	Longit.	Lateral
Energy	Elec.	Nuclear	Range	Strag.	Strag
170.00 keV	1.789E+00	1.136E+00	2232 Å	682 Å	540 Å
180.00 keV	1.833E+00	1.107E+00	2359 Å	709 Å	565 Å
200.00 keV	1.914E+00	1.054E+00	2612 Å	761 Å	615 Å
225.00 keV	2.008E+00	9.960E-01	2928 Å	823 Å	674 Å

- This table shows that we can implant the n-well with a peak at 2500Å (250 nm) using Phosphorus ions at **190 keV** (interpolating between the two ranges shown). Close this window with the Table.
- Before leaving the *Stopping and Range* window, look at the other Help messages for the **S & R Tables** (press **?** buttons).
- Press **Main Menu** button to return to the Home page of SRIM.

Damage Production by Phosphorus ions at 190 keV

- On the Main Menu, there is a Help beside the button TRIM Calculation. Press this to read the Help, **?**, for this program.
- TRIM (Transport of Ions in Matter) is a very complicated program that describes not only the range of ions into matter, but also details many other aspects of the damage done to the target during the slowing-down process. It will allow you to see the ions penetrating into the target with full animation, and also shows recoil cascades and target atoms mixing together. It makes the calculation for one ion at a time, in order to make precise evaluations of the physics of each encounter between the ion and a target atom. This calculation may be time consuming – from a second to a few minutes for

each ion. The accuracy is determined by the number of ions followed. Typically, a calculation for 1000 ions will give better than 10% accuracy.

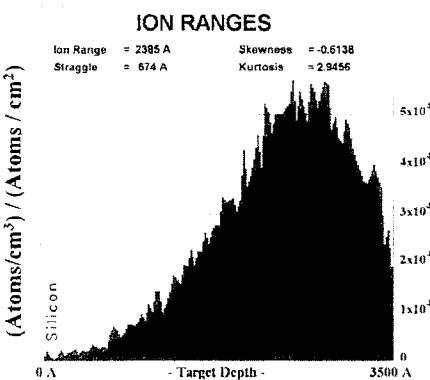
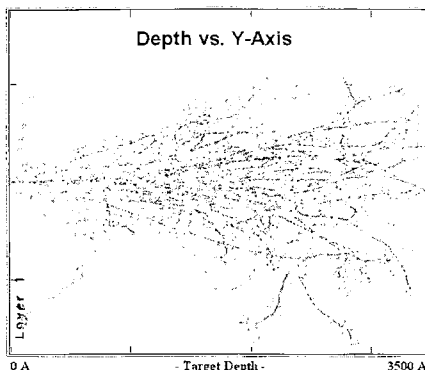
- Click **Trim Calculation** on Main Menu
 - The next window is for the TRIM Setup for the calculation. It contains more options than the simpler Table of Ranges, since we have to include many details about the target structure.
 - Go to ION DATA and click on **PT** button. Select **Phosphorus**. Note that other ion parameters are automatically filled in.
 - On this same ION DATA line, in the box under “Energy (keV)” enter **190**. This was the energy that we found using the SR Tables to put the Phosphorus peak about 250 nm deep into the silicon target.
 - Go down to TARGET DATA. This window can get very complicated since we can have many target layers (up to 20) made up of complex compounds. We will study this in a later Tutorial, but we will only use a simple silicon substrate in this exercise.
 - Find the **PT** button for the target. Open the Periodic Table window and select **Si**.
 - Go to the LEFT side of this line, and for “**Width**” enter **3500 Ang**. This is the layer width of the target. Since we don’t care what happens much deeper than 250 nm, this is an adequate target thickness.
 - Go to the LEFT side of the TARGET DATA input, and for “**Layer Name**” enter “**Silicon**” (instead of *Layer 1*)
 - Next we will consider what kind of calculation is needed. TRIM can be used for simple calculations such as used in the Stopping and Range (SR) Tables, which executes in less than a second, to detailed calculations of every interaction of the ions with the target, which may take a few hours to calculate 100 ions. The type of calculation is setup using the two drop-down menus under the title “Type of TRIM Calculation”.
 - Go to the TOP-RIGHT box “**DAMAGE**”. On the right is the Help box, **[?]**. Press this to read about the types of damage calculations that are available. Although it may seem complex, over the next lessons you will use most of these for special applications.
 - Scroll down the DAMAGE to select “**Detailed Calculation with Full Damage Cascades**”.
 - Below this are Basic Plots which are available. You can ignore this for now. We will use various plots, but we will call them up during the calculation as needed.
 - Finally, on the far right, near the middle of the window, near the boxes called “**Damage (eV)**” there is another Help box, **[?]**. Look at this so you can see various energies that are needed to describe specific damage types. We will go into this in the next Tutorial, but you should begin to learn the terms: Displacement energy, Surface binding energy and Lattice binding energy.
 - The setup is complete. Look at all the boxes to see if you can understand them. Press the Help buttons for explanations.
 - Finally, press **Save Input and Run TRIM**
-

TRIM Calculation Results for Damage

The TRIM calculation begins. There is a pause as TRIM generates internal tables which describe your target. Then you see the first ion track. The ion track shows a red dot

wherever the ion creates a vacancy (knocks a silicon atom away from its lattice site). The green dots are vacancies caused by recoiling silicon atoms.

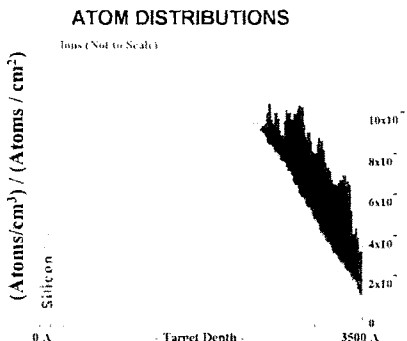
- Note that the ion creates damage constantly (red dots), while there are clusters of green dots where recoiling silicon atoms cause what is called a *recoil cascade*.
- Every time the phosphorus hits a silicon atom hard, it will transfer a significant portion of its energy. This is true because the mass of P is almost the same as the mass of Si. If the ion / target atom masses are very different, then there is much less energy transferred to the target atom. This is basic physics of the elastic collision of two particles. Every time there is a hard ion/silicon hit, and a green cascade is formed, there is a good chance that the ion changes direction. Since you are only seeing two axes, some deflections may not be apparent.
- Almost every time the ion has a collision with a target atom, there is one vacancy created (a red dot). The target atom then recoils and all its collisions which cause vacancies are plotted as green dots. A single recoil atom may cause up to a 1000 vacancies (green), while the ion only gets 1 vacancy plotted (red).
- On the left side of this **TRIM Calculation Window** are various buttons in a table called **DISTRIBUTIONS**. The left hand column of buttons, [?], are *Help* for each of the plots. The second column of buttons, [File], generate files on the hard disk (don't click them). The third column, [Plot], (white squares) are for plots. We will use these for the bullet items below. When you click on any button, there is a pause until the calculation for the current ion completes. Then the command is executed. So you have to be patient. The calculation continues while you look at any plots, and these plots will be updated after each successive ion.



- The top plot is the **ION DISTRIBUTION**. Read the Help, [?]. The terms should be familiar to you. Now click on the plot box for this item. A plot will appear titled: **ION RANGES**. You will see the distribution of phosphorus ions (190 keV) building up in the silicon target. The "Ion Range" should be about 2400-2500 Å. We set up the target depth at 3500Å to be able to catch most of the ions in the plots. Note the Ordinate

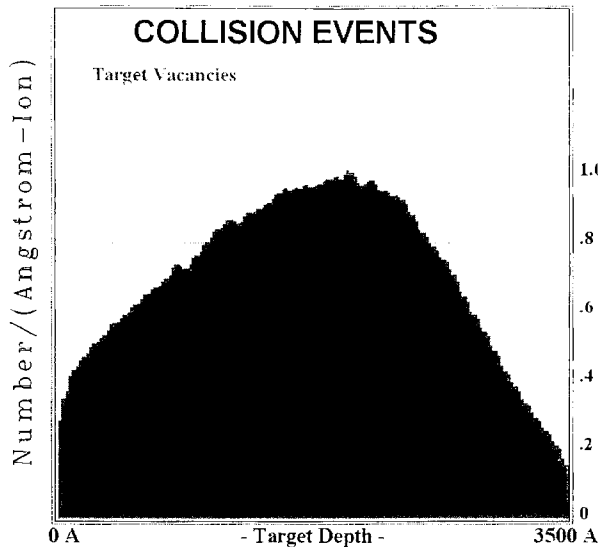
units: “(Atoms/cm³)/ (Atoms/cm²)”. Although these units appear strange, when you multiply by an implantation dose (ions/cm²), you will end with the impurity concentration (atoms/cm³) vs. depth. This is GOOD. You want a peak impurity concentration of $\sim 5 \times 10^{18}/\text{cm}^3$. See if you can determine that an implant dose of 10^{14} phosphorus/cm² will be adequate. This is perfect doping for an n-well.

- If you wanted a peak dopant concentration of $10^{17}/\text{cm}^3$, what would be the required dose for the phosphorus implant?
- Note that the higher moments of the distribution are also given on the plot (straggle, skewness, kurtosis). These are briefly discussed in the Help for the plot. For more details, click on the top tab “Help, FAQ and Scientific Explanations”, then “TRIM FAQ and Solutions”, then “Statistics of Range Distributions”. Read this to get an understanding that these range terms are various statistical methods which describe the final ion distribution.
- Close this Range plot window (every open plot window slows down the calculation).
- Next we will look at the **Ion/Recoil Distribution**. Press the Help [?] button for a description. At the bottom of this Help window is a copy of a typical harddisk file.¹
- Select the plot for the **Ion/Recoil Distribution**. Note that the “Ion” plot (red) is identical to that shown in the Ion Distribution. The green plot shows the silicon recoil distribution. These are all the silicon atoms knocked out of their lattice sites, creating vacancies. Note that the distribution of silicon recoils (green) has a shallower peak than that for the phosphorus ions. Near the end of the phosphorus tracks, the ions do not have enough energy to create massive cascades. The two peaks are about the same size, so they both contribute about equally to the total damage to the target.
- The units of this plot are also “(Atoms/cm³)/ (Atoms/cm²)”. Near the peak of the Si recoil distribution, the value is 10^8 . The density of silicon is about 5×10^{22} atoms/cm³. With a little math, you can derive that for a dose of 5×10^{14} P atoms/cm², you will average one displacement per target atom at the peak of the damage distribution. This would indicate that a crystal target should go amorphous, except at room-temperature about 99% of the silicon crystal damage almost instantly anneals and most of this damage disappears. This will be discussed in more detail below.



¹ Note: If the characters in this datafile look weird, then the font “MS-LineDraw” has not been installed on your PC. This must be done before you continue. It has been included in the SRIM software, and has been put into the directory: C:/WINDOWS/FONTS. Use Windows Explorer to find it. Select it, and press FILE and then “INSTALL NEW FONT”. These instructions may vary with different editions of Windows.

- A second plot will help you to understand details of these collisions. The plot called "Collision Events" plots the number of Target Vacancies as a function of depth (the plot is generated by clicking on *Damage Events* in the TRIM Calculation window and selecting *Total Vacancies*). Note that the peak also is about 1.0 vacancies per Å-ion, in agreement with the Recoil distribution on the previous figure ($10^8 \text{ Å} = 1 \text{ cm}$). This subject will be covered in more detail in Tutorial #4.



Does the Phosphorus Create an Amorphous Layer ?

We can estimate whether the phosphorus can create an amorphous layer. At the PEAK of the damage plot created above, the vacancy rate is about 1 vacancy/target atom. But we are assuming that 99% of the damage instantly anneals, leaving only 1% damage. Using the above plot, with an implant dose of $10^{15}/\text{cm}^2$ ions, that makes 10^{13} stable vacancies / Angstrom-cm². Converting this, using: $10^8 \text{ Angstrom} \equiv 1 \text{ cm}$, gives a vacancy density of 10^{21} vacancies/cm³.

The density of silicon is 5×10^{22} atoms/cm³. The calculated damage is 10^{21} vacancies/cm³. Hence the silicon target is damaged to about 2%, and the implant layer is not amorphous. This conclusion is not quite accurate because the displacement energy for silicon (discussed in Tutorial-4) will decrease as damage accumulates. This means that once you have partial damage, it is easier to create more damage because the lattice is more loosely coupled and atoms are easier to dislodge. These changes in the crystal integrity are not included in TRIM, so the damage may be underestimated.

Tutorial #2 – Target Mixing and Sputtering

The previous Tutorials has covered how to setup TRIM, determine which ion and energy to specify for a n-well implantation, and how to evaluate the damage during the implantation. This Tutorial will show other effects of ion/solid interactions.

Interface Mixing and Sputtering

Interface Mixing is the transport of atoms from one layer of a target into another layer. This is usually an undesirable effect. We have seen how ions can transfer significant energy to recoil atoms, and these can move long distances and create significant collision cascades (see Tutorial #4). When a recoil atom crosses from one target layer to another, the second layer is contaminated.

However, there are special cases where recoil mixing is used to modify materials on purpose, and this process is called “**recoil implantation**”. This technique is used for materials which are either difficult or dangerous to handle. An example is the fabrication of materials containing radioactive substances. For example, a thin layer of calcium may be deposited on a target of silicon, and then it is placed in a nuclear reactor to convert the calcium to a radioactive isotope. The silicon is then placed in an ion implanter, and a high dose of Xe ions are implanted into the calcium layer. The Xe atoms knock some of the radioactive material into the silicon, where it is trapped. After removing any remaining surface Ca, the silicon with implanted radioactive calcium can be safely handled. Such a target is useful to provide a sample which emits a radioactive particle (here from the Ca) but which is far less dangerous than a pure sample of radioactive Ca.

Sputtering is the opposite of Recoil Implantation. Here, surface atoms are removed from the target by creating recoil cascades that come back out of the target, and which give surface atoms enough energy so that they are driven away from the target. There is a binding force which holds atoms to the target, and this is called the **Surface Binding Energy**, E_{surf} . An atom at the target surface is not confined on one side, so the energy required to remove it from its lattice site is less than if it was inside the solid and surrounded by other atoms. A surface atom has fewer electronic bonds which must be broken. E_{surf} is usually less than the Displacement Energy, E_{disp} , for the solid.

-
- Open SRIM by clicking on its icon on your desktop.
 - In the window, click on **TRIM Calculation** to open the TRIM Setup window.
 - Press **TRIM DEMO**. This window will generate the input for 12 examples which show how TRIM can be used for different applications. Press the button for: **Xe into Si/Pt/Si (Mixing a Marker)**. Look at the various inputs to the TRIM calculation. Then press **Save Input ant Run TRIM**. The window will close, and TRIM will immediately start.

Target Mixing

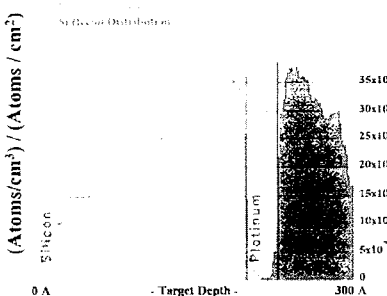
This example shows a thin Pt layer, inside a target of silicon. It was chosen to show how large the effects of interface mixing might become.

Click on the plot: ***Ion/Recoil Distribution***. In the sub-menu that appears, select “2 – ***Silicon Recoil Distribution***” and “4 – ***Silicon Recoil Distribution***” and then ***Plot***. The two silicon recoil distributions will be in different colors to separate the two contributions. After just a few ions, less than 100, the gap holding the platinum layer will start filling up with silicon atoms. By 400 atoms, this layer will be almost 5% silicon. The transfer of atoms into this layer is very efficient for a heavy ion such as Xe (atomic number = 54). Close this plot window.

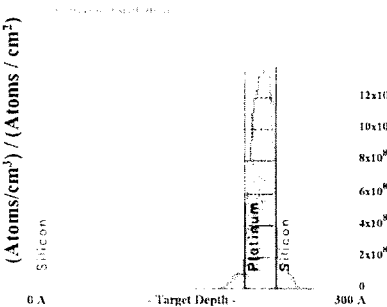
Again, click on the plot: ***Ion/Recoil Distribution***. In the sub-menu that appears, select 3 – ***Platinum Recoil Distribution***, and then ***Plot***. This plot shows the platinum layer atoms, and how many have moved into the silicon. Of particular note is that the number of platinum atoms displaced towards the surface is quite large, at least 50% as large as the platinum atoms driven deeper into the target. This is remarkable! The ions are flying deep into the target, and all the initial recoils are generally starting in the same direction, i.e. deeper into the target. How can atoms end up at a shallower position than where they start?

To see the answer, click on the ***XY Longitudinal*** plot that shows each ion and the displacements that it causes (This plot button is in the section ***Collision Plots***). At the bottom of this plot is a button marked ***Clear***. This will clear the plot so that you can see individual ions and the recoil cascades that are generated. The ion track is a thin line of red dots, where all recoil cascades must start. Each recoil cascade (not the ion’s cascades) begins in a forward direction, but rapidly spreads out into almost random directions. The dense cascades look like balls of green dots, with no special direction. The cascades involve so many particles that any “knowledge” of the original ion direction is rapidly lost. The cascade becomes an isotropic event, i. e. the atoms go in every direction. (Note: for high performance PCs, it may be necessary to press “***Clear***” and then press “***Pause***” at the top of the TRIM window. This will stop the display after the next ion.)

ATOM DISTRIBUTIONS

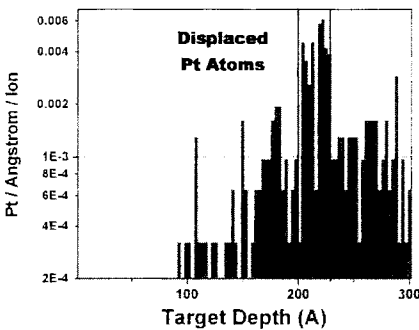


ATOM DISTRIBUTIONS



This is what causes backward moving Pt atoms, which move towards the target surface. The big cascades rapidly lose any forward direction and become isotropic. The degree that this happens is indicated by the difference in the number of Pt atoms which are forward scattered, deeper into the silicon, and the number scattered back towards the target surface.

A second feature to note is the large distance that the platinum atoms will move. The original Pt layer is 30 Angstrom thick. Within 500 incident ions, you will begin to see platinum atoms driven more than 30 Å from the Pt layer.



If you go to the TRIM DISTRIBUTIONS box and press the *File* button command for ***Ion/Recoil Distributions***, you will get a numerical table which shows more details than the plot. This file is placed in the SRIM folder: ***./SRIM Outputs***, and it is called ***RANGE.txt***. It shows that some Pt atoms have recoiled far back from the Pt layer – within 100 Å of the surface, and others have reached the back edge of the target. The recoil mechanism is so efficient that Pt atoms are driven throughout the silicon target with fewer than 500 incident ions. If TRIM is continued for several thousand ions, some of the Pt atoms will be found to have moved back through the target surface, and are lost from the target.

Let the above TRIM calculation continue until more than 1000 ions are completed. You can increase the speed of calculation by closing all plot windows, which slow down the calculation.

Target Sputtering

Sputtering is the removal of near-surface atoms from the target. When a cascade gives a target atom an energy greater than the "surface binding energy" of that target, the atom may be sputtered. To actually be sputtered, the atom's energy normal to the surface must still be above the surface binding energy when it crosses the plane of the surface. The sputtering of a surface is described by a "Sputtering Yield", which is defined as the mean number of sputtered target atoms per incident ion. If the target is made of several elements, there is a separate sputtering yield for each element.

Sputtering Yield = (Number of Sputtered Atoms) / (Number of Incident Ions)

The surface binding energy (SBE) of an atom to a surface is known only for a few materials, but it is common to use the ***heat of sublimation*** as an estimate. Typical values are: Ni (4.46 eV), Cu (3.52 eV), Pd (3.91 eV), Ag (2.97 eV), Pt (5.86 eV) and Au (3.80 eV). Values will be suggested when you set up the TRIM calculation.

Comments on Sputtering

- Only the cascades which come back to the target surface are important to sputtering, so it is usually adequate to use only a thin target to simulate sputtering. For heavy ions, e.g. heavier than 20 amu, a target thickness of 300 Å is usually adequate. Using a very thin target reduces the time spent calculating cascades which will not contribute to sputtering. For light ions, e.g. He, it will be necessary to use thicker targets, as much as 1000 Å, since these ions may backscatter from deeper in the target and cause sputtering as they exit from the target surface. The target depth needed for a calculation may be estimated by running several quick cases and seeing at which target depth the sputtering yield remains constant.
- The sputtering yield is very sensitive to the surface binding energy (SBE) which you input to the calculation. Be aware that for real surfaces, this energy changes under bombardment due to surface roughness and damage, and also due to changes in the surface stoichiometry for compounds. The sensitivity of sputtering yield to surface binding energy may be displayed during the calculation by using the plotting menu. The plots of sputtering yield to SBE are accurate to about 30%.

[For cascades within the target at very low energy (which is a major contributor to sputtering) TRIM uses the hard-sphere model for scattering as described in J. P. Biersack and W. Eckstein, Appl. Phys., A34, 73-94 (1984). See figure 3 of this paper, for example.]

It is possible that some of the recoil cascade atoms which exit the target have originated from deeper inside the target than just the surface. We will see that some Pt atoms are seen to sputter from collisions that begin more than 200 Angstroms inside the target.

Now look at the right side of the TRIM window at the section called **SPUTTERING YIELD (SY)**. This gives the number of atoms which have been sputtered per incident ion. You will see that ~ 6 or 7 silicon atoms are sputtered for each incident ion. The ions are actually digging a hole, for more atoms are leaving than arriving, by 6 to 1! Further, if you have run at least 1000 ions, you will see that there is even a number of platinum ions which have sputtered. The Pt sputtering yield is shown as =.005324 (about 1 every 200 ions). They started 200 Angstroms inside the target, and some of the cascades have been so energetic that the platinum atoms were transported back through the top surface!

SPUTTERING YIELD		
	Atoms/Ion	eV/Atom
TOTAL	6.463	
Si	6.46	74.75
Pt	0.005324	6422.23
Si	0.000000	0.00

Save every ions

- Pause the TRIM calculation by pressing **PAUSE** at the top of the TRIM window.
- At the left, under **DISTRIBUTIONS**, press the plots: **Integral** and **Differential Sputtered Atoms**

Look first at the plot called **Sputtering (Integral)**. The plot name is shown at the top of the plot window. This plot shows the energy of every recoiling atom which reaches the target surface. The ordinate has units of *Atoms/Ion*, so each ion will produce about this number of recoiling atoms which reach the surface. There is a vertical bar marked *3.1 eV*, which is the average **Surface Binding Energy**, E_{surf} , which was entered for silicon in this target. To the left of this bar is an arrow with the legend *Not Sputtered*. At 3.1 eV, the number of atoms which reached the surface with more than this energy is about 7. This is the number of atoms sputtered, and it agrees with the number we saw in the **SPUTTERING YIELD** table above.

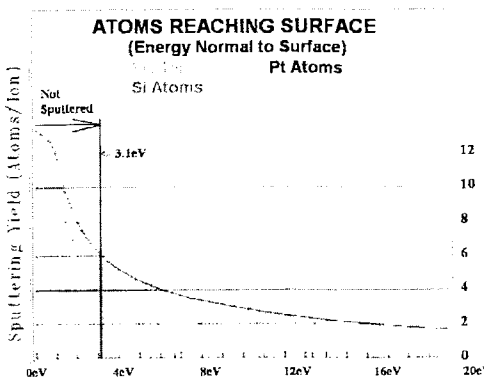


Figure 11-1 – Integral Sputtering Yield

One comment should be made about the Surface Binding Energy. This is the minimum energy which an atom must have to be sputtered. It should be clear that only the *normal component* of the ion's energy should be counted. That is, an ion which reaches the surface with a trajectory of 45° to the surface, will actually need $1.4 \times E_{surf}$ to be sputtered. In the plots that you will create below, this correction is automatically included. The atom energies shown are always the normal component of the atom's energy, not its total energy.

The value of the Surface Binding Energy probably changes with irradiation. This is because the sputtering of a target makes it rough and damaged, and rough targets tend to have reduced Surface Binding Energies. As the target roughens, the sputtering yield will go up as each surface atom is tethered to the surface by fewer electrons. Hence the calculation of sputtering does not include all effects – especially a surface binding energy that changes with time as the beam roughens the surface. But this plot allows us to estimate how much this Sputtering Yield might change with time. We can see that if the Surface Binding Energy would be reduced in half, the sputtering would increase less than 2x. And even if the Surface Binding Energy would be

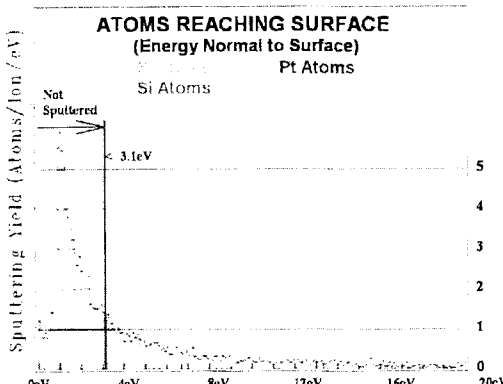


Figure 11-2 – Differential Sputtering Yield

Look first at the plot called **Sputtering (Integral)**. The plot name is shown at the top of the plot window. This plot shows the energy of every recoiling atom which reaches the target surface. The ordinate has units of *Atoms/Ion*, so each ion will produce about this number of recoiling atoms which reach the surface. There is a vertical bar marked *3.1 eV*, which is the average **Surface Binding Energy**, E_{surf} , which was entered for silicon in this target. To the left of this bar is an arrow with the legend *Not Sputtered*. At 3.1 eV, the number of atoms which reached the surface with more than this energy is about 7. This is the number of atoms sputtered, and it agrees with the number we saw in the **SPUTTERING YIELD** table above.

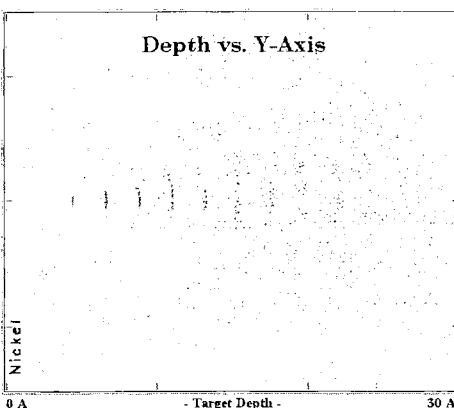
reduced to ZERO, the sputtering yield would increase only by 2x. So the calculation will be accurate within 2x, no matter what happens to the target surface.

Click on the plot **SPUTTERING (Differential)** to bring it to the top. This plot is the differential of the previous Integral plot. The Integral Plot shows the number of atoms reaching the surface with a given energy of more. This plot shows the distribution of atom energies reaching the surface. The most common energy is very low, about 1 to 2 eV.

Stop the TRIM calculation. You can do this either by pressing the windows Close box **X** in the upper right of the window, or by pressing **File** and **Exit**. When asked if you want to SAVE the calculation, press **NO**. The TRIM calculation window will close, and you will return to the TRIM setup window.

- Try a different calculation by pressing **TRIM DEMO** and then select **Sputtering: Xe into Nickel**. This calculation will show an extreme example of sputtering.

As the calculation proceeds, in the starting plot called **XZ Longitudinal**, you will see that the red dots showing displacements by the ion begin to cluster in vertical lines. The spacing between atoms in Nickel is slightly more than 2 Angstroms, and this is the separation between the groups of crescent red dots. The incident ion can only have one collision for each monolayer of target, so when you look at this plot (the total target width is less than 15 atoms) you can see actual atomic structure. After a period of time, the green dots will also begin to show the same striations. Again, this is due to the atomic spacing of the target.



Press the DISTRIBUTIONS plot: **Integral Sputtering**. This plot indicates that more than 10 atoms are sputtered for each incident ion. But the slope of the integral of atom energies is much steeper than for the previous silicon target. If the surface roughens, and the Surface Binding Energy of the target is reduced, the sputtering yield may go up 2x or even 3x. Hence for this case, the sputtering calculation is only a rough estimate because we can not predict the surface roughening. Such roughening depends, for example, on the grain size of the poly-crystalline nickel. This effect can not be incorporated into TRIM.

Detailed data about all sputtered atoms can be recorded by pressing the File button. This creates a file called "SRIM Outputs\SPUTTER.txt". A typical example of this file is shown below. (Note that this file must be formatted using the font MS-LineDraw to get the various lines and boxes in the report.)

SUMMARY : Mixing and Sputtering Calculation:

- Interface Mixing can be a large effect with atoms moving more than 100A from initial position.
 - Significant number of atoms move towards the surface. These also can move long distances.
 - Sputtering can rapidly erode the surface with more than 5 atoms leaving for each incident ion.
 - Some atoms which sputter come from deep in the target, as seen for the Pt atoms which sputter from more than 200 Angstroms below the surface.
-

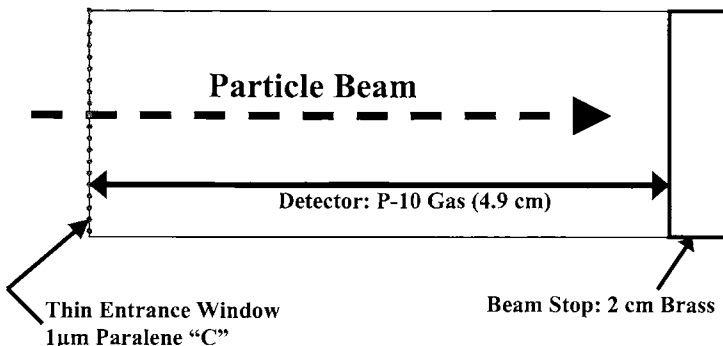
Example of datafile SPUTTER.txt

SPUTTERING CALCULATION							
=====							
=	AXIS DEFINITIONS: X=Depth, Y,Z= Lateral plane of target surface.	=					
=	Shown are: Ion Number	=					
=	Sputtered atom type (atomic name) and energy (eV)	=					
=	(Note: SBE is NOT subtracted from atom energy)	=					
=	Point of ejection relative to ion entrance point.	=					
=	Trajectorial cosines of ejected atom.	=					
=	Cosine (X) is negative indicating motion away	=					
=	from the target surface.	=					
=	Cosine (Y) and Cosine (Z) are transverse motion.	=					
=====							
CALCULATION DATA							
=====							
Xe(1 keV) ==> Si(100 A)							
Ion	Atom	Energy	Depth	Lateral-Position		Atom	Direction
Numb	Numb	(eV)	X(A)	Y(A)	Z(A)	Cos(X)	Cos(Y)
1	1	2219	00E+00	-.397E+01	.174E+02	-.73966	-.45399
1	1	2281	00E+00	-.391E+01	.143E+02	-.56877	-.43337
1	1	222	00E+00	-.758E+01	.161E+02	-.92030	.02871
1	1	223	00E+00	-.835E+01	.152E+02	-.39997	.77688
							.48627

Tutorial #3 – Building Complex Targets

Mixed Gas/Solid Targets – Gas Ionization Chamber

Previous Tutorials have covered how to setup TRIM, determine which ion and energy to specify for a semiconductor n-well implantation, and how to evaluate the damage during an implantation into a semiconductor. This Tutorial will show how to build a complex target: a Gas Ionization Detector for energetic ions with both Gas and Solid volumes.



The apparatus consists of a long cylinder. It has a very thin entrance window, on the left, made of a polymer called Paralene "C". This thin film is only $1 \mu\text{m}$ thick, and it allows the beam to enter the detector with minimal energy loss. The detector itself is made of a special gas called P-10, which is a mixture of 10% Methane (CH_4) and 90% Argon. The argon is ionized by the particles, and the ejected electrons are swept off by electric fields (not shown). There is a chance that the stream of ionized gas might lead to breakdown, and the 10% methane "quenches" any excessive charge buildup. Finally, there is a "Beam Stop" at the end. The beam should stop entirely within the P-10 gas, but a thick end plate is usually included for safety.

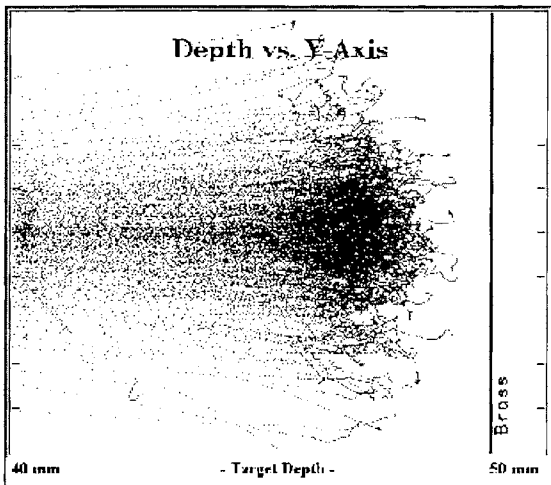
We wish to build this detector in SRIM so that we can evaluate what happens when a beam enters the detector. This is an exercise in building a complex target, and we are only using the detector as an example.

Start SRIM by clicking on its icon.

- Select **TRIM Calculation**
- In the upper left, press **TRIM Demo**
- Select the target at the bottom of the 2nd column:
He (5 MeV) into Gas Ionization Detector
- Press **Save Input and Start TRIM**. You may get a warning about the target density.
Press **Yes** to keep the value suggested.
- TRIM starts using this target

This setup will give you the target details of a Gas Ionization Detector. Several things to note:

- o The ions all stop just before they reach the brass Beam Stop at the bottom.
- o The plot shows only part of the target. Note the abscissa shows depths from 40 mm to 50 mm. That is, you have expanded this deep part of the target so that you see the final ion paths in greater detail.
- o The thin entrance window is not shown. It is there, but when we expand the deep section, this first layer no longer shows on the plot.



You might look at several of the calculation plots. There are no recoils or sputtering atoms because we have omitted these for this calculation. When you are done looking at plots, **close TRIM without saving the data**. This puts you back in the TRIM setup screen.

We shall build an identical setup manually to show how to build a complex target in TRIM. Down at the bottom of this window is a button to clear all entries. Press **Clear All**.

Enter the **ION DATA**:

- In the line called Ion Data, enter Helium, atomic number 2. You may use the **PT** button.
- Enter the Ion Energy (keV) as 5000 (5 MeV)
- The angle of incidence is “normal” so leave this angle as zero.

Enter the **TARGET DATA**. The target will have three layers: the surface thin film, the long cylinder of gas, and the brass Beam Stop.

- The first layer is a plastic film made of Paralene “C”. There is a short-cut for entering this complex material. On the right of the TARGET DATA is a button called **Compound Dictionary**. Press this.
 - o Listed in this directory are more than 300 compounds. Paralene “C” is a trade name, and you either have to know its real name or else look through the long listing of trade names. Click on **PLASTICS / POLYMERS**.
 - o The listing expands, and down this list you will find: “**Polychloro-p-xyllylene / Paralene-C**”. Note that the listing tells you that it contains C₈H₇Cl, and it has a density of 1.289. In the yellow window in the bottom is a long description of the

material, including a chemical diagram of its structure. (If the yellow window contains weird characters, then the font *Linedraw* has not been installed on your computer. See note at end of this lesson.) **Important:** the description includes a correction for the stopping of He ions in this substance, +3.5%, based on the bonding of the compound. Select Paralene-C by clicking on it. Then press the button **Add to Current Layer**. You will be asked if you want to use the Stopping Correction for this compound. Answer **Yes**

- You will see that Layer #1 is fully filled in. The layer is now described as Paralene-C, and the atomic structure is included. The only item left is the **Width**, which is 10000 Angstroms. This is the default, so for a 10 μm thickness it does not have to be changed. We can now construct the second layer.
- Press the button **Add New Layer**. You will be asked for a short Layer Name. Enter: **P-10 Gas**
- We will construct this gas directly. Go to the right part of the TARGET DATA window and get the Periodic Table by pressing **PT**. Find **Ar** and click on it. The first element is specified as argon.
- We now need to add Methane to this gas. Press the button **Add New Element to Layer**. For this second element, again press **PT**. Select **H** and click on it. This enters hydrogen as part of the target.
- Press the button **Add New Element to Layer**. For this third element, again press **PT**. Select **C** and click on it. This enters carbon as part of the P-10 Gas.
- Now we have to specify the amounts of each. P-10 gas is 90% Ar and 10% methane, CH₄. These percentages are by weight, and SRIM uses atomic percents. Use the relative number of atoms as: Ar:64, C:7, H:29. Find the target column labeled **Atom. Stoich**. Enter the stoichiometries of the three atoms, placing **64** next to Argon, **29** next to Hydrogen, and **7** next to Carbon. SRIM will automatically normalize these to the correct ratios.
- Next, on the left side, for this second layer (**P-10 Gas**), there is a small box marked **Gas**. You need to check this box. This modifies the stopping calculations since gases have higher stopping powers than solids. Now we need to change the layer **Density (g/cm³)**. SRIM calculates a density assuming a solid. However, P-10 is a gas. Change the Density to read: **.00125**.
- The last item to enter is the target width. We wish this width to be 49 mm. There is a drop-down menu next to the **Width** column. Click on this and specify “**mm**”. Then under Width, enter: **49**.
- Press the button **Add New Layer**. You will be asked for a short Layer Name. Enter: **Brass**
- To simplify this entry, again open **Compound Dictionary**. Click on **METAL / ALLOYS**.
- Find the entry **Brass (typical)**. Click on this. Then click on **Add New Element to Layer**. You will be asked if you want to add “Brass to Brass”. It is asking you if you

want to add Brass to the current layer, which you called *Brass*. If you say NO, then you could place it in a different layer. But we wish to include it in the 3rd layer, called *Brass*, so press **YES**.

- Brass contains Cu, Zn and Pb. All the details are filled out for you, except the layer width. Go to the *Width* column, and enter **2.5 mm**. Remember to pull down the units menu to specify "mm".

This completes the setup for the calculation. Note that we have not changed the "*Type of TRIM Calculation*" at the upper right of the window as we did before (Lesson #2). We are using "Quick Calculation of Damage" for now since we want to see what happens when we run the calculation. Specifically, we are not sure that we have made the gas thick enough to stop all the ions, and we will run TRIM to see what happens and then adjust the dimensions.

You have completed the entry of a target with three layers and a total of nine elements. Good job!

Press **Save Input and Run TRIM**.

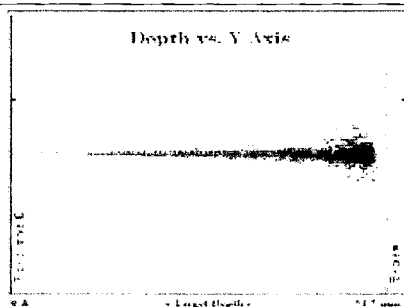
You should see a plot that looks like →→→

If you don't see this, you have put in a wrong entry. You must go back to the beginning and review all the entries.

When you get this plot, you will then modify the calculation to see more details.

- Press **PAUSE** at the top of the TRIM window.
- Press **Change TRIM**.
- We want to see the details at the very end of the range of ions. To do this we will expand the window of the plot. On the left hand side you can find a table called *PLOT Window*. Under this are the numbers **0 A - 515010000 A**. This means that the plot shows the target from the surface, 0 Angstroms, to the deepest target point, 51.5 mm. Change the *left window* to read 40 mm = **400000000 A** (there are 8 zeroes). Change the right window to read 50 mm = **500000000 A**. (8 zeroes). This will make a window that concentrates on the very end of range.
- At the top of the window, press **End Edit**. A window will pop up saying that you will have to restart TRIM. Press **YES**.
- Press **Continue**. TRIM should restart. [There is a chance of a crash. If so, you will be put back in the TRIM Setup window. Just press **SAVE Input and Run TRIM**. Then repeat the above commands to change the plot-window depths.]

At this point your plot should be identical to that of the DEMO that you executed. Note that the ions are well behaved until the very end of their travel. Their initial high velocity prevents strong interactions with the target. Conduction electrons in a target have velocities equivalent to about 25 keV/amu (the velocity of He ions at 100 keV, since He ions have a mass of 4 amu). This is energy that has the maximum strength of interaction between He



and the target electrons. The interactions between He and the target nuclei are only significant below this energy. So the He beam remains tightly focused until the He energy drops below 100 keV, or 2% of its original energy of 5 MeV.

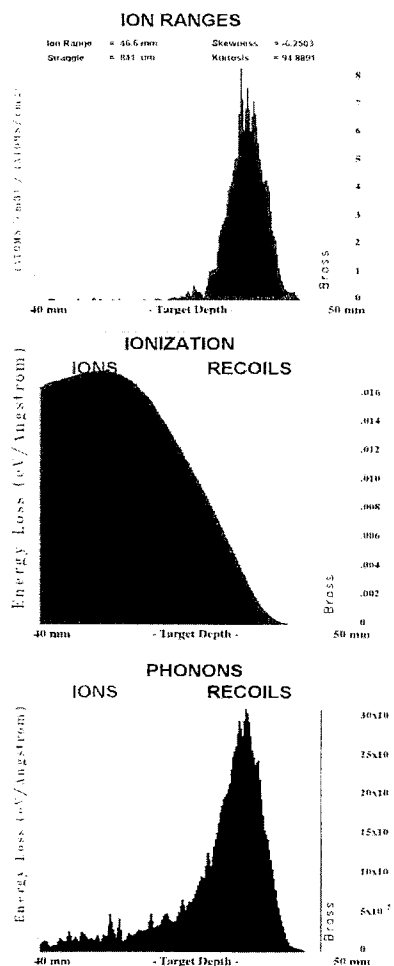
Let's look at a couple of plots. Press

Pause TRIM,

- Click on **Ion Distribution**. You will see a nice Gaussian shape, centered on 46.6 mm. It is very narrow with the straggling being less than 2% of the depth.
- Click on **Ionization**. This plot shows the energy dissipated to target electrons. Note that at the very bottom of the plots is the tiny ionization contribution from the recoils (blue line). More than 99% of the energy loss to electrons is by direct interaction with the ions.
- Click on **Phonons**. This plot shows the exact opposite trend for the production of target phonons. The target recoils now dominate this energy loss. However, one should note the units on the ordinate. The phonon energy loss is about 1% of the ion's energy loss to the target electrons. In fact, the contribution of the recoils to the target electrons is about the same as to phonons (loss to the target atoms). The energy loss by the ions to phonons is almost zero (see faint red dotted line on plot). If you look at the table on the right of the window called "**% ENERGY LOSS**", you will see the relative distribution of energy loss. Direct losses to the target electrons accounts for 99% of the ion's energy loss, and everything else is rather insignificant.

You are now done with this example. Close TRIM. When asked to **SAVE** the calculation, answer **YES**. Save the calculation in the **Default SRIM Directory**.

When you return to the TRIM setup window, press **Clear All** to begin a new session.



You may restart the last calculation by clicking on the small box in the lower-right marked “***Resume saved TRIM calc***”. Try this now. When asked, say “***Restore TRIM from SRIM Directory***”. A new box will pop up showing where you stopped the last calculation. Press **OK**.

Now resume the calculation by pressing the pink box: **Resume Saved TRIM**. The calculation will resume where it last left off. The plot of the ions will start over, since this plot is not saved. (If you get an error message, try this step a second time.)

NOTE: Only the last saved TRIM can be restored unless you save the calculation in a location different from the SRIM default location, the SRIM subdirectory: “***../SRIM Restore***”. If you save it elsewhere, you can always restart the calculation from its last point.

Special Notes about the TRIM Setup Window

- At the lower-left is a command “***AutoSave at Ion #***” with an entry box. TRIM automatically saves the calculation after a certain number of ions. Often, TRIM is run overnight, and this feature makes sure that some information is saved even if there is a power failure. The **default is 10,000 ions**. You can see what has been calculated by using the command **Resume Saved TRIM**.
 - Next is the command ***Total Number of Ions*** (default = **99999**). This command is useful to compare identical calculations with slight ion or target differences. When the calculation finishes the complete set of ions, it saves the calculation and stops.
 - Next is the command ***Random Number Seed*** (default = blank). It is possible for an artifact (weird event) to be calculated. For example, there may be only one chance in 10,000 that the ion will have a hard collision with a surface atom, creating a large cascade. If you want to save typical plots, sometimes these rare events make abnormal plots. Enter any number (**1** is OK) and you will get a totally different calculation. The default seed if no number is entered is 16381, which is a number of mythical reverence to those who delve deeply into random number theory.
-

Note: The font “***LineDraw***” is required to view some of the details of the TRIM setup program. If you find that part of the TRIM setup uses the wrong font, follow these directions.

You can find a copy of the missing font in the directory: ***..SRIM 2003/Data/Linedraw.ttf***. All you need to do is to copy this file, **Linedraw.ttf**, into the system font folder: C:/Windows/Fonts. For Windows XP systems, the font will be automatically activated. In prior Windows systems, the Font directory may be in a different location, and you may have to manually activate the font by (1) moving the font **Linedraw.ttf** into the system font directory and (2) in Windows Explorer, double click on the font name. A window will open asking if you wish to install this font.

Tutorial #4 - Calculations of Target Damage

SRIM Tutorial #1 showed how to construct a CMOS n-well in silicon that would give a peak concentration of n-type dopants of about $\sim 5 \times 10^{18}$ atoms/cm³, with the peak depth being 250 nm. The question was to select the correct dopant, and to find the implantation energy and dose (ions/cm²) to achieve this n-well structure. The Tutorial ended with the selection of phosphorus ions at 190 keV, with an implant dose of about 10^{14} ions/cm².

This tutorial will expand on the complicated subject of target damage by ions, and will use the target of Tutorial #1 for this discussion.

Normally, implanting at room-temperature, 300°K, will cause most of the implantation damage to “self-anneal”. The target damage disappears because at room temperature, the lattice atoms have adequate energy to allow simple target damage to regrow back into its original crystalline form. In general, metals self-anneal faster, and insulators slower than the semi-conductor silicon, so a silicon target makes a good example. However, there are no thermal effects in SRIM, so the damage which is calculated is that which would happen for an implantation at 0°K. Ignoring thermal effects changes the quantity of final damage, but the basic damage types which are discussed will still occur.

First, set up the same calculation in SRIM as was used in Lesson #1 :

- Click on the SRIM icon on your desktop.
 - In the opening window, click on **TRIM Calculation**.
 - Go to ION DATA and click on **PT** button. Select **Phosphorus**.
 - On this same ION DATA line, in the box: “**Energy (keV)**” you need to enter **190**.
 - Go down to TARGET DATA. Find the **PT** button for the target. Select **Silicon**.
 - Go to the LEFT side of this line, and for “**Width**” enter **3500 Ang**.
 - Go to the LEFT side of this line, and for “**Layer Name**” enter “**Silicon**” (instead of “**Layer 1**”)
 - Go to the TOP-RIGHT box “**DAMAGE**”. Scroll down to select “**Detailed Calculation with Full Damage Cascades**”.
 - The setup is complete. Look at all the boxes to check that you have entered the right numbers. Also look at some of the other entries. Press the Help button, **?**, for each item to obtain full explanations of that entry.
 - Finally, press **Save Input and Run TRIM**
-

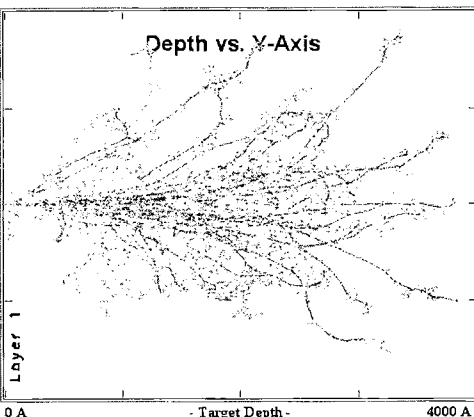
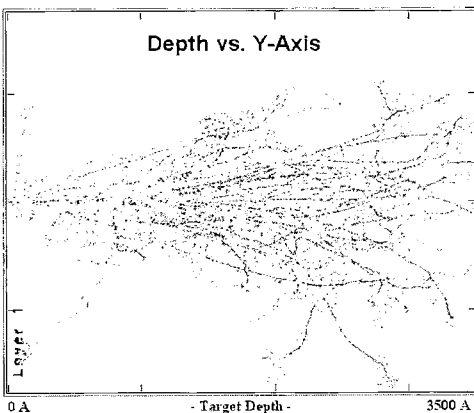
TRIM opens and the calculation immediately begins.

There is a plot in the center that shows the calculation results for each ion. The red dots are those collisions between the ion and target atoms in which the target atoms are knocked from their lattice sites. The green dots are collisions between recoiling target atoms, silicon, and other target atoms. The recoiling target atoms cause collision cascades which dominate the damage process. The dot is only plotted if the transferred energy is large enough to displace the atom hit from its lattice site. Thus the plot shows the number of displacements which have occurred. There is a different color used to show where each ion stops, but this single black pixel is so small on modern high-resolution screens that it is hard to see.

Note the upper left "ION" box, which repeats the Ion data. Note the "TARGET DATA" window, which contains all target information (you may have to expand this window with your cursor). Some of this information you did not enter, such as Displacement Energy (15eV), Surface Binding Energy (4.7eV), and Lattice Binding Energy (2eV). The values given are the default values for silicon. These will be explained later in this lesson.

First, we will play with some TRIM controls so that you can understand its flexibility. Pause the calculation by pressing **Pause**. Now press **Change TRIM**. This will allow you to change the input values to modify the calculation. For example, let's change the color of the recoiling silicon atoms from green to blue. (*Note that the colors mentioned may differ on your PC if someone has previously altered the default colors for SRIM*). Click on the colored square labeled "**Moving Atom Colors**". A palette of colors will appear. Pick a blue. Press **OK**. Press **End Edit**. Press **Continue**. The new recoiling silicon atoms will be colored blue when they make a vacancy. This blue dots are overwhelmed by the green silicon "stopping atom" dots, but you should see a few in the collision cascades.

Notice in the plot of the ion tracks, that some of the ions appear to be leaving the target to the right. The target is not deep enough to capture all the ions. To correct this, pause the calculation by pressing **Pause**. Now press **Change TRIM**. Click in the *Target Data* window: **Width (A)** **3500**. A popup menu will appear so that you can change this target depth to 4000. You will also need to change the **Plot Window** displayed on the left in the *Plots* window. This should also be changed to 4000 so that you will be looking at the full target depth. After making this change, press **End Edit**. Press **Continue**. Since we are making a fundamental change in TRIM, the calculation restarts from the beginning. The plot has changed so that it is now showing a depth of 0-4000Å. And the ions are now all stopping before they go off the plot.



The purpose of this exercise was to show that you don't need to know all the variables to start TRIM. Perhaps you are unsure about what is the maximum depth of the furthest ion. You can start TRIM with approximate values, and then change them to more suitable values after you see what happens.

Let the TRIM calculation continue while you read the next two pages of explanation.

Scientific Background – “The Physics of Recoil Cascades”

This section discusses terms used in evaluating the damage caused by energetic ions to a solid target. We need first to define basic terms.

The various parts of target damage are defined as:

- ***Displacement*** = The process where an energetic incident atom knocks a lattice atom off its site.
- ***Vacancy*** = A empty lattice site (without an atom). Originally all lattice sites are occupied, and displacements cause vacancies.
- ***Interstitial Atoms*** = Atoms which were knocked out of their original site, and come to a stop in the solid. Also the incident ions, when they stop, are considered interstitial atoms.
- ***Replacement Collisions*** = Atom sites with new atoms, identical to their original atom (this is discussed below). This is the only mechanism in which a vacancy may be re-occupied.
- ***E_{disp} = Displacement Energy***, the minimum energy required to knock a target atom far enough away from its lattice site so that it will not immediately return. This minimum energy produces a “Frenkel Pair” = a single vacancy and a nearby interstitial atom, which is the most fundamental type of damage caused by an ion.
- ***E_{latt} = Lattice Binding Energy***, the minimum energy needed to remove an atom from a lattice site. It takes energy to break electronic bonds and displace an atom from a lattice site, so this part of the energy transferred to a recoiling atom is lost. The lattice binding energy must be smaller than the Displacement Energy.
- ***E_{surf} = Surface Binding Energy***. An atom at the target surface is not confined on one side, so the energy required to remove it from its lattice site is less than if it was inside the solid and surrounded by other atoms. A surface atom has fewer electronic bonds which must be broken. This energy is especially important for calculating sputtering (removal of surface atoms).
- ***E_{final} = Final Energy of a moving atom***, below which it is considered to be stopped. The calculation of ion kinetics has to end at some minimum energy. The various energy loss processes tend to become smaller as an ion slows down, and a minimum energy creates a more efficient calculation. The Final Energy is an energy below any of the above energies.

For silicon targets, the default values are: $E_{\text{disp}} = 15 \text{ eV}$, $E_{\text{latt}} = 2 \text{ eV}$, $E_{\text{surf}} = 4.7 \text{ eV}$ and $E_{\text{final}} = 2 \text{ eV}$.

If a moving atom hits a target atom, and it transfers more than E_{disp} , the target atom will be ejected from its lattice site. Its recoil energy, $E_{\text{recoil}} = E_{\text{disp}} - E_{\text{latt}}$, since it will lose E_{latt}

energy to the lattice. The target recoil atom, if its energy is greater than E_{disp} , may go on and create further vacancies by hitting other target atoms.

There is special damage type that must be considered. If the incident atom is the same element as the atom that it hits, then the incident atom might transfer its energy to the target atom, knock it out of its lattice site, and the incident atom will then take its place in the lattice, while the hit atom moves on. This is called a **Replacement Collision**. Although this may sound complicated, this mechanism may reduce the total vacancies by up to 30%. **Three different elements must be met for a Replacement Collision.**

- (1) The moving atom must be identical to the target atom.
- (2) The incident atom must end with less energy than E_{final} (it must stop).
- (3) The struck atom must have enough energy to move on, i.e. its energy is greater than E_{disp} .

The calculation of cascades, target displacements, replacement collisions, etc. makes certain assumptions which are defined explicitly below:

- Assume an incident atom has atomic number Z_1 , and energy E . It has a collision within the target with an atom of atomic number Z_2 . After the collision, the incident ion has energy E_1 and the struck atom has energy E_2 .
- An **Atomic Displacement** occurs if $E_2 > E_{\text{disp}}$ (the hit atom is given enough energy to leave the site). A **vacancy** occurs if both $E_1 > E_{\text{disp}}$ and $E_2 > E_{\text{disp}}$ (both atoms have enough energy to leave the site). Both atoms then become moving atoms of the cascade. The energy, E_2 , of atom Z_2 is reduced by E_{latt} before it has another collision. If $E_2 < E_{\text{disp}}$, then the struck atom does not have enough energy and it will vibrate back to its original site releasing E_2 as **phonons** (energy deposited into crystal lattice vibrations).
- After a collision, if $E_1 < E_{\text{disp}}$ and $E_2 > E_{\text{disp}}$ and $Z_1 = Z_2$, then the incoming atom will remain at the site and the collision is called a **replacement collision** with E_1 released as **phonons**. The atom in the lattice site remains the same atom by exchange. This type of collision is common in single element targets with large recoil cascades. If $E_1 < E_{\text{disp}}$ and $E_2 > E_{\text{disp}}$ and $Z_1 \neq Z_2$, then Z_1 becomes a stopped **interstitial** atom.
- Finally, if $E_1 < E_{\text{disp}}$ and $E_2 < E_{\text{disp}}$, then Z_1 becomes an **interstitial** and $E_1 + E_2$ is released as **phonons**. If your target has several different elements in it, and each has a different displacement energy, then E_{disp} will change as each atom of the cascade hits different target atoms.

These sum of these damage types are related. If you understand these two equations, then you have a good grasp of the above definitions.

$$\text{Displacements} = \text{Vacancies} + \text{Replacement Collisions} \quad (\text{Eq. 1})$$

$$\text{Vacancies} + \text{Replacements} = \text{Interstitials} + (\text{Atoms which leave the target volume}) \quad (\text{Eq. 2})$$

If a cascade atom leaves the target volume, it is no longer followed. That is, if it leaves the target front surface or the rear surface, it is discarded. TRIM will follow atoms indefinitely as they go sideways, even though they leave your screen. But if they go through either target surface they are discarded and not counted. So vacancies occur within the target, and the final resting place of a moving recoil atom can be some distance from its vacancy. If a recoil atom leaves the target, clearly the sum of interstitials will be less than the number of

vacancies by the loss of that atom. Each replacement collision reduces the number of vacancies and the number of interstitials by one, leaving Eq. (1) in balance.

For those using the TRIM "quick" calculation of target damage, TRIM uses the Kinchin-Pease analytic solution for target damage as modified by two later authors. This topic is covered in the TRIM textbook, see Chapter 7 "The Scientific Background of TRIM".

The following references can be used for background:

1. Kinchin and R. S. Pease, Rep. Prog. Phys., vol. 18, 1 (1955).
2. P. Sigmund, Rad. Eff., vol. 1, 15 (1969).
3. M. J. Norgett, M. T. Robinson and I. M. Torrens, Nucl. Eng. Design, vol. 33, 50 (1974).

Questions- See if you can answer the below questions without looking back. Then check your answers. (Answers at the end of this Tutorial)

(1) Does every displacement of a target atom lead to an interstitial ?

(2) What is the difference between the Lattice Binding Energy and the Surface Binding Energy of a target atom?

(3) If you implant silicon ions into a silicon target, can the incident silicon ion become a "Replacement Collision"? Why?

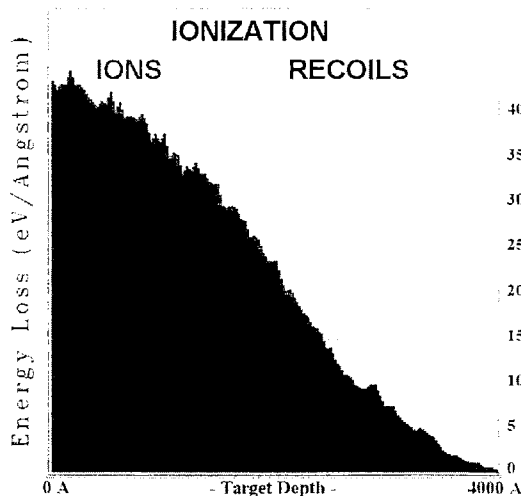
Energy Loss to Ionization and Phonons

We will now look at two simple plots: ***Ionization*** and ***Phonons***.

Ionization is energy loss to the target electrons. The electrons of the target absorb energy from the fast moving ions and recoil atoms, and then release it as heat if the target is a metal, or as phonons if the target is an insulator. The plot shows ionization from the incident ions and also from recoiling target atoms.

Phonons are energy stored in atomic vibrations in a crystal.

Since all the atoms in a crystal are linked, when you start vibrating one of them, then many of the other atoms start vibrating. This mass vibration is described as a phonon, since it is somewhat quantized (certain vibration modes are preferred).



We are assuming that TRIM has been running while you have been reading all of the above definitions and explanations.

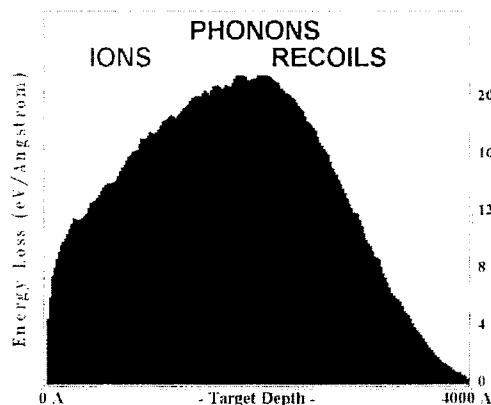
Open the ***Ionization*** plot by clicking on its box in the *Plot* window. (See plot on previous page.) There are two distinct plots, one for electronic energy loss from the incident ions, and one for energy loss from recoiling target atoms. In general, the ions have more ionization energy loss, but this is not true for all ion/target combination. The electrons tend to absorb energy most efficiently from particles whose velocity is similar to their velocity. The ions are moving much faster than the recoiling silicon target atoms, so the ions lose more energy to the target electrons.

Close the ***Ionization*** plot, and open the ***Phonon*** plot.

This plot shows the energy loss to phonons to be very different than that for Ionization. You can barely see the energy loss to phonons from the ions (red line at the bottom of the plot), and the phonons are produced almost exclusively by the recoiling target atoms. Where do these recoil-phonons come from? We don't know quite yet (it will be explained by another plot), but you can look at the window called *Calculation Parameters* on the right. The section called "% Energy Loss" shows how the incident energy of each ion (190 keV) is dissipated. The row called ***Phonons*** shows that the Ions are losing only a small amount of their energy, $\sim 0.44\%$, to phonons ($190 \text{ keV} \times 0.44\% = 836 \text{ eV}$), while the Recoils are depositing $\sim 30\%$ of the energy into phonons ($190 \text{ keV} \times 29\% = 55 \text{ keV}$).

How are phonons made? The phonons come from several sources. When an atom is knocked out of its lattice site, its binding energy, $E_{\text{latt}} = 2 \text{ eV}$, is deposited into phonons produced by the recoils. If you look at the upper right box in TRIM, you will see how many vacancies are produced by each ion, Vacancies/Ion = ~ 2300 . So for each ion, displacements by the ion or recoil cascades cause $2300 \times 2 \text{ eV} = 4,600 \text{ eV}$ of phonons.

- The rest of the phonons are caused by either the ion or a recoil hitting a lattice atom and transferring less than E_{disp} of energy. At least E_{disp} must be transferred to a target atom to eject it from its site. What happens if less than this energy is transferred? Then the target atom recoils and vibrates for a while, but it doesn't have enough energy to bounce out of its site, and the energy is finally given to new phonons.
- The TRIM box on the right called "% Energy Loss" allows you to divide the incident ion energy into various types, including phonons. The ions generate phonons with 0.44% of their incident energy of 190 keV, and the recoiling atoms contribute an additional



% ENERGY LOSS	Ions	Recoils
Ionization	44.31	23.77
Vacancies	0.13	2.51
Phonons	0.44	28.85

$28.8\% = 29.2\%$ (total). Multiplying by the total ion energy, $190 \text{ keV} \times 29.2\% = 55 \text{ keV}$ of phonons per incident ion. Assuming phonons add directly to target temperature, this can make the target quite hot. *Close the Phonon Plot.*

Damage Creation in the Target

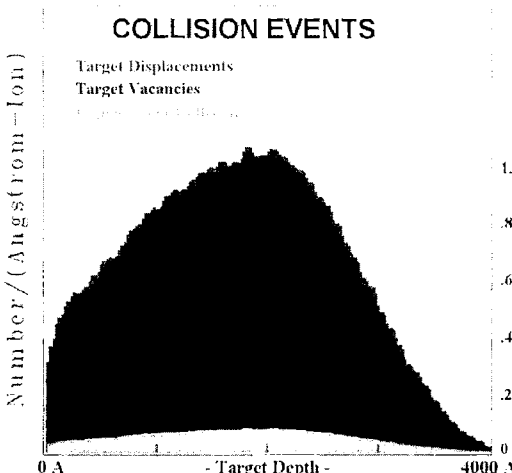
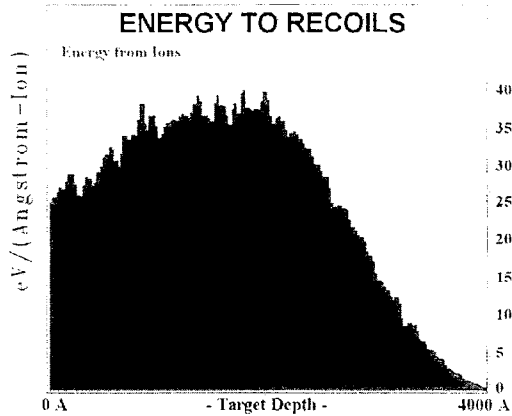
The next two available plots will show how the target damage is being created. In the *Plot* window, click the plot box: **Energy to Recoils**. A box will open asking whether you want to plot **Energy from Ions**, or **Energy absorbed by Silicon atoms**. You can pick either one. This selection is important if there are more than one element in the target, and you want to find out how much each type absorbed. For our simple case, there is only one plot because all the energy deposited by the ions will be absorbed by silicon atoms. Both plots are identical for a single element target.

The energy transferred to target atoms is fairly constant down to the mean range of the ions, $\sim 2500 \text{ \AA}$, and then it falls off as the ions stop. Other ion/target combinations may be quite different.

How much energy is transferred to the recoil cascades? Looking at the “% Energy Loss” box again, we can add up the energy deposited by the recoils: $\sim 24\% + 3\% + 29\% = 56\% = 106 \text{ keV}$. So the ion deposits 44% of its energy directly to the target, and give up 56% to recoil cascades. Close the **Energy to Recoils** plot.

Open the plot: **Damage Events**.

A menu pops up which contains all the damage details. Press the plots #1 (**Total Displacements**), #2 (**Total Vacancies**), and #3 (**Replacement Collisions**). Then press :



Show Plot Numbers 1 2 3.

The higher curve shows the **Total Target Displacements**. This is the number of atoms knocked off their target lattice site. The next lower curve shows the **Target Vacancies**. This is lower than the Target Displacements curve, showing that there are fewer vacancies than displacements.

Why are there fewer vacancies than displacements?

The lowest curve shows the **Replacement Collisions**. These are displacements in which the incident atom gives up almost all of its energy, and it does not have enough to continue further, and it falls into the vacancy left by the recoiling target atom. That is, it knocks out a target atom, and then replaces it in the lattice. Since it is the same element, there is no change in the target. As you can see, *the sum of the lower two curves equals the upper curve of Displacements*. Remember the equation shown in the **Physics of Recoil Cascades** section:

$$\text{Displacements} = \text{Vacancies} + \text{Replacement Collisions}$$

In this case, almost 10% of the displaced atoms do not leave vacancies, but instead are replaced by another silicon atom.

Are Replacement Collisions a significant portion of the target displacements?

How much do they reduce target damage in this example?

Answers to Questions in this Tutorial:

Remember the two basic equations of target damage:

$$\text{Displacements} = \text{Vacancies} + \text{Replacement Collisions} \quad (\text{Eq. 1})$$

$$\text{Vacancies} + \text{Replacements} = \text{Interstitials} + (\text{Atoms which leave the target volume}) \quad (\text{Eq. 2})$$

(1) Does every displacement of a target atom lead to an interstitial ?

No. When we combine Eq. (1) and (2) we can obtain:

$$\text{Displacements} = \text{Interstitials} + (\text{Atoms which leave the target volume})$$

As long as the collision cascades remain within the target volume, then every displacement will yield an interstitial. If recoiling atoms leave the target, then they are not counted as interstitials. The total number of interstitials may be increased if you also count the incident ions that end within the target, but this is an exception to the general rule counting the displaced atoms minus any atoms that leave the target volume.

(2) What is the difference between the Lattice Binding Energy and the Surface Binding Energy of a target atom?

Lattice Binding Energy is the minimum energy needed to remove an atom from a lattice site. It takes energy to break electronic bonds and displace an atom from a lattice site.

Surface Binding Energy. An atom at the target surface is not confined on one side, so the energy required to remove it from its lattice site is less than if it was inside the solid and surrounded by other atoms. A surface atom has fewer electronic bonds which must be broken, so it is usually considered to be less than the Lattice Binding Energy.

(3) If you implant silicon ions into a silicon target, can the incident silicon ion become a “Replacement Collision”? Why?

Yes. Although normally one defines *Replacement Collision* as a recoiling target atom knocking out another target atom of the same element, and replacing it in the lattice. Hence it replaces the atom since it is the same element, there is no change in the target lattice site. However, if your ion is the same element as one of the target atoms, it can also knock out one of these atoms and replace it. But this is not a common occurrence, and usually one expands the definition of *Replacement Collision* to include these rarer events.

SRIM - References

- 1804 Benjamin Robins, "New Principles in Gunnery", London (1807). The only copy available in the United States is the 2nd Edition (1842) at the United States Military Academy, West Point, NY.
- 00 a Mme. Pierre Curie, Comptes Rendus, 130, 76 (1900).
- 03 a J. J. Thomson, "Conduction of Electricity Through Gases," Cambridge University Press. (1903).
- 05 a W. H. Bragg and R. Kleeman, Phil. Mag., 10, 318 (1905).
- 09 a H. Geiger and E. Marsden, Proc. Roy. Soc., 82, 495 (1909).
- 11 a E. Rutherford, Phil. Mag., 21, 212 (1911); ibid, 21, 699 (1911).
- 12 a J. J. Thomson, Phil. Mag., 6-23, 449 (1912).
- 12 b J. Stark, Z. f. Physik, 13, 973 (1912).
- 12 c C. G. Darwin, Phil. Mag., 23, 901 (1912).
- 13 a N. Bohr, Phil. Mag., 25, 10 (1913).
- 14 a L. Flamm, Sitzungsber. d. K. Akad. d. Wiss. Wien, Mat. -nat. Kl., 123, 1393 (1914).
- 15 a N. Bohr, Phil. Mag., 30, 581 (1915).
- 27 a E. Fermi, Z. f. Physik, 29, 315 (1927).
- 30 a H. A. Bethe, Ann. Physik, 5, 325 (1930).
- 31 a N. F. Mott, Proc. Camb. Phil. Soc., 27, 553 (1931).
- 32 a H. A. Bethe, Z. f. Physik, 76, 293 (1932).
- 32 b A. Sommerfeld, Z. f. Physik, 78, 283 (1932).
- 32 c W. Lenz, Z. f. Physik, 77, 713 (1932); H. Jensen, Z. f. Physik, 77, 722 (1932).
- 32 d C. Moller, Ann. Physik, 14, 531 (1932).
- 32 e A. Sommerfeld, Z. f. Physik, 78, 283 (1932).
- 32 f W. Lenz, Z. f. Physik, 77, 722 (1932).
- 32g H. Jensen, Z. f. Physik, 77, 722 (1932).
- 33 a F. Bloch, Ann. Physik, 16, 287 (1933).
- 33 b F. Bloch, Z. f. Physik, 81, 363 (1933).
- 34 a H. A. Bethe and W. Heitler, Proc. Roy. Soc., A146, 83 (1934).
- 38 a W. F. G. Swann, J. Frank. Inst., 226, 598 (1938).
- 39 a E. J. Williams, Proc. Roy. Soc., 169 (1939).
- 39 b O. Hahn and F. Strassman, Naturwiss., 27, 11 (1939).
- 40 a L. A. Turner, Rev. Mod. Phys., 12, 1 (1940).
- 40 b W. E. Lamb, Phys. Rev., 58, 696 (1940).
- 40 c E. Fermi, Phys. Rev., 57, 485 (1940).
- 40 d N. Bohr, Phys. Rev., 58, 654 (1940).
- 40 e E. J. Williams, Phys. Rev., 58, 292 (1940).
- 41 a N. Bohr, Phys. Rev., 59, 270 (1941).
- 41 b J. Knipp and E. Teller, Phys. Rev., 59, 659 (1941).
- 41 c J. H. M. Brunnings, J. Knipp and E. Teller, Phys. Rev., 60, 657 (1941).
- 47 a G. Moliere, Z. f. Naturforschung, A2, 133 (1947).
- 47 b E. Fermi and E. Teller, Phys. Rev., 72, 399 (1947).
- 48 a N. Bohr, Mat. Fys. Medd. Dan. Vid. Selsk., 18, No. 8 (1948).
- 48 b A. Bohr, Mat. Fys. Medd. Dan. Vid. Selsk., 24, No. 19 (1948).
- 49 a P. Gombas, "Die Statistische Theorie des Atoms und ihre Anwendungen," Springer-Verlag, Austria (1949).
- 50 a T. Hall, Phys. Rev. 79, 504 (1950).
- 50 b N. H. Marich, Proc. Cambridge Phil. Soc., 46, 356 (1950).
- 52 a M. C. Walske, Phys. Rev. 88, 1283 (1952).
- 52 b Sternheimer R. M., "The Density Effect for the Ionization Loss in Various Materials",

SRIM - References

- Phys. Rev. 88, 854-859.
53 a H. A. Bethe, Phys. Rev. 89, 1256 (1953).
53 b J. Lindhard and M. Scharff, Mat. Fys. Medd. Kgl. Dan. Vid. Selsk., 27, No 15 (1953).
54 a J. Lindhard, Mat. Fys. Medd. Dan. Vid. Selsk., 28, No. 8 (1954).
54 b N. Bohr and J. Lindhard, Mat. Fys. Medd. Dan. Vid. Selsk., 28, No. 7 (1954).
54 c A. Erdelyi, "Table of Integral Transforms", McGraw-Hill, London (1954).
55 a J. Neufeld and R. H. Ritchie, Phys. Rev., 98, 1632 (1955); ibid. 99, 1125 (1955).
55 b J. A. Philips, Phys. Rev., 97, 404 (1955).
55 c Kinchin and R. S. Pease, Rep. Prog. Phys., 18, 1 (1955).
56 a W. Brandt, Phys. Rev. 104, 691 (1956).
56 b M. C. Walske, Phys. Rev. 101, 940 (1956).
56 c U. Fano, Phys. Rev., 103, 1202 (1956).
56 d W. Barkas, W. Birnbaum and F. M. Smith, Phys. Rev., 101, 778 (1956).
56 e P. Gambas, "Statistische Behandlung des Atoms", in *Encyclopedia of Physics*, 36, (1956).
57 a O. B. Firsov, Zh. Eksp. Teor. Fiz., 32, 1464 (1957).
57 b O. B. Firsov, Zh. Eksp. Teor. Fiz., 33, 696 (1957).
57 c H. Bichsel, R. F. Mozley and W. A. Aron, Phys. Rev., 105, 1788 (1957).
58 a O. B. Firsov, Zh. Eksp. Teor. Fiz., 34, 447 (1958).
58 b O. B. Firsov, JETP, 7, 308 (1958).
58 c W. Whaling, "Handbuch der Physik, Bd. XXXIV", 13, Springer-Verlag, Berlin
58 d S. K. Allison, Rev. Mod. Phys., 30, 1137 (1958).
59 a O. B. Firsov, Zh. Eksp. Teor. Fiz., (Transl.: Sov. Phys. JETP, 9, 1076 (1959)).
59 b R. H. Ritchie, Phys. Rev., 114, 644 (1959).
59 c O. B. Firsov, Zh. Eksp. Teor. Fiz., 36, 1517 (1959).
60 a H. Bichsel and E. A. Uehling, Phys. Rev., 119, 1670 (1960).
60 b R. M. Sternheimer, Phys. Rev., 117, 485 (1960).
60 c L. C. Northcliffe, Phys. Rev., 120, 1744 (1960).
60 d J. A. Davies, J. Friesen and J. D. McIntyre, Can. J. of Chem., 38, 1526 (1960).
61 a H. Bichsel, Tech. Report #3, Dept. of Physics, Univ. of So. Calif. (1961).
61 b J. Lindhard and M. Scharff, Phys. Rev., 124, 128 (1961).
62 a F. W. Martin and L. C. Northcliffe, Phys. Rev., 128, 1166 (1962).
62 b J. D. Jackson, "Classical Electrodynamics," Chapt. 13, Wiley, New York (1962, 1975).
63 a J. Lindhard, M. Scharff and H. E. Schiott, Mat. Fys. Medd. Dan. Vid. Selsk., 33, No. 14 (1963).
63 b U. Fano, Ann. Rev. Nucl. Sci., 13, 1 (1963).
63 c L. C. Northcliffe, Ann. Rev. Nucl. Sci., 13, 67 (1963).
63 d F. Herman and S. Skillmann, "Atomic Structure Calculations," Prentice-Hall (1963).
63 e M. T. Robinson and O. S. Oen, Appl. Phys. Lett., 2, 30 (1963).
63 f W. McChback and S. K. Allison, Phys. Rev., 132, 294 (1963).
63 g J. Lindhard, V. Nielsen, M. Scharff and P. V. Thomsen, Dansk Videnskab. Mat.-Fys. Medd., 33, no. 10 (1963).
63 h H. Bichsel, p. 8, "Amer. Inst. of Phys. Handbook", McGraw-Hill Co., New York (1963).
64 a J. Lindhard and A. Winther, Mat. Fys. Medd. Dan. Vid. Selsk., 34, No. 4 (1964).
64 b M. Abramowitz and I. A. Stegun, eds. "Handbook of Mathematical Functions", N.B.S. Applied Mathematics Series, No. 55, Washington, D.C. (1964). See pages 374-379, Eq. 9.8.5 and 9.8.6.
64 c J. P. Biersack, Hahn-Meitner Report, HMI-B37 (1964).

SRIM - References

- 65 a W. Booth and I. S. Grant, Nucl. Phys., 63, 481 (1965).
65 b J. H. Ormrod, J. R. MacDonald and H. E. Duckworth, Can. J. Phys., 43, 275 (1965).
65 c F. Eisen, Can. J. Phys., 46, 570 (1965).
65 d P. M. Porter and R. B. Moore, Can. J. Phys., 43, 1904 (1965).
65 e G. Leibfried, "Bestrahlungseffekte in Festkörpern", Teubner, Stuttgart (1965).
66 a J. F. Janni, U.S. Air Force Weapons Lab., Tech. Rpt. 65-150 (1966). (out of print)
66 b C. D. Moak and M. D. Brown, Phys. Rev., 149, 244 (1966).
66 c H. E. Schiott, Mat. Fys. Medd. Dan. Vid. Selsk., 35, No. 14 (1966).
67 a E. Bonderup, Kgl. Danske Vid. Sels. Mat. Fys. Medd., 35, No. 17 (1967).
67 b H. Bichsel, Tech. Report No. USC-136-120, Univ. S. California (1967).
67 c P. T. Wedepohl, Proc. Phys. Soc., 92, 79 (1967)
67 d T. L. Loucks, "Augmented Plane Wave Method", Benjamin Press, New York (1967).
68 a J. Lindhard, V. Nielsen and M. Scharff, Mat. Fys. Medd. Dan. Vid. Selsk., 36, No. 10 (1968).
68 b J. Lindhard, V. Nielsen, M. Scharff and P. V. Thomsen, Mat. Fys. Medd. Dan. Vid. Selsk., 33, No. 10 (1968).
68 c C. Tschalar, Nucl. Inst. and Meth., 61, (1968); ibid 64, 237 (1968).
68 d T. E. Pierce and M. Blann, Phys. Rev., 173, 390 (1968).
68 e K. B. Winterbon, Can. J. Phys., 46, 2479 (1968).
68 f H. E. Schiott, Can. J. Phys., 46, 449 (1968).
68 g J. B. Sanders, Can. J. Phys., 46, 455 (1968).
68 h S. Roosild, R. Dolan and B. Buchanan, J. Elec. Soc., 115, 307 (1968).
68 i B. L. Crowder, J. Electrochem. Soc., 46, 455 (1968).
69 a P. Sigmund, Rad. Eff., 1, 15 (1969).
69 b B. Carnahan, H. A. Luther and J. O. Wilkes, "Applied Numerical Methods", Wiley, New York (1969).
69 c D. E. Harrison, W. L. Gay and H. M. Effron, J. Math. Phys., 10, 1179 (1969).
70 a L. C. Northcliffe and R. F. Schilling, Nucl. Data Tables, 7, 233 (1970).
70 b C. C. Rousseau, W. K. Chu and D. Powers, Phys. Rev., A4, 1066 (1970).
70 c K. B. Winterbon, P. Sigmund and J. B. Sanders, Mat. Fys. Medd. Dan. Vid. Selsk., 37, No. 14 (1970).
70 d C. Varelas and J. P. Biersack, Nucl. Inst. and Meth., 79, 213 (1970).
70 e H. Bichsel, Amer. Inst. of Phys. Handbook, 3rd. Ed. (1970).
70 f W. S. Johnson and J. F. Gibbons, "Projected Range Statistics in Semiconductors," Stanford University Bookstore, Stanford, CA, 1970 (out of print).
70 g W. Brandt and J. Reinheimer, Phys. Rev., 2B, 3104 (1970).
70 h H. Bichsel, Phys. Rev., 1B, 2854 (1970).
70 i V. I. Gaydaenko and V. K. Nikulin, Chem. Phys. Lett., 7, 360 (1970).
70 j M. T. Robinson, "Nuclear Fission Reactors", British Nuclear Energy Society, London, 364 (1970).
70 k G. Ryding, A. Wittkower and P. H. Rose, Particle Accel., 6, 23 (1970).
71 a V. K. Nikulin, Zh. Tekh. Fiz., 4, 41 (1971) [Sov. Phys. - Tech. Phys. 16, 28 (1971)].
71 b W. D. Wilson and C. L. Bisson, Phys. Rev., B3, 3984 (1971).
71 c E. Bonderup and P. Hvelplund, Phys. Rev., A4, 562 (1971).
71 d M. Inokuti, Rev. Mod. Phys., 43, 297 (1971).
71 e C. W. Gear, "Numerical Initial Value Problems in Differential Equations", Prentice Hall (1971).
72 a P. Sigmund, Rev. Roum. Phys., 17, 823 (1972); ibid, 17, 969 (1972); ibid, 17, 1079 (1972).

SRIM - References

- 72 b H. D. Betz, Rev. Mod. Phys., 44, 465 (1972).
- 72 c H. Bichsel, "American Institute of Physics Handbook", 8-142, McGraw Hill, New York (1972).
- 72 d K. B. Winterbon, Rad. Effects, 13, 215 (1972).
- 72 e J. D. Jackson and R. L. McCarthy, Phys. Rev., B6, 4131 (1972).
- 72 f W. K. Chu and D. Powers, Phys. Lett., A40, 23 (1972).
- 72 g J. C. Ashley, R. H. Ritchie and W. Brandt, Phys. Rev., B5, 2393 (1972).
- 72 h R. G. Gordon and Y. S. Kim, J. Chem. Phys., 56, 3122 (1972).
- 72 i M. D. Brown and C. D. Moak, Phys. Rev., B6, 90 (1972).
- 72 j K. Guttner, H. Ewald and H. Schmidt, Rad. Eff., 13, 111 (1972).
- 72 k I. M. Torrens, "Interatomic Potentials", Academic Press Co., New York (1972).
- 72 l P. C. Gehlen, J. R. Beeler jr. and R. I. Jaffee, "Interatomic Potentials and Simulation of Lattice Defects", Plenum Press, New York, (1972).
- 73 a J. C. Ashley, R. H. Ritchie and W. Brandt, Phys. Rev., A8, 2402 (1973).
- 73 b T. M. Buck, G. H. Whitley and L. C. Feldman, Surf. Science, 35, 345 (1973).
- 73 c R. A. Johnson, J. Phys. F3, 295 (1973).
- 73 d J. C. Ashley, R. H. Ritchie and W. Brandt, Phys. Rev., A8, 2402 (1973).
- 73 e G. Basbas, W. Brandt and R. Lambcrt, Phys. Rev., 7A, 983 (1973).
- 73 f G. Basbas, W. Brandt and R. H. Ritchie, Phys. Rev., 7A, 1971 (1973).
- 74 a J. F. Ziegler and W. K. Chu, Atomic Data and Nucl. Data Tables, 13, 463 (1974).
- 74 b H. H. Andersen, "Studies of Atomic Collisions in Solids by Means of Calorimetric Techniques", Univ. Aarhus, Denmark (1974).
- 74 c B. M. Latta and P. J. Scanlon, Phys. Rev., 10A, 1638 (1974).
- 74 d Y. S. Kim and R. G. Gordon, J. Chem. Phys., 60, 4323 (1974).
- 74 e M. T. Robinson and I. M. Torrens, Phys. Rev., B9, 5008 (1974).
- 74 f C. Castaing, P. Baruch and C. Picard, LeVide, 171, Suppl. 61 (1974).
- 74 g M. J. Norgett, M. T. Robinson and I. M. Torres, Nucl. Eng. Design, 33, 50 (1974).
- 74 h E. S. Mashkova and V. A. Molchanov, Rad. Eff., 23, 215 (1974).
- 75 a J. D. Jackson, "Classical Electrodynamics," Chapt. 13, Wiley, New York (1962, 1975).
- 75 b P. Sigmund, Chapt. 1, "Radiation Damage Processes in Materials," ed. by C. H. S. Du Puy, Noordhoff, Leyden (1975).
- 75 c W. Brandt, p261, "Atomic Collisions in Solids", Plenum Press, 1 (1975).
- 75 d J. P. Biersack and D. Fink, page 737, "Atomic Collisions in Solids", Plenum Press (1975).
- 75 e D. K. Bricc, "Ion Implantation Range and Energy Deposition Distributions, vol. 1, High Energies," Plenum Press, New York (1975).
- 75 f K. B. Winterbon, "Ion Implantation Range and Energy Deposition Distributions, vol. 2, Low Energies," Plenum Press, New York (1975).
- 75 g J. F. Gibbons, W. S. Johnson and S. W. Mylroie, "Projected Range Statistics: Semiconductors and Related Materials," 2nd Edition, Halsted Press, Stroudsbury, PA, USA (1975).
- 75 h D. G. Simons, D. J. Land, J. G. Brennan and M. D. Brown, Phys. Rev., 12, 2383 (1975).
- 75 i W. Brandt, "Atomic Collisions in Solids", Plenum Press, 1, 261 (1975).
- 75 j D. Issacson, "Compilation of r_s Values", New York University Doc. #02698, National Auxiliary Publication Service, New York (1975).
- 75 k B. M. Latta and P. J. Scanlon, Phys. Rev., 12A, 34 (1975).
- 75 l L. F. Shampine and M. K. Gordon, "Computer Solutions to Differential Equations", W. H. Freeman Inc., San Francisco (1975).
- 75 m W. Neuwirth, W. Pietsch, K. Richter and U. Hauser, Z. Physik A 275 (1975).

SRIM - References

- 76 a** J. Lindhard, Nucl. Inst. and Meth., 132, 1 (1976).
76 b S. Matteson, E. K. L. Chau and D. Powers, Phys. Rev., A14, 169 (1976).
76 c S. Kalbitzer, H. Oetzmann, H. Grahmann and A. Feuerstein, Z. f. Physik, A278, 223 (1976).
76 d B. M. Latta and P. J. Scanlon, Nucl. Inst. and Meth., 132, 133 (1976).
76 e J. S. Forster, D. Ward, H. R. Andrews, G. C. Ball, G. J. Costa, W. G. Davies and I. V. Mitchell, Nucl. Inst. and Meth., 136, 349 (1976).
76 f J. E. Robinson, K. K. Kwok and D. A. Thompson, Nucl. Inst. and Meth., 132, 667 (1976).
76 g W. K. Chu, Phys. Rev., A13, 2057 (1976).
76 h W. Brandt and R. H. Ritchie, Nucl. Inst. and Meth., 132, 43 (1976).
76 i M. B. Latta and P. J. Scanlon, Phys. Stat. Sol., 74B, 711 (1976).
76 j N. W. Ashcroft and N. D. Mermin, "Solid State Physics", Holt, Rinehart and Winston Co., New York (1976).
76 k D. J. Land and J. G. Brennans, Nucl. Inst. and Meth., 132, 89 (1976).
76 l C. O. Amblandh, U. von Barth, Z. P. Popovic and M. J. Scott, Phys. Rev., 14B, 2250 (1976).
76 m M. Kaminski and S. K. Das, J. Nucl. Matl. (Letters), (1976).
76 n O. S. Oen and M. T. Robinson, Nucl. Inst. Meth., 132, 647 (1976).
76 o M. Inokuti, Rev. Mod. Phys., 43, 297 (1976).
77 a H. H. Andersen and J. F. Ziegler, "Hydrogen Stopping Powers and Ranges in All Elements", vol. 3 of series "Stopping and Ranges of Ions in Matter," Pergamon Press, New York (1977).
77 b H. H. Andersen, "Bibliography and Index of Experimental Range and Stopping Power Data", vol. 2 of series "Stopping and Ranges of Ions in Matter," Pergamon Press, New York (1977).
77 c W. D. Wilson, L. G. Hagmark and J. P. Biersack, Phys. Rev., 15B, 2458 (1977).
77 d B. Smith, "Ion Implantation Range Data for Silicon and Germanium Device Technologies", Research Studies Press, Forest Grove, Oregon, USA (1977).
77 e W. A. Grant, D. Dodds, J. S. Williams, G. E. Christodoulides, R. A. Baragiola and D. Chivers, "Proc. 5th Int. Conf. on Ion Implantation in Semicond. and Other Matl.", Plenum Press (1977).
77 f W. D. Wilson, L. G. Hagmark and J. P. Biersack, Phys. Rev., 15, 2458 (1977).
77 g H. H. Andersen, J. F. Bak, H. Knudsen, P. M. Petersen and B. R. Nielsen, Nucl. Inst. and Meth., 140, 537 (1977).
77 h J. F. Ziegler, Appl. Phys. Lett., 31, 544 (1977).
77 i T. L. Ferrell and R. H. Ritchie, Phys. Rev. 16B, 115 (1977).
77 j S. Datz, J. Gomez del Campo, P. F. Dittmer, P. D. Miller and J. A. Biggerstaff, Phys. Rev. Lett., 38, 1145 (1977).
77 k H. H. Andersen, J. F. Bak, H. Knudsen and B. R. Nielsen, Phys. Rev., 16A, 1929 (1977).
77 l L. Meyer, M. Klein and R. Wedell, Phys. Stat. Sol., 83B, 451 (1977).
77 m D. J. Land, J. G. Brennan, D. G. Simons and M. D. Brown, Phys. Rev., A16, 492 (1977).
77 n M. C. Cross, Phys. Rev., 15, 602 (1977).
77 o E. Zaremba, L. M. Sander, H. B. Shore and J. H. Rose, J. Phys., F7, 1763 (1977).
77 p W. Moller, M. Hufschmidt and D. Kamke, Nucl. Inst. and Meth., 140, 157 (1977).
77 q W. K. Chu, R. H. Kastl, R. F. Lever, S. Mader and B. J. Masters, Phys. Rev., 16B, 3851 (1977).
77 r J. P. Biersack and W. Kruger, "Ionenimplantation", by H. Ryssel and G. Ruge, B. G. Teubner Press, Stuttgart (1978).
78 a J. F. Ziegler, "Helium Stopping Powers and Ranges in All Elements," vol. 4 of series

SRIM - References

- "Stopping and Ranges of Ions in Matter," Pergamon Press, New York (1978).
- 78 b** J. F. Ziegler, Nucl. Inst. and Meth., 149, 129 (1978).
- 78 c** H. H. Andersen, K. N. Tu and J. F. Ziegler, Nucl. Inst. and Meth., 149, 247 (1978).
- 78 d** V. L. Moruzzi, J. F. Janak and A. R. Williams, "Calculated Electronic Properties of Metals", Pergamon Press (1978).
- 78 e** N. H. Sabelli, M. Kantor, R. Benedek and T. L. Gilbert, J. Chem. Phys., 68, 2767 (1978).
- 78 f** B. S. Yarlagadda, J. E. Robinson and W. Brandt, Phys. Rev., 17B, 3473 (1978).
- 78 g** R. H. Ritchie and W. Brandt, Phys. Rev., 17A, 2102 (1978).
- 78 h** M. Inokuti, Y. Itikawa and J. E. Turner, Rev. Mod. Phys., 50, 23 (1978).
- 78 i** J. Arponen and E. Pajanne, J. Phys., C12, 3013 (1978).
- 79 a** W. K. Chu, p. 179, "Proceedings of 1978 Intl. Conf. on Ion Beam Mod. of Materials", Hungarian Academy of Sciences, Budapest, Hungary (1979).
- 79 b** S. Kalbitzer, *ibid*, page 3.
- 79 c** D. Ward, H. R. Andrews, I. V. Mitchell, W. N. Lennard and R. B. Walker, Can. J. Phys., 57, 645 (1979).
- 79 d** G. J. lafrate and J. F. Ziegler, Jour. Appl. Phys., 50, 5579 (1979) plus errata available from the authors.
- 79 e** P. M. Echenique, R. H. Ritchie and W. Brandt, Phys. Rev., A20, 2567 (1979).
- 79 f** N. H. Savelli, R. Benedek and T. L. Gilbert, Phys. Rev., A20, 677 (1979).
- 79 g** P. Loftager, F. Besenbacher, O. S. Jensen and V. S. Sorensen, Phys. Rev., A20, 1443 (1979).
- 80 a** J. F. Ziegler, "Handbook of Stopping Cross Sections for Energetic Ions in All Elements," vol. 5of series "Stopping and Ranges of Ions in Matter," Pergamon Press, New York (1980).
- 80 b** U. Littmark and J. F. Ziegler, "Handbook of Range Distributions for Energetic Ions in All Elements," vol. 6of series "Stopping and Ranges of Ions in Matter," Pergamon Press, New York (1980).
- 80 c** P. E. Batson, Sol. State Comm., 34, 477 (1980).
- 80 d** J. P. Biersack and L. G. Haggmark, Nucl. Inst. and Meth., 174, 257 (1980).
- 80 e** S. P. Ahlen, Rev. Mod. Phys., 52, 121 (1980).
- 80 f** J. C. Ashley, Nucl. Inst. and Meth., 170, 197 (1980).
- 80 g** S. A. Cruz, C. Vargas and D. K. Brice, Nucl. Inst. and Meth., 170, 208 (1980).
- 80 h** H. Ryssel, G. Lang, J. P. Biersack, K. Muller and W. Kruger, IEEE Trans. Elec. Dev., ED-27, 58 (1980).
- 80 i** M. J. Berger et al., "Radiation Quantities and Units", ICRU-33, International Commission on Radiation Units, Bethesda, MD, USA (1993).
- 80 j** D. I. Thwaites, Phys. Med. Biol., 25, 865 (1980).
- 80 k** F. Hubert, A. Fleury, R. Bimbot and D. Gardes, Ann. de Phys., 5, 1 (1980).
- 81 a** A. H. Agajanian, "Ion Implantation: A Bibliography", 6, IBM Tech. Comm. Rpt. # TR22.2374, East Fishkill, New York, (1981).
- 81 b** U. Littmark and J. F. Ziegler, Phys. Rev., 23A, 64 (1981).
- 81 c** S. Kreussler, C. Varelas and W. Brandt, Phys., Rev., 23B, 82 (1981).
- 81 d** A. Mann and W. Brandt, Phys. Rev., 24, 4999 (1981). Note: Figure 3 of this paper can not be reproduced. It contains serious computational errors. The conclusions based on the figure must be considered unproven.
- 81 e** M. Kitagawa, "Recent Theoretical Developments in Atomic Collisions in Solids", Strasbourg, France (1981).
- 81 f** P. M. Echenique, R. M. Nieminen and R. H. Ritchie, Sol. Stat. Comm., 37, 779 (1981).
- 81 g** W. Brandt, Nucl. Inst. and Meth., 191, 453 (1981).
- 81 h** S. A. Cruz, L. T. Chadderton and J. C. Barthelat, Nucl. Inst. and Meth., 191, 479 (1981).

SRIM - References

- 81 i N. E. B. Cowern, Phys. Lett., 82A, 200 (1981).
81 j J. P. Biersack, Nucl. Inst. and Meth., 182/183, 199 (1981).
81 k J. A. Golovshenko, A. N. Goland, J. S. Rosner, C. E. Thorn, H. E. Wegner, H. Krendsen and C. D. Moak, Phys. Rev., 23B, 957 (1981).
81 l N. R. Arista and W. Brandt, Phys. Rev., A23, 1898 (1981).
81 m F. Guinea, F. Flores and P. M. Echenique, Phys. Ref. Lett., 47, 604 (1981).
81 n D. J. Isaacson, Ph.D. Thesis, New York University, (1981). (unpublished)
81 o F. Jahnel, H. Ryssel, G. Prinke, K. Hoffman, K. Muller, J. P. Biersack and R. Henkelman, Nucl. Inst. and Meth., 182/183, 223 (1981).
82 a W. Brandt and M. Kitagawa, Phys. Rev., 25B, 5631 (1982).
82 b J. P. Biersack and J. F. Ziegler, "Ion Implantation Techniques," Springer-Verlag, p. 122 (1982).
82 c N. E. B. Cowern, Nucl. Inst. and Meth., 194, 101 (1982).
82 d D. Fink, J. B. Biersack, K. Tjan and V. K. Cheng, Nucl. Inst. and Meth., 194, 105 (1982).
82 e G. Basbas and R. H. Ritchie, Phys. Rev., 25A, 1943 (1982).
82 f J. P. Biersack and J. F. Ziegler, Nucl. Inst. and Meth., 194, 93 (1982).
82 g P. Sigmund, Phys. Rev., 26A, 2497 (1982).
82 h N. E. B. Cowern, Phys. Rev., A26, 2518, (1982); ibid A25, 604 (1982).
82 i R. Ishiwari, N. Shiomi and N. Sakamoto, Phys. Rev., A25, 2524 (1982).
82 j W. Brandt, Nucl. Inst. and Meth., 194, 13 (1982). Note that figure 4 of this paper contains a serious error and that the Hc ion data, if plotted correctly, fails to fall with the heavy ion data.
82 k V. I. Shulga, Rad. Eff., 62, 237 (1982).
82 l E. S. Mashkova, V. A. Molchanov and V. I. Shulga, Rad. Eff., 62, 107 (1982).
82 m J. P. Biersack and M. Stadelc, Rad. Eff., 64, 51 (1982).
82 n D. Fink, J. P. Biersack, K. Tjan and V. K. Cheng, Nucl. Inst. and Meth., 194, 105 (1982).
82 o J. F. Janni, Atomic Data and Nucl. Data Tables, 27, No. 2-5, 1 (1982).
82 p D. J. O'Connor, Nucl. Inst. and Meth., 196, 493 (1982).
82 q J. P. Biersack, Z. f. Physik, A-95, 305 (1982).
82 r P. Mertens and Th. Krist, Nucl. Inst. and Meth., 194, 57 (1982).
82 s E. C. Montenegro, S. A. Cruz, C. Vargas-Aburto, Phys. Lett., 92A, 195 (1982).
83 a J. P. Biersack and P. Mertens, "Charge States and Dynamic Screening of Swift Ions in Solids," p 131, Oak Ridge Rpt. No. CONF-820131, Oak Ridge (1983).
83 b W. N. Lennard, H. R. Andrews, I. V. Mitchell, D. Phillips and D. Ward, ibid, p 136 (1983).
83 c H. Bichsel, Phys. Rev., A28, 1147 (1983).
83 d J. Berthold and S. Kalbitzer, Phys. Lett., 91A, 37 (1982).
83 e Y. H. Ohtsuki, "Charged Beam Interactions with Solids", Taylor and Francis, London (1983).
83 f D. Fink, J. P. Biersack, M. Stadelc, K. Tjan, V. K. Cheng, Nucl. Inst. and Meth., 218, 171 (1983); ibid 817 (1983)..
83 g M. J. Puska and R. M. Nieminen, Phys. Rev., B27, 6121 (1983).
83 h I. Nagy, J. Laszlo and J. Giber, Appl. Phys., A31, 153 (1983).
83 i D. I. Thwaites, Rad. Res., 95, 495 (1983).
83 j G. Both, R. Krotz, K. Lohman and W. Neuwirth, Phys. Rev., A28, 3212 (1983)
84 a J. F. Ziegler, J. P. Biersack, U. Littmark, "The Stopping and Range of Ions in Solids," vol. 1 of series "Stopping and Ranges of Ions in Matter," Pergamon Press, New York (1984).

SRIM - References

- 84 b J. P. Biersack and W. Eckstein, Appl. Phys., A34, 73 (1984).
84 c H. Kitagawa Nucl. Inst. and Meth., B2, 123 (1984).
84 d M. J. Berger et al., "Stopping Powers and Electrons and Positrons", ICRU-37, International Commission on Radiation Units, Bethesda, MD, USA (1984).
85 a D. J. O'Conner, R. McDonald and J. P. Biersack, Nucl. Inst. and Meth., XX, xxx (1985).
85 b M. Behar, P. Fichtner, C. A. Olivieri, J. P. deSouza, F. Zawislak, J. P. Biersack and D. Fink, Rad. Eff. Lett., 85, 117 (1985).
85 c J. Mahanty, K. N. Pathak and V. V. Paranjape, Sol. State Comm., 54, 649 (1985).
85 d R. Wedcill, Nucl. Inst. and Meth., B12, 17 (1985).
85 e I. Nagy, J. Laszio and J. Giber, Nucl. Inst. and Meth., A321, 221 (1985).
85 f P. Bauer, D. Semrad and P. Mertens, Nucl. Inst. and Meth., B12, 56 (1985).
85 g L. E. Porter, Nucl. Inst. and Meth., B12, 50 (1985).
85 h D. I. Thwaites, Nucl. Inst. and Meth., B12, 84 (1985).
86 a P. M. Echenique, R. M. Nieminen, J. C. Ashley and R. H. Ritchie, Phys. Rev., A-33, 897 (1986).
86 b J. C. Ashley, A. Gras-Marti and P. M. Echenique, Phys. Rev., A-34, 2495 (1986).
86 c J. Mahanty, K. N. Pathak and V. V. Paranjape, Phys. Rev., B32, 2333 (1986).
86 d A. Gras-Marti, P. M. Echenique and R. H. Ritchie, Surf. Sci., 173, 310 (1986).
86 e D. Semrad, P. Mertens and P. Bauer, Nucl. Inst. and Meth., B15, 90 (1986).
86 f I. Nagy, J. Laszio and J. Giber, Nucl. Inst. and Meth., B15, 8 (1986).
86 g D. J. O'Conner and J. P. Biersack, Nucl. Inst. and Meth., B15, 14 (1986).
86 h H.Q. Woodward and D. R. White, British J. of Radiology, vol. 59, 1209-1219 (1986).
86 i Fishman & Moore, S.I.A.M.-J.S.C., vol. 7, 24 (1986))
87 a M. Aono and R. Souda, Nucl. Inst. and Meth., B27, 55 (1987).
87 b E. W. Kuipers and A. L. Boers, Nucl. Inst. and Meth., B29, 567 (1987).
87 c S. I. Easa and A. Modinos, Surf. Sci., 183, 531 (1987).
87 d J. C. Ashley and P. M. Echenique, Phys. Rev., B35, 1521 (1987).
87 e J. R. Sabin and J. Oddershede, Nucl. Inst. and Meth., B27, 280 (1987).
87 f L. E. Porter, Rad. Res., 110, 1 (1987).
87 g D. I. Thwaites, Nucl. Inst. and Meth., B27, 293 (1987).
88 a A. Arnau, P. M. Echenique and R. H. Ritchie, Nucl. Inst. and Meth., B33, 138 (1988).
88 b M. Kato, T. Ititaka and Y. H. Ohtsuki, Nucl. Inst. and Meth., B33, 432 (1988).
88 c K. J. Snowdon, Nucl. Inst. and Meth., B33, 365 (1988).
88 d I. Nagy, A. Arnau and P. M. Echenique, Phys. Rev., B38, 9191 (1988).
88 e K. J. Snowdon, D. J. O'Connor and R. J. MacDonald, Phys. Rev. Lett., 61, 1760 (1988).
88 f C. D. Hu and E. Zaromba, Phys. Rev., B37, 9268 (1988).
88 g K. Schonhammer, Phys. Rev., B37, 7735 (1988).
88 h D. Boutard, W. Moller, B. M. U. Scherzer, Phys. Rev., B38, 2988 (1988).
88 i W. Eckstein and M. Hou, Nucl. Inst. and Meth., B31, 386 (1988).
88 j S. T. Nakagawa and Y. Yamamura, Radiation Effects, 105, 239 (1988).
88 k J. P. Biersack, Nucl. Inst. Methods, B35, 205-214 (1988).
88 l P. L'Ecuyer, C.A.C.M., vol. 31, 742-749, 774-776 (1988), "An Efficient and Portable Combined Random Number Generator"
89 a P. M. Echenique, I. Nagy and A. Arnau, Intnl. J. Quantum Chem., 23, 521 (1989).
89 b P. M. Echenique and J. B. Pendry, Prog. Surf. Sci., 32, 111 (1989).
89 c H. Derkx, A. Narmann and W. Heiland, Nucl. Inst. and Meth., B44, 125 (1988).
89 d F. Shoji, K. Oura and T. Hanawa, Nucl. Inst and Meth., B36, 23 (1989).
89 e J. Burgdorfer, J. Wang and J. Muller, Phys. Rev. Lett., 62, 1599 (1989).
89 f T. Ititaka and Y. H. Ohtsuki, Surf. Sci., 213, 187 (1989).

SRIM - References

- 89 g H. Mikkelsen and P. Sigmund, Phys. Rev., A40, 101 (1989).
89 h I. Nagy, A. Arnau and P. M. Echenique, Phys. Rev., A40, 987 (1989).
89 i Hubert, F., Bimbot, R., and Gauvin, H., (1989). Nucl. Instr. and Meth. B36, 357; (1990). At. Data Nucl. Data Tables, 46, 1.
89 j "The Stopping of Ions in Compounds", by J. F. Ziegler and J. M. Manoyan, published in Nuclear Instruments and Methods, Vol. B35, 215-228 (1989)
90 a A. Narman, R. Monreal, P. M. Echenique, F. Flores, W. Heiland and S. Schubert, Phys. Rev. Lett., 64, 1601 (1990).
90 b A. Arnau, M. Penalba, P. M. Echenique, F. Flores and R. H. Ritchie, Phys. Rev. Lett., 65, 1024 (1990).
90 c P. M. Echenique, F. Flores and R. H. Ritchie, Sol. State Phys., 43, 229 (1990).
90 d M. Hasagawa, T. Uchida, K. Kimura and M. Mannami, Phys. Lett., A-145, 182 (1990).
90 e Y. Yamazaki, Nucl. Inst. and Meth., B48, 97 (1990).
90 f T. Iiaka, Y. H. Ohtsuki, A. Koyama and H. Ishikawa, Phys. Rev. Lett., 65, 3160 (1990).
90 g A. Koyama, Y. Sasa, H. Ishikawa, A. Misu, K. Ishii, T. Itatka, Y. H. Ohtsuki and M. Uda, Phys. Rev. Lett., 65, 3156 (1990).
90 h Y. Susuki, H. Mukai, K. Kimura and M. Mannami, Nucl. Inst. and Meth., B48, 347 (1990).
90 i H. Esbensen and P. Sigmund, Ann. Phys., 201, 152 (1990).
90 j A. H. Sorensen, Nucl. Inst. and Meth., B48, 10 (1990).
90 k H. Bichsel, Phys. Rev., A41, 3642 (1990).
90 l Bauer, P., (1990). Nucl. Instr. and Meth. B45, 673.
90 m Hubert, F., Bimbot, R., and Gauvin, H., (1989). Nucl. Instr. and Meth. B36, 357; (1990). At. Data Nucl. Data Tables, 46, 1.
90 n G. Schiwietz, Phys. Rev. 42A, 296, (1990)
91 a A. Narmann, W. Heiland, R. Monreal, F. Flores, P. M. Echenique, Phys. Rev., 44B, 2003 (1991).
91 b A. Narmann, Mod. Phys. Lett., B5, 561 (1991).
91 c R. Medenwalt, S. P. Moller, E. Uggerhoj, T. Worm, P. Hvelplund, H. Knudsen, K. Elsener and E. Morenzoni, Nucl Inst. and Meth., B58, 1 (1991).
91 d K. Shima, N. Kuno, M. Yamanouchi and H. Tawara, Natl. Inst. for Fusion Sci., #NIFS-DATA-10, (1991).
91 e R. Medenwalt, S. P. Moller, E. Uggerhoj, T. Worm, P. Hvelplund, H. Knudsen, K. Elsener and E. Morenzoni, Phys. Lett., A-155, 155 (1991).
91 f S. A. Cruz and J. Souillard, Nucl. Inst. and Meth., B61, 433 (1991).
91 g W. Eckstein, "Computer Simulation of Ion-Solid Interactions", Springer-Verlag, Berlin (1991).
91 h H. Paul, D. Semrad and A. Swilinger, Nucl. Inst. and Meth., B61, 261 (1991).
92 a M. Penalba, A. Arnau and P. M. Echenique, Nucl. Inst. and Meth., B67, 66 (1992).
92 b M. Penalba, A. Arnau, P. M. Echenique, F. Flores and R. H. Ritchie, Europhysics Lett., 19, 45 (1992).
92 c F. J. Garcia de Abajo and P. M. Echenique, Phys. Rev., 46, 2663 (1992).
92 d A. Narmann, H. Franke, K. Schmidt, A. Arnau and W. Heiland, Nucl. Inst. and Meth., B69, 158 (1992).
92 e P. Bauer, F. Kastner, A. Arnau, A. Salin, P. D. Fainstein, V. H. Ponce and P. M. Echenique, Phys. Rev. Lett., 69, 1140 (1992).
92 f A. Arnau, M. Penalba, P. M. Echenique and F. Flores, Nucl Inst. and Meth., B69, 102 (1992).
92 g S. A. Cruz and J. Souillard, Nucl. Inst. and Meth., B71, 387 (1992).

SRIM - References

- 92 h H. Bichsel, Phys. Rev., 46A, 5761 (1992).
- 92 i H. Bichsel and T. Hiroka, Nucl. Inst. and Meth., B66, 345 (1992).
- 92 j P. Bauer, W. Rossler and P. Mertins, Nucl. Inst. and Meth., B69, 46 (1992).
- 93 a J. M. Pitarke, R. H. Ritchie, P. M. Echenique and E. Zaremba, Europhysics Lett., 24, 7 (1993).
- 93 b J. M. Pitarke, R. H. Ritchie and P. M. Echenique, Nucl. Inst. and Meth., B79, 209 (1993).
- 93 c P. M. Echenique and A. Arnau, Phys. Scripta, T49, 677 (1993).
- 93 d M. J. Berger et al., "Stopping Powers and Ranges for Protons and Alpha Particles", ICRU-49, International Commission on Radiation Units, Bethesda, MD, USA (1993). See pages 82-105 for a length discussion of experimental methods and their limitations.
- 94 a P. Sigmund, Phys. Rev. A, 50, 3197-3201 (1994).
- 94 b A. N. Narmann and P. Sigmund, Phys. Rev. A, 49, 4709-4715 (1994).
- 95 a P. Sigmund and A. N. Narumann, Laser and Part. Beams, 13, 281-292 (1995).
- 95 b Turner, J. E., "Atoms, Radiation and Radiation Protection", Wiley, New York, 2nd Ed.
- 97 a L. Glazov and P. Sigmund, Nucl. Inst. Methods, B125, 110-115 (1997).
- 98 a P. Sigmund, Nucl. Inst. Methods, 135B, 1-15 (1998).
- 98 b P. Sigmund and L. Glazov, Nucl. Inst. Methods, B136-138 (1998)
- 98 c Konac, G., Kalbizer, S., Klatt, C., Niemann, D. and Stoll, R. (1998a). Nucl. Instr. and Meth., B138, 159.
- 98 d Konac, G., Klatt, C. and Kalbizer, S., (1998b). Nucl. Instr. and Meth. B146, 106.
- 2000 a Bransden B. H. and Joachain C. J., "Quantum Mechanics", Prentice Hall, Harlow, 2nd Ed. (2000)
- 2000 b Sigmund P. and Schinner A., "Binary Stopping Theory for Swift Heavy Ions", Europ. Phys. J. D12, 425-434 (2000).
- 2000 c Sigmund P., "Shell Correction in Bohr Stopping Theory", Europ. Phys., D12, 111-116 (2000).
- 2000 d Schinner A. and Sigmund P., "Polarization Effect in Stopping of Swift Partially Screened Heavy Ions: Perturbative Theory", Nucl. Inst. Meth., B164-165, 220-229.
- 2000 e Pitarke J. M. and Campillo I., "Band Structure Effects on the Interaction of Charged Particles with Solids", Nucl. Inst. Meth., B164, 147-160 (2000).
- 2000 f Arbo N. R., Gravielle M. S. and Miraglia J. E., "Second Order Born Collisional Stopping of Ions in a Free-Electron Gas", Phys. Rev. A62, 32901-1-7 (2000)
- 2000 g Glazov L. G., "Energy Loss Spectra of Swift Ions", Nucl. Inst. Meth., B161, 1-8.
- 2000 h Hiraoka, T. and Bichsel, H., (2000). Medical Standard Dose, Chiba, Japan 5 (Suppl.1),1.
- 2001 a Wieszczycka W. and Scharf W. H., "Proton Radiotherapy Accelerators", World Scientific, New Jersey, USA (2001).
- 2001 b Paul, H. and Schinner, A., (2001). Nucl. Instr. and Meth. B179, 299.
- 2002 a Sigmund, P. and Schinner A., "Binary Theory of Electronic Stopping", Nucl. Inst. Meth.m, B195, 64-90 (2001).
- 2002 b Bichsel H., "Shell Corrections in Stopping Powers", Phys. Rev. A-65, 1-11 (2001)
- 2002 c Arista N. R., "Energy Loss of Heavy Ions in Solids: Non-Linear Calculations for Slow and Swift Ions", Nucl. Inst. Meth., B195, 91-105 (2001)
- 2002 d Grande P. L. and Schwietz G., "The Unitary Convolution Approximation for Heavy Ions", Nucl. Inst. Meth., B195, 55-63 (2001)
- 2002 e Glazov L. G., "Energy Loss Spectra of Swift Ions- Beyond the Landau Approximation", Nucl. Inst. Meth., B192, 239-248 (2001).
- 2002 f Grande, P.L. and Schwietz, G., (2002). Nucl. Instr. and Meth. B195, 55 (2002).
- 2002 g Maynard, G., Sarrazin, M., Katsonis, K., and Dimitriou, K., (2002). Nucl. Instr. and Meth.

SRIM - References

- B193, 20 (2002).
- 2002 h** Paul, H. and Schinner, A., (2002). Nucl. Instr. and Meth. B195, 166 (2002).
- 2002 i** Sigmund, P. and Schinner, A., (2002). Europ. Phys. J. D23, 201; Nucl. Instr. and Meth. B195, 64; Nucl. Instr. and Meth. B193, 49 (2002).
- 2003 a** Geant4 collaboration (2003). Nucl. Instr. and Meth. A506, 250 (2003).
- 2003 a** Cohen S. M., “Bethe Stopping Power Theory for Heavy Element Targets and Relativistic Projectiles”, Phys. Rev., A 68, 12720 (2003)
- 2003 b** Paul, H. and Schinner, A., (2003). Nucl. Instr. and Meth. B209, 252.
- 2003 c** Paul, H. and Schinner, A., (2003). At. Data Nucl. Data Tables 85, 377.
- 2003 d** Sigmund, P., Fettouhi, A. and Schinner, A., (2003). Nucl. Instr. and Meth. B209, 19.
- 2004 a** Cabrera-Trujillo R. and Sabin, J. R., Ed. “Theory of the Interaction of Swift Ions with Matter”, Part 1, vo. 45, , Adv. Quantum Chem., Elsevier, Amsterdam.
- 2004 b** Cabrera-Trujillo R. and Sabin, J. R., Ed. “Theory of the Interaction of Swift Ions with Matter”, Part 2 vo. 46 , Adv. Quantum Chem., Elsevier, Amsterdam.
- 2004 c** Sigmund, P., “Stopping of Heavy Ions”, vol. 204 of Springer Tracts of Modern Physics, Springer Co., Berlin.
- 2004 d** Cohen S. M., “Aspects of Relativistic Sum Rules”, Adv. Quantum Chem., 46, 241-265
- 2004 e** Sharma A., Fettouhi A., Schinner A. and Sigmund P., “Electronic Stopping of Swift Ions in Compounds”, Nucl. Inst. Meth., B218, 19-28.
- 2004 f** Ziegler, J.F., (2004). Nucl. Instr. and Meth. B219-220, 10
- 2005 a** ICRU, Vol. 73 of ICRU Reports, “Stopping of Ions Heavier than Helium”, Oxford Univ. Press, Oxford, UK.
- 2005 b** Basko M. M., “On the Low-Velocity Limit of the Bohr Stopping Formula”, Europ. Phys. J. D 32, 9-17.
- 2005 c** Sigmund P., Sharma A., Schinner A. and Fettouhi A., “Valence Structure Effects in the Stopping of Swift Ions”, Nucl. Inst. Meth., B230, 1-6.
- 2005 d** Cohen S. M., “Simple and Accurate Sum Rules for Highly Relativistic Systems”, J. Chem. Phys., 122, 104-105.
- 2005 e** Paul, H. and Schinner, A., (2005). Nucl. Instr. and Meth. B227, 461.
- 2006 a** Sigmund, P., “Particle Penetration and Radiation Effects”, vol. 151 of Springer Tracts of Solid State Sciences, Springer Co., Berlin.
- 2006 b** Sigmund P. and Schinner A., “Shell Correction in Stopping Theory”, Nucl. Inst. Meth., B243, 457-460.
- 2006 c** Allison et al. (2006). IEEE Transactions on Nuclear Science 53, 270.
- 2006 d** Paul, H., (2006). Nucl. Instr. and Meth. B247, 166.
- 2006 e** Paul, H. and Schinner, A., (2006). Nucl. Instr. and Meth. B249, 1.

Professor Helmut Paul (Univ. Linz) has digitized and plotted most existing experimental data of the stopping powers of ions in matter. His work has made accessible a century of experimental results, and this is a major contribution to the understanding of the stopping of ions in matter. See his website :

www.exphys.uni-linz.ac.at/Stopping/

SRIM - Index

A

Accuracy of PRAL Tables	10-8 to 10-11
Ahlen, S.	1-12, 1-17, 4-3
Air, He Ranges in	5-23
Algorithm for Ion's Range	10-4 to 10-12
Angle of Incidence of Ion,	8-5
TRIM	
Animated Plots in TRIM	9-41
Anomalous Peaks and Dips,	8-26 to 8-27
TRIM	
Atom, Bohr	2-18, 2-22
Atom, Hartree-Foch	2-10, 2-16 to 2- 25, 3-8
Atom, Lenz-Jenzen	2-20
Atom, Moliere	2-20
Atom, Moruzzi, Janak and	2-10, 2-17 to 2- 25
Williams	
Atom, Thomas-Fermi	2-10, 2-16 to 2- 25
Atom-Atom scattering	2-10 to 2-33, 7- 3 to 7-7
Atomic Electron Exchange	2-12 to 2-15, 2- 24 to 2-25
Energy	
Auto-Saving of TRIM	8-8
Calculation	

B

BACKSCAT.txt Datafile	9-18 to 9-19
Backscattered Ions Datafile	9-18 to 9-19
Backscattered Ions in TRIM	8-8
Barkas-Andersen Correction	4-7, 4-22 to 4- 32
Batch Mode, Running TRIM	8-27 to 8-30
in	
Bethe, H.	1-9, 1-12, 3-3
Bethe-Bloch Corrections	4-33 to 36
Bethe-Bloch Equation	4-2 to
Bichsel, H.	1-17, 4-3
Bichsel, Shell Corrections	4-10 to 4-20
Biersack's <i>Magic Formula</i>	2-38 to 2-43, 7- 3 to 7-7
Binary Collisions	2-10 to 2-33
Binary Scattering - <i>Magic</i>	2-38 to 2-43
<i>Formula</i>	
Biologic Targets in TRIM	8-4
Bloch Correction, Stopping	3-3, 4-7, 4-30 to 4-33
Bloch F.	1-9, 1-12

Bohr Atom	2-18, 2-22
Bohr Straggling	6-5 to 6-6
Bohr, Neils	1-5 to 1-21, 2-1, 3-3, 2-10, 4-2
Bonding Corrections to	5-3 to 5-23
Stopping	
Bragg's Rule	Ch 5
Brandt, W.	1-16
Brandt-Kitagawa Theory	3-29 to 3-40
Building Complex Targets,	11-15 to 11-20
Tutorial #3	

C

Center of Mass Coordinates.	2-2 to 2-8, 6-2
to 6-5	
Charge Distributions, Solid	2-15, 2-17
State	
Charge State - Hydrogen Ion	3-9 to 3-10
Charge state of ion	1-12 to 1-20
Collision Data - High	8-22
Resolution	
COLLISON.txt (Full	9-38 to 9-39
Cascades)	
COLLISON.txt (No Cascades)	9-36 to 9-37
COLLISON.txt (Quick	9-32 to 9-36
Damage)	
COLLISON.txt datafile	8-9, 8-19, 9-3
Colors of TRIM Plots	8-30, 9-41
COM Coordinates	2-2 to 2-8
Complex Targets, Tutorial #3	11-15 to 11-20
Compound Stopping	5-6 to 5-20
Corrections, Examples	
Compounds in TRIM	Ch 5, 8-6, 8-11
Coordinates, Center of Mass	2-2 to 2-8, 6-2
to 6-5	
Corc-and-Bond Corrections	5-3 to 5-23
Corrections to Bethe-Bloch	4-33 to 36
Corrections, Core and Bond	5-3 to 5-23
Curie, Marie	1-2

D

Damage Calculations in TRIM	7-26 to 7-28, 8- 7, 8-9 to 8-10
Damage in Target, Tutorial #4	11-21 to 11-28
Damage, Kinchin-Pcase Model	7-27 to 7-28, 8- 7, 8-9 to 8-10
Datafile of Ion's 3-D Path	8-23 to 8-24, 9- 14 to 9-15
Datafile: 3-D Stopping	9-17 to 9-18
Distribution	

SRIM - Index

Datafile: BACKSCAT.txt	9-18 to 9-19	
Datafile: COLLISON.txt	9-3	Energetic Ion Stopping Ch 4
Datafile: COLLISON.txt	8-9, 9-17 to 9-18,	Energy Degraders 8-20 to 8-22
Datafile: COLLISON.txt		Energy to Recoils, Tutorial #4 11-21 to 11-28
Datafile: COLLISON.txt (Full Cascades)	9-38 to 9-39	Error #62 in TRIM 8-15
Datafile: COLLISON.txt (No Cascades)	9-36 to 9-37	Error in TRIM, Regional Settings 8-5
Datafile: COLLISON.txt (Quick Damage)	9-32 to 9-36	Error in TRIM.DAT 8-15
Datafile: IONIZ.txt	9-25 to 9-26	Error , TRIM Recoil Cascade Size 8-31 to 8-32
Datafile: LATERAL.txt	9-15 to 9-17	Ethylene, Stopping in 5-8
Datafile: NOVAC.txt (Replacement Collisions)	9-27 to 9-31	Exchange Energy between Electrons 2-12 to 2-15, 2-24 to 2-25
Datafile: PHONON.txt	9-26 to 9-27	
Datafile: RANGE 3D.txt	9-14 to 9-15	
Datafile: RANGE.txt	9-11 to 9-12	
Datafile: SPUTTER.txt	9-21 to 9-23	
Datafile: TDATA.sav	9-7 to 9-8	
Datafile: TRANSMIT.txt	9-19 to 9-20	
Datafile: TRIM.cfg for TRIM Colors	8-30	
Datafile: TRIM.IN	9-5 to 9-7, 8-27 to 8-30	Fano, U. 1-12, 1-17, 4-3 to 4-47
Datafile: TRIMOUT.txt	9-24	FAQs for TRIM 9-41
Datafile: VACANCY.txt	9-27 to 9-30	Fermi, Enrico 1-8, 1-10, 3-3
Datafiles from TRIM	Ch 9	Firsov Interatomic Potential 2-29
DaVinci, L and SRIM	1-1	Formvar, Stopping in 5-10
Definitions used in Book	1-1	Free Electron Gas 1-12, 3-3 to 3-6
Density Effect in Stopping	4-6, 4-20 to 4-21	Free Flight Path (FFP) in TRIM 7-7 to 7-17
Displacement Damage in TRIM	7-27 to 7-28, 8-7, 8-9 to 8-10	Free Flight Path and Experiments 7-12 to 7-13
Displacement Energy in TRIM	8-7, 8-9 to 8-10	Full Damage Calculation in TRIM 8-4
Displacements, Tutorial #4	11-21 to 11-28	
E		
Effective Charge in Stopping	3-25 to 3-40, 4-8	Gas / Solid Targets in TRIM 8-6, 8-11, 8-22 to 8-23
Electron Exchange Energy	2-12 to 2-15, 2-24 to 2-25	Gas / Solid Targets, Tutorial #3 11-15 to 11-20
Electron Induced Cascades in TRIM	8-4, 8-16 to 8-18	Gas Phase Corrections 5-6 to 5-7, 5-21
Electronic Stopping	Ch 2 to Ch 4	Gases, Stopping in Ch 5
Electronic Stopping - Straggling	Ch 6, 7-24 to 7-26	Gciger, H. 1-5
Electronic Stopping, 3-D Plots	8-19	
Electronic Stopping, Lindard	3-4 to 3-6	
Electronic Straggling in TRIM	Ch 6, 7-24 to 7-	
H		
Hartrree-Foch Atom		Hartree-Foch Atom 2-10, 2-16
He ions in Air – Range		He ions in Air – Range 5-23
Heavy Ion Stopping, BK Theory		Heavy Ion Stopping, BK Theory 3-29 to 3-40
Heavy Ion, Scaling of Stopping		Heavy Ion, Scaling of Stopping 3-24 to 3-40
Helium Ion – Stopping		Helium Ion – Stopping 3-10 to 3-16
Help during TRIM Calculation		Help during TRIM Calculation 9-41
History of Stopping and Ranges		History of Stopping and Ranges Ch 1
History of Stopping Theory		History of Stopping Theory 4-2
Hydrocarbons, Stopping in		Hydrocarbons, Stopping in 5-2 to 5-3, 5-10

SRIM - Index

Hydrogen Ion – Stopping	3-10 to 3-20	Layered Structures in TRIM	7-33
Hydrogen Ion, Charge State	3-9 to 3-10	LDA and Shell Corrections	4-10 to 4-20
I			
Impact Parameter and Free Flight Path	7-15	Legal Notice about SRIM	8-33 to 8-34
Impulse Approx. in Free Flight Path	7-14 to 7-17	Lenz-Jenzen Atom	2-20
Input Parameters to TRIM	Ch 8	Light Ion Stopping	Ch 4
Input Window in TRIM	8-2 to 8-3	Lindhard Interatomic Potential	2-30
Interatomic Potential, Firsov	2-29	Lindhard Stopping	4-37 to 4-44
Interatomic Potential, Lindhard	2-30	Lindhard, J	1-12, 3-4 to 3-6
Interatomic Potentials	2-10 to 2-33	Liquid, Stopping in	5-6 to 5-7, 5-21
Interatomic Potentials, Universal	2-27 to 2-33, 2-44 to 2-47	Local Density Approximation (LDA)	3-6 to 3-10, 4-37 to 4-44
Interstitial Atoms in TRIM	8-7, 8-9 to 8-10	LSS Theory	1-15
Interstitial Production in TRIM	7-27 to 7-28, 8-7, 8-9 to 8-10	M	
Ion Energy Reducers (Degraders)	8-20 to 8-22	Magic Formula	7-3 to 7-7
Ion Mixing Calculations	8-22	<i>Magic Formula</i> for Binary Scattering	2-38 to 2-43
Ion Mixing, Tutorial #2	11-8 to 11-14	Marsden, E	1-5
Ion Range, 3-D Plot	9-13	Masking Effects in TRIM	7-34, 9-13
Ion Ranges, Tutorial #1	11-2 to 11-7	Mixing of Layers, Tutorial #2	11-8 to 11-14
Ion Screening Length	3-29	Moliere Atom	2-20, 3-8
Ion Straggling	Ch 6	Monolayer Collisions Steps in TRIM	8-4
Ion Trajectory – Random Walk	10-2	N	
Ion's 3-D Path in Target	8-23 to 8-24	Neutron Induced Cascades in TRIM	8-4, 8-16 to 8-18
Ion's Range – Algorithm	10-4 to 10-12	New Principles of Gunnery (1848)	1-1
Ionization in Target, Tutorial #4	11-21 to 11-28	Northcliffe, L.	4-3
Ionization Plot in TRIM	9-25 to 9-26	Nuclear Fission	I-5
Isotopically Enriched Targets	8-20	Nuclear Stopping	Ch 2
K			
Kinchin-Pease Damage in TRIM	7-27 to 7-28, 8-7, 8-9 to 8-10	Nuclear Stopping, Straggling of	10-18 to 10-19
Kohn, Core and Bond Model	5-2 to 5-3	Nuclear Stopping, Universal	2-34 to 2-36, 10-15 to 10-18
Kurtosis	6-1, 6-10 to 6-20, 8-24 to 8-25	Nuclear Straggling	2-36 to 2-38, 6-1, 6-10 to 6-20
L			
Laboratory Coordinates	2-3	P	
Lamb, Willis	1-8, 1-11	Parameters of the Magic Formula	7-5 to 7-7
Landau Straggling	6-6 to 6-7	Peaks and Dips in TRIM	8-26 to 8-27
Lateral Range Distribution Plot	9-15 to 9-17	Periodic Table in TRIM	8-5
LATERAL.txt Datafile	9-15 to 9-17	Phase Corrections	5-6 to 5-7, 5-21
Lattice Binding Energy in TRIM	8-7, 8-9 to 8-10	Phonon Plot in TRIM	9-26 to 9-27
Lattice Binding Energy, Tutorial #4	11-21 to 11-28	Phonons in Target, Tutorial #4	11-21 to 11-28
		Phonons in TRIM	8-7, 8-9 to 8-10
		Photon Induced Cascades in TRIM	8-4, 8-16 to 8-18
		Physics of Recoil Cascades	8-9

SRIM - Index

Plot, 3-D Ion Ranges	9-13	TRIM	
Plot, Ion Ranges under a Mask	9-13	Screening Function, Definition	2-18
Plot, Lateral Range Distribution	9-15 to 9-17	Screening Length of Ions	3-29
Plots, Changing Colors	8-30, 9-41	Screening Length, Thomas-Fermi	2-18
Plots, TRIM Ion Ranges	9-9 to 9-12	Setup of TRIM Calculation	Ch 8
Plots, TRIM Recoil Distributions	9-10 to 9-12	Setup Window in TRIM	8-2 to 8-3
Polyimide, Stopping in	5-10	Shell Correction to Stopping	4-6 to 4-20
Polystyrene, Stopping in	5-9	Shell Corrections, Bichsel	4-10 to 4-20
Polysulphone, Stopping in	5-10	Shell Corrections, LDA	4-10 to 4-20
Potentials, Universal Interatomic	2-44 to 2-47	Sigmund, Peter	1-17, I-18, 3-1, 4-3, 5-2, 6-18
Powers, D.	5-1 to 5-3	Skewness	6-1, 6-10 to 6-20, 8-24 to 8-25
PRAL Software	Ch 10	Solid / Gas Targets in TRIM	8-22 to 8-23
PRAL Tables, Accuracy	10-8 to 10-11	Solid / Gas Targets, Tutorial #3	11-15 to 11-20
Projected Range – Algorithm	10-4 to 10-12	Solid State Charge Distributions	2-10 to 2-33
Projected Ranges	7-19 to 7-20, 8-24 to 8-25	Sommerfeld, E.	2-10
R			
Radial Ranges	7-19 to 7-20, 8-24 to 8-25	SPUTTER.txt Datafile	9-21 to 9-23
Random Number Seed in TRIM	7-35	Sputtered Atom Datafile	9-21 to 9-23
Randomness in Ion Trajectory	10-2	Sputtering	7-28 to 7-32, 8-4, 8-8, 8-10 to 8-11
Range of Ions – Algorithm	10-4 to 10-12	Sputtering, Tutorial #2	11-8 to 11-14
Range Straggling	Ch 6	SRIM as a Subroutine	8-32 to 8-35
RANGE.txt, TRIM Datafile	9-10 to 9-12	SRIM Definitions	1-1
RANGE-3D.txt, TRIM Datafile	9-14 to 9-15	SRIM History	1-1 to 1-23
Ranges, He in Air	5-23	SRIM Legal Notice	8-33 to 8-34
Ranges, History of	Ch 1	SRIM Module	8-32 to 8-35
Recoil Cascades, Tutorial #4	11-21 to 11-28	SRIM Tutorials	Ch 11
Recoil Energy Plot in TRIM	9-31 to 9-32	SRIM, Bonding Corrections	5-3 to 5-23
Regional Settings in TRIM	8-5	Stopping and Range Tables	Ch 10
Relativistic Stopping	3-3, Ch 4	Stopping and Range Tables, Accuracy	10-8 to 10-11
Replacement Collisions in TRIM	7-27 to 7-28, 8-7, 8-9 to 8-10	Stopping Force	1-18
Replacement Collisions, Tutorial #4	11-21 to 11-28	Stopping in Ethylene	5-8
Replacements, Plot in TRIM	9-27 to 9-31	Stopping in Formvar	5-10
Ritchie, R.	1-12	Stopping in Gas Phase	5-6 to 5-7, 5-21
Robins, Benjamin	1-1	Stopping in Hydrocarbons	5-2 to 5-3, 5-10
Rutherford, Ernst	1-5	Stopping in Polyimide	5-10
S			
Sabin, J.	5-2 to 5-3	Stopping in Polystyrene	5-9, 5-19
Scaling of Heavy Ion Stopping	3-24 to 3-40	Stopping in Poisylphone	5-10
Scientific Background of	Ch 7	Stopping in Water	5-6 to 5-7
		Stopping Number, Definition	4-7
		Stopping of Helium Ions	3-10 to 3-16
		Stopping of Hydrogen Ions	3-10 to 3-20
		Stopping, 3-D Plots	8-19, 8-23 to 8-25

SRIM - Index

Stopping, Barkas-Andersen Correction	24, 9-14 to 9-15 4-7, 4-22 to 4-32	Tables, Stopping and Range Target Damage in TRIM	Ch 10 7-26 to 7-28, 8-7, 8-9 to 8-10
Stopping, Bloch Correction	4-7, 4-30 to 4-33	Target Damage, Tutorial #4 Target Phase in TRIM Target Roughness and Stopping Target Sputtering in TRIM	11-21 to 11-28 8-6, 8-11 6-18 7-28 to 7-32, 8-10 to 8-11
Stopping, Bonding Corrections	5-12 to 5-17	TDATA.sav, TRIM Datafile	9-7 to 9-8
Stopping, Brandt-Kitagawa Theory	3-29 to 3-40	Teller, E.	1-8, 1-11, 3-3
Stopping, Density Effect	4-6, 4-20 to 4-21	Texture Effects on Stopping	6-18
Stopping, Effective Charge	4-8	Thomas Fermi Atom	1-13 to 1-15, 2-10, 2-20, 3-25
Stopping, Effects of Roughness	6-18	Thomas-Fermi Screening Length	2-18, 2-23
Stopping, Effects of Texture	6-18	Thompson, J. J.	1-2 to 1-5
Stopping, Electronic	Ch 2, 3 and 4	Three Dimension Ion Ranges	9-13
Stopping, Energetic Light Ions	Ch 4	Three Dimensional Stopping Data	8-23 to 8-24
Stopping, History	Ch 1, 4-2	Three Dimensional Stopping Datafile	9-17 to 9-18
Stopping, LDA Calculation	4-37 to 4-44	Three-Dimension Plots of Stopping	8-19
Stopping, Lindhard	3-4 to 3-6, 4-37 to 4-44	TRANSMIT.txt Datafile	9-19 to 9-20
Stopping, Nuclear (Universal)	Ch 2, 10-15 to 10-18	Transmited Ions Datafile	9-19 to 9-20
Stopping, Shell Correction	4-6 to 4-20	Transmited Ions in TRIM	8-8
Stopping, Straggling in	Ch 6	TRIM – Target Damage	7-26 to 7-28, 8-7, 8-9 to 8-10
Stopping, Straggling in Nuclear	10-18 to 10-19	TRIM Backscattered Ions	9-18 to 9-20
Stopping,, Compounds and Gases	Ch 5	TRIM Data in Two Dimensions	7-21 to 7-22, 7-34
Straggling	Ch 6	TRIM Datafile:	9-38 to 9-39
Straggling in Nuclear Stopping	10-18 to 10-19	COLLISON.txt (Full Cascades)	
Straggling in TRIM Ranges	7-18 to 7-23	TRIM Datafile:	9-36 to 9-37
Straggling using Energy Degraders	8-20 to 8-22	COLLISON.txt (No Cascades)	
Straggling, Bohr	6-5 to 6-6	TRIM Datafile:	9-32 to 9-36
Straggling, Elecctronic in TRIM	7-24 to 7-26	COLLISON.txt (Quick Damage)	
Straggling, Landau Theory	6-6 to 6-7	TRIM Datafile: IONIZ.txt	9-25 to 9-26
Straggling, Nuclear	2-36 to 2-38, 6-1, 6-10 to 6-20	TRIM Datafile: LATERAL.txt	9-15 to 9-17
Straggling, Vavilov	6-7 to 6-10	TRIM Datafile: NOVAC.txt	9-27 to 9-31
Subroutine, Making SRIM into a	8-32 to 8-35	(Replacement Collisions)	
Surface Binding Energy in TRIM	8-7, 8-9 to 8-10	TRIM Datafile: PHONON.txt	9-26 to 9-27
Surface Binding Energy, Tutorial #4	11-21 to 11-28	TRIM Datafile: RANGE.txt	9-11 to 9-12
T		TRIM Datafile: RANGE-3D.txt	9-14 to 9-15
Tables of Ion Ranges – Algorithm	10-4 to 10-12		
Tables of Ranges, Accuracy	10-8 to 10-11		

SRIM - Index

TRIM Datafile: TDAT.A.sav	9-7 to 9-8		7, 8-9 to 8-10
TRIM Datafile: TRIM.IN	8-27 to 8-30		8-7, 8-9 to 8-10
TRIM Datafile: TRIMOUT.txt	9-24		7-33 to 7-34
TRIM Datafile: VACANCY.txt	9-27 to 9-30		9-41
TRIM Error, Recoil Cascade Size	8-31 to 8-32		8-31 to 8-32
TRIM Error, Regional Settings	8-5		Cascade Size Error
TRIM FAQs	9-41		TRIM, Mixed Solid/Gas
TRIM Free Flight Path (FFP)	7-7 to 7-17		Targets
TRIM Output Datafiles	Ch 9		TRIM, Modifying During
TRIM Plot: Ion Ranges	9-9 to 9-12		Calculation
TRIM Plot: Recoil Distribution	9-10 to 9-12		TRIM, Neutron Induced
TRIM Range Straggling	7-18 to 7-23		Cascades
TRIM Setup Window	8-2 to 8-3		TRIM, Periodic Table
TRIM Sputtered Atoms	9-21 to 9-23		TRIM, Phonon Plot
TRIM, 3-D Datafile of Ion's Path	8-23 to 8-24		TRIM, Phonons
TRIM, 3-D Datafile of Stopping	8-23 to 8-24		TRIM, Projected Range
TRIM, 3-D Plots of Stopping	8-19		TRIM, Radial Range
TRIM, Anomalous Peaks and Dips	8-26 to 8-27		TRIM, Random Numbers
TRIM, Auto-Saving Calculation	8-8		TRIM, Ranges under a Mask
TRIM, Backscattered Ions	8-8		TRIM, Replacements Plot
TRIM, Biological Targets	8-4		TRIM, Running in Batch
TRIM, Changing Plot Colors	8-30, 9-41		Mode
TRIM, Compound Dictionary	8-6, 8-11		TRIM, Scientific Background
TRIM, Displacement Energy	8-7, 8-9 to 8-10		TRIM, Scientific Explanations
TRIM, Electron Induced Cascades	8-4		TRIM, Solid or Gas Target
TRIM, Electronic Straggling	7-24 to 7-26		TRIM, Sputtered Atoms
TRIM, Energy to Recoils Plot	9-31 to 9-32		TRIM, Sputtering in
TRIM, Error #62	8-15		7-28 to 7-32, 8- 10 to 8-11
TRIM, Error in TRIM.DAT file	8-15		TRIM, Surface Binding
TRIM, Help	9-41		Energy
TRIM, High Resolution Collision Data	8-22		TRIM, the Magic Formula
TRIM, Input / Setup	Ch 8		7-3 to 7-7
TRIM, Interstitial Atoms	8-7, 8-9 to 8-10		TRIM, Transmitted Ions
TRIM, Ion Angle of Incidence	8-5		8-3 to 8-4
TRIM, Ion Mixing Calculations	8-22		TRIM, Vacancy Plot
TRIM, Ionization Plot	9-25 to 9-26		8-4, 8-13 to 8- 18
TRIM, Isotopically Enriched Targets	8-20		TRIM, Various Ion Energies
TRIM, Kinchin Pease Damage	7-27 to 7-28, 8-		8-4, 8-13 to 8- 18
			TRIM, Various Ion Starting
			Positions
			8-4, 8-13 to 8- 18
			TRIM, Viewing Window
			8-7
			TRIM. Datafile TRIM.IN
			9-5 to 9-7
			TRIM.DAT setup file
			8-4, 8-13 to 8- 18
			TRIM.IN datafile
			8-27 to 8-30, 9- 5 to 9-7
			TRIMOUT.txt
			9-24
			Tutorial #1, Ion Ranges, Doses
			11-2 to 11-7
			Tutorial #2, Layer Mixing,
			11-8 to 11-14

SRIM - Index

Sputtering		
Tutorial #3, Complex Targets	11-15 to 11-20	
Tutorial #4, Target Damage	11-21 to 11-28	
Tutorials on SRIM	Ch 11	
Two Atom Scattering, <i>Magic Formula</i>	2-10 to 2-33, 2-38 to 2-43	
Two Dimensional TRIM Plots	7-21 to 7-22, 7-34	
Two-Atom Scattering	Ch 2	
Two-Body Collisions and Scattering Angles	7-7 to 7-8	
U		
Universal Interatomic Potential	2-27 to 2-33, 2-44 to 2-47	
Universal Nuclear Stopping	2-34 to 2-36, 10-15 to 10-18	
V		
Vacancies in Target, Tutorial #4		11-21 to 11-28
Vacancy Plot in TRIM		9-27 to 9-30
Vacancy Production in TRIM		7-27 to 7-28, 8-7, 8-9 to 8-10
Vacancy Production using Kinchin-Pease Model		7-27 to 7-28, 8-7, 8-9 to 8-10
Vavilov Straggling		6-7 to 6-10
Viewing Window in TRIM		8-7
W		
Water, Stopping in		5-6 to 5-7
Weird Distributions in TRIM		8-26 to 8-27
Whaling, W.		1-17
Windows, Regional Settings		8-5
Z		
ZBL Potential		2-27 to 2-33

SRIM Book - Version Number

This SRIM book is being published using what is called “Print on Demand”. This means that the publisher (LuLu.com) has no inventory of books, but only prints a book once it is sold. The printing usually takes 2 days, but for hard covers (such as this book) the text pages must be sent to another factory for the hard cover. This usually takes 10-14 days. The total time to delivery may be 3 weeks after an order is placed. The advantage of this kind of publishing is two-fold:

- (1) This business model results in a reduction of total manufacturing costs by over 40% since there are no unsold books.
- (2) The book can be updated at any time by just uploading a new digital content file. This allows typos, poorly written text and especially unclear figures to be corrected at any time.

Below are the changes incorporated into this SRIM book. Almost all changes have been to clarify figures which contained three or more curves which were not clearly identified. The version number of this book (that you are looking at) is the last version listed below, and is indicated by a number on the spine of the book cover.

The authors are particularly indebted to Gyorgy Vizkelety (GV), Helmut Paul (HP), Nuno Barradas (NB) and Watson Newhauser (WN) for many suggestions and pointing out typos, omissions, and vague language in the text. Their contributions are noted below.

Date / Version	Page	Changes
01/03/2008 / v01		Opened for SALE.
01/16/2008 / v02	0-4, 12-18 1 - 17-24 2-25 4-35 4-36 5-08 5-20	Added Version Numb/Date to title page, and pg 12-18 Added several Notes about important Citations after 1985. Figure 2-10 - Moved “Molierc” to proper curve. Added captions to Figure 4-19. (WN) Added captions to Figure 4-20. (WN) Changed caption to Figure 5-6 to clarify. (WN) Changed caption to Figure 5-10 to clarify. (WN)
2/19/2008 / v03	1-24, 12-11 Cover 9-9 to 9-12 11-2 to 11-14	Added citation to H. Paul’s website on experimental stopping powers. (HP) Added Version Number to Title page and book spine. Changed Figs and Tables to be same as SRIM2008.04 with new ordinate units on Ion/Recoils Distribution plots/tables. Changed SRIM software so that plots of distributions of Ions and Recoils will both have plot Ordinates of (Atoms/cm3)/(Atoms/cm2). Updated Tutorials 1 & 2 so figures and discussion have same units.
06/01/2008 / v04	1-1 1-3 1-7 1-8	Changed spelling of Di Vinci to Da Vinci, and LaPlace to Laplace. Also noted that Robins’ work came after Euler, Laplace and Lavoisier, (HP) Inserted word “used” in sentence about electrometer.(HP) Suggested to change “amu” units to “u”. “Amu” was correct up to 1961. In a history chapter, I think this usage is OK. “amu” is still widely used in U.S. (HP) Changed spelling of Strassman to Strassmann. (HP)

Date / Version	Page	Changes
06/01/2008 / v04 (con't)	1-15, 1-17, 3-2, 3-3, 3-7. 1-13, 2-18 Eq.2.71-2.73; 6- 36, 10-39 3-2 4-26 5-12 5-14 7-6 7-24, Eq. 7-46 and 7-47 Fig. 10-9 10-15	Minor typos corrected. (HP) Changed Bohr Radius to 0.529E-10 m = 0.529 Å. (GV) Changed screening constant from 0.8854 to 0.8853 (GV) Figures 3-6 to 3-10: Added comment to caption about solid line called "Barkas Fit". (HP) Fig. 4-13 – Caption modified to explain "Barkas Fit" curve in figure. (NB) Two citations added to Koln research on CAB approach to stopping in compounds (NB) Bcsenbachker citation added to References. (NB) Table 4-1. Coef. C4, and C5 need to be exchanged. (GV) Changed "B" to " β " (GV) Caption is on wrong figure. Corrected with new caption. (NB) Reference is made to CD-ROM of textbook. All this is now part of SRIM software. See: " <i>../SR Module/HELP – SR Module.rtf</i> " (NB)
12/15/2008 / v05	2-10,2-14,2- 18,3-4,3-5,3- 7,4-7,4-8,4- 23,4-29,4-39,7- 5,7-19,7-28	Numerous typos corrected and several definitions expanded to increase clarity. All these corrections were suggested by a class taught by Col. Don Gillich of Rensselaer Polytechnic Institute and of the United States Military Academy at West Point, USA.

